Characterising alluvial architecture using physical models, subsurface data and field analogues

By

David James Moreton

Submitted in accordance with the requirements
for the degree of Doctor of Philosophy

School of Geography and School of Earth Sciences
University of Leeds

May 2001

The candidate confirms that the work submitted is his own and that appropriate credit has been given where reference has been made to the work of others.

Abstract

This thesis presents an integrated subsurface, field analogue and scaled physical modelling approach to the investigation of the autocyclic and allocyclic controls on braided river morphology and preserved alluvial architecture at both the channel-belt and within channel-belt scales.

The prediction of inter-well alluvial architecture in the continental Barren Red Beds of the Upper Carboniferous, Lower Ketch Member, Southern North Sea, UK, presents difficulties. Subsurface data from the Tyne Field is subdivided into coarse-grained sandbodies (60%) alternating with siltstone lithofacies (40%). A depositional model is proposed representing an aggrading alluvial plain traversed by a series of 100 to 1100 m wide channel-belts with palaeochannel depths of between 1.5 and 3.5 m, and supplied with a fine grain size distribution (D_{50} = 0.08 mm). A seasonal climatic regime probably promoted crevasse splay deposition and development of extensive floodplains. The Tyne model can nest within a regional depositional setting where: (1) the predominant sediment supply was from the north; and (2) proximal to distal trends exhibit a grain size diminution, and a lowering of net-to-gross and connectivity.

This thesis provides the first complete comparative study between the Tyne Field and an onshore analogue, the Eocene Escanilla Formation, Southern Pyrenees, Spain. New evidence is presented to suggest a fluvio-lacustrine setting for the Escanilla Formation. A marked qualitative and quantitative similarity between the two sedimentary sequences gives confidence in the analogue and permits the use of geometrical datasets, including sandbody width/thickness ratios, frequency distributions, channel-belt orientation and connectivity to be used in the construction of geological reservoir models of the Lower Ketch Member. Empirical estimates of channel-belt width in the prediction of sandbody geometry overestimate ~75 % of the channel-belt sandbody widths measured from the outcrop, because estimates fail to account for: (1) different channel patterns, (2) any autocyclic and allocyclic controlling mechanisms, and (3) vertical and lateral channel-belt stacking.

Grain size is a key control on alluvial architecture at both the within channel-belt and channel-belt scale. Physical modelling of the Ashburton River, Canterbury Plains, New Zealand has allowed the impact of grain size to be isolated from other controlling

parameters. Three reach-scale, generic Froude-scaled modelling experiments, incorporating a fourfold change in grain size have been undertaken in a flume facility that permits aggradation. Comparisons between model and field studies suggest grain size is not the most influential control on channel geometry. The modern Ashburton River exhibits no change in channel geometry downstream. However, a halving then quartering of the grain size distribution in the Ashburton River model resulted in: (1) channel geometries first deepening then widening, (2) the proportion of overbank sheet flow increasing, and (3) the duration of channel occupancy remaining constant. Under the boundary conditions imposed in the experimental study, grain size limits are recognised for scaled physical models, which suggest that physical models cannot reproduce Lower Ketch Member grain size distribution ranges.

The preserved alluvial architecture from the Ashburton model is classified and quantified into six architectural elements. Architectural elements from the Ashburton River model show that alluvial architecture is dominated by channel fill deposits. An increase in primary channel fill width and thickness, an increase in splay widths, a higher proportion of preserved splay deposits, and a decrease in the size and frequency of occurrence of fine-grained architectural elements may all be attributed to a quartering of the grain size distribution.

A methodology is presented to link permeability to the architectural elements of the Ashburton model, in order to supply data from the preserved stratigraphy of physical models to serve as inputs for the construction of both static and dynamic (fluid flow) reservoir models. In addition, the potential of an aggrading physical model to examine the impact of sampling frequency and up-scale averaging in the construction of reservoir models is explored.

Acknowledgements

I like to thank NERC and ARCO British Ltd. for providing the funding for this research. I would also like to thank James Parr for setting up this project at ARCO British Ltd., to Peter O'Mara for his time and helpful input to the development of ideas on aspects of hydrogcarbon geology. Thanks go to BP for their continuation of support in the few months prior to submission. John Turner and all the staff at the Core Store are thanked for their help in accessing core data.

My greatest thanks goes to Professors Phil Ashworth and Jim Best, for their ideas for and during the project, continued enthusiasm, dedication, endless opportunities to add skills to my CV, tremendous sense of humour and friendship. I should also like to thank them for their help during fieldwork in New Zealand and the opportunity to incorporate jet boating, quad biking, flying and ladder climbing into my fieldwork, and finally for making time in Leeds extremely enjoyable.

For the great services on fieldwork in Spain I like to thank Phil Ashworth, Jim Best, Mum and Dad, Lisa Burton, and in New Zealand, Phil Ashworth, Jim Best, Merren Jones, Stuart MacQuarrie, Ben Sheets and Chris Paola. For all their help and support in logistics, friendly hospitality and shooting practise a special thanks goes to Don and Pauline Wilson. I would like to thank also to Pete MacManus and Neil Cundall for the production of thin sections; Bob Bows for his construction of the automated laser trolley; Lisa Burton and Linda Gregorash for their grain size analysis. Particular thanks go to Steve Mardon and Merren Jones for continued help throughout my research especially during flume runs when eight tonnes of sediment needed moving and mixing. Thanks go to David Ashley for all his support and help during my time here, Mark Franklin for help with video analysis and Bob Finch for help and support in Earth Sciences. I should also like to thank Andy Evans and Andy Turner for all their web help, Alison Manson, Mark Newcombe, Lois Wright, David Appleyard and Adam Davenport in the Graphics Unit for all their tremendous diagrams.

I should also like to thank a host of people for helpful discussions, many through that great medium email, in helping to sharpen my thoughts and help direct my research; in no particular order thanks go to Merren Jones, Steve Mardon, Andy Howard, Jamie

Woodward, Chris Paola, Richard Collier, Jeff Peakall, Janes Francis, Mike Leeder, Paul Wright, Andy Pulham, Stuart MacQuarrie, Paul Wignall, Rob Raiswell, Mary Kraus, Tom Dreyer, Robert Riding, Matt Davis, Ben Sheets, Ian Lunt, Neville Morrison, Colin Jones and Andrea Moscariello. Thanks go also to my Research Support Committee: Richard Collier, Jamie Woodward, Andy Howard, Peter O'Mara and James Parr. Thanks go to Chris Howells and Al Scott for thought provoking discussions on applications to reservoir modelling and inputs.

For members that have passed through the Zoo during my time in Leeds, including Gary (Biffa), Ruth, Sherryl, Eilidh, Jamie, Suzie, Sim, Lia, Sue and last but not least Frank, for office banter, good laughs and many good nights out in the early years of my PhD! In Earth Sciences thanks go to Jo, Zahir, Chris, Richard, James, Steve, Claire, Claire, Omar and Rufus. Thanks to Sarah Fuller for her help and friendship during my degree and PhD. Zahir and Najat are thanked for their friendship and Jo Horton for continued coffee breaks and lengthy discussion. Thanks go to my housemates and other friends over the years for all their friendship, including Mike, Dan, Afraz, Alan, Naveed, Stam, Paula, Paul, Madeleine, Anna, Claire, Rob, Tom and Sue.

Thanks go to my Brother for inspiring me to finish and live on a Pacific Island, also my sister, Paula Wood and Dan Compton for their hospitality during my stays in London. I would also like to thank Martin, Pauline and Richard for all their friendship over the years. My parents are thanks for all their support during my time at University. An enormous thanks goes to Paula Wood for her continued support, help and particularly her understanding in times when I had to spend my weekends locked away in the Geography basement.

Contents

ABSTRACT.....II

ACKNOWLEDGEMENTS.....IV

CONTENTS.....VI

LIST OF FIGURES AND TABLES.....XV

LIST OF SYMBOLS.....XXVI

LIST OF ACRONYMS.....XXVIII

Chapter 1. Introduction and background to the study

1.1 INTRODUCTION..... 1

1.2 CONTROLS ON ALLUVIAL ARCHITECTURE 1

1.3 APPLICATIONS WITHIN THE HYDROCARBON INDUSTRY 3

1.4 RESEARCH OBJECTIVES..... 5

1.6 THESIS STRUCTURE..... 5

Chapter 2. Controls on alluvial architecture and the assessment of hydrocarbon reservoir heterogeneity

2.1 SYNOPSIS 8

2.2 INTRODUCTION TO CONTROLS ON ALLUVIAL ARCHITECTURE 8

2.2.1 CLIMATIC AND SEA-LEVEL CHANGES 10
2.2.2 TECTONICS 14
2.2.3 SUBSIDENCE AND AGGRADATION RATE 16
2.2.4 COMPACTION 20
2.2.5 AVULSION AND CHANNEL MIGRATION 21
2.2.6 INCISION AND SCOUR 26
2.2.7 GRAIN SIZE, LITHOLOGY AND FLOODPLAIN SEDIMENTATION 28

2.3 DOWNSTREAM FINING CONCEPTS 31

2.3.1 SOURCE LITHOLOGY, GRAIN SIZE AND SEDIMENT SUPPLY RATE 34
2.3.2 TRIBUTARIES 34
2.3.3 DOWNSTREAM CHANNEL GRADIENT 35
2.3.4 AGGRADATION AND SUBSIDENCE 35

2.4 DISCUSSION AND UNRESOLVED ISSUES 36

2.5 INFLUENCE OF ALLOCYCLIC AND AUTOCYCLIC CONTROLS ON WITHIN CHANNEL-BELT RIVER RESPONSE 39

2.6 RELATIONSHIP OF CHANNEL PATTERN TO ALLUVIAL ARCHITECTURE 41

2.6.1 PREDICTION OF SANDBODY GEOMETRIES 45

2.7 SANDBODY INTERCONNECTEDNESS 49

2.8 TECHNIQUES USED TO EVALUATE SUBSURFACE ALLUVIAL ARCHITECTURE 50

2.8.1 WELL DATA 53
2.8.2 OUTCROP ANALOGUES 54
2.8.3 MODERN ANALOGUES 57
2.8.4 EMPIRICAL EQUATIONS 57
2.8.5 GROUND PENETRATING RADAR 58
2.8.6 SEISMIC PROFILING 58
2.8.7 PHYSICAL MODELLING 59
2.8.8 NUMERICAL MODELS 59

2.9 SCALES OF HETEROGENEITY 60

2.10 GEOLOGICAL RESERVOIR MODELS 61

2.11 THE INCORPORATION OF PETROPHYSICS 65

2.12 UP-SCALING AND DYNAMIC SIMULATION MODELLING 67

2.13 SUMMARY 68

Chapter 3. The sedimentology and depositional environment of the Lower Ketch Member, Tyne Field, Southern North Sea, UK

3.1 SYNOPSIS 68

3.2 INTRODUCTION 68

3.3 BACKGROUND TO THE TYNE FIELD 70

3.3.1 LITHOSTRATIGRAPHIC NOMENCLATURE OF THE UK SOUTHERN NORTH SEA 72
3.3.2 SEISMIC, CHEMOSTRATIGRAPHIC AND BIOSTRATIGRAPHIC SUBDIVISION OF THE TYNE FIELD 73

3.4 REGIONAL GEOLOGICAL SETTING 74

4.4.1 REGIONAL PALAEOCLIMATE 76
3.4.1 THE SILVER PIT BASIN 79

3.5 DATA BASE 80

3.6 FACIES ANALYSIS FROM CORE 82

3.7 VERTICAL FACIES ASSOCIATIONS AND SANDBODY TYPES 87

3.7.1 THICKNESS OF SANDBODIES 90

3.8 ESTIMATES OF FORMATIVE CHANNEL DEPTHS AND CHANNEL-BELT WIDTHS 91

3.8.1 ASSUMPTIONS OF CHANNEL DEPTH ESTIMATES 94

3.9 SIGNIFICANCE OF RED BEDS FOR ENVIRONMENTAL INTERPRETATION 94

3.10 DEPOSITIONAL MODEL FOR THE LOWER KETCH MEMBER: A DISCUSSION 96

3.10.1 CHANNEL-BELTS WITHIN THE LOWER KETCH MEMBER 96
3.10.2 CONTROLS ON THE ALLUVIAL ARCHITECTURE OF THE LOWER KETCH MEMBER 98
3.10.3 SUMMARY OF THE DEPOSITIONAL MODEL IN THE TYNE FIELD 99
3.10.4 INCORPORATION INTO THE REGIONAL DEPOSITIONAL MODEL 101

3.11 ESTIMATES OF CONNECTIVITY AND SANDBODY GEOMETRY 102

3.12 IMPACT OF COMPACTION ON LOWER KETCH MEMBER ALLUVIAL ARCHITECTURE 104

3.12.1 COARSE FRACTION: CHANNEL-BELT SANDSTONES 105
3.12.2 FINE FRACTION: OVERBANK MUD/SILTSTONES 107

3.13 STRATIGRAPHIC AND LITHOLOGICAL OUTCROP ANALOGUES 108

3.14 GRAIN SIZE DISTRIBUTION 109

3.15 LITHOFACIES UNITS AND PETROPHYSICS RELATIONSHIPS 112

3.16 SUMMARY 114

Chapter 4. A low net to gross analogue for the Tyne Field: The Escanilla Formation, Southern Pyrenees, Spain

4.1 SYNOPSIS.....115

4.2 INTRODUCTION.....115

4.4 BACKGROUND AND STRATIGRAPHY OF THE ESCANILLA FORMATION.....116

4.3 REGIONAL GEOLOGICAL SETTING.....118

4.5 AINSA BASIN FIELD SITE.....119

4.6 DATA ACQUISITION AND METHODOLOGY.....120

4.7 LITHOFACIES ANALYSIS FROM OUTCROP.....122

4.8 SIGNIFICANCE OF OVERBANKS FOR ENVIRONMENTAL INTERPRETATION.....125

4.8.1 PALAEOSOLS.....125
4.8.2 GYPSUM BEDS.....126
4.8.3 ONCOIDS.....126
4.8.4 LIMESTONES.....128
4.8.5 TRACE FOSSILS.....129

4.9 CLASSIFICATION OF SANDBODIES AND VERTICAL LITHOFACIES ASSOCIATIONS.....131

4.10 PALAEOCURRENT INDICATORS.....137

4.11 ESTIMATES OF FORMATIVE CHANNEL DEPTH AND CHANNEL-BELT WIDTH.....138

4.12 GRAIN SIZE DISTRIBUTION OF THE ESCANILLA FORMATION.....139

4.13 A REVIEW OF THE DEPOSITIONAL MODEL FOR THE ESCANILLA FORMATION.140

4.13.1 CONTROLS ON THE ALLUVIAL ARCHITECTURE OF THE ESCANILLA FORMATION.....142
4.13.2 EVIDENCE FOR BASE-LEVEL OR PROGRADATIONAL CHANGES IN THE ESCANILLA FORMATION.143

4.14 IMPACT OF COMPACTION ON ESCANILLA FORMATION ALLUVIAL ARCHITECTURE.....147

4.15 ESTIMATE OF SANDBODY CONNECTIVITY.....148

4.16 TWO-DIMENSIONAL SANDBODY GEOMETRY.....149

4.16.1 COMPLETE AND PARTIAL SANDBODY DIMENSIONS.....149

4.17 COMPARISONS BETWEEN GEOSTATISTICS FROM THE ESCANILLA FORMATION AND DOCUMENTED OUTCROP STUDIES.....155

4.17.1 CHANNEL-BELT SANDBODY GEOMETRIES.....155
4.17.2 SPLAY LOBE GEOMETRIES.....157
4.17.3 THREE-DIMENSIONAL CHANNEL SANDBODY GEOMETRIES.....158
4.17.4 THREE-DIMENSIONAL SPLAY GEOMETRIES.....159

4.18 COMPARISON BETWEEN MEASURED AND PREDICTED CHANNEL-BELT SANDBODY WIDTH.....159

4.19 GEOMETRIES OF THE OVERBANK DEPOSITS (NON-RESERVOIR COMPONENT)..160

4.20 APPLICATION OF SANDBODY GEOMETRIES TO THE LOWER KETCH MEMBER..160

4.21 THE ESCANILLA FORMATION: AN ANALOGUE TO THE LOWER KETCH MEMBER 161

4.21.1 LIMITATIONS OF THE ESCANILLA OUTCROP STUDY AND FUTURE RECOMMENDATIONS.....164

4.22 REQUIREMENTS FOR FULL ANALOGUE COMPARISON AND VALIDATION 165

4.23 SUMMARY.....166

Chapter 5. Experimental study of the impact of sediment supply grain size on down-basin braided alluvial architecture: rationale and methodology

5.1 SYNOPSIS 168

5.2 INTRODUCTION 168

5.3 PRINCIPLES OF FROUDE-SCALED PHYSICAL MODELLING 170

5.3.1 SCALING OF TIME 173
5.3.2 SCALING OF DISCHARGE 173

5.4 SCALED PHYSICAL MODELLING OF FINE GRAINED SYSTEMS: THE LOWER KETCH MEMBER 174

5.5 JUSTIFICATION FOR THE USE OF THE CANTERBURY PLAINS 176

5.5.1 REGIONAL GEOLOGICAL SETTING 177
5.5.2 STRATIGRAPHY 180
5.5.3 CANTERBURY PLAINS FIELD SITE DESCRIPTION 181

5.6 DATA ACQUISITION FOR PHYSICAL MODELLING INPUT PARAMETERS 182

5.6.1 DOWNSTREAM FINING IN THE ASHBURTON RIVER 183
5.6.2 QUANTIFYING DOWNSTREAM FINING RATE FOR THE ASHBURTON RIVER 183
5.6.3 DOWNSTREAM MODIFICATION OF THE GRAIN SIZE DISTRIBUTION IN THE ASHBURTON RIVER 184
5.6.4 QUANTIFICATION OF BULK GRAIN SIZE FOR PHYSICAL MODELLING 186
5.6.5 ASHBURTON RIVER CHANNEL GEOMETRIES 188
5.6.6 ASHBURTON RIVER CHANNEL GRADIENTS 188
5.6.7 QUANTIFICATION OF ALLUVIAL ARCHITECTURE IN THE CANTERBURY GRAVELS 189

5.7 IMPLICATIONS OF THE CANTERBURY FIELD STUDY FOR PHYSICAL MODELLING 189

5.8 THE FLUME BASIN FACILITY AND EXPERIMENTAL PROCEDURE 190

5.8.1 WATER DELIVERY, CONTROL AND RECIRCULATION 192
5.8.2 MODELLED GRAIN SIZE DISTRIBUTIONS 193
5.8.3 FEED RATE AND AGGRADATION 195
5.8.4 USE OF DISCHARGE AND SEDIMENT HYDROGRAPHS 196

5.9 DESCRIPTION OF EXPERIMENTS 197

5.10 MEASUREMENTS TAKEN DURING THE EXPERIMENTAL RUNS 201

5.10.1 VIDEO IMAGING 201
5.10.2 SURFACE VELOCITY FLOATS 202
5.10.3 SEDIMENT SURFACE MEASUREMENTS 202
5.10.4 SUSPENDED SEDIMENT AND BEDLOAD 204

5.11 SECTIONING OF THE PRESERVED SEDIMENT SEQUENCE FOR QUANTIFYING ALLUVIAL ARCHITECTURE 204

5.12 IMPLICATIONS OF PHYSICAL MODELLING FOR FUTURE ALLUVIAL ARCHITECTURE STUDIES 205

5.13 SUMMARY 206

Chapter 6. The influence of sediment supply grain size on alluvial architecture

6.1 SYNOPSIS.....207

6.2 INTRODUCTION AND BACKGROUND TO THE BRAIDED RIVER EXPERIMENTS 207

6.3 DATA ANALYSIS: FIELD AND FLUME.....209

6.4 COMPARISON OF HYDRAULIC FLOW PARAMETERS: FIELD AND FLUME.....210

6.5 SURFACE FORM AND CHANNEL MORPHOLOGY: FIELD AND FLUME.....211

6.5.1 ASHBURTON RIVER CHANNEL GEOMETRIES 211
6.5.2 THE GEOMETRY OF THE ASHBURTON MODEL CHANNELS 213

6.6 CHANNEL OCCUPANCY 215

6.7 DURATION OF CHANNEL OCCUPANCY 217

6.8 SEDIMENT SURFACE GRADIENTS.....217

6.9 SURFACE MORPHOLOGICAL FORMS.....220

6.9.1. BEDFORM GENERATION.....222

6.10 ANALYSIS OF CUT-FACES.....225

6.10.1 CLASSIFICATION OF ARCHITECTURAL ELEMENTS.....225

6.11 FREQUENCY OF OCCURRENCE OF ARCHITECTURAL ELEMENTS 230

6.12 TWO-DIMENSIONAL ARCHITECTURAL ELEMENT GEOMETRY.....233

6.12.1 DEPOSITION OF FINE-GRAINED ARCHITECTURAL ELEMENTS.....239

6.13 PRESERVATION POTENTIAL 242

6.14 A SUMMARY OF THE IMPACT OF GRAIN SIZE ON WITHIN CHANNEL-BELT CHANNEL MORPHOLOGY AND ALLUVIAL ARCHITECTURE.....243

6.15 THREE-DIMENSIONAL ELEMENT ARCHITECTURE 244

6.16. COMPARISON OF PROTOTYPE AND MODEL ALLUVIAL ARCHITECTURAL 244

6.17 SCALING WITHIN PHYSICAL MODELLING AND APPLICATION TO ANALOGUE/RESERVOIR STUDIES.....246

6.18 COMPARISONS BETWEEN GEOSTATISTICS FROM PHYSICAL MODELLING AND DOCUMENTED OUTCROP STUDIES 248

6.19 DISCUSSION.....249

6.19.1 CHANNEL GEOMETRY.....250
6.19.2 BEDFORM GENERATION.....251
6.19.3 ALLUVIAL ARCHITECTURE AND PRESERVATION POTENTIAL.....252
6.19.4 ALLUVIAL ARCHITECTURE MODELS 254
6.19.5 PRESERVATION OF FINE-GRAINED DEPOSITS 254
6.19.6 UP-SCALING OF PHYSICAL MODEL DATASETS 255

6.20 LIMITATIONS AND POTENTIAL BENEFITS OF FUTURE PHYSICAL MODELLING.255

6.21 SUMMARY.....256

Chapter 7. Application of combined core-physical modelling-outcrop approach to reservoir simulations: future potential

7.1 SYNOPSIS 258

7.2 INTRODUCTION 258

7.3 SCALES OF HETEROGENEITY 259

7.4 QUANTITATIVE DATA NEEDS FOR PETROLEUM ENGINEERING 260

7.5 ADVANTAGES OF USING PHYSICAL MODELS OVER CONVENTIONAL METHODOLOGIES 261

7.6 APPLICATION OF PHYSICAL MODELLING TO THE CHARACTERISATION OF ALLUVIAL RESERVOIRS 262

7.6.1 Relationships between petrophysical properties and lithofacies 262

7.7 A METHODOLOGY FOR COLLECTING DATA FROM PHYSICAL MODELLING EXPERIMENTS FOR RESERVOIR EVALUATION 265

7.7.1 Vertical proportion curves 267

7.8 DATA FROM PHYSICAL MODELS AS INPUT TO OBJECT- AND PIXEL- BASED RESERVOIR SIMULATION MODELS 270

7.8.1 Altering grid size and sample averaging 272

7.9 ALTERNATIVE ANALYSIS TECHNIQUES 276

7.10 RECOMMENDATIONS 279

7.11 SUMMARY 280

Chapter 8: Conclusions and recommendations for further work

8.1 CONCLUSIONS 281

8.1.1 CARBONIFEROUS OF THE UK SOUTHERN NORTH SEA 281
8.1.2 ONSHORE ANALOGUES FOR THE UK SOUTHERN NORTH SEA 282
8.1.3 QUANTITATIVE PREDICTION OF ALLUVIAL ARCHITECTURE 282
8.1.4 PHYSICAL MODELLING OF FINE-GRAINED SYSTEMS 284
8.1.5 THE IMPACT OF GRAIN SIZE ON ALLUVIAL ARCHITECTURE 284
8.1.6 INTEGRATED APPROACHES TO FLUVIAL RESERVOIR EVALUATION 286

8.2 RECOMMENDATIONS FOR FUTURE WORK 287

REFERENCES 291

APPENDIX A: TYNE FIELD SEDIMENTARY CORE LOGS 349

APPENDIX B: KRUSKAL-WALLIS TEST: ANALYSIS OF VARIANCE BY RANKS 358

APPENDIX C: GRAIN SIZE FOR SUSPENDED SEDIMENT SAMPLES 359

APPENDIX D: SUPPLEMENTARY CD 360

List of figures and tables

Chapter 1. Introduction and background to the study

Figure 1.1. Controls on the fluvial system and alluvial architecture (from Marriott, 1999)..... 2
Figure 1.2. Scales of fluvial heterogeneity required for full reservoir evaluation (from Bristow, 1996)..... 4

Chapter 2. Controls on alluvial architecture and the assessment of hydrocarbon reservoir heterogeneity

Figure 2.1. Summary diagrams illustrating the relationship between shoreface and fluvial architecture as a function of base-level change (from Shanley and McCabe, 1993). 12
Figure 2.2. Simulated cross section from Bridge and Leeder (1979) showing increased sandbody connectivity to the area of maximum tectonic subsidence. The speckled units represent channel-belt sandbodies with the surrounding material representing floodplain deposits. 15
Figure 2.3. Simulated cross-sections from experiments by Bridge and Leeder (1979). Vertical exaggeration is 25. Mean avulsion period is 445 years in these examples; mean channel-belt aggradation rates are (A) 0.02 m year^{-1}, (B) 0.01 m year^{-1}, (C) 0.005 m year^{-1}. Note the change in stacking patterns and the reduction in connectivity as aggradation rate increases. The speckled units represent channel-belt sandbodies with the surrounding material representing floodplain deposits. 17
Figure 2.4. The effect of variation in the sediment supply versus accommodation ratio on sandbody interconnectedness (P = palaeochannel axis) (from Dreyer, 1993). Dashed areas represent channel-belt sandbodies. 17
Figure 2.5. Model stacking patterns for a fore-tilted basin with local avulsion and slow (left) versus rapid (right) subsidence rates. The relation between avulsion frequency and sedimentation rate is $f_a = r^{0.2}$. Proximal and distal cross-sections are positioned to be equally spaced in both basins, but with proximal sections being the same thickness. Sandbody thickness is set by the local sedimentation rate and the relationship between avulsion frequency and sedimentation rate. The downstream change in stacking pattern is a function of the rate of change of subsidence downstream. The speckled units represent channel-belt sandbodies with the surrounding material representing floodplain deposits. (from Heller and Paola, 1996)..... 18
Figure 2.6. Diagrammatic representation of the avulsion, and vertical and horizontal migration of a channel-belt axis. Note the effect of the processes on the amount and distribution of potential reservoir sand (from Leeder *et al.*, 1993)..... 22
Figure 2.7. (a) avulsion frequency versus sediment-feed rate for four experiments and (b) normalised by their values for the lowest feed rate. The fitted line has a power-law exponent of 5.87 showing avulsion frequency increases with sediment feed rate (from Bryant *et al.*, 1995)..... 22
Figure 2.8. Relation between channel-belt stacking density and sedimentation rate for three possible regimes defined by the exponent β in a power-law relation between avulsion frequency and sedimentation rate. Black represent channel-belt sandbodies; dashed pattern represent floodplain deposits. The top panel corresponds to a regime in which avulsion frequency is taken to be independent of sedimentation rate. The bottom panel is that suggested where an increase in sedimentation rate leads to higher switching rates, more effective removal of floodplain fines, and higher density of sandbodies (from Bryant *et al.*, 1995)..... 23
Figure 2.9. Sketch section normal to regional palaeoflow to illustrate the major alluvial architectural effects resulting from a major episode of incision as sectioned relatively close the position of initial base-level fall (from Leeder and Stewart, 1996) 26
Figure 2.10. The influence of intrinsic scour: (A) during flood events a river channel may be locally scoured to a depth in excess of the average bankfull depth. Later waning of the flood allows the scour pool to be partially filled by channel sediment; (B) abandonment of the channel without net aggradation will produce a sandbody whose thickness is in excess of original (BF) depth. Thickening of the sandbody in this case is purely due to scour. (C) shows the depositional form if the sandbody is abandoned after limited aggradation the proportional thickening due to scour will be less important. Note the bankfull depth is again a poor measure of sandbody thickness (from Salter, 1993)..... 27
Figure 2.11. Downstream changes in the mean grain size of bed material, an example from the River Noe, England (a) showing an exponential change in mean grain size and (b) showing how sedimentary links between tributary inputs create a stepped downstream fining trend (from Knighton, 1998)..... 31
Figure 2.12. Facies models showing down-basin change in the type and proportion of facies observed in a terminal fan sequence (from Kelly and Olson, 1993)..... 31
Figure 2.13. Active bulk layer grain size distributions from the Allt Dubhaig. (A) Measured grain size distributions. (B) Adjusted psi sizes computed by adjusting the mean of all the samples to be the same as that at 0.22 km (from Hoey and Bluck, 1999)..... 33

Figure 2.14. Example of the sandbody stacking patterns as a function of aggradation rate, lateral channel migration and channel-belt avulsion (from Bristow and Best, 1993). 36
Figure 2.15. Classification of channel patterns (after Schumm, 1981). Note the difference in channel planform for different grain size classifications. 39
Figure 2.16. Vertical profile models for braided stream deposits (from Miall, 1977). Facies codes are to the left of each column. Arrows show small-scale cyclic sequences. 42
Figure 2.17. The eight basic architectural elements in fluvial deposits (from Miall, 1988a,b). 43
Figure 2.18. Terminology devised by Friend *et al.* (1979) to describe sandbody geometry based on a width/thickness ratio of 15:1. 45
Figure 2.19. Sandbody types and their relation to channel pattern (from Fielding and Crane, 1987)..... 45
Figure 2.20. Schematic block diagram showing large-scale depositional geometries. (A) Idealised cross-section of an internode, showing relative ages (1-oldest, 3-youngest) of channel-point-bar couplets based on crosscutting relationships, and coarse-grained point-bar deposits and mostly fine-grained fill in abandoned channels. (B) At the larger scale, node-internode geometry can result in swelling and thinning of channel deposits in the floodplain. (C) Wide and narrow channel deposits in vertical outcrop (from Harper and Jones, 1998). 47
Figure 2.21. Channel depth versus channel-belt width (perpendicular to palaeocurrent) relationships for types of modern and ancient fluvial channel deposits showing a large amount of scatter and therefore pose great difficulties in the application of general trend lines (from Fielding and Crane, 1987). 47
Figure 2.22. Prediction of the most likely channel-belt width from measured thickness data using the geometric mean of all the data in Figure 2.21 (from Fielding and Crane, 1987). 48
Figure 2.23. Problems of determining depositional width from a measurement of depositional thickness are illustrated in vertical log profiles from Bridge and Tye (2000) showing that identification of basal erosional surface between the centre and left vertical log profiles may be ambiguous. 49
Figure 2.24. Sandstone body interconnectedness as a function of the net sand fraction of the sequence (from Fielding and Crane, 1987). Note that at 0.6 the sandbodies become fully connected. 50
Figure 2.25. (A) Two-dimensional stratigraphic simulation of fluvial channel-belts (stippled) in the Travis Peak Formation, North Appleby field, East Texas basin (zone 1 of Tye, 1991; Davies *et al.*, 1993). (B) Wireline logs and channel-belt sandbodies of zone 1 as originally correlated by Tye (1991). (C) Revised well-to-well correlations using same data as in (B), but constrained to recalculated channel-belt widths. Note that limiting channel-belt widths decreases sandbody connectivity in two dimensions. (from Bridge and Tye, 2000). 52
Figure 2.26. Idealised wireline log characteristics for facies analysis in the subsurface (from North, 1996). 54
Figure 2.27. Steps for stochastic simulation of sand channels in a cross-section (From Srivastava, 1994). 62
Figure 2.28. Vertical proportion curves (solid line) experimental results (black dots), and example section through two different object-based models condition on the proportion data (from Deutsch and Wang, 1996). 64
Figure 2.29. Geometrical shapes representing fluvial sandstone bodies, which are used in object-based modelling: (A) channel-belts, (B) with overbank sandstones, and (C) crevasse channels (from Hirst *et al.*, 1993). 64
Figure 2.30. Distribution of values of permeability (ln K) for sediment samples from various hydrofacies in the Quaternary Stoughton gravel deposit (from Anderson *et al.*, 1999) showing the direct link between facies type and petrophysical attributes. 66

Table 2.1. Examples of published studies documenting the range of allocyclic and autocyclic controls influencing a fluvial system. These controls are linked with both positive and negative feedback effects. 9
Table 2.2. Architectural elements in fluvial deposits (from Miall, 1996). 43
Table 2.3. Example of the range of quantitative alluvial architectural datasets available from outcrop and flume studies. 56
Table 2.4. Scales of heterogeneity for consideration of fluvial reservoir performance. 61

Chapter 3. The sedimentology and depositional environment of the Lower Ketch Member, Tyne Field, Southern North Sea, UK

Figure 3.1. Location of the Tyne Field, Southern North Sea, showing the three main gas accumulations at the top Lower Ketch depth map (modified from Cooper, 1995)..... 71
Figure 3.2. Stratigraphic nomenclature of the Southern North Sea and location of the Tyne reservoir interval (modified from Cooper, 1995)..... 73
Figure 3.3. Simplified structural map of the (a) Western European Carboniferous Basin (modified Maynard *et al.*, 1997), and (b) the Southern North Sea (modified from Bailey *et al.*, 1993)..... 78
Figure 3.4. Structural cross-section based on a 3-D random track Tyne South-Tyne North of the Southern North Sea Upper Carboniferous deposits. Note: the main reservoir target of the Tyne reservoir interval is the Lower Ketch Member (modified from Cooper, 1995)..... 79
Figure 3.5. Lower Ketch Member reservoir thickness from north to south of the Tyne Field, SNS. Note that the wells have been corrected for deviation, but not structural effects such as faulting, folding or unconformities. A general increase in reservoir thickness to the south is observed as late Carboniferous unroofing occurred leading to a truncation of the Schooner Formation to the north..... 80
Figure 3.6. Random track plot showing the variation in Net-to-Gross of the Lower Ketch Reservoir interval from north to south of the Tyne Field calculated from well data..... 82
Figure 3.7. Examples of facies types observed within the cored intervals of the Lower Ketch Member, Tyne Field, SNS. Facies codes are shown on core (for full facies description refer to Table 3.2). Note: All cores are 3 inches in diameter and some are deviated. Dashed lines represent basal sandbody contact..... 86
Figure 3.8. Characteristic vertical profiles through the three sandbody types (A-C) observed within cores from the Lower Ketch Member, Tyne Field, SNS. The fourth category, Type D results from the stacking of sandbody types A-C forming a composite sandbody profile..... 88
Figure 3.9. Histogram to show types of sandbodies (A-D) observed within the Lower Ketch reservoir interval (n = 33). Refer to text for full description of sandbody types..... 90
Figure 3.10. Thickness-frequency distribution for Lower Ketch Member sandbodies (n = 24) that have been subdivided into Type A-D classifications. Refer to text for full description of sandbody types..... 91
Figure 3.11. Schematic block diagram to represent the depositional environment of the Lower Ketch Member in the UK Southern North Sea.....100
Figure 3.12. Schematic block diagram to show the palaeogeographic setting for depositional units 1-3 of the Ketch and Schooner Fields at the distal end of a broad alluvial plain (modified from Stone and Moscariello, 1999). The boxed area represents a more proximal position in the basin where sediments of the Tyne Field were deposited.....102
Figure 3.13. Grain size distribution for the Lower Ketch Member reservoir interval (D_{50} = 0.078mm)..111

Table 3.1. Well cores from the Tyne Field used in the analysis of the Lower Ketch Member reservoir interval..... 81
Table 3.2. Lithofacies units observed within the Lower Ketch Reservoir, Tyne Field. Note the cores in the Tyne field are biast towards the reservoir quality rock. * Note no distinction has been made between K_v and K_h. Facies are coded with the classifications modified from Miall (1977, 1978). Examples of lithofacies from the Lower Ketch Member are shown in Figure 3.7 and provided in the supplementary CD (Appendix D)..... 83
Table 3.3. Description of sandbody types found within the Lower Ketch Member based on vertical lithofacies associations..... 89
Table 3.4. (a) Estimates of dune height, channel depth and channel-belt width from cross-set data in the Lower Ketch Member reservoir interval, and (b) estimates of channel depth from channel fills in the LKM. *cbw* = channel-belt width..... 93
Table 3.5. Step-by-step procedure for calculation of a composite grain size distribution for the Lower Ketch Member reservoir interval.....110
Table 3.6. Lithofacies groups used for construction of the Lower Ketch Member grain size distribution.....110
Table 3.7. Statistics for porosity and permeability for each lithofacies type observed within the Lower Ketch Member of the Tyne Field. Refer to Table 3.2 for lithofacies descriptions.....113

Chapter 4. A low net to gross analogue for the Tyne Field: The Escanilla Formation, Southern Pyrenees, Spain

Figure 4.1. Tertiary stratigraphic framework of the Ainsa Basin, Southern Pyrenees, Spain. Chronostratigraphy has been taken from Hartland *et al.* (1990) GT589 timescale and lithostratigraphy adapted from Bentham (1992). The bar indicates the interval investigated for comparisons with the Lower Ketch Member, SNS. Note the general increase in net-to-gross up sequence. 117
Figure 4.2. Geological map of the Ainsa Basin, Southern Pyrenees, Spain, showing the two outcrop sections used in the study (modified from Bentham, 1992)....118
Figure 4.3. Escanilla Formation exposure in the Ainsa Basin with boxed areas showing where alluvial architectural datasets were collected (View SE from the village of Eirpol). 121
Figure 4.4. Palaeosol development within the Escanilla Formation showing (a) horizonation and (b) horizontal bedding picked out by subtle changes in the grain size within the overbank deposits. 125
Figure 4.5. Oncoids observed within the Escanilla Formation. (a) a cylindrical oncoid with a length of 1.6 m, (b) oncoids showing a concentric growth pattern, and (c) an oncoid showing a silty internal fill. 128
Figure 4.6. (a) Limestone bed within the overbank deposits and thin sections taken through the limestones showing (b-c) freshwater gastropods and (d) ostracods indicating the occurrence of lacustrine depositional systems on the floodplain. 129
Figure 4.7. Trace fossils observed within the Escanilla Formation: (a) Domichnia traces in overbank fines, (b) Domichnia traces in stacked sandbodies, and (c) a bedding plane view of continental trace fossils. 130
Figure 4.8. Comparison of vertical facies profiles through sandbody types in both the Lower Ketch Member and Escanilla Formation. Note the marked similarity of log profiles. For a description of vertical profiles refer to the text. 133
Figure 4.9. Comparison of cumulative percentage grain size distributions for the Lower Ketch Member and the Escanilla Formation. 140
Figure 4.10. Schematic block diagrams to represent the depositional environments for the Escanilla Formation. 146
Figure 4.11 (a). Comparison of sandbody thicknesses between the Lower Ketch Member and the Escanilla Formation, and (b) adjustment of the thicknesses following decompaction using Retallack's expression of the Sclater-Christie (1980) equation. Both sequences were assummed to have an initial solidity of 0.6. Note only complete thicknesses were used in the Lower Ketch Member cored interval. 148
Figure 4.12. Probability density functions of the sandbodies widths within the Escanila Formation following the conditioning method of Visser and Chessa (2000a, b). Showing the (a) raw, (b) complete and (c) adjusted data. 152
Figure 4.13. Width class PDF's defined into sandbody types (see Figure 4.3 for descriptions). Showing (a) raw, (b) complete and (c) adjusted datasets used to condition sandbody width by methods of Visser and Chessa (2000a,b). 153
Figure 4.14. Box and whisker plots of (a) width/thickness ratios, (b) thickness and (c) width for sandbody types measured within the Escanilla Formation sequences, showing the considerable range in sandbody geometries within the Escanilla Formation. 154
Figure 4.15. Cross plot of Escanilla Formation sandbody geometries (n = 136) plotted against sandbody dimension data from the Escanilla Formation by Dreyer *et al.* (1993)....156
Figure 4.16. Width versus thickness cross plot for channel pattern types taken from Fielding and Crane (1987) compared to the Escanilla Formation sandbody geometries....156
Figure 4.17. Width versus thickness cross plot for splay lobes from the Escanilla Formation compared to those defined in the Jurassic Saltwick and Scalby Formations (Walderhaug and Mjos, 1991).157
Figure 4.18. Cross plot of adjusted sandbody geometrical data from the Escanilla Formation with a best fit line plotted (n = 136). Note the considerable scatter and the ambiguity in the application of general trend lines to the cross plot dataset....161

Table 4.1. Lithofacies units observed within the Escanilla Formation, Spain. Facies are coded based on Miall (1977, 1978) classification scheme....123
Table 4.2. Step-by-step procedure for sandbody classification and quantification....131
Table 4.3. Sandbody types observed within the Escanilla Formation, Spain. Examples of sandbody types are illustrated in Figure 4.9. Dimension data is outlined in Table 4.8....134

Table 4.4. Summary of cross-set data from the conglomerates and pebbly sandstone lithofacies within the Escanilla Formation, which represent bar and dune deposition respectively. 138
Table 4.5. Estimates of channel depths and channel-belt widths in both the Lower Ketch Member and the Escanilla Formation, using equations outlined by Bridge and Tye (2000). 138
Table 4.6. Estimates of flow depth from channel fill deposits within the Lower Ketch Member and the Escanilla Formation. 139
Table 4.7. Comparison of grain size data from the Lower Ketch Member and the Escanilla Formation. 140
Table 4.8. Statistic for sandbody dimensions from the Escanilla Formation based on complete measurements (n =44) and (italics) recalculated datasets using the Visser and Chessa (2000a) width conditioning method (n =136). 151
Table 4.9. Statistics from measured thicknesses for overbank mud/siltstones from the Lower Ketch Member and the Escanilla Formation. 160
Table 4.10. Summary of criteria used to assess the viability of the Escanilla Formation as an analogue to the Lower Ketch Member reservoir interval. 163
Table 4.11. List of minimum data requirements for full subsurface reservoir to outcrop analogue comparisons. 166

Chapter 5. Experimental study of the impact of sediment supply grain size on down-basin braided alluvial architecture: rationale and methodology

Figure 5.1. Modified Shields curve from Ashworth *et al.* (1994) to show that the critical threshold above which the flow becomes hydraulically rough occurs where values of Re* are in the range of 5-70 based on calculations using grain size D_{90}. 172
Figure 5.2. (a) Modern Ashburton River Mouth (~1.2 km across) discharging into the Pacific Ocean, (b) The present day retrogradational Canterbury Cliff line composed of late Quaternary Gravels. Showing ~10 km of coastline and the Rangitata River Mouth at the top of the figure..... 177
Figure 5.3. Location maps for (a) the Canterbury Plains field sites, and (b) sites of Wolman grain size sampling along the modern Ashburton River..... 179
Figure 5.4. Late Quaternary History of the Canterbury Plains, based on Suggate (1963, 1965) and Brown *et al.* (1988). 180
Figure 5.5. Downstream fining curves plotted for D_{50} and D_{90} for the South Branch of the Ashburton River. 183
Figure 5.6. Grain size distribution curves for sample sites on the South Branch Ashburton River showing a conservation of grain size distribution shape downstream. All samples taken are of the gravel fraction only (>5.6mm)..... 185
Figure 5.7. Adjusted downstream grain size distributions by normalising the D_{50} sizes of all the samples to the D_{50} value at the Inverary Road (66.7 km). The distribution becomes similar downstream of 43.9 km from the modern Ashburton River Mouth. This may be associated with the change in channel pattern to a single thread channel to a braided channel between Mt. Somers and Thompsons Track (Figure 5.3b). 185
Figure 5.8. Bimodal grain size distribution for bulk samples taken from the Canterbury Gravels at the Rangitata and Wakanui sites (See Figure 5.3 for site locations). With the grain size distribution taken from Smalls Road superimposed for the gravel fraction >5.6 mm. 187
Figure 5.9. Shift in grain size distributions for the three proposed modelling scenarios, series F, M and C. 188
Figure 5.10. Diagram showing the experimental basin facility set-up used in the three experimental runs. 191
Figure 5.11. Calibration curve for the pump used for the physical modelling experiments..... 192
Figure 5.12. Grain size distribution curves for series C, M and F (sampled from mixed batches) used for the physical modelling compared to a 1:50 scaled bulk grain size distribution taken from the Canterbury Gravels. 194
Figure 5.13. Calibration curves for the AccuRate sediment feeder for sediment mixes used in series F and C used in the physical modelling experiments. Note that higher feed rates were obtainable from series C sediment as a result of the a higher bulk density..... 195
Figure 5.14. (a) Discharge and (b) sediment input hydrographs used in the physical modelling experiments. Data taken from the October 1990 Ashburton River flood and scaled according to scaling laws detailed in Sections 5.3.1 and 5.3.2..... 196
Figure 5.15. Oblique view of the Leeds flume facility (a) after initial water was turned on and (b) during experiment C. Flow enters the basin from the central feeder channel at the top and drains at the bottom of the image. 200
Figure 5.16. Photograph of the Selcom SL5070 laser unit mounted on an aluminium bridge and used for the measurement of surface braidplain topography..... 202
Figure 5.17. Diagram to show the plan view of the Leeds flume basin and the location of laser profiles and cut-section lines 1-26. 203
Figure 5.18. Sectioning procedure for the FSM sediment sequence (a) showing the section face being photographed following cutting of the aggraded sediments and (b) an example of the 2 m wide section exposure of alluvial architecture cut perpendicular to flow. 205

Table 5.1. Summary of data collected for input and validation of the Ashburton River physical model. 182
Table 5.2. Diminution coefficients reported for braided streams α_d where the diminution coefficient is expressed as the reduction in particle phi size per kilometre (ψ km^{-1}). Note all field study coefficients are for median or mean size of surface material..... 184
Table 5.3. Channel gradient data taken at four river reaches along the modern Ashburton River. 189
Table 5.4. Summary of experiments performed investigating two different sediment supply grain size distributions, series C and Series F..... 198

Chapter 6. The influence of sediment supply grain size on alluvial architecture

Figure 6.1. Exponential downstream fining curve based on D_{50} values for the modern Ashburton River with the superposition of the D_{50} values of the three scaled grain size distributions from series C, M and F. 209
Figure 6.2. Box and whisker plots for the depth, width and width/depth ratios for three sites along the course of the Ashburton River, representing position (A) at 0 km (the Ashburton mouth), (B) 18 km (Ashburton Town) and (C) 43 km (Thompsons Track, North and South Branches) upstream from the present coastline. 212
Figure 6.3. Probability density functions of channel widths for (a) the modern Ashburton River and physical modelling series (b) F, (c) M, and (d) C. Note: widths have been scaled up from the flume. 214
Figure 6.4. Box and whisker plots for depth, width and width/depth ratio distribution data from series C, M and F. Note the increase in width and depth between series C and F, but without a change in width/depth ratios. Note: widths have been scaled up from the flume. 214
Figure 6.5. Examples of overhead images from (a) Rakaia River, Canterbury Plains and (b) series C modelling experiment to show the marked similarity of form between the two scales. Flow direction in both (a) and (b) is from right to left. 215
Figure 6.6. Comparisons of channel occupancy between the three experiments taken at a discharge of 1.67 l s^{-1}. An increasing proportion of the floodplain is occupied by sheet flow between series C and F. 216
Figure 6.7. Duration of channel occupancy (see text for description) for series C, M and F, showing no significant difference between the three experiments. Note: the frequency of sampling was 1 hour, therefore any channel shifts below 1 hour will not be identified. 217
Figure 6.8. The development of downstream sediment surface gradients during the 125 hour experiment. The area between the lines represents sediment accumulation during four hour intervals. The bold line indicates where the grain size distribution was quartered. The gap in the line represents a section where no data were collected 218
Figure 6.9. Box and whisker plots showing the range, upper and lower quartiles, mean and median values for downstream sediment surface gradients measured in series C, F and M. 218
Figure 6.10. Examples of overhead video images showing the surface depositional forms described in Table 6.5, (a) from series C and (b) series F. Scale bar = 1 m. Flow direction is from right to left. Each image represents an area 2.5 m x 2 m. 221
Figure 6.11. Overhead image of the braidplain showing the bedforms that form at low flow stage in series F and M (example from series F). Flow direction is from right to left and the images represents an area of braidplain of 2.5 m x 2 m. 222
Figure 6.12. Phase diagram from Allen (1983a) showing the calculated dimensionless boundary shear stress for D_{50} and D_{90} values from experiment series F, M and C. 223
Figure 6.13. Overhead images of (a) a plan view and (b) an oblique view looking upstream following instantaneous drainage of the flume facility at 1.67 L s^{-1}, confirming that bedforms that disappear at higher shear stresses are ripples (see Figure 6.12). Black arrows indicate the flow direction. 224
Figure 6.14 (a) Examples of architectural elements types A-F taken from the sections cut perpendicular to palaeoflow in the series C and F, where flow direction is into the page. Where A = primary channel fills, B = secondary channel fills, C = splay, D = fine-grained channel fills, E = erosional remnants, and F = overbank fines. Refer to Table 6.6 for sedimentary descriptions. The dashed line represents the boundary between series C at the base and series F at the top and the scale bar in each case is 20 mm. 228
Figure 6.15. Frequency of occurrence for architectural elements observed in cut-sections from series F, M, and C. 231
Figure 6.16. Vertical proportion curves for series F experiments, indicating an increase in the proportion of splay deposits towards the top of the sequences where the deposits became abandoned. 231
Figure 6.17. Geometrical information for architectural element A, primary channel fills. 234
Figure 6.18. Geometrical information for architectural element B, secondary channel fills. 234
Figure 6.19. Geometrical information for architectural element C, splays. 235
Figure 6.20. Probability density functions for width distributions of coarse-grained architectural elements (a) primary channel fills, (b) secondary channel fills, and (c) splays observed within the three experiments. Note the similarity of series C and M, but an extended width distribution of series F in (a) and (c). 236

Figure 6.21. Probability density functions for the width distributions of fine-grained architectural elements (a) channel fills, (b) erosional remnants, and (c) overbank fines observed within series C, M and F.....237
Figure 6.22. Probability density functions for width/thickness ratio distributions of coarse-grained architectural elements (a) primary channel fills, (b) secondary channel fills, and (c) splays observed within the three experiments. Note the similarity of distributions between series C, M and F.....238
Figure 6.23. Running mean of suspended sediment concentrations by weight for series C and F, measured during at minimum discharge (0.31 l s^{-1}). Note the higher rates for series F compared to C.....240
Figure 6.24. Calculated fall velocities for particles in suspension in series C and F based on sediment concentration presented in Figure 6.23. Note: the vertical exaggeration.....241
Figure 6.25. Examples of architectural elements observed within the Canterbury Gravels, New Zealand. Where A = primary channel fills, B = secondary channel fills, C = splay, D = fine-grained channel fills, E = erosional remnants, and F = overbank fines. White scale bars represent 0.5 m. 245

Table 6.1. Summary of imposed conditions for the three FSM experiments used to compare the impact of sediment supply grain size on channel morphology and alluvial architecture.....208
Table 6.2. A summary of mean key flow parameters calculated for the Ashburton River field study and physical modelling experiments series C, M and F. 210
Table 6.3. Comparison of channel geometries measured at four sites along the course of the modern Ashburton River.....211
Table 6.4. Description of flow types observed within each of the three braided experimental runs. 216
Table 6.5. Summary of surface depositional forms from the three experiments, series F, M and C described from analysis of overhead video footage.....220
Table 6.6. Architectural elements observed within the flume sections and Quaternary Gravels of the Canterbury Plains. Elements A-C may include openwork deposits in field examples. Geometries for each of the architectural elements are presented for individual experiments in Tables 6.7 and 6.8.....226
Table 6.7. Geometrical dimensions for the coarse-grained architectural elements observed in the sections of the three experiments of series C (standard text), M (italics) and F (bold) grain size distributions.....233
Table 6.8. Geometrical dimensions for the fine-grained architectural elements observed in the sections of the three experiments of series C (standard text), M (italics) and F (bold) grain size distributions. 233
Table 6.9. Comparisons of formative channel width and depth data with preserved channel fill width and thickness data from the Ashburton model. The mean values of maximum channel depth were used.....242
Table 6.10. Summary information on the statistical differences using the Kruskal-Wallis test between series C - M - F, showing at the 95 % confidence limit the + represents a significant increase and – a significant decrease in the variables. Where no symbol is present, no significant differences between the series was found. 243
Table 6.11. Two-dimensional geometries of coarse-grained channel fill architectural elements B measured from the Ashburton model and the Canterbury Gravels as documented in Ashworth *et al.* (1999). 246

Chapter 7. Application of combined core-physical modelling-outcrop approach to reservoir simulations: future potential

Figure 7.1. Photograph from Anderson *et al.* (1999) showing lithofacies Gs, Gm, and Sh within the Stoughton Gravel deposits used to apply permeability information to architectural elements from the Ashburton model. 264
Figure 7.2. Vertical proportion curves for series C, showing a possible cyclicity with an increasing percentage of splay deposits (architectural element C) around the 2.25 m level, with two peaks either side of increased primary channel deposits (A). Note the sequence has been up-scaled by 1:50 (n =60)....269
Figure 7.3. Vertical proportion curve for series F showing the dominance of channel fill deposition and an increase in the proportion of splay deposits towards the top of the sequences, reflecting the reworking towards the top of the sequence. Note the sequence has been upscaled by 1:50. 270
Figure 7.4. The effects of averaging the vertical facies data, whilst keeping the sampling frequency constant. Where A = Primary channel fills, B = Secondary channel fills, C = Splays, D = fine-grained channel fills, E = erosional remnants, and F = overbank fines. The small scale cyclicity that may be encountered in the (a) and (b) is lost when and averaged over greater vertical thicknesses (c and d). Also, because the data are averaged, the finer-grained architectural elements are distributed through the entire sequences (c and d) and not just concentrated in the centre of the sequences as shown in (a) and (b)....274
Figure 7.5. A diagram to illustrate the impact of the progressive doubling the vertical grid spacing (reducing the sampling frequency) using the model section data (a-d). Where A = Primary channel fills, B = Secondary channel fills, C = Splays, D = fine-grained channel fills, E = erosional remnants, and F = overbank fines. The most apparent differences are that as sampling frequency is reduced, primary channel fill deposits become over represented and a loss of some of the fine-grained elements (D and E) occurs....275
Figure 7.6. An example of the sectioned alluvial architecture from unscaled models from the experimental facility at St. Anthony Falls, University of Minnesota. Note palaeoflow direction was out of the page (Courtesy of Ben Sheets, University of Minnesota)....276
Figure 7.7. Examples of how the techniques using greyscale pixel analysis of Davis *et al.* (2000) to assign permeabilities could be employed on sections from the scaled Ashburton physical model (Chapter 6). Sections are cut perpendicular to the palaeoflow direction. (a), (b), and (c). 278

Table 7.1. Scales of heterogeneity for consideration of fluvial reservoir performance, showing how different techniques provide data at different scales that complement each other as various aspects of the reservoir model are constructed. 260
Table 7.2. Assignment of permeability classes based on calibration of Soughton Outwash Gravels (from Anderson *et al.*, 1999) to architectural elements described in Chapter 6, Table 6.6....264
Table 7.3. A step-by-step methodology required to collect data from stratigraphic physical models to serve as inputs to object-based geological simulations. 267
Table 7.4. Typical input parameters for a current fluvial reservoir modelling software simulators, ROXAR - RMS/STORM. The versatility of the physical modelling dataset allows provision of all parameters to cover a spectrum of methods for reservoir evaluation....271

Appendix

Figure A1. Core log for well 44/18-1, Tyne Field, SNS.....350
Figure A2. Core log for well 44/18-T1, Tyne Field, SNS. 351
Figure A3. Core log for well 44/18-T2, Tyne Field, SNS. 352
Figure A4. Core log for well 44/18-2Z, Tyne Field, SNS. 353
Figure A5. Core log for well 44/18-T3a, Tyne Field, SNS.....354
Figure A6. Core log for well 44/18-4A, Tyne Field, SNS.....355
Figure A7. Core log for well 44/18a-T5, Tyne Field, SNS.....356
Figure A8. Core log for well 44/18a-5, Tyne Field, SNS.....357

Table C1. D_{50} values for samples of suspended sediment taken from series C and F.....359

List of symbols

c	Volume concentration of grains in the falling dispersion (%)
C	Compaction
D	Grain size diameter (m)
D_0	Initial grain size diameter (m)
D_{50}	The 50th percentile of the grain diameter (m)
D_{90}	The 90th percentile of the grain diameter (m)
D_b	Depth of burial (km)
d	Formative channel depth (m)
d_m	Mean bankfull flow depth (m)
e	Base of natural logarithms
ew	Expected sandbody width (m)
F	Proportion of prototype floodplain (%)
fc	Hydrography duration compression factor
Fr	Froude number
g	Gravitational constant (m s^{-2})
h	Average flow depth (m)
h_m	Mean dune height (m)
Hy_m	Model hydrograph duration (hr)
Hy_p	Prototype hydrograph duration (hr)
K	Permeability (mD)
K_h	Horizontal permeability (mD)
K_v	Vertical permeability (mD)
K_S	Surface roughness (m)
L	Sandbody length (m)
Q_m	Discharge of the model (m)
Q_p	Discharge of the prototype (m)
m	model
n	Exponent for fall velocity
N^w_c	Number of complete sandbody widths
p	prototype
R	Hydraulic radius (m)
Re	Reynolds number

Re*	grain Reynolds number
$Re*_{crit}$	Critical grain Reynolds number
S	Bed slope
S_b	Buried solidity (%)
S_i	Initial solidity (%)
S_m	Mean cross set thickness (m)
U	Downstream velocity ($m\ s^{-1}$)
U_*	Shear velocity ($m\ s^{-1}$)
W	Characteristic weight (kg)
W	Sandbody width class (m)
w	Partially observed sandbody width (m)
W_0	Initial particle weight (kg)
W_m	Width of the flume facility (m)
W_p	Maximum field prototype floodplain width (m)
Q_{max}	Maximum discharge ($m^3\ s^{-1}$)
Qp	Prototype discharge ($m^3\ s^{-1}$)
U_f	Fall velocity ($mm\ s^{-1}$)
v_g'	Fall velocities of a spherical particle in a dispersion of falling grains ($mm\ s^{-1}$)
v_g	Fall velocity of a single grain in an otherwise grainless fluid ($mm\ s^{-1}$)
x	Downstream distance (km)
α	Diminution coefficient ($mm\ km^{-1}$)
α_d	Diminution coefficient for characteristic grain size ($mm\ km^{-1}$)
λ	Outcrop length (m)
$\lambda_l^{0.5}$	Length scale for time
$\lambda_Q^{2.5}$	Scaling of time for discharge
λ_t	Scaling ratio of time between prototype and model
$(\lambda_t)_V$	Time scale for mean flow velocity
ρ	Density of the fluid ($kg\ m^{-3}$)
ρ_S	Density of the sediment ($kg\ m^{-3}$)
σ	Surface tension ($N\ m^{-1}$)
τ	Shear stress ($N\ m^{-2}$)
τ^*	Dimensionless shear stress
τ_c^*	Critical dimensionless shear stress
μ	Dynamic viscosity of the fluid ($kg\ m^{-1}\ s^{-2}$)

List of acronyms

BRB	Barren Red Beds
CBW	Channel-belt width
FSM	Froude-scale model
GFSM	Generic Froude-scale model
GPR	Ground penetrating radar
LKM	Lower Ketch Member
MNSH	Mid North Sea High
PDF	Probability density function
Series C	Coarse grain size distribution
Series M	Medium grain size distribution
Series F	Fine grain size distribution
SNS	Southern North Sea

Chapter 1. Introduction and background to the study

1.1 Introduction

Fluvial systems are found in almost all latitudes, altitudes and topographic gradients, developing under a spectra of sedimentary environments. Defining, understanding and isolating the primary allocyclic (extrinsic) and autocyclic (intrinsic) controls acting within these different alluvial environments is paramount to the construction of stratigraphic models and prediction of alluvial architecture. Many hydrocarbon reservoirs are located in fluvial sequences (cf. Martin, 1993). Interpretation of alluvial architecture is often undertaken in the hydrocarbon industry from one-dimensional well datasets with spacings of ~0.5 km (e.g. Lorenz *et al.*, 1985; Begg *et al.*, 1989; Atkinson *et al.*, 1990; Lui *et al.*, 1996; Eschard *et al.*, 1998; Tye *et al.*, 1999; Vaughan *et al.*, 1999). Successful prediction of alluvial architecture, in terms of depositional geometries, frequency of occurrence and, crucially, interconnectedness has economic implications for improving subsurface reservoir prediction and recovery. Well-to-well correlation is commonly based on the occurrence of marker horizons, an assessment of the palaeodepositional environment, and the assignment of geometrical and spatial heterogeneity datasets within the reservoir interval across a range of scales. Accurate prediction of the alluvial architecture requires the geologist to undertake several key steps during reservoir evaluation: (1) establishing the main controls on the fluvial system; (2) quantifying river morphology at the time of deposition; (3) linking surface form and processes to subsurface alluvial architecture; (4) quantifying the alluvial architecture; and (5) linking all of the above to the reservoir properties (e.g. petrophysics) at a range of scales. Often this process is undertaken in reverse in order to compare and assign analogue datasets to the fluvial sequence concerned.

1.2 Controls on alluvial architecture

Fluvial systems respond to a range of allocyclic and autocyclic controls (Figure 1.1), including, but not exclusive to: climate and base-level (Leeder, 1993; Koss *et al.*, 1994; Leeder and Stewart, 1996), tectonics (Miall, 1981; Alexander and Leeder, 1987; Peakall, 1998, Kraus and Middleton, 1987; Shuster and Steidmann, 1987), sediment supply and aggradation rate (Bentham *et al.*, 1993; Germanoski and Schumm, 1993; Ashworth *et al.*, 1999), and channel and channel-belt avulsion (Leddy *et al.*, 1993;

Bryant *et al.*, 1995; Bridge and Mackey, 1995; Heller and Paola, 1996; Field, 2001). Sedimentary successions are the subsurface expression of the complex interaction between these controls. Isolation, quantification and characterisation of these controls in any sedimentary sequence have always been the goal of the geologist. The interpretation of ancient sedimentary sequences requires knowledge drawn from analogue studies, which has often been restricted to qualitative descriptions. With technological advances now allowing stratigraphic computer models to be built, the effect of allocyclic and autocyclic controls on alluvial architecture needs to be isolated and quantified.

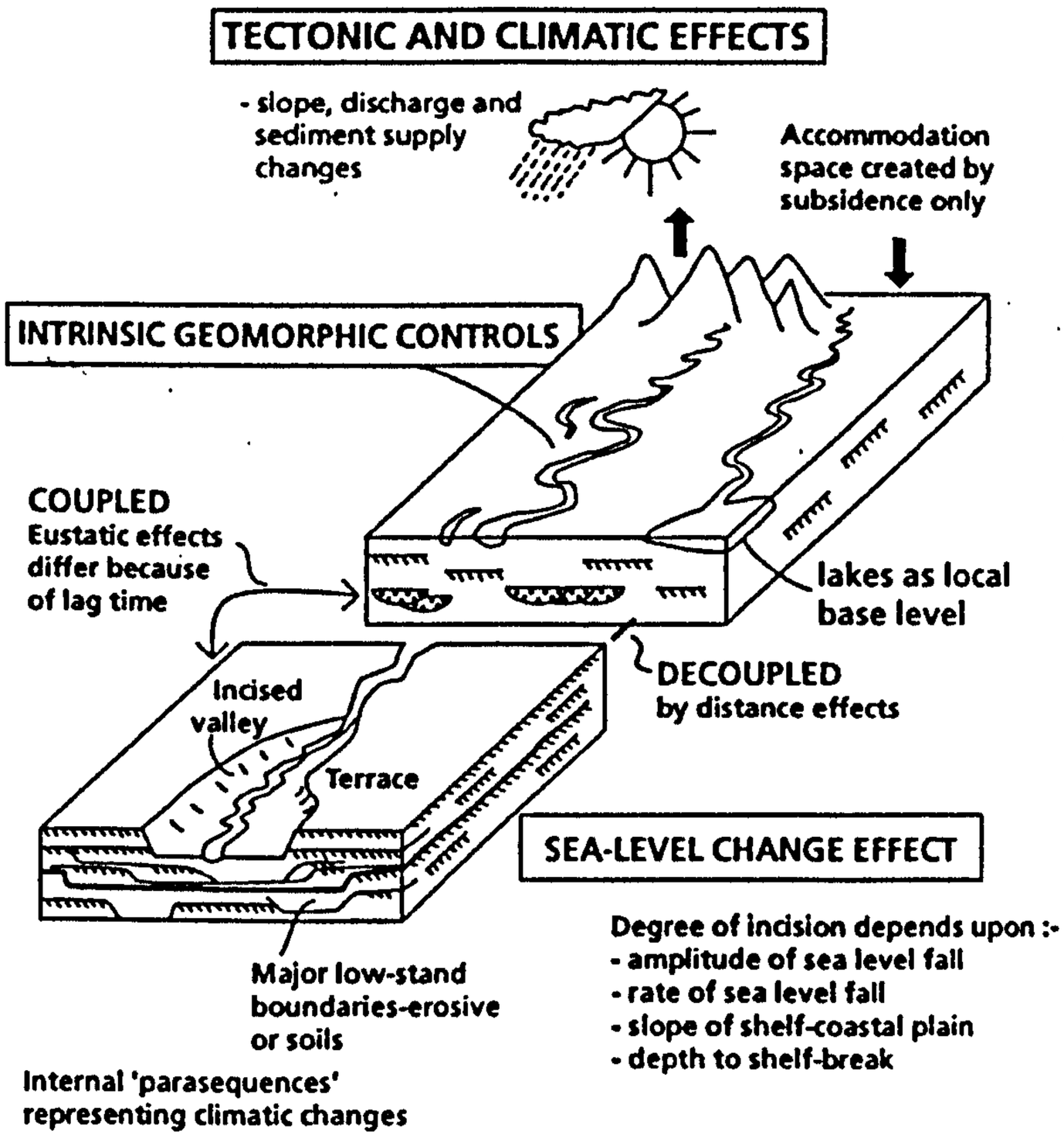

Figure 1.1. Controls on the fluvial system and alluvial architecture (from Marriott, 1999)

One of the key controls of fluvial depositional style is the sediment supply grain size (Wolcott, 1988) and the subsequent modification of the grain size distribution downstream. The impact of sediment supply grain size on rivers has been qualitatively shown to influence river morphology (Schumm, 1981; Simons and Simons, 1987; Leopold, 1992; Friend, 1993). Many studies of modern and ancient fluvial systems have documented the diminution of sediment grain size downstream (e.g. Brierley and Hickin, 1985; Dawson, 1988; Werritty, 1992; Hoey and Bluck, 1999; Rice, 1999). However, the link to the subsurface alluvial architecture has been rarely discussed;

exceptions including Heller and Paola (1996). Grain size is also a primary control on the petrophysical properties of individual lithofacies units/architectural elements (Hazen, 1893; Freeze and Cherry, 1979; Domenico and Schwartz, 1990; Miller *et al.*, 1990; Brayshaw *et al.*, 1996). Consequently, as grain size can be quantified in both modern and ancient environments and linked to reservoir properties, understanding how grain size influences subsurface architecture will significantly enhance conceptual, stratigraphic and reservoir models of fluvial systems.

1.3 Applications within the hydrocarbon industry

Fluvial sedimentary sequences provide host to some of the most important hydrocarbon reservoirs (Martin, 1993). Over the past 15 years there has been renewed interest in the Southern North Sea as a major gas producing region. Particular attention in the Upper Carboniferous Red Bed sequences (e.g. Tyne, Ketch and Schooner Fields of the Silverpit Basin) has sparked a great interest in fluvial sequences where the net-to-gross ratio is

extraction (Fogg, 1986; Fielding and Crane, 1987; Bridge and Mackey, 1993a). With the lack of biostratigraphic and seismic control (Mijnssen, 1997; Stone and Moscariello, 1999), interpretation of these low net-to-gross sequences is often limited to chemostratigraphic or pedofacies analysis (Pearce *et al.*, 1999; Stone and Moscariello, 1999). While these techniques may provide vertical subdivision of the reservoir interval, they lack the lateral resolution. Cross plots of sandbody width and thickness are often used to provide information on sandbody geometries from onshore outcrop analogues (e.g. Fielding and Crane, 1987; Dreyer, 1993; North and Taylor, 1996; Robinson and McCabe, 1997; Bridge *et al.*, 2000). However, problems associated with gathering outcrop datasets and cross plots with wide data scatter result in poorly constrained channel-belt sandbody geometries being used to evaluate the inter-well reservoir architecture. Considerable uncertainty also lies in using published data to build geological models (static models) and provide petroleum engineers with quantitative data with which to construct flow simulations (dynamic models).

As hydrocarbon reservoir development projects move into secondary stages of production, more information is needed on the within channel-belt alluvial architecture (the individual channel and bar scale, Figure 1.2). Often the lack of quantitative data

available at the channel-belt and within channel-belt scale results in petrophysical characteristics being up-scaled to the seismic scale of information causing changes in the permeability balance (Mansoori, 1994; Davis *et al.*, 2000). The need to address all the scales of heterogeneity (van der Graff and Ealey, 1989; Cross, 1991), exhibited in any particular fluvial reservoir interval is paramount to complete static and dynamic reservoir modelling. Conventional techniques, such as the use of outcrop analogues, may best provide information on the channel-belt scale sandbody geometries, while smaller internal heterogeneities have often been limited to qualitative descriptions (e.g. Miall, 1977, 1978; Collinson, 1978; Miall, 1985). Techniques such as physical modelling, numerical modelling and ground penetrating radar may provide quantification of the scale of heterogeneity needed to satisfy the gap in currently available datasets.

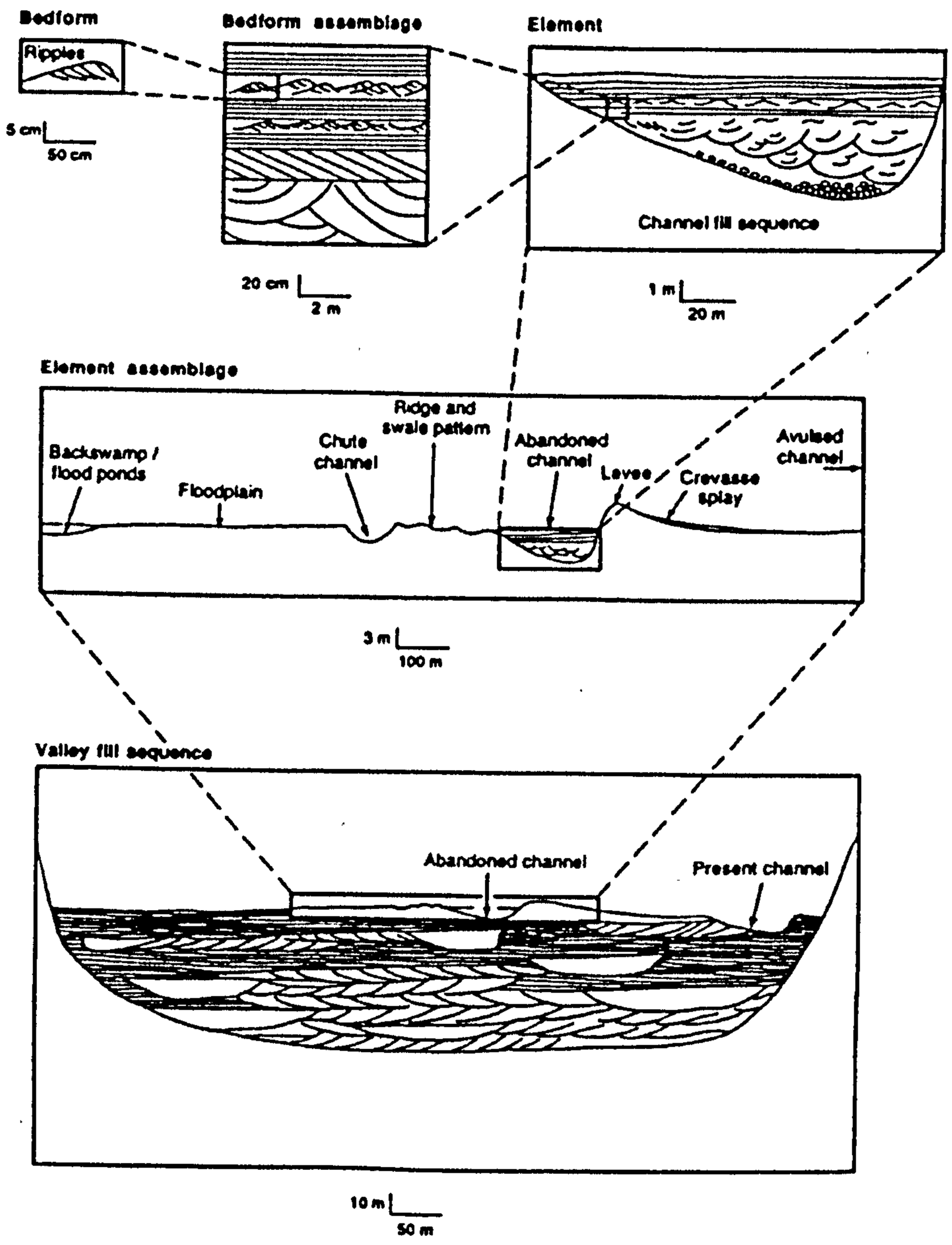

Figure 1.2. Scales of fluvial heterogeneity required for full reservoir evaluation (from Bristow, 1996).

1.4 Research objectives

The objectives of this research are sixfold:

1. To review the controlling mechanisms responsible for the construction of alluvial architecture and the techniques employed for hydrocarbon reservoir evaluation.
2. To highlight areas of data shortage for quantitative alluvial architecture models.
3. To examine the alluvial architecture and depositional environment of the Lower Ketch Member reservoir interval, Tyne Field, Southern North Sea, UK, and establish the main controlling mechanisms on deposition.
4. To assess the suitability of UK onshore analogues for the Tyne Field and evaluate the benefits of the outcrop analogues versus published datasets for the prediction of subsurface reservoir alluvial architecture in low net-to-gross systems.
5. To isolate and quantify the control of grain size on the surface channel morphology and subsurface alluvial architecture of braided rivers using field studies and physical modelling.
6. To assess the use of an integrated core, field and physical modelling approach to improve understanding of different scales of alluvial architecture in order to provide high resolution, spatially-intensive datasets for quantitative reservoir evaluation.

1.6 Thesis structure

Chapter 2 reviews the autocyclic and allocyclic controls on fluvial systems and discusses current models of alluvial architecture. The concepts of downstream fining and sediment supply grain size are critically reviewed and trends highlighted. The chapter documents the history of vertical facies models and their link to surface channel morphology. A review of the move to a more quantitative approach to sedimentological characterisation is highlighted and the techniques now being used to provide data for subsurface evaluation are critically appraised. Finally, the shortcomings of reservoir simulation models are shown to be often the result of a paucity of geologically-constrained input. The review summarises on the best data sources from current techniques in addressing input parameters needed for different scales of reservoir heterogeneity.

Chapter 3 investigates the Carboniferous Lower Ketch Member of the Tyne Field, Southern North Sea and discusses the sedimentology, lithofacies and depositional environment of an aggrading alluvial plain where both channel-belt and floodplain deposition occurred coevally. The Tyne depositional model is incorporated into the regional palaeogeographic setting for the Silver Pit Basin. Quantitative data are provided for sandbody thicknesses, channel depths, channel-belt widths and grain size distribution. A review of the influence of compaction on the prediction of the lateral extent of sandbodies is provided. Lithological analogues have been critically appraised and chosen in preference to stratigraphic analogues to provide information on the inter-well architecture.

Chapter 4 tests the Eocene Escanilla Formation, Ainsa Basin, Spain, for use as an outcrop analogue to the Lower Ketch Member. The channel-belt sandbodies are classified using a quantitative methodology and demonstrate that a variety of channel-patterns may have existed on the alluvial plain. The sedimentological, lithofacies interpretations and depositional model of Bentham *et al.* (1993) are reviewed. Two-dimensional channel-belt geometries are presented and adjusted for exposure based on methodologies of Visser and Chessa (2000a,b). Qualitative and quantitative comparisons of sequences show an understanding of the Lower Ketch Member may benefit from datasets gained from the Escanilla Formation.

Chapter 5 describes the rationale, experimental equipment and procedure for an experimental study of the impact of sediment supply grain size on braided alluvial architecture. The principles of physical modelling are briefly reviewed and a discussion on the problems of scale modelling fine-grained systems, such as the Lower Ketch Member and the Escanilla Formation, is provided. Field data from the modern Ashburton River and Quaternary Gravels, Canterbury Plains, New Zealand are used to supply the necessary prototype input parameters for two experiments, which used a bimodal grain size distribution that was reduced in magnitude by 75 % in an experimental flume basin that permits aggradation.

Chapter 6 quantifies the impact of sediment supply grain size on the surface channel morphology and resultant within channel-belt alluvial architecture from three experiments incorporating a fourfold change in grain size magnitude. The flow parameters from the physical model are quantified and assessed. Channel geometries,

channel occupancy, duration of channel occupancy, and sediment surface slope are quantified and compared between experiments and the field prototype. The surface processes are discussed and linked to a six-fold scheme of architectural element classification via analysis of overhead video footage. Horizontal proportion curves of frequency of occurrence and width/thickness measurements of architectural elements are used to explain architectural trends resulting from changes in sediment supply grain size and a quantitative model is proposed. The model alluvial architecture is compared to the Canterbury Gravels and application to other documented outcrop and reservoir studies is discussed.

Chapter 7 examines the application of an integrated core, outcrop and physical modelling approach to the geological characterisation of reservoirs. The benefit of each of these techniques in addressing different scales of reservoir heterogeneity is considered. A methodology for gaining quantitative data from physical models in order to serve as input to object-based models is presented, founded on the relationship between architectural elements/facies and petrophysical properties. The effects of sampling frequency and averaging are reviewed and alternative methods of analysis are introduced.

Chapter 8 provides a summary of the main conclusions and presents recommendations for future work.

Some supporting material is provided on the enclosed CD (Appendix D).

Chapter 2. Controls on alluvial architecture and the assessment of hydrocarbon reservoir heterogeneity

2.1 Synopsis

This chapter reviews and describes the range of allocyclic and autocyclic controls influencing the fluvial system. The controls are discussed with respect to their resultant depositional form. The role of sediment supply grain size is reviewed and established in the context of down basin fining trends and depositional architecture. Surface-to-subsurface relationships and the development of facies schemes and architectural models are discussed. The assignment of characteristic sandbody geometries from specific depositional environments is demonstrated to carry considerable conditions for their application. The move to a more quantitative approach in sedimentological characterisation is highlighted and the techniques now being used to provide data for subsurface reservoir evaluation are critically appraised. Finally, the shortcomings of reservoir simulation models are shown to often be the result of a paucity of geologically-constrained inputs. This review indicates the optimal data sources from current techniques to address input parameters needed for different scales of reservoir heterogeneity.

2.2 Introduction to controls on alluvial architecture

Fluvial systems respond to external (allocyclic) and internal (autocyclic) controls (Table 2.1) influencing both the regional (basin scale) architecture and the local channel scale architecture. Our understanding of the controls on alluvial architecture requires the recognition of their influence in the stratigraphic record, often in one-dimension as vertical profiles (e.g. Collinson, 1978) or two-dimensions as channel-belt sandbodies (e.g. Friend *et al.*, 1979). In any particular sequence it is often unclear as to which of these allocyclic and autocyclic mechanisms are the primary controls on alluvial architectural style. Autocyclic mechanisms (e.g. channel avulsion and migration) may modify the short-term character of the fluvial system, leading to the change in the position of the channel. Only long-term allocyclic events (tectonics, base-level change, climate and sediment supply) may alter channel width, channel depth, sediment calibre,

sediment discharge, slope, and planform causing major architectural changes (Miall, 1996). The complex interplay between controlling variables led Hartley (1993) to state:

"In order to assess the importance of any one allocyclic mechanism on the alluvial architecture of a basin-fill sequence the mechanism should be studied in isolation from another, a situation difficult to achieve".

Table 2.1. Examples of published studies documenting the range of allocyclic and autocyclic controls influencing a fluvial system. These controls are linked with both positive and negative feedback effects.

Controlling Factors	Effects	Author (s)
Base-level and climate change	Controls channel incision, aggradation, sediment supply, hydrological regime and preservation potential	Friend (1978), Leeder (1993), Koss *et al.* (1994), Leeder and Stewart (1996), Newell *et al.* (1999)
Tectonics	Controls subsidence rates, tilting creates channel -belt stacking	Miall (1981), Alexander and Leeder (1987), Kraus and Middleton (1987), Groll and Steidmann (1987), Shuster and Steidmann (1987), Hartley (1993), Leeder (1993), Peakall (1998), Peakall *et al.* (2000)
Basin type and geometry	Basin wide alluvial architecture and channel-belt slope and palaeoflow	Miall (1981)
Aggradation rate	Controls stacking pattern, interconnectedness of sandbodies and preservation potential	Germanoski and Schumm (1993), Bentham *et al.* (1993) Ashworth *et al.* (1999)
Sediment supply and provenance	Grain size distribution, downstream fining rate, channel slope	Weber (1980), Germanoski and Schumm (1993)
Compaction	Controls stacking pattern and distortion of architectural elements	Athy, 1930; Maxwell, 1964; Baldwin, 1971; Sclater and Christie, 1980; Shinn and Robbin, 1983; Baldwin and Butler, 1985; Fielding, 1986; Collier, 1989; Caudill *et al.*, 1997
Avulsion frequency and type	Controls stacking patterns, channel fill and distribution	Leeder (1978) Allen (1978), Leddy *et al.* (1993), Tornqvist (1994), Bridge and Mackey (1995), Bryant *et al.* (1995), Heller and Paola (1996)
Incision and scour	Controls preservation of deposits and interconnectedness of sandbodies	Grissinger and Murphey (1983), Salter (1993), Alexander and Gauthorpe (1993), Leeder and Stewart (1993), Best and Ashworth (1997)
Flood magnitude and frequency	Discharge, controls sediment supply, nature of floodplain deposits and repetition of sequences	Miall (1978)
Vegetation and bank strength	Channel pattern and confinement	Gibling and Rust (1990), Huang and Nanson (1998)

Understanding the controls on alluvial architecture is fundamental to the construction of well-constrained stratigraphic models and the successful exploitation of many hydrocarbon reservoirs. More detail on the internal architecture is needed during the development of a hydrocarbon reservoir, to include the channel-belt and within channel-belt (individual bar and channel) scale.

The main aims of this chapter are:

1. To review the allocyclic and autocyclic controls on channel morphology and alluvial architecture.
2. To evaluate the impact of sediment supply grain size into a drainage basin and establish the manner in which grain size sorting occurs down a river course.
3. To review the relationship between depositional environment and alluvial architecture for the prediction of subsurface geometries.
4. To critically appraise the different techniques used to predict reservoir alluvial architecture and highlight any gaps in the current datasets on alluvial architecture.
5. To establish the current progress of reservoir simulation modelling techniques and their data requirements.

2.2.1 Climatic and sea-level changes

Climate coupled with lithology control the flux of sediment into the basin, with climate controlling the vegetation type and density, the magnitude and frequency of discharge regimes, the degree of weathering and the sediment supply rate. In addition, base-level will control the accommodation space in the basin. Base-level may be defined as the imaginary horizontal level or surface to which sub-aerial erosion proceeds (Schumm, 1993) and this is commonly sea-level. Many regional base-level controls have been deemed the result of eustatic sea-level changes that have been attributed to Milankovitch cycles of precession, obliquity and eccentricity of the earth, which create cyclical climate changes as the amount of solar radiation influencing the earth alters (Hays *et al.*, 1976, Imbrie *et al.*, 1984). The pronounced coupling of climate and base-level controls with periods of ice expansion during glaciation creating a global sea-level fall, alternating with ice retreat generating a sea-level rise, has been identified as the forcing mechanisms for many of the cyclical changes in alluvial sequences (e.g. Olsen, 1990). Climate and base-level relationships are often the founding principles for sequence stratigraphic models, such as those developed at Exxon (Vail *et al.*, 1977). Climatic and sea-level changes may cause local transgressional or regressional sequences to form when fluvial systems advance or retreat, aggrade or degrade, creating different architectural styles (Leeder, 1993). For example, in sediment-starved systems incision may occur, while in periods of increased sediment flux, aggradation will occur (Jones *et al.*, 1999). The rate at which these changes operate will determine the frequency of

changes in both the downstream and vertical stratigraphic development of a basin. Increases in the density of channel deposits may be related to base-level changes, although could equally be a result of other allocyclic or autocyclic controls (Leeder and Stewart, 1996).

Base-level change has been investigated using physical models (e.g. Koss *et al.*, 1994, Paola, 2000) and field outcrop (e.g. Kvale and Vondra, 1993). In addition, the use of computer models that simulate base-level change have been shown to produce outputs in broad agreement with outcrop data (Marriott, 1999). Base-level fall may create incision and erosion creating a sediment bypass zone. Incisional events have been identified as more subtle boundaries in the geologic record, separating fluvial deposits with distinctly different architectures (Shanley and McCabe, 1993, Figure 2.1). Results from Kvale and Vondra (1993), Koss *et al.* (1994) and Paola (2000) indicate that when base-level drops too rapidly for sedimentation to keep pace, deposition occurs as a prograding fluvial braidplain with minimum vertical build up. While during base-level standstill and rise, fluvial aggradation occurs that produces a vertical build-up of the shelf. A base-level rise and standstill may also induce incision, with rivers adjusting their downstream slopes to meet coastal erosion (Leckie, 1994; Leatherman *et al.*, 2000). The wide contradictions in the fluvial response to climate and base-level change imply that the balance between the rate of change in climate and sea-level will determine the nature and response of the fluvial system in any particular basin.

The key to distinguishing the changes in fluvial outcrop sequences is to isolate climate and base-level controls against other forcing mechanisms discussed in the following sections. Analysis of the modern Canterbury Plains, New Zealand, reveals incisional river systems that are bèing driven by rapid tectonic uplift of the Southern Alps in the proximal reaches. In the medial reaches there is a zone of minimal erosion, whilst in distal reaches incision is being driven by a current sea-level standstill and rapid (~ 1 m yr^{-1}) coastal erosion, forcing rivers to modify their downstream gradient to meet this retrogradational coastline (Leckie, 1994).

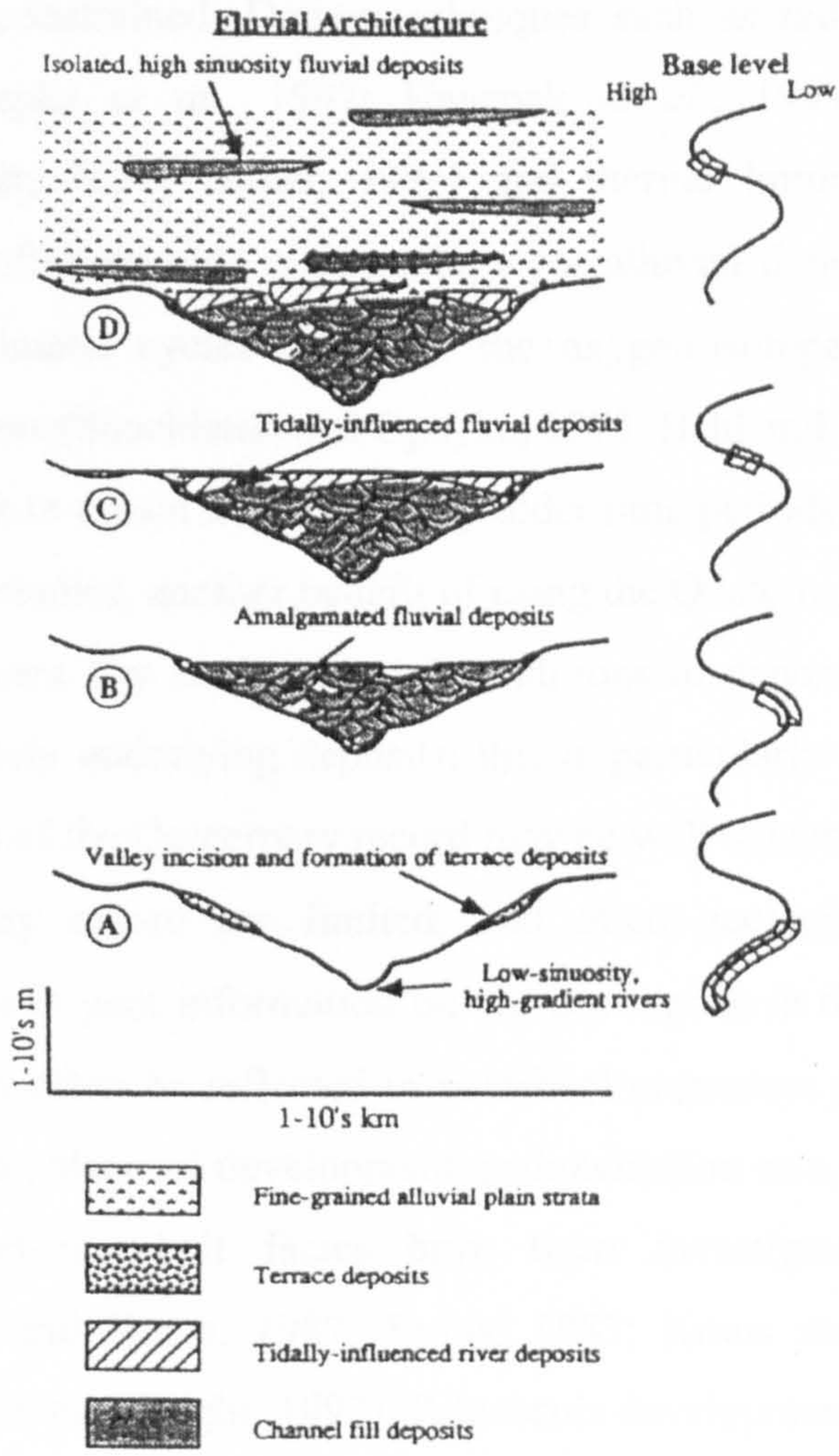

Figure 2.1. Summary diagrams illustrating the relationship between shoreface and fluvial architecture as a function of base-level change (from Shanley and McCabe, 1993).

Climate influences the prevailing discharge regime, which in turn controls the sediment load and sorting downstream. Changes in discharge and sediment controlling variables have been shown to affect cross-sectional and planform geometry (reviewed in Richards, 1982; Brierley, 1996; Knighton, 1998), to include geometric changes to width, depth, width/depth ratio, sinuosity and slope. Changes in channel geometry influence the geometry, magnitude and frequency of occurrence of depositional facies. For example, Olsen (1990) attributed two cyclical changes in meandering sandbody thickness in the Andersson Land Formation of East Greenland to reflect climatically driven changes in discharge regime related to Milankovitch cycles. Smith (1994) also suggested that changes in sandbody geometry, net-to-gross, sediment accumulation and palaeosol development in tectonically quiescent periods might reflect climate change.

Much of the work concerning the role of climate and sea-level changes on fluvial architecture has focused on the Quaternary record (Blum and Törnqvist, 2000) since the

chronology is well constrained. Dating techniques such as radiocarbon, cosmogenic (Bierman, 1994; Repka *et al.*, 1997; Hancock *et al.*, 1999), optical stimulated luminescence (Berger, 1988; Duller, 1996) and thermo luminescence (Clarke and Rendell, 2000) can often provide a chronology for alluvial deposits. This chronology can be linked to climatic cycles based on the oxygen-isotope record from marine sediments and ice cores (Shackleton and Opdyke, 1973; Behl and Kennett, 1996), which may be more difficult to obtain in geologically older time periods (Blum and Törnquist, 2000). In some field studies, another benefit of using the Quaternary record concerns the similarity of the present day environmental conditions to depositional conditions that formed the immediately underlying deposits; this is particularly true for the Holocene record. While studies of the Quaternary record may be well constrained, climatic studies of the pre-Quaternary record are limited, and often geologists have reverted to alternative techniques to gain information on climate regime at the time of deposition. Climatic controls can often be reflected in palaeosol sequences (Retallack, 1984) and relationships between palaeosol development, sedimentation rate, floodplain hydrology and proximity to channel-belt facies have been investigated using pedofacies relationships (Bown and Kraus, 1987; Kraus, 1987; Kraus and Bown, 1993), and palaeocatena relationships (Wright, 1992). Palaeosols development on terraces has been used to imply a reduction in discharge resulting in floodplain abandonment (Blum and Valastro, 1994). Leeder (1975) proposed a method for determining floodplain sedimentation rates from calcrete development. However, this approach has to be considered with caution (Wright, 1990) as, again, much of the present knowledge of palaeosol development is based on the Quaternary record, resulting in uncertainty concerning the length of time palaeosols take to form. Further complications arise in the interpretation of sequences such as red beds, which may have been formed during a variety of humid to arid climatic settings (Turner, 1980) and have to be analysed in conjunction with other sedimentological features to constrain the depositional setting. Much of the identification of climatic and base-level controls in the subsurface hinges on the observation of sedimentary features that are specific to the forcing mechanisms. In the following sections it will become apparent that more than one controlling mechanism may ultimately determine the alluvial architecture and these may be indistinguishable.

2.2.2 Tectonics

Tectonic activity and subsidence provide the basin scale controls on river behaviour, influencing the three-dimensional distribution of channel-belt sandbodies by controlling shape, size and orientation of the basin (reviewed in Miall, 1996). The influence of tectonics on alluvial architecture has been demonstrated from outcrop (Leeder *et al.*, 1996), modern rivers (Peakall, 1998, Peakall *et al.*, 2000) and physical models (Burnett and Schumm, 1983; Ouchi, 1985) who advocate that the style of channel response reveal that channel-belts and their associated deposits are sensitive indicators of active tectonic regimes. Additionally, tectonics can affect sediment calibre and volume supplied from the hinterland, which in turn controls channel-belt avulsion (Section 2.2.5). Many studies of basin tectonics have focused on the role of faulting as a primary control on channel behaviour.

Surface expressions of fault activity have strong local effects on river orientation and gradient and thus alluvial architecture. Several studies have documented the response of channel-belt to gradient changes created by tectonic tilting (Todd and Went, 1991; Olsen and Larson, 1993, Peakall *et al.*, 2000). Tilting of a floodplain has been shown to result in slow channel-belt migration incision or sudden avulsion in a down-dip direction towards the active fault, consequently, altering the style of alluvial architecture stacking patterns (Leeder, 1993; Leeder *et al.*, 1996; Peakall, 1998; Peakall *et al.*, 2000). Gordon and Heller (1993) demonstrated lithofacies had a marked asymmetry due to syntectonic deposition in the Pine Valley, Nevada. Alexander and Leeder (1987) established that the primary influence of tectonic activity on floodplain behaviour is tilting, varying spatially and temporally. The rate of tilting appears to control the style of channel movement, with a threshold between ~7.5 x 10^{-4} and 7.5 x 10^{-3} radians k yr^{-1} separating avulsion or gradual down-dip migration respectively (Peakall *et al.*, 2000), which may influence the geometry of the resultant channel deposits (i.e. ribbon versus sheet sandstones). Syndepositional faulting can deflect channels around the upthrown fault (Groll and Steidtmann, 1987) and the net result of continued tilting may be to create a concentration of channel sandbodies close to the axis of maximum subsidence (Figure 2.2, Bridge and Leeder, 1979).

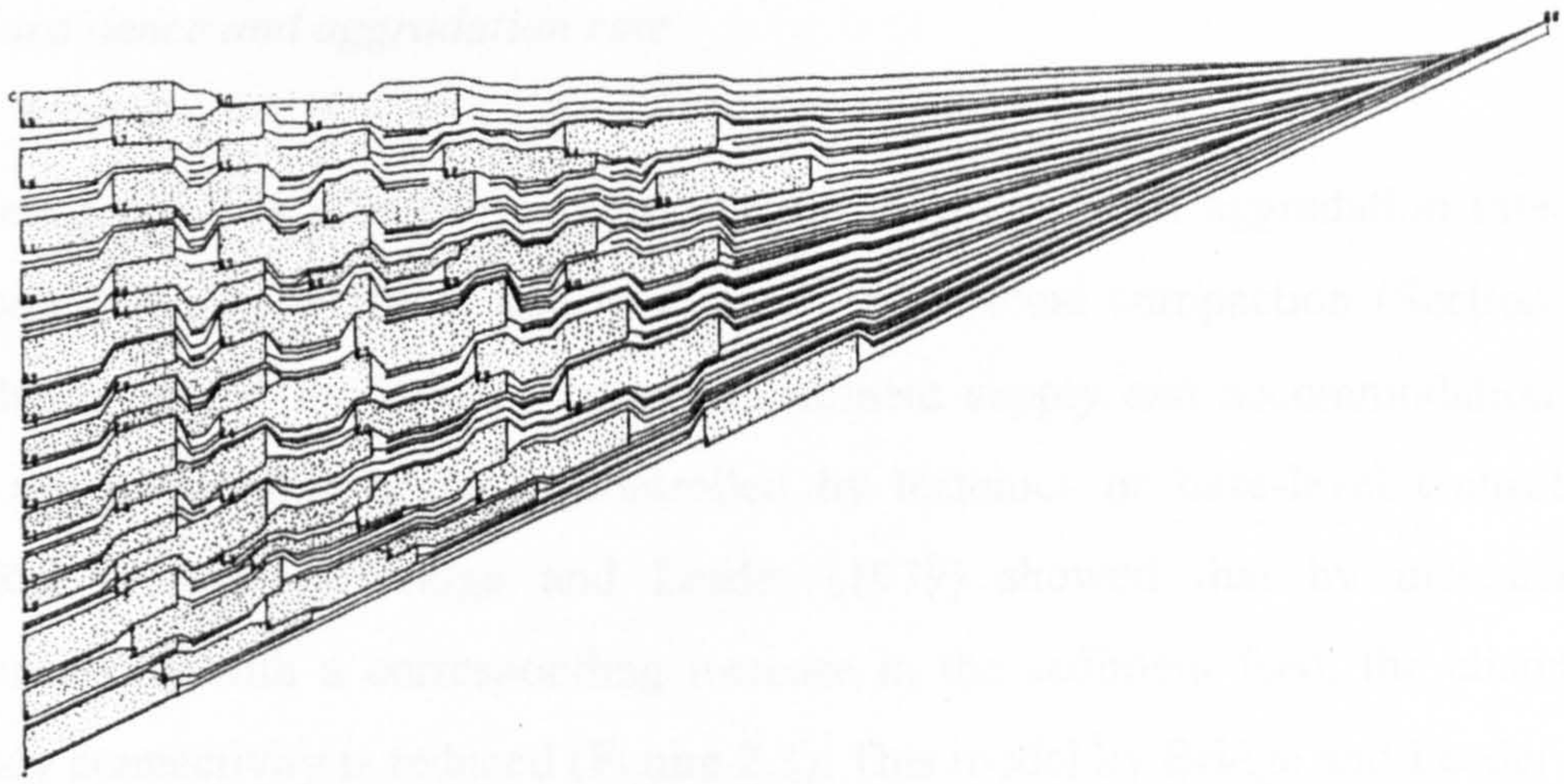

Figure 2.2. Simulated cross section from Bridge and Leeder (1979) showing increased sandbody connectivity to the area of maximum tectonic subsidence. The speckled units represent channel-belt sandbodies with the surrounding material representing floodplain deposits.

Tectonics studies of basin filling mechanisms (e.g. Miall, 1981; Alexander and Leeder, 1987; Leeder, 1993) indicate that the rate of space creation by tectonic mechanisms will control the volume of sediment introduced into the basin and influence the extent to which sediments prograde or retreat. Changes in uplift rates of the hinterland may cause progradation or retrogradation forming cycles of coarsening and fining-upwards sequences in vertical section respectively (Hartley, 1993; Leeder, 1993). Furthermore, large rivers (100 km long) may cross several tectonic zones during their course, and incorporate complex interaction from eustatic base-level and sediment supply controls. These interactions may alter drainage patterns downstream (e.g. Schumm, 1977, 1981; Miall, 1981) causing superposition of different controlling mechanisms to be reflected in the stratigraphic record (e.g. Lawrence *et al.*, 1990; Olsen and Larson, 1993; Cojan, 1993). The relative impact of various controls acting down the length of the channel may modify with distance from the source, for example, the modern day Canterbury Rivers, New Zealand (Leckie, 1994, refer to Section 2.2.1).

Many of the tectonic models (e.g. Bridge and Leeder, 1979; Leeder *et al.*, 1996) focus on the two-dimensional channel-belt scale architecture. Also worth noting is that in asymmetric half-graben basins, lateral input to the basin may occur as fans draining the basin margin form on an active fault scarp. Consequently, alluvial sequences may record the interplay between both axial and transverse drainage systems within the sedimentary basin (Leeder and Gawthorpe, 1987).

2.2.3 Subsidence and aggradation rate

Subsidence rate has often been considered synonymous with aggradation rate and is often controlled by tectonics and to a lesser extent local compaction (Section 2.2.4). Aggradation rate is the balance between sediment supply and accommodation space, where accommodation space is controlled by tectonics or base-level controls. The numerical models of Bridge and Leeder (1979) showed that by increasing the subsidence rate with a corresponding increase in the sediment feed, the channel-belt sandbody connectivity is reduced (Figure 2.3). This model by Bridge and Leeder (1979) has been incorporated into the interpretation of a host of subsequent outcrop studies exhibiting contrasting architectural styles (e.g. Kraus and Middleton, 1987; Arche and Lopez-Gomez, 1999). These contrasting architectural styles are based on the premise that lower subsidence rates form thick, multi-storey, amalgamated channel-belt sandbodies with scarce overbank deposits, whilst high subsidence rates are characterised by single/isolated or weakly, multistorey, channel-belt sandbodies and the predominance of overbank deposits. The decoupling of avulsion frequency from aggradation rate in the Bridge and Leeder (1979) model has important ramifications for architectural stacking patterns (discussed in Section 2.2.5) and may lead to a re-evaluation of the sequence interpretations base of the original Bridge and Leeder (1979) model. Additionally, models of Bridge and Leeder (1979) keep the ratio between accommodation space and sediment supply rate, termed the *capture ratio* (Paola, 1988), equal to 1. Deviation from this capture ratio of 1 can also dramatically influence the stacking patterns (Dreyer, 1990, Figure 2.4). Complementary work by Heller and Paola (1996, Figure 2.5) suggested that while subsidence rate controlled the rate at which channel-belt alluvial architecture changes in a downstream direction, other controls such as avulsion and sedimentation rate dictate whether the stacking patterns become more or less dense downstream.

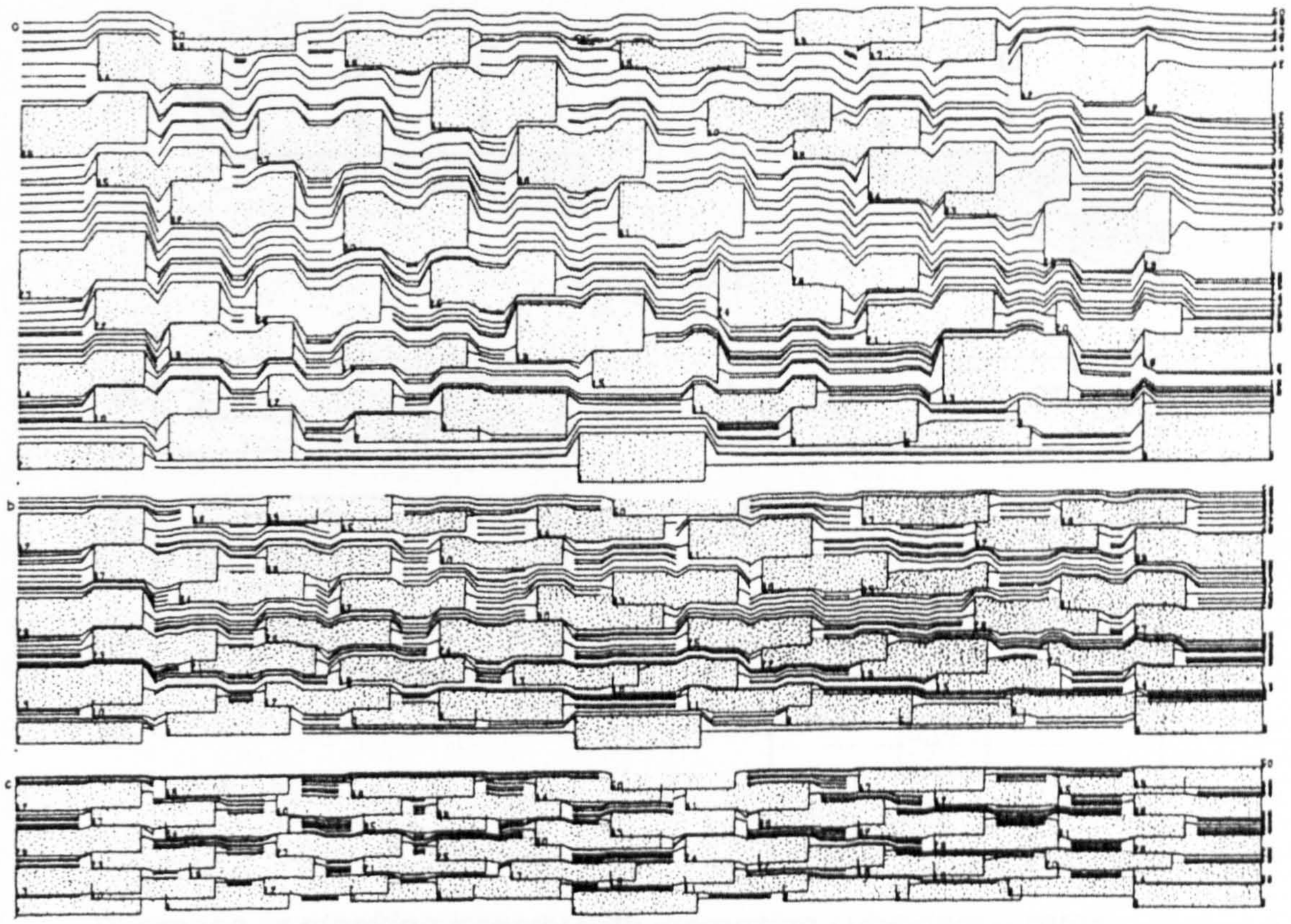

Figure 2.3. Simulated cross-sections from experiments by Bridge and Leeder (1979). Vertical exaggeration is 25. Mean avulsion period is 445 years in these examples; mean channel-belt aggradation rates are (A) 0.02 m year^{-1}, (B) 0.01 m year^{-1}, (C) 0.005 m year^{-1}. Note the change in stacking patterns and the reduction in connectivity as aggradation rate increases. The speckled units represent channel-belt sandbodies with the surrounding material representing floodplain deposits.

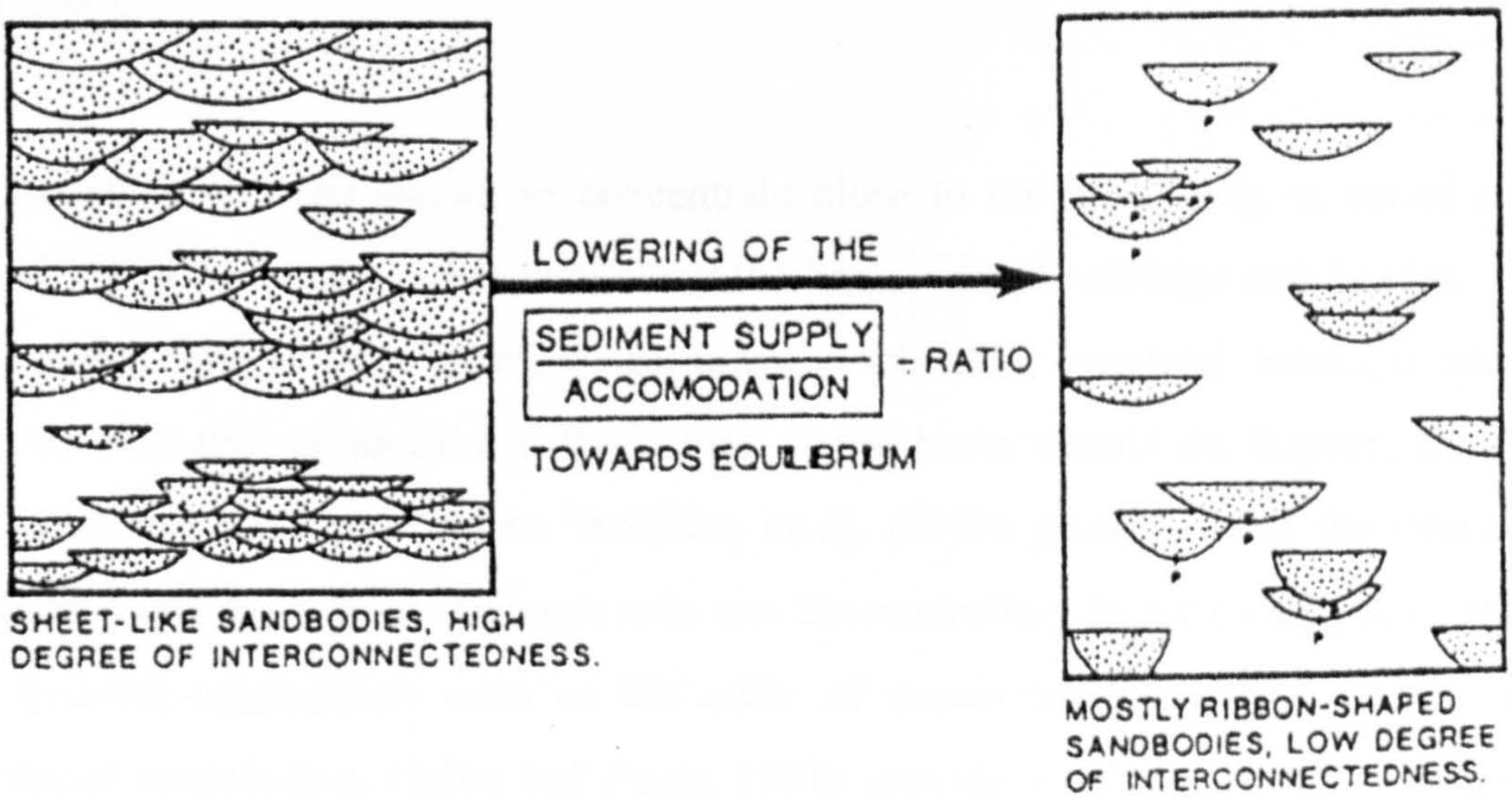

Figure 2.4. The effect of variation in the sediment supply versus accommodation ratio on sandbody interconnectedness (P = palaeochannel axis) (from Dreyer, 1993). Dashed areas represent channel-belt sandbodies.

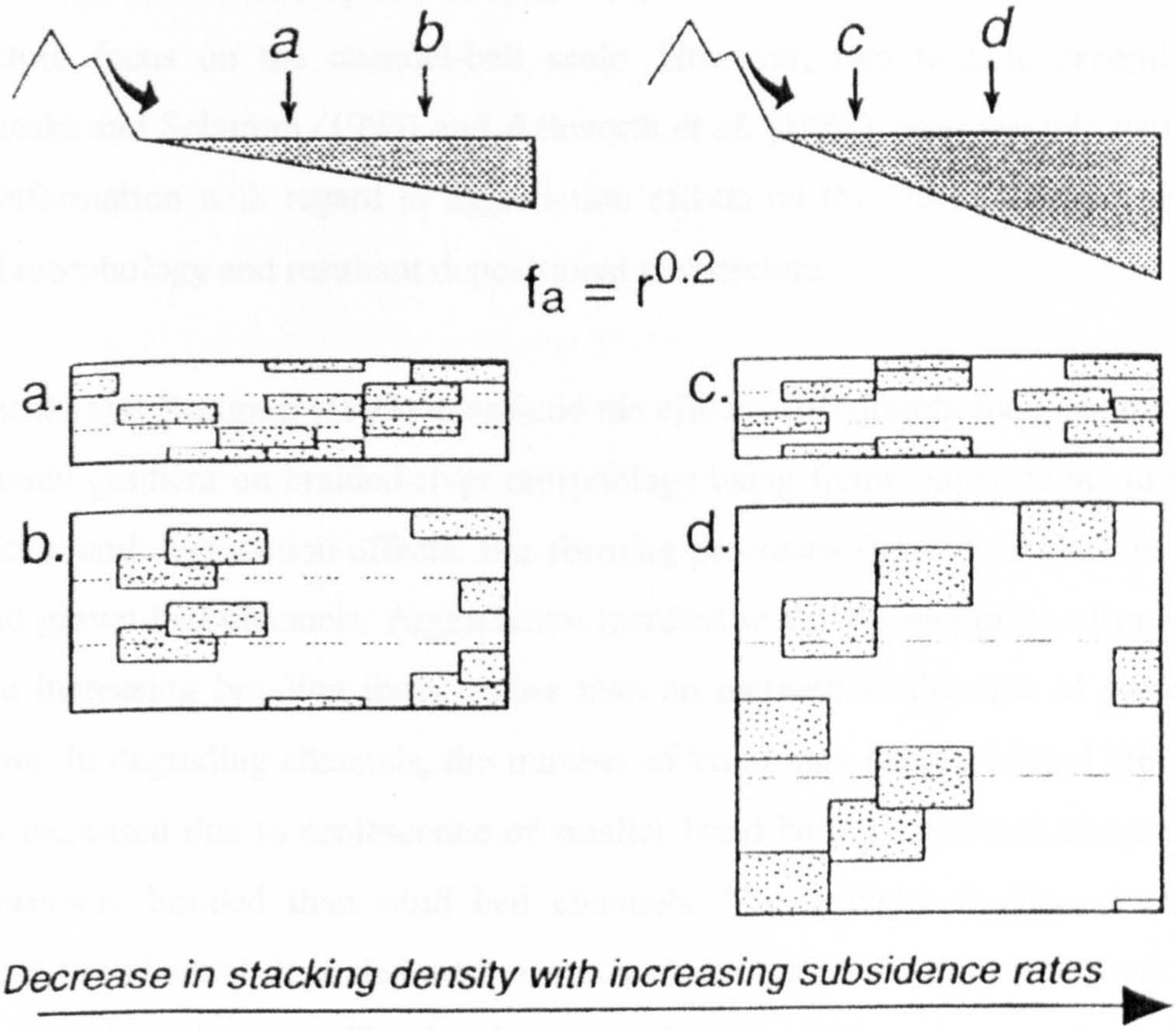

Figure 2.5. Model stacking patterns for a fore-tilted basin with local avulsion and slow (left) versus rapid (right) subsidence rates. The relation between avulsion frequency and sedimentation rate is $f_a = r^{0.2}$. Proximal and distal cross-sections are positioned to be equally spaced in both basins, but with proximal sections being the same thickness. Sandbody thickness is set by the local sedimentation rate and the relationship between avulsion frequency and sedimentation rate. The downstream change in stacking pattern is a function of the rate of change of subsidence downstream. The speckled units represent channel-belt sandbodies with the surrounding material representing floodplain deposits. (from Heller and Paola, 1996).

Sandbodies have been shown to concentrate close to the basin axis in zones of the highest subsidence rates rather than along the basin margins (Bridge and Leeder, 1979; Read and Dean, 1982). Therefore, in actively subsiding synclinal basins it may be expected that the sandbodies in the centre of the basin should be thinner, less well connected and more ribbon-like. Bentham *et al.* (1993) proposed that the decline in subsidence rate away from the basin axis was the controlling factor on aggradation rate, with greatest aggradation rates in the areas of maximum subsidence. While these conceptual models (e.g. Heller and Paola, 1996) provide a link between several points along the length of a basin they fall short of the natural complexity of the system. Therefore, there is a need to incorporate other aspects of individual channel sequences such as grain size distribution, channel and channel-belt sandbody geometry.

Again, many of the conceptual models built to aid our interpretation of alluvial architecture focus on the channel-belt scale. However, two notable exceptions are Germanoski and Schumm (1993) and Ashworth *et al.* (1999), who provide particularly useful information with regard to aggradation effects on the within channel-belt scale channel morphology and resultant depositional architecture.

Germanoski and Schumm (1993) examined the effects of sediment load, sediment size, and channel gradient on braided-river morphology using flume experiments to recreate aggradation and degradation effects. Bar-forming processes showed similarities in both sand and gravel-bed channels. Aggradation resulted in the development of more braid bars and increasing braiding index rather than an increase in the size of pre-existing braid bars. In degrading channels, the number of braid bars decreased and the average bar size increased due to coalescence of smaller braid bars. Gravel-bed channels were more intensely braided than sand bed channels. The gravel-bed channel remained braided as the channel degraded with a much slower response time (i.e. more stable) than the sand bed channels. The development of new braid bars in aggrading channels forced flow to the channel banks and led to an overall increase in total channel-belt width.

This study by Germanoski and Schumm (1993) provides valuable information on impact of aggradation and degradation on surface channel morphology, yet the development of a full stratigraphic model of within channel-belt architecture requires the inclusion of subsequent reworking of the bar and channel deposits. It may be postulated that an increase in the aggradation rate will enhance the preservation potential and reduce reworking of sedimentary deposits. Ashworth *et al.* (1999) tested this presumption using a combined field and flume study to show that braided alluvial architecture at the channel scale is determined by the local, instantaneous aggradation rate related to individual flood events rather than long-term regional aggradation. Moreover, when aggradation rate was increased by a factor of two, no significant observable change in the geometry or frequency of occurrence of fine- or coarse-grained depositional niches was identified. This lead to the conclusion that braided alluvial architecture is independent of aggradation rate and that the regional aggradation rate may have to varied by several orders of magnitude before influencing the alluvial architecture.

2.2.4 Compaction

Compaction of sedimentary deposits occurs as stratigraphy is buried by ensuing aggradation, sediment loading and/or structural emplacement, which reduces the vertical thickness of the sequences. Compaction causes a steady reduction in porosity as depth of burial increases, which is reflected by a reduction in reservoir quality and hydrocarbon recovery efficiency. Compaction can influence the alluvial architecture in several ways during deposition and subsequent burial of the sediment.

A range of depth versus porosity/compaction curves have been developed for particular lithologies (e.g. Perrier and Quiblier, 1974; Shinn and Robbin, 1983; Baldwin and Butler, 1985). The relative difference between the compaction rates of different lithologies, often sand and shales, can result in changes in topographic relief on the floodplain (Allen, 1978), which can control channel avulsion to topographic lows and consequently the stacking patterns (Bridge and Leeder, 1979), and has been termed *facies-dependent differential* compaction (Collier, 1989). Subsequent burial of stratigraphy can result in continued facies-dependent compaction causing architectural distortion as porosities are reduced by grain sorting and packing (Baldwin, 1971). In addition, subsequent burial diagenesis may both enhance and reduce final burial porosity. The second component of differential compaction is *basement topography-induced compaction differential* (Collier, 1989), which allows different thicknesses of sedimentary deposits to aggrade over a varied basement topography resulting in differential loading on the buried sequence at different positions in the basin. Standard compaction curves (e.g. Sclater and Christie, 1980; Baldwin and Butler, 1985) assume shales undergo significantly more compaction than sands and this can result in an increase in the proportion of channel-belt sandstone deposits at greater depths (Bridge and Mackey, 1993). However, channel-belt sandbody interconnectedness may not be affected by compaction (Leeder, 1978). More recent work on continental sequences (e.g. Retallack, 1993; Caudill *et al.*, 1997) established that in continental shales, where palaeosol development was evident differential compaction between sands and shales may have been negligible (refer to Chapter 3, Section 3.12). Differential compaction is often difficult to incorporate into simple backstripping models (Giles *et al.*, 1998) especially in sequences with highly heterogeneous sediments. Sediment loading and compaction can have significant effects on subsidence (Reynolds *et al.*, 1991) and tend

to amplify tectonic controls (Heller and Paola, 1992). Thinning can be attributed to compaction alone (Baldwin, 1971) and therefore some assessment of compaction in an alluvial sequence must be made in order to use analogue data for subsurface interpretation. Additionally, the estimation of channel-belt sandbody widths is commonly based on sandbody width versus thickness relationships and failure to quantify the effect of burial compaction on the sandbody thickness will result in a reduction in the estimate of sandbody width with increasing burial depth.

2.2.5 Avulsion and channel migration

A channel-belt may alter its position on an alluvial plain by three mechanisms: (1) vertical incision, (2) migration and asymmetric incision, and (3) avulsion, which result in different depositional styles (Figure 2.6). Vertical incision is dealt with in Section 2.2.6 and not considered further here. Alexander and Leeder (1987) broke down the lateral changes in channel position further into: (1) instantaneous downtilt avulsion triggered by a single tectonic event, producing sudden hydraulic events in response to a seismic event; (2) topographically triggered avulsion; and (3) slow migration of a channel-belt by processes of preferential downslope erosion and meander cut-off or anabranch abandonment. The division between the occurrence of avulsion and gradual downdip migration of the channel-belt is linked to the tilt rate of the floodplain (Peakall *et al.*, 2000). Periodic avulsion, rather than sweeping from side to side, is the principal mechanism by which rivers deposit laterally extensive sheets of channel-belt sediments (Bridge, 1985). The tectonic triggering mechanisms for avulsion and channel-migration are discussed in Section 2.2.2, while avulsion processes caused by topography are presented here.

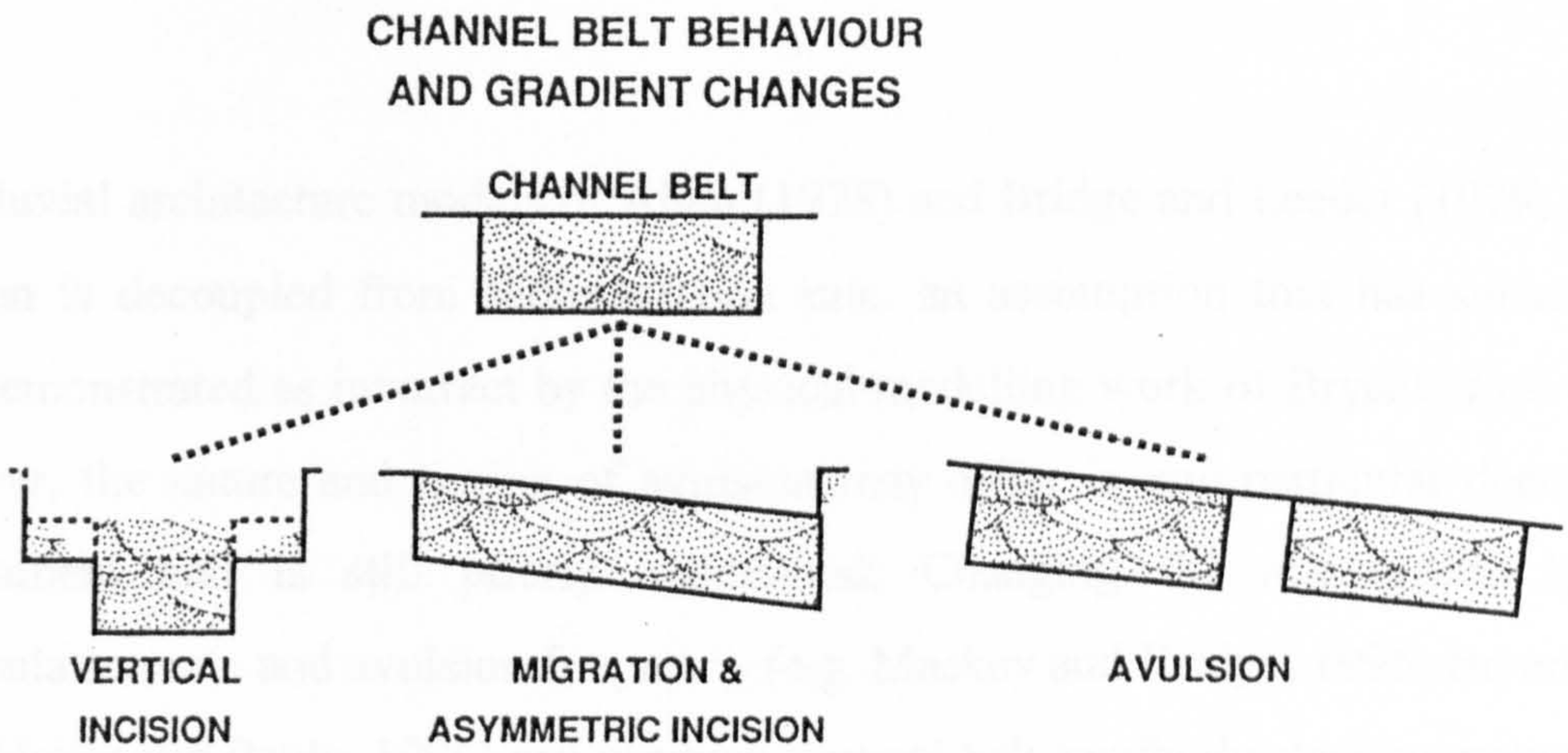

Figure 2.6. Diagrammatic representation of the avulsion, and vertical and horizontal migration of a channel-belt axis. Note the effect of the processes on the amount and distribution of potential reservoir sand (from Leeder *et al.*, 1993).

Avulsion is the abrupt switching and lateral shift of the channel-belt across the floodplain and is controlled by factors, including tectonics (Section 2.2.2), flood magnitude and frequency, and bank erodability. Avulsion can change the course of a short segment of the river or the entire channel-belt (Leeder, 1978) and therefore, has implications for both channel-belt and within channel-belt scale architecture. Topographically triggered avulsion is driven by superelevation of some part of the channel or channel-belt above its surroundings, which occurs as high sedimentation rates near the channel decline distally over the floodplain away from the channel margin (Bryant *et al.*, 1995). At a critical level of elevation above the floodplain the channel avulses in favour of a lower channel position. As sediment supply rate increases the channel reaches the critical level of topographic elevation in progressively shorter time periods. Consequently, as sediment feed rate increases the likelihood of avulsion also increases (Figure 2.7, Bryant *et al.*, 1995).

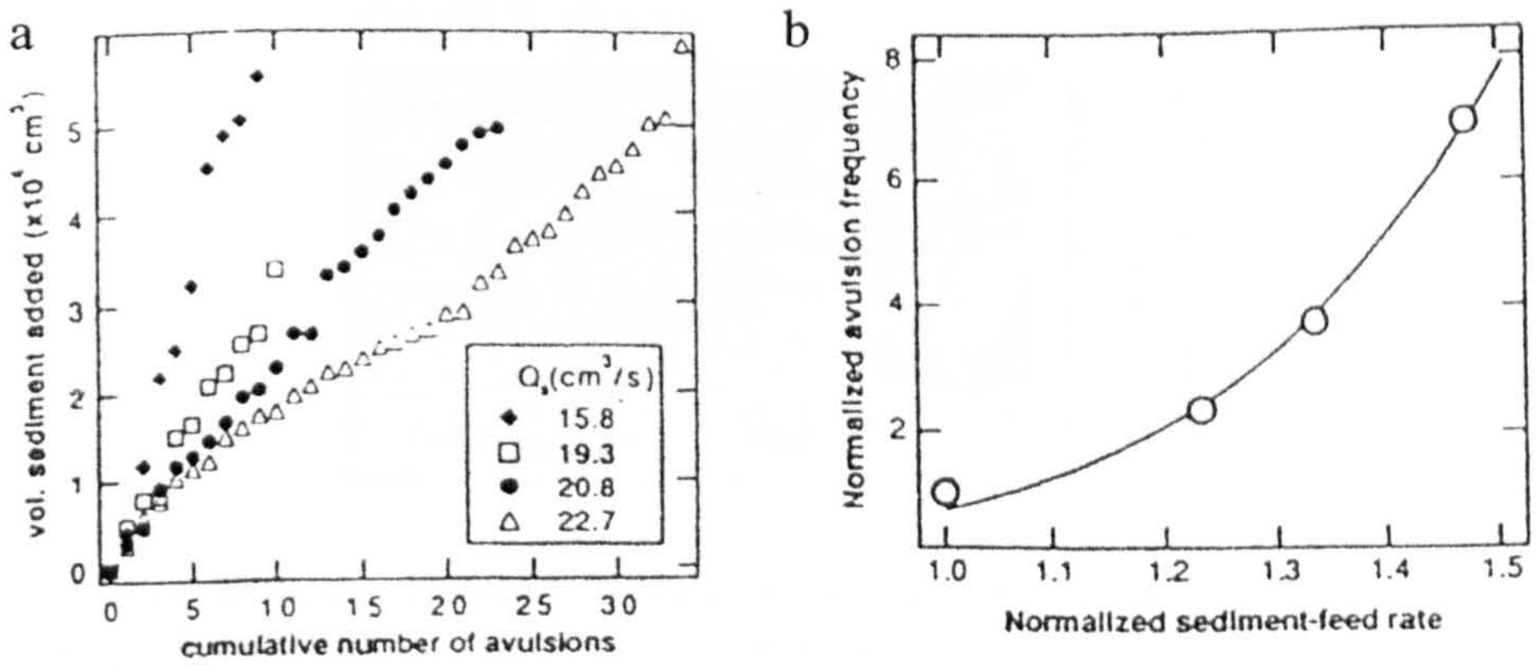

Figure 2.7. (a) avulsion frequency versus sediment-feed rate for four experiments and (b) normalised by their values for the lowest feed rate. The fitted line has a power-law exponent of 5.87 showing avulsion frequency increases with sediment feed rate (from Bryant *et al.*, 1995).

The alluvial architecture models of Allen (1978) and Bridge and Leeder (1979) assume avulsion is decoupled from sedimentation rate, an assumption that has subsequently been demonstrated as incorrect by the physical modelling work of Bryant *et al.* (1995). However, the nature and timing of avulsion may differ in any particular depositional environment and is still poorly understood. Changing the relationship between sedimentation rate and avulsion frequency (e.g. Mackey and Bridge, 1995; Bryant *et al.*, 1995; Heller and Paola, 1996) can produce channel-belt sandbody stacking patterns that are both consistent and contradictory to stratigraphic models of Allen (1978) and Bridge and Leeder (1979) (compare Figure 2.8 and Figure 2.3). Hence, outcrop studies are required to verify the conceptual stratigraphic models of Bryant *et al.* (1995) in order that they may be up-scaled to interpret analogue sequences.

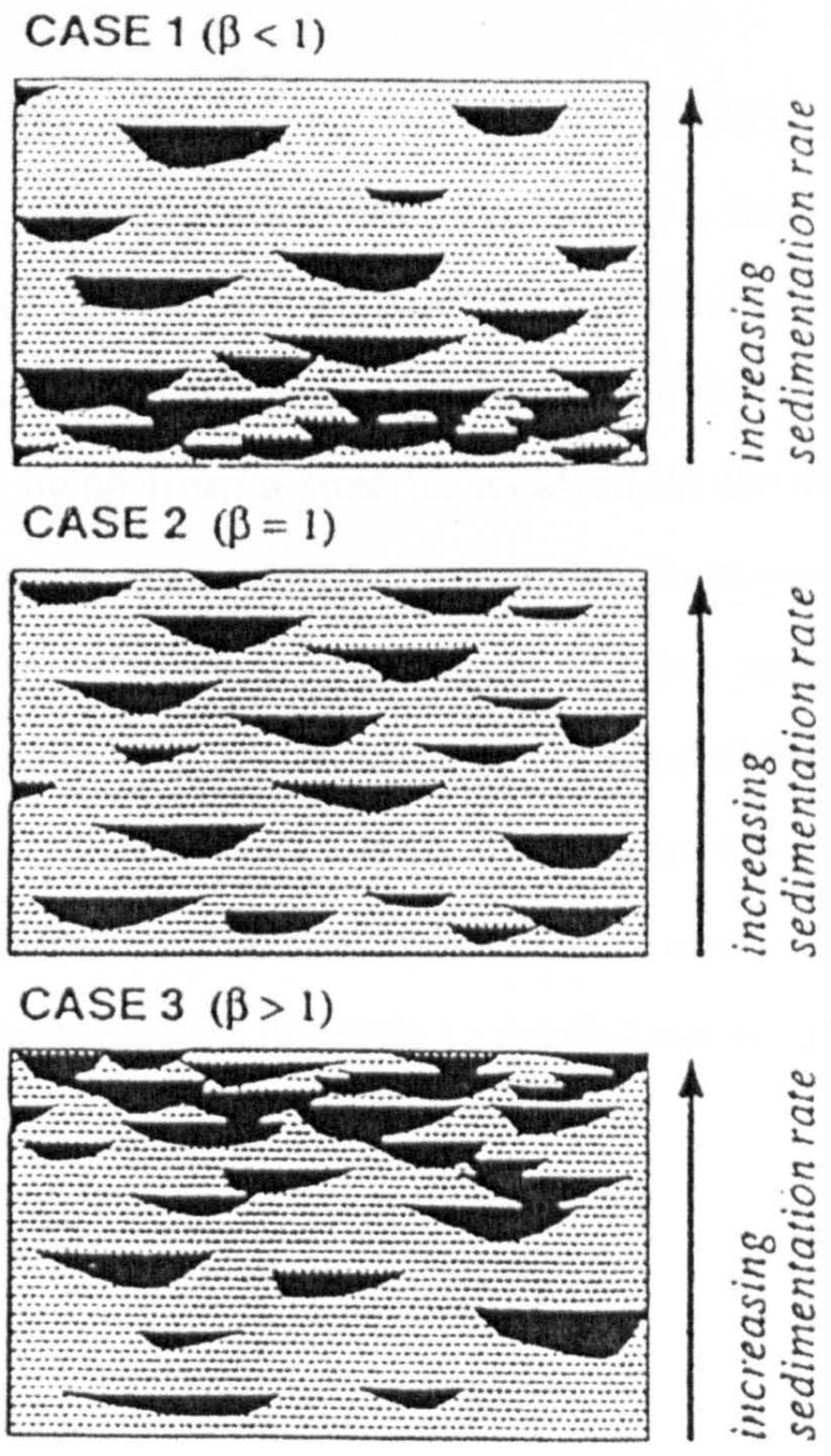

Figure 2.8. Relation between channel-belt stacking density and sedimentation rate for three possible regimes defined by the exponent ß in a power-law relation between avulsion frequency and sedimentation rate. Black represent channel-belt sandbodies; dashed pattern represent floodplain deposits. The top panel corresponds to a regime in which avulsion frequency is taken to be independent of sedimentation rate. The bottom panel is that suggested where an increase in sedimentation rate leads to higher switching rates, more effective removal of floodplain fines, and higher density of sandbodies (from Bryant *et al.*, 1995).

Theoretical stratigraphy models such as those produced by Bryant *et al.* (1995) and Heller and Paola (1996) have been concerned with the channel-belt scale architecture with limited reference to how the planform and cross-sectional geometry of a channel is modified with styles of avulsion. The impact of avulsion frequency at the channel scale is often termed *anabranch avulsion*. The type and rate of avulsion will determine the nature of deposition in the abandoned channel. For example, rapid channel plugging can create internally massive sandstone bodies, while gradual channel abandonment and avulsion causes passive infilling creating a layered fining upwards sequence (Dreyer, 1990). Leddy *et al.* (1993) defined three mechanisms of anabranch avulsion in braided rivers: (1) choking, (2) constriction, and (3) apex avulsion. Leddy *et al.* (1993) suggested that avulsion deposits may be dominated by coarse sediment plugs that have rapidly blocked the channel, which is followed by a more passive fine-grained sediment fill in the abandoned channel. The difficulty in verifying these relationships in the field stems from the difficulties in access to field areas during avulsion events.

Kraus and Bown (1993) and Kraus and Wells (1999) showed how palaeosol development sequences, termed *pedofacies relationships*, may be used in determining proximity to the channel margin and thus avulsion behaviour, which are particularly useful in cored reservoir intervals. The pedofacies relationship relies on the assumption that as channels migrate away from a specific location on the floodplain, and over time the soils will show an increasing maturity up-sequence in response to lower aggradation rates away from the channel margin. Interpretation of these pedofacies relationships may be complicated by: (1) locally high aggradation rate caused by the deposition of splays halting soil development; (2) composite soils forming in between two active channels; and/or (3) subtle changes in topography and water table across the floodplain. Grain size can be used in addition to palaeosol analysis to predict proximity to channel sandbodies (Guccione, 1993).

2.2.6 Incision and scour

There are two scales of alluvial incision: channel scour and larger scale erosion of valleys within the alluvial settings; both mechanisms lead to removal of a time sequence of sediment causing entirely unrelated deposits to overlie each other (Leeder and Stewart, 1996). Fluvial scour and incision may influence the three-dimensional geometry of fluvial sandbodies by creating an increase in local or widespread sandbody thickness (Figure 2.9). Valley incision responds to allocyclic controls to include: (1) increased discharge and stream power, as a result of climate change; (2) tectonic uplift within the mid-stream and upstream portion of the drainage basin; (3) decreased stream load as a result of climate change, which may all result in sediment bypass and localised unconformities; and (4) base-level changes (Emery and Myers, 1996). Incision caused by allocyclic forcing mechanisms creating entrenched valleys is known as *extrinsic incision* (Salter, 1993) and can affect the river system over considerable distances. For example, Shanley and McCabe (1993) postulate that sea-level control typically extends 100-150 km inland from the related shoreline.

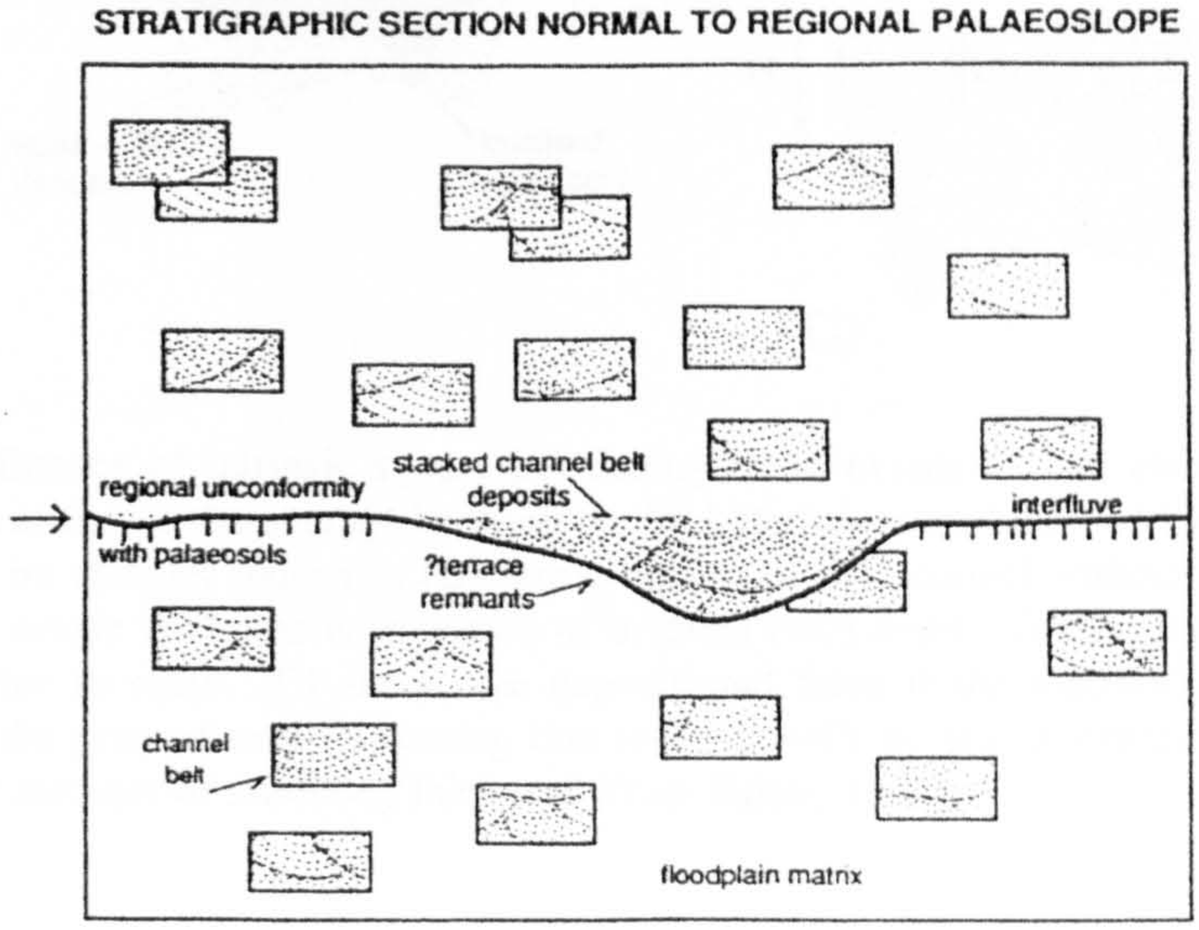

Figure 2.9. Sketch section normal to regional palaeoflow to illustrate the major alluvial architectural effects resulting from a major episode of incision as sectioned relatively close the position of initial base-level fall (from Leeder and Stewart, 1996)

Incision may also be an autocyclic process promoted by constriction and curvature of confluences within major channels, termed *intrinsic scour* (Salter, 1993). Scouring promotes downward thickening of the sandbody and increased interconnectedness, without net vertical aggradation. Intrinsic scour at channel confluences has the potential

to rework large proportions of the channel base creating thick channel deposits (Best and Ashworth, 1997). At low aggradation rates sandbody thickness may exceed the bankfull depth by 100 % due to scour (Figure 2.10). Fielding and Crane (1987) noted that preserved sandbody thickness will often exceed the maximum formative channel depth, but attributed this solely to ensuing aggradation. Ultimately, sandbody thickness will be controlled by extreme depths while average depths will control internal stratification (Salter, 1993). Modification of sandbody thickness by scour can hinder application of empirical width/thickness relationships from analogue deposits that require an estimation of channel depths. Consequently, measurement of internal stratification may be more appropriate for reservoir – outcrop analogue comparisons. Interconnectedness of sandbodies is largely due to downward erosion by sandbody bases by extrinsic incision, while intrinsic scour becomes more important during relative sea-level fall or standstill (Salter, 1993).

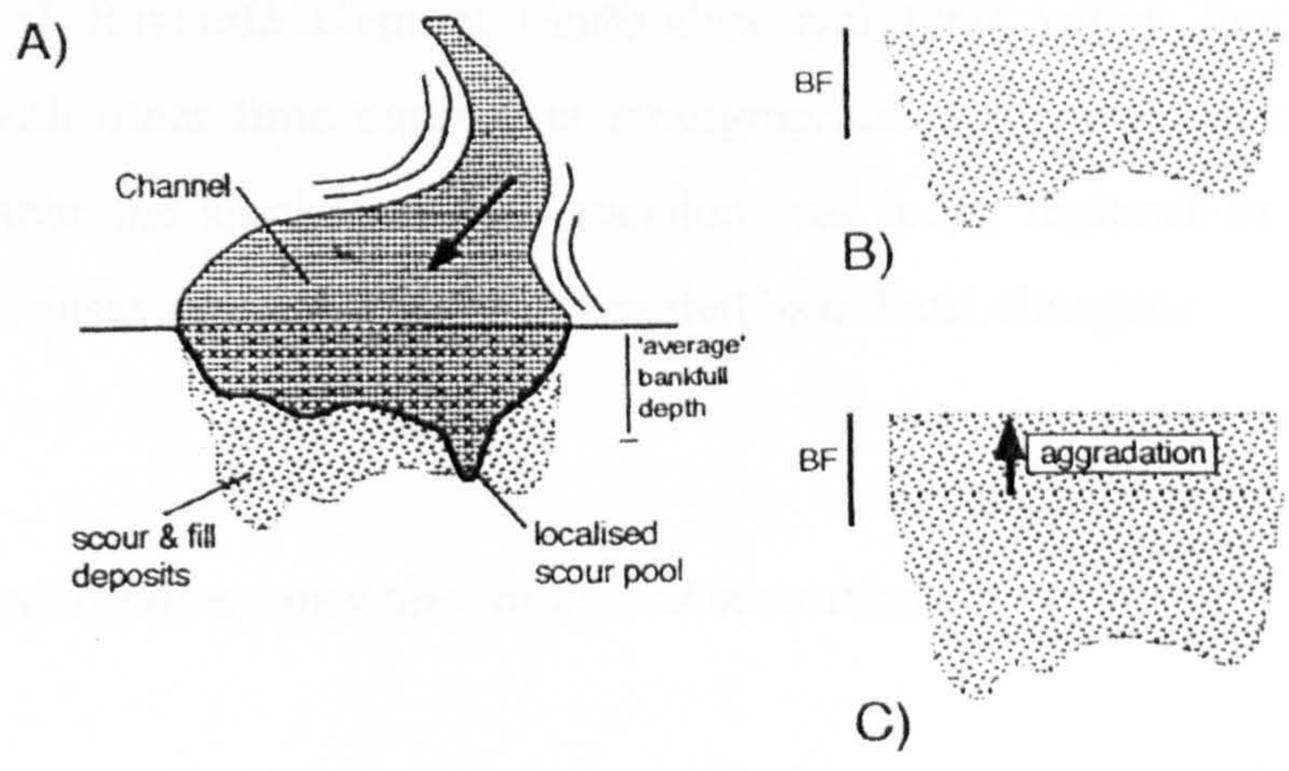

Figure 2.10. The influence of intrinsic scour: (A) during flood events a river channel may be locally scoured to a depth in excess of the average bankfull depth. Later waning of the flood allows the scour pool to be partially filled by channel sediment; (B) abandonment of the channel without net aggradation will produce a sandbody whose thickness is in excess of original (BF) depth. Thickening of the sandbody in this case is purely due to scour. (C) shows the depositional form if the sandbody is abandoned after limited aggradation the proportional thickening due to scour will be less important. Note the bankfull depth is again a poor measure of sandbody thickness (from Salter, 1993).

Recognising the point along a river profile at which external incision due to sea-level fall can be distinguished from intrinsic scour is a key to interpretation of the sedimentary record. Alexander and Gawthorpe (1993) highlight the difficulty in differentiating between allocyclic incision-induced erosion and intrinsic scour erosion produced by a newly-avulsed channel. Large-scale extrinsic incision must be recognised as having a larger spatial extent than more localised channel scour in the sedimentary record. Best and Ashworth (1997) showed that boundaries in ancient alluvial deposits that have

previously been assumed to be the result of sea-level drop may be the result of deep basal erosion surfaces caused by scour at channel confluences and bends. In order to unambiguously define extrinsic incision from intrinsic scour in a fluvial sequence the erosive surface should be at least five times the mean channel depth and extend for distances greater than the floodplain width, possibly being traceable between different basins (Best and Ashworth, 1997). While sound in theory, in practice correlation of incision surfaces is particularly challenging to recognise in well data or scattered outcrop exposure. The identification of extrinsic incision has been assisted by the recognition of distinct bounding surfaces such as palaeosol horizons, resulting from alluvial floodplain abandonment and formation of terraces (e.g. Blum and Valastro, 1994; Leeder and Stewart, 1996).

In summary, to recognise incision in the rock record it is therefore necessary to: (1) identify incised fluviatile channel sandbodies and their valley margins; (2) make correlations with other time equivalent stratigraphical sequences, in order to try and establish whether the spatial scale of incision was local, regional or global; and (3) determine the causes of local, regional or global base-level changes.

2.2.7 Grain size, lithology and floodplain sedimentation

A notable characteristic of many alluvial architecture models (e.g. Bridge and Leeder, 1979; Mackey and Bridge, 1995; Heller and Paola, 1996) is the almost universal inclusion of two very distinct grain size modes, sand/gravel and mud/silt, which in turn form channel-belt sandbodies and floodplain deposits respectively. While this tentative division of grain size may be applicable to outcrop sequence, for example, the Escanilla Formation (Bentham *et al.*, 1993; Dreyer *et al.*, 1993) and the Green River Formation (Ryder *et al.*, 1976), many other fluvial drainage systems do not receive this particular mixture of fine- and coarse-grained sediments. Proglacial outwash streams are fluvial systems that fall into this category and studies such as Ashworth *et al.* (1999) show a bimodal distribution of sand and gravels within the Ashburton River, New Zealand, with a pronounced absence of sediment finer than sand grade. Moreover, proglacial rivers in New Zealand show significant floodplain development (Reinfelds and Nanson, 1993; Warburton *et al.*, 1993), although floodplains are not identified within the subsurface.

The supply of fine-grained sediment to the system is linked to climate (Section 2.2.1) and the lithology of the hinterland. The presence of a large volume of fine-grained material within the fluvial system can affect bank strength and consequently channel cross-sectional form and pattern. Increased bank strength can be attributed to a number of floodplain characteristics, including vegetation development (Smith, 1976; Marsden, 1981), clay content (Schumm and Khan, 1972) and duricrust formation (Gibling and Rust, 1990), which inhibits lateral channel migration forming deeper narrower channels (Huang and Nanson, 1998). Alternatively, any lack of sediment binding during the deposition may decrease the cohesion of the channel banks and discourage incision of the channels; this is particularly true for the Devonian Old Red Sandstone (Tunbridge, 1981).

In summary, channel-belt scale alluvial architectural models (e.g. Bridge and Leeder, 1979) simplify grain size distributions by using a single division of coarse and fine grain sizes to represent channel-belt and floodplain deposits respectively. However, in natural systems the shape of grain size distributions varies and therefore deserves more attention. The incorporation of grain size characteristics into any depositional model first requires a review of the two principal factors influencing grain size distribution at any particular point in the basin: (1) the source lithology of any basin has a major influence on the observed grain size distribution supplied to the most proximal position of the basin (Wolcott, 1988); and (2) the modification of this grain size distribution downstream as a result of abrasion, chemical weathering and/or selective sorting. Alteration of either the magnitude or sorting of the grain size distribution at any particular point on the long profile of the fluvial channel-belt may result in a change in channel behaviour and depositional architecture. For example, Parker (1979) predicted that a 30 % increase in gravel load, for a given discharge, leads to a 40 % increase in channel width and a 25 % reduction in centre depth. Sambrook Smith (1996) proposed that when surface sand content in bimodel fluvial bed sediments exceeded 30 % the bed changed from behaving as a gravel bed to behaving as a sand bed (based on the work of Iseya and Ikeda, 1987). The source lithology will be somewhat consistent in supplying the basin with a particular grain size distribution, while subsequent modification of this initial distribution is subject to a wider range of controls. It is therefore pertinent to review the concepts of downstream fining.

2.3 Downstream fining concepts

Clastic components of braided rivers decrease in size away from the source (Figure 2.11a) as a result of abrasion, hydraulic sorting and chemical weathering. This downstream fining relationship is often broadly incorporated into proximal to distal trends in sedimentary facies models (e.g. Kelly and Olsen, 1993, Figure 2.12). While the supplied grain size distribution will be determined by the hinterland lithology (Wolcott, 1988), the nature of downstream fining will be influenced by a range of variables including: sediment supply, discharge regime, channel width/depth ratios, channel gradient, vegetation, climate and tributary input, which are reviewed in the proceeding four sections.

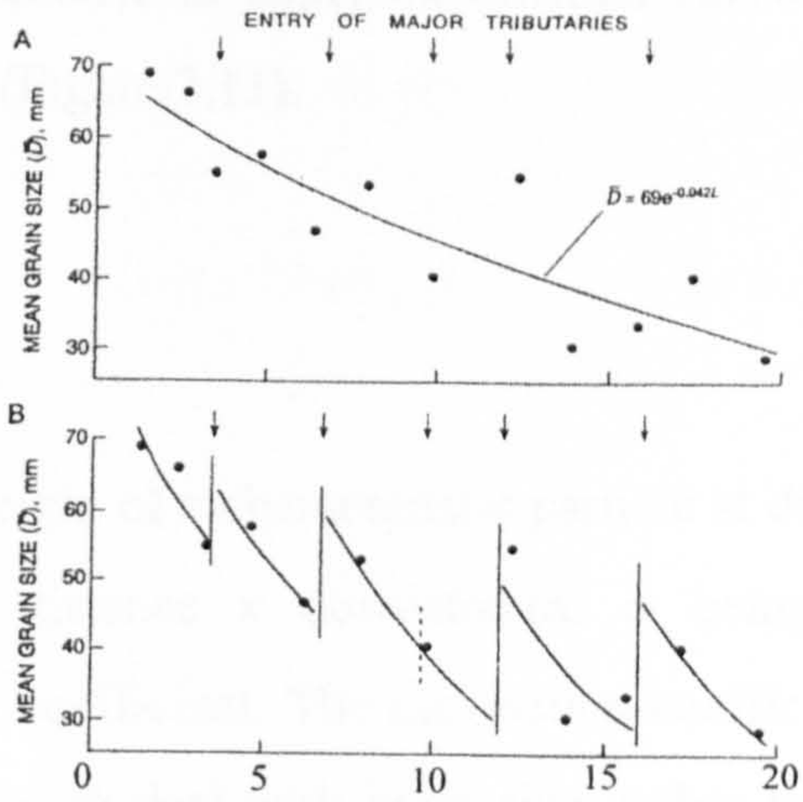

Figure 2.11. Downstream changes in the mean grain size of bed material, an example from the River Noe, England (a) showing an exponential change in mean grain size and (b) showing how sedimentary links between tributary inputs create a stepped downstream fining trend (from Knighton, 1998).

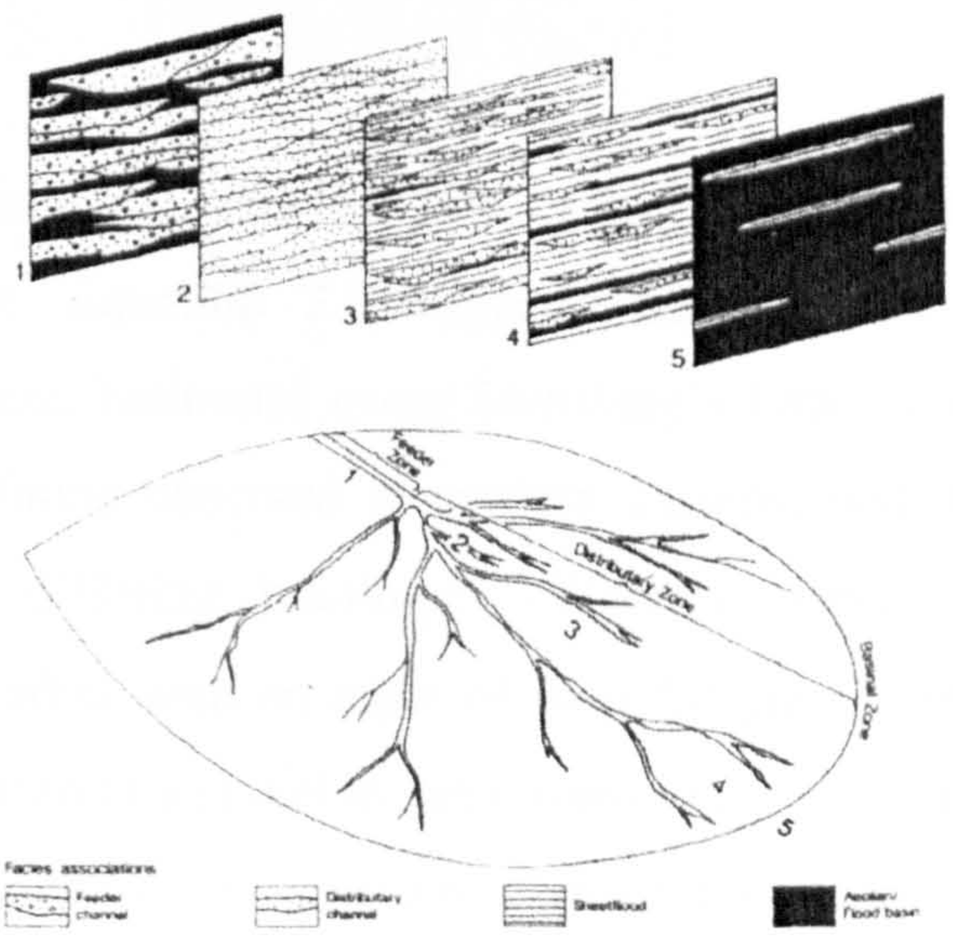

Figure 2.12. Facies models showing down-basin change in the type and proportion of facies observed in a terminal fan sequence (from Kelly and Olson, 1993).

Downstream fining operates at a variety of scales both in the field (Rice, 1999) and flume (Paola *et al.*, 1992), with downstream fining rates showing a large variation in diminution coefficients (α), which is defined as the rate of decline in characteristic particle size weight per unit distance (Sternberg's, 1875). Diminution coefficients range over several orders of magnitude (e.g. 10^{-5} to 10^{-1}, Rice, 1999). Downstream fining has been observed in rivers exhibiting different channel patterns and examples from braided streams include the Squamish River, British Columbia (Brierley and Hickin, 1985) and the Sunwapta River, Alberta, Canada, (Dawson, 1988). The early work by Sternberg's (1875) saw the development of an exponential model (Equation 2.1) for downstream fining caused by abrasion. In many subsequent studies Sternberg's law has been applied and it is now common practise to apply exponential curves to datasets to constrain downstream fining trends (Figure 2.11).

$$W = W_0 e^{-\alpha x} \qquad \text{Equation 2.1}$$

where W_O is the initial weight of a characteristic particle at distance zero, and W is the characteristic weight at distance x downstream, α being the 'weight reduction coefficient' or diminution coefficient. The diminution coefficient (α) using weight has been subsequently modified to deal with grain size, rather than weight (Equation 2.2, Hoey and Bluck, 1999).

$$D = D_0 e^{-\alpha x} \qquad \text{Equation 2.2}$$

where D is some characteristic grain size (D_{50} or D_{90}), D_0 is its initial value, and α is the diminution coefficient. Equation 2.2 suggests that the rate of clast attrition is proportional to clast size. Estimates using Sternberg's Law commonly do not account for the magnitude of fining observed in modern streams, with the exception being in rivers supplied with differing lithologies (Werritty, 1992; Smith *et al.*, 1994). Experimental flume studies with an input of bimodal gravel feed resulted in a gravel fining and then production of a gravel to sand transition over 21 m distance (Paola *et al.*, 1992), with selective deposition being the dominant process for downstream fining, while abrasion was negligible over this distance. Follow up work by Seal *et al.* (1997) suggested basin length is the major control on fining rate.

Often river studies use the D_{50} or D_{90} grain size values to constrain the downstream fining rate for a particular river and whilst these values may yield the gross downstream diminution rate, the overall sorting of the distribution may alter along the river course. Sediment can become more bimodal downstream as a result of selective sorting (Sambrook Smith and Ferguson, 1995). This sorting trend is particularly pronounced at the gravel-sand transition, which can occur within a distance of 10 km in large rivers to 0.2 km in small rivers (Sambrook Smith and Ferguson, 1995). At the gravel-sand transition the grain size modes are significantly altered with an increased proportion of the sand fraction. Similar gravel-sand transition trends have been observed in both field (Shaw and Kellerhals, 1982; Ferguson *et al.*, 1996) and flume studies (Paola *et al.*, 1992, Sambrook Smith and Ferguson, 1996). Alternatively, a conservation of the grain size distribution sorting may be recorded downstream (Figure 2.13) associated with downstream fining; such a trend has been documented in the Allt Dubhaig River, Scotland (Hoey and Bluck, 1999). Consequently, no one trend can be applied to the downstream fining models without a full assessment of the controlling variables.

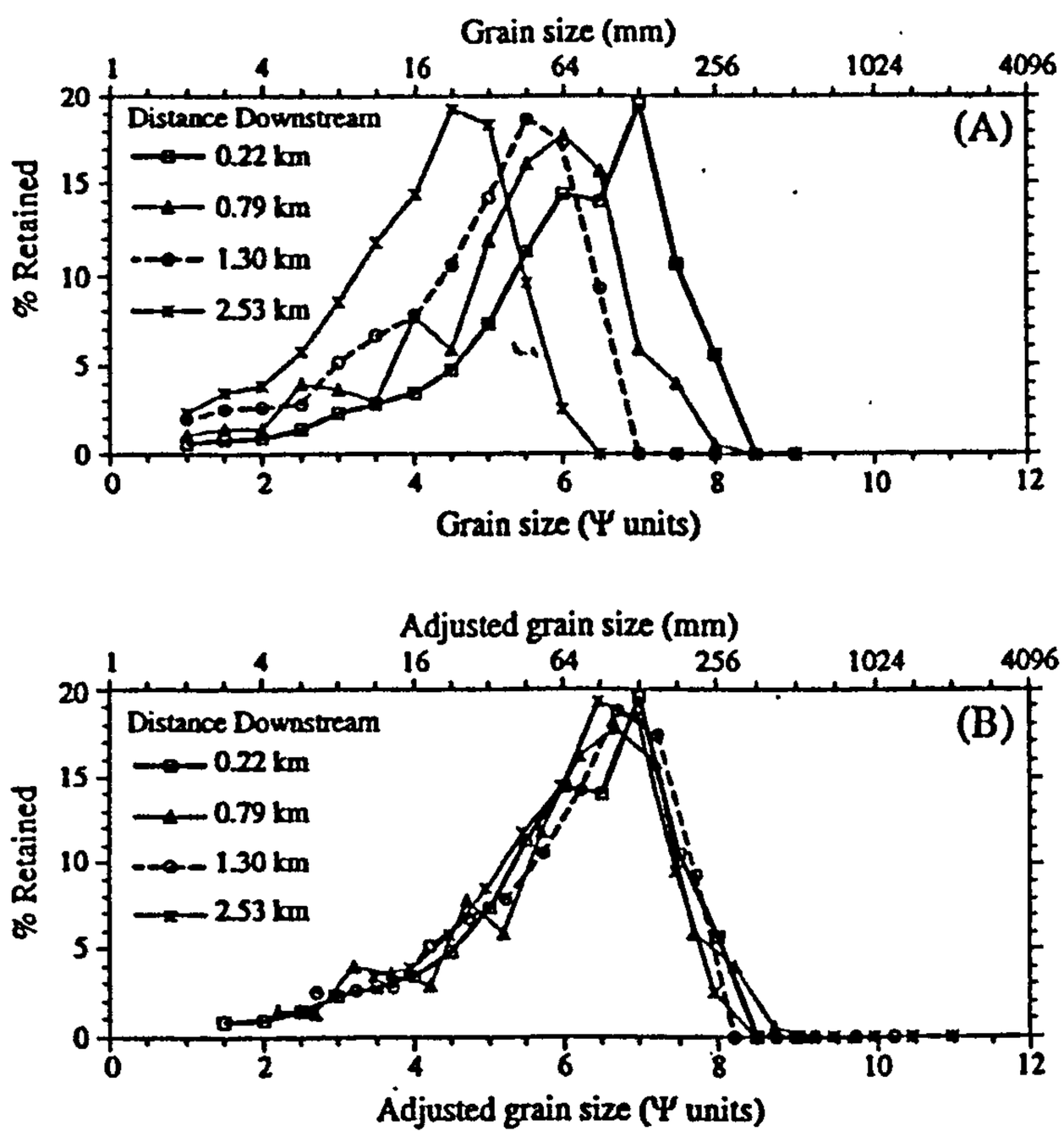

Figure 2.13. Active bulk layer grain size distributions from the Allt Dubhaig. (A) Measured grain size distributions. (B) Adjusted psi sizes computed by adjusting the mean of all the samples to be the same as that at 0.22 km (from Hoey and Bluck, 1999).

2.3.1 Source lithology, grain size and sediment supply rate

The supply and rate of fining will be dependent on the lithology of the sediment source (Wolcott, 1988). Ferguson *et al.* (1996) noted that as more poorly sorted distributions are introduced to the system, stronger proximal and overall fining occurs downstream. The effect of lithology on downstream fining has been addressed by Werritty (1992) and Kodama (1994a,b). Kodama's (1994) work on the Watarase River, Japan, suggested grain size changes may correlate to differences in the resistance to breakdown and that longitudinal changes in composition show selective transport by lithology. Abrasion is more influential in a mixed lithology system. Work by Werritty (1992) in a gravel-bed river in Southern Poland found a distinct relationship between the downstream fining rate and lithology of gravel clasts, concluding that fining rate increased in softer limestones, with progressively less fining occurring in granitoids and quartzites respectively.

2.3.2 Tributaries

During the course of a river, tributaries supply fresh sediment load and water discharge to the main channel, which can disrupt the channel-belt downstream fining trend (Church and Kellerhals, 1978; Richards, 1982; Rice and Church, 1998; Rice, 1999). These tributary inputs may cause local aggradation and channel adjustment, thereby producing a more stepped downstream fining trend (Figure 2.11b). The length of channel-belt segments between tributary inputs are referred to as *links* (Rice, 1999) and individual links can exhibit individual fining trends. Complex fining trends have been isolated and correspond to tributary inputs (e.g. Rice, 1999). Tributary inputs can also increase discharge downstream and Ferguson *et al.* (1996) noted that downstream fining develops more rapidly at higher discharge events, although this is often offset by lower frequencies of occurrence of higher discharge events. Recognition of tributary inputs in the sedimentary record is an extremely difficult task, although sediment provenance work may permit identification of some of these inputs (e.g. Hamlin *et al.*, 2000).

2.3.3 Downstream channel gradient

Rapid changes in grain size have been shown to be associated with changes in gradient (Rice, 1999) and often a decline in slope is associated with a rapid downstream fining followed by an abrupt transition from gravel to sand (Ferguson and Ashworth, 1991). Downstream sorting is caused by the concavity of the profile (Ferguson and Ashworth, 1991). Hoey and Ferguson (1994) report that a strong concavity in the profile forces rapid downstream fining, which agrees with Parker's (1991a,b) results from the Red Deer River and correlations from Morris and Williams (1999). Fining trends can be established in flume experiments where no changes in slope or discharge were imposed (Paola *et al.*, 1992). The downstream decrease in channel gradient and increase in the sand proportion is consistent with the experimental work by Iseya and Ikeda (1987), who showed that once the sand fraction exceeded 30 % of a bimodel fluvial gravel distribution the slope needed to transport the sediment was reduced.

2.3.4 Aggradation and subsidence

Hoey and Ferguson (1997) state that as aggradation rate decreases (reduced sediment supply), the lower the initial concavity, which reduces the sensitivity of fining response, leading to a coarsening of the bed and a reduction in downstream fining. This conclusion agrees with Robinson and Slingerland (1998) who suggest that subsidence rate and sediment supply are the most important controls on downstream fining. Studies on the Pocono Formation (Central Appalachian Basin) indicate that the increased slope increases the ability to transport coarser sediment (Robinson and Slingerland, 1998). When the sediment discharge is reduced better sorting occurs, which enhances downstream fining trends. Lower rates of fining in proximal and medial subreaches of the Sunwapta River were attributed to lower rates of aggradation and possibly net degradation (Dawson, 1988). This theory conflicts with Brierley and Hickin (1985) who proposed that the rate of fining increased with the rate of deposition, with highest rates observed on rapidly aggrading alluvial fans. However, experimental results indicate that there was very little difference in the overall fining pattern during a fourfold change in the rate of deposition (Seal *et al.*, 1998).

2.4 Discussion and unresolved issues

Several underlying themes for investigation arise from this review of autocyclic and allocyclic controls, which require subsequent clarification. One clear point evident from the preceding sections is that no single autocyclic and allocyclic controlling mechanism may be responsible for the reaction of rivers and/or be diagnostic for any particular stacking pattern. Additionally, two or more different controls may produce the same resultant effect on alluvial architecture. For example, a base-level shift or a change in tectonic subsidence may both result in a change in the accommodation space, and, depending on the relationship of these changes to sediment supply rate, they may produce similar or dissimilar stratigraphy. In the same way, the relationship between sediment supply rate and avulsion frequency can produce comparable and contrasting architectural stacking patterns (cf. Bridge and Leeder, 1979, Figure 2.3; Bryant *et al.*, 1995, Figure 2.8; Heller and Paola, 1996, Figure 2.5). Figure 2.14 illustrates how fluvial sequences that are controlled by high channel migration and low aggradation rate may exhibit a similar architectural style to fluvial sequences formed from high avulsion frequency and low aggradation rate.

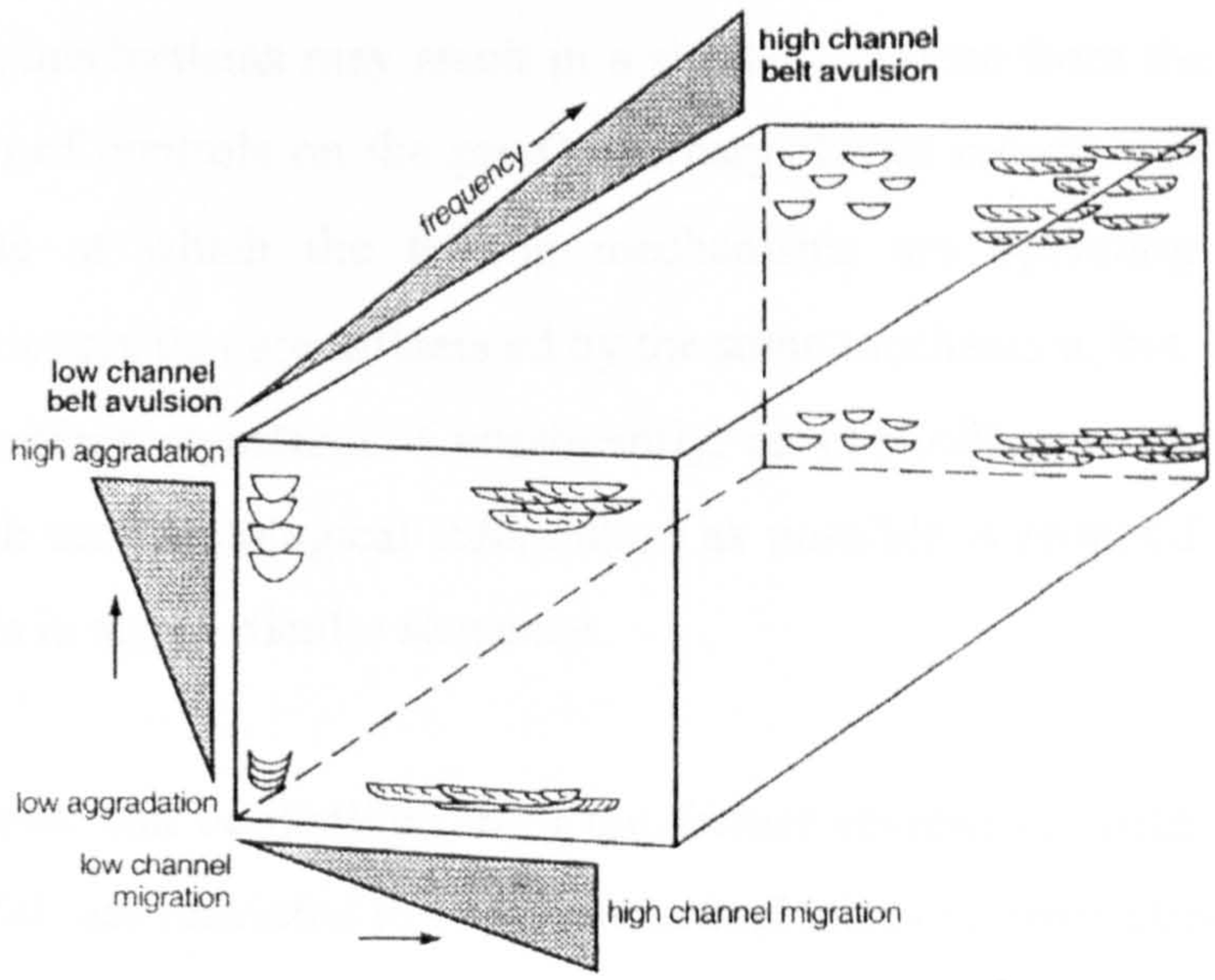

Figure 2.14. Example of the sandbody stacking patterns as a function of aggradation rate, lateral channel migration and channel-belt avulsion (from Bristow and Best, 1993).

In the pre-Quaternary record this process of identifying the controlling mechanisms is further hindered by the lack of well-constrained climatic data, which is so prevalent in the Quaternary. Consequently, the use of palaeosol analysis to establish environmental controls on the fluvial system is often employed. While palaeosols have the power to

provide a large amount of information about the climate, aggradation rate and hydrology of the depositional environment, their interpretation also carries considerable uncertainty. The presence and maturity of calcretes has been used to estimate aggradation rate (e.g. Leeder, 1975; Allen and Wright, 1989) although Wright (1990) argues that many studies of calcrete development are based on the Quaternary and therefore estimates of aggradation rate have to be approached with caution. Furthermore, assignment of climatic and hydrologic conditions based on palaeosol analysis is often difficult. For example, the reddening of palaeosols has been attributed to a range of climatic settings (cf. Turner, 1980; Pye, 1983; Dubiel and Smoot, 1994) and reddening can also take place by secondary diagenetic processes (e.g. Johnson *et al.*, 1997). However, with a paucity of laterally correlative marker horizons the use of palaeosols can guide interpretation of the depositional environment. Yet, in the absence of any other evidence to indicate climatic setting most sedimentary sequences are indistinct (Miall, 1996).

On reflection, the results from the preceding review on allocyclic and autocyclic controls on the fluvial system reveal that three main relationships can be established: (1) different forcing mechanisms may result in a similar response from the fluvial system; (2) identification of controls on the pre-Quaternary fluvial record is often ambiguous; and (3) the rate at which the forcing mechanisms are operating may result in depositional sequences that are influenced by the same mechanism, but have completely contrasting subsurface signatures. Consequently, as controlling mechanisms are case specific, as much sedimentological information as possible is required to establish the principal controls in any particular sequence.

Three further issues can be distilled from the former review: (1) many of the alluvial architecture models are restricted to two-dimensional slices of cross-stream stratigraphy, exceptions are the models of Mackey and Bridge (1995); (2) alluvial architecture models focus on the channel-belt scale sandbody architecture; and (3) alluvial architecture models assume that the drainage system is supplied by equal proportion of fine-grained floodplain and coarse-grained sandstone material, while making no incorporation of the differences in initial sediment supply grain size and modification of this grain size distribution downstream.

To elaborate on the second point, the majority of theoretical and outcrop based models for stacking patterns have focused on the channel-belt scale architecture, namely channel-belt sandbodies and fine-grained floodplain deposits (e.g. Bridge and Leeder, 1979; Bryant *et al.*, 1995; Mackey and Bridge, 1995; Heller and Paola, 1996; Leeder *et al.*, 1996). The key to developing comprehensive alluvial architecture models lies not only with the quantification of the channel-belt scale architecture, but also the understanding of the smaller scale within channel-belt scale architecture. Information at the within channel-belt scale has often been confined to vertical facies profiles and qualitative descriptions of architectural elements. Therefore this individual channel scale architecture needs quantification.

In relation to the third point, much of the work focusing on downstream changes in grain size has been concerned with the supply of sediment into a single channel-belt and how the grain size distribution responds or causes changes in channel form. An appreciation of other allocyclic and autocyclic controls is required before the impact of grain size can be isolated on the within channel-belt river response. For example, studies of modern rivers (e.g. Goff and Ashmore, 1994) and physical models (e.g. Hoey and Sutherland, 1991; Warburton and Davies, 1994) have noted the adjustment in channel morphology as a result of changes in sediment supply rate and transport processes. Therefore, the following section reviews current understanding of other controls on the river response within a single channel-belt. Isolation and quantification of the impact of grain size will assist in incorporating downstream facies trends into three-dimensional alluvial architecture models.

The remainder of this chapter is designated to: (1) the analysis and terminology used in the recognition of formative channel patterns responsible for the deposition of a particular fluvial sequence; (2) the quantification and prediction of sandbody geometry and interconnectedness; and (3) the range of techniques used in subsurface reservoir evaluation.

2.5 Influence of allocyclic and autocyclic controls on within channel-belt river response

During its course a river may undergo several morphological changes as a result of variation in factors such as grain size, discharge and channel gradient. As a consequence of these changes in controls a single river can display braided, meandering and straight channel pattern characteristics (e.g. Singh *et al.*, 1993, Brierley, 1996; Ferguson and Brierley, 1999; Deodhar and Kale, 1999). Many classification systems have been developed to distinguish between channel pattern type by identifying characterising parameters including: sediment supply rate, discharge, and grain size characteristics that include sediment size and sorting (e.g. Figure 2.15, Schumm, 1977, 1981; Schumm and Brakenridge, 1987; Orton and Reading, 1993). This section discusses the controlling factors on channel pattern and the relative importance of grain size on channel pattern and the final depositional architecture.

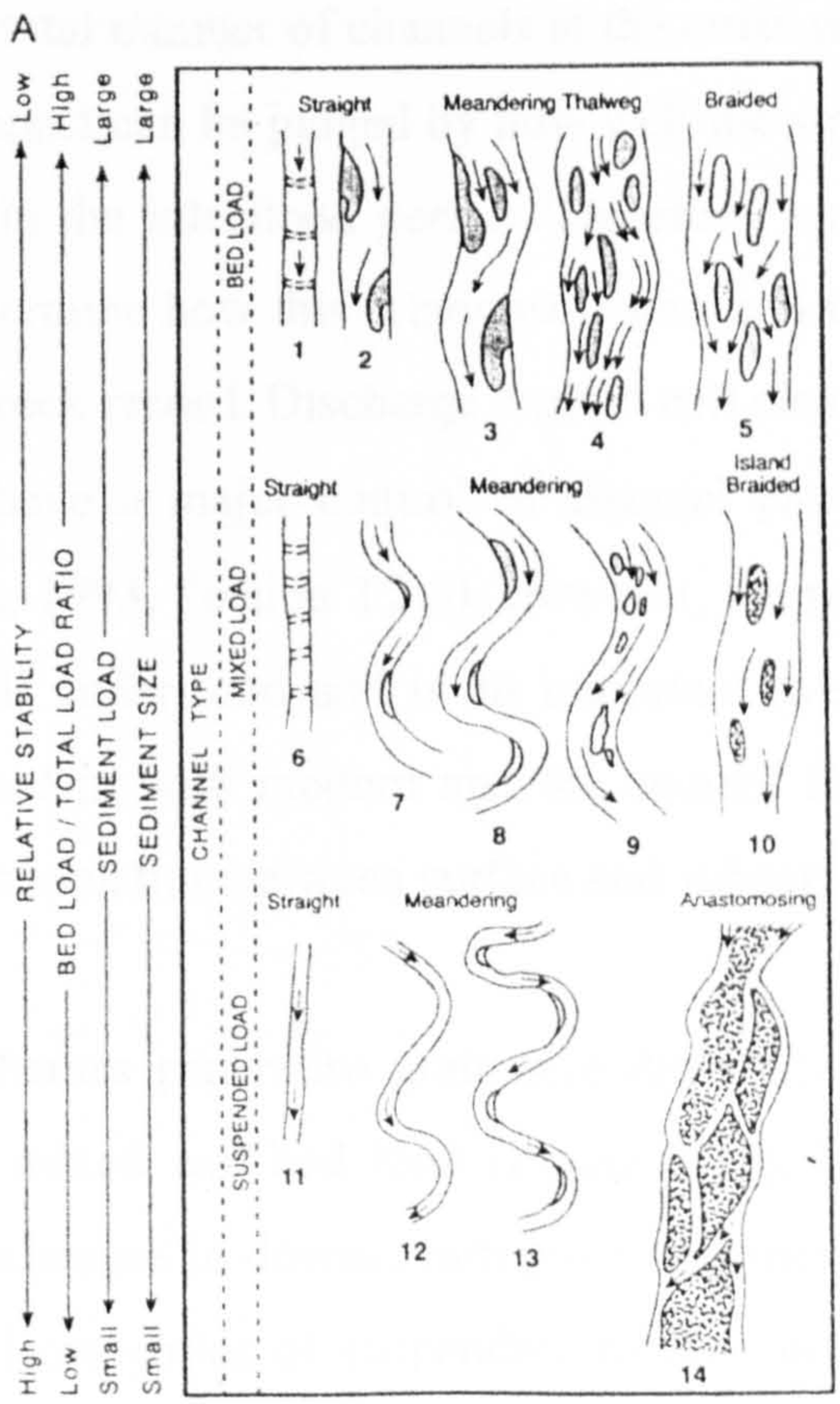

Figure 2.15. Classification of channel patterns (after Schumm, 1981). Note the difference in channel planform for different grain size classifications.

Cross-sectional (e.g. width/depth ratio) and plan view geometry adjusts to accommodate prevailing discharge, supplied sediment load and bed slope conditions (e.g. Leopold and

UNIVERSITY
LIBRARY
LEEDS

Wolman, 1957; Chitale, 1970; Schumm and Khan, 1972; Leeder, 1973; Knighton, 1998). Channels commonly show an increase in width downstream as a result of increased discharge in conjunction with a reduction in grain size, channel depth and slope (Shaw and Kellerhals, 1982). In more arid terminal fan drainage systems, evaporation and infiltration of water discharge along the rivers course can result in a decrease in discharge and corresponding reduction in channel size downstream (Newell *et al.*, 1999). Additionally, the occurrence of high magnitude flood events can play a major role in determining the channel morphology (Gupta, 1983) and channel-belts may also respond to accommodate an increasing flood discharge by widening the channel (Gupta and Fox, 1974) or increasing the number of channels (e.g. Schumm and Lichty, 1963; Harvey, 1969; Warburton *et al.*, 1993). Controlled release from a dam on the Ohau River, New Zealand showed that as discharge is increased the channels become wider and deeper and merge to become a single larger channel (Mosley, 1982). Supplementary channels are generated with similar characteristics to those existing at lower discharges and the total number of channels at the cross-section remains constant (Mosley, 1982). Flood impact can be judged by how well the smaller flows can modify the form of the channel in the interflood period. Therefore, an important concept for sedimentologists is to determine how this relationship between the flood and interflood flows is expressed in the rock record. Discharge regime will also influence the sediment supply rate, which can have a major control of channel pattern and response (e.g. Germanoski and Schumm, 1993, Section 2.2.3). However, the relationship of grain size characteristics is less well understood and is an important avenue to pursue because grain size can be measured in both modern and the ancient fluvial systems and may therefore, allow direct extrapolation between surface and subsurface.

Channel classification schemes generalise grain size distributions by portraying them often just as suspended, mixed and bed load (Figure 2.15). Yet, within a particular channel-belt more subtle changes in downstream grain size may occur (refer to Section 2.3) within the individual categories of suspended, mixed and bed load, and channel response may be less pronounced than a complete channel pattern change and may occur as more gradational changes in channel geometry. Several studies have noted changes in channel geometry or channel behaviour as a result of distinct changes in grain size (e.g. Schumm, 1960; Sambrook Smith, 1996; Whipple *et al.*, 1998). Schumm (1960) measured the average grain size on channel banks and found that grain size correlated

well with width/depth ratio of channel cross-sections indicating that channels with a higher weight percentage of mud had higher bank strengths and subsequently lower width/depth ratios. Experimental work by Whipple *et al.* (1998) complements the findings of Schumm (1960). Whipple *et al.* (1998) suggested that the degree of channelisation is dependent on water discharge and grain size, but independent of sediment supply rate. Increasing the proportion of fine sediment in the system had the effect of progressively enhancing flow channelisation, which was attributed to the onset of significant suspended sediment transport and the effective cohesion of the channel banks. Bluck (1987) also noted that the control of slope on bar form type was a more important determining parameter than grain size. Much of the work on the channel response to the impact of grain size is still qualitative and requires isolation and quantification from other controls.

If channel pattern is to be used to provide definition for the assignment of quantitative datasets to interpret subsurface sequences, channel pattern must first be recognised in the subsurface before characteristic geometrical information can be used for a particular channel type. Moreover, whilst controls such as discharge, sediment supply and grain size may be investigated in relation to surface morphology and channel pattern, any alluvial architecture models based on these controls require the incorporation of subsequent reworking of the original form.

2.6 Relationship of channel pattern to alluvial architecture

Alluvial architecture models are based largely on vertical lithofacies associations (Miall, 1977, Collinson, 1978, Figure 2.16). These qualitative models have been developed to interpret the depositional environment and, subsequently, geologists have used these schemes to develop models for specific fluvial sequences. Application of vertical facies schemes often involves adapting them in order to classify the particular sequence being studied, leading to a new model for every real-world example (Dott and Bourgeois, 1983). In order that the lateral variability of sandbodies is captured, often several vertical profiles are taken from cored well data, multiple logs at intervals along a single outcrop, or several pits dug in a modern river, then general vertical trends are picked out

and matched to a particular depositional environment/channel pattern (e.g. Collinson, 1978, Cant and Walker, 1978; Bentham *et al.*, 1993).

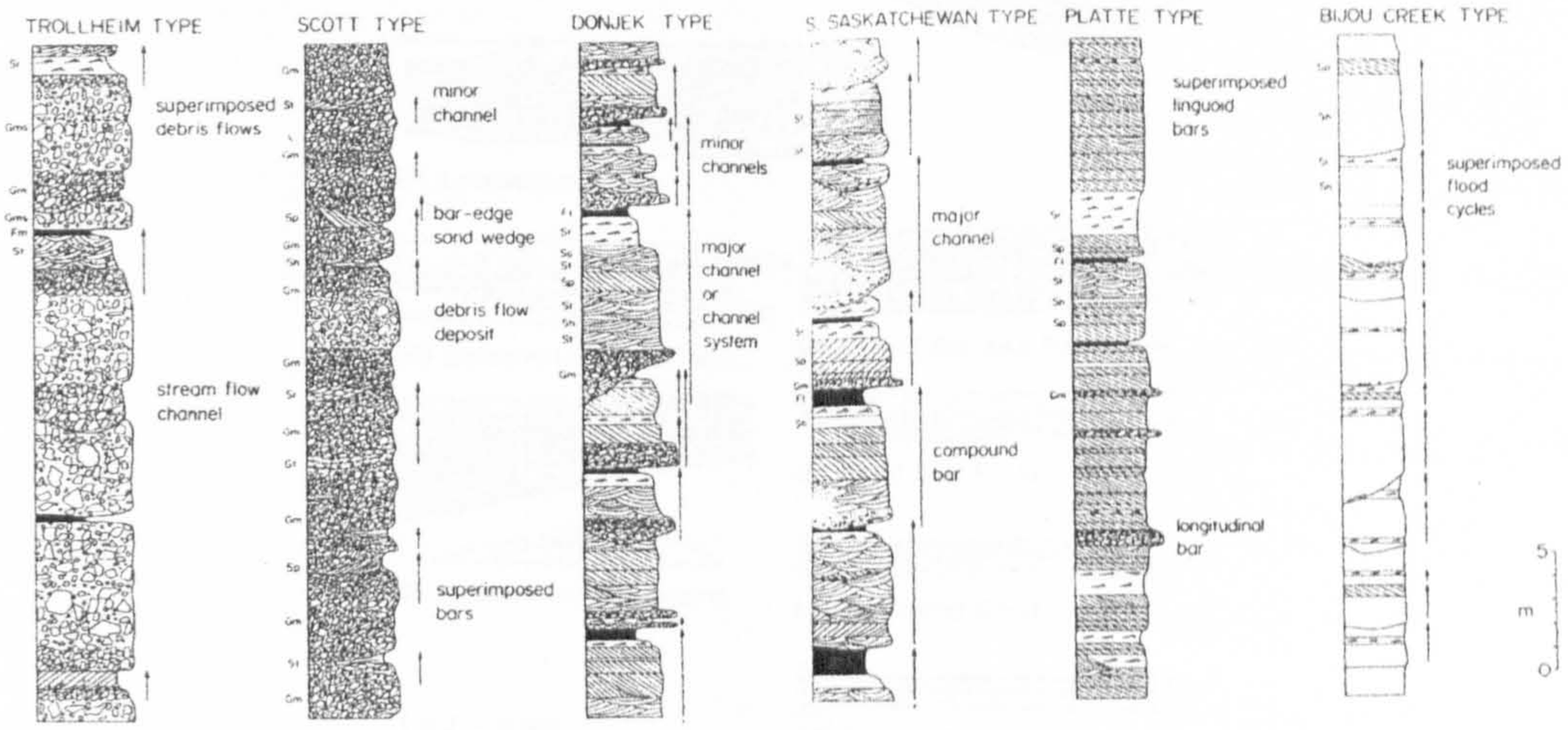

Figure 2.16. Vertical profile models for braided stream deposits (from Miall, 1977). Facies codes are to the left of each column. Arrows show small-scale cyclic sequences.

While vertical facies profiles permit comparison between fluvial sequences and provide a first solution to the interpretation of depositional environment, these models are one-dimensional. Allen (1983a) investigated the Devonian Brownstones fluvial sequence and classified the alluvial architecture based on the definition of a hierarchy of essentially two-dimensional bounding surfaces, a method that was adopted and developed by Miall (1985) and Wizevich (1993). Miall (1985a) developed the concept of architectural element analysis, which involved assigning a two-dimensional shape to the facies type (Figure 2.17, Table 2.2). Architectural elements form the basic building blocks of all fluvial sequences, although the overall geometry and stacking patterns may differ between sequences. Fielding (1993) highlighted the need to adapt the hierarchy of architectural elements to the particular sequence being studied, such that outcrop studies (e.g. Miall, 1988a,b; Eberth and Miall (1991); Hornung and Aigner, 1999; Klingbeil *et al.*, 1999) have adapted this architectural element classification scheme to apply to specific fluvial sequences. In an attempt to increase understanding of alluvial architecture a number of studies have employed a combination of vertical facies, architectural elements, and bounding surface schemes to characterise alluvial architecture in a qualitative way (e.g. Cant and Walker, 1978; Allen, 1983a; Bridge and Diemer, 1983; Alexander and Gawthorpe, 1993; Cadle and Cairncross, 1993; Steel and Thompson, 1983; Willis, 1993a,b; Wizevich, 1993; Willis and Behrensmeyer, 1994).

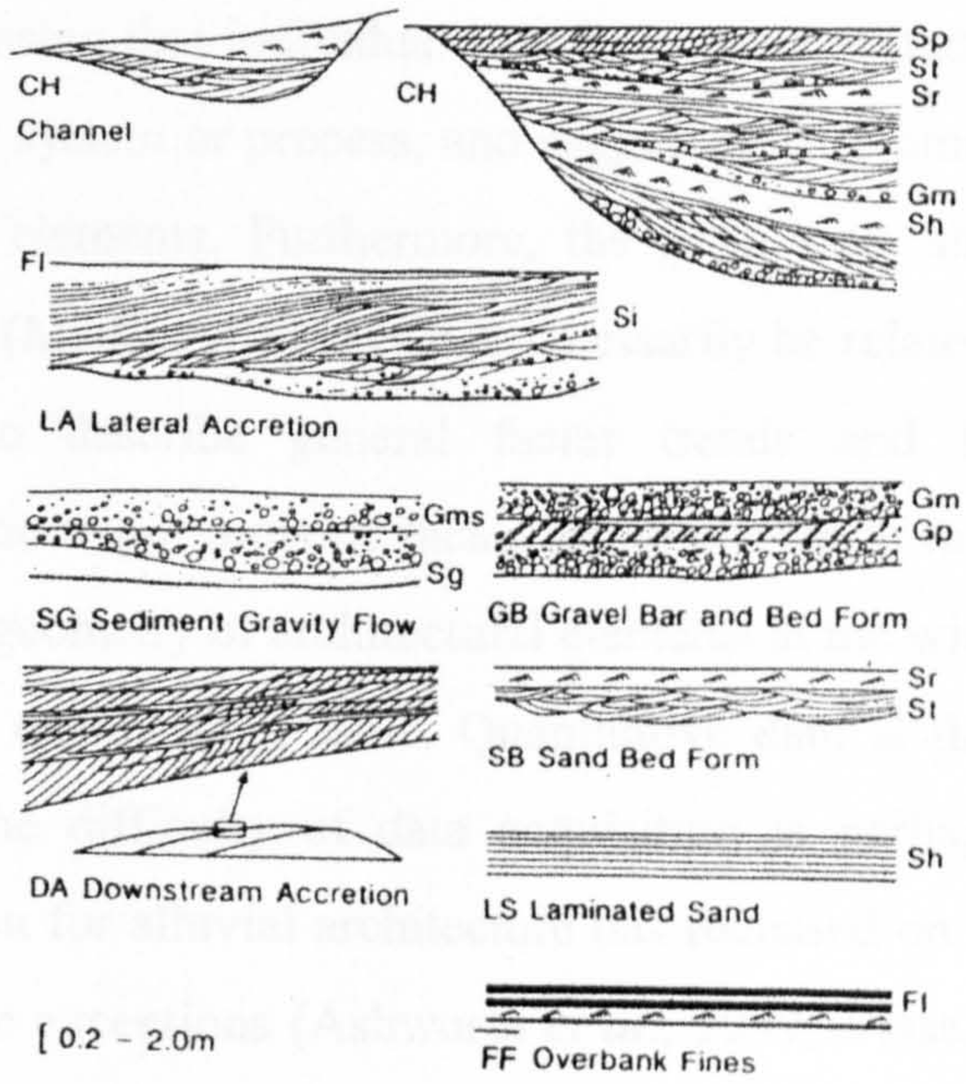

Figure 2.17. The eight basic architectural elements in fluvial deposits (from Miall, 1988a,b).

Table 2.2. Architectural elements in fluvial deposits (from Miall, 1996).

Element	Symbol	Principal facies assemblage	Geometry and relationships
Channels	CH	Any combination	Finger, lens or sheet; concave-up erosional base; scale and shape highly variable; internal concave-up 3rd-order erosion surfaces common
Gravel bars and bedforms	GB	Gm, Gp, Gt	Lens, blanket; usually tabular bodies; commonly interbedded with SB
Sandy bedforms	SB	St, Sp, Sh, Sl, Sr, Se, Ss	Lens, sheet, blanket, wedge, occurs as channel fills, crevasse splays, minor bars
Downstream-accretion macroform	DA	St, Sp, Sh, Sl, Sr, Se, Ss	Lens resting on flat or channeled base, with convex-up 3rd-order internal erosion surfaces and upper 4th-order bounding surface
Lateral-accretion macroform	LA	St, Sp, Sh, Sl, Se, Ss, less commonly Gm, Gt, Gp	Wedge, sheet, lobe; characterized by internal lateral-accretion 3rd-order surfaces
Scour hollows	HO	Gh, Gt, St, Sl	Scoop-shaped hollow with asymmetric fill
Sediment gravity flows	SG	Gmm, Gmg, Gci, Gcm	Lobe, sheet, typically interbedded with GB
Laminated sand sheet	LS	Sh, Sl; minor Sp, Sr	Sheet, blanket
Overbank fines	FF	Fm, Fl	Thin to thick blankets; commonly interbedded with SB; may fill abandoned channels

Facies classification from Miall (1978b).

Bridge (1985, 1993a) has criticised the use of lithofacies and architectural element analysis schemes, stressing that individual lithofacies are not mutually exclusive to any particular depositional system or process, and suggests that geometric names be used to describe architectural elements. Furthermore, the grain size, shape and geometry of architectural elements (Miall, 1985) may not necessarily be related to time. While these models are useful to describe general facies trends and links to depositional environment, one of the major aims of facies interpretation is to quantitatively predict the three-dimensional geometry of architectural elements at the within channel-belt scale and sandbodies at the channel-belt scale. Quantitative data at the within channel-belt scale is scarce and the difficulty of data acquisition is perhaps why much of the geometrical information for alluvial architecture has focussed on the channel-belt scale architecture, with some exceptions (Ashworth *et al.*, 1999; Visser and Chessa, 2000a). Commonly, the geometries of individual architectural elements within a particular sequence are defined solely by minimum and maximum width and thickness values (e.g. Hornung and Aigner, 1999) yet within fluvial systems a hierarchy of channels can exist (Williams and Rust, 1969) resulting in a hierarchy of depositional geometries. Therefore, quantification of the distribution of individual architectural element geometries is required to predict the probability of an architectural element with particular geometrical attributes occurring within a defined fluvial sequence. Understanding the geometrical distribution of architectural elements allows the assignment of lateral dimensions to vertical facies profiles. While geometrical information at the channel-belt scale is continually being presented in the literature, the information at the within channel-belt scale is slow to follow and here lies the data gap. With reservoir simulation models requiring high resolution, spatially intensive quantitative datasets at all scales, this within channel-belt architecture is required for future reservoir modelling by both petroleum and aquifer engineers.

While there appears to be a data gap in the quantitative architectural analysis, the prediction of channel-belt sandbody geometries now warrants further review. Channel-belt sandbody geometries are often gathered from analogue outcrop studies to aid subsurface interpretation over inter-well distances and are often founded on the principle that channel patterns in particular depositional environments will create a characteristic distribution of sandbody geometries.

2.6.1 Prediction of sandbody geometries

The goal in understanding channel pattern from vertical log profiles lies with the prediction of channel and channel-belt sandbody geometries (e.g. Fielding and Crane, 1987; Dreyer *et al.*, 1993; North and Taylor, 1996; Robinson and McCabe, 1997). Traditionally, sandbody geometries have been described as ribbon and sheet sandbodies (Figure 2.18) based on a division in width/thickness ratio of 15:1 (Friend *et al.*, 1979).

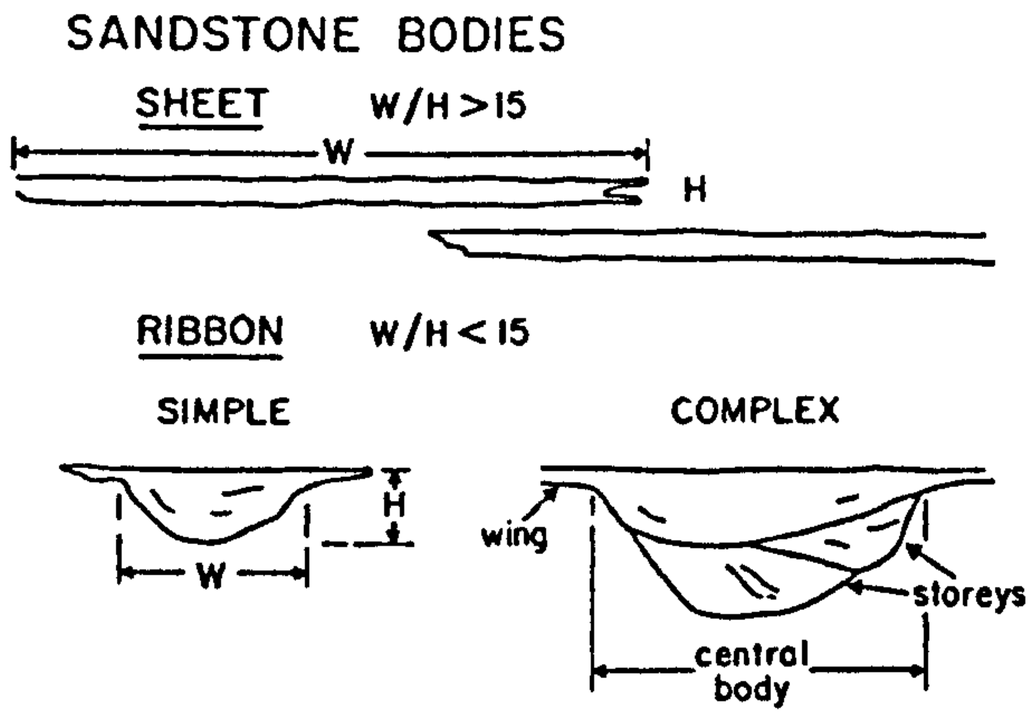

Figure 2.18. Terminology devised by Friend *et al.* (1979) to describe sandbody geometry based on a width/thickness ratio of 15:1.

The division of sheet and ribbon sandbodies has often been assigned to specific formative channel patterns (Fielding and Crane, 1987; Figure 2.19). This has led to a stereotyping of particular channel patterns to diagnostic channel-belt sandbody geometry. Subsequent studies have used these characteristic geometries to interpret inter-well alluvial architecture.

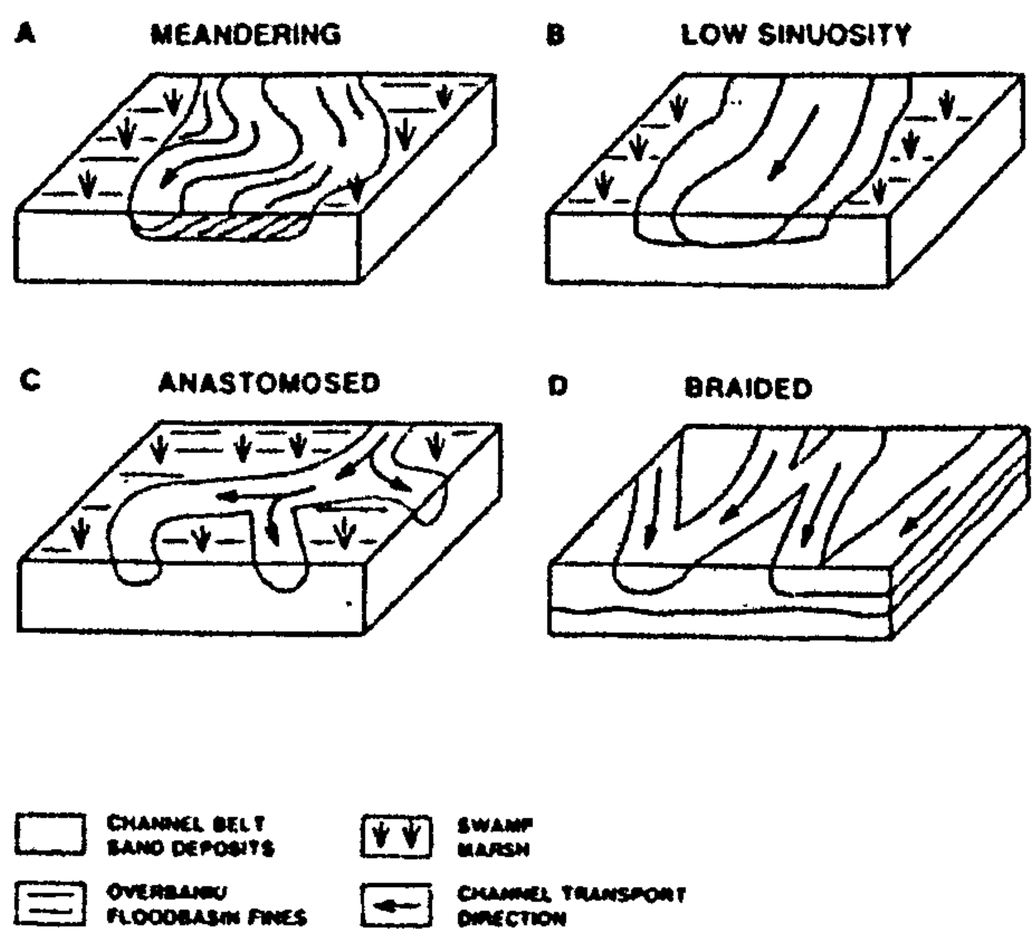

Figure 2.19. Sandbody types and their relation to channel pattern (from Fielding and Crane, 1987).

Several studies have highlighted the potential pitfalls with the approach of assigning characteristic sandbody geometries based on an assessment of channel pattern. Brierley and Hickin (1991) showed similarity in depositional architecture excavated within reaches of meandering, wandering and braided river channels and postulated that river planform is not a control on deposited sedimentary sequences, either at the bedform-scale facies or the floodplain assemblage scale. Advocates of the non-link between channel pattern and vertical facies profiles include Bridge (1985) and Bridge and Tye (2000) who indicate that similar vertical profiles can be formed by different allogenic and autogenic processes and therefore different channel patterns (Miall, 1996). For example, lateral accretion deposits have been used to define point-bar migration and interpreted as meandering channels. However, lateral accretion deposits can also be formed in braided rivers and consequently, lateral accretion deposits that may have been traditionally interpreted as the result of meandering rivers (Bristow, 1987, 1993a; Stear, 1983) may have been the result of braided channel deposition. The use of characteristic sandbody geometry is also complicated by the observation in some sequences of a range of sedimentary features, which indicate that a combination of channel patterns may have coexisted during the deposition of those particular sequences. Consequently, the resulting alluvial architecture shows the presence of a large range of sandbody geometries within the individual formation (e.g. Dreyer *et al.*, 1993).

Furthermore, studies such as Jones and Harper (1998) have demonstrated how channel avulsion events of point-bar deposits form nodes and internodes in planform on the meandering Rio Grande River, and have resulted in the formation of both wide and narrow channel sandbodies in outcrop (Figure 2.20). Peakall *et al.* (2000) attributed changes in channel-belt sandbody geometry to regional-scale tectonic tilting mechanisms within meandering rivers (Section 2.2.2). Analogue width and thickness cross plot data such as those shown in Figure 2.21 have been used to construct predictive models of most likely sandbody width (Figure 2.22). In light of the studies such as Jones and Harper (1998) and Peakall *et al.* (2000), which introduce significant uncertainties to the prediction of channel-belt sandbody geometries, the application of these models has to be approached with caution. In order to apply sandbody geometries to analogue sequences with confidence, geologists must look to evaluate all aspects of the alluvial architecture, including: lithofacies, architectural elements, grain size

distribution, palaeosol analysis, biostratigraphy, basin type, and-critically-the scale of the system.

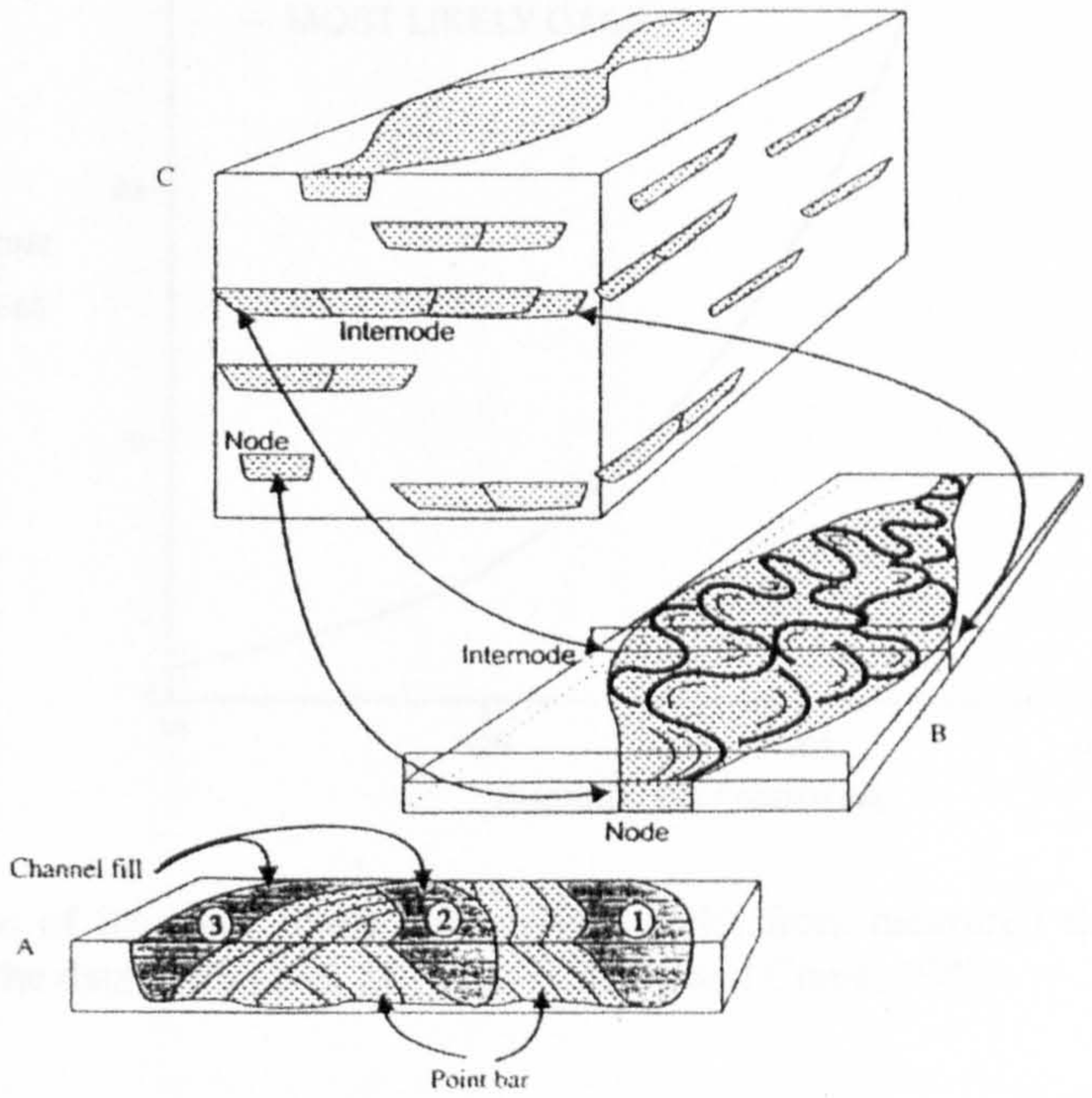

Figure 2.20. Schematic block diagram showing large-scale depositional geometries. (A) Idealised cross-section of an internode, showing relative ages (1-oldest, 3-youngest) of channel-point-bar couplets based on crosscutting relationships, and coarse-grained point-bar deposits and mostly fine-grained fill in abandoned channels. (B) At the larger scale, node-internode geometry can result in swelling and thinning of channel deposits in the floodplain. (C) Wide and narrow channel deposits in vertical outcrop (from Jones and Harper, 1998).

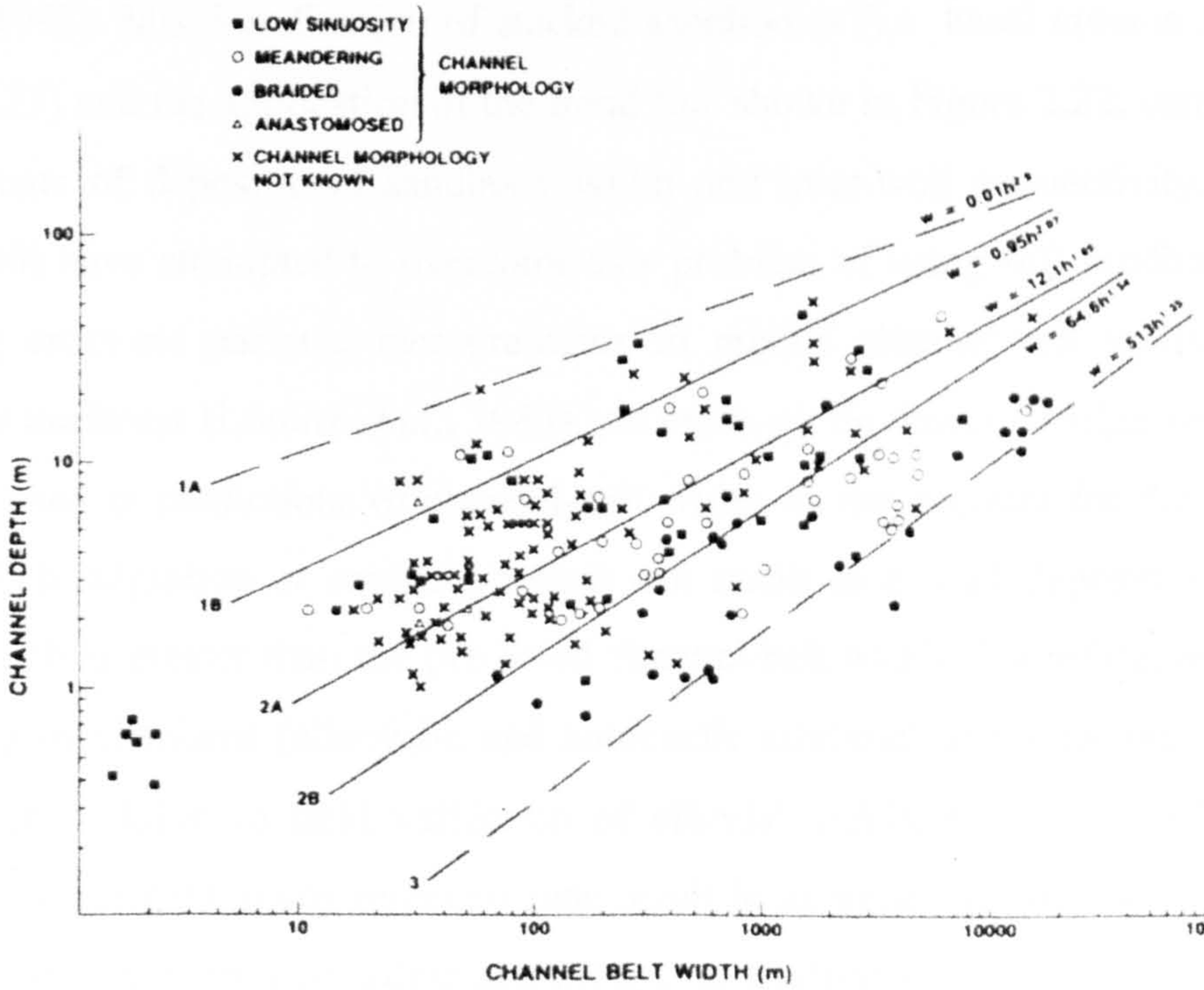

Figure 2.21. Channel depth versus channel-belt width (perpendicular to palaeocurrent) relationships for types of modern and ancient fluvial channel deposits showing a large amount of scatter and therefore pose great difficulties in the application of general trend lines (from Fielding and Crane, 1987).

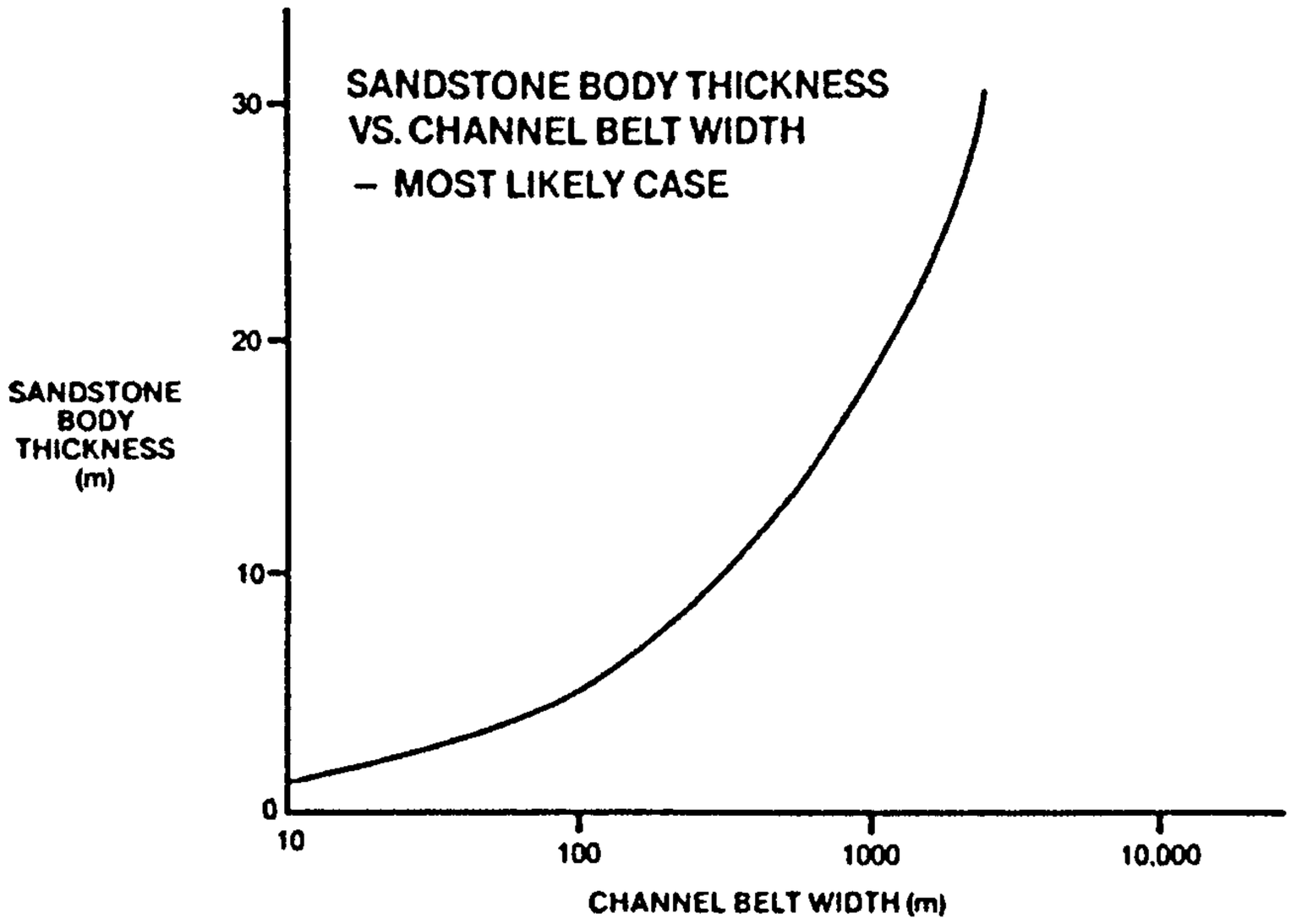

Figure 2.22. Prediction of the most likely channel-belt width from measured thickness data using the geometric mean of all the data in Figure 2.21 (from Fielding and Crane, 1987).

Models such as Figure 2.22 are often used in inter-well reservoir prediction to determine the lateral extent of sandbodies based on an assessment of sandbody thickness (e.g. Lorenz *et al.*, 1985). So far, sandbodies described in this section have been treated as isolated bodies, however, in many sequences sandbodies are stacked. This stacking has been the focus of many stratigraphy models (e.g. Bridge and Leeder, 1979; Mackey and Bridge, 1995). Misidentification of stacked sandbodies (i.e. basal erosion surfaces, see Figure 2.23) and the application of the trend line shown in Figure 2.22, can result in the overestimate of depositional sandbody width and inter-well connectivity. Bridge and Tye (2000) have attempted to overcome this problem of using full sandbody thickness by using cross-set package measurements to predict channel-belt width. Both total sandbody thickness (Lorenz *et al.*, 1985) and cross-set thickness (Bridge and Tye, 2000) methods used in predictions of channel-belt width do not account for the processes of channel-belt migration or stacking, which can result in a final depositional sandbody width which is greater than the predicted channel-belt width. Therefore, an assessment of forcing mechanisms (allocyclic and autocyclic controls) active during deposition is required in addition to field validation of alluvial architecture. Extrapolation of the wrong analogue data to any reservoir may result in an underestimate or overestimate of the sandbody geometries with dramatic effects on sandbody connectivity.

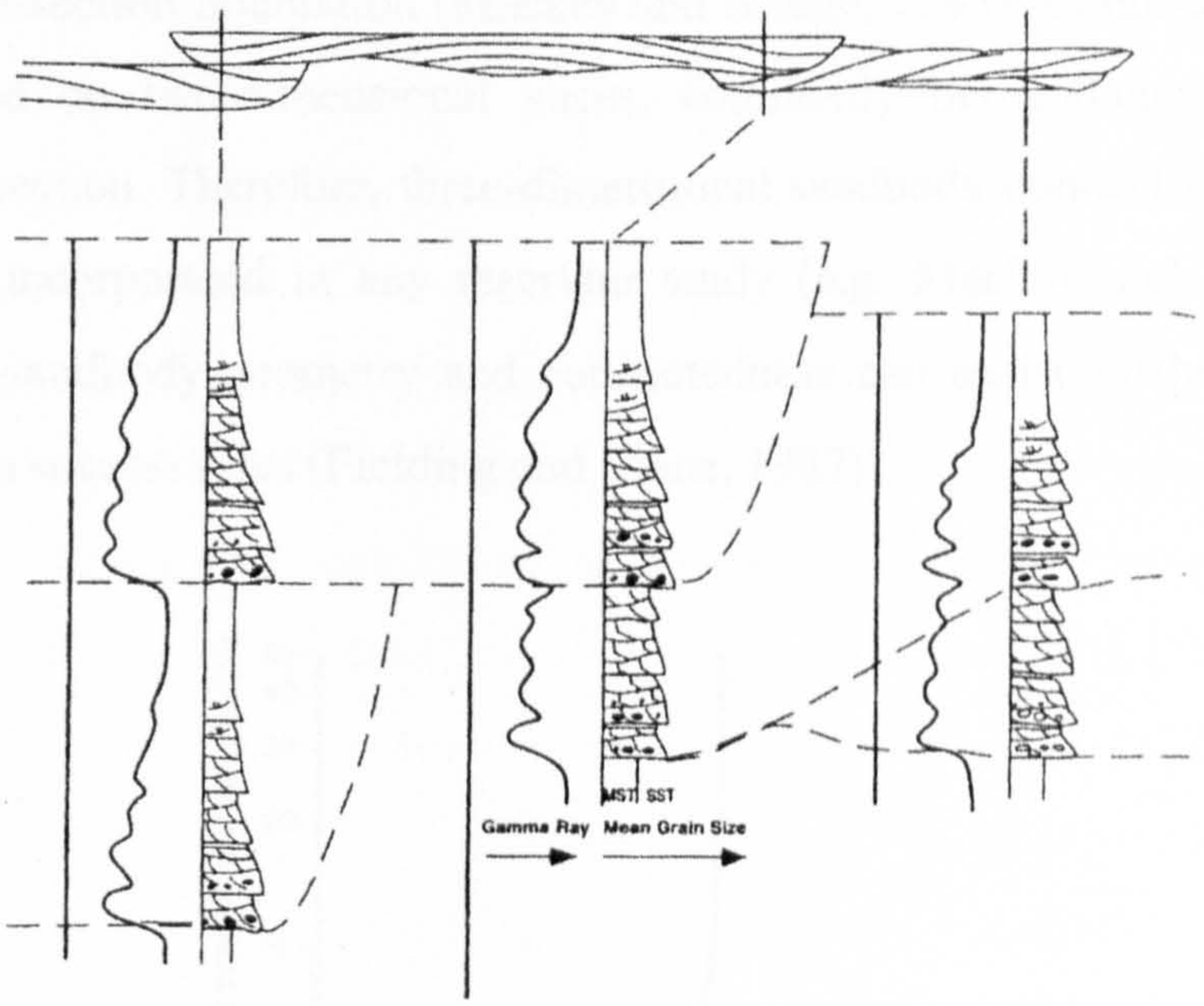

Figure 2.23. Problems of determining depositional width from a measurement of depositional thickness are illustrated in vertical log profiles from Bridge and Tye (2000) showing that identification of basal erosional surface between the centre and left vertical log profiles may be ambiguous.

2.7 Sandbody interconnectedness

Permeability often contrasts strongly between channel-belt sandbodies (reservoir) and confining overbank (non-reservoir) deposits (Fogg, 1990). Futhermore, the interconnectedness of sandbodies will control fluid flow patterns within the reservoir and is paramount to the successful extraction of hydrocarbons. The ratio between the reservoir quality and non-reservoir quality rock is expressed as the *net-to-gross*. Allen's (1978) theoretical model shows that if the percentage of overbank fines in a sequence was greater than 50 % the sandbodies would be virtually unconnected. Fogg (1986) shows sandbodies to be isolated at net-to-gross values of <20 % and amalgamated at >60 %. Further work by Fielding and Crane (1987, Figure 2.24) and Bridge and Mackey (1993b) illustrate that channel sandbodies are relatively isolated where the proportion of channel facies is < 40 % with connectivity increasing at proportions between 40-75 %, with values above 75 % being highly connected. The orientation of these sandbodies is often not quantified and studies of the Schooner Formation (Mijnssen, 1997) suggested channel sandbody orientation to be the primary control on sandbody connectivity. Channel-belt sandstone connectivity has been shown to be influenced by controls including tectonics (Bridge and Leeder, 1979; Peakall *et al*, 2000), incision (Leeder and Stewart, 1996), avulsion and migration (Leeder *et al*., 1993; Bryant *et al*.,

1995) and cross-section orientation (Mackey and Bridge, 1995). Connectivity estimates are often based on two-dimensional slices, commonly perpendicular to the main channel-belt direction. Therefore, three-dimensional sandbody connectivity needs to be addressed and incorporated in any reservoir study (e.g. Mackey and Bridge, 1995).. Understanding sandbody geometry and connectedness can assist in the prediction of well-penetration success rates (Fielding and Crane, 1987).

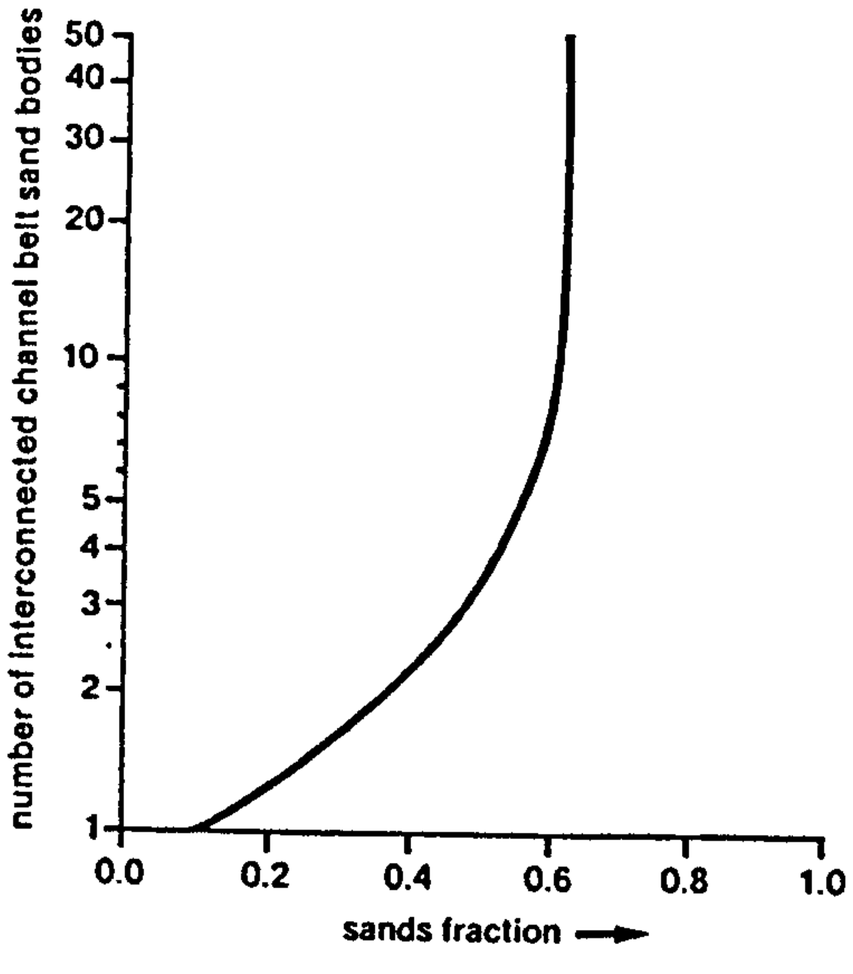

Figure 2.24. Sandstone body interconnectedness as a function of the net sand fraction of the sequence (from Fielding and Crane, 1987). Note that at 0.6 the sandbodies become fully connected.

2.8 Techniques used to evaluate subsurface alluvial architecture

A primary objective in reservoir characterisation is the accurate prediction of hydrocarbon flow through heterogeneous sediments based on datasets from scattered wells (with separation distances in the order of ~ 0.5 km). In order to evaluate and predict reservoir performance accurately, the correlation of reservoir sandbodies between wells is required. The application of an appropriate dataset for subsurface interpretation is paramount to successful prediction of alluvial architecture. This section outlines the range of techniques that are employed to evaluate alluvial architecture. Good summaries are also discussed in Bryant and Flint (1993), North (1996) and Bridge and Tye (2000).

In many reservoir evaluations a stage is reached when a conceptual depositional model is developed, and this is effectively a mental image of the depositional environment and the deposits under evaluation. The depositional model is re-evaluated and refined during the development of the field, as more data become available. This process is subjective, but is often necessary to steer geologists to the quantitative datasets required for modelling (MacDonald and Holland, 1993). The importance of reservoir re-evaluation in alluvial architecture is illustrated in Bridge and Tye (2000) who show a two-dimensional correlation of channel sandbodies predicted from numerical modelling (Figure 2.25a) and traditional inter-well correlation (Figure 2.25b) for the Travis Peak Formation (Tye, 1991). Figure 2.25c displays the re-evaluated channel-belt sandbody widths and shows the initial interpretations vastly overestimated sandbody connectivity.

Traditionally, decisions on reservoir management have been made based on the geologist's experience of inter-well alluvial architecture using a variety of techniques to correlate units, such as core and well interpretation. In secondary recovery stages there is a need for the geologist to gain quantitative data from analogue studies. In addition, as reservoir simulation modelling techniques become more sophisticated and can incorporate finer scales of detail, there is a growing need for high resolution, spatially-intensive geostatistical data on river morphology and alluvial architecture. With this in mind, two key shortfalls are drawn out of the current quantitative datasets addressed in Section 2.6, these are: (1) geologists often use channel-belt scale width/thickness dimensions to provide data on geometries for reservoir engineers and the use of these data for reservoir evaluation carries considerable conditions with its application; and (2) quantitative datasets on within channel-belt architecture is scarce, but necessary for full reservoir evaluation. The techniques discussed in the following sections may aid in their solution.

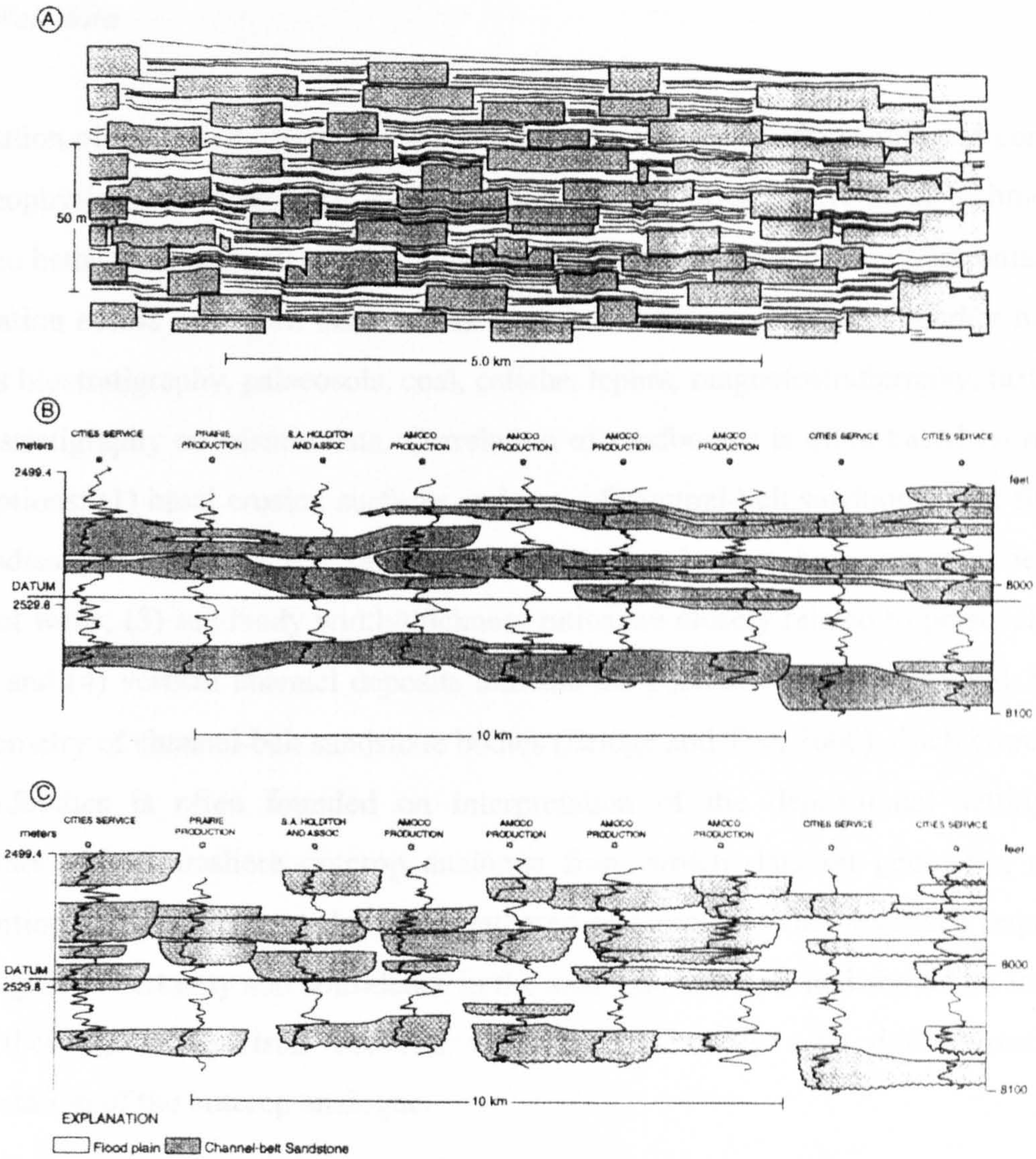

Figure 2.25. (A) Two-dimensional stratigraphic simulation of fluvial channel-belts (stippled) in the Travis Peak Formation, North Appleby field, East Texas basin (zone 1 of Tye, 1991; Davies *et al.*, 1993). (B) Wireline logs and channel-belt sandbodies of zone 1 as originally correlated by Tye (1991). (C) Revised well-to-well correlations using same data as in (B), but constrained to recalculated channel-belt widths. Note that limiting channel-belt widths decreases sandbody connectivity in two dimensions. (from Bridge and Tye, 2000).

2.8.1 Well data

Correlation of inter-well reservoir architecture and interconnectedness requires core data and geophysical measurements. The spatial resolution of the correlation technique is often no better than the well spacing and there is more vertical data than horizontal data. Correlation across inter-well distances is often based on a reference or marker horizon such as biostratigraphy, palaeosols, coal, caliche, tephra, magnetostratigraphy, tuff beds, chemostratigraphy or seismic data. Correlation of sandbodies is often based on several assumptions: (1) basal erosion surfaces and tops of channel-belt sandbodies are flat; (2) sandbodies positioned at the same stratigraphic level must be connected between adjacent wells; (3) sandbody width/thickness ratios are closely related to palaeochannel depth; and (4) vertical channel deposits indicate the palaeochannel pattern and, hence, the geometry of channel-belt sandstone bodies (Bridge and Tye, 2000). Such correlation of sandbodies is often founded on interpretation of the depositional setting and assignment of an onshore outcrop analogue from which data on geometry, spatial distribution and interconnectedness are gathered and applied. This approach requires a high degree of certainty and confidence in the analogue selected, and should be founded on a thorough comparison between well data (primarily core descriptions) and interpretation of the outcrop analogue.

Geometrical data from core are the foundation for studies regarding depositional environment, stratigraphy and reservoir evaluation. There is a lack of core data presented in the literature containing quantitative estimates of channel depths and sandbody thicknesses. A major challenge therefore is to extrapolate vertical/sub-vertical core data to lateral architecture (Lorenz *et al.*, 1985). Core data provides both a vertical description of the facies present in the wells and details on petrophysical attributes within the well for flow simulations.

Core data are often sparse and correlation often relies upon calibration with wireline well data (Serra, 1987; Rider, 1990; Worthington, 1990, Lovell *et al.*, 1998). Attempts have been made to assign idealised wireline log characteristics to determine facies types (e.g. Richardson *et al.*, 1987a; Richardson *et al.*, 1987b; North, 1996, Figure 2.26; North and Taylor, 1996) in non-cored reservoir intervals. Superposition of channel-belts is often difficult to determine from wireline log and core data, and misinterpretation of

stacked sandbodies may result in overestimates of channel-belt sandbody width, net-to-gross and connectivity.

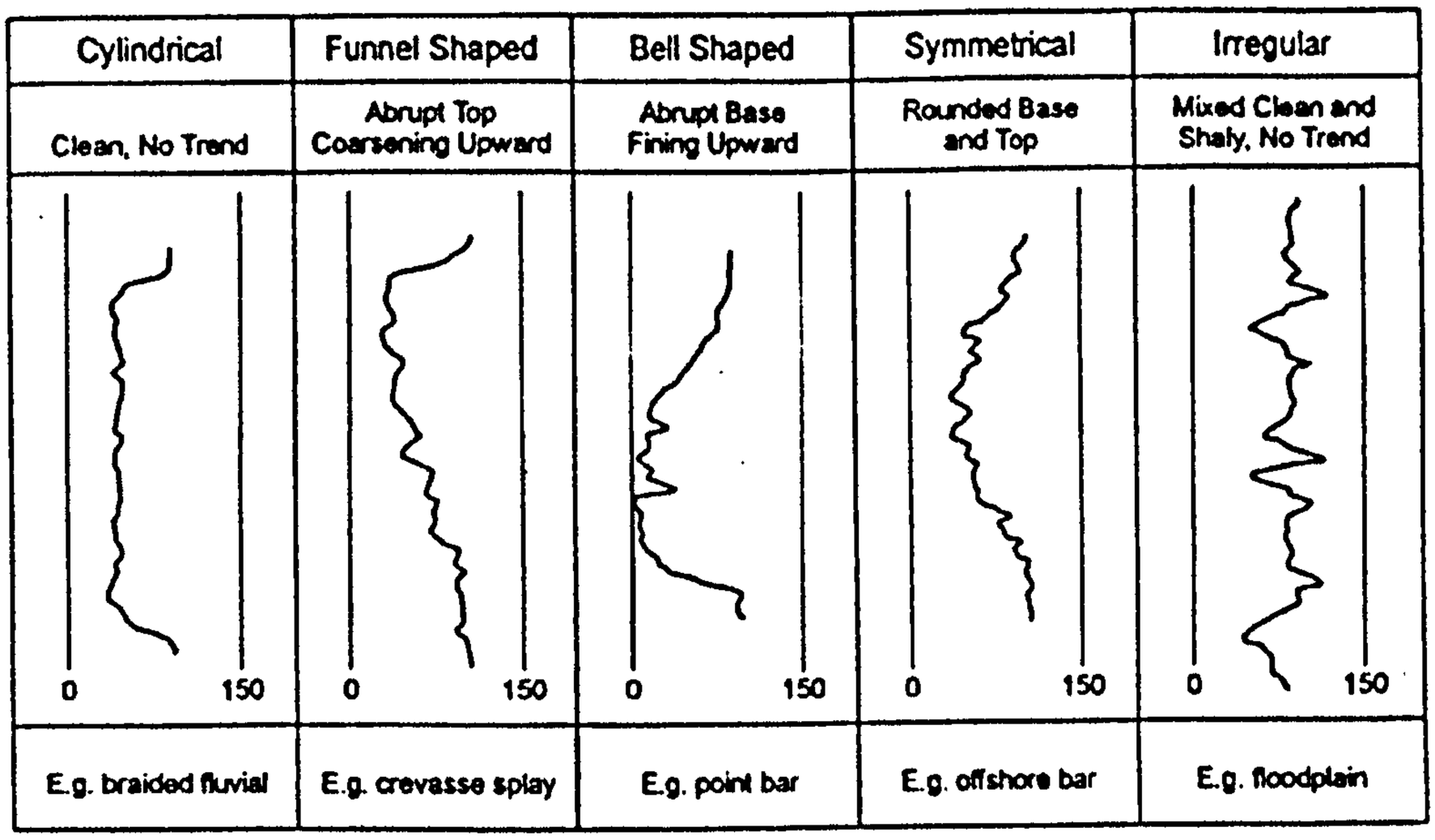

Figure 2.26. Idealised wireline log characteristics for facies analysis in the subsurface (from North, 1996).

Supplementary techniques, including dip meters (Williams and Soek, 1993), Formation MicroScanner (FMS) and other image logs (e.g. Luthi, 1990; Mercadier and Livera, 1993) can be employed with core data to aid interpretation of depositional sequences. A requirement in the application of all the geophysical techniques is that they are calibrated with cored intervals.

2.8.2 Outcrop analogues

Outcrop analogues have traditionally been used to determine inter-well alluvial architecture. The assignment of an onshore outcrop analogue to any subsurface reservoir is often determined on an evaluation of the depositional environment based on facies descriptions from core and a lithological and/or stratigraphic match with an exposed sequence (e.g. Lui *et al.*, 1996; Bridge *et al.*, 2000). The shortcomings of using outcrop analogues have been discussed in Geehan (1993), Alexander (1993) and Bridge and Tye (2000). Outcrops are rarely so well exposed to allow full quantification of the complete hierarchy of architectural geometries in three-dimensions. Outcrops with lateral exposure less than the average well spacing can also be difficult to apply to

subsurface datasets, since the same problems of predicting the connectivity in wells are encountered. Outcrops are also often two-dimensional, although attempts to quantify the three-dimensional extent of the channel-belt sandbodies have been performed by drilling series of vertical wells behind the outcrop face (Ravenne *et al.*, 1989; Mathieu *et al.*, 1995).

Published literature (Table 2.3) commonly detail channel-belt scale geometrical attributes of alluvial architecture from outcrop studies, with very few studies reporting measurements from either within channel-belt fines or overbank deposits (excluding splays). Often measurements have come from sequences where there is a clear distinction between overbank deposits and the channel sandbodies such as in the Escanilla Formation (Dreyer *et al.*, 1993), the Esplugafreda Formation (Dreyer, 1993) and the Chubut Group (Bridge *et al.*, 2000). However, many studies do not give an estimate of the accuracy of measurements, nor do they give geometric dimensions with reference to the mean palaeocurrent direction. There is also often an inconsistency in various facies descriptions when comparing studies, and little consideration is normally given to the effect of burial compaction or estimates of burial depth. Few studies in the literature provide data on width, length and thickness of sandbodies (Mjos *et al.*, 1993a,b; North and Taylor, 1996) with the majority only providing two-dimensional geometrical data. Additionally, photographic distortion is often ignored when sandbody measurements are taken from photomontages, yielding significant errors (cf. Wizevich, 1991; Arnot *et al.*, 1997).

Table 2.3. Example of the range of quantitative alluvial architectural datasets available from outcrop and flume studies.

Author(s)	Date	Geological Formation	Geological age	Depositional environment	Number of data points
Aitken, J. F., Quirk, D. G., & Guion, P. D.	1999	Mexborough Rock	Westphalian A-C	Sandy braided	32
Ashworth, P. J., Best, L. J., Leddy, J. O., & Geehan, G. W.	1994	Ivishak Formation	Triassic/Permian	Proglacial braided stream	2608
Ashworth, P. J., Best, L. J., Peakall, J., & Lorsong, J. A.	1999	Ashburton River gravels	Quaternary	Proglacial braided stream	4898
Beer, J. A. & Jordan, T. E.	1989	Jarillal/Huachipampa/Quebreda Fm.	Mid-Miocene	Ephemeral braided	6
Collinson, J.	1978	Various	N/A	Meandering	41
Cuevas Gozalo, M. C. & Martinius, A. W.	1993	Loranca Basin, Spain	Tertiary	Meandering/distal fan	63
Davies, D. K., Williams, B. P. J. & Vessell, R. K.	1992	Travis Peak Fm.	Lower Cretaceous	Meandering/Braided	4
Dreyer, T.	1990	Saltwick Fm./Aspelintoppen Fm.	Jurassic/Eocene	Delta plain channels	37
Dreyer, T.	1993	Esplugafreda Fm.	Palaeocene	Ephemeral stream	119
Dreyer, T., Falt, L. M., Hoy, T., Knarud, R., Steel, R., & Cuevas, J. L	1993	Escanilla Fm.	Eocene	Semi-arid braided/ meandering	27
Fielding, C. R. & Crane, R. C.	1987	Various	N/A	Various	115
Friend, P. F., Slater, M. J., & Williams, R. C.	1979	Various	Oligocene/Miocene	Various	5
Friend, P. F., Mahmood, R. S., Geehan, G. & Sheikh, K. A.	2001	Chinji Fm. Siwalik Group	Miocene	Various	194
Gibling, M. R. & Rust, B. R.	1990	Waddens Cove Formation	Pennsylvanian	High sinuosity channel	3
Hirst, J. P. P.	1991	Huesca System	Miocene	Fluvial fan	36
Lorenz, J. C., Heinze, D. M., Clark, J. A. & Searls, C. A.	1985	Mesaverda Group	Cretaceous	Meandering	273
Mjos, R., Walderhaug, O. & Prestholm, E.	1993	Various	N/A	Various	16
Nami, M. & Leeder, M. R.	1978	Scalby/ Saltwick Fm.	Middle Jurassic	Meandering/Braided	
North, C. P. & Taylor, K. S.	1996	Kayenta Formation	Lower Jurassic	Ephemeral stream	54
Putnam, P. E.	1983	Mannville Group	Lower Cretaceous	Anastomosing channels	2
Reynolds, A. D.	1999	Various	N/A	Various	41
Robinson, J. R. & McCabe, P. J.	1997	Morrison Fm.	Upper Jurassic	Sandy braided	129
Stear, W. M.	1983	Lower Beaufort Group	Permian	Splay	1
van der Neut, M. & Eriksson, P. G.	1999	Wilgerivier Fm.	Precambrian	Braided	73
Walderhaug, O. & Mjos, R.	1991	Scalby/ Saltwick Fm.	Middle Jurassic	Fluvial/delta plain	75
Visser, C. A. & Chessa, A. G.	2000	Cutler Formation	Upper Permian	Fluvial/aeolian	38

2.8.3 Modern analogues

Modern depositional fluvial systems can supplement outcrop studies by providing data that cannot easily be obtained from vertical cliff sections, including channel depths and widths, braiding patterns and sinuosities. Such information is currently used in reservoir modelling software. Studies such as Cant and Walker (1978) have investigated the depositional architecture immediately beneath the surface in the South Saskatchewan River, Canada. These modern river studies provide surface-to-subsurface links to aid in our understanding of the depositional architecture, which can be more difficult to establish in ancient outcrop sequences.

2.8.4 Empirical equations

Empirical relationships are often based on modern fluvial systems and extrapolations made to the subsurface. Empirical equations have been employed to relate palaeochannel depth, channel width and channel-belt width (Lorenz *et al.*, 1985) based on published formulae (Leopold and Wolman, 1960; Carlston, 1965) first used to calculate meander bend amplitudes and then channel-belt width. Estimates of channel width and channel-belt width of rivers are subsequently used to predict sandbody geometry. For example, by using uncompacted channel-bar deposits (Lorenz *et al.*, 1985), formative dune height cross-strata (Leclair *et al.*, 1997; Bridge, 1997) and point-bar dip angle and channel depth and width (Leeder, 1973), quantitative relationships have been derived between mean dune height and flow depth (Yalin, 1964; Allen, 1970). Misinterpretation of the depositional environment however, may lead to the inappropriate application of these formulae to depositional sequences.

2.8.5 Ground Penetrating Radar

Ground Penetrating Radar (GPR) is a non-invasive geophysical technique that can be used to constrain the three-dimensional within channel-belt scale architecture of fluvial sequences. The versatility of the GPR technique has been demonstrated in a number of studies (e.g. Gawthorpe *et al.*, 1993; Huggenberger, 1993; Aigner *et al.*, 1996; Bridge *et al.*, 1995, 1998; Aspiron and Aigner, 1999). GPR works on similar principles to seismic methods by emitting short pulses of electromagnetic energy which propagate into the ground. Some of this energy is reflected back from stratal reflectors of primary depositional fabric (e.g. bar foresets) to a receiving antenna. Data are received as two-way travel time, which can be used in conjunction with outcrop (e.g. Huggenberger, 1993) and vibracore (e.g. Bridge *et al.*, 1995) data to calibrate two-way travel time to true vertical depth. GPR data are processed and displayed in a similar format to seismic reflection techniques. These GPR techniques can allow the three-dimensional quantification of architectural elements behind an outcrop face. The limitation of GPR is that a choice has to be made between the depth of penetration and the architectural resolution gained from the sequence (i.e. resolution depletes at greater depths). Therefore, studies of fluvial deposits are often restricted low-level subsurface analysis of channel scale architecture (few metres to 10's metres).

2.8.6 Seismic profiling

Two-dimensional seismic profiling is commonly used to determine large-scale reservoir structure (e.g. 100 m vertical thickness). The resolution of seismic profiling is largely determined by the present reservoir depth and cannot therefore be employed in all situations. Seismic resolution becomes lower than the studied architecture at greater subsurface depth. At depths below several kilometres, resolution is generally no better than a few hundred metres and the internal architecture becomes seismically transparent (e.g. Mijussen, 1997). Three-dimensional seismic profiling has been used to determine the geometries of channel-belt sandbodies, providing information on channel-belt width and sinuosity (Weber, 1993; Brown, 1986; Burnett, 1996). To resolve channel sandbodies in the subsurface, the thickness generally has to exceed 10 m (Bridge and Tye, 2000). Seismic studies do not therefore capture the within channel-belt

architectural scale. Seismic techniques also suffer from problems of gas shadows, which can alter the seismic impedance and reduce the resolution of the architecture beneath.

2.8.7 Physical modelling

Previous physical modelling has focused on planform replication of the fluvial system (e.g. Schumm, 1977; Ashmore, 1982). During the early 1990s the construction of several experimental basin facilities allowing the preservation of an aggraded sediment sequence were developed at the University of Leeds, University of Minnesota and University of Utrecht. Aggrading physical models have the advantage of being able to recreate stratigraphy under precisely known, repeatable conditions. These have allowed the isolation and quantification of controls on the alluvial stratigraphy. Previous experiments have focused on the occurrence of fine-grained elements (Ashworth *et al.*, 1994), influence of lateral titling (Peakall, 1995), aggradation rate (Ashworth *et al.*,1999), and subsidence rate and pattern (Paola, 2000; Stokstad, 2000). The use of these physical models may provide insight into the most influential controls on the fluvial system. In recent years, the incorporation of aggradation into models has shown that physical modelling can not only provide information on the controls on alluvial architecture and heterogeneity (e.g. Ashworth *et al.*, 1994; Peakall *et al.*, 1996; Ashworth *et al.*, 1999; Paola, 2000, Stokstad, 2000) but can also be calibrated with outcrop studies (Ashworth *et al.*, 1999). Additionally, data from scaled models can provide the within channel-belt geometrical information (Table 2.3) required to fill the current data gap for reservoir simulation techniques.

2.8.8 Numerical models

Process-based numerical models have been developed to predict the distribution and geometry of channel-belt sandbodies within alluvial successions in two-dimension (e.g. Allen, 1978; Leeder, 1978; Bridge and Leeder, 1979) and more recently three-dimensions (e.g. Mackey and Bridge, 1995; Webb and Anderson, 1996). Process-based models are also used to examine the various allocyclic and autocyclic controls on

alluvial architecture and have been employed to interpret outcrop sequences. For example, the alluvial stratigraphy model of Bridge and Leeder (1979) has been used to interpret fluvial architectural styles in the Green River basin, Wyoming (Shuster and Steidtmann, 1987). While these numerical models involve simplification of the input parameters, they still offer a first order solution to the influence of controls on alluvial architecture. Models such as those of Bridge and Leeder (1979) were concerned with single thread channel-belts traversing an alluvial plain to construct two-dimensional stratigraphy. Development of three-dimensional models by Mackey and Bridge (1995) reveal that channel-belt proportion, connectedness and width and thickness of sandbodies are critically dependant on cross-section orientation and distance from the point of avulsion, factors which are not incorporated into two-dimensional models. The continual development of these models and the incorporation of factors such as multiple channel-belt systems and within channel-belt alluvial architecture is needed in future models.

2.9 Scales of heterogeneity

Cross (1991) highlights the need to treat and analyse each scale of heterogeneity within a reservoir to complement each other. The need to assess heterogeneity and predict reservoir performance from individual sandstone packages is clearly vital (Van der Graaff and Ealey, 1989). Physical modelling can quantify heterogeneity at the scale of the genetic sandbody (>0.001 to 0.5 km), which Van der Graaff and Ealey (1989), Lasseter *et al.* (1986) and Weber (1986) have defined. Physical modelling data may fill the gap between petrophysical scale data and channel-belt scale architecture, such as those modelled by Allen (1978), Bridge and Leeder (1979), and Mackey and Bridge (1995), and the scale of outcrop analogues studies, such as the Escanilla Formation (Dreyer *et al.*, 1993). Heterogeneity increases with decreasing scale of facies unit and increased mud/shales in the system (Galloway and Sharp, 1998).

On the smaller scale, features such as openwork deposits (e.g. Anderson *et al.*, 1999) have been identified as potential 'thief' zones for hydrocarbons and therefore need to be considered in any heterogeneity model. Failure to account for the within channel-belt

scale heterogeneities, which may form high and low permeability conduits, can result in the implementation of management techniques that cause early breakthrough of injected water in the reservoir (Weber, 1986).

Often several techniques will be used in a full appraisal of the subsurface architecture of any particular reservoir block. The different techniques described in this chapter provide data at different scales of heterogeneity to enhance reservoir understanding and Table 2.4 summarises where the most appropriate source of analogue data are available.

Table 2.4. Scales of heterogeneity for consideration of fluvial reservoir performance.

Scale		Example	Most appropriate data source
Field scale	1 - 10 km	Formation scale	Seismic
Reservoir scale	0.1 - 1 km	Channel-belt complexes	Outcrop analogue, seismic
Genetic sandbody scale	0.01 - 0.5 km	Architectural elements	Physical modelling experiments and field analogue Ground Penetrating Radar
Small scale	0.1 - 1 m	Petrophysical properties/sedimentary structures	Physical modelling experiments, well data and outcrops

2.10 Geological reservoir models

Reservoir hydrocarbon geologists and hydrogeologists are linked by common aims and consequently common modelling data needs. A large volume of literature now exists that addresses the needs of these two disciplines. Comprehensive reviews on hydrocarbon approaches to modelling are found in Bryant and Flint (1993) and Yaris and Chambers (1994), and for aquifer modelling in Fraser and Davies (1998) and the special issue of Sedimentary Geology (1999).

As subsurface datasets consist of scattered well data, appraisal of any reservoir requires the interpretation of the inter-well architecture. Inter-well alluvial architecture may be constructed using stochastic modelling techniques (Stanley *et al.*, 1990; Rudkiewicz *et al.*, 1990) based on a series of geologically constrained input parameters. Stochastic models generate a series of outputs (termed *realisations*) to complete the inter-well information about the reservoir architecture. Each realisation may be different, but

outcomes are common in their statistical regularity (Haldorsen and Damsleth, 1990). However, these stochastic models must honour the well data and statistical probabilities that they are conditioned on (Figure 2.27).

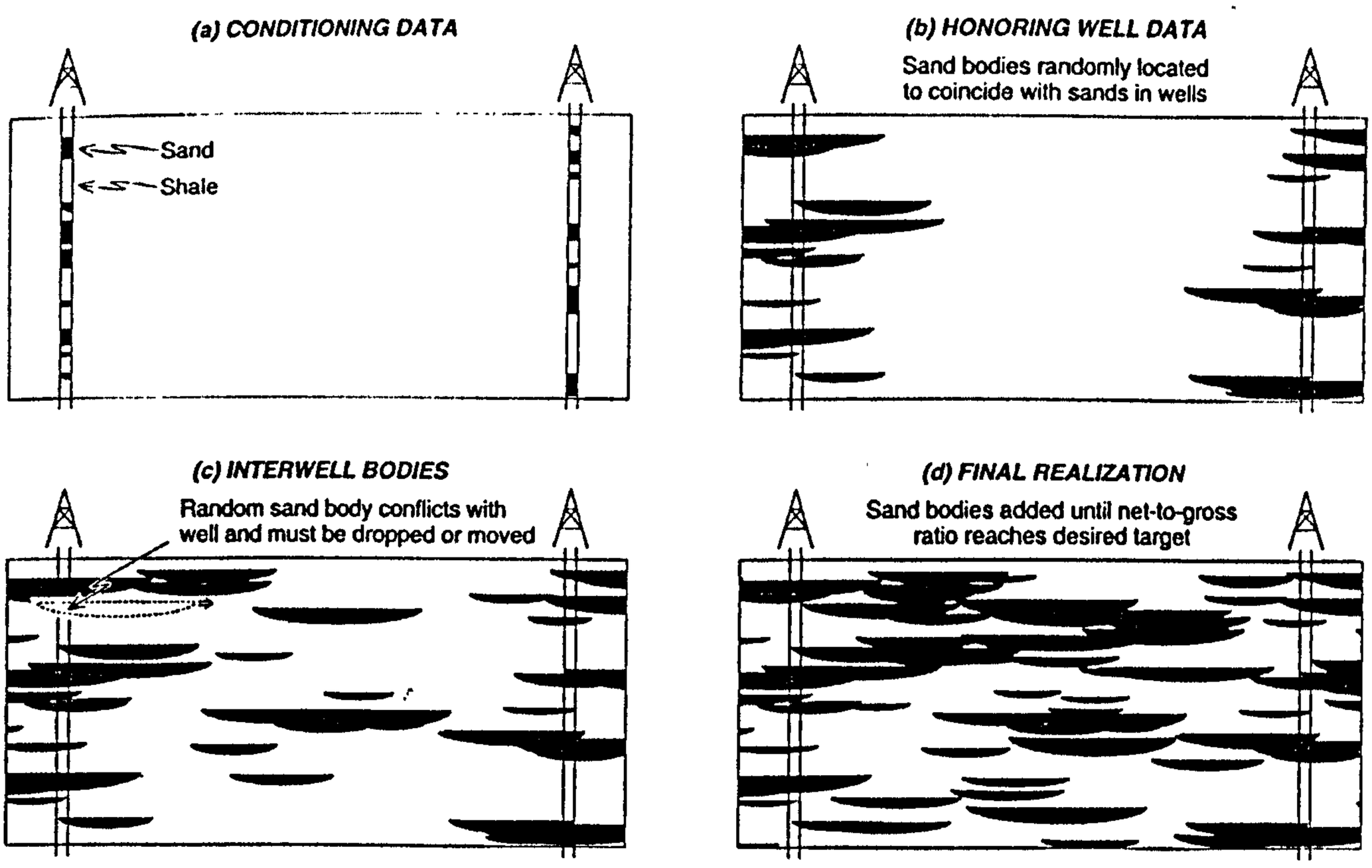

Figure 2.27. Steps for stochastic simulation of sand channels in a cross-section (From Srivastava, 1994).

The procedure of reservoir modelling generally uses a two stage approach: (1) the construction of a geological model (*Static* model) based on geologically constrained input data from wells and outcrop information; and (2) the incorporation of petrophysical information to allow a flow model to be constructed (*Dynamic* model). This reservoir modelling procedure may be accomplished using two general techniques; pixel-based and object-based modelling. These two techniques are addressed in the following section.

1. Pixel-based modelling is the simplest modelling technique and relies on data from core plugs on porosity and permeability to populate a particular reservoir block. Generally pixel-based modelling requires no information on the depositional geometries of the system. Stop data from vertical proportion curves can be used to populate the reservoir block with particular values of porosity and permeability data. Also particular petrophysical properties can be assigned to sit next to other values. This method takes no account of the depositional form and facies relationships to build the models, although by default it must incorporate some representation of the depositional form, because studies have shown there to be a link between petrophysical properties and grain size, and in turn, grain size and facies type (Begg *et al.*, 1989; Atkinson *et al.*, 1990; Lui *et al.*, 1996; Eschard *et al.*, 1998; Klinbeil *et al.*, 1999; Tye *et al.*, 1999; Vaughan *et al.*, 1999).
2. Object-based modelling (Deutsch and Wang, 1996, Figure 2.28) is a method whereby deterministic data from well-core, seismic lines and geophysical techniques are used to condition the stochastic simulation process (Storstad *et al*, 1999). The reservoir volume is populated with objects defined on a set of criteria such as width:length:thickness data. Flow cells are given a three-dimensional shape (defining volume) and petrophysical characteristics. Assignment of porosity and permeability data within objects can be calibrated based on facies-petrophysical relationships. The arrangement of objects can be defined using relationships of architectural elements to each other, for example, splays are always attached to channel margins (cf. Hirst *et al.*, 1993, Figure 2.29). Porosity and permeability data can be distributed within objects by pixel-based modelling approaches. These models can also incorporate erosional information, allowing one object to erode into the surface of another object. Many of these models are used to define the heterogeneities on the scale of the channel-belt architecture. The smaller-scale within channel-belt architecture is commonly not available for geological modelling. The limitations of current computing power often means smaller scale heterogeneities used in building a geological model are lost in the averaging and up-scaling procedure required to run fluid flow simulations. Studies such as Ashworth *et al.* (1994, 1999) have started to gain information on the individual channel-scale architecture by measuring the coarse- and fine-grained depositional niches in a scaled model of the Ivishak Formation and Ashburton River respectively.

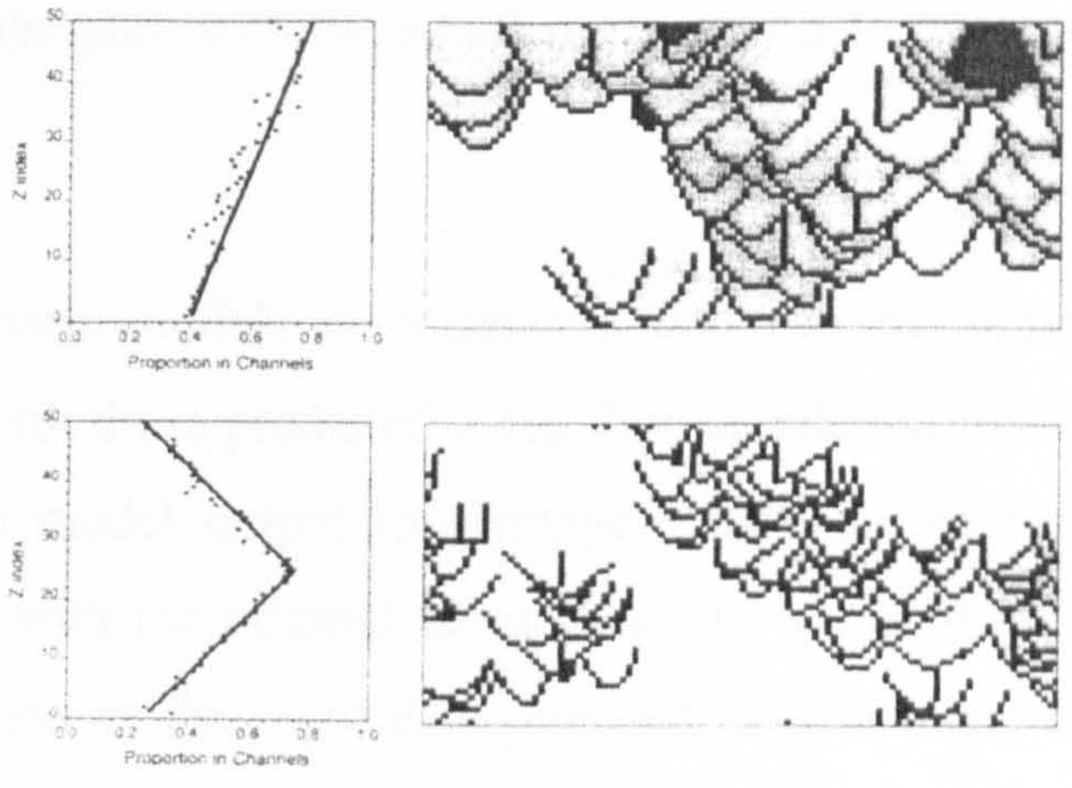

Figure 2.28. Vertical proportion curves (solid line) experimental results (black dots), and example section through two different object-based models condition on the proportion data (from Deutsch and Wang, 1996).

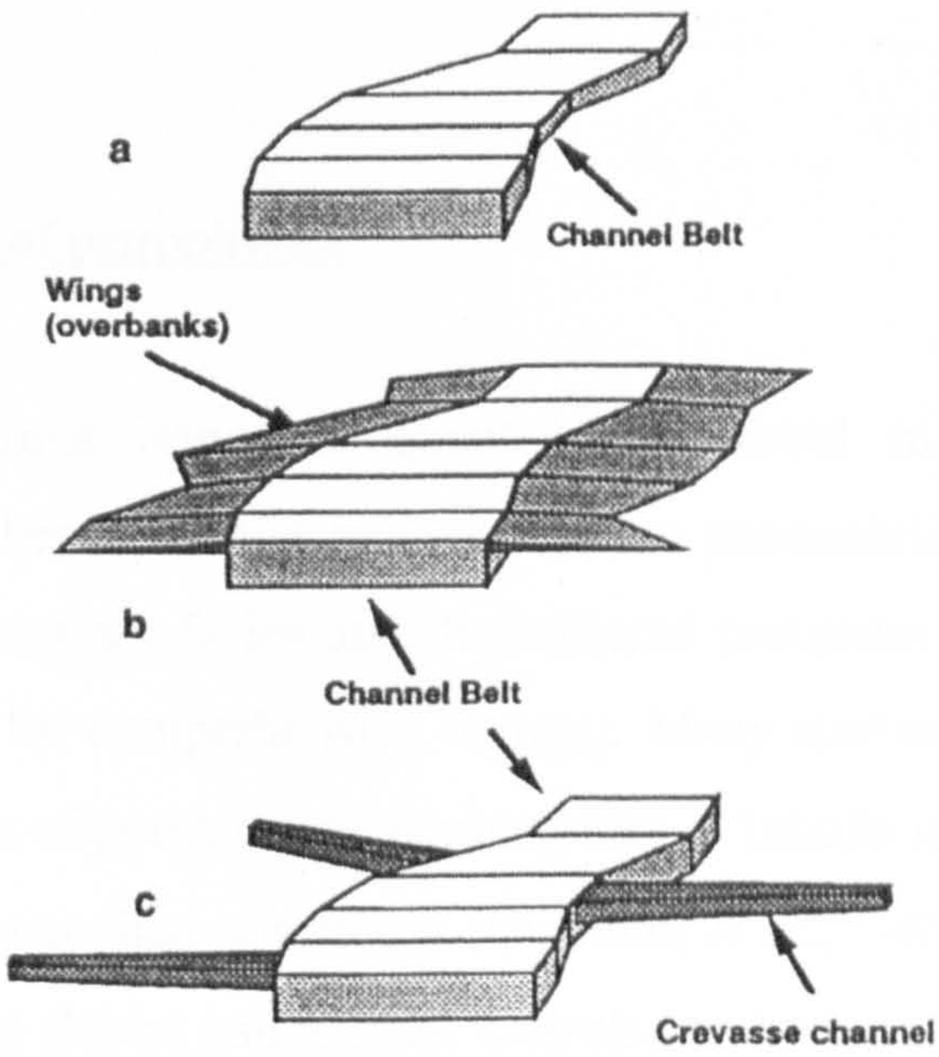

Figure 2.29. Geometrical shapes representing fluvial sandstone bodies, which are used in object-based modelling: (A) channel-belts, (B) with overbank sandstones, and (C) crevasse channels (from Hirst *et al.*, 1993).

A study by Seifert and Jensen (2000) found that the reservoir modelling outputs from pixel- and object-based reservoir modelling approaches for a braided river system were different, and a combination of the two approaches proved the most satisfactory in recreating braided river deposits. Pixel- and object-based approaches require no input on the formative processes to construct a three-dimensional reservoir block, and rely on the ability to simulate the subsurface architecture in the form of cells from geological examples from reservoir and outcrop studies. The way these cells from pixel- and object-based simulations knit together will create a pattern of high and low permeability

zones, resulting in the ability of the simulated reservoir to transmit fluids through the cells for extraction.

Validation of reservoir models is paramount and can be achieved by monitoring production curves with those predicted using flow simulation models, or by comparing the statistics of the model output (percentage occurrence of facies, geometries and interconnectedness) with the original input data. The value of any reservoir model is, however, only as good as the input data provided, and in many cases the models are conditioned by data from well logs, core and seismic lines, which have restricted resolution.

2.11 The incorporation of petrophysics

Permeability is the most important quantifiable control in reservoir fluid flow simulations and a number of studies assume that the permeability distribution patterns are a function of sedimentary facies and depositional processes (see Alexander, 1993; Brayshaw *et al.*, 1996 for comprehensive review). Many studies have tried to link the petrophysical properties of porosity and permeability to lithofacies types in a number of environments, including aeolian sandstones (Chandler *et al.*, 1989), carbonate reservoirs (Sahin *et al.*, 1998) and fluvial sandstones. Correlation between fluvial lithofacies and petrophysical attributes has been documented in both reservoir wells (Begg *et al.*, 1989; Atkinson *et al.*, 1990; Lui *et al.*, 1996; Eschard *et al.*, 1998; Tye *et al.*, 1999; Vaughan *et al.*, 1999) and onshore analogues (Ravenne *et al.*, 1987: Dreyer *et al.*, 1990; Jacobsen and Rendall, 1991). For example, the South Belridge Field (Miller *et al.*, 1990) shows a direct correlation between permeability and grain size. Grain size and sorting are the major controls on petrophysical properties (Brayshaw *et al.*, 1996). Therefore, the collection of geometrical facies data from analogues can be used to in conjunction with petrophysical-facies relationships (e.g. Figure 2.30) for extrapolation to the subsurface.

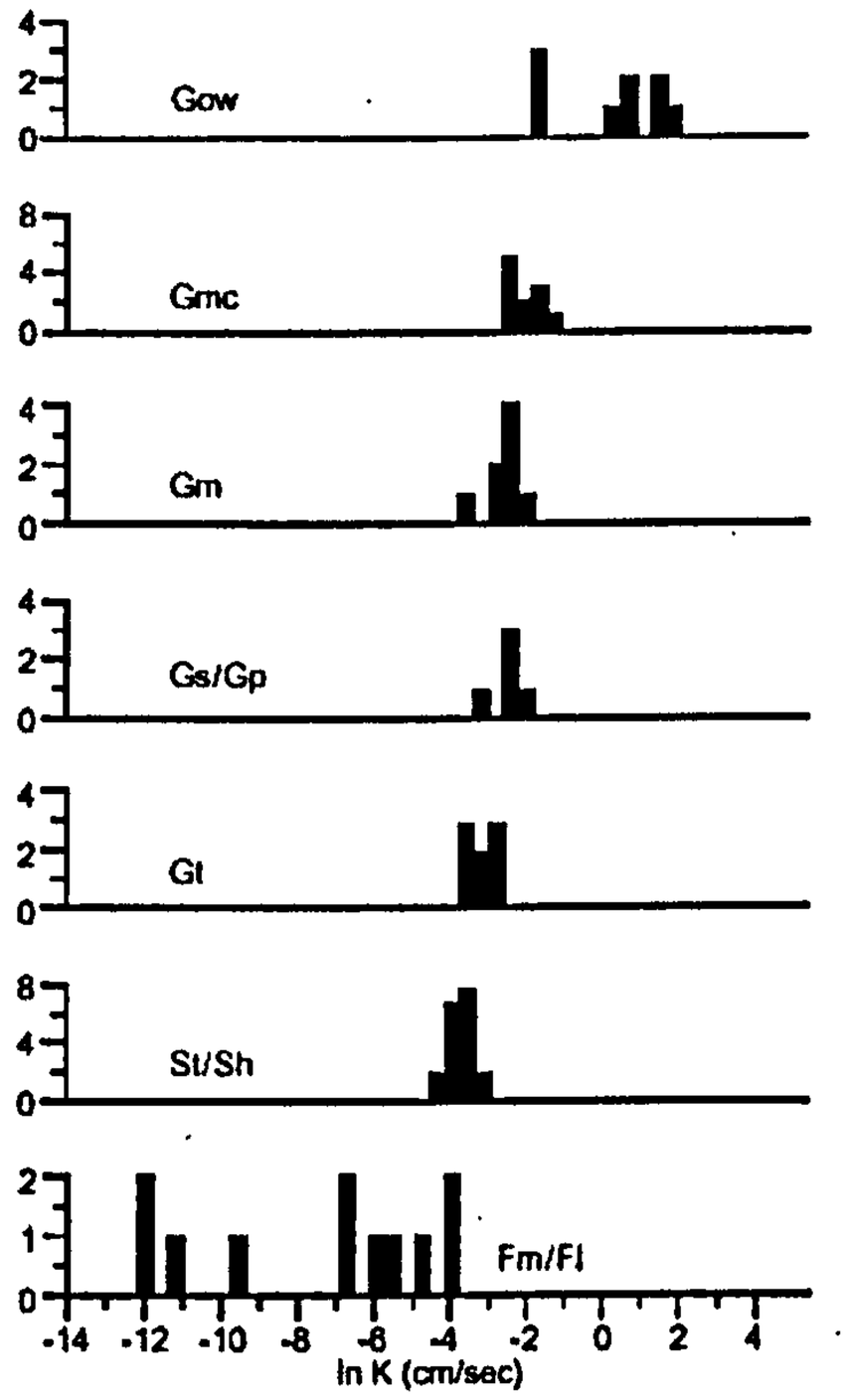

Figure 2.30. Distribution of values of permeability (ln K) for sediment samples from various hydrofacies in the Quaternary Stoughton gravel deposit (from Anderson *et al.*, 1999) showing the direct link between facies type and petrophysical attributes.

Typically, the needs of reservoir engineers have been difficult to fulfil with qualitative facies descriptions and so the usefulness of constructing a depositional model has been put into question. In order to provide useful sedimentological information: (1) a relationship between facies and petrophysical characteristics must be established; (2) facies must be given a three-dimensional shape; and (3) the distribution and frequency of occurrence of facies must be quantified.

To expand on points one and two, full hydrogeological characterisation of a sedimentary body must include a detailed description of its three-dimensional internal geometry (Webb, 1994). These architectural elements with characteristic petrophysical properties have been termed *hydrofacies* in the aquifer literature (Anderson *et al.*, 1999). This data requirement is forcing the development of quantitative facies models (Dominic *et al.*, 1998) and the quantitative datasets gained from studies are being collected for flow simulations (Willis and White, 2000).

Difficulties in identification of the two- and three-dimensional shape and frequency distribution of facies from subsurface and outcrop studies is being combated by the use

Difficulties in identification of the two- and three-dimensional shape and frequency distribution of facies from subsurface and outcrop studies is being combated by the use of geostatistical information techniques such as vertical and horizontal proportion curves (Ravenne and Beucher, 1988) and variograms (Davis *et al.*, 1993; Kupferberger and Deutsch, 1999), which allow rapid characterisation of trends and distributions of alluvial architecture. These data are commonly being used to assess facies within a reservoir in a quantitative way to provide inputs to geological reservoir models (Davis *et al.*, 1993).

2.12 Up-scaling and dynamic simulation modelling

Following the construction of a geological model, the reservoir block is exported into a flow simulation package to develop a dynamic model. Up-scaling of the three-dimensional geological model is carried out to enable flow simulation modelling to be performed. This up-scaling procedure involves reducing the geological detail, which results in the channel-belt architecture being lost while petrophysical properties are averaged within flow cells. This up-scaling methodology is routinely carried out, although there has been limited investigation into the three-dimensional within channel-belt architecture influence on flow behaviour. Up-scaling studies show that different scale heterogeneities have significant effects on multiphase flow behaviour (Lasseter *et al.*, 1986; Mansoori, 1994). Development of heterogeneity modelling software is out-pacing the collection of input parameters to test and validate the modelling. As computing power increases, the smaller scale heterogeneities will be incorporated into models. Once flow cell size is reduced by one or two orders of magnitude (architectural element scale) there will be a need for a host of within channel-belt architecture information.

2.13 Summary

This chapter has highlighted the following points:

1. Alluvial architectural trends are the result of a complex combination of allocyclic and autocyclic controls that are inherently linked, many of which are often inferred from alluvial sequences. Disentangling these controls from outcrop studies is often difficult. No single autocyclic and allocyclic controlling mechanism may be attributed to the response of rivers and/or be diagnostic for any particular stacking pattern. Additionally, two or more controls may produce the same resultant effect. The task of ranking autocyclic and allocyclic controls in order of importance for any particular fluvial system needs to start with the isolation of individual controls via physical or numerical modelling.
2. Grain size has been identified as a key variable and control on within channel-belt and channel-belt alluvial architecture. Alluvial architecture models commonly assume that the drainage system is supplied by two distinct grain size populations, which form fine-grained floodplain and coarse-grained channel-belt sandstones deposits, while making no incorporation of the differences in initial sediment supply grain size and modification of this grain size distribution downstream. Additionally, while many studies have considered the controls on, and rate of, downstream fining in relation to downstream changes in channel pattern and morphology, the link to the subsurface has been largely unexplored and requires quantification for realistic three-dimensional alluvial architectural models to be constructed.
3. Field and reservoir studies have established the link between facies type and petrophysical properties. Therefore, any downstream changes in the magnitude and sorting of grain size distribution may affect the geometry and frequency of occurrence of facies, and consequently the petrophysical properties. Hence, without a full understanding of architectural element geometries associated with these downstream trends, conceptual and quantitative stratigraphic models are limited.
4. The prediction of subsurface geometrical characteristics from any particular fluvial sequence carries considerable prerequisites before application. Sandbody geometry is determined by channel pattern, autocyclic and allocyclic controlling mechanisms and stacking pattern. As a result, sandbody geometries may vary significantly within the same depositional sequence. The prediction of channel-belt sandbody geometries

and their distributions requires a full quantitative and qualitative characterisation of any reservoir sequence and outcrop analogue study.

5. A compilation of the literature reveals a paucity of quantitative architectural studies and those documented are often limited to two-dimensional outcrop studies at the channel-belt scale. Consequently, alluvial architecture models have focused on the channel-belt scale sandbody alluvial architecture. The development of pixel- and object-based geological reservoir simulation and flow simulation software is driving the need to provide well-constrained quantitative datasets on smaller scale within channel-belt architecture. These data may be provided using a variety of techniques and the benefits of an integrated approach show how subsurface heterogeneity can be more successfully evaluated.

Chapter 3. The sedimentology and depositional environment of the Lower Ketch Member, Tyne Field, Southern North Sea, UK

3.1 Synopsis

This chapter examines core data from the Lower Ketch Member (Westphalian C-D), Tyne Field, Southern North Sea, UK. Investigation of alluvial architecture shows a depositional sequence comprising of channel-belt sandstones containing subordinate amounts of conglomerate (60%) alternating with shales (40%), which have been reddened by multiphase oxidation. Sedimentology is discussed and a fourfold sandbody classification scheme based on vertical facies profiles is proposed. A depositional model is outlined for an aggrading alluvial plain where channel-belt and floodplain deposition occurred coevally. Floodplain areas were periodically inundated with floodwaters and may have formed ephemeral lakes. The net-to-gross ratio suggests that in parts of the reservoir interval the sandbody connectivity is problematic for hydrocarbon extraction. The lack of correlative marker horizons make the prediction of channel-belt scale sandbody geometries difficult. UK onshore analogues are evaluated and their use for providing geometrical data rejected. Finally, a direct correlation between facies type and permeability is established, which would permit the incorporation of facies into dynamic fluid flow modelling.

3.2 Introduction

In recent years there has been renewed interest in the Southern North Sea (SNS) as a major gas producing region. In particular the top Carboniferous Barren Red Beds have yielded several important gas reservoirs (e.g. Mijnssen, 1997; Stone and Moscariello, 1999). Description and quantification of inter-well stratigraphy is paramount to successful reservoir development strategies of these Barren Red Bed sequences during secondary development phases. The Barren Red Beds are seismically transparent (Mijnssen, 1997) and, therefore, predicting the alluvial architecture is even more difficult. The Barren Red Beds are composed of coarse-grained sandbodies alternating with pervasively reddened overbank fines, which correspond to the reservoir rock and non-reservoir rock, respectively. Studies such as Besly *et al.* (1993) have speculated that the sandstone bodies of the Ketch Member were mainly deposited as incised valley fills

and have a predominantly shoe-string form and poor lateral continuity. More recent studies by Mijnssen (1997) and Stone and Moscariello (1999) suggest that sandbodies within these red beds represent a combination of incised valley fills and aggrading braided channel-belts. Alluvial architectural models (e.g. Bridge and Leeder, 1979; Shanley and McCabe, 1993), reviewed in Chapter 2, may predict different stacking pattern scenarios for incised valley fills where channels-belts are laterally confined, as opposed to rapidly aggrading braided channel-belts, which may avulse and migrate across the developing braidplain. Consequently, in order to reliably predict the alluvial architecture of the Barren Red Beds, an assessment of the depositional environment is required and, critically, channel-belt sandbody geometry needs to be quantified.

This chapter documents the results gained from the examination of eight well cores (total of core length: 909.15', with deviations from the vertical between 0 to 64°, Appendix A, Figures A1-8), combined with an extensive literature search on the sedimentology and depositional environment of the Westphalian age Tyne reservoir, SNS.

The aims of this investigation are:

1. To characterise the sedimentology, lithofacies, hydrofacies and sandbody types present within the Lower Ketch Member, Tyne Field, Southern North Sea.
2. To determine a depositional model for the Lower Ketch Member and fit this model into the regional palaeogeography for the Southern North Sea region.
3. To predict sandbody geometry and connectivity to aid interpretation of the inter-well alluvial architecture within the Lower Ketch Member reservoir interval.
4. To evaluate outcomes of 1-3 to suggest a suitable onshore analogue for the Lower Ketch Member.

3.3 Background to the Tyne Field

The Tyne Gas Field is located in Quadrant 44, Block 18, SNS, and lies within the Silver Pit Basin north of the Sole Pit inversion (Figure 3.1). The reservoir deposits are late Carboniferous in age, Westphalian C-D (~311-305 Ma) within the Schooner Formation. The reservoir sequence is composed of thick fluvial sands and conglomerates (60 %) alternating with thick overbank shale zones (40 %). The upper surface of the Tyne reservoir zone is bounded by an unconformity beneath the Permian Rotliegend Group (Silver Pit Formation). The Basal Permian Silver Pit shales provide a regional top seal. The underlying coal measures provide the source rock for the reservoir. The Schooner Formation is dominated by red beds that are informally divided into the *Upper* and *Lower* Ketch Member (Cameron, 1993). The principal reservoir zone is the Lower Ketch Member with a maximum thickness of 150 m at a depth of ± 3700 m true vertical distance (tvdss). The Upper Ketch Member provides an additional reservoir unit in the North Tyne, although this is not the focus in this thesis. The Upper Ketch sands are thinner than those found in the Lower Ketch interval (Collinson and Jones, 1997) and the sequence has a lower net-to-gross than the Lower Ketch Member. The higher shale proportion results in the Upper Ketch acting as seal horizon rather than a reservoir horizon. The contact between the Lower and Upper Ketch Members can be observed in well 44/18a-5, core depth 12526.8' (Appendix A, Figure A8).

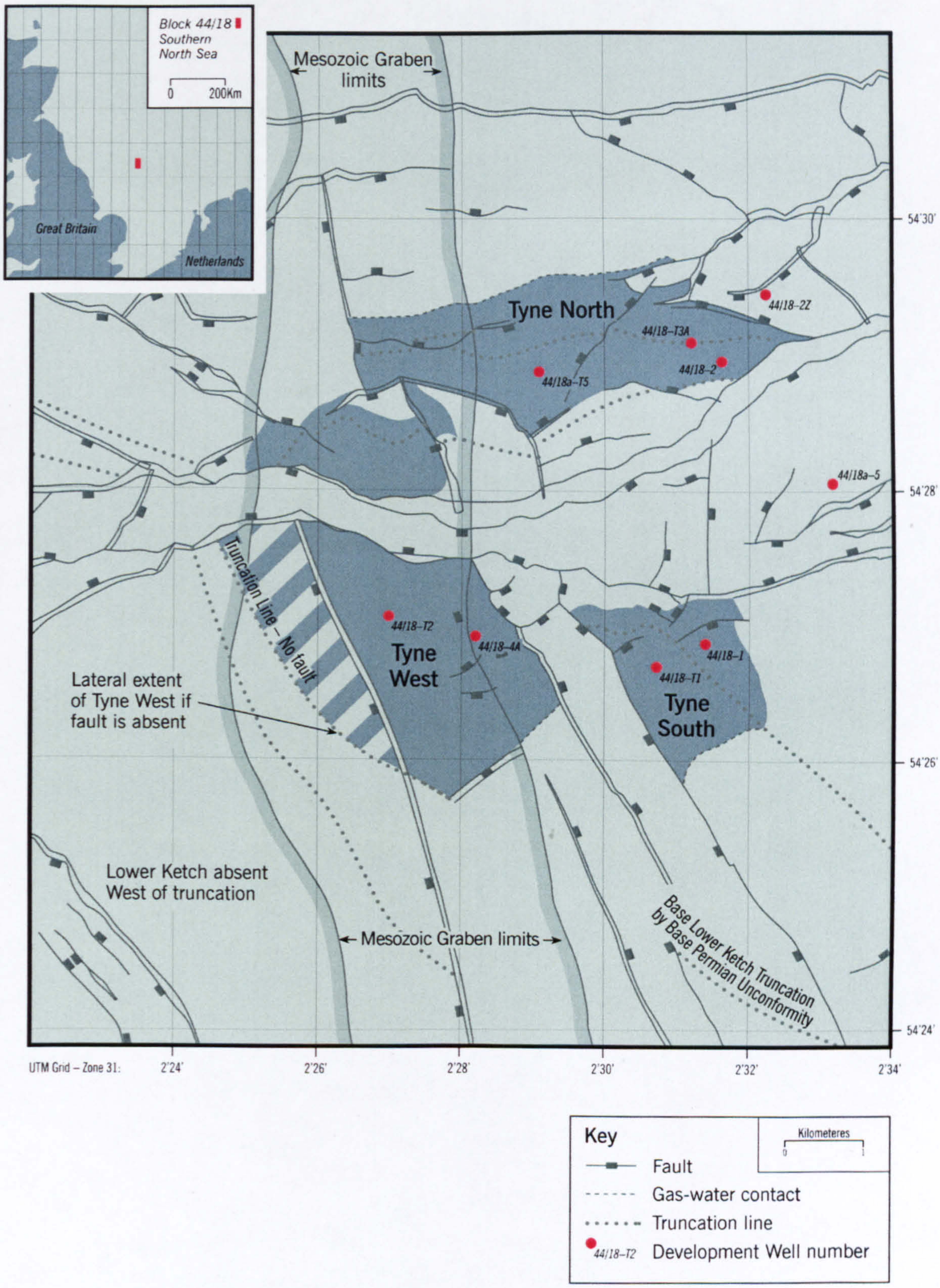

Figure 3.1. Location of the Tyne Field, Southern North Sea, showing the three main gas accumulations at the top Lower Ketch depth map (modified from Cooper, 1995).

3.3.1 Lithostratigraphic nomenclature of the UK Southern North Sea

A comprehensive nomenclature scheme has been constructed for the North Sea (Cameron, 1993) to provide a lithostratigraphic framework to facilitate stratigraphic correlation and inter-well interpretation across fields. The Lower Ketch Member is part of the Schooner Formation, which forms the top part of the Conybeare Group, and which also comprises the Caister Coal Formation and the Lower Westoe Coal Formation (Figure 3.2). In some parts of the Silver Pit Basin the Conybeare Group is more than 1500 m thick. Seismic and biostratigraphic data highlight an unconformity overlaying the Westphalian B aged Westoe Coal Formation, corresponding to high energy coarse-grained sediments that have been deposited over a flat lying deltaic plain environment. The Schooner Formation is a composite of sandy coal measures of deltaic origin (e.g. Fielding, 1984, 1986) and overlying primary red beds of Westphalian C age. These changes in facies resulted from a gradual elevation in land surface providing better drainage conditions.

The Schooner Formation is described as having alternating mudstones and channel-fill sandstones. Deposits have been previously named the 'Barren Red Beds' (Rhys, 1974), 'Barren Red Measures' (Leeder and Hardman, 1990), and 'Barren Red Group' (Besly, 1990). The Ketch Member has a maximum thickness of 550 m in the Silver Pit Basin area. The Lower and Upper Ketch Members of the Tyne Field correlate with onshore UK stratigraphic analogues of the Etruria (Besly, 1988; Glover *et al.*, 1993) and Keele Formations of Central England (Besly *et al.*, 1993) respectively. The Etruria and Keele Formations exhibit different facies trends to those observed in the Lower and Upper Ketch Members (cf. Besly and Turner, 1983). This is discussed further in Section 3.13. Westphalian strata were gently folded, faulted and variably eroded prior to the deposition of overlying Lower Permian desert sediments.

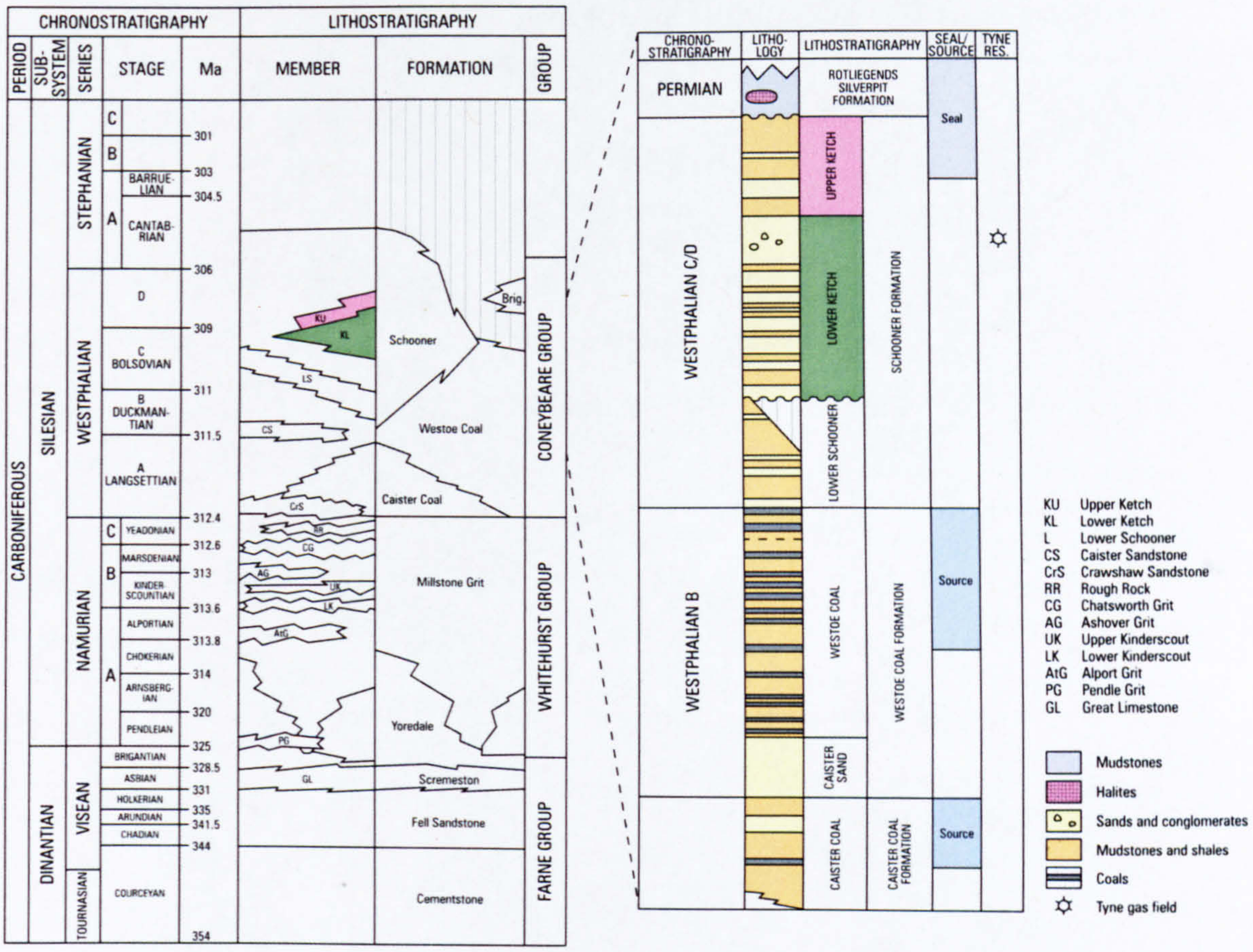

Figure 3.2. Stratigraphic nomenclature of the Southern North Sea and location of the Tyne reservoir interval (modified from Cooper, 1995).

3.3.2 Seismic, chemostratigraphic and biostratigraphic subdivision of the Tyne Field

The Barren Red Bed reservoir zones of the SNS are noted for being seismically transparent (Mijnssen, 1997, Stone and Moscariello, 1999). The resolution of seismic data is limited to the definition of unconformities at the top and base of the reservoir and not the internal sandbody architecture. Consequently, alternative methods have been previously employed to refine the resolution of the internal architecture of the reservoir interval. Chemostratigraphy has been used to subdivide the Barren Red Beds both onshore (Pearce *et al.* 1999) and offshore (Stone and Moscariello, 1999; Pearce, 1995). Reservoir subdivisions are restricted to the base of the Upper Ketch Member and the T-horizon, which is the transitional zone from the higher net-to-gross Lower Ketch interval to the low net-to-gross Upper Ketch Member. Additionally, the continental deposits of the Ketch Member are devoid of marine marker horizons, which enhances difficulties in chronological correlation. Palynological analysis on well cores from 44/18 - T1 (Mclean, 1996) revealed that preservation of palynomorph samples was

barren to poor, particularly in the grey coarse to very coarse sandstones, which are traditionally viewed as unsuitable for palynology. Organic maceral recovery within samples from core 44/18-1 is very poor. Organic material has been destroyed by the oxidising conditions prevailing at time of deposition (Lake, 1992) and therefore, biostratigraphic control on the Lower Ketch sequence is scarce.

In summary, although broad subdivisions can be defined within the Tyne reservoir using the methods outlined above, the definition of channel-belt sandbody scale depositional architecture is limited. Therefore, comparison of core data with outcrop analogue sequences may be more appropriate.

3.4 Regional geological setting

In the late Devonian and early Carboniferous the broadly east-west convergence of Laurussia and Gondwana (Leeder, 1988a, 1988b) caused northerly subduction of the oceanic crust and the onset of an extensional regime, which created the Variscan mountains and developed the Western European Carboniferous Basin (WECB) (Figure 3.3a). The WECB extended in an east-west trending zone from Germany across Europe to Ireland. At this time much of Britain and the North Sea were lying in a paralic sedimentary environment (Ziegler, 1990; Evans *et al.*, 1992). The Southern North Sea area developed into a broad back arc-region (Hollywood and Whorlow, 1993) within this extensional regime and extensional faulting occurred. This back-arc extension had largely ceased by the Westphalian B and had been replaced by thermal subsidence. Thermal subsidence is thought to have produced a more uniform subsidence pattern and consequently more a uniform distribution of sediment thickness in the Westphalian (Leeder, 1987; Leeder, 1988, Leeder and Hardman, 1990; Maynard *et al.*, 1997). With continued northward advancement of the of the Variscan mountain front, the tectonic regime changed from a passive thermal subsidence to one of compressional tectonics, causing the formation of a flexural foreland basin, and leading to the closure of the Rheic Ocean (Besly, 1990). Consequently, the SNS basin had a restricted inflow of ocean water (Quirk and Aitken, 1997) with depocenters that were controlled by earlier Carboniferous rift faults (Leeder and Hardman, 1990). From mid-Westphalian B, compressional tectonics continued to dominate the patterns of sedimentation, causing increased folding and faulting, which elevated the land surface and created a regional

unconformity in the late Westphalian C and D. During the Westphalian C sedimentary facies changed from coal-bearing delta plain to alluvial plain environments (Hollywood and Whorlow, 1993) with associated red bed formation. Fluvial systems expanded and migrated south during the Westphalian C and D and increasingly dominated the basin fill sequences (Leeder, 1988). The SNS basin was bounded by Pennine uplift to the west, the Mid-North Sea High (MNSH) to the north and the London-Brabant Platform to the south (Glennie and Boegner, 1981). Major river systems from the northern Laurentian-Fenno-Scandian High provided the main source of sediment supply to the SNS basin (Cowen, 1989; Leeder *et al.*, 1990; Besly *et al.*, 1993; Collinson *et al.*, 1993; Quirk, 1993) with additional supplies from the Anglo-Brabant Massif to the southeast and the Variscan Mountains in the south (Leeder *et al.*, 1990; Besly *et al.*, 1993; Collinson *et al.*, 1993; Quirk, 1993). Mijnssen (1997) identified that channel orientations within the Schooner Formation were predominantly NE-SW with some SE-NW and much of the sand delivered to the basin was from the north. Additional sand deposited within the SNS basin resulted from intra-basinal reworking by the erosion of growth folds (Leeder and Hardman, 1990).

Deposition in the SNS basin resulted in Westphalian sandstone strata thinning to the south and disappearing south of latitude 54°45' (Collinson and Jones, 1997) where zones became dominated by lacustrine sedimentation. Fluvial sandstones reappear further south near to the Variscan front as a result of southerly supplied fluvial systems. The Tyne Field gas accumulations lie between latitudes of 54°25' - 54°30' (Figure 3.1) and are therefore situated in the area dominated by lacustrine sediments. Collinson and Jones (1997) documented a decrease in sandbody size from north to south. Basin inversion during the final stages of the Variscan deformation caused a gradual elevation in the area causing subaerial exposure and subsequent erosion before burial beneath the base Permian sediments. During the late Westphalian to early Permian the foreland basin was subjected to the Saalian rifting event, which led to the formation of E-W and NW-SE normal faults that tilted and offset Westphalian strata. This active faulting during the end of Westphalian C/D may have resulted in local uplift and subaerial exposure of the Lower Ketch and Westoe Coals Formation associated with the Variscan Orogeny, which were eroded and redeposited in the Upper Ketch (Cooper and Merryweather, 1994). South of latitude 54°, Westphalian strata thicken, caused by post-depositional unroofing during erosion in the base Permian (Quirk and Aitken, 1997).

While facies patterns of onshore late carboniferous red beds show strong tectonic control (Besly, 1988), the influence offshore is more ambiguous. The Westphalian strata are uniform and were not affected by syn-depositional faulting and folding (Quirk and Aitken, 1997). Syn-depositional fault activity affected facies distribution in a subtle way and therefore, evidence of syn-depositional faulting within the area of the Tyne Field may be difficult to quantify and over few kilometre distances may be negligible. However, the relationship between faulting and sediment distribution requires more investigation when considering the regional facies distributions. The quality of seismic within the Carboniferous is variable and much of the timing of the faulting and folding is poorly constrained. In addition to this, post-depositional uplift and erosion has caused the removal of the Westphalian sediments creating difficulties in regional correlation. In summary, while uncertainties lie with the syn-sedimentary impact on sediment accumulation, it is recognised that tectonics can have a significant affect on alluvial architecture (see Chapter 2) and therefore, future studies must attempt to improve the understanding on the tectonic-sedimentation relationships in the SNS basin.

4.4.1 Regional palaeoclimate

The British Isles and offshore UK situated north of the Hercynian orogenic belt lay at an equatorial to sub-equatorial latitude during the Carboniferous. Towards the end of the Carboniferous there was a change in climate associated with a general drying trend. The removal of the low-latitude moisture source changed rainfall patterns to a more seasonal (monsoonal) regime (Rowley *et al.*, 1985). Rainfall would have been concentrated along the coastlines of Tethys and western high mid latitudes. Patterns would produce climatic zones that were more parallel to the continental outline (Francis, 1994), creating unsteady discharge patterns with flood events that were able to carry coarse sediment in channels and induce overbank flooding and splays. Although climate was drying out and becoming more arid (Hedemann and Teichmuller, 1971) in the Westphalian D, vegetation was still present on the land surface (Quirk, 1997). Changes in floodplain flora may have resulted from changes in the late Carboniferous climate. In Euroamerica, a change from lycopod dominated to tree-fern dominated floras were related to a drying phase at the Westphalian/Stephanian boundary (Francis, 1994). Often vegetation was limited to Calamites and only incipient soils formed before burial curtailed soil development. Changes in vegetation may have controlled channel stability of the fluvial

drainage system. During late Westphalian C-D times basin infill was predominantly non-marine and saw the expansion of alluvial plain deposition resulting from a progressive southward migration of an arid climate belt. This climate shift led to an improvement in drainage conditions and the establishment of an alluvial plain in place of the former waterlogged plains of the underlying Westoe Coals deposits (Lopez-Gamundi *et al.*, 1993). Red beds acquired their pigmentation by syn-depositional oxidation of the alluvial overbank deposits in relatively well-drained soil profiles. Long-term climate variations created a fluctuating groundwater table, causing the oxidation of sediments close to the surface (Besly and Turner, 1983). The SNS basin was situated in the rain shadow of the Hercynian mountains (Besly, 1988), causing extreme aridity in the lee of these mountains (Glennie, 1983). However, the main sediment source area, which was several 100 km to the north, would have remained relatively unaffected by climate change during the late Carboniferous (Quirk, 1997). In summation, a general drying trend is evident throughout the late Westphalian and early Permian, which was punctuated by smaller scale climate fluctuation. These smaller scale climate fluctuations may have influenced the alluvial architecture of Lower Ketch Member.

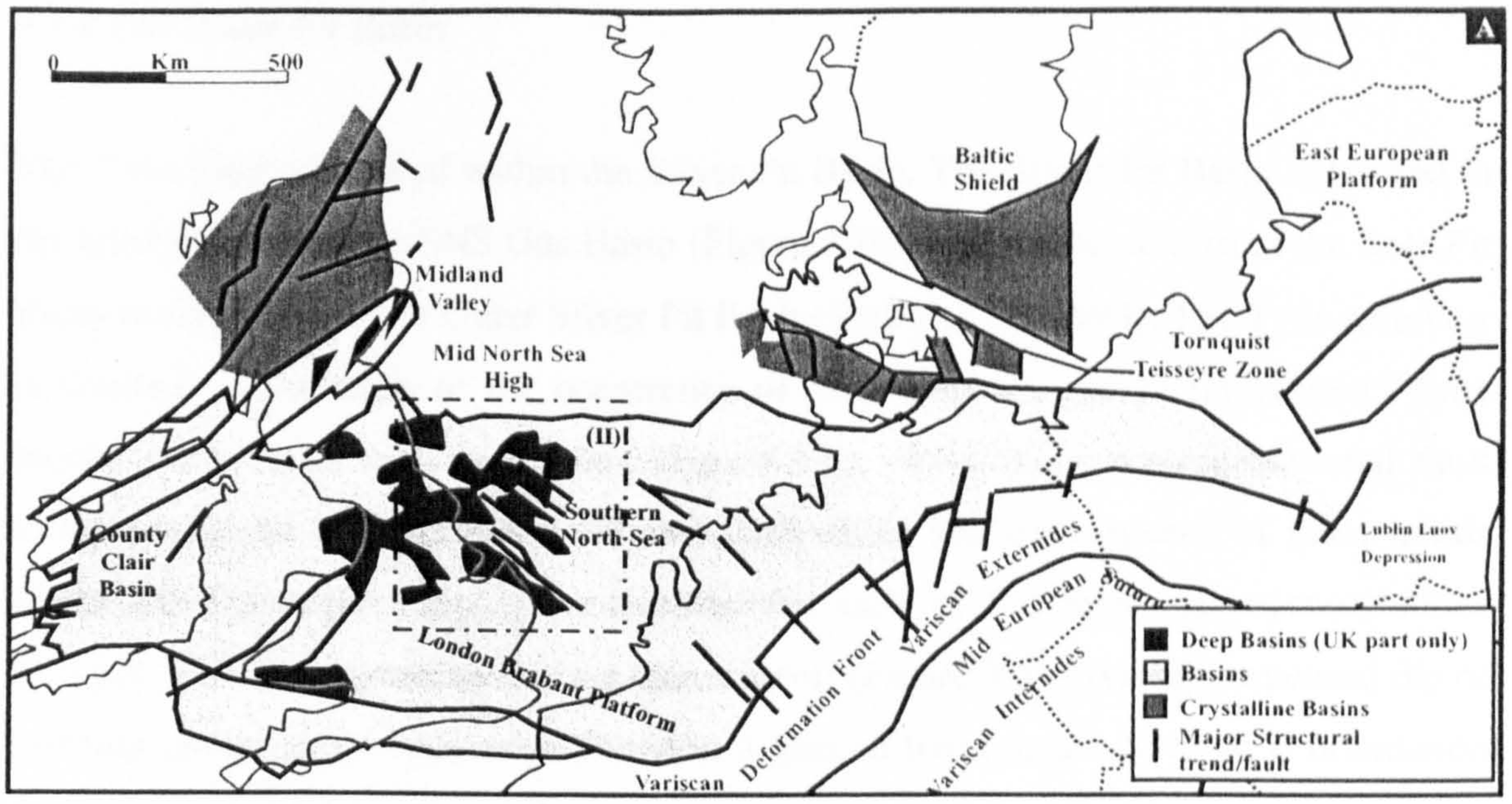

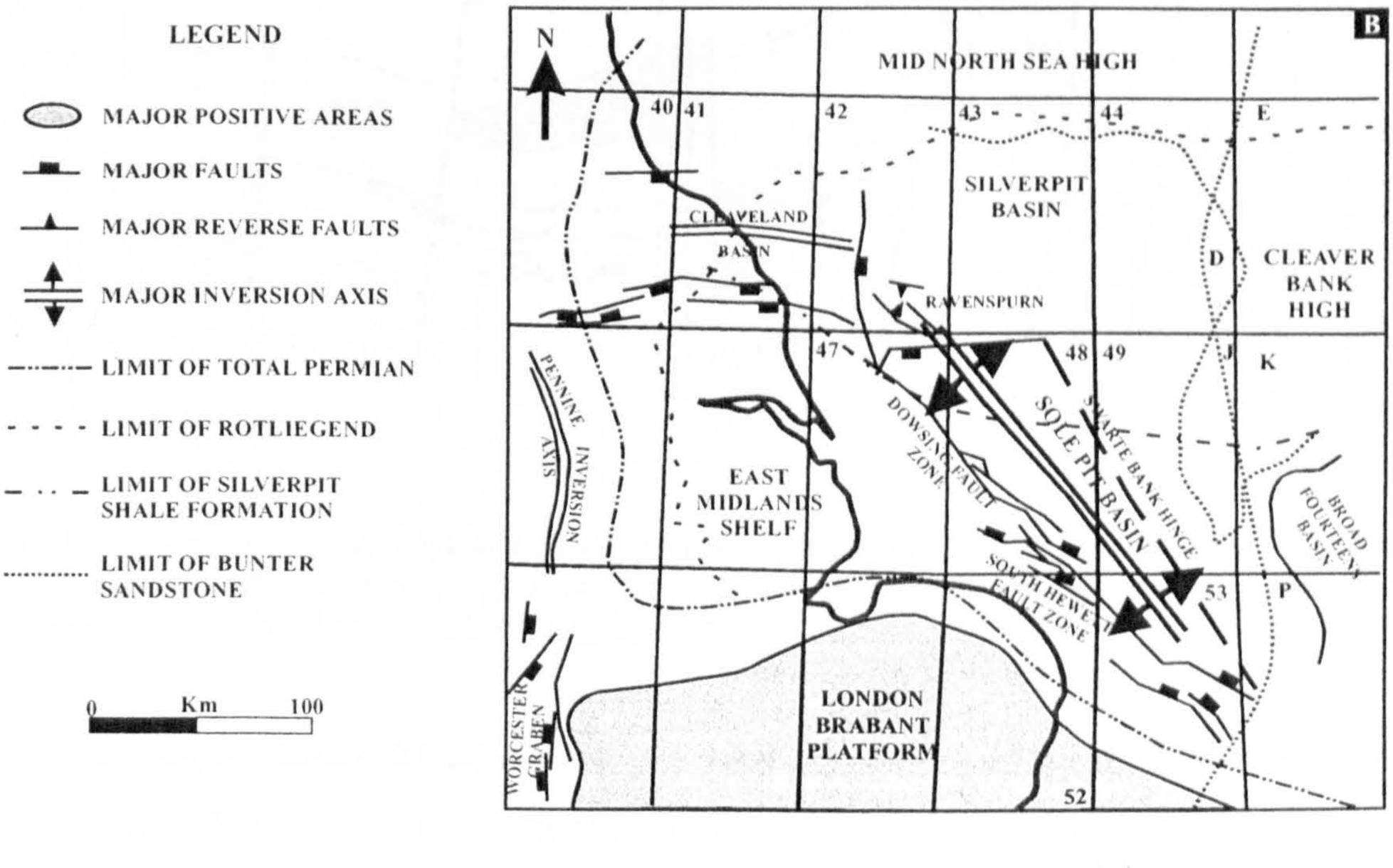

Figure 3.3. Simplified structural map of the (a) Western European Carboniferous Basin (modified Maynard *et al.*, 1997), and (b) the Southern North Sea (modified from Bailey *et al.*, 1993).

3.4.1 The Silver Pit Basin

The Tyne Field is located within the Silver Pit Basin. The Silver Pit Basin is located in the northern part of the SNS Gas Basin (Figure 3.3b) and is separated from the Sole Pit Basin to the south by the Outer Silver Pit Fault (Bailey *et al.*, 1993). The Tyne reservoir is divided on the basis of the occurrence of three separate gas accumulations: Tyne North, Tyne South and Tyne West (Figure 3.1). Two main post-depositional fault trends are found in the basin: E-W and NNW-SSE. The convergence of these trends forms the structural trapping mechanism for each of the three gas accumulations (Cooper, 1995), compartmentalising the reservoir (Figure 3.4). Average structural dip of bedding planes show beds are inclined in a general trend to the NNE to E orientation with dips ranging from 4° to 16°.

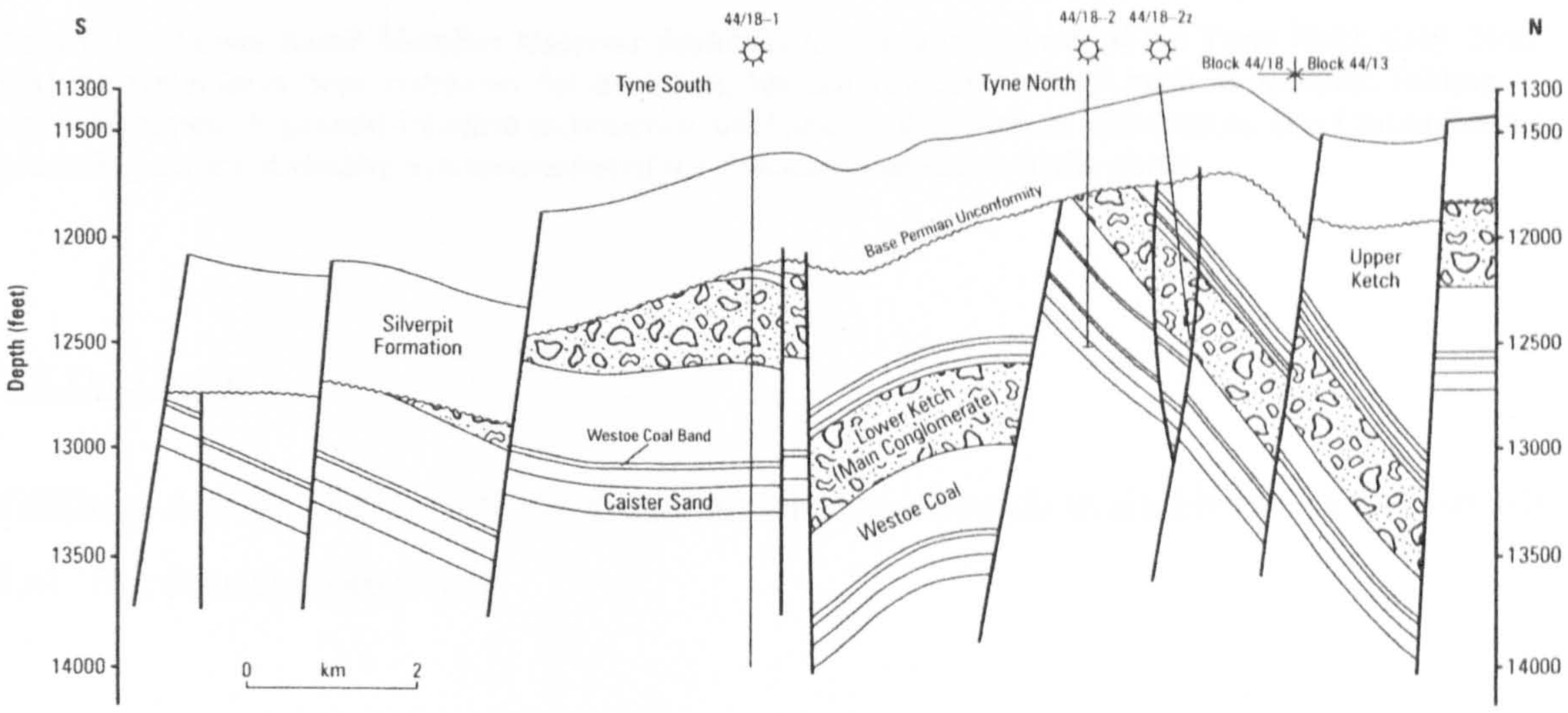

Figure 3.4. Structural cross-section based on a 3-D random track Tyne South-Tyne North of the Southern North Sea Upper Carboniferous deposits. Note: the main reservoir target of the Tyne reservoir interval is the Lower Ketch Member (modified from Cooper, 1995).

Lower and Upper Ketch Members are progressively truncated by the Base Permian unconformity. This progressive truncation has caused the Upper Ketch Member to be completely removed from the crest of the Tyne North Structure. In the Tyne North the Silver Pit Formation and Upper Ketch Member act as top seals for the Lower Ketch reservoir. A wedge of Upper Ketch shales beneath the Permian sequence forms the stratigraphic sealing of the Tyne West and Tyne South. Removal of parts of the Lower Ketch Member in the north results in a progressive, structurally controlled, thickening of the interval to the south (Figure 3.5). The post-depositional structural control on the Tyne Field is not the focus for this thesis and is not discussed further.

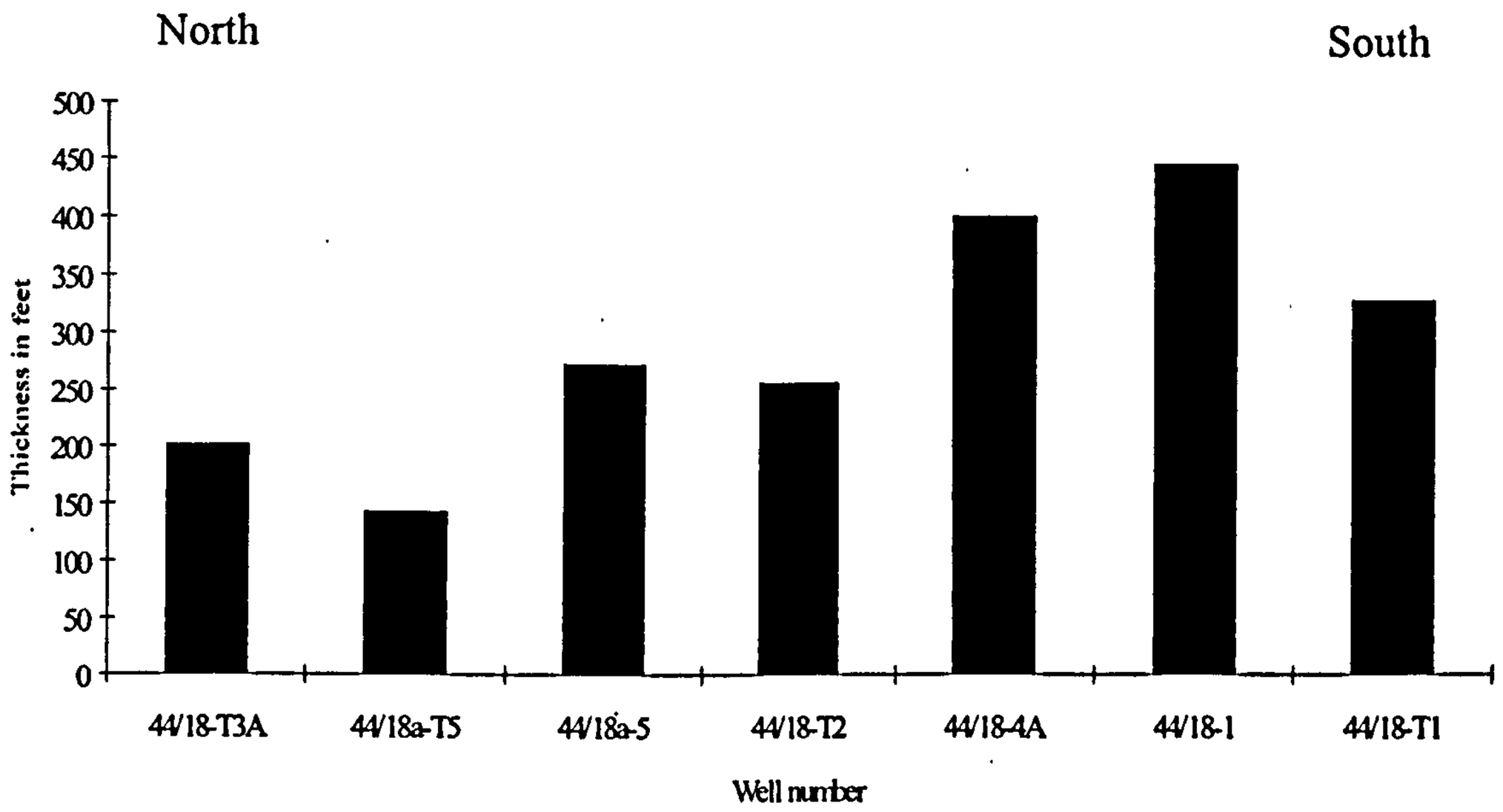

Figure 3.5. Lower Ketch Member reservoir thickness from north to south of the Tyne Field, SNS. Note that the wells have been corrected for deviation, but not structural effects such as faulting, folding or unconformities. A general increase in reservoir thickness to the south is observed as late Carboniferous unroofing occurred leading to a truncation of the Schooner Formation to the north.

3.5 Data base

Offshore data for the Tyne Field, Quadrant 44/18 were made available by ARCO British Ltd. The datasets comprised:

- Core data from eight wells (Table 3.1) (total core length 909.15') were provided as 2-3" diameter slabbed cores and set in epoxy resin. Core data available from each well varied from 36.3 ft to 161.2 ft and formed the primary data for facies analysis. Cored intervals were biased towards coarse-grained reservoir quality rock. Cored intervals in adjacent wells were not confined to equivalent horizons making lateral correlation difficult.
- 28 thin sections sampled from core plugs and used for grain size analysis.
- Eight wireline well completion logs (for the wells shown in Table 3.1) were used to gain quantitative net-to-gross data on the entire reservoir interval.
- Biostratigraphic (Mclean, 1996) and Palynological (Lake, 1992) reports were used to assist palaeoenvironmental reconstruction.
- In-house development project report was used to provide background information.

Table 3.1. Well cores from the Tyne Field used in the analysis of the Lower Ketch Member reservoir interval.

Well Number	Core number	Core depth (decimal feet)	Total core length (decimal feet)	Well deviation (degrees)	Gas accumulation
44/18 -T1	2	14582.00 - 14630.90	48.90	28	Tyne South
	3	14630.90 - 14706.00	75.1		
44/18 -1	1	12393.00 - 12408.90	15.9	4	Tyne South
	2	12409.00 - 12427.20	18.2		
	3	12427.00 - 12429.20	2.2		
44/18-T2	1	13236.00 - 13297.00	61	24	Tyne West
	2	13297.00 - 13306.50	9.5		
	3	13306.50 - 13397.20	90.7		
44/18 -2z	1	12892.00 - 12909.00	17	45	Tyne North
	2	12911.00 - 12926.10	15.1		
	3	12939.00 - 13000.15	61.5		
	4	13249.00 - 13265.00	16		
44/18-T3A	1	21154.00 - 21215.50	61.5	64	Tyne North
	2	21223.00 - 21256.50	33.5		
44/18 -4A	1	12208.00 - 12284.00	76	4	Tyne North
	2	12288.00 - 12341.85	53.85		
	3	12342.00 - 12374.20	32.2		
	4	13172.00 - 13232.10	60.1		
44/18a-5	1	12455.00 - 12566.00	111	0	Tyne West
44/18a-T5	2	18058.00 - 18142.50	84.5	54	Tyne North
	3	18148.00 - 18173.50	25.5		

3.6 Facies analysis from core

Lithofacies are divided into two distinct members: (1) a coarse-grained member comprising sandstones containing pebbles and a small percentage of conglomerates, and (2) a fine-grained member comprising pervasively reddened muds and silts, forming the reservoir and non-reservoir rock respectively, with a mean net-to-gross of 60 % (Figure 3.6). Nine lithofacies units have been identified in the well cores (Appendix A, Figures A1-A8) from the Lower Ketch Member (Table 3.2, Figure 3.7). Lithofacies units have been given facies codes based on a classification scheme modified from that developed by Miall (1977, 1978), to allow comparison with analogue deposits.

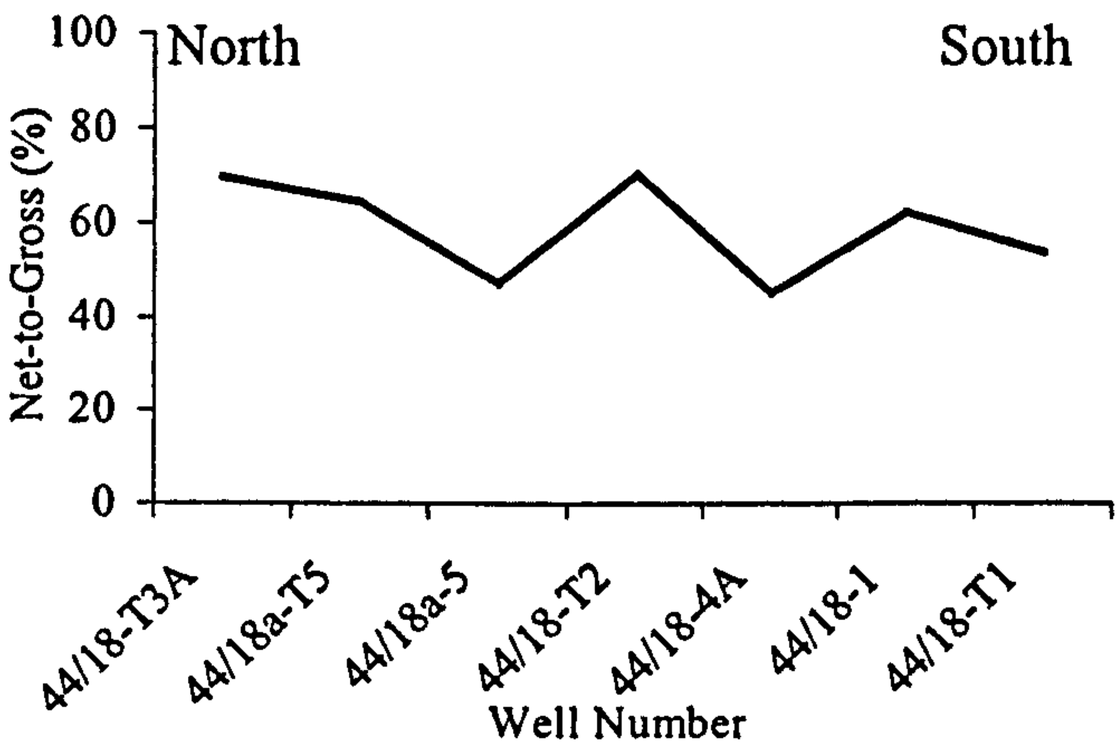

Figure 3.6. Random track plot showing the variation in Net-to-Gross of the Lower Ketch Reservoir interval from north to south of the Tyne Field calculated from well data.

Analysis of the coarse-grained fraction of the Lower Ketch Member in the cored interval reveals a series of stacked sandstones and conglomerate facies (codes GC, PS, SS), which exhibit random interbedding of trough and tabular cross-bed sets over centimetre scale, often showing reactivation surfaces, local scour and diffuse pebble horizons. Large grain size variation and lenses of bedload sediment (bedded and massive) are common. A systematic change in grain size is only evident at the top of individual sandbodies where fining occurs, which is associated with channel-belt abandonment. The development of lateral accretion deposits that are characteristic of point-bar migration were not noted. The previous description has led to the assignment of a braided channel-belt model with the development of extensive fine-grained floodplains (Table 3.2). However, there still lies considerable uncertainties associated with the identification of distinct channel types from vertical core data (Chapter 2) and studies such as Bridge and Gable (1993) showed that deposits of lateral and point-bars do not differ substantially from those of migrating bars.

Table 3.2. Lithofacies units observed within the Lower Ketch Reservoir, Tyne Field. Note the cores in the Tyne field are biast towards the reservoir quality rock. * Note no distinction has been made between K_v and K_h. Facies are coded with the classifications modified from Miall (1977, 1978). Examples of lithofacies from the Lower Ketch Member are shown in Figure 3.7 and provided in the supplementary CD (Appendix D).

Code	Lithofacies unit	Sedimentary structure / texture	Depositional processes/ interpretation	Percentage of lithofacies in the cored interval	Lithofacies associations	Mean porosity (%) and mean permeability, K (mD) *	Comparison with the literature
GC	Coarse-gravel framework conglomerate	Massive -crudely stratified pale brown to grey units. Sandstone matrix varies from 40 – 80 %. Sub-rounded to rounded clasts, up to 60 mm long axis, crudely imbricated and aligned to bedding. Ranging in thickness from a few clasts to 1 m. Mud matrix conglomerates are rare. Tabular cross-bedding.	Channel lag deposit and coarse bed-load dominated channel deposition within braided streams. Representing gravel bar deposition (bar core/bar margins) and coarse channel lags.	7 %	GC, PS, SS (Fining upwards channel fills, can show stacking)	8.3 % 159.3 mD	Plates A. Figure 1-10 Atkinson *et al.* (1990); Sometimes observed a channel sheet, plate 1.2, Mader, (1985). Gt, Gp, Gh, Gcm Miall, (1977). Similar to gravel facies of Ramos and Sopeña (1983)
PS	Parallel and cross-bedded pebbly sandstone	Pale brown to grey, tabular to trough cross-bedded sandstone. Clasts are often imbricated parallel to bedding. Pebble percentage ranges from 1 – 20%. Predominantly quartz clast with sizes up to 30mm long axis. May show normal grading.	Channel sequences formed by bar and dunes in bed-load channel deposition within braided streams as bar and dune forms migrate. Changing flow stages of an accreting bar form.	26 %	GC, PS, SS (Fining upwards channel fills, can show stacking) Alternatine GC and SS	11.1 % 306.3 mD	Plates B and C. Figure 1-10 Atkinson *et al.* (1990); St, Sp, Sl, Sh Miall, (1977); Plate 2.1 alternating sandstone/gravel Mader, (1985); Sandstone facies of Ramos *et al.* (1986)
SS	Parallel and cross-bedded well-sorted fine to medium sandstone	Pale brown to grey well sorted sandstone with no pebbles with very clear tabular and trough cross-bedding. Slight reddening in some cores. Parallel bedding often forms the top unit in channel-belt sandbodies in a fining up transition from cross-bedding to parallel laminated beds into the overlying overbank deposits.	Channel-belt deposits formed from active bar and dune migration in braided channels. Parallel beds indicate reduced flow stage and channel-belt abandonment.	34 %	GC, PS, SS (Fining upwards channel fills, can show stacking)	12.2 % 193.6 mD	Plates D. Figue 1-10 Atkinson *et al.* (1990); St, Sp, Sl, Sh Miall, (1977); Facies h Ramos *et al.* (1986). Fine -grained deposition niches of Ashworth *et al.* (1999)

Table 3.2. Continued

Code	Lithofacies unit	Sedimentary structure / texture	Depositional processes/ interpretation	Percentage of lithofacies in the cored interval	Lithofacies associations	Mean porosity (%) and mean permeability, K (mD) *	Comparison with the literature
Fwc	Grey laterally confined mud/silts	Fine grey within channel belt mud/silts, laminated with thickness up to a few feet and no pedogenic reddening. Some disturbance is observed. Rare	Channel plugs bounding the top of abandoned channel fill sequences within the channel-belt	<1 %	GC, PS,SS, Fwc (Fining upwards channel plug)	NA NA	Fl, Fsm Miall, (1977); Facies f Ramos *et al.* (1986).
FS	Fine- to medium-grained isolated sandstones	Fine to medium grained pale to grey sandstone within overbank deposits. Planar to cross-stratified with some reddening. Thicknesses between 0.5-2.5 m. Fining-up. Parallel and ripple laminated. Contacts appear to be planar, sharp at the base and diffuse at the top.	Single channels, possibly crevasse channels or splay lobes breaching the channel margin and scouring overbank deposits. Isolated or sheet sandstones.	1 %	FS, SSrc (Single channel scouring out muds/silts)	6.0 % 3.0 mD	Sh, Se, Miall (1977); Facies h Ramos *et al.* (1986). Splays of Bentham *et al.* (1993).
SSrc	Intraformational muds clasts within sandstones	Fine to coarse sandstones containing elongate angular rip-up clasts of mud/silts up to 50 mm long and aligned to bedding. They form part of fining up sequences.	Single crevasse channels or splay lobes breaching the channel margin and scouring overbank deposits, forming an intraformational rip-up lag. Clasts sources from well-poorly drained overbank silts. Eroded by incision or bank collapse.	2 %	FS, SSrc, SS (Single channel scouring out muds/silts)	4.5 % 0.6 mD	
Fob	Parallel laminated muds/silts	Finely laminated red to grey mud/silts with absence of biogenic or pedogenic disturbance. Pervasive haematite reddening masking primary sedimentary structures. Terminal splay ends.	Low flow overbank suspension fallout and deposition without subsequent soil development.	2 %	Fob, Fr (Different paleosol horizons)	2.9 % 0.5 mD	Fl, Sh Miall, (1977)
SSr	Pedogenically modified sandstones	Massive grey/red pedogenically modified fine sands with some preservation of laminae. Thicknesses range from 1 to 3 feet. Lack of lamination suggests mechanical breakdown due to pedogenesis.	Overbank deposition at a proximal position to the channel-belt.	11 %	SSr, Fob, Fr changes in grain size may represent proximity to channel-belt (Kraus and Bown, 1987, 1993)	4.6 % 0.3 mD	

Table 3.2. Continued

Code	Lithofacies unit	Sedimentary structure / texture	Depositional processes/ interpretation	Percentage of lithofacies in the cored interval	Lithofacies associations	Mean porosity (%) and mean permeability, K (mD) *	Comparison with the literature
Fr	Pedogenically modified silts	Pedogenically modified oxidized red mud/silts with pervasive mottling. Rootlet bioturbation and nodular calcretes are present. No preserved vegetation evident. Often shows leaching below sandbodies. Some pryrite with reduction halos are observed. Absence of desiccation cracks.	Low flow overbank suspension fallout and deposition with subsequent soil development with limited horizonation (Aridisols, Entisols). Arid climates or rapid aggradation may have suppressed soil formation. May have been deposited in shallow lakes or distal playa. Nodular calcretes indicate a seasonal climate. Carbonate nodules can be controlled by subtle difference in topography and drainage (<0.5 m). Pyrite indicates reduction of some organic material.	17 %	Fob, Fr (Different palaeosol horizons)	3.2 % 0.9 mD	Fr Miall (1977), Palaeosols are similar to those described by Besly *et al.* (1993) for the Etruria Formation and Driese *et al.* (1995) for the Lochness Formation.

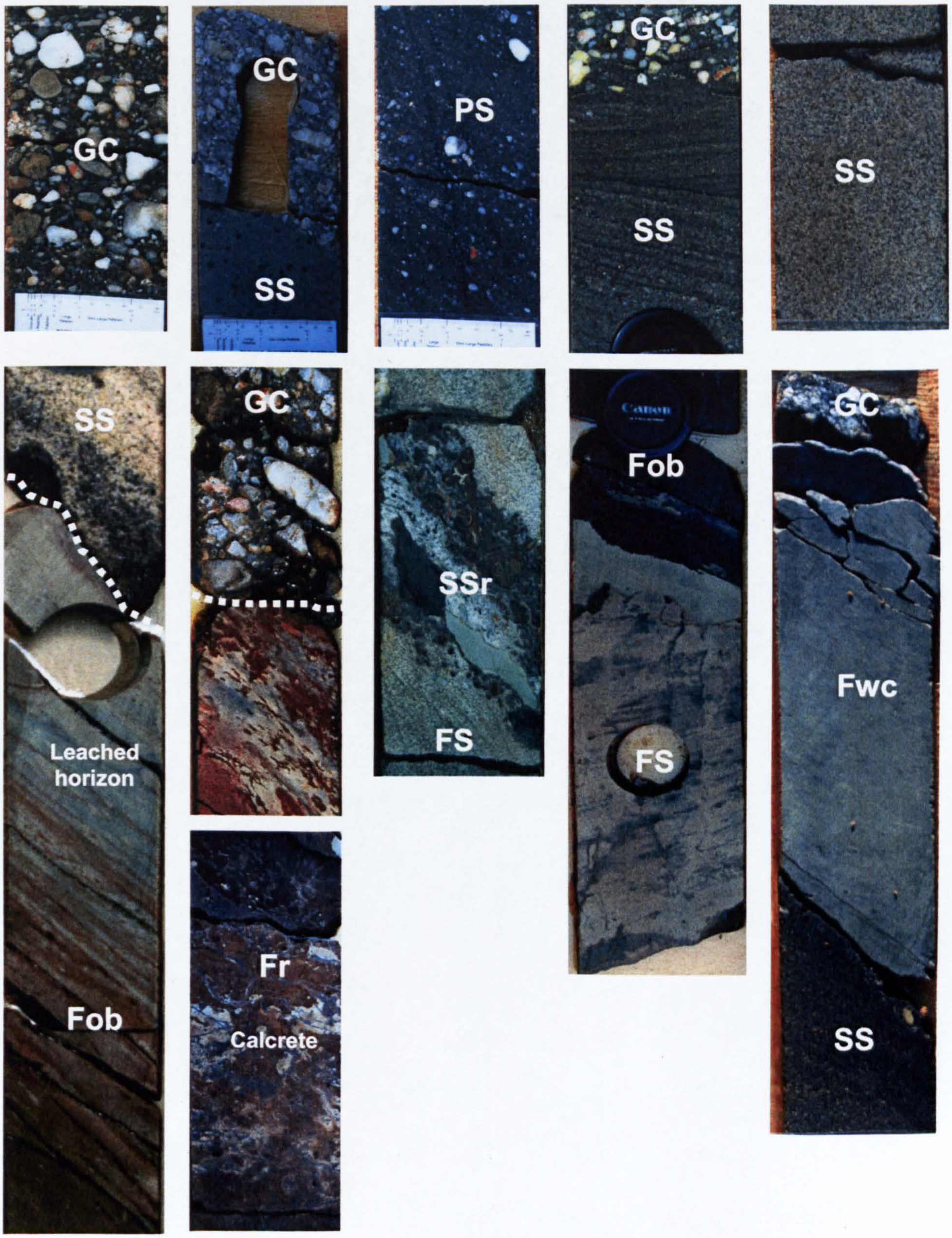

Figure 3.7. Examples of facies types observed within the cored intervals of the Lower Ketch Member, Tyne Field, SNS. Facies codes are shown on core (for full facies description refer to Table 3.2). Note: All cores are 3 inches in diameter and some are deviated. Dashed lines represent basal sandbody contact.

3.7 Vertical facies associations and sandbody types

The term 'sandbody' in this thesis is used to describe all coarse-grained bodies (> sand grade), which may include conglomerate facies. Initial observations from well cores show that the channel deposits exhibit a low degree of vertical connectivity and channel-belt sandbody widths that are generally narrower than well spacing. This section describes the vertical facies associations within the coarse-grained fraction and categorises them into four sandbody types: (A) channel conglomerate-sandstones, (B) channel sandstones, (C) crevasse splay lobes sandstones, and (D) composite sandstones, shown in Figures 3.8a-d and based on log profiles described in Table 3.3. Sandbody types within the Lower Ketch Member have been compared to examples from published literature studies (Table 3.3). Some concern over the use of vertical facies profiles has been expressed by Bridge (1993), but with the analysis restricted to one-dimensional core, vertical facies profiles still provide valuable datasets for comparisons to analogue outcrops.

General sandbody characteristics include a sharp and erosional base, often overlain by basal channel lag deposits of quartzite dominated clasts, above which the sandbody often fines upwards. The percentage occurrence of each sandbody type observed in the cored intervals is displayed in Figure 3.9. These data may be useful in populating reservoir simulation models with the correct proportions of sandbody types.

The shortfalls of using vertical facies profiles to predict channel patterns and subsequently, sandbody width were outlined in Chapter 2. However, application of outcrop analogue data to predict alluvial architecture and sandbody geometries must first start with a good facies match. Comparison of two-dimensional sandbody geometries from the literature and outcrop sequences would allow a more precise sandbody classification scheme to be developed (Chapter 4).

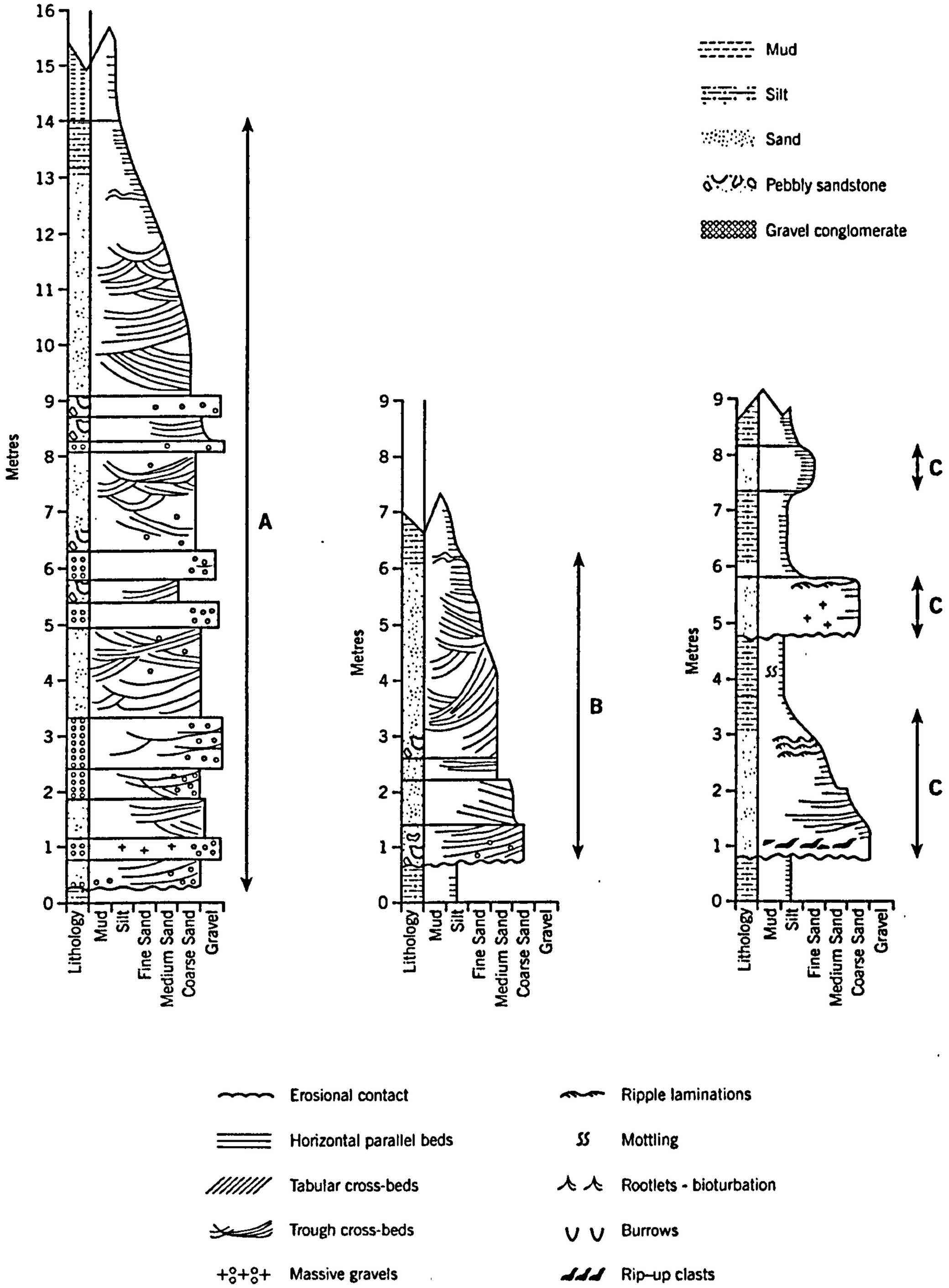

Figure 3.8. Characteristic vertical profiles through the three sandbody types (A-C) observed within cores from the Lower Ketch Member, Tyne Field, SNS. The fourth category, Type D results from the stacking of sandbody types A-C forming a composite sandbody profile.

Table 3.3. Description of sandbody types found within the Lower Ketch Member based on vertical lithofacies associations.

Sandbody Type	Vertical facies associations	Description	Interpretation	Comparison with literature
A (Conglomerates and sandbstones) (Figure 3.7a).	GC, PS, SS	Thick single / multistorey sandbodies comprising parallel and planar/trough cross-bedded sandstones, pebbly sandstones and conglomerates. Sandbodies comprise a series of stacked fining upward units that are often incorporated into a larger fining upward trend. Single facies units consist of a gravel conglomerate basal unit with some interbedded pebbly sandstone and sandstone beds, and thick trough cross-bedded unit grading into overbank fine sands and silts. Occasionally these sandbodies contain siltstone channel plug deposits resulting from passive channel filling events.	Mixed bedload braided river system where dune and bar formation co-existed. Small fining upwards sequences may indicate lateral accretion suggesting high sinuousity channels were also present, although may have existed within braided channel-belts.	Sandbody a, Figure 12 (Smith, 1990) within the deposits of the Triassic Budleigh Salterton Pebble Beds.
B (Sandstones) (Figure 3.7b)	PS, SS	Thick trough cross-bedded and parallel bedded sandstones and pebbly sands bodies that contain very little gravel grade sediment Sandstones are well-sorted and fine-up gradually from a sharp basal contact and may have a sheet or ribbon two-dimensional form.	Sandy braided channel system characterised by dune and sandy bar migration within the channels.	Lateral extent of these units are unclear, but they appear to be of a similar nature to the ribbon and sheet sandbodies described in the system (Martinius, 2000).
C (Splays) (Figure 3.7c)	FS, SSrc	Thin fine-medium grained finely laminated sandstone units that are conformable with the under and overlying floodplain deposits, although sometime exhibit a sharp basal contact. Stacking within sands is defined by thin fining upwards units within the overbank deposits. Deposits exhibit some wavy bedding and current ripples, and can also contain rip-up clasts. Occasional coarsening upwards is exhibited.	Splays formed as crevasse channels breached channel banks and deposited sediment as a lobe on the floodplain. Rip-up clasts suggest rapid channel scouring or bank collapse by crevasse channels into the overbank deposits.	Splay channel and lobe sandbodies described in Mjos *et al.* (1993) and the non-channelised sandbodies of Martinius (2000). These are splay deposits and analogue deposits in the Escanilla Formation would characteristically fine and thin away from the channel margins as a wedge shape.
D (Amalgamated sandbodies)	GC, PS, SS, FS, SSrc	Composite sandbodies, which in their entirety may be composed of a stacked sequence comprising of a number of the sandbodies described above (A-C). For example in well 44/18a-T5 between 18112' and 18058' the sandstones exhibit a stacking of a sheet conglomerate on top of a trough cross-bedded sandstone units.	Combination of depositional environments described for sandbody types A-C.	Laterally these sandbodies may look similar to the amalgamated complex in Figure 5F, Hirst (1991).

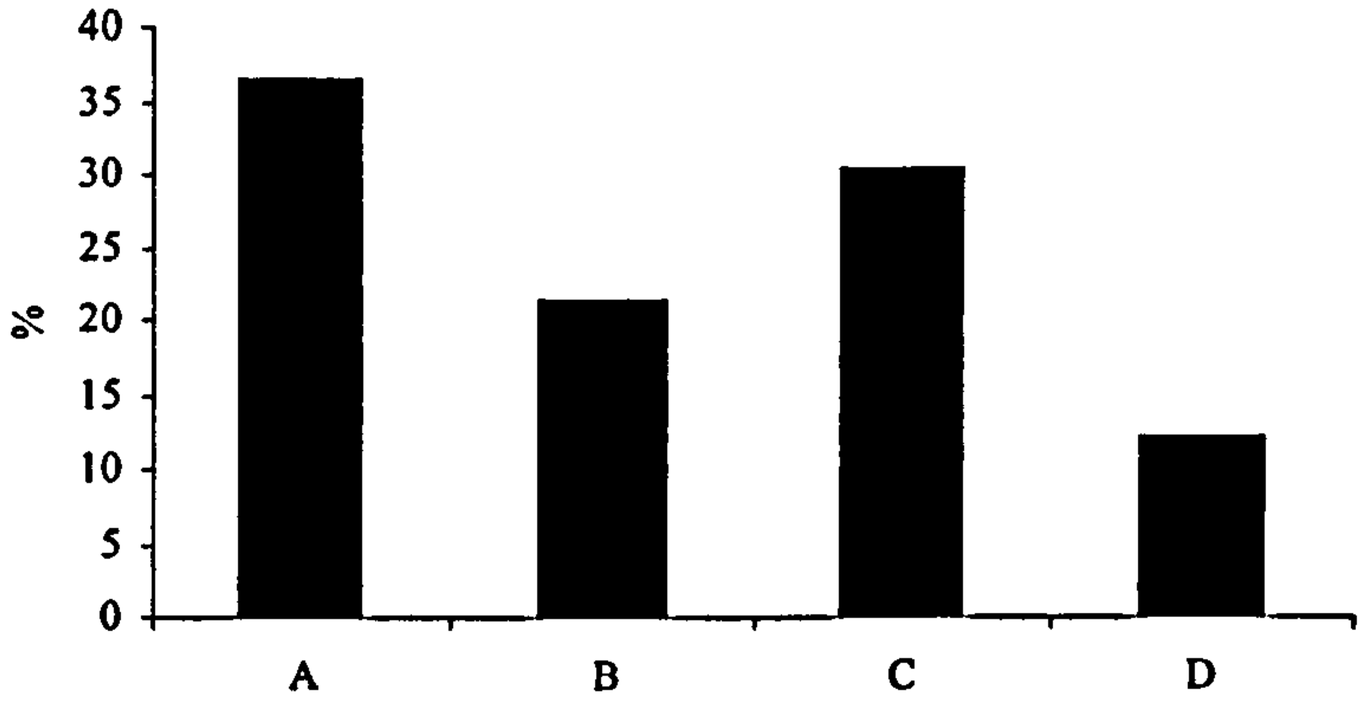

Figure 3.9. Histogram to show types of sandbodies (A-D) observed within the Lower Ketch reservoir interval (n = 33). Refer to text for full description of sandbody types.

3.7.1 Thickness of sandbodies

Measurement of complete sandbody thicknesses was undertaken (Figure 3.10). Complete sandbody thickness was defined by the occurrence of both basal and top contacts within cored intervals of the Lower Ketch Member. Complete sandbodies had a mean thickness of 4.9 m, while the largest partially cored sandbody measured 22+ m. Although sandbody thicknesses have been corrected for well deviation, there is no certainty that the sandbody was penetrated at the position of maximum thickness. The ratio between average and maximum thickness of a sandbody's length is in the range 0.6-0.8 (Hirst *et al.*, 1993). Consequently, the sandbody thickness distribution may be an underestimate of true maximum thickness. Type C splay sandbodies make up the majority of thin sands (< 2 m) and Type B sandbodies are generally below 8 m in thickness, with the sandbodies containing conglomerates representing the thickest sandbodies (> 8 m). This sandbody classification may be inappropriately applied when sandbodies stack vertically as a result of successive channels that may occupy the same site (cf. Morhrig *et al.*, 2000). These stacked sandbodies may be difficult to distinguish in core and lead to an overestimation of channel sandbody thickness.

One goal of the geologist is to predict sandbody widths using thickness as a guide (e.g. Fielding and Crane, 1987). Details outlined in Chapter 2, Section 2.6.1 highlight the huge uncertainties in the prediction of most likely sandbody width (Chapter 2, Figure 2.22) using scattered datasets. It is therefore fitting to review alternative methods of predicting sandbody architecture in the following section, using estimates of cross-set heights to predict formative channel depth and channel-belt width.

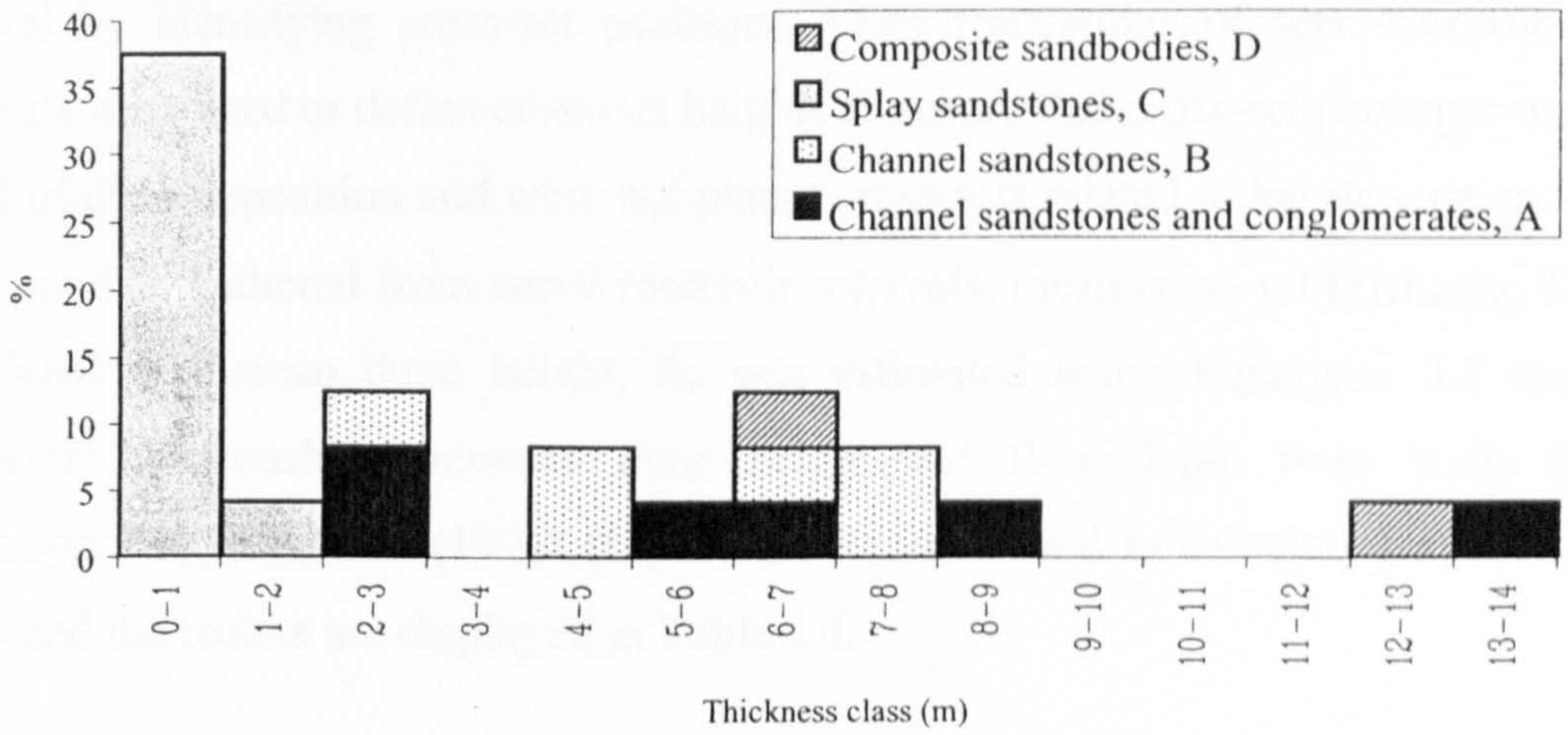

Figure 3.10. Thickness-frequency distribution for Lower Ketch Member sandbodies (n = 24) that have been subdivided into Type A-D classifications. Refer to text for full description of sandbody types.

3.8 Estimates of formative channel depths and channel-belt widths

In order to match correctly the scale of channels that deposited the sandbodies within the reservoir sequence to the scale of channels that were responsible for deposition of any outcrop analogue sequence chosen, an estimate of formative channel depth is required. Failure to match the scale of the depositional systems may result in sandbody geometries being extrapolated between fluvial systems differing in scale over several orders of magnitude. Hence, several measurement techniques have been used to estimate channel depths and channel-belt widths from Lower Ketch Member core data.

Gaining information on formative channel depths is more problematic in cored intervals in comparison to two-dimensional outcrop exposure. However, preserved set heights have been used to gain information on formative channel depth from both core and outcrop (Paola and Borgman, 1991; LeCair *et al.*, 1997; Bridge and Tye, 2000; Alexander *et al.*, 2001). LeClair *et al.* (1997) suggests that most cross-sets are formed by only the highest 10 % of dunes, and formative bed wave heights range from 0.18 to 0.3 m. LeClair *et al.* (1997) also assumes aggradation has a minor influence on cross-set thickness. Using set heights allows comparison between core to outcrop sequences. Different relationships exist between flow depth and bar formation, and flow depth and dune formation (Refer to Todd, 1996, p314). Therefore, measurements were confined to

cross-set heights within trough cross-bedded sandstone within the Lower Ketch cored interval by identifying cross-set packages. Clear truncations of sets over sub-metre intervals were used to define cross-set heights to ensure that cross-set packages were the result of dune deposition and were not planar cross-sets related to bar deposition. Using cross set data gathered from cored reservoir intervals, mean cross set thickness, S_m was calculated and mean dune height, h_m was estimated using Equations 3.1 and 3.2. Empirical relationships between dune height and flow depth from Yalin (1964) (Equation 3.3) and Allen (1970) (Equation 3.4) were used to calculate formative flow depth and the results are displayed in Table 3.4.

$$ß = S_m / 1.8 \qquad \text{Equation 3.1}$$

$$h_m = 2.22ß^{1.32} \qquad \text{Equation 3.2}$$

$$d / h_m = 6 \qquad \text{Equation 3.3}$$

$$d = 11.6\, h_m^{\,0.84} \qquad (0.1\text{ m} < d < 100\text{ m}) \qquad \text{Equation 3.4}$$

Alternatively, the use of preserved channel fill deposits can be used to assess channel depths. In many onshore outcrop sequences complete abandoned channel fill sequences are easy to identify, but often only represent a minor proportion of the facies types observed in any one alluvial sequence (cf. Table 1 in Ashworth *et al.*, 1999). In one-dimensional cores, single channel fill deposits are difficult to distinguish from stacked facies profiles. Paola and Borgman (1991) suggest that preserved channel thicknesses range between 40-75 % of their formative channel depth. Where a clear erosional base, fining upward trend and a fine cap were identified, a single preserved channel sequence was measured. Only two channel fill fining upward sequences were observed within the Lower Ketch Member (well 44/18-T2, 13281.7'-13283.6'; well 44/18a-T5, 18107.4'-18111.2'). Comparisons between the two methods are summarised in Table 3.4a and b.

Table 3.4. (a) Estimates of dune height, channel depth and channel-belt width from cross-set data in the Lower Ketch Member reservoir interval, and (b) estimates of channel depth from channel fills in the LKM. *cbw* = channel-belt width.

Method A	**Lower Ketch Member**
Lithofacies	SS/PS
N	30
Mean set height (Sm) (m)	0.34
Standard deviation (Ssd)	0.26
Applicability test (Ssd/Sm = 0.88 ± 0.3)*	0.78
Mean dune height (hm) (m)	0.24
Depth (Yalin, 1964) equation (m)	1.5
Depth (Allen, 1970) equation (m)	3.5
Estimate of channel-belt widths (cbw)	
Channel-belt width (Bridge & Mackey, 1993) equation 3.5 using Yalin (m)	117
Channel-belt width (Bridge & Mackey, 1993) equation 3.5 using Allen (m)	320
Channel-belt width (Bridge & Mackey, 1993) equation 3.6 using Yalin (m)	578
Channel-belt width (Bridge & Mackey, 1993) equation 3.6 using Allen (m)	1078
Method B	
N	2
Mean channel fill depth (m)	0.9
Minimum flow depth (m)#	1.2
Maximum flow depth (m)#	2.2

* Refer to Bridge and Tye (2000) for applicability test.

Based on estimates of preserved channel fill thicknesses being between 75% and 40% of original flow depth (Paola and Borgman, 1991).

Estimates of channel fill thickness were confined to the cored intervals only to allow direct comparison to outcrop analogues. Estimates from trough cross-bed thickness produce channel depths in the range of 1.5 to 3.5 m, which have a similar order of magnitude to the range of channel depths calculated using Paola and Borgman's (1991) method, yielding depths between 1.2 and 2.2 m.

Channel-belt widths (*cbw*) were estimated based on empirical Equations 3.5 and 3.6 using mean bankfull flow depth, d_m (Bridge and Mackey, 1993a).

$$cbw = 59.9 d_m^{1.8} \qquad \text{Equation 3.5}$$

$$cbw = 192 d_m^{1.37} \qquad \text{Equation 3.6}$$

Channel-belt widths are estimated to range between 117-1078 m. Assuming channel-belt width can be used as a surrogate for sandbody width (as used by Lorenz *et al.*, 1985), the Lower Ketch Member sandbody widths may be similar to those described in the Escanilla Formation (Dreyer *et al.*, 1993). Although the use of these channel-belt

widths may provide minimum sandbody widths they fail to account for sandbodies that comprise multilaterally stacked sandbodies. Additionally, while mean set height is a useful scale comparison between reservoir and analogue, the maximum cross set height may be more appropriate to pick up extreme events, and future work should consider these higher magnitude events.

3.8.1 Assumptions of channel depth estimates

Truncation by erosion of channel fill deposits and drilling of cores which do not penetrate directly through the thickest part of the channel deposit or trough cross-set package may produce an underestimate of channel bankfull depth. Scour of channels can produce sequences that overestimate mean channel depth (Salter, 1993) and burial compaction of sediments can also alter estimates of channel depth and need to be considered (see Section 3.12). Compaction of these coarse deposits will give underestimates of bankfull channel depths if not already corrected for. As the thickness of individual channels increases, the uncompacted channel depths are proportionally increased.

3.9 Significance of red beds for environmental interpretation

Fine-grained deposits are pervasively reddened within the Lower Ketch Member deposits. Red colouration is probably due to the presence of haematite in the matrix and as coatings (Walker, 1967). Oxidized floodplain fines (red beds) have often been regarded as typical of ephemeral stream sedimentation (Miall, 1977). However, the origin of red bed deposits has been attributed to a number of environments and can occur under a spectra of climatic settings from wet to arid (Turner, 1980; Pye, 1983; Dubiel and Smoot, 1994), containing low original organic content (Turner, 1980; Myrow, 1990) and lack of biopreservation. Therefore, as colour may have no palaeoclimatic significance it cannot be used alone to interpret red beds and correlate sequences, and additional information from primary sedimentary structure and facies description are needed for environmental reconstruction.

The degree of reddening caused by rubifaction depends on the length of exposure and on the climate at the time of formation. Reddening is particularly dependent on temperature and the amount of rainfall (Ruhe, 1965; Harden, 1982). Walker (1967) has shown that prolonged periods of exposure are needed for full reddening to occur.

Additional complications arise in the interpretation of the Upper Carboniferous red beds as a result of multiphase reddening. This multiphase reddening occurs as a result of: (1) primary pedogenic reddening and (2) secondary reddening by penetrative oxidation from pre-Permian surface (Besly and Turner, 1983; Turner, 1980). Distinguishing between primary and secondary reddening can be difficult, as they appear similar. Late Carboniferous sequences may be reddened to a maximum depth of 600 m below the Permian unconformity (Trotter, 1953, 1954), therefore base Permian reddening may encompass the entire Lower Ketch reservoir interval. Multiphase reddening has been documented in Johnson *et al.* (1997), where a study of the Westphalian D-Stephanian, Halesowen and Salop Formations in the West Midlands describes two phases of reddening: (1) Deep oxidation in an arid climate following Variscan uplift and erosion in the Permian, resulting in the precipitation of haematite; and (2) Secondary precipitation of haematite resulting from lateral flow of meteoric water through connected permeable sandstone units. Palaeosols in the Lower Ketch Member compare to present-day ferratic palaeosols and show features of warm, reasonably humid but well drained conditions. Palaeosol development has been used in the Schooner and Ketch Fields to yield information on aggradation rates (Stone and Moscariello, 1999) but is not easily defined in the Tyne cores and subsequent palaeosol correlations are not possible within the Tyne reservoir. A strong diagenetic overprint may have reddened the deposits further and masked any pedogenic mottling. In the Lower Ketch Member two phases of reddening and varying well deviations make horizonation difficult to establish. However, the lack of laminations within the fine-grained deposits cored interval of overbank deposits may indicate pedogenic disturbance, suggesting the development of peds and early mechanical breakdown have destroyed the primary sedimentary structures. The colonization of floodplains by vegetation may take place after only a few months following a flood event in some semi-arid climate regimes and consequently soil development will initiate and destroy primary depositional laminae.

Differential leaching and reduction processes related to differences in porosity and permeability within channel-belt deposits (Section 3.15) may be responsible for colour

variations. Sandbodies are the higher permeability strata and provide preferential flow paths for reducing pore waters. The influence of these porewaters may extend out immediately beneath the base of the sandbody. Pedogenic reddening typically increases up through the sandbody profile in association with fining upward trends within the sandbody.

Grey colouration of some of the mud/silt overbank deposits suggests that floodplains were also subjected to some reducing conditions. The presence of siderite indicates poorly drained conditions and pyrite shows a sulphate reduction and porewater diagenesis has occurred. Evidence for reduced conditions within the floodplain deposits may suggest the floodplains were periodically waterlogged during the deposition of the Lower Ketch Member. Evidence for waterlogged conditions is inconclusive due to the strong reddening overprint. While red beds are challenging to interpret, information presented in the preceding sections has allowed a depositional model to be proposed.

3.10 Depositional model for the Lower Ketch Member: a discussion

Analysis of lithofacies within the Lower Ketch Member suggests a depositional environment where northerly supplied sandy, channel-belts traversing an alluvial plain were periodically flooded under a seasonal climate to create extensive floodplains. In order that extensive floodplain deposits were preserved, sediment supply must have been characterised by a very fine grain size distribution (Section 3.14). The Silver Pit Basin was situated close to the equator and was subjected to a semi-arid climate exhibiting seasonal rainfall, which was responsible for periodic inundation of the floodplains and may have formed temporary lakes on the floodplain surface. This section presents a discussion on the depositional environment (Figure 3.10) and sets the Tyne Field in a regional context.

3.10.1 Channel-belts within the Lower Ketch Member

Examination of the coarse-grained deposits reveals distinctive vertical fining upward sequences that can be divided into four sandbody types (A-D). Type A consists of

massive and cross-bedded conglomerates and trough and planar cross-bedded sandstones, indicative of in channel bar and dune migration in a sandy braided river system with a limited supply of pebbly material. The low proportion of gravel grade material in the sequence (< 10%) suggests the type of deposition was probably more consistent with sandy braided river models (e.g. Cant and Walker, 1978; Blodgett and Stanley, 1980; Ramos *et al.*, 1986; Bristow, 1993). The conglomerates that are present within the sandbodies represent coarse lag deposits and deposition during high flow stages. Additionally, small fining upwards sequences in sandbody type A indicate the presence of lateral accretion which in turn may be evidence that meandering channels existed coevally with braided channel-belts during deposition. Type B sandbodies comprise exclusively sandstone and contain predominantly trough cross-bedded or parallel-bedded facies of sandy braided river origin. Lithofacies show a marked similarity with fluvial sequences investigated by Hirst (1991) and Dreyer *et al.* (1993). Similarities between these two studies suggest that a variety of channel patterns may have existed during the deposition of the Lower Ketch Member and therefore, prediction of channel-belt width is ambiguous. Vertical facies profiles derived from ribbon and sheet sandbodies are indistinguishable in core. Consequently, in the absence of any lateral correlation, the assignment of ribbon or sheet geometries to vertical facies associations from the Lower Ketch Member is difficult. However, analysis of cross-set data allows the scale of the rivers to be inferred. Maximum channel depths were between 1.5 and 3 m and channel-belt widths are estimated to range from 120 to1080 m. This wide range in predicted channel-belt widths is consistent with channel-belt sandbody geometries measured from the Escanilla Formation (Dreyer *et al.*, 1993).

Type C sandbodies were formed by overbank splay lobes and commonly exhibit fining upwards sequences and parallel laminations with evidence of current ripples, which grade into overlying overbank fines. Maximum stacked splay sandbody thickness is 2 m and resulted from several phases of overbank deposition. Splay were fed by crevasse channels, which exhibit sharp erosive bases and rip-up clasts horizons. These crevasse channels breached the channel-margins and ensuing scour and incision into the overbank sediments occurred. Fine-grained splay sandbodies that display conformable basal contacts and more gradational upper contacts represent the more distal extent of splay lobe deposition where deposits have fined away from the channel-belt margin in relation to a reduced flow power. Splays crevasse channels and lobes may be similar to those described by Smith *et al.* (1989) and Mjos *et al.* (1993) and have a tabular to

wedge shaped form. Splay processes may have been the preceding mechanism for channel-belt avulsion events (Smith *et al.*, 1989).

3.10.2 Controls on the alluvial architecture of the Lower Ketch Member

Lack of well-defined palaeosol horizons (Aridisols and Entisols) indicates that soil development was suppressed by either high aggradation rates (e.g. Kraus and Middleton, 1987; Shuster and Steidtmann, 1987; and Bentham *et al.*, 1993) or the lack of biogenic activity caused by climate. Extreme climate conditions are capable of suppressing significant soil development. During the late Carboniferous there was an increase in aridity and this may have inhibited soil formation. Therefore, within the Tyne Field, no conclusive evidence is available to determine whether high aggradation rates or extreme climate conditions were responsible for poor palaeosol development. However, the presence of well-defined palaeosol horizons in the Ketch and Schooner Fields (Stone and Moscariello, 1999), suggests that climate was not curtailing soil formation within the Silver Pit Basin. Hence, the weak palaeosol development in the Tyne area may have been attributed to an aggradational system rather than an incisional system.

Several lines of evidence also suggest that the Lower Ketch Member reservoir interval was deposited in an aggrading stream environment. While vertical facies profiles through the channel sandbodies suggest braided river deposition, this evidence alone is inconclusive in determining whether the channel-belts were incising or aggrading, as braided channel patterns can exist in both aggading and degrading systems (Germanoski and Schumm, 1993). For example, the present day braided rivers of the Canterbury Plains, New Zealand are incising, however, previously braided Canterbury Rivers were aggrading (Bal, 1996). Analysis of palaeosol development has been used to estimate relative aggradation rate (e.g. Stone and Moscariello, 1999) and the period of depositional cessation required for palaeosol development has been subject to many debates. The presence of calcretes not only provides evidence for climatic conditions, but also offers estimates of aggradation rate. In modern environments calcretes are most common in warm to hot climates (mean annual temperature 16-20 °C) and marked by low seasonal rainfall (100-500 mm) (Goudie, 1973, 1983). Calcrete precipitation can occur where pauses in sedimentation may have been as little as 10^2 years (Allen, 1986),

and Leeder (1975) predicts floodplain deposition rates in the order of 2×10^{-3} m yr^{-1} as the lower limit of calcrete generation (see discussion in Chapter 2, Section 2.4). The presence of overbank splay sandbodies also agrees with a system that had overbank flooding events and not one of incision and channel-belt confinement.

Lithofacies analysis of the fine-grained overbank deposits also allows several other clues to the depositional environment to be distilled. The presence of pyrite with small reduction halos, siderite (nucleation on limited amounts of organic material) and grey non-oxidized rip-up clasts in an otherwise exclusively oxidized overbank sequence, suggests that some reducing conditions were present within the floodplain environment. Environmental interpretation is clouded by the pervasive multiphase reddening that occurred due to base Permian penetrative weathering (cf. Besly and Fielding, 1989). Consequently, the lack of preserved rootlets, palynomorphs and organic matter within the Lower Ketch interval signifies either a sparsely vegetated floodplain or the subsequent removal of organic material by oxidation. The vegetation that was present during the late Carboniferous may have been confined to the most primitive vascular plants such as small reeds or ferns. These would have been opportunistic, colonising the floodplain during the wet season (because they needed to drop their spores in water) and then dying off in the dry season. Not enough is know about late Carboniferous vegetation to determine their binding capacity of floodplain sediments and impact on channel-belt stability.

Evidence presented in this section suggests the floodplain topography and prevailing seasonal climate conditions of the Silver Pit Basin probably resulted in the co-existence of both waterlogged and well-drained conditions. Collinson and Jones (1997) suggested there is a shift to a more lacustrine setting to the south of the Tyne Field. However, there is a lack of diagnostic criteria to argue for the existence of lakes on the floodplain during the deposition of the Lower Ketch Member in the Tyne Field.

3.10.3 Summary of the depositional model in the Tyne Field

In summary, the Lower Ketch Member sequence resulted from continental deposition on an alluvial plain during basin inversion and relative closure to the open ocean. A model is presented in Figure 3.11 to display the type of sedimentary conditions

responsible for the deposition of the Lower Ketch Member. The sequence is dominated by two distinctive vertical fluvial facies associations: coarse sandstone-gravel units deposited in active channel-belts alternating with finer mud-silt units deposited in inter-distributary floodplain areas. Determining whether climate, sediment supply load, sediment grain size or tectonics controlled the vertical alternation between channel and overbank deposits is problematic.

Several depositional models have been put forward for the Lower Ketch Member, including: (1) an incised valley system (Besly *et al.*, 1993); (2) a low angle arid-humid alluvial fan model (Collinson and Jones, 1997) similar to that observed in the modern Kosi Fan, Indogangetic Plains (cf. Wells and Dorr, 1987; Singh *et al.*, 1993); and (3) braided and anastomosing river systems adjacent to floodplain muds (Mijnssen, 1997, Stone and Moscariello, 1999) from stratigraphic equivalent deposits in the Schooner Field. The evidence presented in this section implies an aggrading stream model may be more appropriate for the deposition of the Lower Ketch Member interval in the Tyne Field. Furthermore, the comparison of data from the Tyne Field and studies of the Ketch and Schooner Fields (Mijnssen; 1997; Stone and Moscariello, 1999) allows depositional environments to be consolidated in a regional model. The establishment of an aggrading stream model has important ramifications for the prediction of channel-belt sandbody stacking patterns and connectivity. These two subjects will be addressed in the following sections.

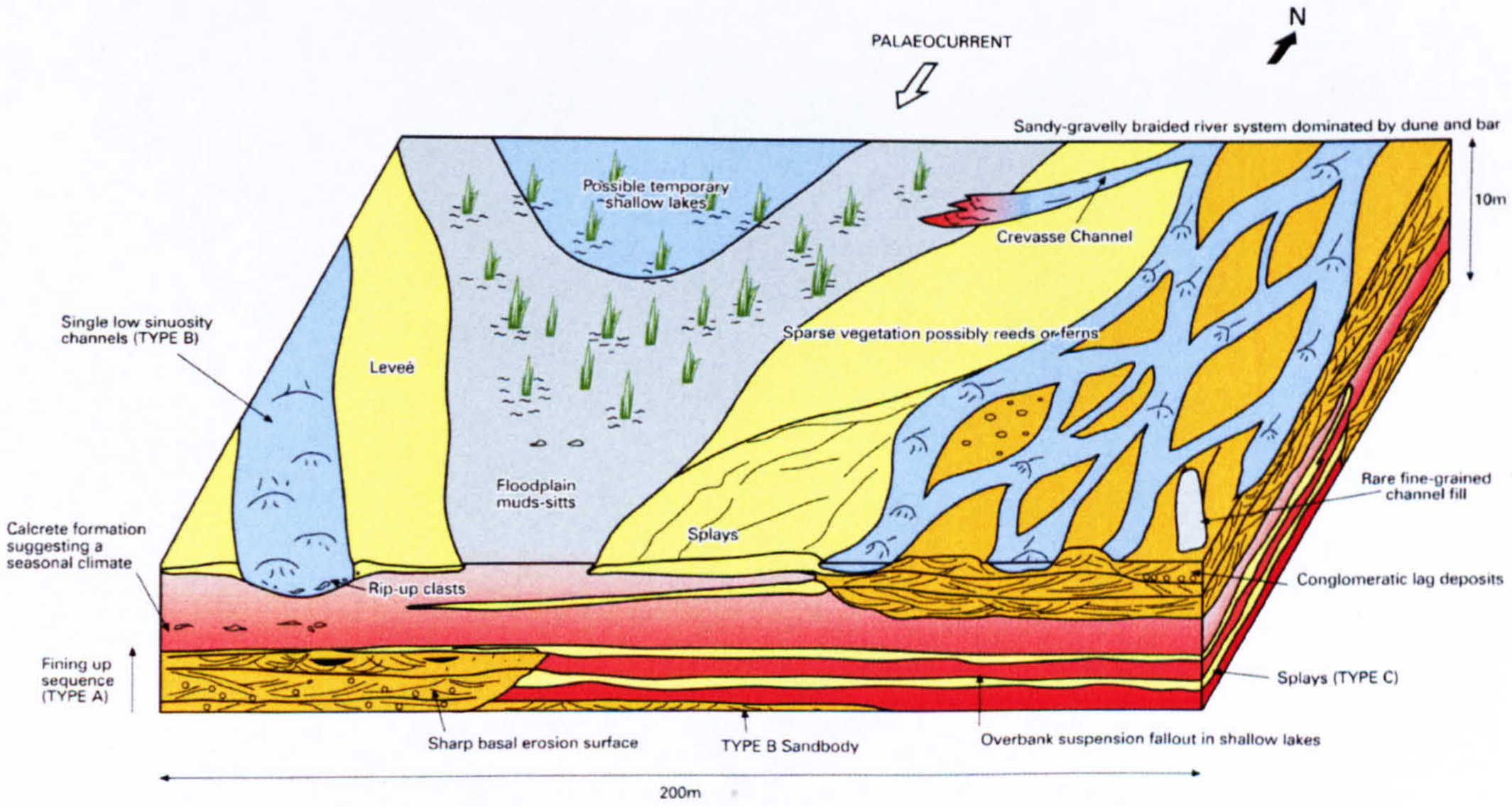

Figure 3.11. Schematic block diagram to represent the depositional environment of the Lower Ketch Member in the UK Southern North Sea.

3.10.4 Incorporation into the regional depositional model

The schematic depositional model presented in Figure 3.11 is well supported by the depositional models for Ketch units 1-3 described in Stone and Moscariello (1999). While climate conditions were conducive to palaeosol formation, the marked differences in palaeosol maturity shown between the north (Tyne Field) and south (Schooner and Ketch Fields) of the Silver Pit Basin imply that either: (1) deposition in the area of the Ketch and Schooner Fields was more susceptible to local base-level controls; (2) a switch between an incising system, where abandoned terraces formed, and an aggrading system occurred between the locations of the Ketch/Schooner Fields and the Tyne field respectively; or (3) relative aggradation rates and avulsion frequency were higher in the north of the basin.

The Stone and Moscariello (1999) study of the Ketch Formation in the Ketch and Schooner Fields, lying to the south of the Tyne Field, shows consistent proximal-distal trends from a dominant palaeosource (i.e. MNSH) to the north, which include: (1) a downstream fining; (2) decreasing net-to-gross, (3) decreasing sandbody connectivity, and (4) increasing palaeosol development. These trends are consistent with the regional study of Collinson and Jones (1997) who noted that the occurrence of sandbodies dies out to the south of the Tyne Field and is replaced by an area dominated by a playa type depositional system. Therefore, the Tyne Fields location represents a more proximal position in the Silver Pit Basin (Figure 3.12). These Ketch Member proximal-distal facies trends may also be similar to the terminal fan model of Kelly and Olsen (1993).

There is no evidence to suggest that local base-level and subsequent channel-belt incision displayed in units 4 and 5 of Stone and Moscariello (1999) propagated so far north as to influence on the Ketch Member deposits of the Tyne Field. No diagnostic criteria are available to determine whether sediment supply, climate or tectonics were the controlling mechanisms for the development of alluvial architectural patterns. Further investigation is needed to integrate the proximal-distal relationships between the Tyne and Ketch/Schooner Fields respectively, and to determine whether units 1-3 of the Ketch and Schooner Fields (Stone and Moscariello, 1999) are stratigraphic equivalents to the Lower Ketch Member of the Tyne Field.

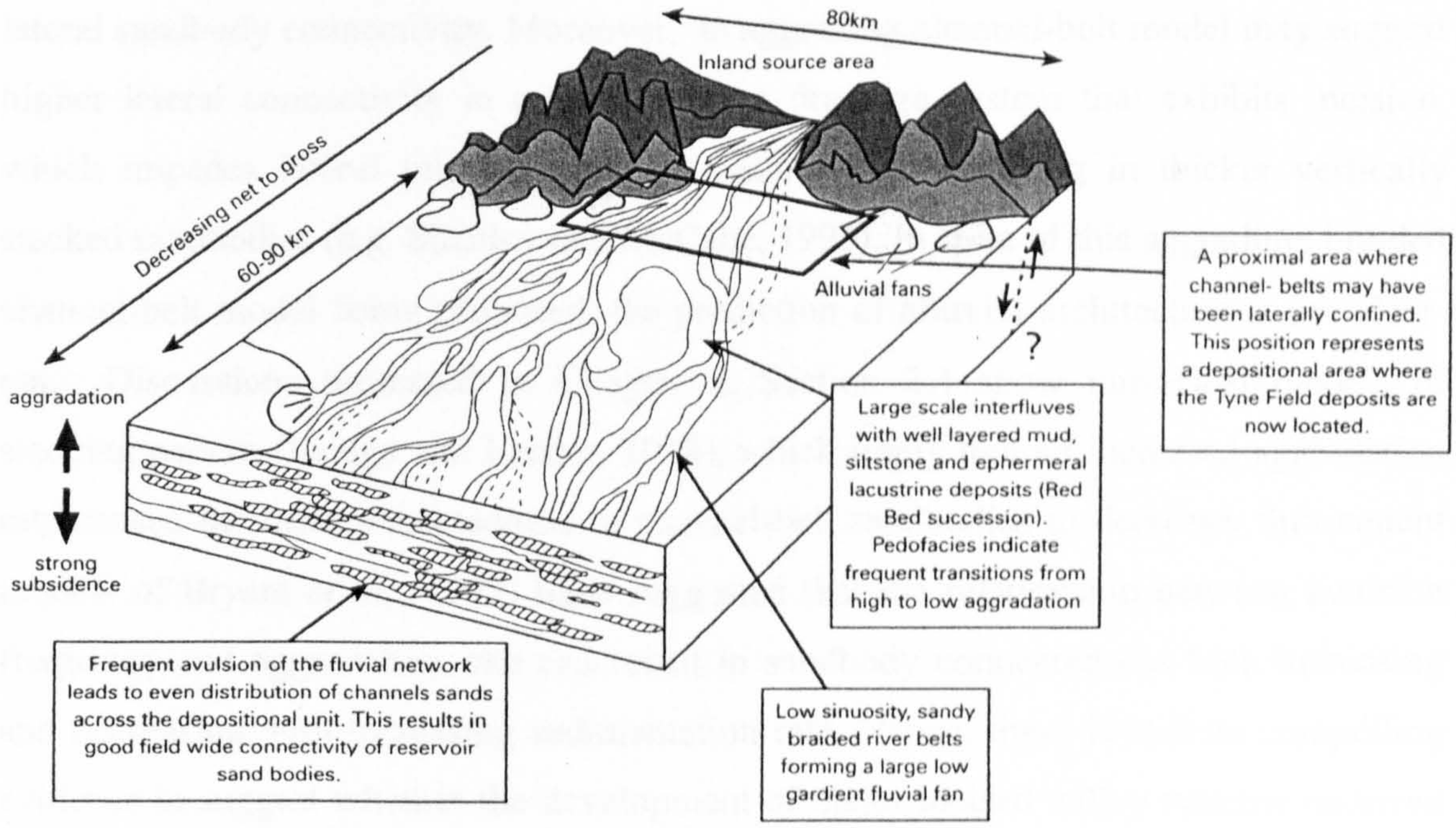

Figure 3.12. Schematic block diagram to show the palaeogeographic setting for depositional units 1-3 of the Ketch and Schooner Fields at the distal end of a broad alluvial plain (modified from Stone and Moscariello, 1999). The boxed area represents a more proximal position in the basin where sediments of the Tyne Field were deposited.

3.11 Estimates of connectivity and sandbody geometry

Large well spacing and the lack of correlatative marker horizons within the Lower Ketch Reservoir interval make prediction of alluvial architecture difficult. The net-to-gross of the Lower Ketch interval is ~60 %, therefore, based on calculations of Fielding and Crane (1987) and Bridge and Mackey (1993a), sandbody connectivity should be relatively high within the Lower Ketch Member interval. However, locally within individual wells the net-to-gross is shown to be as low as ~45 % (Figure 3.6) where connectivity becomes problematic and more precise estimates of sandbody geometry are required.

To enable sandbody connectivity to be more reliably predicted knowledge is required of: (1) depositional environment, and (2) channel-belt sandbody geometries. Evidence presented in this chapter suggests an aggrading stream model for the deposition of the Lower Ketch Reservoir interval. The assignment of an aggradational model over an entrenched system (cf. Stone and Moscariello, 1999) has important implications for

lateral sandbody connectivity. Moreover, an aggrading channel-belt model may suggest higher lateral connectivity in opposition to a drainage system that exhibits incision, which impedes lateral migration of the channel-belt, resulting in thicker vertically stacked sandbodies (e.g. Shanley and McCabe, 1993). In spite of this aggrading, braided channel-belt model being proposed, the prediction of alluvial architecture is not clear-cut. Discussions presented in Chapter 2, Section 2.4 show numerical models of stacking pattern (Bridge and Leeder, 1979), which imply that an increased aggradation rate caused the interconnectedness of channel-belt sandbodies to decrease. Subsequent models of Bryant *et al.* (1995) have suggested that the relationship between avulsion frequency and aggradation rate can result in sandbody connectedness both increasing and decreasing with increasing sedimentation rate. Hence, there is still no compelling evidence to suggest whether the development of major incised valley systems occurred during the deposition of the Lower Ketch Member.

The frequency distribution of channel-belt sandbody geometries will also have important ramifications for the prediction of inter-well connectivity. Collated datasets of sandbody geometries (e.g. Fielding and Crane, 1987), attributed to braided river deposition, show a high degree of scatter, and theoretical equations to derive sandbody width from sandbody thickness are ambiguous (see discussion in Chapter 2, Section 2.6.1). Using sandbody thickness measurement from the Lower Ketch Member and sandbody geometries from a possible outcrop analogue, the Escanilla Formation (Dreyer *et al.*, 1993), minimum and maximum sandbody width can be estimated. The Escanilla Formation sandbodies display width/thickness ratios of between 5 to >100 and provide tentative estimates for Lower Ketch Member channel sandbody widths (excluding splays) in the range of 16 to 2240 m. These sandbody width values are outside the range of channel-belt sandbody widths (117-1078 m) estimated from cross-set data (Section 3.8). Estimates of sandbody geometry from published literature cross plots of width versus thickness and cross-set data still provide only a range of possible sandbody widths. Consequently, field studies are required to match geological attributes between reservoir and outcrop analogue data, in order to provide a frequency distribution of sandbody geometries to constrain reservoir interconnectivity more accurately. The evidence presented in this section has highlighted the need to refine the estimates of channel-belt sandbody geometry by establishing the distinct frequency distributions of geometries for the sandbodies that are present within the Lower Ketch

reservoir interval. In order to achieve this, data from an onshore analogue must be gathered.

Discussion in this section has been limited to two-dimensional cross-stream width and thickness estimates from evidence from scattered core data. Yet channel-belts are three dimensional and downstream connectivity also needs evaluating. Channel orientation was identified as the critical factor affecting sandbody connectivity and gas recovery in the Schooner Field (Mijnssen, 1997). Therefore, future work must focus on the downstream connectivity within the Tyne Field to provide three-dimensional alluvial architecture. The use of wireline log analysis may also help constrain spatial trends within the Lower Ketch reservoir interval.

Burial compaction may also affect the prediction of alluvial architecture, geometries and sandbody connectivity. Sequences comprising of a distinct coarse-grained and fine-grained fraction may suffer from differential compaction, which may distort the subsurface architecture. Compaction is the subject for review in the next section.

3.12 Impact of compaction on Lower Ketch Member alluvial architecture

During post-depositional burial of sediments, compaction initially occurs in response to the pressure of overlying sediments and is assumed to be uniaxial, with no lateral displacement occurring. With studies such as Fielding and Crane (1987) using the relationship of sandbody thickness to sandbody width to predict alluvial architecture in reservoir evaluation, and subsequently using estimated widths in stochastic simulation models, it is now fitting to review the influence of compaction on: (1) sequences containing coarse sandstone and fine overbank facies, and (2) the prediction of sandbody widths based on preserved sandbody thickness or formative channel depth estimates.

Most compaction curves assume mechanical compaction is the only process occurring and no diagenetic effects are in action during burial (cementation and pressure solution). Giles *et al.* (1998) has suggested that compaction factors based on current models have a large error. Subsequently, the inappropriate use of default compaction curves can

introduce significant errors to any calculations of alluvial architecture. This section will introduce some empirically derived compaction estimates for the Lower Ketch Member reservoir interval, which requires information on: (1) the maximum burial depth, and (2) knowledge of the depositional environment. This section outlines some current ideas on how relative compaction of sediments can be calculated and their influence on estimates of formative channel depth and sandbody geometries determined.

A range of porosity - depth trends has been presented by several authors (Athy, 1930; Maxwell, 1964; Baldwin, 1971; Sclater and Christie, 1980; Shinn and Robbin, 1983; Baldwin and Butler, 1985; Caudill *et al.*, 1997) that demonstrate a porosity decrease with increasing burial depth. These trends assume that porosity loss is equal to compaction, assuming the solid volume remains constant, with no dissolution and overgrowth occurring during burial.

In large parts of the SNS basin, Carboniferous rocks are not at their maximum depth of burial at present day (Archard *et al.*, 1998). Therefore, estimates of compaction should be based on the maximum depth of burial that the reservoir interval reached during the basin's history. In outcrop studies, alluvial sequences have been subsequently uplifted, and therefore require burial depths to be ascertained. When using outcrop studies it is also often assumed that compaction effects are non-reversible and no further diagenetic alteration has occurred. Compaction estimates in this section are currently based on a present day burial depth of the Tyne reservoir of ~ 3660 m. The assumption is made that individual compaction estimates for the coarse sandbodies and fine overbanks remain constant over the entire vertical thickness of the reservoir interval (e.g. 150 m). Compaction estimates for coarse (sandstones) and fine fractions have been dealt with separately and estimates of porosity have excluded any diagenetic alteration.

3.12.1 Coarse fraction: channel-belt sandstones

The standard sandstone compaction Equation 3.7 by Sclater and Christie (1980) predicts a buried sandstone solidity of 82 % at burial depths equivalent to that of the Lower Ketch Member reservoir.

$$D_b = 3.7 \ln [0.49/ (1-S_b)] \qquad \text{Equation 3.7}$$

where D_b is depth of burial in km, S_b is buried solidity and assumes a grain density of 2600 kg m^{-3}. Therefore, porosity would equate to 18 %, which is a comparable value to the highest measurements of porosity taken within the coarse sandstones of cored intervals in the Lower Ketch Member reservoir interval (Symonds and van Dijk, 1995). Compaction calculations are based on the assumption that porosity is related to compaction thickness, i.e. solidity can be treated as a fraction or percentage of sediment thickness. Retallack (1993) proposed that initial solidity was the determining factor in calculating compacted sediment thickness at any given depth and therefore, modified the Sclater-Christie (1980) expression to give Equation 3.8 as:

$$C=-S_i/[0.49/(e^{(D/3.7)})-1] \qquad \text{Equation 3.8}$$

where C is compaction and S_i is initial solidity. Estimates of the minimum and maximum initial solidity of uncompacted sands at surface levels for the Lower Ketch Member were based on Beard and Weyl (1973) initial porosity values for unconsolidated sands of 42.5 % in very well sorted sands and 27.9 % in very poorly sorted sands. This range of initial porosity gave rise to initial solidity values in the range of ~0.55 - 0.75 to produce minimum and maximum burial compaction thicknesses for the Lower Ketch Member of 67 % and 92 % of their original thickness respectively.

Retallack's (1993) equation was chosen to calculate compaction estimates for the entire coarse fraction of the Tyne core. There is a low percentage of conglomerates in the Lower Ketch Member cored wells (< 10%) in most cores, with sand being the most predominant coarse fraction grain size. The presence of hydrocarbons and porewaters may preserve porosity during burial and also affect compaction estimates, but are very difficult to quantify. Similarly, grain sorting, grain shape and diagenesis also contribute to the compaction history. Compaction has the effect of decreasing the estimates of formative channel depths outlined in Section 3.8 and is often overlooked when applying information from analogue datasets to reservoir studies.

3.12.2 Fine fraction: overbank mud/siltstones

Traditionally, the compaction of fine-grained deposits (shales) has been considered to be greater than sandstones. Often calibrations of the finer fractions are scarce due to the general paucity of mudstone core samples. Baldwin and Butler (1985) (B-B) provided a power law Equation 3.9 for the compaction of 'normal' shales, based on determining solidity:

$$D_b = 6.02\ S_i^{6.35} \qquad \text{Equation 3.9}$$

where S_i is solidity. For burial depths of 3.7 km, a standard shale using B-B curve compacts to 22 % of its original thickness based on an initial solidity of 20 %. This initial solidity of 20 % may cause vast overestimates of compaction and would introduce significant geometric distortion to subsurface correlations of alluvial architecture in low net-to-gross reservoirs (Baldwin, 1971).

In a dry climate, the soils on a floodplain may dry out and bake hard soon after deposition and expel pore waters before burial occurs, in which case, during subsequent burial, there is limited opportunity for compaction due to dewatering. The non-reservoir overbanks of the Lower Ketch reservoir interval contain evidence of pedogenic alteration, suggesting formation in a semi-arid seasonal climate. Therefore, an initial solidity more characteristic of semi-arid soils, needs to be applied to the fine overbank sediments of the Lower Ketch Member. It is unlikely that the initial solidity of muds was as low as 20 % in this Carboniferous semi-arid climate. Retallack's (1993) estimate of 50 % initial solidity for shales is likely to give a more accurate estimate of initial solidity for the fine-fraction of the Lower Ketch Member.

Caudill *et al.* (1997) used data based on clastic dyke lengths in vertic palaeosols to calibrate thickness of compacted sediments against porosity and solidity in shales. Caudill *et al.* (1997) suggested compaction estimates for vertic palaeosols undergo significantly less burial compaction than is commonly assumed. As a result, vertic calibrated shale compaction curves based on a higher initial solidity of 70 % provide more realistic estimates of compaction for sequences containing palaeosols than standard shale compaction curves. Prior to burial, vertic soils are in a semi-compacted state, with high bulk densities, and may only start to compact at depths greater than 1.5

km. Blodgett (1985) also noted the high bulk densities of vertisols might limit compactability. Caudill *et al.* (1997) analysis of Late Carboniferous palaeosols and non-palaeosols shales at 2.5-3 km depth provides estimates of compaction of between 93 % and 70 % (maximum compactions) of their original thickness respectively. These estimates put compaction values for the fine fraction in a similar range to compaction values calculated for the coarse fraction of the Lower Ketch Member reservoir.

Without an estimate of burial compaction for cored interval and outcrop sequences errors could be significant. Using knowledge of maximum burial depth and depositional environment initial solidity of the fine fraction within the Lower Ketch Member deposits can be predicted to fall between 50 % (Retallack, 1986) and 70 % (Caudill *et al.*, 1997). These fine fraction values fall into a similar vertical compaction range as the coarse fraction within the Lower Ketch Member. Hence, facies-dependent differential compaction (e.g. Collier, 1989) between the coarse and fine factions is considered to be minimal and therefore will not have a large impact on the overall alluvial architecture. However, the topography of the base Lower Ketch Member is poorly constrained and does not allow any estimation of basement topography-induced compaction (e.g. Collier, 1989) to be calculated. The Lower Ketch Member sequence can be deemed to have undergone uniform deformation. Finally, any comparison of reservoir sandbody thickness with an onshore analogue requires the quantification of both maximum burial depth and depositional environment.

3.13 Stratigraphic and lithological outcrop analogues

The uncertainty in the prediction of reservoir connectivity for the Lower Ketch Member presented in Section 3.11 confirmed the need to assign and test an onshore outcrop analogue to the Lower Ketch Member. Application of datasets from sandbody geometries available within the literature has inherent limitations (discussed in Chapter 2, Section 2.6.1). Consequently, the use of documented outcrop studies described in the literature to interpret the lateral inter-well architecture of the Lower Ketch Member are shown to be unsatisfactory. The assignment of a stratigraphically equivalent analogue is preferable to a purely lithological analogue because if controls such as global climate and sea-level changes and development of land flora can be matched between reservoir and analogue, therefore, uncertainties are reduced.

The Lower Ketch Member reservoir interval correlates stratigraphically to the Etruria Formation (Westphalian B/C) (cf. Besly and Turner, 1983; Glover *et al.*, 1993; Besly and Cleal, 1997). The Etruria Formation is a mudstone dominated red bed succession that developed close to the equator under humid tropical climate conditions with seasonal rainfall variation. The presence of coal seams and increased reddening up the Etruria Formation sequence indicate that better drainage conditions prevailed during the late Carboniferous due to progradation of topographically higher, and thus better drained, floodplain environments. Sandbodies display lateral accretion surfaces resulting from deposition by meandering channels containing plant fragments. Comparisons between the documented studies of lithofacies within the Etruria Formation and the Lower Ketch Member suggest the depositional environments were not analogous. In addition, the poor onshore UK exposure prohibits the application of an UK onshore stratigraphic outcrop analogue and forces the testing of a lithological analogue. Similar lithofacies and environments of deposition have been documented for the Escanilla Formation, Southern Pyrenees, Spain (Bentham *et al.*, 1993; Dreyer *et al.*, 1993) and the Green River Formation, USA (Ryder *et al.*, 1976). The application of the Escanilla Formation as an analogue to the Lower Ketch Member is addressed in Chapter 4.

3.14 Grain size distribution

This section describes the methodology and rationale employed to obtain a composite grain size distribution for the Lower Ketch reservoir interval (Table 3.5). Grain size was measured in order to assess the feasibility of running a physical froude-scaled model of the Tyne Field to assist in reservoir characterisation (Chapter 5, Section 5.4) and compare to outcrop analogues. Well data are the primary data source for grain size analysis and an assumption was made that well data was representative of the whole reservoir interval. Cored intervals of conglomerate, pebbly sandstones, and sandstones from all wells were used in the analysis. These data were complemented with data on the < 2 mm grain size fraction using thin sections constructed from core plugs from wells 44/18-T3A, 44/18-T2 and 44/18-T1. For efficient characterisation of grain size, core lithofacies units described in Section 3.6 were reduced to four grain size dependent lithofacies groups (Table 3.6). In calculating grain size distributions for the Lower Ketch reservoir interval burial compaction has not been considered. The resultant grain

size distribution (Figure 3.13) has a D_{50} of 0.078 mm and D_{90} of 0.416 mm, therefore, the majority of the Lower Ketch Member comprises sand grade material or smaller.

Table 3.5. Step-by-step procedure for calculation of a composite grain size distribution for the Lower Ketch Member reservoir interval.

Step	Procedure
	Core analysis
1	Measurement of clasts >2 mm (observed longest axis) in 2-D sliced core. Clasts were measured to the nearest 0.5 mm to a lower limit of 2 mm. Medium axis measurements were also taken. (n = 1565)
2	Areas of an ellipse were calculated for each clast. Area of clasts were summed and divided by the area of the core interval measured. Results estimate the proportion of matrix (<2 mm) to clasts (>2 mm). Steps 1 and 2 were carried out in GC and PS lithofacies individually. PDF's were plotted.
	Thin section analysis
3	Measurement of the sediment fraction (matrix) <2mm using 18 thin sections from core plugs provided by ARCO British Ltd. from wells 44/18-T3A and 44/18-T2. Grains were measured to the nearest 0.01 mm to a lower limit of 0.04 mm under an optical microscope. All coarse reservoir lithofacies were analysed. (n = 1837)
4	Total coarse-grained grain size distribution was calculated by weighting distributions by the clast and matrix proportions.
5	Measurement of the non-reservoir (mudsilt) lithofacies <2 mm using 10 thin sections from core plugs provided by ARCO British Ltd. from all wells. Grains were measured to the nearest 0.001 mm to a lower limit of 0.004 mm under an optical microscope. (n = 1167) A single distribution was produced of all non-reservoir facies.
	Wireline/well completion data analysis
6	Six well completion logs constructed from wireline well data were used to estimate a reservoir to non-reservoir facies proportion.
7	Results from all the distributions were up-scaled to reflect the whole reservoir interval. Ratios of the three coarse lithofacies groups (Table 3.6) were kept in proportion.

Table 3.6. Lithofacies groups used for construction of the Lower Ketch Member grain size distribution.

Description	Grain sizes	Lithofacies units included
Reservoir facies		
Framework supported conglomerate	>2 mm and <2 mm (sand/gravel)	GC
Pebbly sandstones	>2 mm and <2 mm(sand/gravel)	PS
Well sorted sandstone and siltstones	<2 mm (sand)	SS, FS, SSrc
Non-reservoir facies		
Overbank fines	<2 mm (fine sand/silts/mud)	Fwc, Fob, Fr

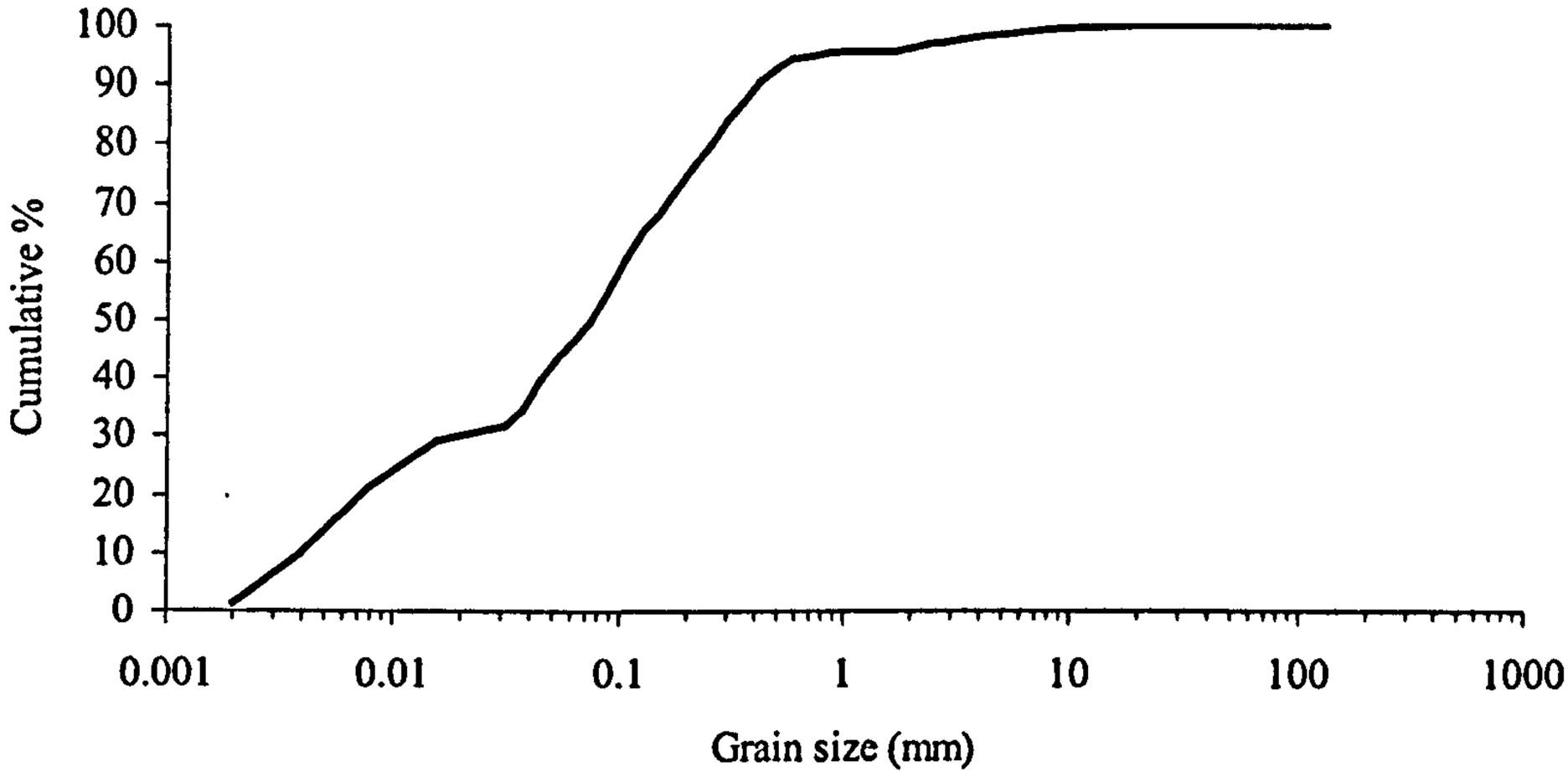

Figure 3.13. Grain size distribution for the Lower Ketch Member reservoir interval (D_{50} = 0.078mm).

The grain size distribution in Figure 3.31 provides a valuable parameter with which to compare the reservoir and any analogue sequence chosen. However, there are several limitations to the analysis of grain size distribution. The resultant depositional grain size distribution may not necessarily reflect the initial grain size distribution supplied to the fluvial system at the time of deposition, because the method employed in Table 3.5 does not account for: (1) sediment that may have been carried through the fluvial system and into the basin as bedload or suspended sediment and therefore were not deposited; (2) the contribution of fine-grained material by illuviation (in-wash of soil material); and (3) aeolian inputs to or removal from the basin. Consequently, future work needs to investigate: (1) the contribution of diagenetic/pedogenic versus detrital clays to the total volume of fine-grained material preserved in the Lower Ketch Member, (2) the influence of aeolian processes, and (3) the proportion of bedload and suspended sediment passing through the fluvial system during deposition, which are not preserved. The use modern analogues are required to constrain the later two. Quantification of illuvium and aeolian processes is difficult and has not been accounted for in reservoir-analogue comparisons for the Lower Ketch Member in this chapter. A change in the ratio of the fines being supplied to the system by the fluvial, aeolian and illuvium processes will have consequences for: (1) the depositional model proposed, and (2) the alluvial architecture at the time of deposition.

3.15 Lithofacies units and petrophysics relationships

Permeability is the most important quantifiable control in reservoir fluid flow simulations and a number of studies assume that permeability distribution pattern is a function of sedimentary facies and depositional process (see Alexander, 1993 for a review). Many studies have tried to link the petrophysical properties of porosity and permeability to lithofacies type (Chapter 2, Section 2.11). In order to evaluate the petrophysical properties of the Lower Ketch Member, dataset were evaluated from core plug samples analysed by ARCO from cores 44/18-T2, 44/18-T3A, 44/18a-5 and collated according to lithofacies units (Table 3.2).

Petrophysical properties (permeability and porosity) display a direct correlation to facies type in the Lower Ketch Member reservoir interval (Table 3.7) and correlations are primarily controlled by grain size, sorting and early pedogenic weathering (cf. Brayshaw *et al.*, 1996). There is a general decrease in reservoir quality with decreasing grain size of the lithofacies units, with the exception of the conglomerates facies (GC). Within the conglomerate facies, poor sorting is the most likely cause for poor reservoir properties. The best reservoir quality is exhibited by the pebbly sandstones (PS). The well-sorted sandstones (SS) have similar petrophysical properties to the pebbly sandstones. The location of these sandstone lithofacies at the top of fining upwards sequences sandbodies where mottling and bioturbation are common may account for a lower permeability than the PS facies. Where correlation between lithofacies and petrophysical properties are weak, diagenetic alteration of petrophysics (e.g. secondary overgrowth or dissolution) may be responsible and therefore must also be evaluated.

Table 3.7. Statistics for porosity and permeability for each lithofacies type observed within the Lower Ketch Member of the Tyne Field. Refer to Table 3.2 for lithofacies descriptions.

Porosity (%)

Facies code	n	Mean	Median	Minimum	Maximum	Standard deviation
GC	54	8.3	8.5	2.4	14.3	2.9
PS	153	11.1	12.1	3.4	17.4	3.6
SS	182	12.2	12.9	0.6	20.9	4.3
Fwc	NA	NA	NA	NA	NA	NA
FS	22	6.0	5.8	1.1	12	2.7
SSrc	5	4.5	5.7	1.8	7.5	2.5
Fob	9	2.9	2.8	0.8	5.2	1.4
SSr	25	4.6	3.8	0.6	10.1	2.9
Fr	8	3.2	3.4	0.8	5.2	1.5
Total	458					

Permeability (mD)

Facies code	n	Mean	Median	Minimum	Maximum	Standard deviation
GC	34	159.3	24	0.16	2000	369.8
PS	109	306.3	60	0.04	3140	544.1
SS	190	193.6	14	0.01	3460	425
Fwc	NA	NA	NA	NA	NA	NA
FS	24	3.0	0.08	0.01	62	12.6
SSrc	5	0.6	0.34	0.09	1.7	0.7
Fob	8	0.5	0.30	0.03	1.1	0.4
SSr	28	0.3	0.03	0.01	6	1.1
Fr	13	0.2	0.02	0.01	1.1	0.4
Total	411					

Identification of this link between lithofacies/architectural elements and petrophysical properties permits the use of these data in reservoir simulation models. Additional information is required on the geometry of lithofacies, which then allows the up-scaling of petrophysical properties in dynamic reservoir modelling.

3.16 Summary

Investigation of the Lower Ketch Member has highlighted several conclusions:

1. The Lower Ketch Member contains nine individual lithofacies units. Coarse deposits (60 %) can be grouped into four vertical facies associations: channel-belt sandbodies (Types A,B), overbank splay sandbodies (Type C) and amalgamated sandbodies (Type D). Sandbodies exhibit a cyclical alternation with heavily oxidized floodplain fines (40 %). A depositional environment is proposed of an aggrading alluvial plain with a series of 120 to 1080 m wide, sandy braided channel-belts and associated overbank crevasse splays and splay lobes deposited coevally with overbank floodplain and possible lacustrine deposits. Palaeochannels within the sandy braided rivers were between 1.5 and 3.5 m in depth. Channel-belts resulted in the deposition of single and stacked sandbodies of thickness between 2.5 and 22+ m. Climate was seasonal and floodplains were both well and poorly drained with limited soil formation due to ensuing aggradation. A fine-grained sediment supply was critical for the preservation of extensive floodplain deposits.
2. Results from the Lower Ketch Member are consistent with a regional model of a northerly supplied aggrading sandy braided river system, where sandbody net-to-gross and connectivity decreased in a southerly direction. Evidence for incised valley formation is inconclusive and predictions of sandbody connectivity are ambiguous. Comparison with the literature suggests that sandbody widths range between 20-2240 m and therefore, require further quantification to gain frequency distributions. Onshore UK stratigraphic analogues exhibit contrasting lithofacies trends and interpreted depositional environment to the deposits of the Lower Ketch Member, Tyne Field, consequently, an alternative outcrop analogue is required.
3. Facies-dependent differential compaction within the Lower Ketch reservoir interval was minimal, and although errors are large, burial compaction estimates suggest the sequence may be ~73 % of the original depositional thickness.
4. The lithofacies units of the Lower Ketch Member show a direct relationship to petrophysical properties and thus permit the incorporation of three-dimensional lithofacies geometry into future static (object-based) and dynamic reservoir models.

Chapter 4. A low net-to-gross analogue for the Tyne Field: The Escanilla Formation, Southern Pyrenees, Spain

4.1 Synopsis

This chapter documents the findings of fieldwork carried out on the Escanilla Formation, Southern Pyrenees, Spain, and discusses the suitability of the Escanilla Formation as an outcrop analogue for the Lower Ketch Member, Tyne Field, SNS (Chapter 3). The Escanilla Formation exhibits comparable vertical facies trends to the Lower Ketch Member, which resulted from the co-existence of several channel-belt types operating in the Ainsa Basin during the deposition of the sequence. Channel-belt types include laterally unconstrained sandy-gravel braided streams, higher sinuosity channels, and laterally confined low sinuosity channels. Overbank flooding of the channel-belts resulted in sheet flows and splay deposition that extended out from the channel margins. Sandbodies are classified as: ribbons, sheet sandstones, sheet sandstone with conglomerates and splays. Overbank deposits comprise 36 % of the Escanilla Formation sequence and represent deposition on a floodplain where lakes existed for periods of time long enough for limestone and algal mat development to occur. Two-dimensional sandbody geometry is quantified and predictions made on Lower Ketch Member inter-well alluvial architecture.

4.2 Introduction

In order to understand subsurface reservoir architecture and aid prediction of heterogeneity, onshore outcrop analogues are used to gain information on sandbody size, geometry (width:length:thickness) and internal structure (e.g. Lorenz *et al.*, 1985; Bridge *et al.*, 2000). The Carboniferous Lower Ketch Member (Chapter 3) is characterised by alternations of coarse-grained sandbodies situated within fine-grained overbank floodplain deposits. Subsurface sandbodies within the Lower Ketch Member were estimated to have formed from channel-belts with widths of between 120-1080 m, and therefore many of the sandbody dimensions are less than the typical well spacing (~ 0.5 km) and cannot be resolved using subsurface techniques. Consequently, the application of a lithological outcrop analogue to evaluate the subsurface architecture of the Lower Ketch Member reservoir interval and validate subsurface well correlations

was chosen because: (1) UK stratigraphic analogues show dissimilar lithofacies characteristics and do not expose enough outcrop to gain geometric data over distances equivalent to well spacing; (2) well correlation, seismic, chemostratigraphic and biostratigraphic datasets poorly constrain internal reservoir architecture; and (3) estimates of channel-belt width from empirical equations (Chapter 3, Section 3.8) predict a wide range of possible sandbody geometries that need to be more accurately forecast.

The lithological analogue chosen was the Eocene Escanilla Formation, Southern Pyrenees, Spain, which was first described by Garrido-Megias (1968). Subsequent work by Bentham (1992), Bentham *et al.* (1992, 1993) and Dreyer *et al.* (1993) describe in detail the stratigraphy and sedimentology of the Escanilla Formation. Using the Escanilla Formation the aims of this chapter are:

1. To characterise the lithofacies units present within the Escanilla Formation and reassess the depositional model put forward by Bentham *et al.* (1993).
2. To assess the Escanilla Formation as an analogue for the Lower Ketch Member deposits from the Tyne Field reservoir, SNS.
3. To quantify channel-belt sandbody geometry and provide estimates of inter-well sandbody connectivity for the Lower Ketch Member reservoir.

4.4 Background and stratigraphy of the Escanilla Formation

The Escanilla Formation is a 750 m thick sedimentary sequence (Figure 4.1) located within the Ainsa and Tremp-Graus Basin complex, Southern Pyrenees, Spain. Escanilla Formation has been interpreted as medial/distal alluvial fan to axial fluvial system deposits (Bentham *et al.*, 1993; Dreyer *et al.*, 1993). The Escanilla Formation is characterised by a range of channel-belt sandbodies set within a sequence of fine-grained overbank deposits. Bentham *et al.* (1993) proposed a new aggrading braided stream model for the Escanilla Formation and attributed the presence of abundant fine-grained material to high aggradation rates of between 0.25-0.35 mm/1000 years (uncompacted).

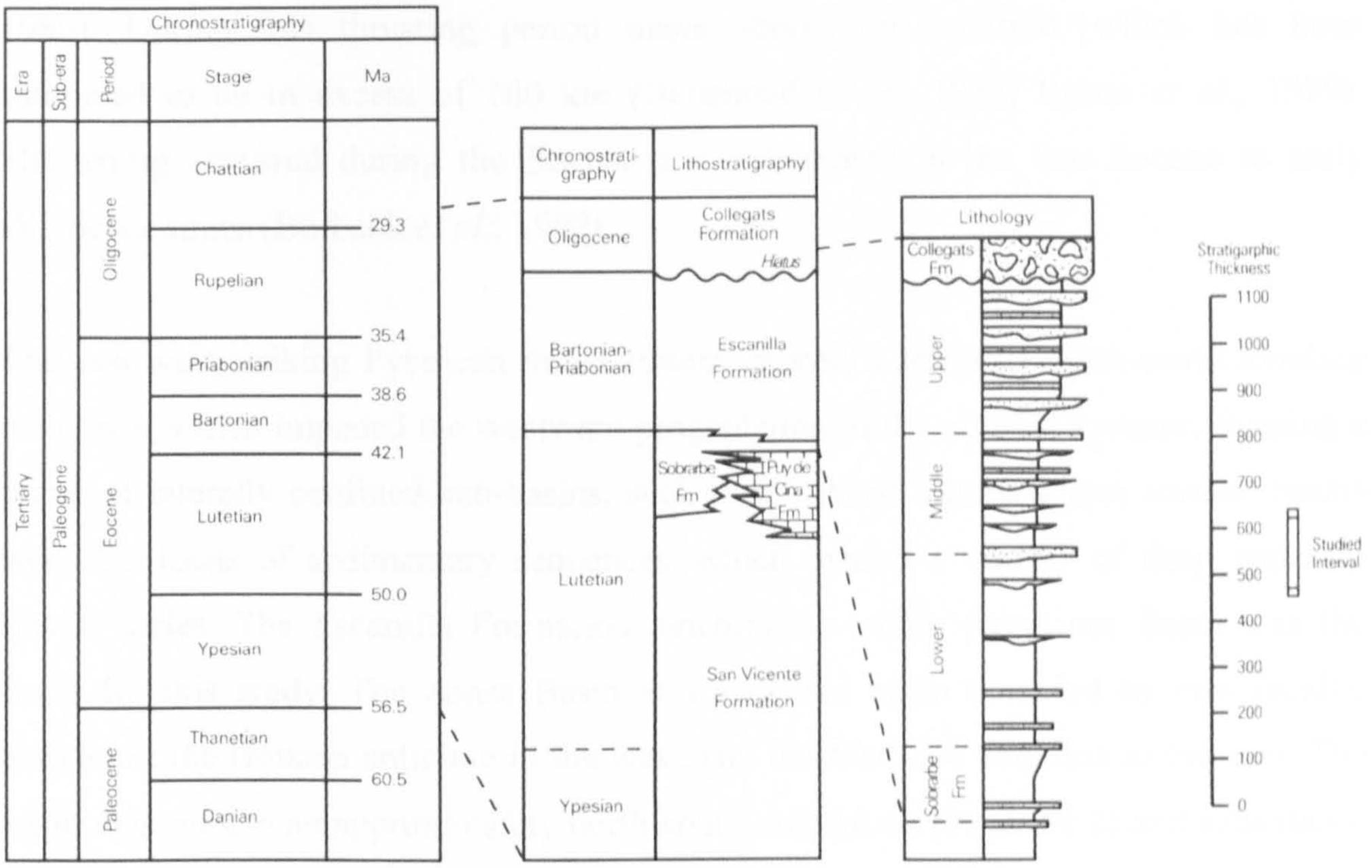

Figure 4.1. Tertiary stratigraphic framework of the Ainsa Basin, Southern Pyrenees, Spain. Chronostratigraphy has been taken from Hartland *et al.* (1990) GT589 timescale and lithostratigraphy adapted from Bentham (1992). The bar indicates the interval investigated for comparisons with the Lower Ketch Member, SNS. Note the general increase in net-to-gross up sequence.

The Escanilla Formation forms the lower part of the Campodarbe Group and is underlain by shallow marine and deltaic units of the Belsue Formation and the Sorbrarbe Formation (Dreyer *et al.*, 1999, Figure 4.1). Bentham (1992) puts the base of the Escanilla Formation at the contact where the sequence is underlain by grey marls containing bivalves and trough cross-stratification. This underlying unit is capped by a horizon of shallow marine nummalitic foraminifera that can be observed on the dirt road between the villages of Olson and Mondot. A progressive unconformity develops towards the anticlines of the Ainsa Basin and the Escanilla Formation is superposed on a marine limestone of Lutentian age (Dreyer *et al.*, 1993). A major sub-regional unconformity bounds the top of the Escanilla Formation, which is overlain by the coarse alluvial conglomerates of the Oligocene Collegates Group (Garrido-Megias, 1973). The Escanilla Formation is divided into three informal members: *Lower*, *Middle* and *Upper* Members (Bentham *et al.*, 1992). A thick 30–40 m basin-wide amalgamated sandbody unit has been taken as the boundary between the Lower and Middle Escanilla Formation (Bentham, 1992) and the sequences immediately above and below this boundary exhibit similar facies.

PAGE NUMBERING AS ORIGINAL

1986). During this thrusting period major shortening occurred, which has been estimated to be in excess of 100 km (Deramond *et al.*, 1985; Roure *et al.*, 1989). Shortening occurred during the Eocene and culminated in the late Eocene to early Oligocene times (Burbank *et al.*, 1992).

The east-west striking Pyrenean thrust system created a series of north-south trending anticlines, which impeded the westward progradation of the alluvial systems, forming a series of laterally confined sub-basins, such as the Ainsa Basin. These smaller basins were the focus of sedimentary sequences, which exhibit a variety of deep water to fluvial facies. The Escanilla Formation outcropping within the Ainsa Basin was the focus for this study. The Ainsa Basin is a synclinal basin bounded by two parallel anticlines: the Boltana anticline in the west, and the Mediano anticline in the east. The basin axis runs in an approximately north-south orientation (Figure 4.2) and subsidence rate increases as a function of distance away from the growing anticlines (Bentham *et al.*, 1993).

Clastic detritus into the southern Pyrenean basin was predominantly derived from the Pyrenean source to the north of the basin. Clastic input from the Catalan ranges to the east and the Iberian ranges to the southwest were volumetrically less important (Turner *et al.*, 1984).

A palaeomagentic study by Smith (1996) suggests the Iberian Peninsular has only undergone approximately 4° northward drift in latitude since middle Eocene times when the basin was situated between 35-40° N latitude. During the Eocene the Ainsa Basin was subjected to a Mediterranean to semi-arid climate (Atkinson, 1983).

4.5 Ainsa Basin field site

The Escanilla Formation outcrops extensively within the small 20 km wide Ainsa Basin, Southern Pyrenees (Figure 4.2). The best exposure is along a prominent generally east-west trending, north facing ridge that outcrops across the entire basin. This ridge is formed by the differential erosion of a large amalgamated sandbody punctuated by a series of gullies. The Escanilla Formation has been mapped out between the villages of

Barcabo in the west, Escanilla in the east, and Castejon de Sobrabe in the north (Bentham *et al.*, 1993, Figure 4.2).

Access to the outcrop is generally good due to differential erosion of the finer overbank lithologies relative to the coarser channel deposits creating a stepped topography. A series of local roads allow access to the outcrops from the main A-138 (Ainsa-Barbastro) Road and the smaller Barcabo-Boltana Road (Figure 4.2), which are orientated parallel to the basin axis.

4.6 Data acquisition and methodology

In order to investigate the alluvial architecture of the Escanilla Formation, two 150 m vertical sedimentary successions were studied at two localities: (1) the centre (Olson), and (2) the western margin (Casa de Coloma) of the Ainsa Basin. These two locations were chosen on the basis of good exposure and access (Figures 4.3). Cross-sectional panels from the two localities provide data on sandbody geometry, size and location. Each section panel was orientated sub-perpendicular to the general north-south palaeoflow direction (Bentham *et al.*, 1993; Dreyer *et al.*, 1993) and extended for a distance of ~1 km, allowing examination of the alluvial architecture on an inter-well scale. Sedimentary logs were taken through the two sectional panels to characterise the vertical and lateral lithofacies trends and provide net-to-gross estimates.

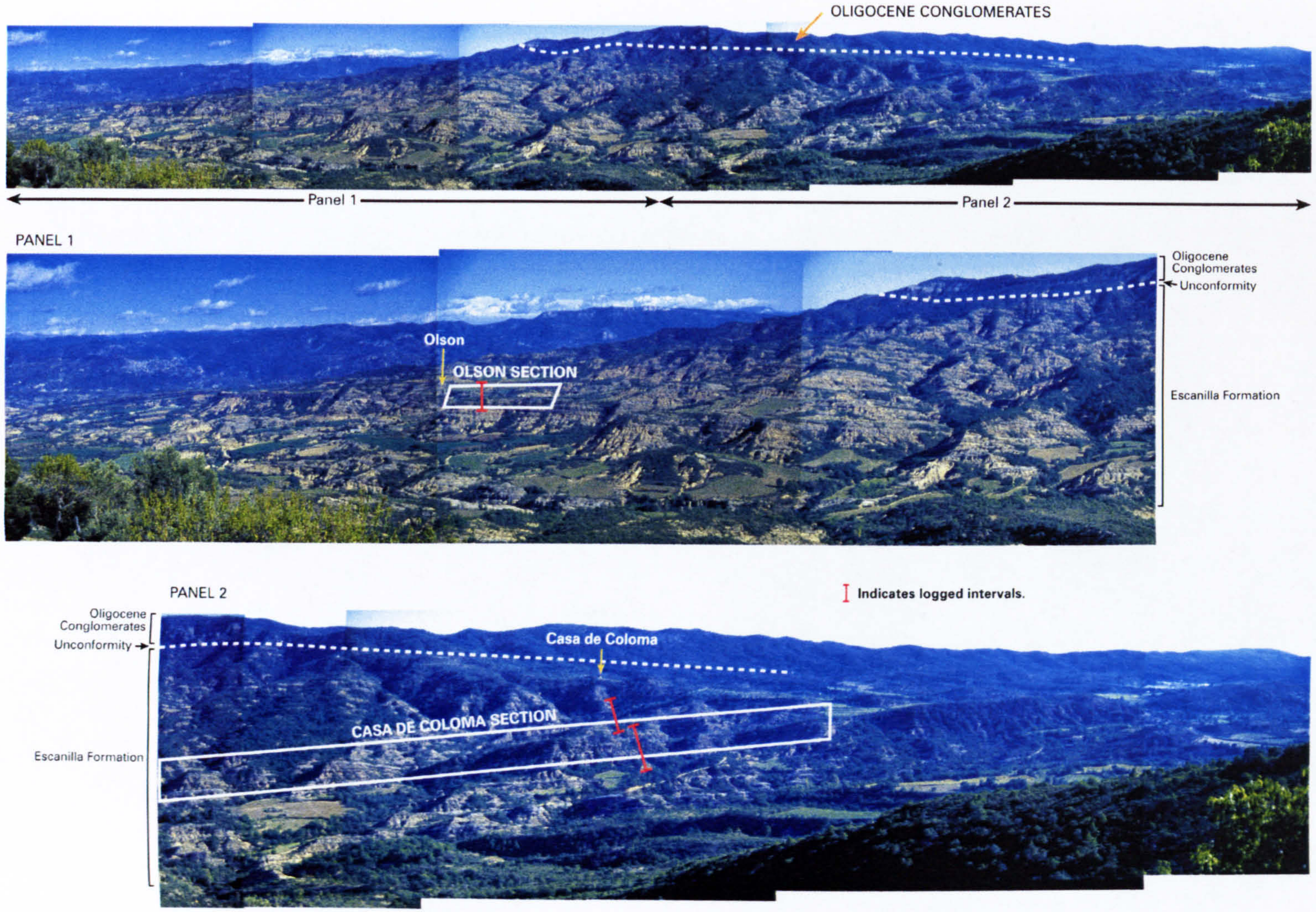

Figure 4.3. Escanilla Formation exposure in the Ainsa Basin with boxed areas showing where alluvial architectural datasets were collected (View SE from the village of Eirpol).

4.7 Lithofacies analysis from outcrop

The deposits of the Escanilla Formation consists of two distinct lithofacies groups: (1) a coarse channel-belt fraction forming discrete sandbodies containing sandstones, pebbly sandstones and conglomerates; and (2) a fine-fraction comprising red-orange overbank silts and muds exhibiting immature palaeosol development. A summary of the lithofacies scheme and interpretation is presented in Table 4.1. Where Escanilla Formation lithofacies analogue lithofacies that were observed within the Lower Ketch Member (Chapter 3, Table 3.2) identical lithofacies codes were assigned.

Much of the facies descriptions from the Escanilla Formation bear similarities to those presented by Bentham *et al.* (1993) and Dreyer *et al.* (1993), although, some new information is presented regarding the palaeontology and limestone beds found within the overbank deposits of the Escanilla Formation.

Initial assignment of the analogue sequence was founded on similarities in grain size fractions (i.e. sandbodies and floodplain deposits) and sedimentary structures between the Escanilla Formation and cored intervals from the Lower Ketch Member, SNS (Chapter 3). The Escanilla Formation lithofacies show a marked similarity to many of the lithofacies documented within the Lower Ketch Member. While matching facies is the foundation for any reservoir analogue study, quantitative geometrical information cannot be extrapolated from outcrop to the reservoir without a full comparison and validation of the two sequences. Consequently, the remainder of this chapter is dedicated to: (1) characterising the sandbody types and vertical facies associations; (2) quantifying the scale of the palaeochannels; (3) reviewing the depositional model; (4) quantifying the sandbody geometries; and (5) assessing the suitability of the Escanilla Formation as an analogue to the Lower Ketch Member.

Table 4.1. Lithofacies units observed within the Escanilla Formation, Spain. Facies are coded based on Miall (1977, 1978) classification scheme.

Code	Lithofacies unit	Sedimentary structure/ Texture	Depositional processes/ interpretation	Percentage of lithofacies in the logged interval	Lithofacies associations	Two-dimensional shape (perpendicular to palaeoflow)	Comparison with the literature
GC	Coarse-gravel framework conglomerate	Massive to crudely bedded. Poorly sorted, containing subrounded clasts up to 15 cm diameter. Bounded at the base by a sharp erosion surface.	Channel lag deposit and coarse bed-load dominated channel deposition within braided streams. Large scale bar migration.	17.5 %	GC, PS, SS (Fining upwards channel fills, can show stacking)	Sheet	Lithofacies A and B, Steel & Thompson, 1983. Plates A. Figure 1-10 Atkinson *et al.* (1990); Sometimes observed a channel sheet, plate 1.2, Mader, (1985); Gt, Gp, Gh, Gcm Miall, (1977). Similar to gravel facies of Ramos and Sopeña (1983); G1, G2, Siegenthaler & Huggenberger (1993)
PS	Trough and planar cross-bedded pebbly sandstone	Medium to coarse sandstone with up to 40% clasts often grading into sandstone. Can occur as sheets of lenses.	Dune and bar migration in a sandy braided river.	7.7 %	GC, PS, SS (Fining upwards channel fills, can show stacking)	Sheet and lenses	Lithofacies C, Steel & Thompson, 1983. Plates B and C. Figure 1-10 Atkinson *et al.* (1990); St, Sp, Sl, Sh Miall, (1977); Plate 2.1 alternating sandstone/gravel Mader, (1985); Sandstone facies of Ramos *et al.* (1986); G3 Siegenthaler & Huggenberger (1993)
SS	Trough cross-bedded well-sorted fine to medium sandstone	Medium to coarse sandstone, well sorted with a few pebbles Trough cross-bedded sandstone can occur as sheets or lenses.	Dune and bar migration in a sandy braided river.	30.1 %	GC, PS, SS (Fining upwards channel fills, can show stacking)	Sheet and lenses	Lithofacies D and E, Steel & Thompson, 1983. Plates D. Figure 1-10 Atkinson *et al.* (1990); St, Sp, Sl, Sh Miall, (1977); Facies h Ramos *et al.* (1986). Fine - grained deposition niches of Ashworth *et al.* (1999)

Table 4.1. Continued

Code	Lithofacies unit	Sedimentary structure/ texture	Depositional processes / interpretation	Percentage of lithofacies in the logged interval	Lithofacies associations	Two-dimensional shape (perpendicular to palaeoflow)	Comparison with the literature
Fwc	Laterally confined mud/silts	Channel plug mud and silt often pedogenically reddened.	Channel plugs bounding the top of abandoned channel fill sequences.	Not encountered in the logged interval used.	GC, Fwc, PS (Fining upwards channel plug)	Lense	Fl, Fsm Miall, (1977); Facies f Ramos *et al.* (1986).
FS	Fine- to coarse-grained isolated planar -rippled sandstones	Fine-to coarse coarse sandstone containing planar laminea, with some ripples. Some mud matrix observed. Fining-up. Rare	Single channels or lobes, possibly crevasse channels breaching the channel margin and scouring overbank deposits. Isolated or sheet sandstones.	8.6 %	FS, SSrc (Single channel scouring out muds/silts)	Sheet, wedge	Sh, Se, Miall (1977,1992); Facies h Ramos *et al.* (1986). Splays of Bentham *et al.* (1993).
SSrc	Intraformational rip-up muds within a fine sandstone units	Fine to coarse sandstones containing elongate angular rip-up clasts of mud/silts up to mm long and aligned to bedding. Rare	Single crevasse channels breaching the channel margin and scouring/ incising overbank deposits, forming an intraformational lag.	Not encountered in the logged interval used.	FS, SSrc (Single channel scouring out muds/silts)	Planar	
F/Fr	Pedogenically modified muds/silts	Pedogenically modified oxidized red mud/silts with pervasive mottling. Destruction of all primary sedimentary structures except under sandstones where horizonation can be observed. Oncoids, dessciation cracks, calcretes and traces fossils observed. Domichnia traces common.	Overbank deposition with subsequent soil development, during periods of relative non-aggradational phases. Some freshwater lacustrine deposition. Insect traces.	36 %	F/Fr, L (Different palaeosol horizons)	Tabular	Fl, Sh Miall, (1977)
L	Limestone	Limestone beds range in thickness from 10 cm to 40 cm and maximum widths of 500 m. Containing small gastropods and ostracods	Freshwater lacustrine deposition in shallow, low energy environment lake.	0.1 %	F/Fr, L	Sheet	Freshwater limestones in similar to those of Nickel (1983)

4.8 Significance of overbanks for environmental interpretation

Fine-grained sandstone and siltstones representing overbank deposition within the Escanilla Formation exhibit pervasive reddening. In addition, very few primary sedimentary structures are preserved as a result of heavy weathering. Analysis of the overbank floodplain deposits reveals several important features, which are described in the proceeding sections and assist in environmental reconstruction.

4.8.1 Palaeosols

Observation of freshly weathered fines beneath sandbodies show cyclic palaeosol horizonation and bedding (Figure 4.4). However, these horizons cannot be traced laterally and therefore, pedofacies relationships (e.g. Kraus and Bown, 1987) cannot be applied. Where palaeosols can be observed, development is immature and characterised by an extensive mottling of the brown and red overbanks into greys, purples, greens and yellows. These poorly developed soils may have been analogous to modern day Aridisols and Entisols. Occasionally, desiccation cracks were observed on bedding surfaces indicating that some subaerial exposure of the floodplain occurred. The poorly developed palaeosol characteristics may indicate high aggradation rates prevailed during the deposition of the Escanilla Formation (Bentham *et al.*, 1993).

a

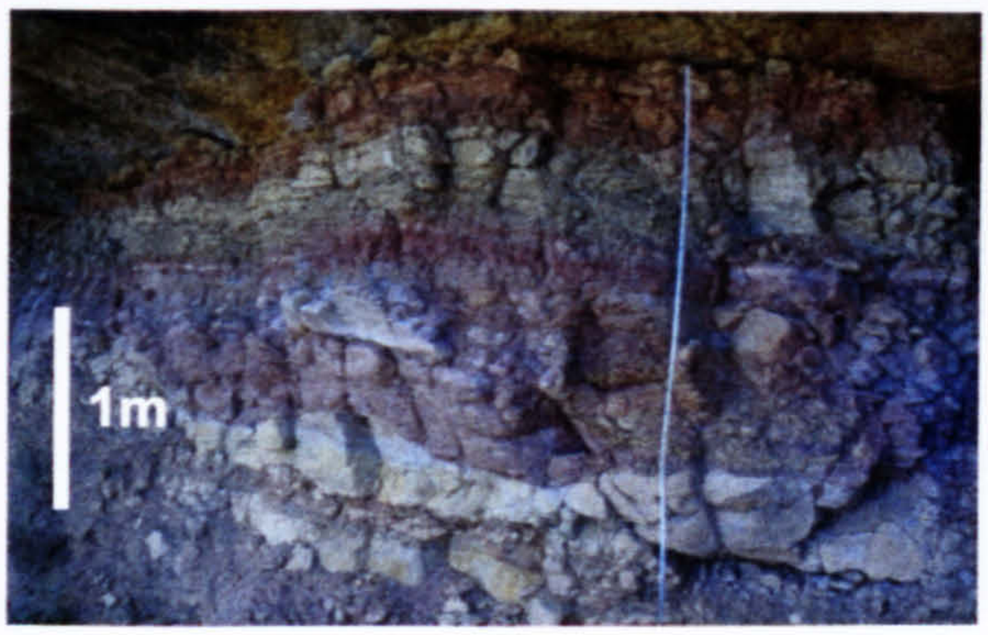

b

Figure 4.4. Palaeosol development within the Escanilla Formation showing (a) horizonation and (b) horizontal bedding picked out by subtle changes in the grain size within the overbank deposits.

4.8.2 Gypsum beds

Gypsum is found in the Lower Escanilla Formation, occurring in vertic structures. Gypsum is rarely present in the Middle and Upper Escanilla Formation. The gypsum may have been present in the Lower Escanilla because sediments represent deposition on a low-lying alluvial plain, which was subjected to marine incursions. Marine incursions replenished sulphate supplies in porewaters allowing gypsum to form. As the alluvial plain prograded basinwards, a shallowing upward sequence was created (Mutti *et al.*, 1988) and the impact of marine incursions would have been less pronounced. Consequently, sulphate supplied to the floodplain was reduced, which resulted in a change from a marine evaporite environment to a shallow freshwater lake environment where carbonate precipitation occurred (e.g. Schreiber, 1980). The reduced sulphate supply to the Upper and Middle Escanilla Members may have inhibited gypsum bed formation.

An alternative explanation for the development of gypsum may be that the vertic structures were produced diagenetically, in which case the Escanilla Formation would not have necessarily have undergone any base-level changes in order to get the change in facies up through the sedimentary sequence. Consequently, the change in facies could have formed as a result of the progressive progradation of the alluvial plain throughout the deposition of the Escanilla Formation sediments. Gypsum may be more similar to the satin spar veins described in Gustavson *et al.* (1994). The origin of the gypsum in the Escanilla Formation requires further investigation.

4.8.3 Oncoids

Cylindrical nodules were observed in clusters within the overbank deposits, commonly found to be preferentially eroded out of the floodplain fines (Figure 4.5). Sizes of nodules range from 0.1-1.6 m in length and 0.02-0.33 m in diameter. The external surfaces were commonly smooth with a concentric internal structure. Preserved nodules are often ellipsoidal in cross-section as a result of anisotropic compaction during burial. These nodules have been interpreted as oncolites, formed by *Cyanophyta* (blue green algae) with centrifugal growth patterns around an intermittently mobile nucleus (cf. Riding, 1983). Nodules are similar to the type C (concentrically stacked layers molding the outline of the core) and type R (randomly stacked more or less concentric layers

with protruding bumps or domal overgrowths) oncoids described in the Eocene Guarga Limestones in the adjacent Tremp-Graus Basin (Nickel, 1983). Oncoids would have formed under similar conditions to those depositing the limestone beds of facies L (Section 4.8.4). The oncoids observed within the Escanilla Formation are unusually large (maximum 1.6 m) and their elongate nature indicate that the algal growth nucleated on twigs, roots or logs that controlled the size and shape of the nodule. The internal fill of the oncoids varies and includes material from the surrounding overbank silts and drusy calcite replacement fill. The later replacement fill of the nucleus suggests the nucleus was soft organic material that has subsequently decayed, although, no evidence for the presence of vegetation for the nucleus was observed within the sequence. Vegetation that allowed oncoid nucleation to occur may have been provided from areas more proximal and at higher elevations within the basin.

Algal mat oncoids indicate shallow continental lacustrine settings. In modern environments oncoids occur on a soft bottom substrate covered with marcophytes, in water depths less than 3 m (Flügel, 1978; Schneider *et al.*, 1983). Oncoids appear to have undergone several phases of growth and been rolled around by wave action. Oncoids alone are not environment specific, having been described in marine (Peryt, 1981), brackish (Monty, 1979) and freshwater (Fritish, 1959; Monty, 1972; Nickel, 1983; Riding and Voronova, 1982; Schneider *et al.*, 1983) environments. Their presence has been noted to represent areas of slow sedimentation rate (Peryt, 1981) and in fluviolacustrine environments they require low sediment load and turbidity of the water (Mouline, 1977). Algal growth would have been stopped by reactivation of channels during flood periods. Periodic agitation is indicated by the oncoids concentric construction and documents the intermittent proximity of a high energy transporting medium to these sediments (Nickel, 1982). Flowing water would have been needed to form a crust on the oncoid. These oncoids probably formed rapidly, in the order of tens of years. Growth rates of up to 2.2 mm yr^{-1} have been noted by Merz-Preiß and Riding (1999), suggesting that the largest Escanilla oncoids could have formed in a minimum of 150 years. In summary, oncoids suggest shallow lakes formed on the floodplain where for significant periods of time there was no influence by fluvial activity.

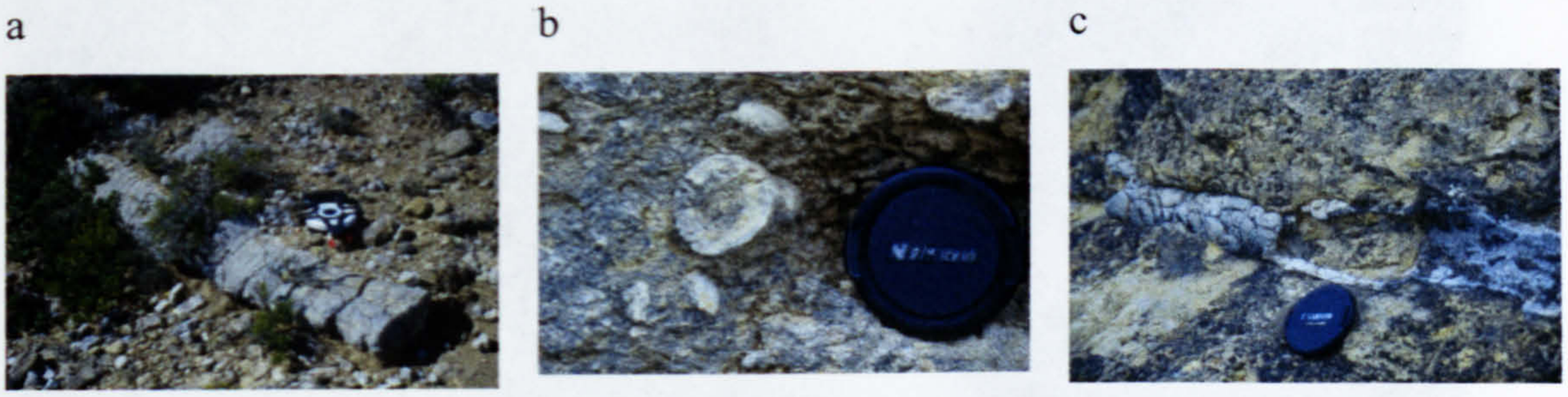

Figure 4.5. Oncoids observed within the Escanilla Formation. (a) a cylindrical oncoid with a length of 1.6 m, (b) oncoids showing a concentric growth pattern, and (c) an oncoid showing a silty internal fill.

4.8.4 Limestones

Whitish grey micritic limestones are observed in 0.1-0.4 m thick beds with lateral extents over 500 m (Figure 4.6a). Thin section analysis exhibits micritic textures and an absence of body fossils in some of the limestone beds. In other samples complete and fragmented gastropod and ostracods shells were observed within a faecal pellet matrix (Figures 4.6b-c). Limestones are analogous to those described as fluviatile/lacustrine distal interchannel carbonate facies in the Guarga Formation in the adjacent Tremp-Graus Basin (Nickel, 1982) and also descriptions presented in Freytet (1973) and Martinius (2000). Low energy shallow lakes, with limited suspended sediment concentration were the depositional setting for the limestone formation. Lakes were periodically separated from any fluvial activity and low clastic sedimentation rates allowed carbonates to form. Persistence of the lakes was controlled by channel-belt migration or avulsion, and their period of existence may have been in the order of 10000 years based on the Guarga limestones (Nickel, 1982). Work by Crouzel and Meyer (1977) suggested that with increasing distance from the apical area of a fluvial fan, the relative contribution of carbonates to the overall clastic sequence would increase. Calcium is probably supplied to the distal parts of the alluvial system by groundwater that drained the southern Pyrenees (Nickel, 1982). These limestone beds indicate temporary ponding of water on the floodplain caused by either tectonically or climatically controlled base-level change.

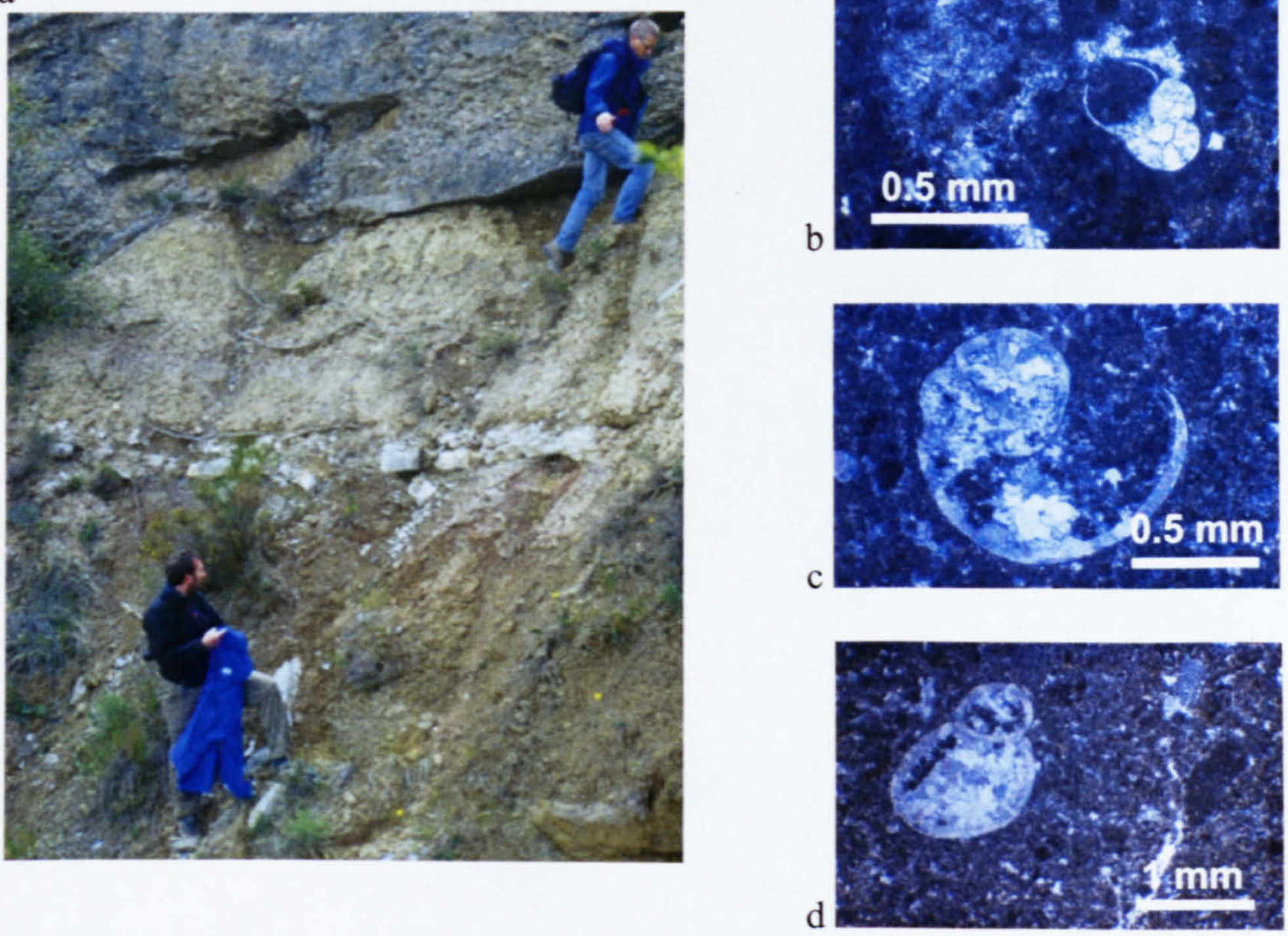

Figure 4.6. (a) Limestone bed within the overbank deposits and thin sections taken through the limestones showing (b-c) freshwater gastropods and (d) ostracods indicating the occurrence of lacustrine depositional systems on the floodplain.

4.8.5 Trace fossils

Vertical burrows, with maximum lengths from 100-200 mm and 10 mm in diameter, occur abundantly within the Escanilla Formation deposits (Figure 4.7a). Preservation is particularly good beneath the basal contacts of major fluvial sandbodies, where burrow fill material is often coarser than the surrounding sediment, forming positive relief casts. Cylindrical structures appear to be coarsely meniscate, with meniscate spacings of approximately 5-10 mm. Burrow orientation is commonly vertical, although they are often twisted. Preserved terminations are rare, gently rounded and do not taper or branch. Burrows from the Escanilla Formation are very similar to the Domichnia Type 8 (Figures 12c/d and 13c) described by Bown (1982) within the fluvial Oligocene Jebel Qatrani Formation, Egypt. Burrows also occur within the fine-grained sandstone bodies, although they are less common, occurring on discrete pause-plain horizons within vertically stacked sandbodies (Figure 4.7b).

Burrows were formed by organisms with little substrate preference or by multiple organism types. Bentham *et al.* (1993) suggested that the cylindrical structures formed

from vegetation such as thick grass or reed rizoliths, which colonised the floodplain. However, the lack of branching, tapering or size diversity argues against rizolith origin. Similar burrows have been documented by Stanley and Fagerstom (1974, p77, Figures 10-11) and have been known to form by insects (e.g. Ratcliffe and Fagerstom, 1980) and spiders (e.g. Ahlbrant *et al*., 1978; Ratcliffe and Fagerstom, 1980).

Other burrows exhibit horizontal feeding traces on exposed overbank bedding surfaces (Figure 4.7c). These traces may have been formed by beetle larva similar to the traces observed in the red bed Wilwood Formation of Wyoming (Andy Pulham, pers. Comm.1998).

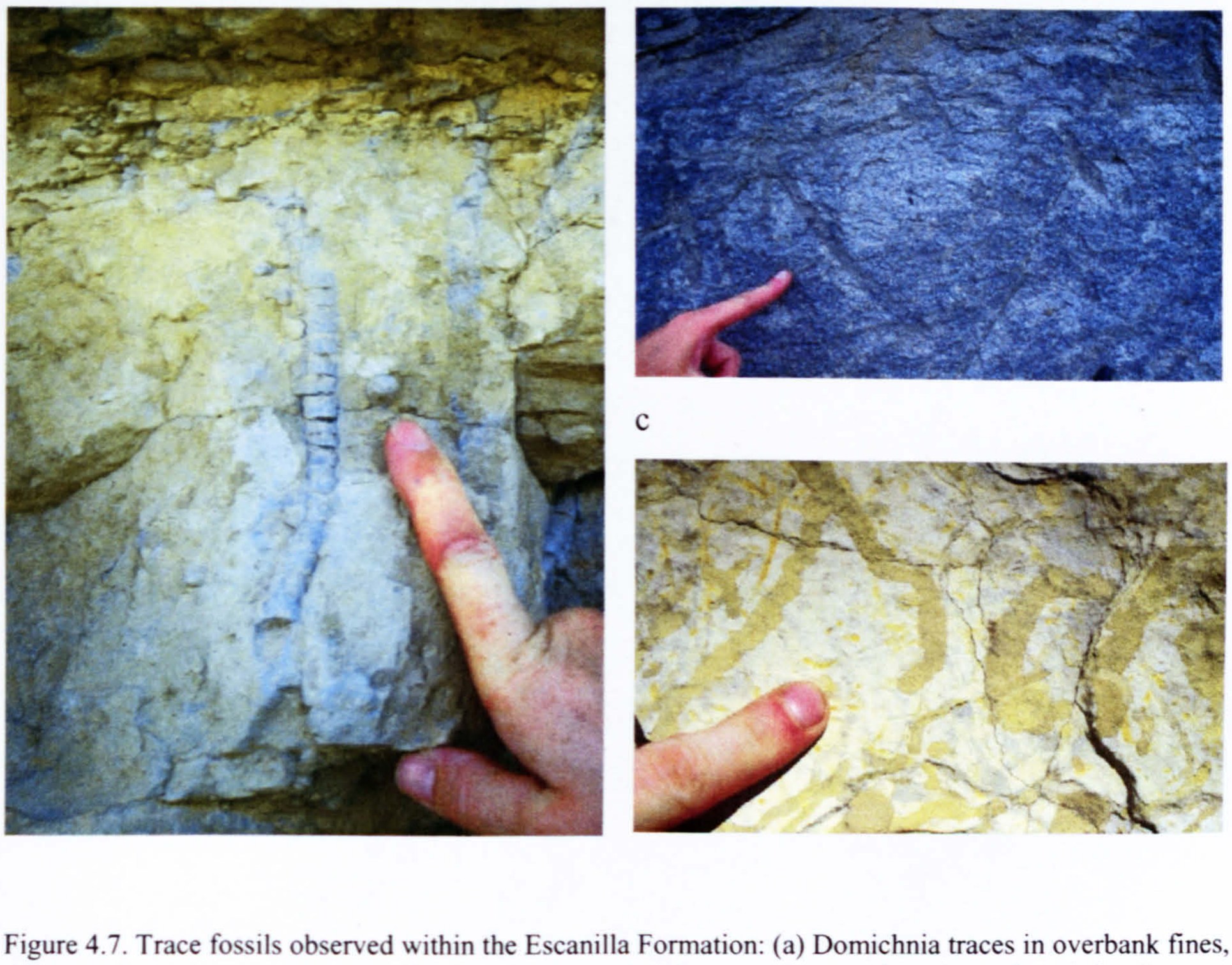

Figure 4.7. Trace fossils observed within the Escanilla Formation: (a) Domichnia traces in overbank fines, (b) Domichnia traces in stacked sandbodies, and (c) a bedding plane view of continental trace fossils.

4.9 Classification of sandbodies and vertical lithofacies associations

Initial qualitative observation of the Escanilla Formation indicates that the channel sandstones exhibit a low degree of vertical and lateral interconnectedness. Sandbodies can often be traced for 100's m forming sheet sandbodies, while other sandbodies appear to pinch out and form ribbon-type geometries (cf. Friend *et al.*, 1979). Sandbodies may taper out into fine splay sandstones that are more laterally extensive. Sandstone bodies vary in thickness from 0.5 to 40 m and show lateral and vertical stacking. Commonly, sandbodies have a sharp basal erosion surface, fine upwards and display great variability in internal facies organisation. Combining vertical facies profiles with two-dimensional geometry can enhance understanding of channel pattern and depositional environment. Therefore, sedimentary logs were used to assess the similarity of vertical lithofacies profiles (Figure 4.8) to the Lower Ketch Member (Types A-D, Chapter 3, Figure 3.7). Sandbody geometry was then characterised and quantified using the methodology outlined in Table 4.2.

Table 4.2. Step-by-step procedure for sandbody classification and quantification.

Steps	Procedure
	Fieldwork
1	Measurement of sandbodies maximum thickness and maximum lateral extent of sandbody outcrop.
2	Measurement of orientation of sandbody outcrop and grid references at each end of the sandbody.
3	Assignment of partial, unlimited or complete codes (Geehan and Underwood, 1993)
4	Classification of sandbody type based on internal structure and grain size.
5	Collection of palaeocurrent data for each study area.
	Office
6	Reorientation of sandbodies to the mean palaeocurrent direction and recalculation of adjusted widths (Haldorsen and Chang, 1986). Minimum lengths parallel to palaeoflow can also be calculated.
7	Sandbodies divided into ribbons and sheets (Friend *et al.*, 1979) based on width to thickness ratios of <15:1 or >15:1 respectively. Using only the completely exposed sandbodies where both ends are observed to terminate.
8	Calibration of partial and unlimited sandbodies with the complete sandbody PDF's (Geehan and Underwood, 1993; Visser and Chessa, 2000a,b) based on sandbody type guided by internal structure and grain size.
9	Comparison and application of corrected sandbody PDF's to the Lower Ketch Member reservoir interval.

Using aerial photographs proved unsatisfactory for the quantification of sandbody geometries. Sandbodies with widths less than 50 m were measured with a tape and those greater than 50 m were mapped on to a 1:50000 map using a three-point compass bearing and a Garmin Global Positioning System. Sandbodies were projected onto a

two-dimensional vertical plane perpendicular to the mean palaeocurrent direction; in order to obtain width and length estimates. Low topographic elevation to the north of the main outcrop ridge in the Ainsa Basin inhibited interpretation using basin-wide photomontages. Therefore, ground mapping was the only true way to provide the resolution required for detailed sandbody measurements and classification.

Sandbodies were classified into four categories based on the scheme outlined in Table 4.2 as: Ribbons, Sheet sandstones, Sheet sandstones and conglomerates and splays (Table 4.3) and generalised vertical facies profiles were characterised for each sandbody type (Figure 4.9). In addition, the frequency of occurrence of each of these sandbody types was quantified (Figure 4.10).

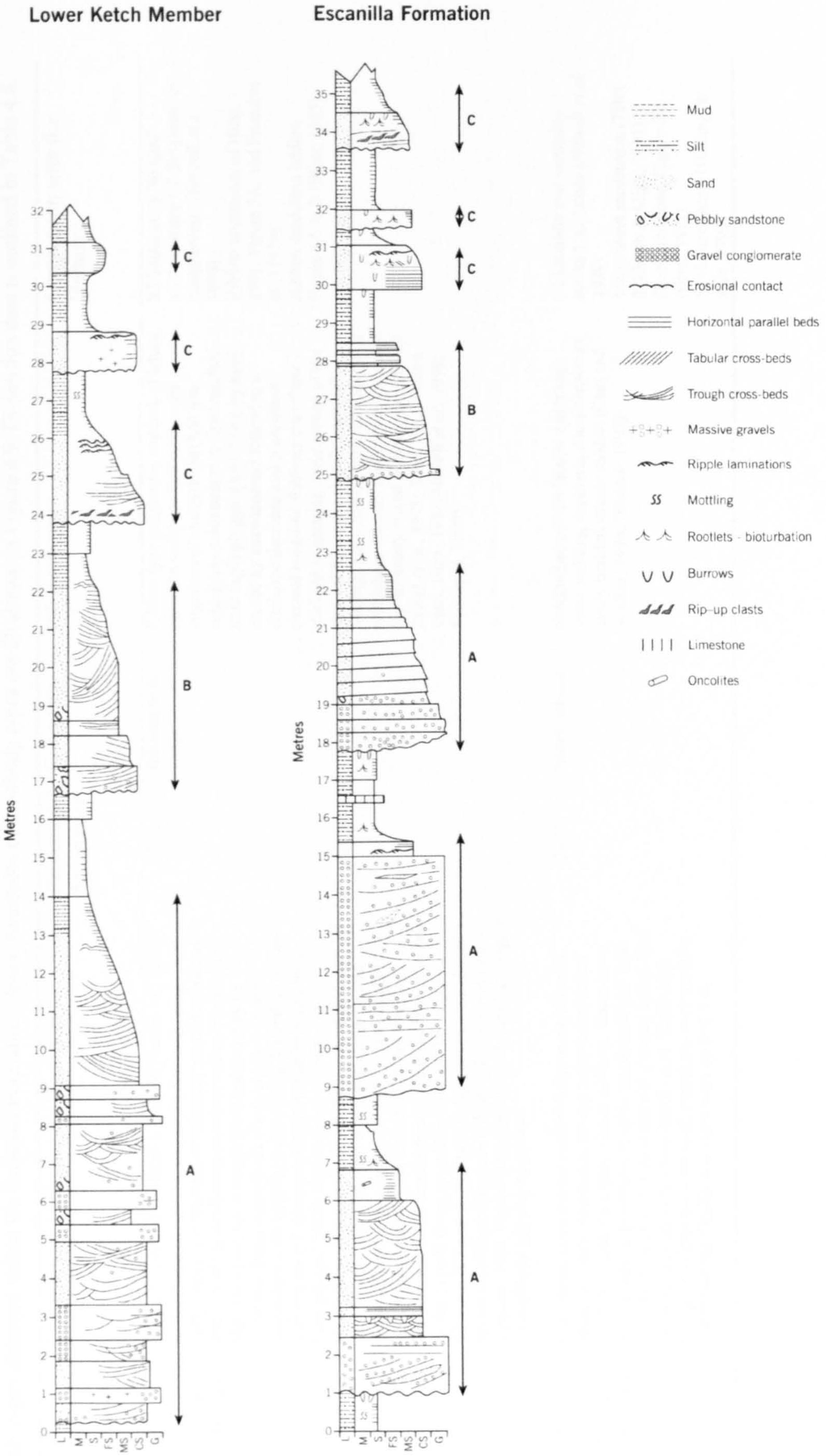

Figure 4.8. Comparison of vertical facies profiles through sandbody types in both the Lower Ketch Member and Escanilla Formation. Note the marked similarity of log profiles. For a description of vertical profiles refer to the text.

Table 4.3. Sandbody types observed within the Escanilla Formation, Spain. Examples of sandbody types are illustrated in Figure 4.9. Dimension data is outlined in Table 4.8.

Sandbody Type	Vertical facies associations	Descriptions / sedimentary structures	Percentage occurrence	Geometry	Interpretation	Comparison with the literature
Ribbon sandbodies (sandstones and conglomerates)	Type B SS, PS usually as coarser base and GC	Laterally confined sandbodies with W/T ratios <15 and terminations of channel margins by levees or wing shape splay deposits. Sedimentary structures are often obscured due to modern weathering processes and unimodal grain size. However, some trough cross-bedding may be observed. Basal contacts are sharp, concave up and sometimes with a pebbly sandstone lag. Lateral migration was limited (cf. Anastomosing) and channels may have been plugged before migration could occur. No interbedded shales are observed. Ribbon conglomerates (cf. Newell *et al.* 1999) are rare within the sequences and internal facies show massive or crudely cross-bedded fills with wings extending out from the channel margins. Ribbon sandbodies have similar vertical facies associations to the Type B fining up profiles from the Lower Ketch Member (Chapter 3, Figure 3.7). Splays and wing shaped levees associated with these ribbons (cf. Smith and Perez-Arlucea, 1994, Figure 7) thin and fine out from the margins of sandbody and may be stacked.	23 %	Ribbons with wings	Ribbon type geometries and lack of lateral accretion indicates limited channel migration of channels that had low sinuosities. Channels may have resulted from rapid plugging and filling by sand caused by abandonment following a discharge decrease and subsequent channel avulsion. Ribbons may show stacking suggesting reoccupation of the channel following abandonment (cf. Morhig *et al.*, 2000, Figure 9B). Single or multiphase channel fill deposits formed in low sinuosity mixed bedload channels (cf. Friend *et al.*, 1979; Stear, 1983; Friend, 1986; Hirst, 1991; Newell *et al.*, 1999; Martinius, 2000).	S3 Single story 'winged' sandstone and G2 Single storey conglomerate (Newell *et al.* 1999) Ribbon sandstones of Hirst, 1991, Figure 5A; and Friend et al., (1979) Ribbon sandstone bodies, Figure 6A & B (Stear, 1983)
Sheet sandstones	Type B (SS, PS usually as coarser base)	Commonly show similar vertical facies associations to those of ribbon sandstones, having larger lateral extent (W/T >15) and sharp planar basal surfaces. Sheets have similar tabular geometries to splay sandstones with little thickness variation, but show internal channel facies. Mud drapes can occur within these sandbodies. Sandbodies comprise of fine to coarse sand, commonly with a pebbly sandstone lag. Depths of erosion were up to 2-3 m.	34 %	Sheet- tabular	Sandbodies exhibit tabular and trough cross-bedding structures characteristic of sandy braided stream models (Cant and Walker, 1978, Bristow, 1993).	S1 Laterally and vertically stacked sandstone (Newell *et al.* 1999) Major sheet sandstones (Table 2, Eberth & Miall, 1991) Sheet sandstone, Figure 5D, (Hirst, 1991) Sandstone sheets (Gibling & Rust, 1990)

Table 4.3. Continued.

Sandbody Type	Vertical facies associations	Descriptions / sedimentary structures	Percentage occurrence	Geometry	Interpretation	Comparison with the literature
Composite sheet sandstone / conglomerates (Amalgamated) can appear with lateral accretion	Type A (SS, PS, GC)	Sheet sandstones with conglomerates (Table 4.3, Figure 4.9) differ from the sheet sandstones by the presence of between 40-90 % conglomerate facies, which incorporates sandstone lenses. Sheet sandstones with conglomerates sandbodies exhibit sharp erosional bases and a fining upward trend incorporating two distinct lithofacies groups: (1) parallel or planar cross-bedded conglomerates facies with sandstone lenses form the basal group that extend across the entire sandbody width, showing similarities to facies observed within the gravel-bed braided river deposits of Ashworth *et al.* (1999) and Ramos and Sopeña (1983); and (2) trough cross-bedded medium to coarse sandstone facies often forms the upper group above a sharp unconformable contact with the underlying conglomerates. These vertical facies groups are comparable to Type A profiles (Chapter 3, Figure 3.7) from the Lower Ketch Member. The largest of the sheet sandbodies can stack up to 40 m thick. Sandbodies can show lateral accretion surfaces indicating lateral channel migration. Lateral accretion can occur in combination with more braided channel architectural elements.	22 %	Sheet -tabular	Basal conglomerate units probably resulted from bar migration within a mixed bedload braided channel system. This transition into well-sorted trough cross-bedded sandstone represents a distinct change in flow discharge or sediment supply. Sandbodies are similar to the Budleigh Salterton Pebble Beds in Figure 12a of Smith (1990) and sheet sandbodies of Hirst (1991). Lateral accretion surfaces are noted within sandbodies and have a maximum thickness of 4 m. Formation of these lateral accretion surfaces may have resulted from point bar or braid bar migration or accretion within a single or anabranch sinuous channel respectively. The coexistence of smaller planar and trough cross-bedding indicates these sinuous channels may have existed in a multi-channel depositional channel-belt.	BSPB, Figure 12a (Smith, 1990) Sheet sandstone, Figure 5C, (Hirst, 1991) G1 Multi-storey sandstone (Newell et al. 1999) BSPB, Figure 12b (Smith, 1990) Amalgamated complex, Figure 5F, (Hirst, 1991) Type 4 sandbody (Dreyer et al., 1993) S3 Lateral accretion sandbody (Newell et al. 1999) Sheet sandstone, Figure 5B, (Hirst, 1991) Type 3 sandbody, Figure 9 (Dreyer et al., 1993)
Splays	Type C (FS, SS, SSrc)	Laterally extensive sandbodies that are internally horizontally bedded (0.1-1 m) indicating sheet flow deposition. Splays can be associated with any of the sandbody types described above. Commonly horizontally bedded, splays show ripples or fine wavy bedding and fine and thin distally away from the channel margin. Often mottled by surrounding overbank pedogenesis. Often units are stacked and may show fine mudstone beds between splays, similar to the composite crevasse splay sandstones of Mjos *et al.* (1993) and may have a lobe like planform. Vertical facies are similar to the Type C profiles of the Lower Ketch Member (Chapter 3, Figure 3.7).	21 %	Wedge lenticular proximal, sheet-like distal	Splay sandbodies represent successive flows entering a standing body of water (cf. Smith *et al.*, 1989) or crevasse splay lobes and are similar to non-channelised sheets (Hirst, 1991; North and Taylor, 1996) and the splay lobe deposits of Walderhaug and Mjos (1991). Wings may represent single splays similar to Mjos *et al.* (1993). Splay sandbodies can connect larger sheet sandbodies across an inter channel-belt floodplain.	Sheet splay deposits (Bentham et al. 1993) Sheet sandstone, Figure 5E, (Hirst, 1991) Non-channelised sheet, Figure 4 (1) North & Taylor, 1996. Crevasse splay sandstones (Mjos et al., 1993) Smith et al. (1989)

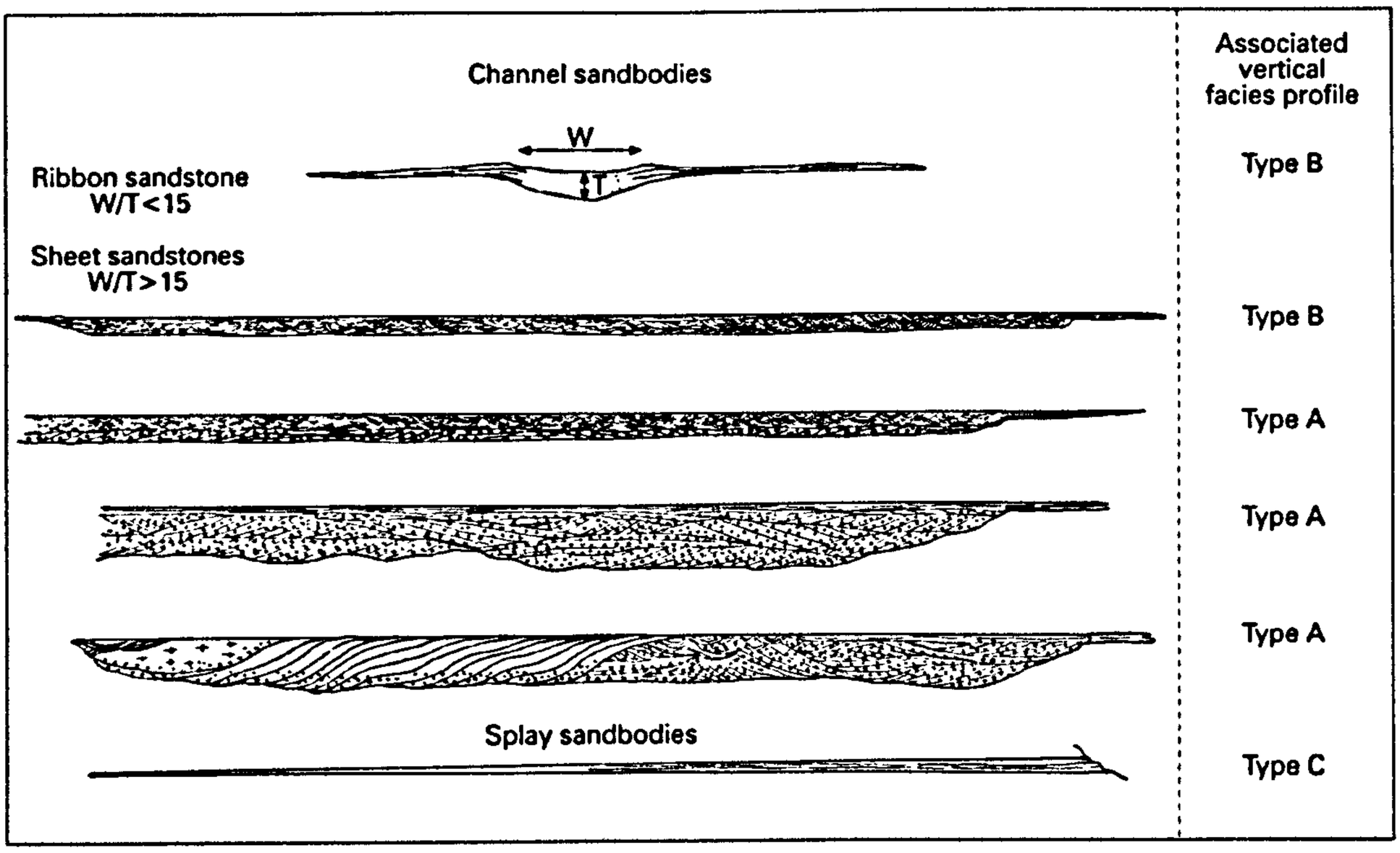

Figure 4.9. Summary of sandstone types from the Escanilla Formation (orientated perpendicular to palaeoflow direction). Vertical lithofacies profiles show similarities with the Lower Ketch Member (Chapter 3)

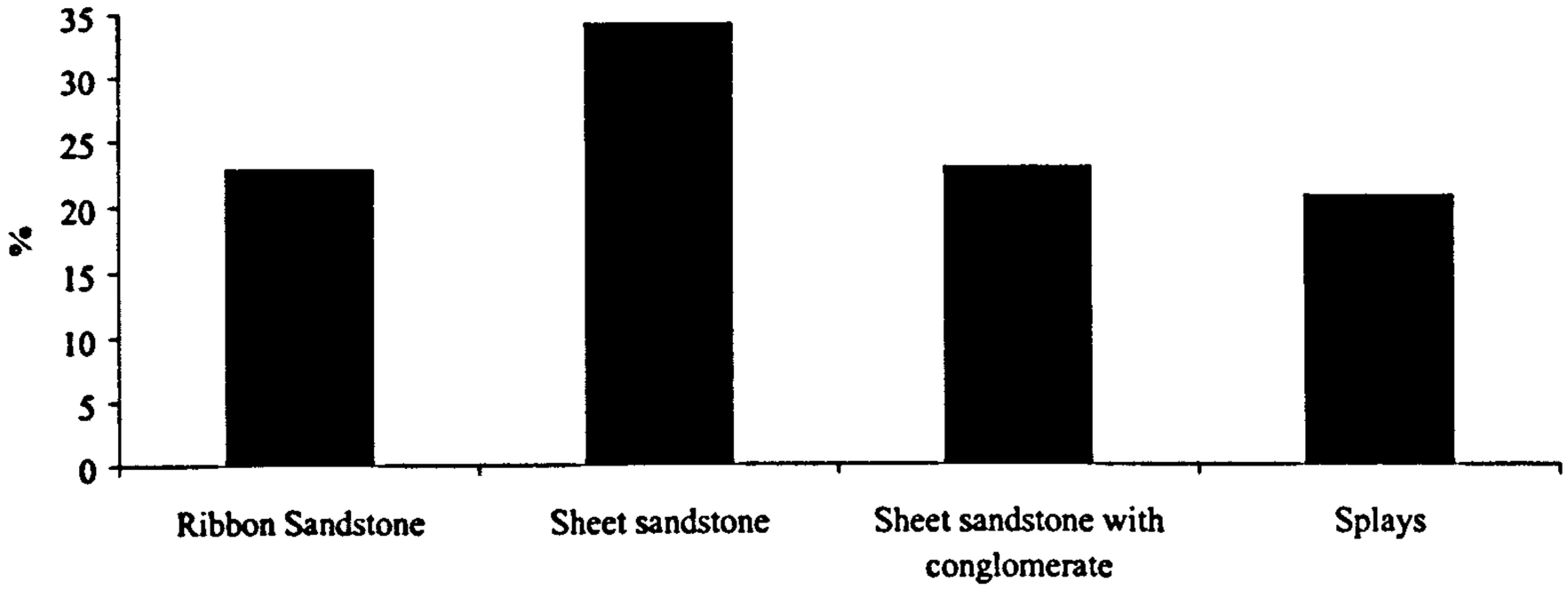

Figure 4.10. Percentage frequency of occurrence for sandbody type within the Escanilla Formation (n = 136).

Vertical facies profiles taken through the Escanilla Formation sandbodies bear similarities with the Lower Ketch Member (Figure 4.8) and therefore, permit the assignment of vertical facies profiles to the two-dimensional sandbody types shown in Figure 4.9. However, both sheet and ribbon sandbodies have Type B vertical facies association signatures, which makes extrapolation of sandbody geometries to the Lower Ketch Member in cored intervals ambiguous. To overcome this uncertainty, information on the relative proportions of sheet and ribbon sandbodies (Figure 4.10) can be used to predict the probability of occurrence of a particular sandbody type.

In some cases, sandbodies can stack laterally and vertically to form composite vertical profiles termed Type D. Composite sandbodies are similar to those described in Nami and Leeder (1972, Figure 3-c) and Cuevas Gozalo and Martinius (1993). These composite sandbodies can often be subdivided into individual channel-belt sandbodies and measured, a procedure more difficult to undertake in one-dimensional cored intervals. Examples of images of the Escanilla Formation sandbodies are shown on the supplementary CD (Appendix D).

4.10 Palaeocurrent indicators

Palaeocurrent data from cross-bedding, gutter casts, current ripples and channel margins indicate a general south south-east trend in the centre of the Basin with a south-south-west trend to the west of the basin. (Figure 4.11). These palaeocurrents are consistent with a northerly-derived palaeosource controlled by active Pyrenean uplift during the Eocene. These data show broad agreement with previous studies (Bentham *et al.*, 1992; Dreyer *et al.*, 1993). Fluvial depositional systems were focused along the core of the Buil syncline and were deflected away from the growing marginal anticlinal structures (Bentham, 1992). These palaeocurrent data were used to derive the mean palaeocurrent direction, which was then used to reorientate sandbody widths, in order to remove any influence of outcrop orientation (Table 4.2) from geometrical statistics.

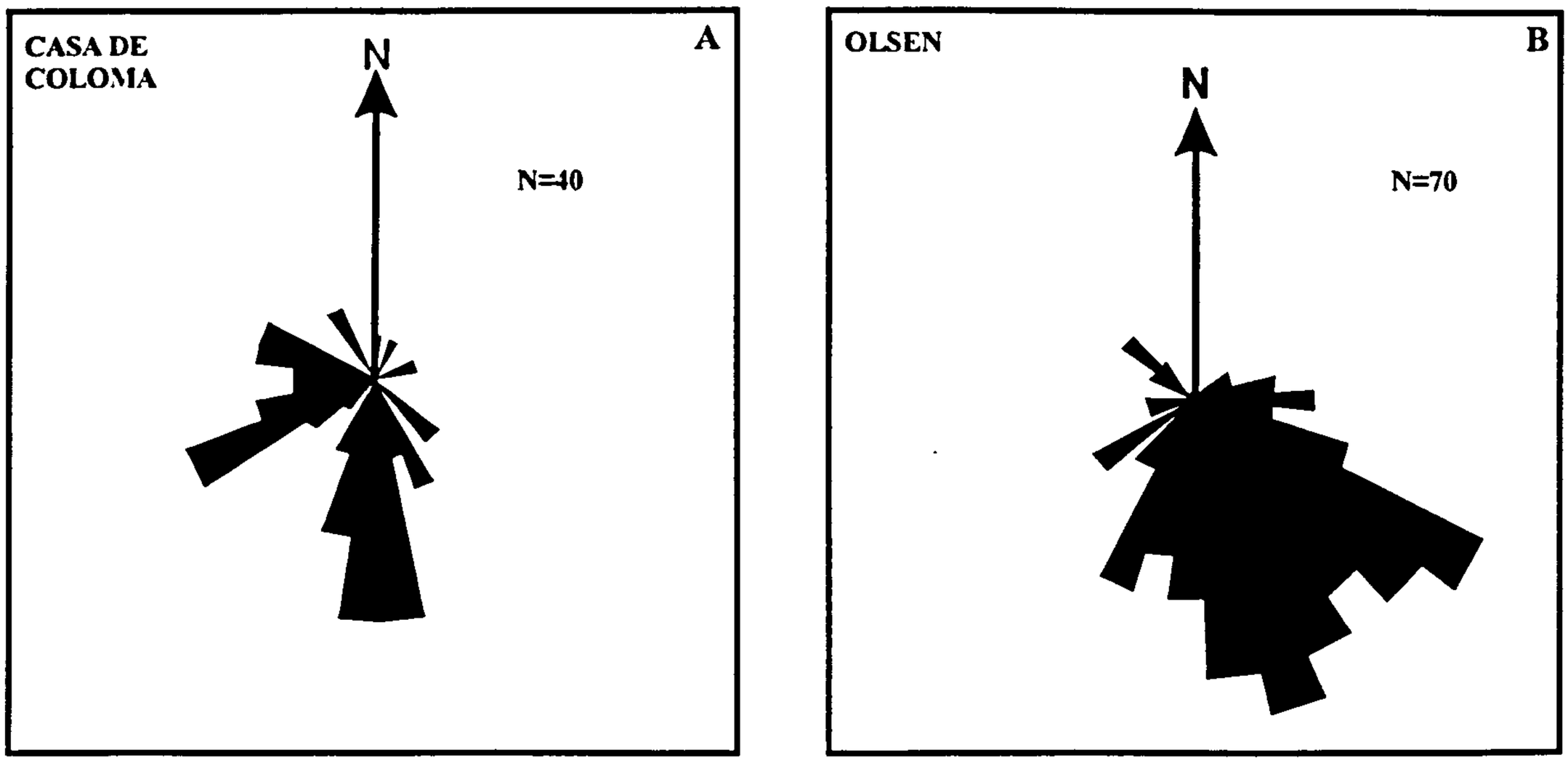

Figure 4.11. Palaeocurrent directions measured within sandbodies at (a) Olson and (b) Casa de Coloma.

4.11 Estimates of formative channel depth and channel-belt width

The same techniques described in Chapter 3, Section 3.8 have been employed to estimate formative channel depths and channel-belt widths for the Escanilla Formation. Measurements were taken from low angle planar cross-bed thickness observed in the gravel facies (cf. Ramos and Sopeña, 1983) and trough cross-bed thickness observed in the sands/pebbly sandstone facies, reflecting deposition by in-channel bar forms (Ashley, 1990) and dunes respectively (Table 4.4). Comparisons between the Escanilla Formation and the Lower Ketch Member were confined to the trough cross-bed measurements because more difficulties exist in defining planar cross-stratification boundaries in core than outcrop and also dunes and bars scale differently to flow depth (see Todd, 1996, p314; Bridge and Tye, 2000). Mean dune height from calculations using the equations of Yalin (1964) and Allen (1970) to estimate flow depths, yield flow depths between 2.5 and 5.5 m for sandstones (Table 4.5).

Table 4.4. Summary of cross-set data from the conglomerates and pebbly sandstone lithofacies within the Escanilla Formation, which represent bar and dune deposition respectively.

	n	Mean (m)	Median (m)	Minimum (m)	Maximum (m)	Standard deviation
Conglomerates	14	1.21	0.75	0.2	4	0.4
Sandstones/Pebbly sandstone	24	0.51	0.35	0.1	1.5	1.04

Table 4.5. Estimates of channel depths and channel-belt widths in both the Lower Ketch Member and the Escanilla Formation, using equations outlined by Bridge and Tye (2000).

	Lower Ketch Member	Escanilla Formation
Lithofacies	SS/PS	SS/PS
N	30	24
Mean set height (Sm) (m)	0.34	0.50
Standard deviation (Ssd)	0.26	0.40
Applicability test (Ssd/Sm = 0.88 ± 0.3)*	0.78	0.79
Mean dune height (hm) (m)	0.24	0.41
Depth (Yalin, 1964) equation (m)	1.5	2.5
Depth (Allen, 1970) equation (m)	3.5	5.5
Estimate of channel-belt widths (cbw)		
Channel belt width (Bridge & Mackey, 1993) equation 1 using Yalin (m)	117	302
Channel belt width (Bridge & Mackey, 1993) equation 1 using Allen (m)	320	657
Channel belt width (Bridge & Mackey, 1993) equation 2 using Yalin (m)	578	1279
Channel belt width (Bridge & Mackey, 1993) equation 2 using Allen (m)	1078	1973

* Refer to Bridge and Tye (2000) for applicability test.

Complete channel fill deposits were rarely observed within the Escanilla Formation and consequently, limited to three measurements (Table 4.6). Complete channel fill deposits

provide estimates of original channel depths of 1.6 to 3.0 m when derived using Paola and Borgman's (1991) range of estimated preserved channel fill thickness. Estimates of channel depth from preserved channel fills are lower than the formative channel depths predicted from cross-set heights and therefore, may only represent the final stages of a channel filling event.

Table 4.6. Estimates of flow depth from channel fill deposits within the Lower Ketch Member and the Escanilla Formation.

	Lower Ketch Member	Escanilla Formation
N	2	3
Mean channel fill depth (m)	0.9	1.2
Minimum flow depth (m)#	1.2	1.6
Maximum flow depth (m)#	2.2	3

Based on estimates of preserved channel fill thicknesses being between 75% and 40% of original flow depth (Paola and Borgman, 1991).

Formative channel depth estimates for the Escanilla Formation when predicted using single channel fill sequences and trough cross-bedding, are between ~36-57 % greater than those derived from the Lower Ketch Member respectively. Underestimates in formative channel depth calculations from the Lower Ketch Member may be caused where bore holes fail to penetrate the maximum cross-set thickness and also because of differences in burial compaction estimates between reservoir and analogue. Both compaction and well penetration location may cause errors in formative channel depth estimates. However, channel depth estimates and subsequent channel-belt width estimates between reservoir and analogue fall into the same order of magnitude.

4.12 Grain size distribution of the Escanilla Formation

The grain size distribution for the Escanilla Formation (Figure 4.13) was calculated using the same methodology employed for evaluating the Lower Ketch Member (Chapter 3, Section 3.14). Results from the two grain size distributions show that D_{50} values (Table 4.7) between reservoir and analogue sequences are comparable, while D_{90} values are greater in the Escanilla Formation. However, comparison of the D_{90} values from both sequences show that both systems are dominated by particles equal to or finer than sand grade. Matching the grain size distribution shape is crucial for the extrapolation of geometrical data from the analogue to the reservoir.

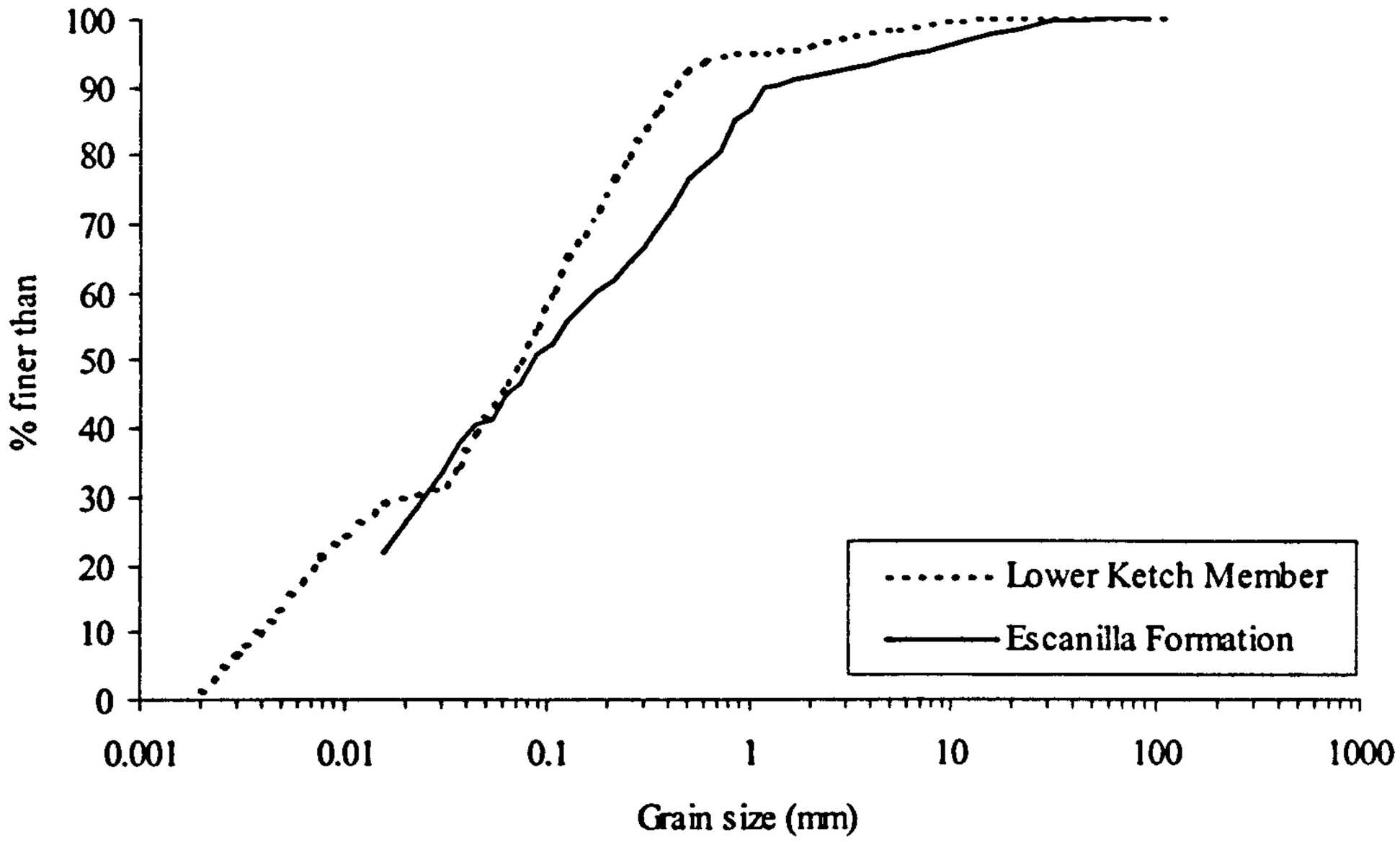

Figure 4.9. Comparison of cumulative percentage grain size distributions for the Lower Ketch Member and the Escanilla Formation.

Table 4.7. Comparison of grain size data from the Lower Ketch Member and the Escanilla Formation.

	Lower Ketch Member	Escanilla Formation
D_{50}	0.075 mm	0.085 mm
D_{90}	0.416 mm	1.227 mm

4.13 A review of the depositional model for the Escanilla Formation

Examination of outcrop data from the Escanilla Formation is reviewed and compared to Bentham *et al.* (1993) model of a rapidly aggrading and avulsing braided stream depositional system for the Lower Escanilla Member. In this section the depositional model (Figure 4.10) presented by Bentham *et al.* (1993) is refined to accommodate new information on: (1) the environmental conditions, especially in relation to lacustrine deposition; (2) the increasing net-to-gross towards the top of the Lower Escanilla and into the Middle Escanilla; and (3) the scale of the formative channels and channel-belts responsible for deposition of the sandbodies.

During the deposition of the Escanilla Formation, a series of varying width channel-belts flowed axially within the north-south orientated Ainsa Basin. Main palaeoflow direction was derived from the north and clastic input was controlled by uplift of the Pyrenean mountain belt. Lithofacies comprise channelised sandstones and extensive

overbank floodplain silts. Bentham *et al.* (1993) interpreted the Lower Escanilla sandbodies as resulting from laterally confined channel-belts capable of rapid vertical aggradation. However, this model may not be applicable to the entire Escanilla Formation. Observations by Bentham *et al.* (1992) show an increase in the proportion of the coarse-grained sandstone bodies in combination with an increase in clast size up through the sequence. The preceding sections have provided evidence from a 150 m thick interval comprising the uppermost part of the Lower Escanilla Member and the lowermost part of the Middle Escanilla Member, and present evidence that is consistent with a general basin wide shallowing upwards model for the Ainsa Basin (Mutti *et al.*, 1988). Thus, this work extends the model of Bentham *et al.* (1993) to include the Middle Escanilla Formation and incorporates some suggestions on the application of alluvial architectural models.

Evidence presented in this chapter documents a fourfold sandbody classification scheme (Table 4.3), which suggests that three types of channel-belt systems occurred during the deposition of the studied interval, to include: (1) laterally confined channels (cf. Bentham *et al.*, 1993); (2) sand-bed braided river systems; and (3) gravel-bed braided river systems. In addition to channel-belt deposition, splay deposition occurred in association with sheet flood events from the margins of all three channel-belt types.

Laterally confined channels produced ribbon-type sandbodies and the sheet sandbodies observed within the sequence exhibit features of both sand-bed and gravel-bed braided rivers. The presence of lateral accretion surfaces also infers the occurrence of higher sinuosity channels at the time of deposition. Sandbodies are observed to stack both vertically and laterally forming amalgamated sheets. Predicted channel depths ranged from 2.5 m to 5.5 m and channel-belt widths are estimated to have ranged from ~300 to 2000 m. Additional splay sands form the fourth sandbody type and are associated with overbank flooding from all the channel-belt types, resulting in the development of splay lobes.

In order to review the controls on the depositional model of the Escanilla Formation further, several key features of the Escanilla Formation need to be addressed: (1) the high proportion of floodplain deposits preserved (36 %); (2) the general coarsening upwards observed between the Lower and Upper Escanilla Members; and (3) the

disappearance of gypsum and appearance of limestone beds at the top of the Lower Escanilla Member. These features shall now be reviewed in the following sections.

4.13.1 Controls on the alluvial architecture of the Escanilla Formation

The low degree of channel interconnectedness displayed within the Lower Escanilla Formation has been attributed to long-term, high aggradation rates (Bentham *et al.*, 1992; Dreyer *et al.*, 1993). The Escanilla Formation is a very fine-grained system and therefore, in part, the composition of the deposited sequence will be a function of sediment supply grain size. Consequently, to attribute the preservation of the overbanks entirely to high aggradation rates, in comparison with other braided river facies models (e.g. Scott, Donjek, South Saskatchewan Rivers described in Miall, 1978) may overlook the impact of sediment source grain size and the sorting of this grain size distribution downstream. Evidence of aggrading coarse-grained gravel-bed braided river systems, such as in the North Canterbury Plains, New Zealand, show development of floodplains between adjacent channel-belts (e.g. Reinfields and Nanson, 1993). Although, examination of the Quaternary alluvial architecture reveals a low preservation potential of fine-grained floodplain material. In addition, aggradation rates for the Escanilla Formation are estimated to be between 0.01-0.57 mm yr^{-1} (Bentham *et al.*, 1992), which are lower or comparable to estimated aggradation rates for deposition of the Canterbury Gravels (0.32-2.85 mm yr^{-1}, Ashworth *et al.*, 1999). Consequently, the difference in grain size being supplied to a particular drainage system is crucial in determining the relationship between channel-belt and floodplain deposits. Hence, the difference in grain size between the Canterbury Gravels comprising of ~20 % sands or finer (Ashworth *et al.*, 1999) and the Escanilla Formation comprising of > 90 % sands or finer (Section 4.12) may be the reason the sequences show a marked difference in the preservation potential of overbank deposits. Subsequently, in order that high volumes of floodplain deposits are preserved, the drainage system must be provided with a high proportion of fine-grained material, either at the source or by modification of the source grain size down the river course.

Bentham *et al.* (1992) suggested that the gradual increase in sandbody proportion upsection is attributed to a gradual slowing down in the sediment accumulation rate, based on numerical stratigraphy models by Bridge and Leeder (1979) and outcrop

studies (e.g. Kraus and Middleton, 1987; Shuster and Steidmann, 1987). Theoretical stacking patterns models of Bryant *et al.* (1995) and Heller and Paola (1996) link channel-belt avulsion frequency to sedimentation rates. Therefore, the increase in sandbody proportion between the Lower and Upper Escanilla Members may substantiate a model of increasing aggradation rate associated with increasing clastic supply and clast size. Evidence for high aggradation rate is reinforced by suppression of palaeosol development. Bentham *et al.* (1993), using work by Retallack (1986), suggested that breaks in deposition were less than 10000 years.

An alternative explanation may suggest that the increase in sandbody proportion between the Lower to the Middle Escanilla Formations in the Ainsa Basin may document a progradation of the downstream fining trend as the foreland basin migrated southwards. Moreover, the Escanilla Formation is representing a shift in facies to a more proximal position, and corresponding increase in the proportion of the coarse-grained material (sands and gravel). Whilst evidence for a change in grain size distribution has been observed at the gravel-sand transition within the channel-belts of gravel-bed rivers (Sambrook Smith and Ferguson, 1995; 1996), the relationship between the sand and silt in more distal sabkha type environments is more poorly understood. For the reason documented above, the change in the proportion of sandbody to overbank deposits is probably due to a change in both aggradation rates (Bentham *et al.*, 1993) in combination with a progradation of the downstream fining trend. However, the relative contribution of the two mechanisms is inconclusive and requires further quantification from modern analogue systems. Furthermore, the incorporation of these downstream fining trends is critical to the development of three-dimensional alluvial architectural models (e.g. Mackey and Bridge, 1995; Heller and Paola, 1996).

4.13.2 Evidence for base-level or progradational changes in the Escanilla Formation

In addition to the increase in the proportion of the coarse-grained fraction upsequence (Bentham *et al.*, 1992), the occurrence of gypsum disappears near to the top of the Lower Escanilla Formation and limestone beds become visible. If the gypsum is the result of marine influence then these observations are consistent with the general shallowing upwards sequence model (Mutti *et al.*, 1988). Gypsum precipitated within the Lower Escanilla sequence may have been formed by sulphate, sourced and

replenished by marine porewaters, which combined with a large available calcium carbonate source from uplift of the Pyrenean hinterland (Bentham, 1992). Limestone formation may have been suppressed during the deposition of the Lower Escanilla Formation because the presence of marine porewaters supplied sulphate to Lower Escanilla sequence, creating a calcium limited system. Consequently, the precipitation of sulphate in the form of gypsum depleted the available calcium reservoirs (see Reading, 1986). The switch from a gypsum forming system to a carbonate forming system is consistent to a general shallowing upward sequence and the change from a supratidal coastal alluvial plain to an alluvial plain. Replenishment of seawater to the alluvial plain of the Lower Escanilla could have been controlled by either regional or local base-level changes, driven by changes in sediment supply and/or tectonic subsidence associated with Pyrenean thrust emplacement or climate. The disappearance of gypsum at the top of the Lower Escanilla indicates a halt to marine supplied porewaters and the loss of a sulphate source at the top of the Lower Escanilla Formation allowed the free calcium to become available to permit limestone beds to form. Alternatively, a general progradation of the alluvial plain could have also caused the coarsening upwards sequence exhibited in the Escanilla Formation. The appearance of limestone beds may be associated with climatic fluctuations during deposition. Investigation is required into the controls on gypsum and limestone formation within the Escanilla Formation.

The observation of nodules within the overbank deposits were initially classified as calcrete horizons by Bentham *et al.* (1993). However, internal structures show concentric or domal algal growth and evidence of fragmentation and regrowth, which suggest a surface rather than soil forming origin. According to estimates based on maximum oncoid size, these oncoids would have formed on the surface in shallow lakes that were present for 150+ years and were subjected to wave activity. The oncoids may have been nucleated on large branches or roots, although, no organic structures are observed within the core of the oncoids. No other evidence for roots or branches is observed within the floodplain deposits. The clustering of the oncoids implies that vegetation debris may have been brought downstream from the hinterland into shallow lakes, which had favourable conditions for cyanobacteria to attach and grow onto the vegetation.

The presence of laterally extensive limestone beds within the floodplain deposits also substantiates the evidence for shallow lake formation. Limestone beds are interpreted as the product of periodic ponding of floodwaters in areas away from the active channel-belts. Lakes may have formed in local topographic floodplain depressions and had maximum depths of ~3 m and lateral extents of over 500 m. In order for both oncoids and limestones to develop, energy conditions must have been low, suspended sediment concentration limited and lake temperatures warm. These conditions suggest that the lake areas were cut-off from much of the channel-belt environment. Several phases of oncoid growth indicate that the lakes were periodically inundated with flowing water from intermittent channel-belt flooding, possibly as a result of a seasonal climate regime. When this flowing water waned, algal growth would have continued. Periodic lake formation may also inhibit the development of soil. Gastopods and Ostracods from the limestone beds provide evidence that indicates the carbonates are of freshwater origin. The presence of limestones and oncoids in an otherwise entirely oxidised sequence may suggest that waterlogged/lacustrine areas developed.

Evidence for a fluvio-lacustrine environment is reinforced by the presence of vertical cylindrical structures, which are thought to be almost exclusively domichnia traces formed by continental fauna living on the floodplain. Development of extensive lakes and the lack of evidence for vegetation or organic matter within the deposits suggest that the level of vegetation on the floodplain may have been minimal and sediment binding may have been limited allowing channel-belts to migrate laterally.

In summary, the depositional model for the Escanilla Formation may show similar facies trends to the terminal fan models of Olsen (1987) and Kelly and Olson (1993). In addition, the increase in sandbody proportions up-sequence may reflect a facies shift from a more distal to a proximal position as the alluvial plain progrades basinward in conjunction with changes in aggradation rate. Moreover, this basinward facies shift reinforces the shallowing and coarsening model of Mutti *et al.* (1988). No conclusive evidence can be found to differentiate between the relative effects of aggradation rate, sediment supply grain size, base-level change and climate on the depositional record of the Escanilla Formation. Further study of the Escanilla Formation examined in this section would benefit greatly from the assignment of a modern day analogue.

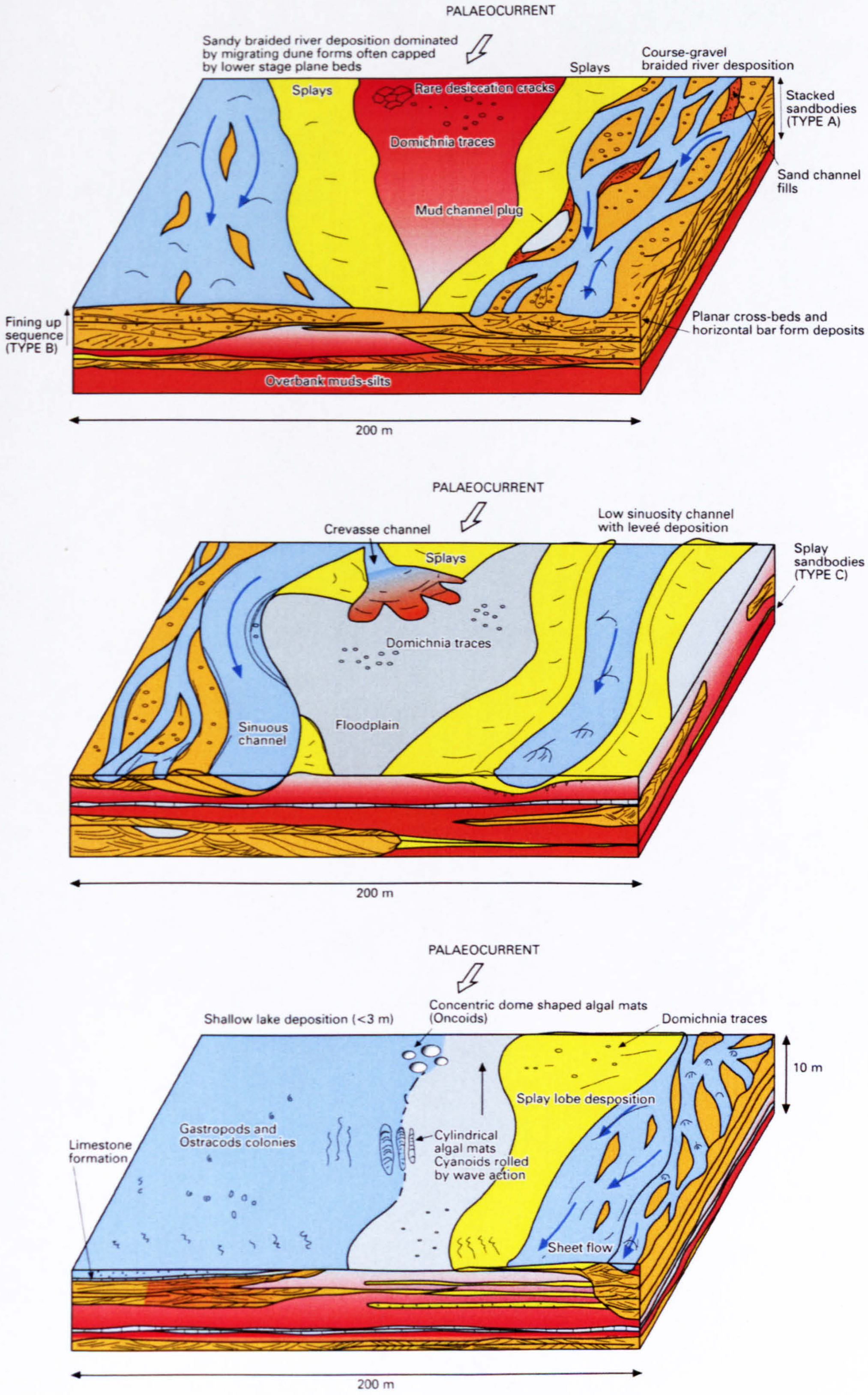

Figure 4.10. Schematic block diagrams to represent the depositional environments for the Escanilla Formation.

4.14 Impact of compaction on Escanilla Formation alluvial architecture

In order to assess the impact of compaction on the alluvial architecture of the Escanilla Formation and use geometrical information from the Escanilla Formation to assist in the prediction of alluvial architecture of the Lower Ketch Member, two issues need to be addressed: (1) the facies-dependent differential compaction between the fine- and coarse-grained fractions (e.g. Collier, 1989) in the Escanilla Formation, and (2) comparison of burial depths and depositional environment between reservoir and analogue. Petrological studies suggest the maximum burial depth reached by the Escanilla Formation is approximately 1.2 km (Tom Dreyer, pers. comm. 2000). To estimate differential compaction for the Escanilla Formation the same arguments hold as those that provided the rationale for calculating compaction of the Lower Ketch Member (Chapter 3, Section 3.13). Evidence suggests climate regime and palaeosol development were comparable to the Lower Ketch Member and therefore, facies-dependent differential compaction was minimal. Additionally, the presence of extensive limestone beds within the overbank deposits can be traced above several adjacent sandbodies and interchannel-belt areas with no observable deformation. These limestones provide further evidence that no facies-dependent differential compaction has occurred between the fine- and coarse-grained deposits. Compaction estimates resulting from differences in burial depth between the Lower Ketch Member and the Escanilla Formation have been calculated using Retallack's (1993) Equation 3.8 modified from the Sclater and Christie's (1980) formula. Calculations assume both formations had initial solidities of 0.6 (based on porosities from unconsolidated sediments from Beard and Weyl, 1973).

Calculations based on a maximum burial depth of 1.2 km for the Escanilla Formation results in burial compaction estimates of 93 % of the original thickness. In comparison, based on a burial depth of 3.7 km, the compaction estimate for the Lower Ketch Member reservoir interval is 73 % of original thickness (Chapter 3, Section 3.12). Readjustment of sandbody thicknesses (Figure 4.11a) to their original depositional thickness (Figure 4.11b) shows that the Lower Ketch Member may have a similar range of sandbody thicknesses to those of the Escanilla Formation.

a

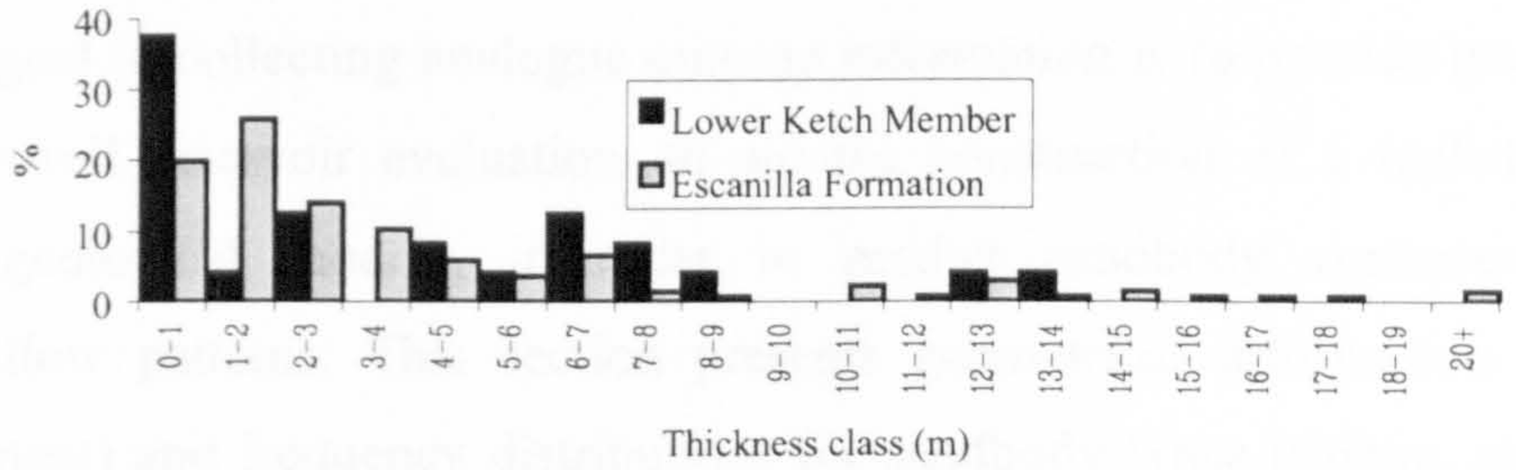

b

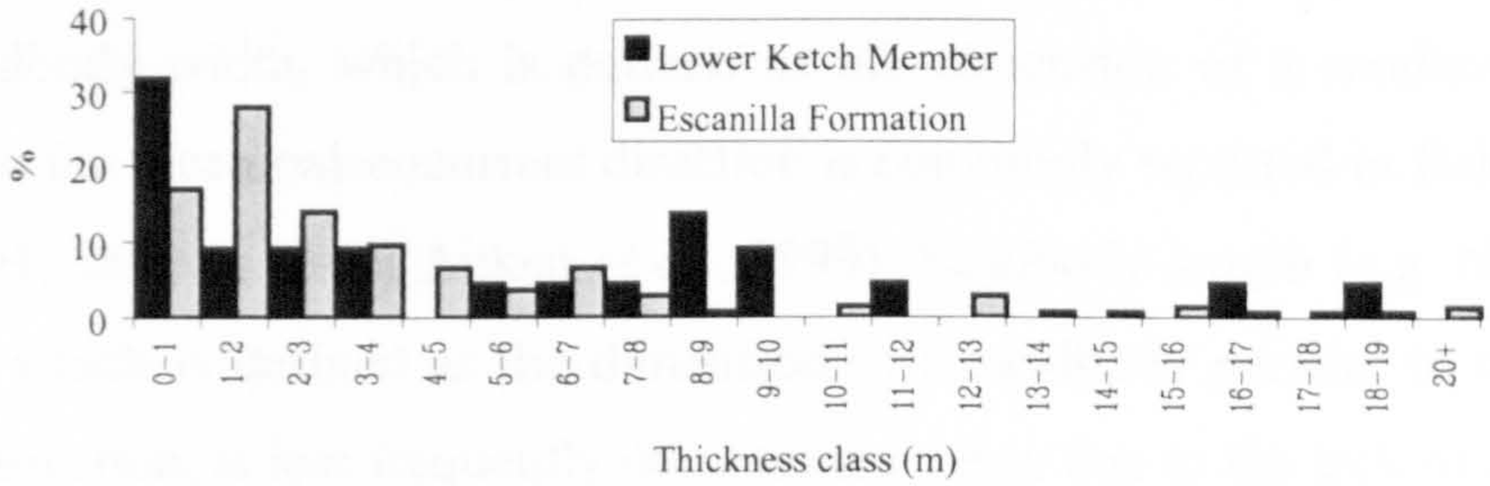

Figure 4.11 (a). Comparison of sandbody thicknesses between the Lower Ketch Member and the Escanilla Formation, and (b) adjustment of the thicknesses following decompaction using Retallack's expression of the Sclater-Christie (1980) equation. Both sequences were assummed to have an initial solidity of 0.6. Note only complete thicknesses were used in the Lower Ketch Member cored interval.

4.15 Estimate of sandbody connectivity

The Escanilla Formation exhibits a net-to-gross of ~0.64, calculated from vertical logged thickness at Olson and Casa de Coloma. Net-to-gross values for the Lower Ketch Member (0.6) are comparable to those of the Escanilla Formation. However, in other areas of the basin and at different heights within the sequence the net-to-gross may vary (Bentham *et al.*, 1992). Theoretical studies suggest that the interconnectedness of channel-belt sandbodies is unlikely if the net-to-gross is below 0.4 (Fielding and Crane, 1987) but certain if the ratio exceeds 0.75 (Bridge and Mackey, 1993b). While net-to-gross values suggest a high level of connectivity, variation in spatial sandbody stacking patterns may cause local reductions in net-to-gross to an extent where connectivity can become problematic. Therefore, quantification of the channel-belt sandbody geometry and frequency distributions of sandbodies and stacking patterns are required before management strategies are made. The following section deals with the quantification of sandbody geometries described in Section 4.9.

4.16 Two-dimensional sandbody geometry

The ultimate goal in collecting analogue outcrop information is to provide quantitative data for inter-well reservoir evaluation, to aid the construction of a realistic three-dimensional geological models, in order to predict sandbody connectivity and hydrocarbon flow patterns. This section presents geometrical information (width : length : thickness) and frequency distributions for sandbody types (ribbon, sheets and splays) identified in Section 4.9 for the Escanilla Formation. The use of these data in interpreting the inter-well alluvial architecture of the Lower Ketch Member is then evaluated. Sandbody width, which is defined as the dimension of a sandbody when perpendicular to the mean palaeocurrent direction is commonly reported in field studies (e.g. Hirst, 1991; Dreyer, 1993; Aitken *et al.*, 1999). Sandbody length (e.g. North and Taylor, 1996), which is defined as the dimension of a sandbody parallel to the mean palaeocurrent direction, is less frequently documented, often due to the lack of available three-dimensional exposure. The distributions of sandbody geometries were collated from the two studied areas in the Ainsa Basin (Figure 4.3), yielding 136 sandbody measurements. Quantification of sandbody geometry is addressed in the following sections.

4.16.1 Complete and partial sandbody dimensions

Quantification of sandbody geometries requires an assessment of the sandbody completeness. The exposure of both margins or one margin of the sandbody defines the sandbody completeness, these are termed complete and partial sandbodies respectively (Geehan and Underwood, 1993). Studies such as that of Nami and Leeder (1978) recorded complete and observed sandbody widths within the Jurassic Scalby Formation. Failure to assess the completeness of sandbodies will result in an underestimate of the widths in the total sandbody frequency distribution. Consequently, the estimates would be a function of the level of exposure of any individual sequence and result in sandbodies with smaller widths having a greater probability of being fully exposed. The Escanilla Formation yielded 68 % partially and 32 % completely exposed sandbody measurements.

Several studies (Geehan and Underwood, 1993; Visser and Chessa, 2000a,b; White and Willis, 2000) have used correction factors to predict individual sandbody widths. These studies used partially exposed sandbody data by adjusting the partial width data according to the complete distribution data, then summing the two distributions to produce an adjusted width-frequency distribution for all the sandbodies. Several of these adjustment techniques have been validated against outcrop studies. For example, the Permian Cutler Group in Visser and Chessa (2000a, b) and the Frewens Sandstone in White and Willis (2000).

The advantage of using the adjusted width distribution technique is that calculation of sandbody widths does not rely on sandbody thickness data, which are discussed in Chapters 2 and 3. Sandbody widths in the Escanilla Formation were corrected for partial lengths using the method proposed in Visser and Chessa (2000a,b) Equation 4.1.

$$ew = \frac{\sum_{l \geq W} W \, lN_c^w/(\lambda - w)}{\sum_{l \geq W} W \, N_c^w/(\lambda - w)} \qquad \text{Equation 4.1}$$

where ew is the expected width for a body with partially observed width w, in an N^w_c is the number of complete width that belong to width class W. Equation 4.1 was repeated for every partial width and the resultant adjusted width estimates were assigned to their corresponding width classes. Adjusted widths were summed with the complete width observations to produce an extended width distribution (Figure 4.12). The approach of Geehan and Underwood (1993) was not used, as the method does not take into account the shape of the outcrop. Figure 4.12 illustrates how use of the adjusted width distribution can add considerable information about the larger width classes. More information can be gained on the distribution when the sandbodies are subdivided into individual type (Table 4.8, Figure 4.13 and 4.14).

However, one drawback of the method is that the classification of partial sandbodies has to be guided by vertical and lateral facies associations (Section 4.8) and not only by geometrical information. This method may be reliably applied to sandbody data when the partial sandbody width/thickness ratios are over 15, but if ratios are below 15 a more subjective classification has to be applied. For example, ribbon and sheet sandstones can both display vertical facies association Type B and therefore present difficulties in the

assignment of two-dimensional geometry. This more subjective sandbody classification was to be applied to 5 % of all the sheet sandstone bodies measured.

Visser and Chessa's (2000a,b) conditioning method does not account for the partial widths that have a greater width than the maximum width of the complete dataset. Therefore, any partial or unlimited sandbody measurements with widths greater than the complete data cannot be adjusted to a greater width when included in the final conditioned dataset. Yet, these larger sandbodies may have a large impact on inter-well connectivity. Therefore, the method may still underestimate the largest sandbody widths observed within the Escanilla Formation.

Table 4.8. Statistic for sandbody dimensions from the Escanilla Formation based on complete measurements (n =44) and (italics) recalculated datasets using the Visser and Chessa (2000a) width conditioning method (n =136).

		Ribbon Sandstone	Sheet sandstone	Sheet sandstone conglomerates	Splays
	N	10	15	10	9
		19	*37*	*37*	*43*
Width (m)	Mean (m)	31	134	217	180
		43	*300*	*334*	*274*
	Median (m)	23	60	181	175
		50	*212*	*325*	*175*
	Standard deviation (m)	25	154	183	157
		22	*252*	*218*	*270*
	Minimum (m)	13	20	20	10
		13	*20*	*20*	*10*
	Maximum (m)	88	525	550	400
		100	*1038*	*875*	*775*
Thickness (m)	Mean (m)	4.2	2.3	4.4	1.4
		4.8	*2.9*	*6.6*	*1.4*
	Median (m)	3.1	1.6	3.9	1.2
		3.0	*2.0*	*4.7*	*0.9*
	Standard deviation (m)	3.8	1.5	3.8	0.6
		6.4	*2.7*	*4.6*	*1.9*
	Minimum (m)	1.5	0.8	1.0	0.8
		1.5	*0.5*	*1.0*	*0.2*
	Maximum (m)	14.0	6.0	13.0	2.3
		30.0	*15.0*	*17.2*	*12.0*
Width /Thickness	Mean	8	58	58	162
		14	*163*	*64*	*340*
	Median	8	27	47	114
		11	*92*	*57*	*161*
	Standard deviation	3	61	47	167
		10	*226*	*45*	*452*
	Minimum	4	16	17	4
		2	*16*	*4*	*5*
	Maximum	13	225	163	453
		48	*1221*	*163*	*1844*
	% occurrence of number	22.7	34.1	22.7	20.5
		14.0	*27.2*	*27.2*	*31.6*

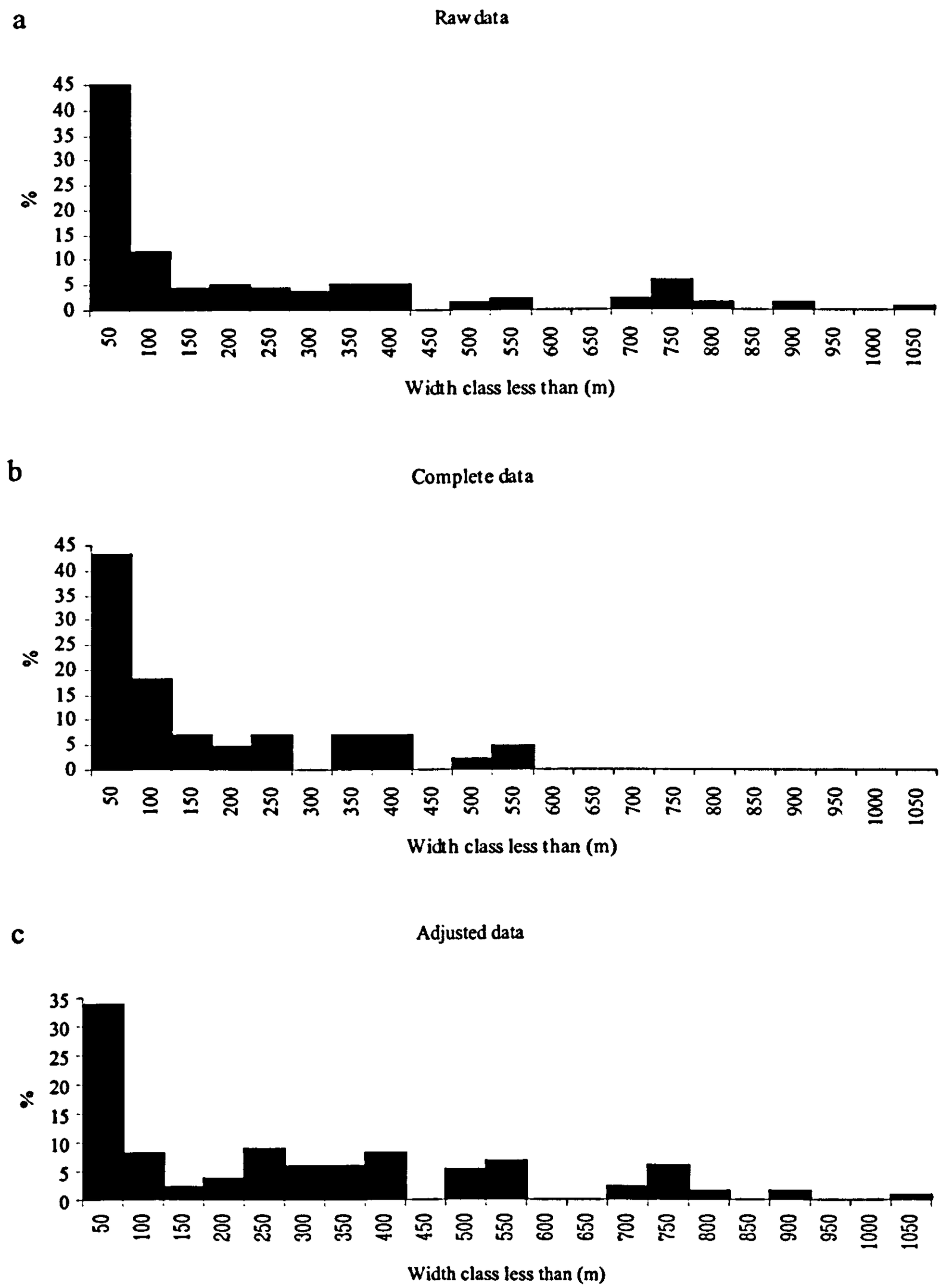

Figure 4.12. Probability density functions of the sandbodies widths within the Escanila Formation following the conditioning method of Visser and Chessa (2000a, b). Showing the (a) raw, (b) complete and (c) adjusted data.

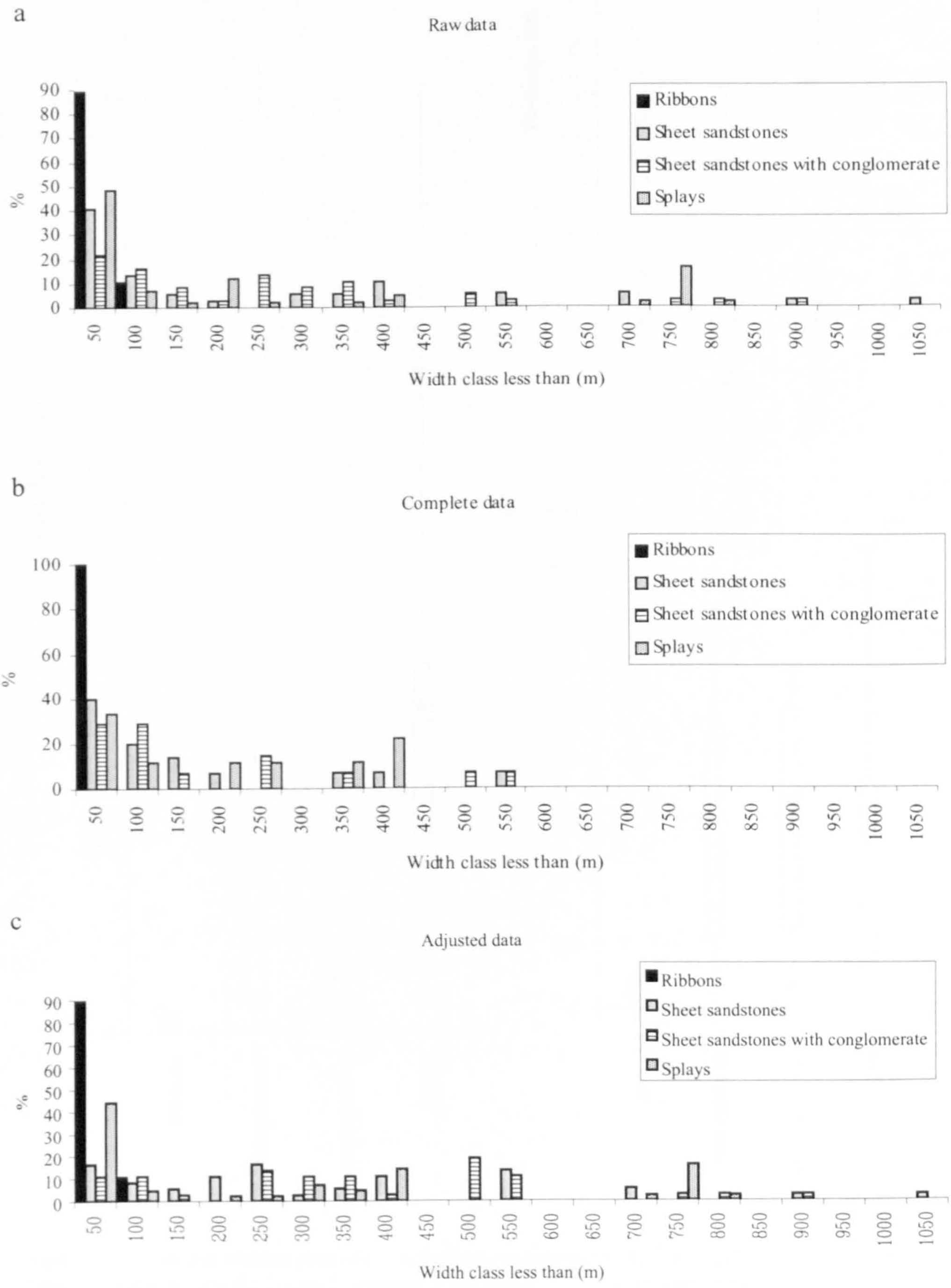

Figure 4.13. Width class PDF's defined into sandbody types (see Figure 4.3 for descriptions). Showing (a) raw, (b) complete and (c) adjusted datasets used to condition sandbody width by methods of Visser and Chessa (2000a,b).

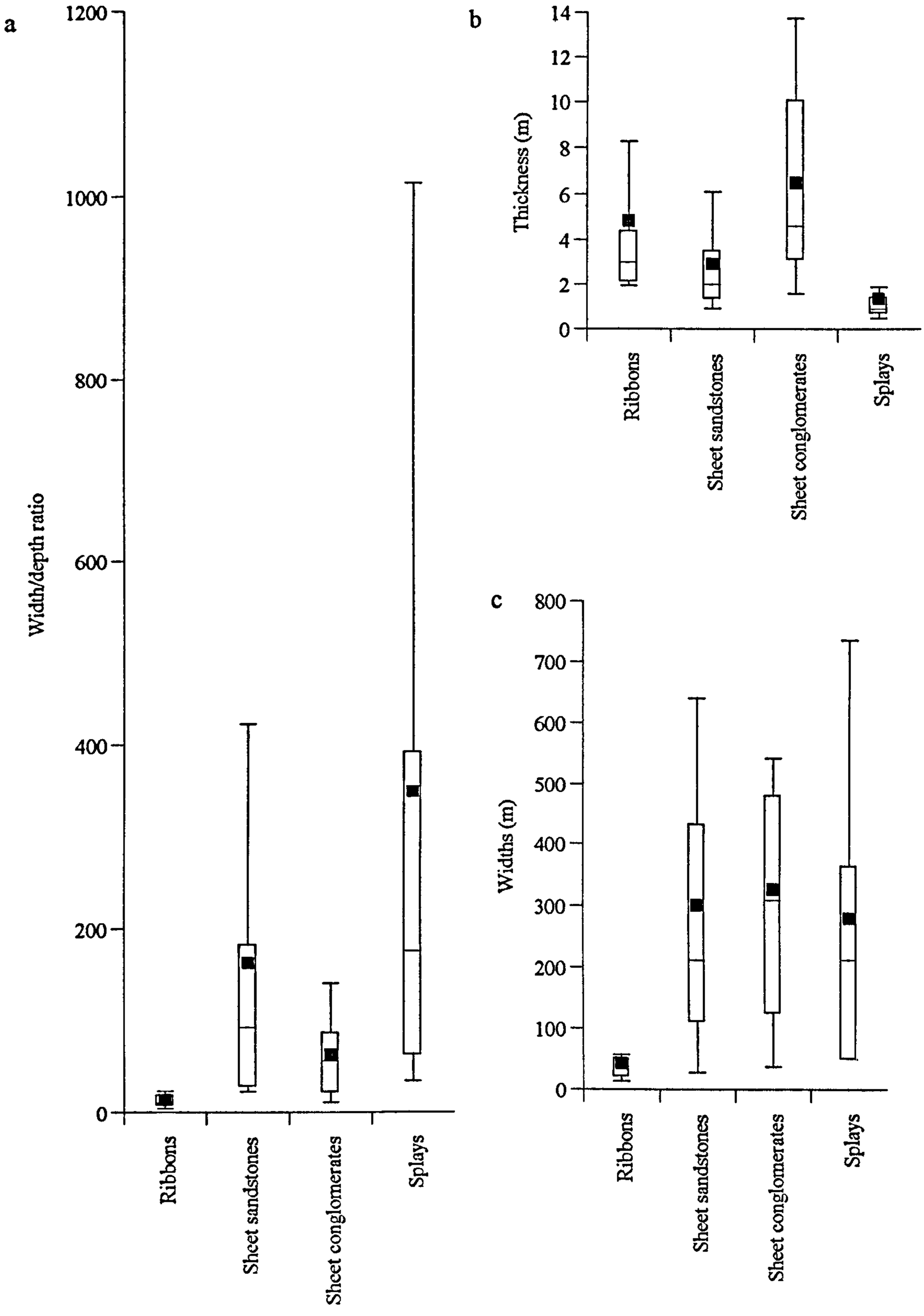

Figure 4.14. Box and whisker plots of (a) width/thickness ratios, (b) thickness and (c) width for sandbody types measured within the Escanilla Formation sequences, showing the considerable range in sandbody geometries within the Escanilla Formation.

4.17 Comparisons between geostatistics from the Escanilla Formation and documented outcrop studies

Geostatistical data from the Escanilla Formation (Table 4.8) were compared to three documented outcrop studies, which focus on channel-belt sandbodies (Fielding and Crane, 1987; Dreyer *et al.*, 1993) and splay sandbodies (Walderhaug and Mjos, 1991). Data from the literature were digitized from the original papers for comparison with datasets from the Escanilla Formation.

4.17.1 Channel-belt sandbody geometries

Dreyer *et al.* (1993) presented a sample of geometrical width versus thickness data from the Escanilla Formation (Figure 4.15) and sandbody geometries fall into the same range of width and thickness data as this study. However, classification of both channel and channel-belt data (Dreyer *et al.*, 1993) are not consistent with the sandbody classification scheme presented in Section 4.9. This highlights the problem that inconsistencies in sandbody classification between studies of the same outcrop sequence can lead to non-comparable datasets.

Inconsistency in sandbody classification is encountered again when the geometrical data from the Escanilla Formation are plotted against width versus thickness data from Fielding and Crane (1987) (Figure 4.16). There is considerable scatter of points between channel pattern types defined by Fielding and Crane (1987) and the Escanilla Formation. The Escanilla sandbodies have not been plotted into sandbody types because classification schemes are not comparable and the Escanilla Formation sandbody data covers the whole spectra of channel types documented in Fielding and Crane (1987). Fielding and Crane's (1987) study takes no account of the depositional environments from any of the compiled datasets and therefore cannot be reliably used. The reliability of any outcrop analogue dataset to interpret channel-belt sandbody reservoir interconnectedness hinges upon the correct interpretation of the depositional environment, including, critically, the scale of the system.

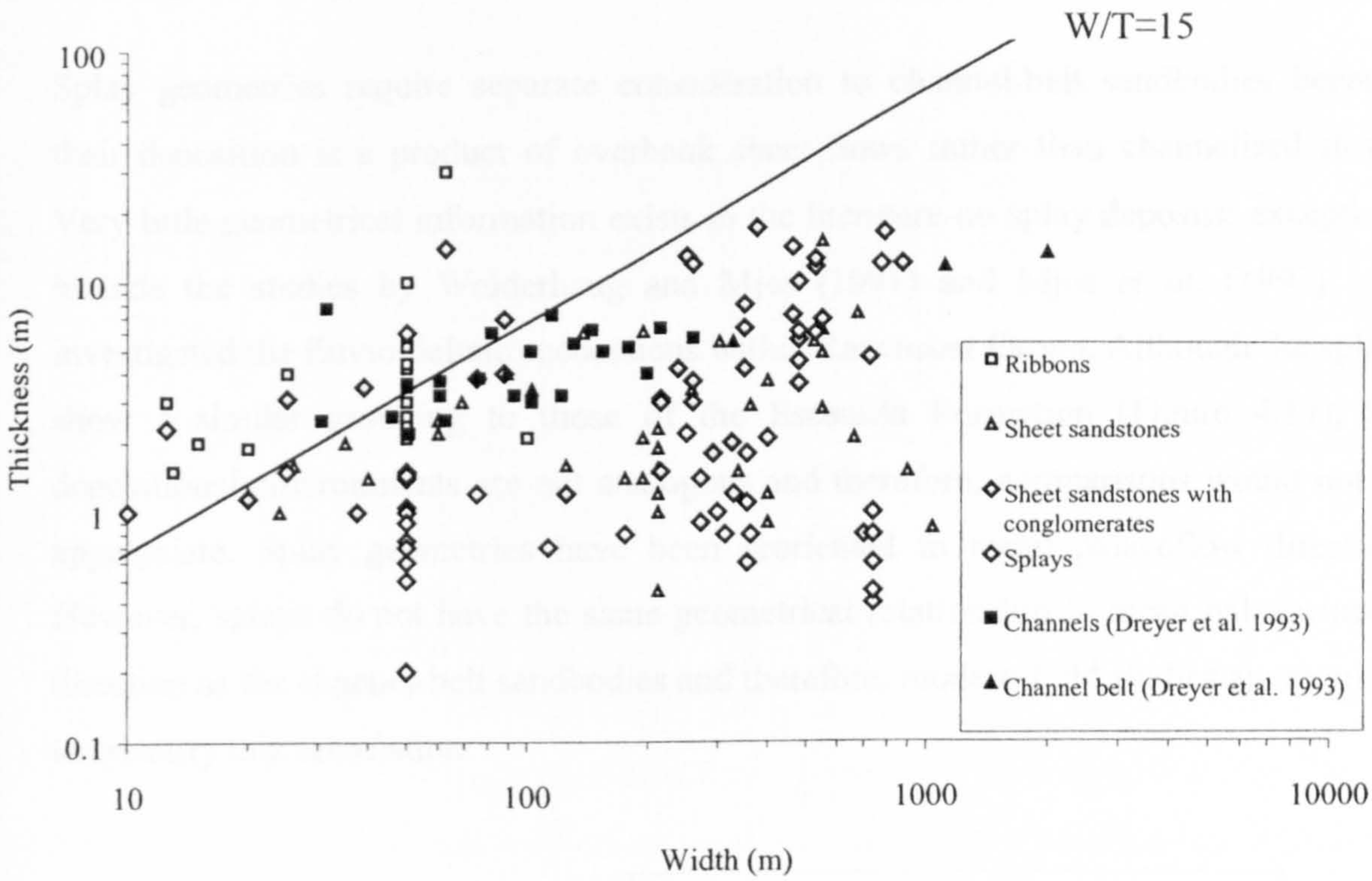

Figure 4.15. Cross plot of Escanilla Formation sandbody geometries (n = 136) plotted against sandbody dimension data from the Escanilla Formation by Dreyer *et al.* (1993).

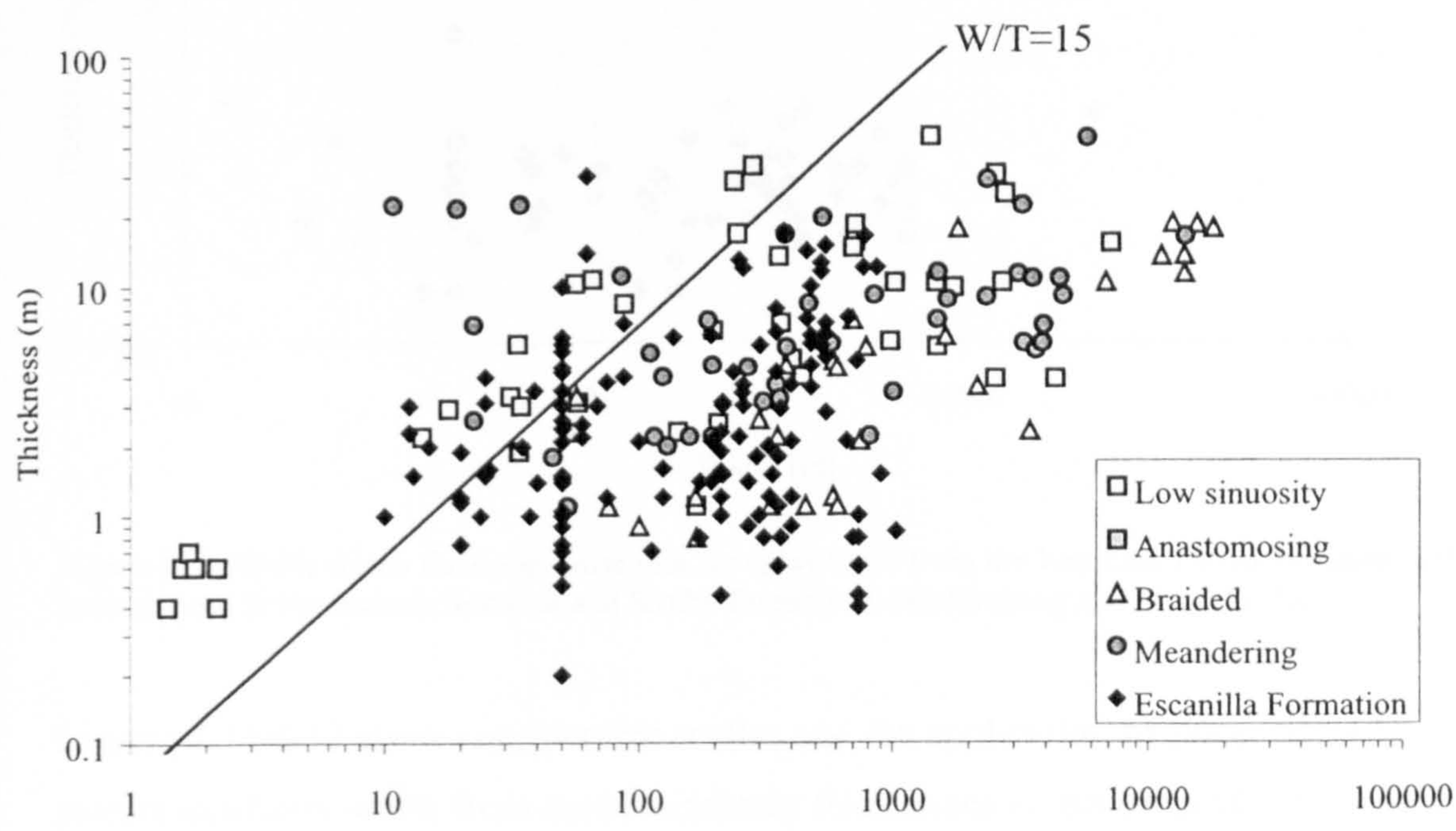

Figure 4.16. Width versus thickness cross plot for channel pattern types taken from Fielding and Crane (1987) compared to the Escanilla Formation sandbody geometries.

4.17.2 Splay lobe geometries

Splay geometries require separate consideration to channel-belt sandbodies because their deposition is a product of overbank sheet flows rather than channelised flows. Very little geometrical information exists in the literature on splay deposits; exceptions include the studies by Walderhaug and Mjos (1991) and Mjos *et al.* (1993) who investigated the fluvio-deltaic successions within Ravenscar Group. Although the splays show a similar grouping to those of the Escanilla Formation (Figure 4.17), the depositional environments are not analogous and therefore, comparisons would not be appropriate. Splay geometries have been reoriented to mean palaeoflow direction. However, splays do not have the same geometrical relationship to mean palaeocurrent direction as the channel-belt sandbodies and therefore, modern field studies are required to quantify this association.

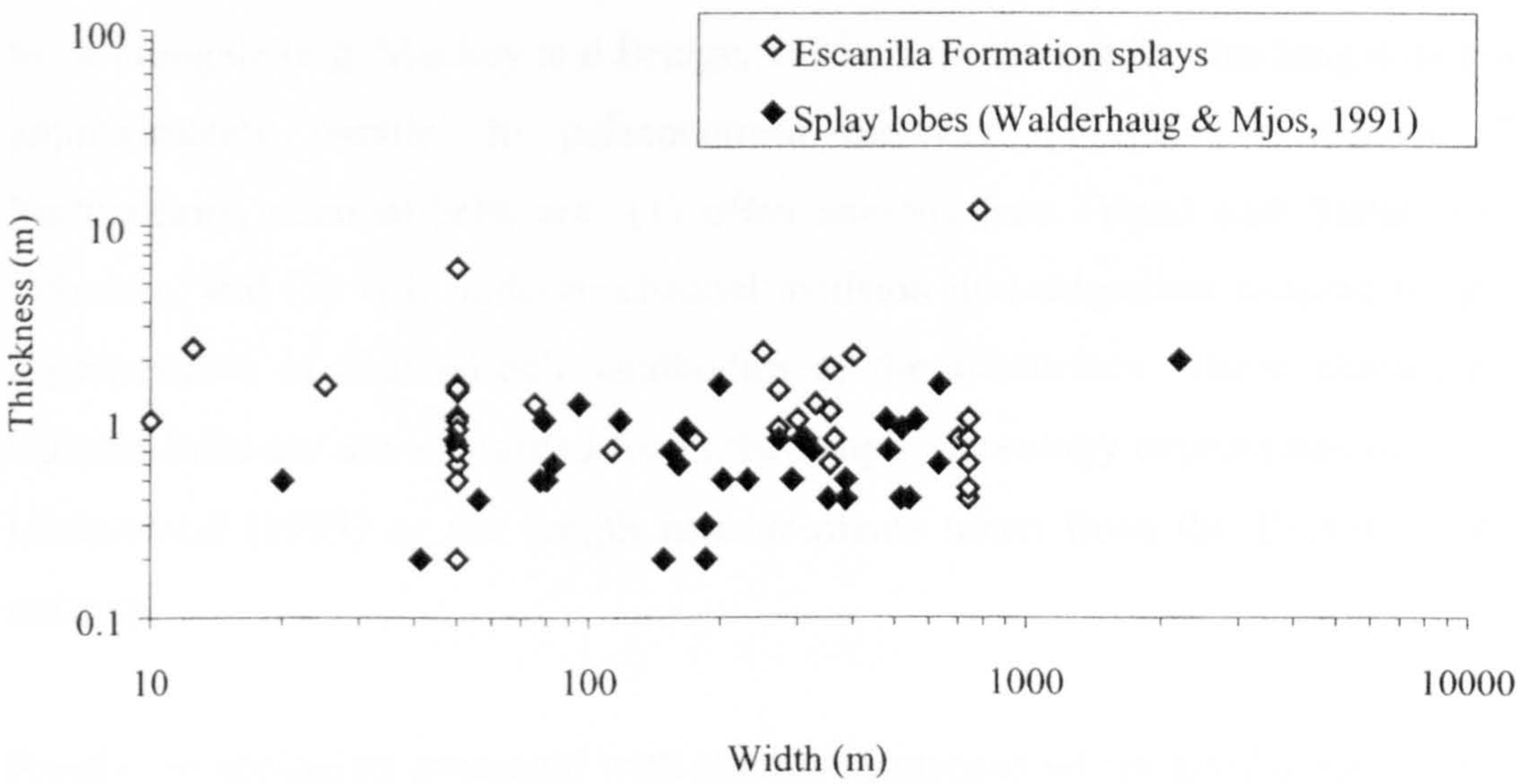

Figure 4.17. Width versus thickness cross plot for splay lobes from the Escanilla Formation compared to those defined in the Jurassic Saltwick and Scalby Formations (Walderhaug and Mjos, 1991).

Figures 4.15-4.17 show considerable scatter and the application of linear trend lines to predict sandbody width from cored sandbody thicknesses is inappropriate. By correctly matching parameters including lithofacies, grain size, sandbody type and depositional model between reservoir and analogue the use of width probably density functions (Figures 4.12 and 4.13) for each sandbody can be employed to predict subsurface reservoir architecture.

4.17.3 Three-dimensional channel sandbody geometries

In the preceding sections geometrical data has been dealt with in two-dimensions. Yet, for complete reservoir evaluation, three-dimensional geometries are required in order that reservoir volumes can be calculated. Data collected from the Escanilla Formation outcrop were reoriented back to a vertical plane perpendicular to mean palaeoflow direction, to yield two-dimensional width measurements. However, outcrop exposure only allowed minimum length measurements to be calculated and the complete sandbody lengths are more difficult to quantify.

Estimates of length frequency distribution from width frequency distributions have been made by Geehan and Underwood (1993) using stereology expressions, which assumed an isotropic shape. Modern channel-belts have greater lengths than widths (e.g. Leckie, 1994). Subsequently, the subsurface expression of channel-belt sandbodies is expected to be elongate (e.g. Mackey and Bridge, 1995), with the sandbodies long axis orientated approximately parallel to palaeocurrent direction (Visser and Chessa, 2000b). Furthermore, channel-belts are: (1) often sinuous (see Friend and Sinha, 1993), (2) bifurcate, and (3) will undergo channel avulsion and migration causing truncation or superposition of channel-belt sandbodies in the subsurface. These characteristics of channel-belts are not accounted for in the simple stereology expressions of Geehan and Underwood (1993) or the length measurements taken from the Escanilla Formation outcrop.

Rarely are geologists presented with alluvial sequences where good outcrop data can be collected perpendicular to mean palaeocurrent direction at two sites in the down-basin direction; exceptions include Newell *et al.* (1999) and Martinius (2000). Mackey and Bridge (1995) and Heller and Paola (1996) have attempted to provide theoretical models to predict down-basin channel-belt sandbody stacking patterns, but these models require field validation. The use of minimum sandbody lengths from this study cannot be reliably used in any predictive model. In order to construct a three-dimensional geological model an assessment of: (1) sandbody width distribution changes down-basin, and (2) sinuosity and connectedness needs to be undertaken. These may provide future opportunity for investigation.

4.17.4 Three-dimensional splay geometries

Splays display different geometries to channel-belt sandbodies and have to be assigned an entirely different shape. Three-dimensional splay shapes may be similar to splays described in modern systems, such as O'brien and Wells (1986) and Smith *et al.* (1989). Geometries may be similar to the wedge and lobe shaped geometries documented in Bridge (1993). Again, the three-dimensional geometry of splays needs further investigation.

4.18 Comparison between measured and predicted channel-belt sandbody width

Using cross-set heights to predict channel-belt widths provides a range of sandbody widths between 300-1980 m (Section 4.11). When compared to sandbody widths measured in the field (13-1038 m) the data shows that 74 % of the sandbody widths measured from the Escanilla outcrop fall below the minimum channel-belt widths predicted from cross-set data. Therefore, empirical estimates may lead to overcorrelation of sandbodies between wells. The maximum measured values from the field are limited by the maximum extent of the outcrop used in the study. Qualitative observations of the outcrop showed that some sandbodies extended for much greater width than the studied section panels (> 2 km). These field observations suggest that some of the sandbodies are also longer than the maximum predicted channel-belt width from cross-set data. These estimates do not account for the lateral migration or stacking of channel-belt deposits within the sequence. Therefore, the use of empirical relationships between cross-set height and channel-belt width does not provide accurate estimates of two-dimensional sandbody geometries within the Escanilla Formation.

4.19 Geometries of the overbank deposits (non-reservoir component)

Quantification of two or three-dimensional architecture for the fine-grained fraction overbank floodplain deposits present inherent difficulties. Often compaction and weathering do not allow palaeosurfaces to be identified within fluvial sequences and therefore, two-dimensional information is scarce. Comparison of vertical overbank deposit thicknesses from well data and onshore analogue give insight into the general vertical stacking patterns between the coarse and fine fraction. Table 4.9 shows that there are similarities between the mean, minimum and maximum thicknesses of overbank deposits for the two sequences, which adds weight to the use of the Escanilla Formation as an analogue to the Lower Ketch Member.

Table 4.9. Statistics from measured thicknesses for overbank mud/siltstones from the Lower Ketch Member and the Escanilla Formation.

	Lower Ketch Member (m)	Escanilla Formation (m)
n	18	101
Mean	4.9	3.9
Median	2.4	2.7
Standard deviation	5.5	3.6
Standard error of mean	1.3	0.36
Minimum	0.16	0.30
Maximum	21.7	22.0

4.20 Application of sandbody geometries to the Lower Ketch Member

Published outcrop dataset, for example, Fielding and Crane (1987) are commonly used to evaluate sandbody continuity in subsurface fluvial reservoirs. Yet, lack of information on the scale of depositional system, palaeoflow direction, climate regime, burial depth and tectonic setting, creates difficulties in the application of these studies as analogues for the Lower Ketch Member reservoir interval. Additionally, standard width versus thickness cross plots (e.g. Lorenz *et al.*, 1985; Fielding and Crane, 1987) use linear relationships to predict sandbody geometries in the subsurface. Width versus thickness cross plots for the Escanilla Formation study (Figure 4.18) in addition to many in the literature (Chapter 2, Table 2.2) show a great scatter of data points. Therefore, the prediction of Lower Ketch Member sandbody widths from an assessment of thickness cannot be undertaken using linear trend lines, because: (1) a variety of channel patterns may have existed during deposition of the sequences, resulting in a

range of channel-belt widths; and (2) estimates rely on the correct measurement of thickness, which can be problematic in core. Therefore, the ambiguity of cross plot datasets suggest that the use of adjusted sandbody width PDF's (Figure 4.16) may provide a more reliable estimate of sandbody width because no reliance is placed on the thickness data from the core.

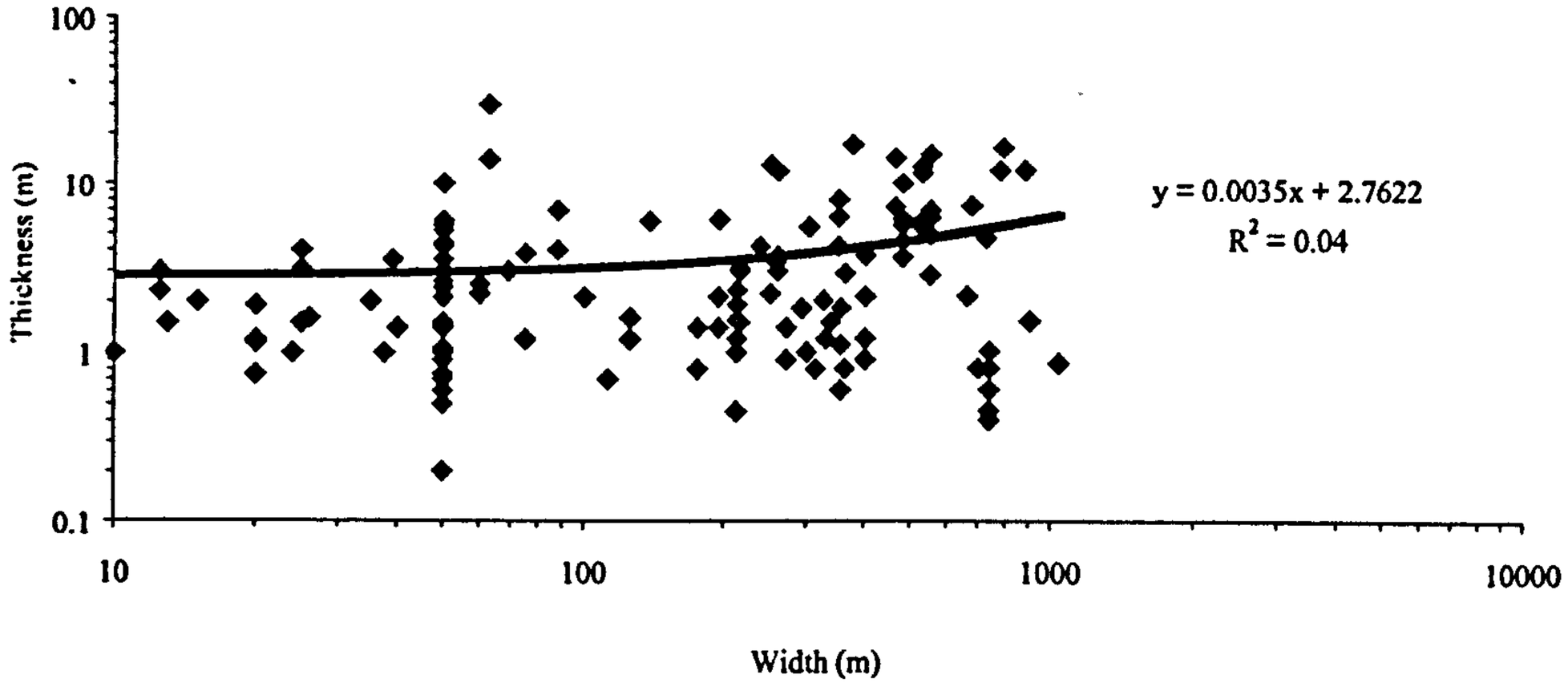

Figure 4.18. Cross plot of adjusted sandbody geometrical data from the Escanilla Formation with a best fit line plotted (n = 136). Note the considerable scatter and the ambiguity in the application of general trend lines to the cross plot dataset.

4.21 The Escanilla Formation: an analogue to the Lower Ketch Member

Analysis of the Escanilla Formation outcrop has proved it to be a good analogue for the Lower Ketch Member, Tyne Field, SNS, and comparisons are summarised in Table 4.10. Consequently, geometric data gathered from the Escanilla Formation may be used in the inter-well interpretation of lateral facies changes within the Lower Ketch Member reservoir.

The Lower Ketch Member and Escanilla Formation sequences exhibit cyclical alternations of vertical and laterally stacked channel sandbodies with pedogenically altered overbank fines. Thicknesses of sandbodies and fine overbanks are comparable in outcrop and core. Basal contacts between the sandstones and underlying fines are sharp and predominantly erosional. Often the sandbodies fine upwards and in many cases exhibit channel stacking. Summary vertical facies logs through the sequences show a

marked similarity between reservoir and analogue. Furthermore, the grain size comparison shows the D_{50} and D_{90} are similar, both exhibiting the same grain size distribution shape, with a dominance of sand grade particles. Matching the grain size distribution is critical to the comparison between the two sequences. In both sequences the proximal to distal trends relate to a decrease in net-to-gross and future study of these downstream trends may reveal vital information on the downstream channel-belt stacking patterns.

Pedogenic indicators display poorly developed, red mottled palaeosols. Lack of correlative marker horizons and pervasive oxidation hinder environmental interpretation of the overbank environment. In both reservoir and analogue evidence is provided that indicates both well-drained (oxidation) and poorly-drained (reduced) soils coexisted within the floodplain. Limestones and oncoids in the Escanilla Formation indicate temporary lakes developed on the floodplain, however, there is no evidence to suggest whether lakes formed on the floodplain during the deposition of the Lower Ketch Member. Trace fossils are rare within the Lower Ketch Member unlike the Escanilla Formation; this difference may be attributed to the development of invertebrates from the Carboniferous to the Eocene. There is no evidence to suggest the floodplains in either sequence were covered with substantial amounts of vegetation, although evidence may have been destroyed by subsequent oxidation and mottling processes.

Grain size distribution has been identified as a major control on the preservation potential of floodplain deposits with the deposits of the Escanilla Formation and the Lower Ketch Member reservoir. However, the identification of the relative impact of allocyclic and autocyclic controls in these two sequences is ambiguous.

Based on the evidence presented in this chapter the use of the Escanilla Formation geometries for the interpretation for the Lower Ketch Member is recommended and definition of reservoir architecture benefits from this analogue study.

Table 4.10. Summary of criteria used to assess the viability of the Escanilla Formation as an analogue to the Lower Ketch Member reservoir interval.

Parameter	Lower Ketch Member, Tyne Reservoir, SNS	Escanilla Formation, Southern Pyrenees, Spain
Age	Carboniferous (Westphalian C-D)	Middle-Upper Eocene (38-39.5 Ma)
Thickness	150 m	500-750 m
Data set	8 wells (Total of 905' core)	Onshore outcrop
Net to Gross	60% (Based on entire wireline log dataset)	64 % in the two logged intervals (150 m)
Grain size distribution	D_{50} = 0.075 mm, D_{90} = 0.416 mm	D_{50} = 0.085 mm, D_{90} = 1.227 mm
Lithofacies/ sedimentary structures	GC) Massive crudely stratified coarse-gravel framework conglomerates PS) Parallel to cross-bedded pebbly sandstone SS) Parallel to cross-bedded medium to coarse-grained sandstone Fwc) Isolate laterally confined muds/silts FS) Fine to coarse-grained isolated sandstones SSrc) Intraformational rip-up clast muds within sandstones Fl) Parallel laminated muds/silts SSr) Pedogenically modified sandstones Fr) Pedogenically modified mud/silts	GC) Large planar and parallel bedded coarse-gravel framework conglomerates PS) Parallel to cross-bedded coarse-grained pebbly sandstone SS) Parallel to cross-bedded medium to coarse-grained sandstone Fwc) Isolate laterally confined muds/silts FS) Fine to coarse-grained isolated parallel laminated sandstones SSrc) Intraformational rip-up clasts within sandstones SSr/Fr) Fine-grained pedogenically modified siltstones and fine sandstones L) Limestones
Thickness of channel sandbodies (compacted)	0.1-22.4+ m (mean = 3.9 m)	0.2-30 m (mean = 3.7 m)
Thickness of overbanks (compacted)	0.16-21.7 m (mean = 4.9 m)	0.3-22 m (mean = 3.9 m)
Formative channel depths	1.5-3.5 m	2.5-5.5 (using SS lithofacies only)
Width of sandbodies	Unknown	10-1037.5 m *
Channel-belt width using empirical relationships	117-1078 m	302-1973 m
Sandbody width:thickness ratios	Unknown	10-300:1
Largest clast size	20-80 mm	20-150 mm
Depositional rate (undecompacted)	Unknown	0.25-0.35 m/1000 years (Bentham *et al.*, 1993) 0.53 m/1000 years (Dreyer *et al.*, 1993)
Climate	Semi-arid/Humid (Equatorial) (Rowley *et al.*, 1985)	Mediterranean semi-arid climate (35-40°N latitude. (Atkinson, 1986)
Bioturbation	Root disturbance	Domichnia traces, algal mats, gastropods, ostracods and oncoids
Palaeosols	Immature – well drained and within lacustrine sequences	Immature – well drained and within lacustrine sequences
Main source area	Fenno-Scandinavian high, 100's km to the north. MNSH (Stone & Moscariello (1999)	Pyrenees mountain belt approximately 60 km north.
Basin type	Foreland (Quirk and Aitken, 1997)	Foreland
Burial depths	3650 m	1200-2000m
Depositional model	Fine-grained depositional multichannel channel-belt with overbank deposition.	Braided and meandering stream channel-belt undergoing overbank deposition.

*Maximum outcrop length used in study area.

4.21.1 Limitations of the Escanilla outcrop study and future recommendations

This chapter has raised several opportunities for further work.

- Examinations of the Escanilla Formation and the Lower Ketch Member provide very little evidence for the development of vegetation on the floodplain during deposition. Whether this is a result of a poorly vegetated floodplain or subsequent destruction and lack of preservation of the vegetation is inconclusive. A study of modern analogue is required to establish how vegetation affects the binding capacity of floodplain sediments and channel-belt migration. Additionally, quantification of plant development from Carboniferous and Eocene times is required to determine the likely affect on the prevailing drainage systems.

- The Escanilla Formation onshore analogue study provides a two-dimensional dataset of the cross-stream channel-belt architecture, but this study fails to provide full three-dimensional alluvial architecture, which includes: downstream geometry, stacking patterns and connectivity. Future work may investigate and quantify basin-wide spatial variations in stacking patterns.

- Sandbody geometries have been calculated based on a rectangular form. Further work is required to quantify the shapes of individual sandbodies in order that reliable stacking patterns be developed.

- The study also fails to quantify the within channel-belt scale architecture, due to: (1) lack of continuous, good quality lateral exposure as sandbodies are heavily weathered; (2) lack of common consensus on definitions of within channel-belt alluvial architecture (cf. Miall, 1985; Bridge, 1993); and (3) complexity of the three-dimensional shape and orientation of the within channel-belt architectural elements.

- The lateral variability of the within channel-belt alluvial architecture of the Escanilla Formation sandbodies may result in the inappropriate application of vertical facies models. Future field studies may highlight the range of vertical facies profiles present within individual sandbodies types.

4.22 Requirements for full analogue comparison and validation

Difficulties in sandbody correlation between wells due to problems in establishing reference horizons in fluvial environments and the scarcity of biostratigraphic indicators, results in the application of outcrop analogues to improve the geological resolution. This chapter has highlighted several problems with the application of published outcrop geometrical datasets (refer to Chapter 2, Table 2.2) for subsurface prediction of alluvial architecture, which are outline below:

- Most literature studies only provide two-dimensional sandbody geometries as a consequence of: (1) sandbodies from large outcrop sections often being measured from photomontages, which may inhibit the collection of three-dimensional datasets, and (2) complete three-dimensional exposure of outcrops are rare.
- Many published outcrop studies ignore the impact of burial compaction and do not apply any estimates of maximum burial depths and resultant compaction.
- Studies do not state whether measured widths are partial (observed) or complete, which may result in a case where thicknesses are measured as maximums and widths are measured as minimums, which may bear no relationship to depositional process, rather to extent of exposure. Correction for outcrop orientation to mean palaeoflow is frequently not defined.
- Correction for distortion of photomontages is not often presented, although this can produce significant errors (cf. Wizevich, 1991; Arnot, 1997, Caracuel *et al.*, 2000).
- Sandbody types are commonly not classified in a comparable way between studies and critically the *scale* of the depositional systems is often not considered.
- Few published studies provide quantitative data for within channel-belt scale alluvial architecture (an exception is the study by Van der Neut and Eriksson, 1999), often due to difficulties in definition and exposure as architectural elements grade laterally into each other.

Many of these problems arise because datasets are poorly constrained. Therefore, a list of the minimum requirements to enable reservoir-analogue studies to be compared is documented in Table 4.11, and must be included with future published geometrical datasets.

Table 4.11. List of minimum data requirements for full subsurface reservoir to outcrop analogue comparisons.

Steps	Data required
	Qualitative data
1	Lithofacies descriptions and classification to guide depositional model.
2	Bioturbation and palaeosol assessment for prediction of climate.
3	Source and basin setting classification.
	Quantitative data
4 *	Measurements of width, length and thickness of channel-belt sandbodies with estimates of distortion and a full description of the measurement techniques.
5	Orientation data of sandbodies.
6	Characterisation of complete, observed and unlimited lengths. Conditioning observed data to complete sandbody datasets.
7	Measurement of overbank thickness.
8	An estimate of burial depth and compaction for both sandbodies and overbanks.
9	Calculation of Net-to-Gross ratio and grain size distribution.
10^	Calculation of net aggradation rate.
11	Calculation of formative channel depths to determine the scale of the system.

*If exposure is good then measurements of within channel-belt scale architectural elements are also needed.

^ Only acts as a guide as rate is often dependant on the time over which the sequence is averaged (Sadler, 1981)

4.23 Summary

Conclusions from the comparative study between Lower Ketch Member and Escanilla Formation are:

1. The depositional model proposed by Bentham *et al.* (1992, 1993) has been expanded by this field study. New information is presented regarding the occurrence of limestones containing freshwater biota and the presence of oncoids, which suggest shallow lakes were pervasive on the floodplain. Channel-belts are estimated to have been between 300-2000 m in width, containing channels with depths of 3.5 to 5.5 m. The disappearance of gypsum at the top of the Lower Escanilla Formation was consistent with the general shallowing upward signature exhibited within the Ainsa Basin, and more specifically, the increase in the proportion of sandbodies during the deposition of the Escanilla Formation. However, it is postulated that the grain size distribution is critical in the development of substantial overbank deposition. While aggradation rates may play a part in the modification of channel-belt sandbody proportions throughout the sequence, there is no evidence to suggest that changes is

alluvial architecture could not have also resulted from a basinward facies progradation of the downstream fining trend as the foreland basin migrated southwards.

2. The difference between burial depth of the Lower Ketch Member reservoir and Escanilla Formation outcrop analogue suggest that the range of sandbody thickness is comparable when decompacted to original depositional thickness.
3. Analysis of the Escanilla Formation provides a good analogue to the alluvial architecture of the Lower Ketch Member, Tyne Field, SNS. Conditioning methods of Visser and Chessa (2000a,b) have been successfully used to adjust the complete Escanilla Formation sandbody distributions and provide an order of magnitude more data than can be obtained from the partially exposed sandbody geometries. Without conditioning, the sandbody distributions would provide an underestimate of sandbody widths, leading to a smaller well spacing being chosen. Empirical estimates of channel-belt width overestimate ~75 % of the measured sandbody widths within the Escanilla Formation. From the data presented in this chapter the use of geometrical information from the Escanilla Formation is recommended for prediction of alluvial architecture in the Lower Ketch Member.
4. This chapter highlights the shortcoming of much of the literature where data are poorly-constrained, and suggests comparison must include, but not be limited to: depositional environment, climate, grain size, lithology, facies associations, palaeochannel depth, orientation, sandbody and overbank geometries, basin setting, and burial depth. Consequently, a list of minimum requirements for full reservoir and analogue comparisons is presented to facilitate the communication and application of geometrical datasets between sedimentary sequences.

Chapter 5. Experimental study of the impact of sediment supply grain size on down-basin braided alluvial architecture: rationale and methodology

5.1 Synopsis

This chapter details the rationale and methodology used for three experiments of a 1:50 generic-Froude scaled model (GFSM) of the braided Ashburton River, New Zealand. Physical modelling was employed to isolate the impact of grain size on surface channel morphology and alluvial architecture. Principles of physical modelling are reviewed and the modelling of fine-grained fluvial sediments appraised. Experiments were carried out in a flume facility, which allows the aggradation of fluvial sediments, followed by excavation and quantification of resultant depositional architecture. Details are presented on data acquisition methods from a field study of the Canterbury Gravels and modern Ashburton River, New Zealand that serve as prototype inputs and verify the model. Physical modelling employed the use of a bimodal sediment mix (~20 % sand, ~80 % gravel). Three experiments were conducted with identical boundary conditions except for a fourfold change in sediment supply grain size. Details are provided on the measurements taken during each experimental run.

5.2 Introduction

Quantitative measurement of down-basin change in within channel-belt alluvial architecture is often difficult to gain from subsurface reservoir or outcrop studies, which suffer from the inherent limitations addressed in Chapter 2. Understanding how sediment grain size and alluvial architecture changes down-basin as a result of downstream fining processes is particularly important for hydrocarbon flow models.

Studies that have focused on the downstream changes in channel morphology and pattern have been concerned with modern fluvial systems, linking channel change downstream to factors such as discharge (Leopold and Maddock, 1953; Harvey, 1969; Stevens *et al.*, 1975; Knighton, 1987b), hydraulic regime (Osterkamp, 1980; Yu and Wolman, 1987) and sediment characteristics (Pickup, 1976; Parker, 1979) (reviewed in Chapter 2). While these modern field studies provide a good insight on the range of

controls influencing the fluvial system, they fail to quantify the relative importance of each controlling factor on channel morphology and depositional architecture.

Few studies have focused on the downstream changes in the internal architecture of alluvial deposits in relation to grain size changes. Robinson and Slingerland (1998) looked at grain size trends in the Pocono Formation, Central Appalachian Basin and concluded that subsidence rate and sediment supply are the most important controls on downstream fining profiles. Other studies have looked at down-basin facies changes for a range of outcropping fluvial and fan systems (e.g. Kelly and Olson, 1993; Martinius, 2000). Studies such as Heller and Paola (1996) considered the changes to the down-basin architecture of channel-belt scale sandbodies within fine-grained overbank deposits in relation to subsidence rate and avulsion frequency. Often the link between grain size and depositional form is only tentatively made by linking the percentage of coarse- to fine-grained deposits to architecture on the gross scale. Understanding the within channel-belt architecture addressed in this chapter is paramount to the construction of stratigraphic and reservoir simulation models, and bridges the gap between the petrophysical scale and channel-belt scale (see Chapter 7). Physical modelling provides one of the only ways of disentangling these controls on alluvial architecture by varying a single controlling variable while keeping all other boundary conditions constant. Therefore, the objectives of the physical modelling were:

1. To quantify the impact of grain size on braided river channel morphology.
2. To isolate the control of grain size on within-channel-belt alluvial architecture.
3. To explore the role of physical modelling as a complementary technique to well, outcrop and modern datasets addressing a scale of information that is difficult to quantify using any other method.

In order to undertake FSM, a robust rationale was required to establish the most appropriate prototype to provide input parameters to the physical model and therefore, the aims of this chapter are to: (1) chose suitable modern and ancient analogue prototypes for FSM; (2) establish a characteristic source grain size distribution to model; and (3) determine how the source grain size distribution is modified (magnitude and modes) in a downstream direction. Since the choice of a suitable prototype hinges on satisfying scaling laws for hydraulic models, it is therefore appropriate to review the underlying principles of physical modelling.

5.3 Principles of Froude-scaled physical modelling

Physical modelling techniques have been employed to study fluvial processes for many years (see reviews in Ashmore, 1982; Schumm, 1987). Experiments have become increasingly sophisticated and more recently have been used to investigate autocyclic and allocyclic controls on sediment deposition and preservation (e.g. Ashworth *et al.*, 1994, 1999; Paola, 2000; Stokstad, 2000).

Modelling approaches usually encompass the need for simplifications and assumptions, and provide a physical representation of form and evolution of a landform while compressing time and scale. This section briefly outlines the principles of physical modelling. More details on physical modelling of open channels are available in Henderson (1966), Mosley and Zimpfer (1978), French (1985) and Peakall *et al.* (1996).

Physical models have been classified by how closely they replicate a prototype and by the controlling boundary conditions (Chorley, 1967; Schumm *et al.*, 1987). The physical modelling described in this chapter is concerned with movable-bed models where the substrate is free to move within a constrained flume basin and where scaling laws for both sediment and water are satisfied (see Yalin, 1971; Langhaar, 1980).

Scaled models are based on similarity theory, whereby a series of dimensionless parameters that fully categorise the flow are evaluated, which maintain geometric, kinematic (motion) and dynamic (force) similarity between model and prototype. Controlling variables (Yalin, 1971) for open channel flow with a fixed-bed are expressed as: the dynamic viscosity (μ) and density (ρ) of the fluid; boundary conditions of the channel, normally the hydraulic radius (R) and surface roughness (k_S); bed slope (S), downstream velocity (U), and gravitational constant (g). In movable-bed models, the flow can be considered as a two-phase flow containing both fluid and particles. Therefore, two parameters, which describe the sediment characteristics, ρ_S (the sediment density) and D, (the characteristic grain size of the sediment) must also be incorporated together with the specific dimensionless properties of the fluid. These variables are used to calculate the three main dimensionless flow parameters: Froude number (Fr) Equation 5.1; flow Reynolds number (Re) Equation 5.2; and grain Reynolds number

(Re*) Equation 5.3. Grain Reynolds number is a measure of the roughness of the bed relative to the thickness of the viscous sub-layer based on D_{90}.

$$\mathrm{Fr} = \frac{U}{\sqrt{gR}} \qquad \text{Equation 5.1}$$

$$\mathrm{Re} = \frac{\rho R U}{\mu} \qquad \text{Equation 5.2}$$

$$\mathrm{Re}^* = \frac{\rho U_* D}{\mu} \qquad \text{Equation 5.3}$$

where U_* is shear velocity. Since the parameters of acceleration due to gravity (g), density of sediment ($_s$) and water ( ), and fluid viscosity (μ) are constant in the model ($_m$) and prototype ($_p$) and assuming a constant temperature, the flow Reynolds number (Re) may be relaxed, whilst keeping the flow within the fully turbulent regime (Re > 2000). The Froude number (Fr) must be kept in the same range between model and prototype. If dynamic similarity is achieved, geometric and kinematic similarity are also assumed (Warburton and Davies, 1998). This modelling technique is known as Froude Scaled Modelling (FSM) and has been successfully employed to model fluvial systems (Ashmore, 1982; 1991a; Warburton and Davies, 1998).

FSM requires the scaling of Re* to ensure hydraulically rough flow conditions. Equation 5.4 expresses the Shields (1936) relationship that is normally rearranged as:

$$\tau^* = \frac{\tau}{(\rho_s - \rho) g D} \qquad \text{Equation 5.4}$$

where τ is the bed shear stress responsible for initiating sediment entrainment for a particular grain-size, D, and τ^* is the dimensionless shear stress. The Shields entrainment diagram (Figure 5.1) uses τ^* and Re* to define an entrainment threshold known as the critical shear stress, τ_c^*, above which a flow is capable of entraining sediment. The Shields diagram also shows τ_c^* becoming constant (approximately 0.056) at high values of Re*. The scatter of points has caused an ongoing debate

concerning the critical threshold value of Re* where the flow may be considered to be fully rough and turbulent and independent of viscous forces (Re^*_{crit}). Ashworth *et al.* (1994) noted that this value occurs at Re* = 5-70. Once these flow parameters have been fully scaled, the scaling of time and hydrographs needs to be addressed using the relevant prototype data (Sections 5.3.1 and 5.3.2).

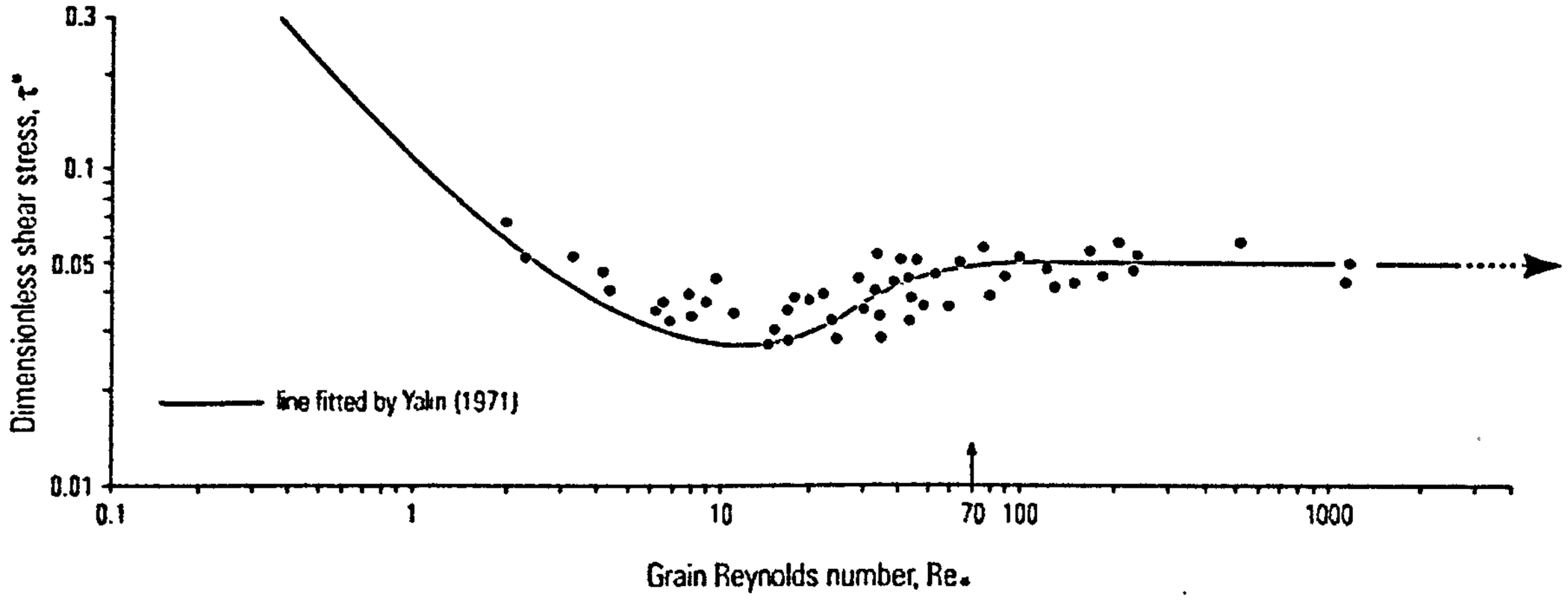

Figure 5.1. Modified Shields curve from Ashworth *et al.* (1994) to show that the critical threshold above which the flow becomes hydraulically rough occurs where values of Re* are in the range of 5-70 based on calculations using grain size D_{90}.

FSM studies may not allow full replication of the fluvial system and some consideration must be given to how other factors that may control the depositional system, such as: (1) vegetation (Smith, 1976; Marsden, 1981) and cohesion (Schumm and Khan, 1972), which may affect binding of the floodplain sediment and increase channel stability; (2) climate, which may alter during the deposition of a complete sequence; (3) compaction, affecting the resultant geometry of the alluvial architecture; (4) base-level (Wood *et al.*, 1993a,b; Koss *et al.*, 1994), which can influence incision rates; and (5) ground water.

Validation and testing of the model is one of the most important steps in model construction. Measurements are made during the experiments and flow parameters calculated to validate the similarity of the model with the prototype. In experiments where aggradation is imposed, the subsurface depositional architecture can be characterised and verified by examination against field outcrop (Ashworth *et al.*, 1999).

5.3.1 Scaling of time

One of the advantages of physical modelling is they enable the study of long-term fluvial changes that would otherwise take place over time periods too long to be studied in the field. Two different approaches to the modelling of time are possible; one based on dimensional analysis and the other on magnitude-frequency analysis (see Peakall *et al.*, 1996). No single scale is used to translate model time into geologic time, nonetheless Paola (in Stokstad, 2000) argues that physical models provide a distorted glimpse of time using real grains and water exhibiting processes that occur in nature. The time scale for mean flow velocity $(\lambda_t)_V$ (Equation 5.6) is given by:

$$(\lambda_t)_V = \lambda_l^{0.5} = \lambda_t \qquad \text{Equation 5.6}$$

where λ_l is the length scale being used in the physical model (e.g. 1:50) and λ_t is the scaling ratio of time between prototype and the model.

5.3.2 Scaling of discharge

Wolman and Miller (1960) showed that there is a good correlation between dominant discharge and the bankfull discharge. Most physical models use constant discharge that approximates to bankfull (Leopold and Wolman, 1957; Ashmore, 1982). Many fluvial processes such as overbank sedimentation and avulsion (Leddy *et al.*, 1993) occur with fluctuating discharge and the use of hydrographs and sediment discharge improves the realism of the model (Ashworth *et al.*, 1994). The scaling for discharge (Equation 5.7) has been given as (Peakall *et al.*, 1996):

$$\lambda_Q^{2.5} = \frac{Q_m}{Q_p} \qquad \text{Equation 5.7}$$

where Q_m is the length of the model, Q_p is the length of the prototype and λ_Q is the scaling ratio for discharge. Before scaling of time and discharge can be performed, the collection of data from suitable field studies is required to serve as prototype data for

physical modelling. The choice of prototype used in physical modelling is discussed in the following sections.

5.4 Scaled physical modelling of fine grained systems: the Lower Ketch Member

Previous physical scale models have commonly been based on coarse proglacial gravel-bed rivers (e.g. Ashmore, 1982; Ashworth *et al*, 1994, 1999; Warburton and Davies, 1994) and little attention has been directed towards the modelling of fine-grained rivers. A series of calculations were performed to determine the theoretical hydraulic flow parameters (described in Section 5.3) for physical modelling of modern or ancient rivers exhibiting a very fine-grained grain size distribution. This section evaluates the potential of using FSM to investigate fine-grained reservoirs such as the Lower Ketch Member.

The D_{90} estimate for the entire Lower Ketch reservoir interval grain size distribution is 0.416 mm. Using a 1:50 length scaling between the model and prototype provides a D_{90} value for a model of the Lower Ketch Member of 8.3 μm. Input values for the calculation of hydraulic flow parameters were based on: (1) channel depths of 1.5-3.5 m based on empirical relationships derived from mean cross-set data in cored intervals (Chapter 3, Section 3.8); (2) channel widths based on a width/depth ratio of 30 (within the range documented by Parker, 1979); (3) a bed slope of 0.01; (4) mean flow velocities of 0.29 m s^{-1} from previous modelling experiments (Peakall, 1995); and (5) a peak discharge of 3.2 l s^{-1} based on the maximum obtainable in the flume facility.

Theoretical calculations of Re* for the Lower Ketch Member produce a value of 0.1, which is below the critical grain Reynolds number (15-70) required for flow to be hydraulically rough (cf. Ashworth *et al.*, 1994). White silica flour (<40 μm) is the smallest commercially available grain size and therefore, the use of the Lower Ketch Member grain size distribution (D_{90} value of 8.3 μm) for FSM would result in most of the D_{90} sediment comprising silica flour.

Ashworth *et al.* (1994) coarsened the scaled grain size distribution whilst keeping the same grain size distribution curve shape, to avoid low Re* values. This method could not be employed with the grain size distribution from the Lower Ketch Member because

the range of particle sizes in the grain size distribution is too wide to incorporate into a physical model (i.e. mud to conglomerate clasts up to 80 mm). Alternatively, a smaller length scaling ratio could be used (e.g. 1:20) to increase the magnitude of grain size distribution used. However, even at a 1:20 scaling ratio the majority of sediment in the model would consist of silica flour. The use of a smaller scaling ratio also reduces the proportion of the braidplain that can be investigated in the flume facility.

In summary, FSM of fine-grained fluvial systems with a high mud/silt content such as the Lower Ketch Member is impractical without introducing a high degree of model distortion. Therefore, modelling of fine-grained prototypes may be restricted to generic models with some relaxation on the scaling of the grain size magnitude or the construction of a larger flume facility. In order to investigate specifically the impact of sediment supply grain size on surface channel morphology and alluvial architecture a different prototype was used. Prototype data for physical modelling was gathered from the modern Ashburton River and the late Quaternary Gravels of the Canterbury Plains, New Zealand. Successful physical modelling work focusing on the control of aggradation rate on alluvial architecture has been previously undertaken using the Canterbury Plains as a prototype by Ashworth *et al.* (1999).

Taking the Canterbury Plains as a prototype, physical modelling was used to establish the role of grain size on the channel morphology of braided rivers and within channel-belt alluvial architecture. The proceeding sections provide field data and evidence from published studies to establish and justify the most appropriate manner in which to model a change in grain size distribution in braided river systems. Two factors need to be taken into consideration: (1) the initial grain size distribution supplied to the river, and (2) the modification of this initial grain size distribution down the rivers course. These two factors are quantified for the modern Ashburton River in the following sections.

5.5 Justification for the use of the Canterbury Plains

Many ancient fluvial sequences have been exhumed following burial, compaction, tectonic deformation to provide outcrop analogues. In order that these analogues may be modelled, the assignment of a depositional model is required, together with an assessment of the processes acting within the system at the time of deposition. Subsequently, the aim is to find a modern day analogue for the outcrop to gain hydraulic and morphological data (e.g. hydrograph type, magnitude and channel dimensions) for inputs to the physical model. Gaining this information from outcrop studies suffers from inherent uncertainties (Alexander, 1993) and inappropriate application of this modern to ancient analogue link would seriously hinder any interpretation. The advantage of using the Canterbury Plains as a prototype system for modelling lies in the access to both modern and ancient datasets to provide prototype information for scaled modelling. Uniquely, the overlying modern day Canterbury braided river systems are very similar to those responsible for deposition of the braided river sediments of the Canterbury Gravels (Bal, 1996) and were chosen as a prototype for physical modelling for several reasons:

1. Exposure of the late Quaternary braided river gravels allows quantification of the alluvial architecture.
2. Modern gravel-bed braided rivers are (Figure 5.2a) forming in the same basin setting and supplied with the same source material as the underlying gravel-bed braided rivers deposits (Figure 5.2b). Access to the modern rivers allows the measurement of hydraulic parameters for input to and validation of the physical modelling. However, during the deposition of the Canterbury Gravels climate and discharge may have changed and these are more difficult to quantify from outcrop sequences.
3. The characteristic grain size distribution is within the gravel range that satisfies all the Froude-scale modelling laws.
4. The results from the physical modelling can be applied to a range of gravel-bed braided rivers documented for modern (e.g. Dawson, 1988; Warburton *et al.*, 1993), outcrop (e.g. Steel and Thompson, 1983; Ramos *et al.*, 1986; Siegenthaler and Huggenberger, 1993) and subsurface (e.g. Atkinson *et al.*, 1990) studies.

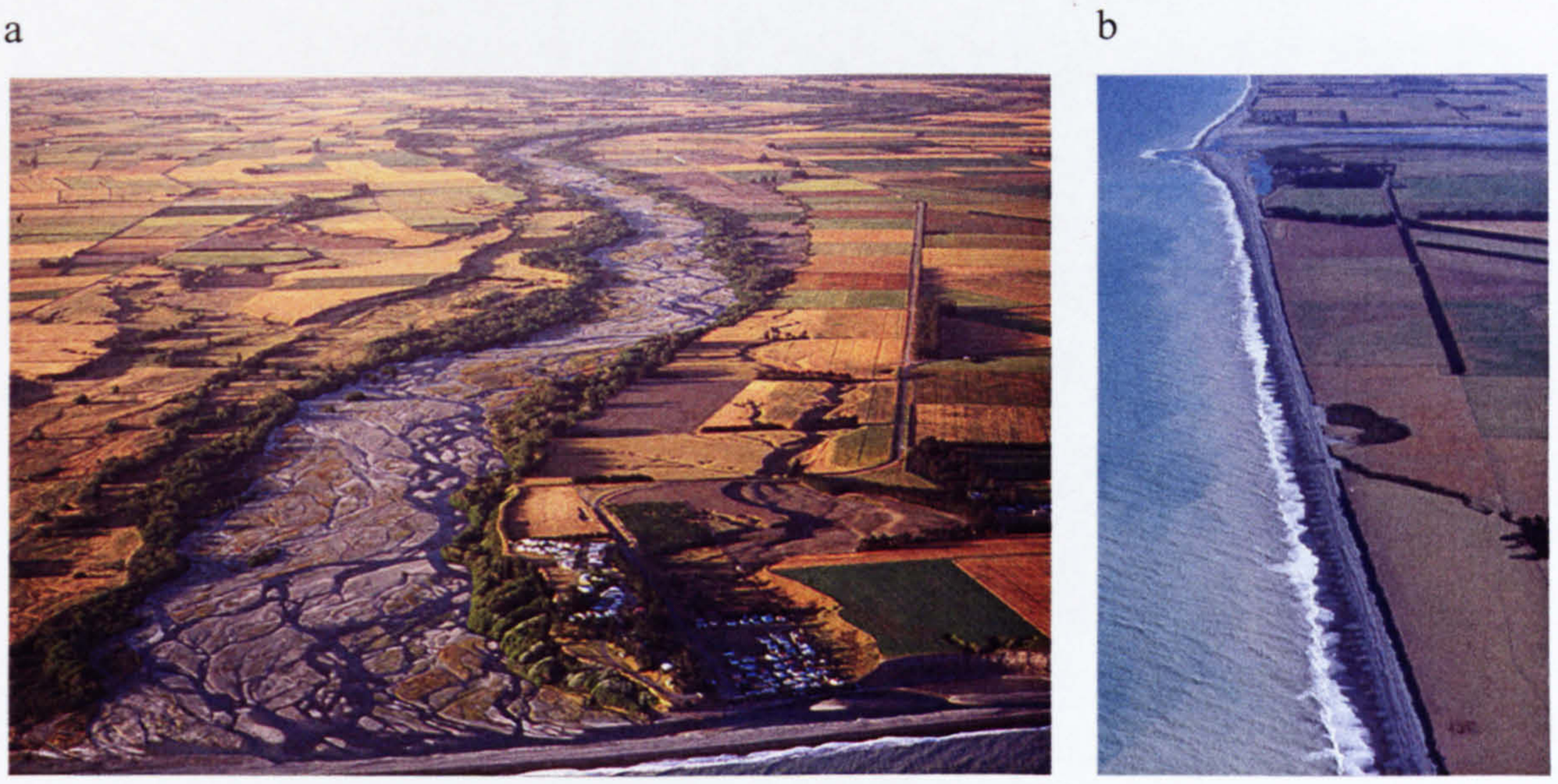

Figure 5.2. (a) Modern Ashburton River Mouth (~1.2 km across) discharging into the Pacific Ocean, (b) The present day retrogradational Canterbury Cliff line composed of late Quaternary Gravels. Showing ~10 km of coastline and the Rangitata River Mouth at the top of the figure.

5.5.1 Regional geological setting

The Canterbury Plains are located in the Canterbury Basin to the east of the Southern Alps, New Zealand and extend over an area 70 km wide and 185 km long (Figure 5.3a). Uplift of the Alps is caused by oblique convergence of the Pacific and Indian plates, which initiated during the late Cenezoic. The Southern Alps are being uplifted at a rate of between 0.8-10 mm yr^{-1} (Wellman, 1979; Tippett and Kamp, 1995) in the central portion. This rate of uplift approximately equals denudation rate (Adams, 1980). Glacio-isostatic forces contribute about 10 % of the total uplift (Mathews, 1967). Uplift rates decline away from the Alpine transform fault and the Canterbury Plains are subsiding at a maximum of 0.2-0.3 mm yr^{-1} (Lensen, 1975; Wellman, 1979), which causes the Quaternary/Tertiary boundary to deepen towards the coast. The Mesozoic basement lies less than 500 m below sea-level at 105-120 m from the Canterbury coast. This basement deepens abruptly at the coast to 3000 m below sea-level and then gradually rises to the east (Atkins and Hicks, 1979).

The Canterbury Plains are composed of a thick succession of unconsolidated late Quaternary fluvio-glacial and fluvial gravels and sands, here termed the Canterbury

Gravels, which have a maximum thickness of over 700 m (Atkins and Hicks, 1979; Wilson, 1985). This stratigraphy has been constructed as a series of broad glacial and interglacial outwash fans sourced from glacial fed rivers propagating from the Southern Alps. Deposition of much of the Canterbury Gravels is attributed to sedimentation during glacial episodes (Soons and Gullentops, 1973), although, deglaciation from *c.*18 ka caused rapid deposition of fluvial gravels (Suggate, 1965). Glacial deposits were then reworked as glaciers retreated (Mabin, 1987). The occurrence of interglacial and glacial cycles has been linked to periods of incision following deglaciation and valley filling during glacial periods (Bal, 1996). These valley fills have been recognised in the top 10-200 m of Canterbury Gravels by the presence of several high permeability corridors, 5-10 km wide, that trend sub-perpendicular to the current Canterbury coastline. These corridors are interpreted as the result of valleys formed during the last interglacial stage (130-75 ka) along a retrogradational coastline, which were subsequent infilled during the last glacial stage (Bal, 1996).

During the last glacial maximum (~20 ka, known as the Otira Glaciation) the braidplain prograded ~55 km out into Canterbury Basin from the present coastline and sea-level was 135 m below the present level (Chappell, 1983; Gibb, 1986; Brown *et al.*, 1988). Between the last glacial maximum and 6.5 ka sea-level rose and since 6.5 ka has remained relatively stable (Gibb, 1986).

The lithology of the mountain catchments of the Canterbury rivers is almost entirely indurated Mesozoic sandstone and mudstone (greywacke and argillite, respectively) (Gibb and Adams, 1982; Brown *et al.*, 1988). Abrasion of greywacke gravels in the Canterbury Rivers produces mud with only small amounts of sand being generated (Adams, 1980).

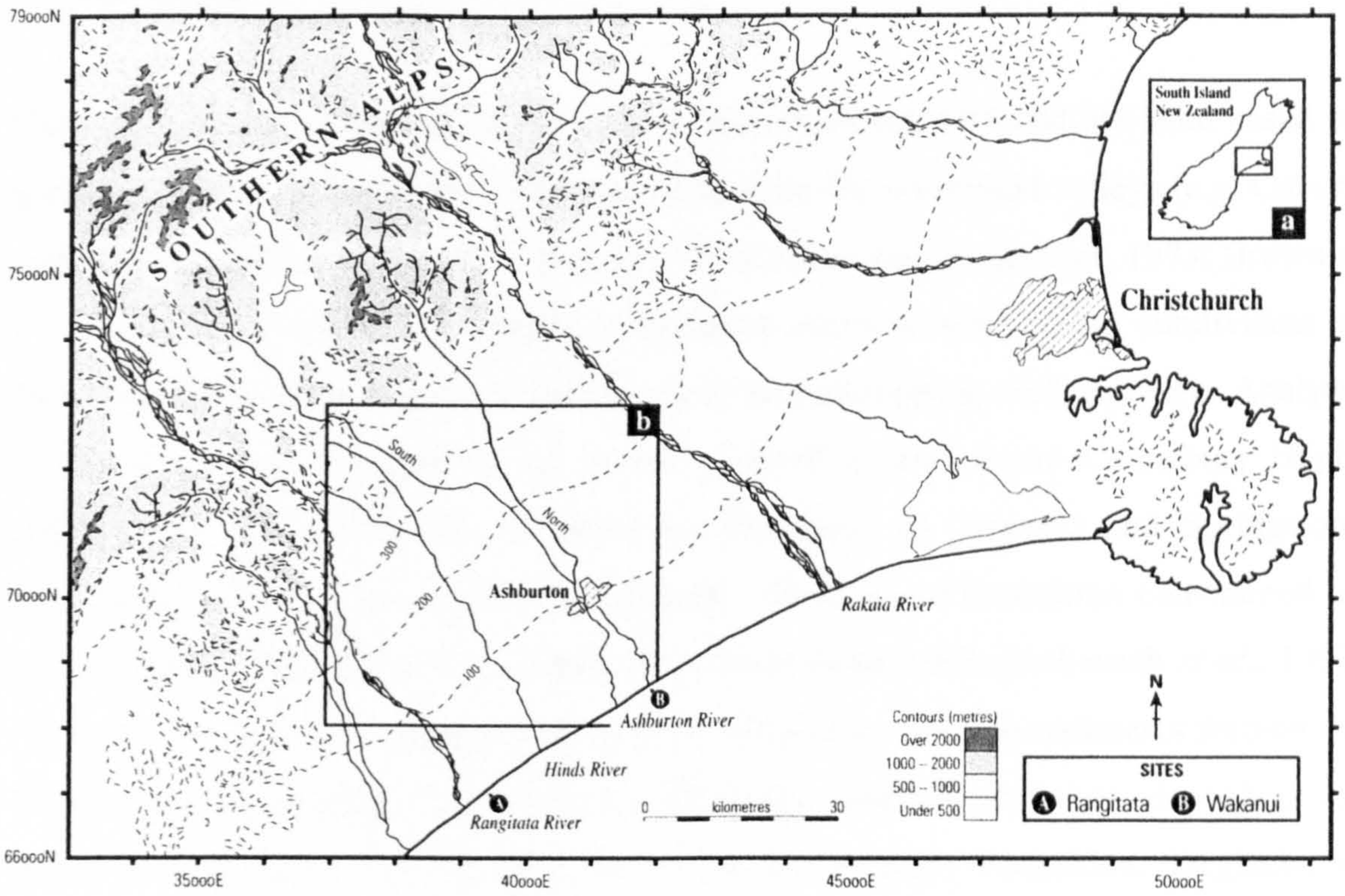

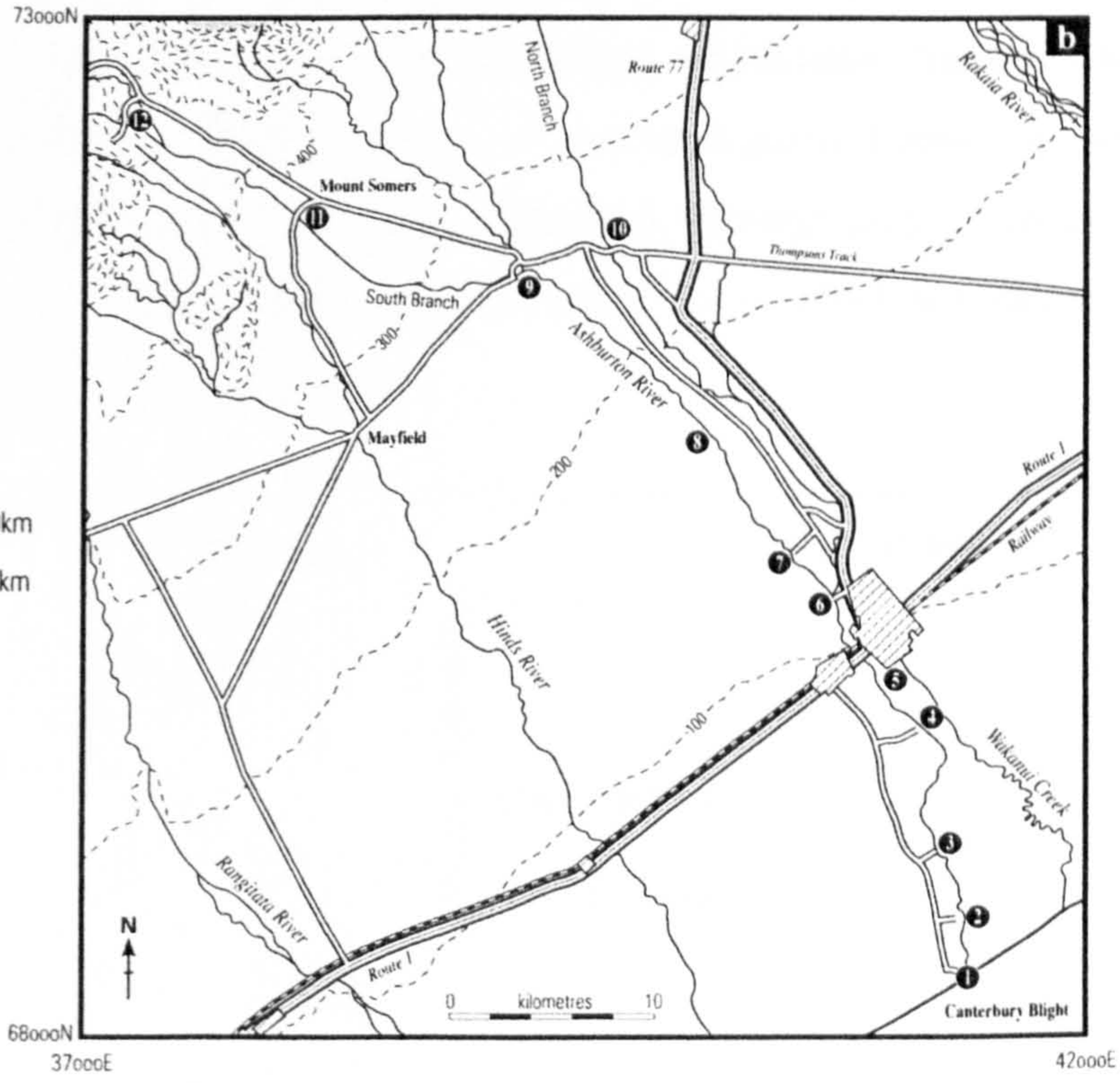

1. Ashburton River mouth 0.3km
2. Croys Road 2.7km
3. Smalls Road 6.3km
4. Boundary Road 13.4km
5. Ashburton Town 18.4km
6. Melrose Road 21.5km
7. Hills Road 24.5km
8. Ollivers Road 30.7km
9. Thompson Track. South Branch 43.9km
10. Thompson Track. North Branch 44.9km
11. Mount Somers 57.4km
12. Inverary Road 66.7km

Figure 5.3. Location maps for (a) the Canterbury Plains field sites, and (b) sites of Wolman grain size sampling along the modern Ashburton River.

5.5.2 Stratigraphy

The nomenclature of the Canterbury Gravel deposits is complex and has been based on glacial advances, terminal moraines and Formations for individual valleys (e.g. Osborn and Suggate, 1959; Soons, 1963; Suggate, 1963; Soons and Gullentops, 1973; Brown *et al.*, 1988). Moreover, the similarity of sediment characteristics makes subdivision of formations very difficult to distinguish within the outcropping cliff exposure. Analysis in this thesis was confined to the gravels exposed in the current Canterbury Blight cliffline, which includes the Windwhistle, Burnham, St. Bernard and Springstone Formations (Figure 5.4) representing between ~30-35 ka of deposition constrained by optical stimulated luminescence dating of the base of the cliffs (Ashworth *et al.*, 1997, 1999). During the early advances of the Otira Glaciation outwash sediments formed the Windwhistle Formation. Subsequently, the Otira Glacial maximum deposited the Burnham Formation conformably above the Windwhistle Formation. Deglaciation commenced at ~18 ka, with several smaller readvances occurring between 18 ka and 14 ka producing rapid deposition of the St. Bernard Formation outwash gravels (Suggate, 1965). During sea-level rise and coastal transgression (Flandrian transgression) associated with deglaciation, the fluvial gravels of the Springston Formation were deposited unconformably above the St. Bernard Formation. A large proportion of the gravels are capped with a layer of fine loess deposits (wind borne), which was deposited over a large portion of the Canterbury Plains.

Formation	Date	Climatic event		Deposits
No deposition	6 k.a. – present	Deglaciation		Fluvial incision
Springston	14–6 k.a.	Deglaciation	Aranui Postglaciation Erosion surface?	Fluvial & fan
St. Bernard	18–14 k.a.	Glacial readvance		Outwash
Burnham	25–18 k.a.	Maximum last glacial	Otira Glaciation	Outwash
Windwhistle	70–25 k.a.	Early glacial advance		Outwash

Figure 5.4. Late Quaternary History of the Canterbury Plains, based on Suggate (1963, 1965) and Brown *et al.* (1988).

5.5.3 Canterbury Plains field site description

This section describes the current field setting where information was gathered in order to perform physical modelling. Sediment is supplied to the present day Canterbury Basin via four main rivers in the study area, the Rakaia, Rangitata, Ashburton and Hinds River. Rivers exit the foothills of the Southern Alps onto the Plains via narrow gorges and discharge some 50-70 km downstream directly into the Canterbury Blight (Pacific Ocean). The Rangitata River meanders downstream of the gorge for a few kilometres before becoming braided (Carson, 1984a,b), while the Rakaia River emerges from its gorge to become fully braided. River mouths are characterised by spit formation (Figure 5.2a), constructed by the strong northerly longshore drift (Carter and Herzer, 1979; Gibb and Adams, 1982). During river floods, these spits are breached and rebuilt as flow wanes (Leckie, 1994). Deltas are not formed off the present day coastline as all sediment is removed by the strong ocean currents and transported northwards around the Bank Peninsular to Pegasus Bay (Carter and Herzer, 1979).

The present sea-level highstand is creating a retrogradational coastline, which is driving coastal erosion (Leatherman *et al.*, 2000). Maximum coastal erosion rates are 1 m yr^{-1} (Wilson, 1976; Gibb, 1978; Basher *et al.*, 1988) and have resulted in the loss of 55 km of coastline, which has exposed up to 25 m of late Quaternary gravels near to the Ashburton River Mouth. The cliff height decreases to the north and south creating a broad convex fan. Incision has occurred as a result of shortening of the river long profiles as the rivers meet base-level. Rates of river down-cutting incision at the coast are 2.7 - 3.3 mm yr^{-1} (Leckie, 1994). At the foothills of the Southern Alps rivers incision is driven by tectonic and isostatic uplift. In an area 8-15 km from the coastline almost parallel to Highway 1, a zone where terraces converge and incision is minimal prevails, termed by Leckie (1994) as the Zone of Minimum Erosion.

50 km of coastal cliffs section between the Rakaia and Rangitata Rivers was studied (Figure 5.3a). A gravel beach provides access to the cliffs through a series of gullies intersecting the current cliff line. Strong winter storms cause cliff erosion and provide freshly weathered gravel exposure.

5.6 Data acquisition for physical modelling input parameters

In order to provide input data for the scaled physical model a number of parameters were measured in the field. A summary of data collected from the Canterbury Plains' field site is presented in Table 5.1, which are discussed in full detail in the proceeding sections.

Table 5.1. Summary of data collected for input and validation of the Ashburton River physical model.

Data collected	Technique	Reason for collection
Grain size from the Ashburton River	Wolman (>5.6 mm)	Quantifying downstream fining rate and downstream modification of grain size shape.
Grain size from the Canterbury Gravels	Bulk sieving	Surface-subsurface comparisons and input grain size to the model.
Channel geometries	Survey	Calculation of hydraulic flow parameters and comparison with the physical model.
Channel gradient	Survey	Imposed model slope, calculation of hydraulic flow parameters and comparison with the physical model.
Alluvial architecture of cliff sections	Photographed	Comparison with preserved sections from the sediment sequence in all flume models.

Physical modelling requires the scaling down of the full prototype grain size distribution. FSM of a full grain size distribution is necessary to allow the reproduction of bed morphology, which also implies the reproduction of sedimentary structures (Warburton and Davies, 1998). Therefore, sampling of grain size was carried out in the modern Ashburton River channel-belt and on the Canterbury Gravels exposed at the current coastline.

The Wolman sampling method was carried out on the surface deposits of the modern Ashburton River to obtain a downstream fining rate. A truncation limit of 5.6 mm was imposed because representative samples could not be taken of particles below 5.6 mm. Consequently, bulk grain size sampling was undertaken on the exposed Canterbury cliffs to provide a full grain size distribution (including the sand mode) for physical modelling. The following sections describe the techniques used to obtain grain size data for physical modelling.

5.6.1 Downstream fining in the Ashburton River

$_d$) defined as the reduction in phi size per kilometre (ψ km^{-1}) for the South Branch Ashburton River where sampling sites were chosen on the basis of access to the river by road (Figure 5.3b). Sites were sampled transverse to the main channel-belt and incorporated the sampling of bar-tops, channel banks, channel beds, slackwater areas and abandoned channels. Particles were sampled at 1 m intervals along each transect, yielding between 100-500 measurements at each site. Care was taken to avoid any influence from possible anthropogenic activity in the channel-belt.

5.6.2 Quantifying downstream fining rate for the Ashburton River

Downstream fining trends for the Ashburton River were constrained by plotting D_{50} and D_{90} values against distance from the Ashburton River Mouth (Figure 5.5) and then fitting an exponential trend line to the data (cf. Sternberg, 1875). Quantification of downstream fining trends were confined to the South Branch of the Ashburton River. The Ashburton River downstream fining trend displays an exponential diminution coefficient of 0.0322 ψ km^{-1}, which falls into the range observed in braided rivers documented in the literature (Table 5.2).

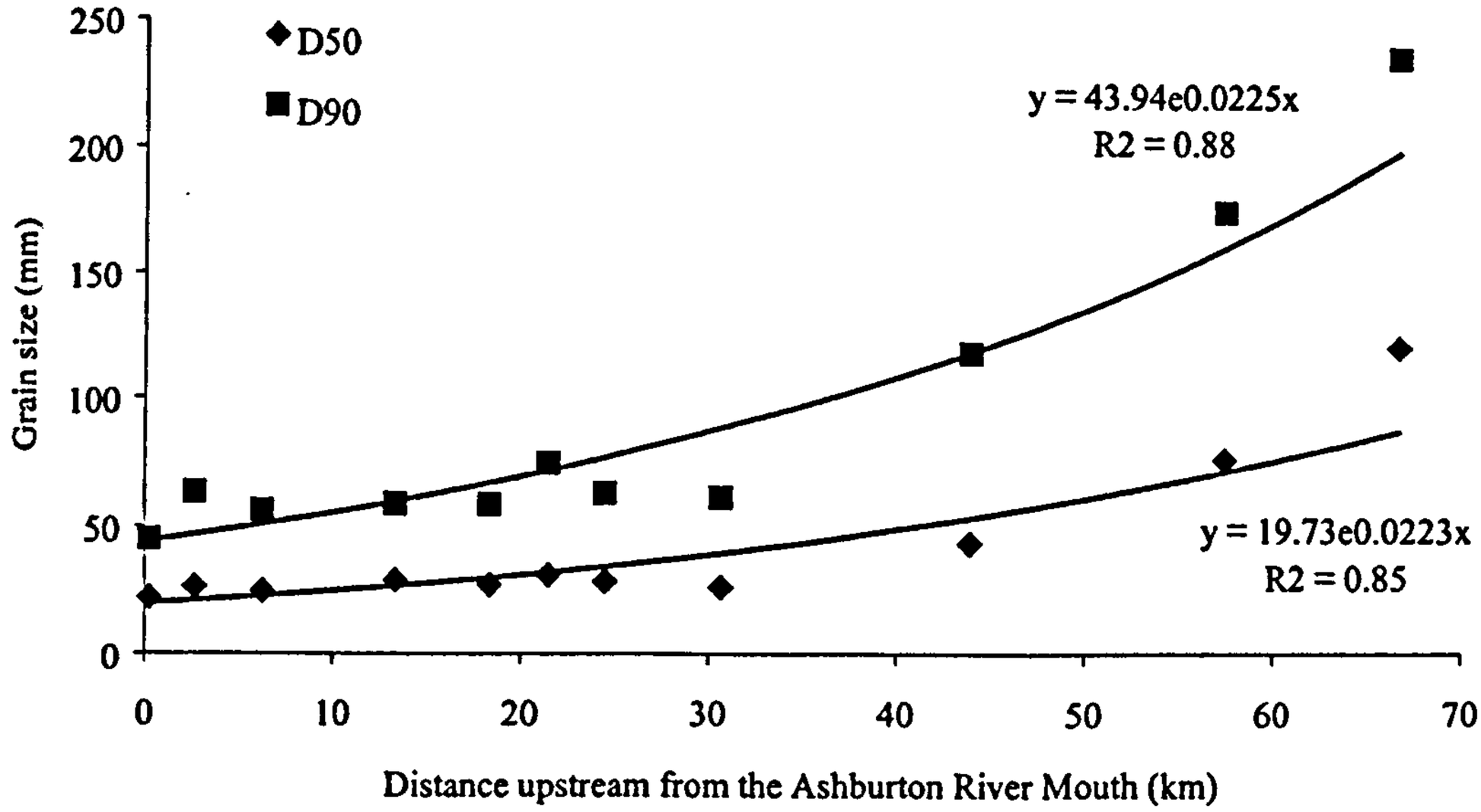

Figure 5.5. Downstream fining curves plotted for D_{50} and D_{90} for the South Branch of the Ashburton River.

Table 5.2. Diminution coefficients reported for braided streams α_d where the diminution coefficient is expressed as the reduction in particle phi size per kilometre (ψ km^{-1}). Note all field study coefficients are for median or mean size of surface material.

Stream	Diminution coefficient α_d(ψ km^{-1})	Source
Sunwapta River	0.2278-0.9982	Dawson, 1988
Squamish River	0.056	Brierley & Hickin, 1985
South Saskatchewan River	0.00147	Shaw & Kellerhals, 1982
North Saskatchewan River	0.0017	Shaw & Kellerhals, 1982
Waimakariri River	0.0102	Hoey & Bluck, 1999
Ashburton River, South Branch	0.0322	This study

5.6.3 Downstream modification of the grain size distribution in the Ashburton River

Results from the Wolman sampling are plotted in Figure 5.6 and show a downstream consistency in the overall grain size distribution shape of the gravel mode (>5.6 mm) between Thompsons Track and the Ashburton River Mouth sites. When these grain size distribution data are normalised to the D_{50} value at the uppermost sampling site, Inverary Road (Figure 5.7), deviation from this consistent trend is only evident in sampling sites more proximal than Thompsons Track (43 km upstream). Between Mount Somers and Thompsons Track (Figure 5.7) the channel becomes braided and the grain size distribution maintains a more consistent shape downstream. This maintenance of the grain size distribution shape has been noted in studies of the Allt Dubhaig (Hoey and Bluck, 1999, see Chapter 2, Figure 2.13), Bow-South Saskatchewan River (Shaw and Kellerhals, 1982), and the Watarase River (Kodama, 1994a). Hoey and Bluck (1999) suggested that the process of size selective sorting retains the overall sorting of the size distribution down the rivers course while the magnitude changes.

Wolman sampling on the Ashburton River was restricted to measurements of the gravel fraction above 5.6 mm. Therefore, in order to obtain the full grain size distribution, bulk sampling from the exposed cliff Canterbury Gravels was undertaken.

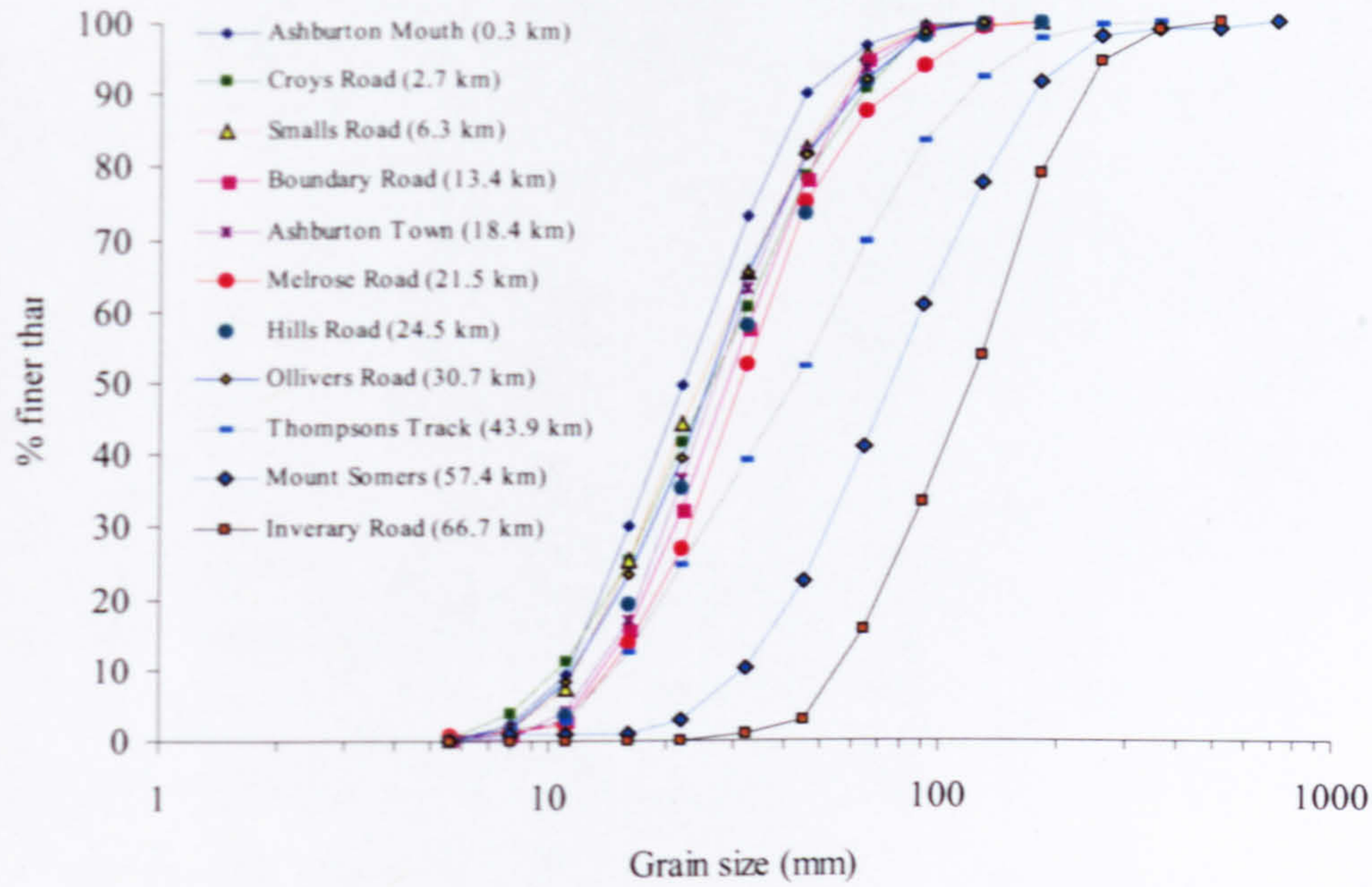

Figure 5.6. Grain size distribution curves for sample sites on the South Branch Ashburton River showing a conservation of grain size distribution shape downstream. All samples taken are of the gravel fraction only (>5.6mm).

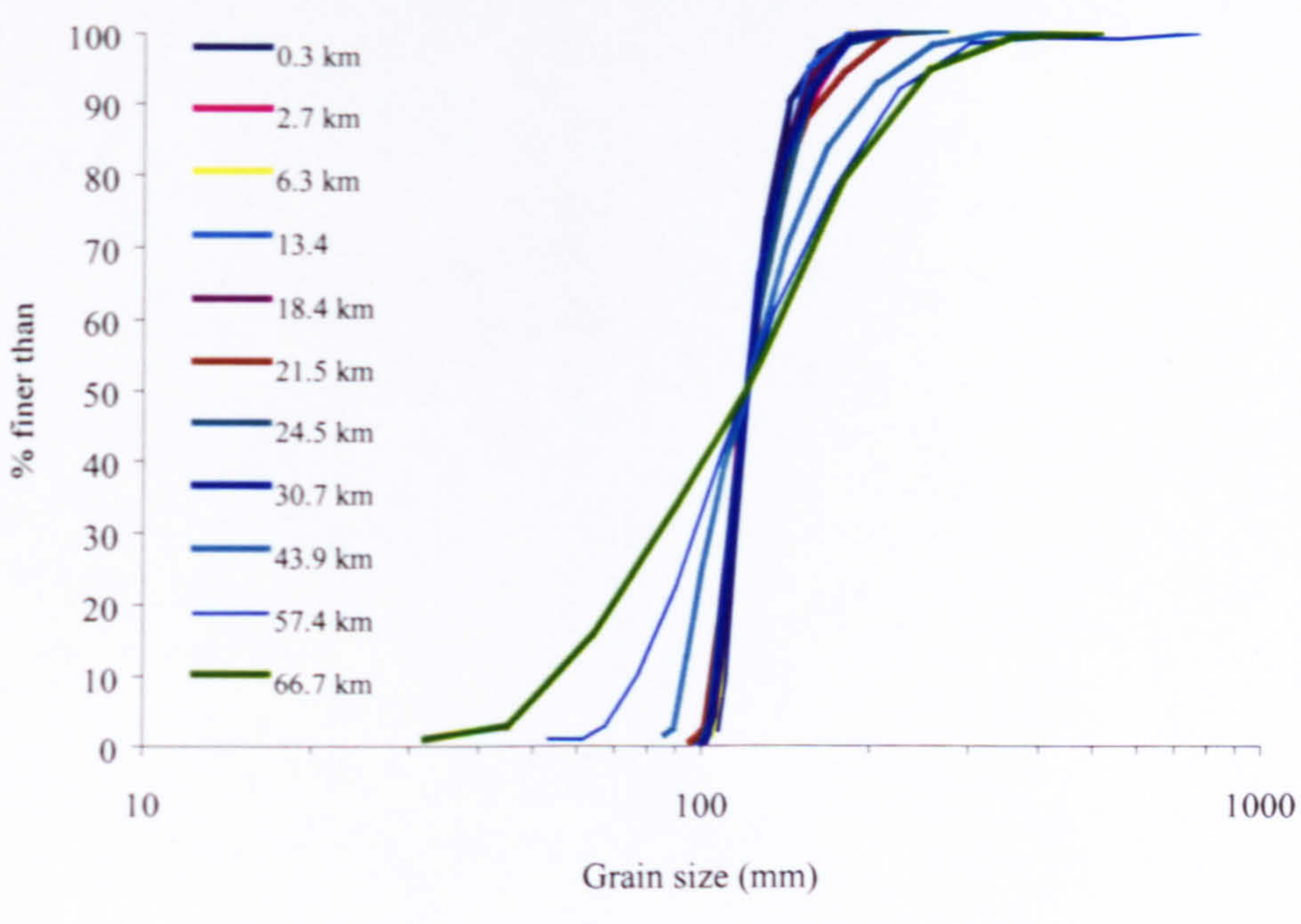

Figure 5.7. Adjusted downstream grain size distributions by normalising the D_{50} sizes of all the samples to the D_{50} value at the Inverary Road (66.7 km). The distribution becomes similar downstream of 43.9 km from the modern Ashburton River Mouth. This may be associated with the change in channel pattern to a single thread channel to a braided channel between Mt. Somers and Thompsons Track (Figure 5.3b).

5.6.4 Quantification of bulk grain size for physical modelling

Five bulk grain size samples were taken from the late Quaternary Gravels at the Wakanui and Rangitata field locations, these represent the thick central portion and thinner margins of the current fan cross-section, respectively (Figure 5.3). Samples were taken from a range of coarse-grained (gravel) architectural elements (Chapter 6, Table 6.6) that included planar and cross-set gravels, together with massive homogeneous gravels and lag deposits. All the coarse-grained elements contained interstitial sand. Gravels were sorted down to 8 mm using Wolman sampling techniques and weighed, while particles less than 8 mm were sieved then weighed. Grains less than 2 mm were measured using a Beckman-Coulter L5230 instrument.

Grain size samples were also collected from the fine-grained architectural elements (sand fraction) and included: channel fills, bar margin fines, erosional remnants and bar top splays (Ashworth *et al.*, 1999). The relative proportion of the sand to gravel was calculated by summing the surface area for each sandbody against the total area of the section panels under investigation. These data were summed with the bulk samples from the coarse-grained architectural elements to produce a composite grain size distribution for use in the physical modelling. The final grain size curve used in the modelling was based on the combined average of the grain size distribution at both the Wakanui and Rangitata field locations (Figure 5.8) and exhibited a strongly bimodal distribution, with the total sandbody fraction accounting for ~20 % of the cumulative grain size curve. Bimodal grain size distributions in fluvial gravels have been documented in both modern and ancient braided systems (e.g. Wolcott, 1988; Sambrook Smith, 1996).

Grain size samples collected from the Ashburton River channel were compared to samples taken from the Canterbury Gravels. Superposition of the gravel fraction from the Ashburton River at Smalls Road (6.25 km upstream of the Ashburton River Mouth) onto the full grain size distributions from the Canterbury Gravels showed a direct match between the gravels fractions with particles above 5.6 mm (Figure 5.7). This suggests the downstream fining rate has undergone minimal change over ~35 ka. Collection of the grain size distribution from the Canterbury Gravels adds information on the faction below 5.6 mm, which was not obtained in river sampling (Figure 5.7). This similarity

between surface and subsurface grain size distributions has also been noted by Dietrich *et al*. (1989).

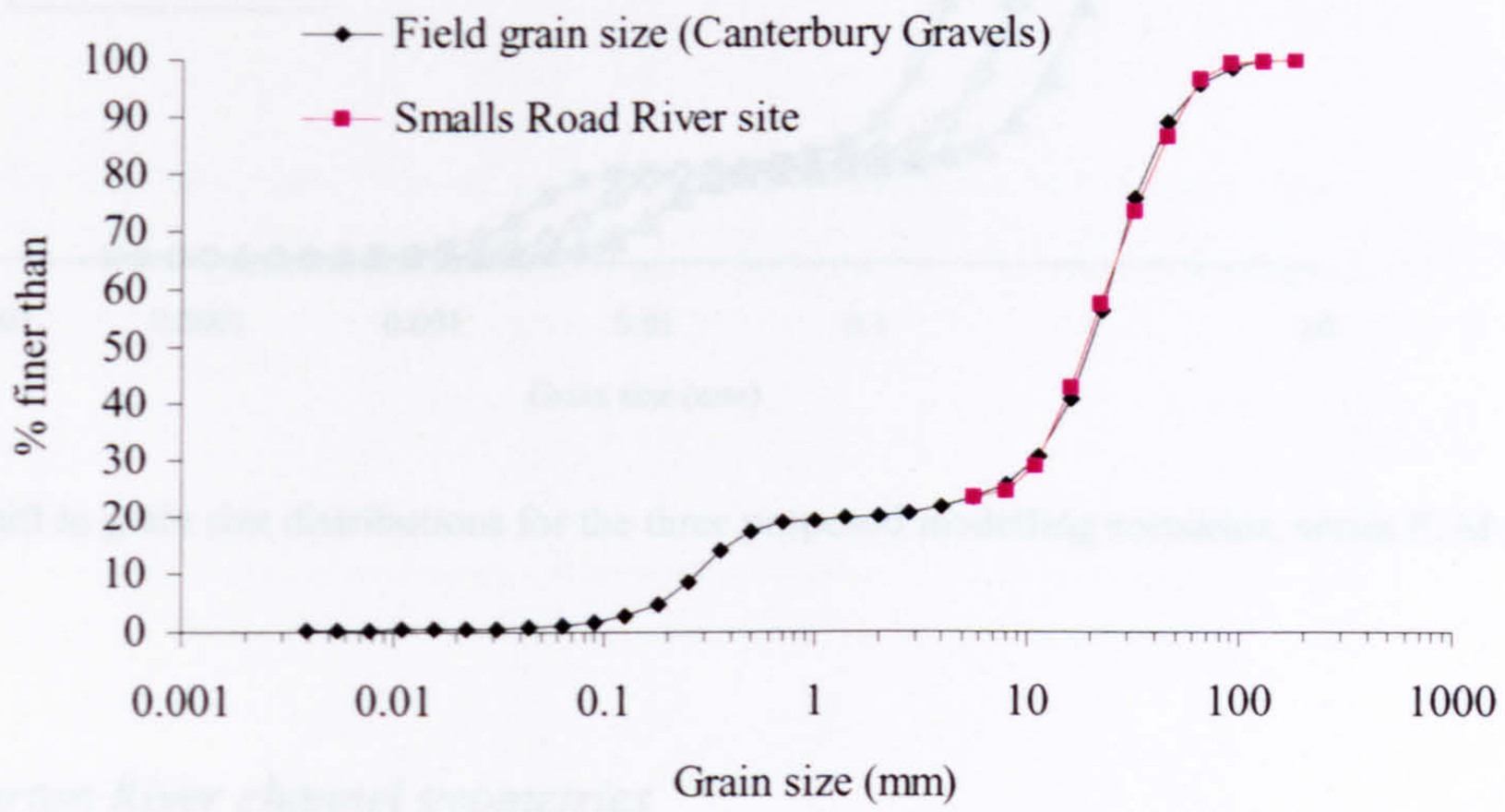

Figure 5.8. Bimodal grain size distribution for bulk samples taken from the Canterbury Gravels at the Rangitata and Wakanui sites (See Figure 5.3 for site locations). With the grain size distribution taken from Smalls Road superimposed for the gravel fraction >5.6 mm.

A scaling of 1:50 was imposed on the grain size distribution measure at the present day coastline (D_{50} = 20 mm) to give a model D_{50} of 0.39 mm (series M). To isolate the effects of changing sediment supply grain size, the distribution was shifted by doubling and halving the magnitude of the distribution calculated for the present day coastal gravels. This shift resulted in two scaled grain size distributions with D_{50} = 0.78 mm (series C), which based on fining rates for the Ashburton River, is equivalent to moving 32 km up the long profile, and D_{50}= 0.19 mm (series F), equivalent to moving 32 km down the long profile (i.e. offshore) (Figure 5.8). Projection of the downstream fining curve offshore represent a period of time during the last Glacial maximum when the coastal gravel plain extended a further ~55 km offshore from the present day coastal cliffline position and assumes a continuation of the grain size diminution rate offshore. Due to the extreme bimodality of the distribution of the deposits measured in the cliff section, a fourfold change in the median grain size only alters the sand to gravel ratio by ~3 %.

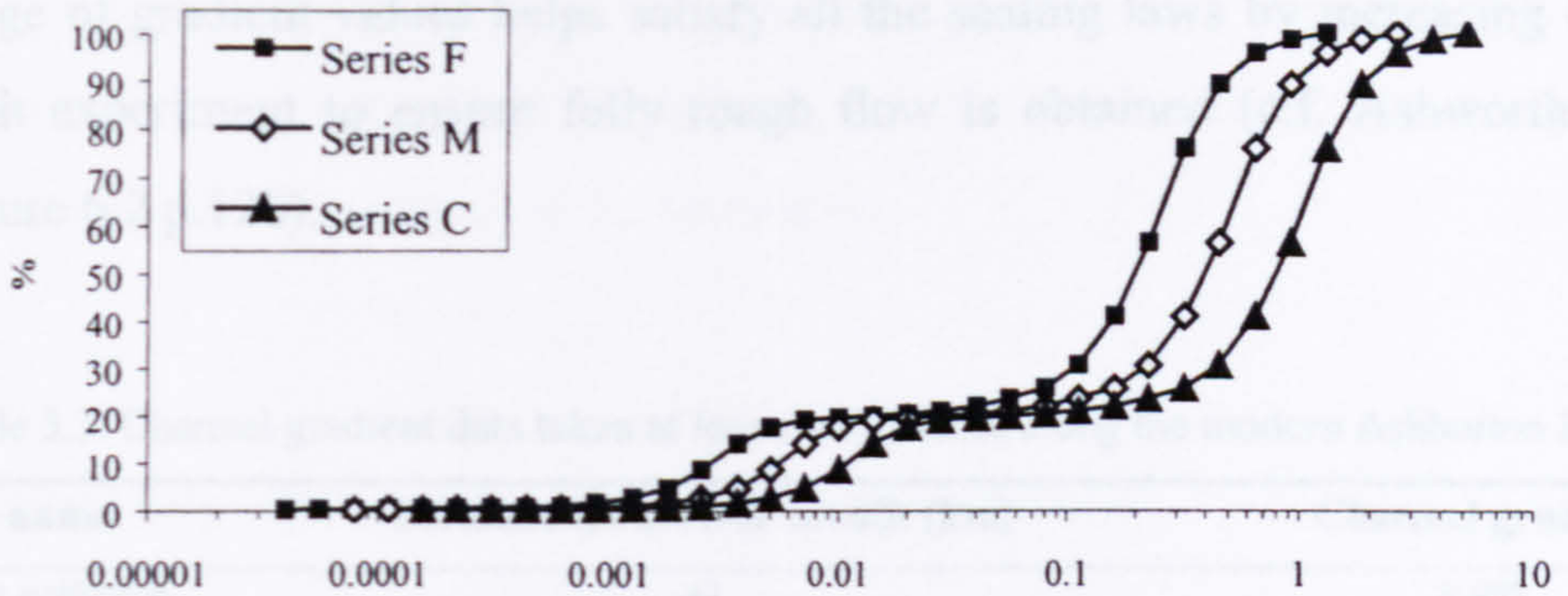

Figure 5.9. Shift in grain size distributions for the three proposed modelling scenarios, series F, M and C.

5.6.5 Ashburton River channel geometries

In order to validate the FSM, morphological data were collected from the modern Ashburton River. Surveys were carried out using a Spectra Precision Geodimeter® 608S Autolock Total Station on several sites of the modern Ashburton River (Figure 5.3b, sites 1, 5, 9). Channel geometries were measured at the three sites along the river long profile, in order to establish if any down-basin change in channel morphology occurs as a result of downstream fining. Bankfull channel depths were defined using the method of Williams (1978a). Data on channel dimensions were compared to measurements taken during the physical modelling. Results from the analysis of channel geometries are detailed in Chapter 6.

5.6.6 Ashburton River channel gradients

Channel gradient data were collected from four sites along the Ashburton River to constrain an appropriate basin gradient for the flume model. Results (Table 5.3) show an approximate halving of the channel gradient between 43 and 18 km upstream of the Ashburton River Mouth. Changes in long profile slopes have been associated with changes in channel pattern and sediment fining (Mackin, 1948; Ferguson and Ashworth, 1991; Sambrook Smith and Ferguson, 1995). Therefore, for modelling purposes an initial basin gradient of 0.01 was selected for all experiments. Initial gradient was above the range of the Ashburton River 0.0046-0.009 because it was necessary to ensure full

braiding and active channel shifting. In addition, keeping the basin gradient at the higher range of gradient values helps satisfy all the scaling laws by increasing Re* values of each experiment to ensure fully rough flow is obtained (c.f. Ashworth *et al.*, 1994, Figure 6.2 p.120).

Table 5.3. Channel gradient data taken at four river reaches along the modern Ashburton River.

Site name	Distance from river mouth (km)	Channel gradient
North Ashburton	43	0.009
South Ashburton	43	0.0074-0.0084
Ashburton Town	18	0.0046
Ashburton Mouth	0.5	0.0049

5.6.7 Quantification of alluvial architecture in the Canterbury Gravels

Fifty kilometres of coastal outcrop were studied between the Rakaia and Rangitata River Mouths (Figure 5.3). Investigation of alluvial architecture was confined to the coastal outcrop as inland exposure was scarce and restricted to a few small gravel pits and vegetated terraces. The aims of the field study were to define architectural elements within the depositional architecture of the Canterbury Gravels to compare by and validate the physical modelling. Previous studies have investigated the geometries of depositional architecture observed within the Canterbury Gravels (Ashworth *et al.*, 1999).

5.7 Implications of the Canterbury field study for physical modelling

Grain size may be an important control on alluvial architecture (Chapter 2) and physical modelling was employed to isolate the control of grain size on alluvial architecture. The Canterbury field study provided information that the Ashburton physical model should firstly, incorporate a bimodal grain size distribution, and secondly, any change in magnitude of the grain size distribution between experiments would retain the grain size distribution shape. As a result of these conditions, three grain size distributions (series F=fine, M=medium and C=coarse) incorporating a fourfold change in the median grain size were scaled for physical modelling. Series C and F were conducted together, while

series M was performed in a previous experiment under *identical* conditions. The following section is devoted to: (1) an explanation of the flume facility used to undertake the FSM, (2) a description of the experiments, and (3) details of the measurements taken during the experiments.

5.8 The flume basin facility and experimental procedure

A flume basin of 5.5 m in length, 3.65 m in width and 0.5 m depth was used for the experimental work (Figure 5.10). The side walls and base of the flume tank are constructed of 10 mm thick industrial sheet plastic (Darvic), which is supported on a steel girder framework, with adjustable legs. The downstream wall of the flume is composed of a galvanised steel mesh with 3 mm diameter holes, overlain by a polyester mesh with 2 mm diameter holes. This mesh design allows the passage of both water and bedload from the active channels into a collection trough while permitting the floodplain to aggrade and minimising draw-down effects that may cause headward erosion. Water also passes through the sediment pile as groundwater throughflow and is allowed to pass through the mesh. Interlocking steel blocks mounted on plinths at the four corners of the flume support the weight of the flume and were set to provide a basin floor slope of 0.01. Two steel girder bridges are mounted on rails that run parallel to the flume sides and span the width of the flume. Bridge 1 allows access to the overhead mounted video cameras and the mounting of the sectioning guillotine. Bridge 2 is used for mounting a lightweight aluminium trolley on two precision rails, which supports a Selcom 5070 laser-profiler unit for measuring topographic profiles of the bed surface (Section 5.10.3).

Water and sediment are fed into the flume basin from a feeder channel of dimensions 2.4 m long, 0.4 m wide and 0.1 m deep, supported on a cradle by an outer frame. The feeder channel is attached to the centre of the upstream wall of the flume basin. Pulses controlled by LabView software supply a racking system driven by two electric DC stepper motor, which raise the inner channel to provide space in the flume basin, and in turn promotes aggradation of the sediment.

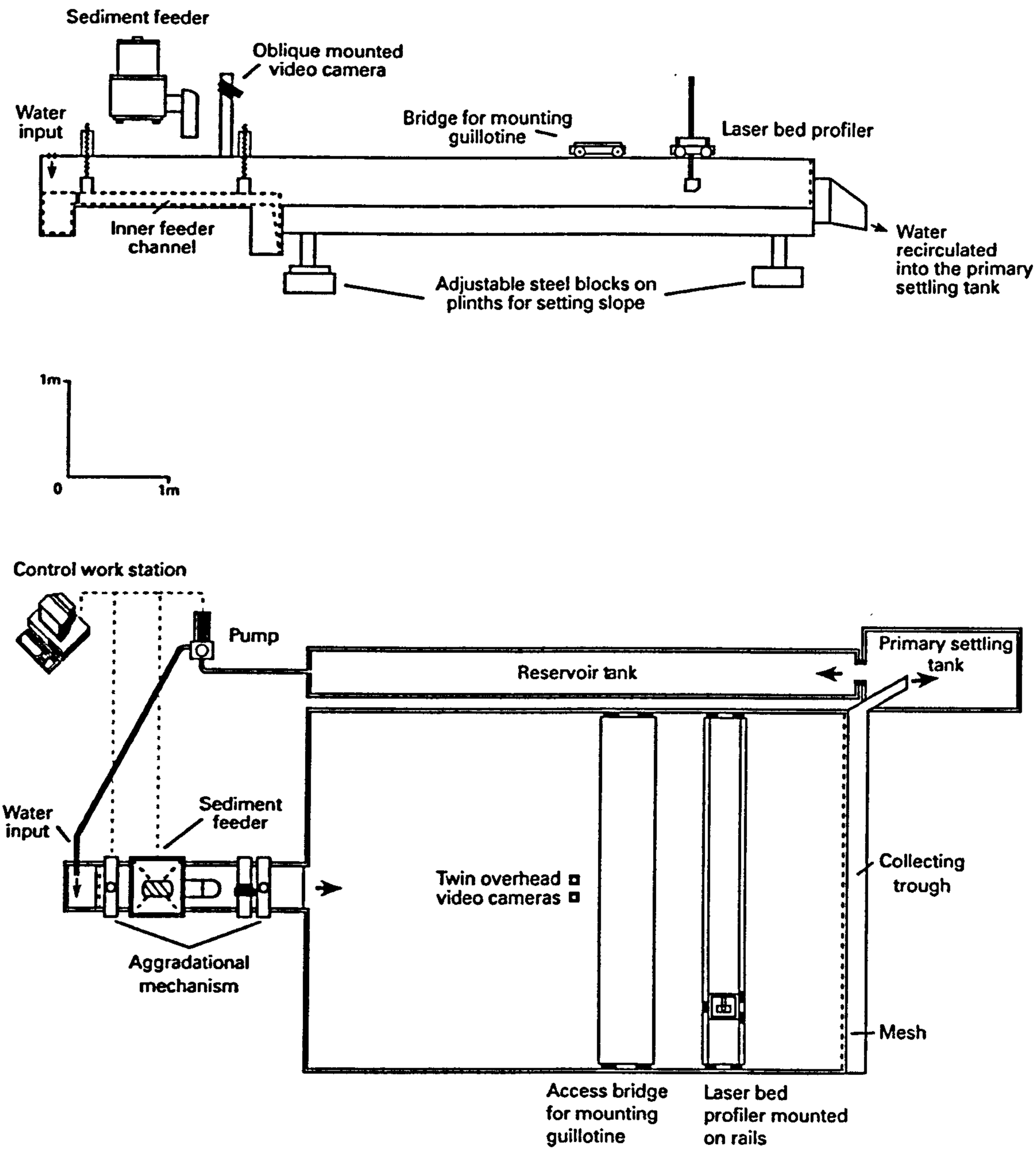

Figure 5.10. Diagram showing the experimental basin facility set-up used in the three experimental runs.

5.8.1 Water delivery, control and recirculation

The flume basin is supplied by water through a pump with a discharge range from zero to 3.23 l s^{-1}, controlled by a 4-20 mA control unit via the LabView computer software. Discharge was calibrated by timing measured volumes of water at 0.5 mA increments. Twenty-six measurements were taken and the data characterised by fitting a sixth order polynomial. The resultant pump calibration curve (Figure 5.11) was used as the reference point in the LabView programme. The desired discharge is loaded into the programme and the computer calculates the required mA output in order to adjust the pump valve opening.

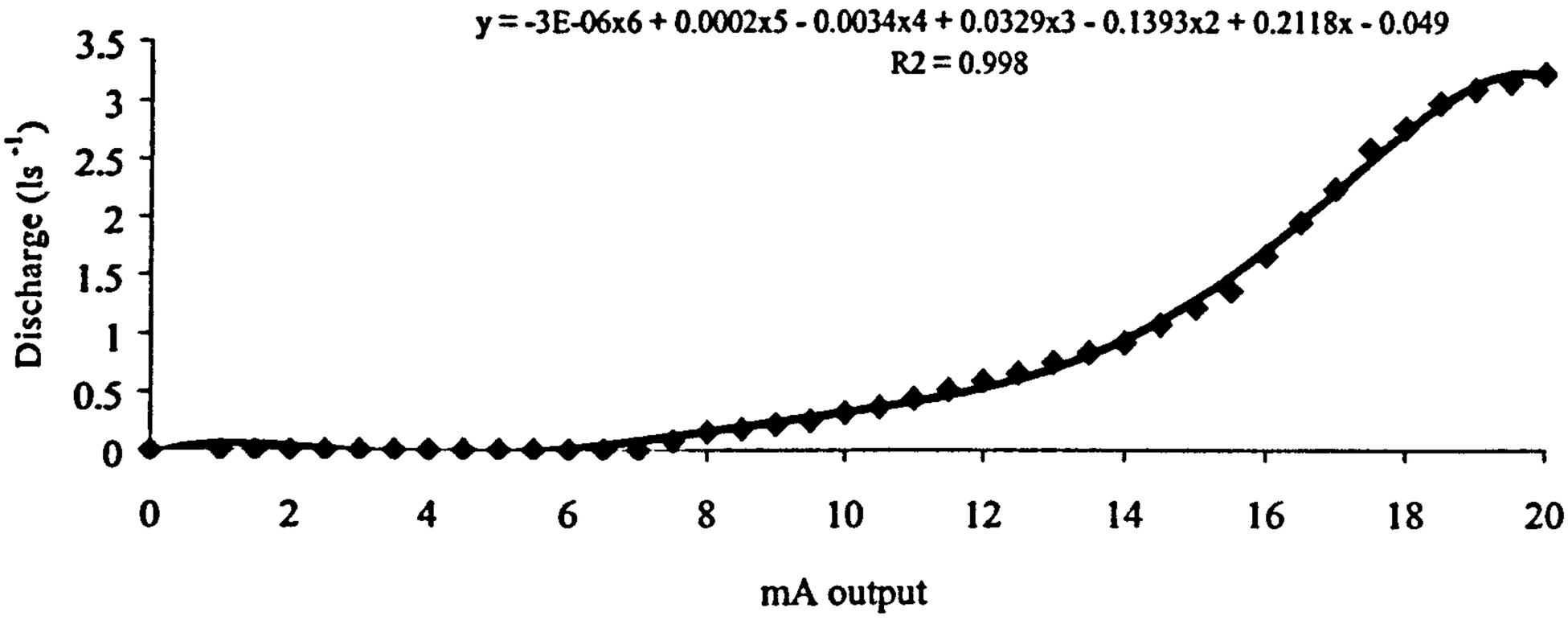

Figure 5.11. Calibration curve for the pump used for the physical modelling experiments.

Water is supplied to the flume from a 1.3 m^3 reservoir tank. Discharge passes into the dampener box at the upstream end of the feeder channel through flexible tubing. The dampener box allows water turbulence to be reduced before passing into the main flume basin. Water passes through a double notch weir within the feeder channel. Sediment is then dropped into the water where it mixes in the feeder channel before entering the main basin. Water and sediment exit the flume via a twin mesh system. Occasionally, sediment needs to be cleared from the end mesh to prevent water ponding. Sediment and water pass into a 0.11 m wide, 0.2 m deep trough that feeds the primary settling tank. The primary settling tank removes much of the bedload sediment passing through the system, also allowing the settling out of a significant amount of suspended sediment from the system. Water then passes into the main reservoir tank where suspension fallout continues before water is recirculated back into the feeder channel.

5.8.2 Modelled grain size distributions

Experiments were carried out using a 1:50 scale grain size distribution of the Canterbury Gravels, New Zealand (Figure 5.9). Series C and F represent the two end members of a downstream fining profile that incorporates a fourfold change in the magnitude of the grain size distribution, where series C has a D_{50} of 0.78 mm (bulk density =1800 kg m^{-3}) and the series F has a D_{50} of 0.19 mm (bulk density =1500 kg m^{-3}).

The grain size of the two scaled distributions were then matched with commercially available sediment (Figure 5.12). Individual distributions were mixed to provide a close match to the prototype distribution. Sediment was mixed in batches in a concrete mixer to achieve homogeneity of the grain size distribution.

Five different coloured sediments, termed 'Chroma F®' with a grain size of 0.2-0.6 mm were added sequentially during every fourth hydrograph to act as time horizons. Coloured sediment was added immediately preceeding the peak discharge to allow particles to be transported and deposited over the entire flume basin. The addition of coloured sediment facilitates the identification of alluvial architecture exposed in the cut sections and the correlation of stratigraphy with laser profiles taken every 4 hours (refer to Section 5.10.3). Following each laser survey a layer of coloured sediment was sprinkled evenly over the central portion of the flume basin, encompassing an area ~2 m x ~2.5 m. To avoid flocculation of the coloured sediment a 5 % calgon solution was sprayed over the layer.

The results from a third experiment, series M were used to complement data from series C and F and provide a mid-point between the two end members of the grain size distributions taken from the Canterbury Plains field prototype. Series M employed the same 1:50 scaled grain size distribution (D_{50} = 0.39 mm) analogous to the grain size distribution sampled from the present day coastal gravels (Figure 5.12) and was conducted under *identical* imposed boundary conditions as those of series C and F.

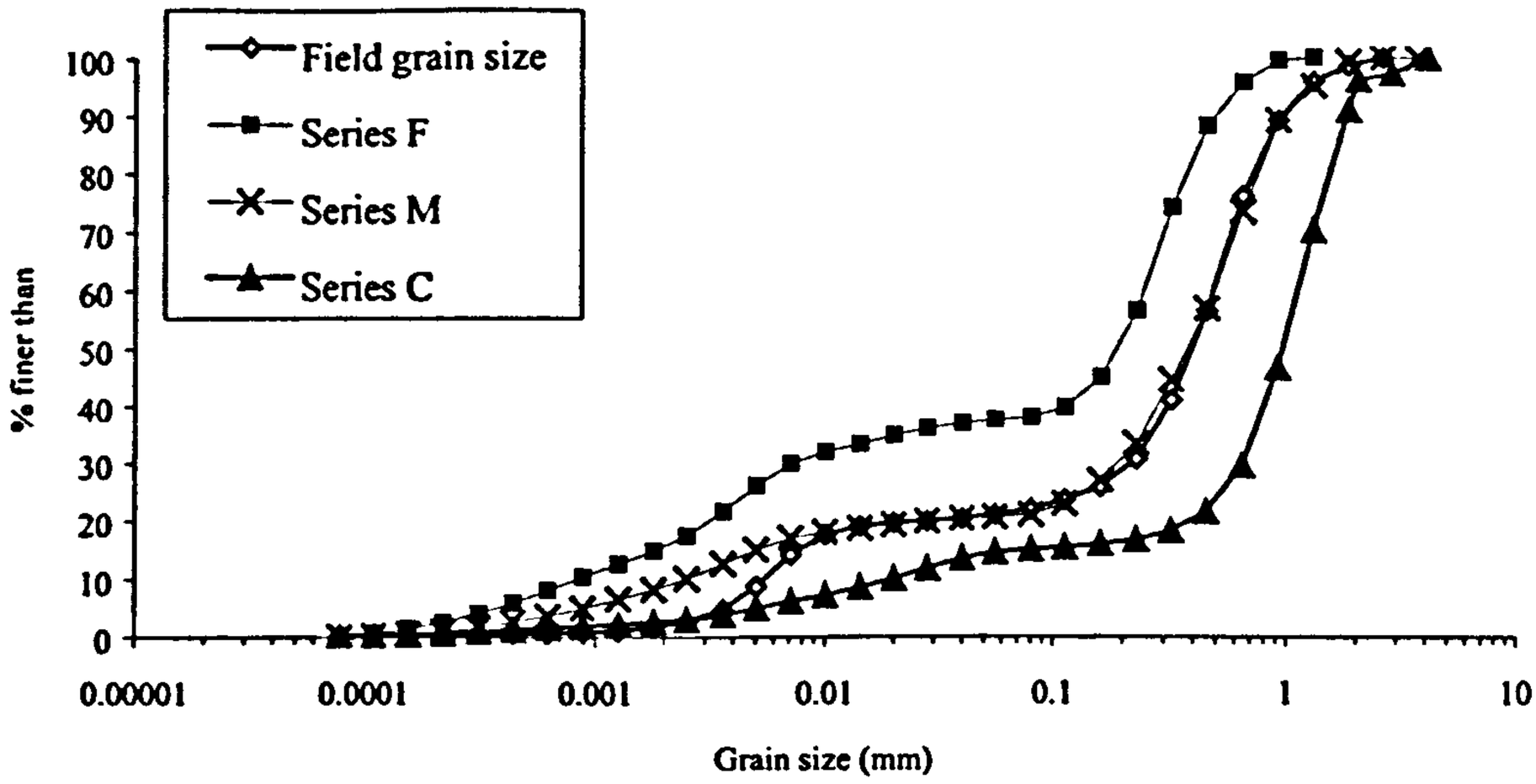

Figure 5.12. Grain size distribution curves for series C, M and F (sampled from mixed batches) used for the physical modelling compared to a 1:50 scaled bulk grain size distribution taken from the Canterbury Gravels.

A 55 mm bed of the grain size distribution used in series C was laid down on the flume basin floor to prevent incision and scour down to the base of the flume during the experiment. Sediment was levelled with a metal beam spanning the entire flume width attached to the platform bridge and dragged across the sediment surface. Once levelled a 0.4 m wide by 0.015 m deep central channel was dredged into the surface. Both the sediment surface and the channel base had an initial slope of 0.01.

Dry sediment was loaded into a stainless steel 602 AccuRate volumetric feeder with a total capacity of 95 litres. The dimensions of the feeder are 0.552 x 0.552 x 0.762 m with a 0.0178 m feeder nozzle. The feeder is supported above the feeder channel on a self-supporting steel stand. Sediment is gravity fed into a stainless steel rotating helix (auger–type). The sediment sits in a Flexible walled Tuf-Flex ® vinyl hopper, which is externally agitated by two paddles. The agitation action stops any material from adering to the walls of the hopper through electrostatic forces and maintains a uniform bulk density into the helix, by ensuring a constant helix fill.

The sediment feeder is computer controlled using LabView 4.0 software, providing a 4-20 mA supply allowing feed rate to vary synchronously with a hydrograph form. Feed rates calibrations were performed at 0.5 mA increments for dry bulk densities of series F and C (Figure 5.13). A sixth order polynomial provided calibration equations for the LabView programme.

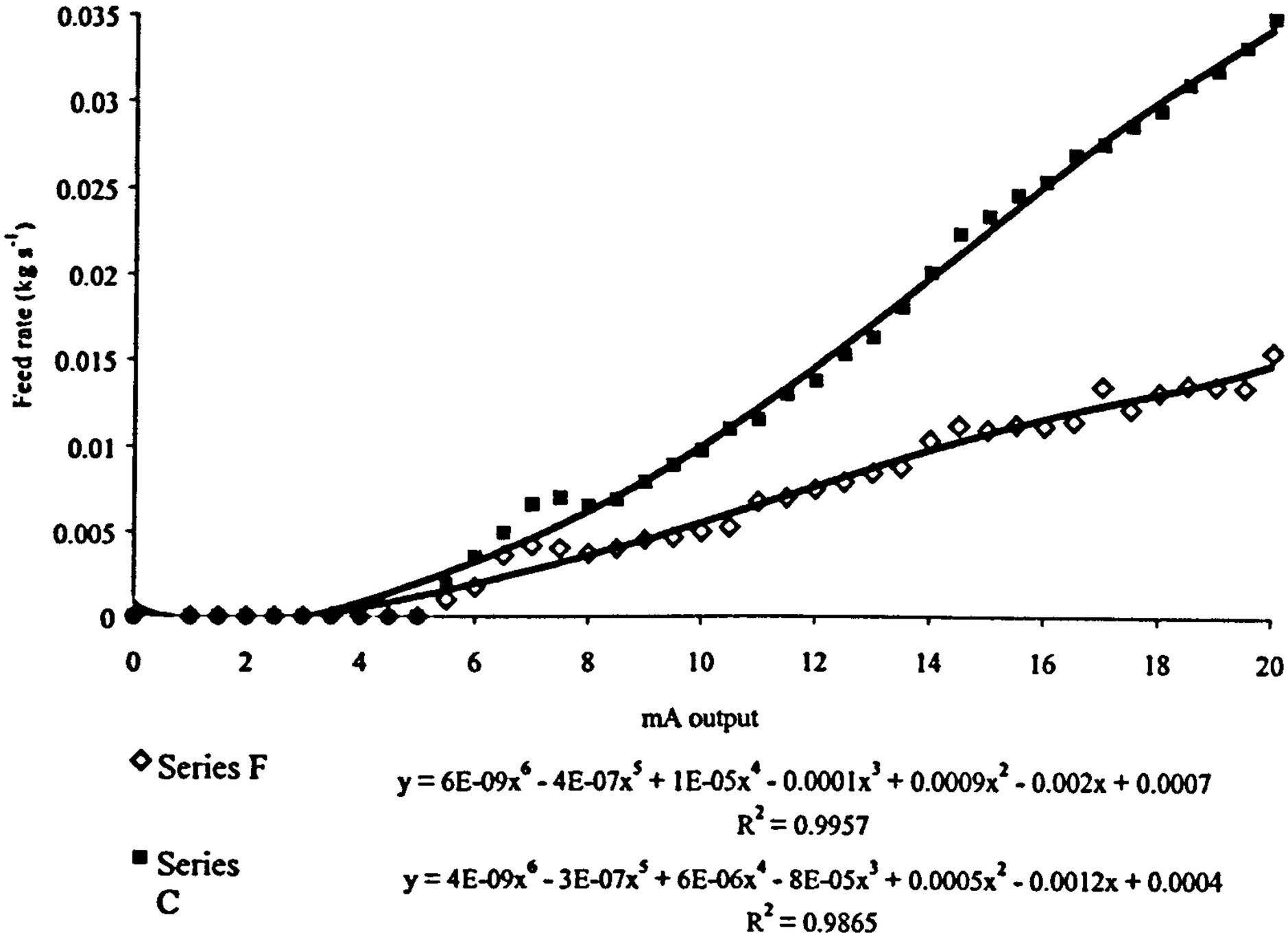

Figure 5.13. Calibration curves for the AccuRate sediment feeder for sediment mixes used in series F and C used in the physical modelling experiments. Note that higher feed rates were obtainable from series C sediment as a result of the a higher bulk density.

5.8.3 Feed rate and aggradation

The feed rate was based on a system with no net aggradation or degradation taking place in the flume basin. Sediment input was based on a *capture ratio* of 1 from Paola (1988), where the capture ratio is defined as the ratio of sediment flux to the rate of creation of cross-sectional area in the basin. Feed rate for the total mass of sediment required for one hydrograph was calculated in proportion to the shape of the discharge hydrograph (Figure 5.14). The feed rates vary between the two grain size distributions as a result of different bulk densities (Figure 5.13). Experiments were run with an imposed aggradation rate of 1 mm hr^{-1}. Aggradation rate was stepped at 0.5 mm increments at 30 minutes intervals through the experiment.

5.8.4 Use of discharge and sediment hydrographs

The use of scaled hydrographs based on the October 1990 flood for the Ashburton River, were employed in each of the experiments C, M and F to improve the realism of the modelling. During the October 1990 flood the flow reached a maximum of 360 m^3s^{-1}. Equation 5.6 and 5.7 were used to scale both discharge and time for each hydrograph to represent one annual flood event and compressed time to a model hydrograph duration of 1 hour (Figure 5.14). 125 hydrographs were run sequentially, incorporating a quartering of the grain size after hydrograph 80 (Table 5.4). Sediment input was supplied synchronously with discharge. However, during the experiment sediment would accumulate in the feeder channel at low discharges. At peak discharges this accumulated sediment was flushed out from the feeder channel, creating a lag in the sediment supply to the flume basin. This lag may be more representative of the time-lag of sediment behind the discharge peak experienced in modern fluvial systems.

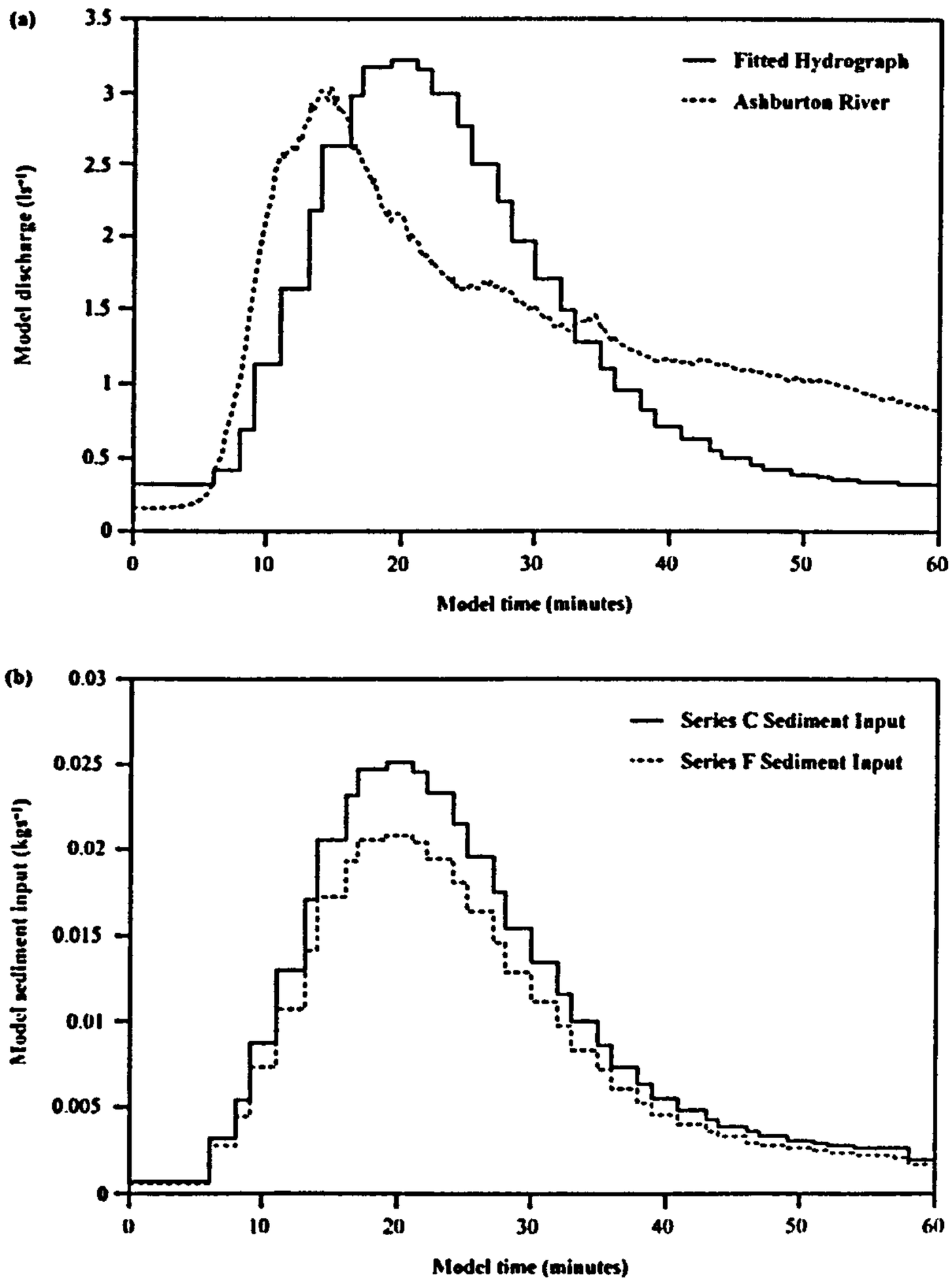

Figure 5.14. (a) Discharge and (b) sediment input hydrographs used in the physical modelling experiments. Data taken from the October 1990 Ashburton River flood and scaled according to scaling laws detailed in Sections 5.3.1 and 5.3.2.

5.9 Description of experiments

A series of five sequential experiments (Table 5.4) were performed to establish the role of sediment supply grain size on surface channel morphology and resultant depositional architecture. From an initial flattened bed surface (Figure 5.15a) sediment feed rate (0.004 kg s^{-1}) and discharge (1.8 l s^{-1}) were kept constant for 21 hours to initiate braiding. Sediment was adding during this initial experiment to balance input with output to avoid incision at the upstream end of the flume or cause any net aggradation. After the initial run of 21 hours where no aggradation was imposed on the system the braiding had reached the side walls and therefore, was deemed to have braided significantly (Figure 5.15b) to start running the aggradation experiments. Following the initial braiding experiment, 125 sequential one-hour hydrographs were run (Table 5.4), incorporating a quartering of the grain size distribution after hydrograph 80. Aggradation imposed during these two runs totalled 125 mm. Following every fourth hydrograph, the discharge was stopped and the braidplain allowed to drain. Once drained a series of laser profiles (Section 5.10.3) were taken to obtain a map of the surface topography. Before starting the next four hydrographs, the discharge was gradually increased for 10 minutes to fill drained sediment pore spaces.

Table 5.4. Summary of experiments performed investigating two different sediment supply grain size distributions, series C and Series F.

Experiment number	Description	Discharge	Feed rate (mean)	Aggradation rate	Grain size distribution	Data collected
Run 1* (Series C)	Initiation of braiding: coarse grain size. Feed rate was altered to balance input to output with no net aggradation. No aggradation was imposed on the system. Purple sediment added at the end of the run.	1.8 l s^{-1}	0.004 kg s^{-1}	0	Coarse	• Initial topographic profile. • Suspended sediment samples at the end of the run (x2) at the inlet and outlet. • Two bedload samples at the end of the run from the end trough. • Temperature every 30 minutes. • Velocity floats at varying discharges. • Video footage (x3 cameras). • Topographic laser profiles every 4 hours at 0.1 m section intervals over a 2.5 m x 2m grid (26 sections).
Run 2* (Series C)	80 x 1 hour hydrographs. Sediment feed rate was proportional to discharge. Coloured sediment added every fourth. Purple sediment added at the end of the run.	Hydrograph 0.3-3.2 l s^{-1}	0.010 kg s^{-1}	1 mm hr^{-1}	Coarse	• Suspended sediment samples every 2 hours (2x inlet and 2x outlet) Total: 120. • Temperature every 30 minutes. • Bedload samples (x2) every 2 hours from the end trough. (HY 1-40 = 22 samples). • Video footage (x3 cameras). • Topographic laser profiles every 4 hours at 0.1 m section intervals over a 2.5m x 2m grid (26 sections). • Suspended sediment samples taken at 5 minute intervals through hydrographs 47 and 79 (2x inlet and 2x outlet) Total = 104 samples. • Velocity floats at varying discharges.
Run 3* (Series C)	Sediment feed rate was proportional to discharge.	Constant discharge (0.313, 1.765, 3.217 l s^{-1})	0.010 kg s^{-1}	1 mm hr^{-1}	Coarse	• Video footage (x3 cameras). • Water surface laser profiles at 0.5 m intervals over a 2.5 m x 2 m grid (6 sections) during the run. After draining dry surface profiles were taken at the same interval. • Velocity floats at the three discharges.

*= Water was changed in the main reservoir tank at the end of the run.

Table 5.4. Continued.

Experiment number	Description	Discharge	Feed rate (mean)	Aggradation rate	Grain size distribution	Data collected
Run 4 (Series F)	44 x 1 hour hydrographs. Sediment feed rate was proportional to discharge. Coloured sediment added every fourth hydrograph.		0.008 kg s^{-1}	1 mm hr^{-1}	Fine	• Suspended sediment samples every 2 hours (2x inlet and 2x outlet) Total: 120. • Suspended sediment samples taken at 5 minute intervals through hydrographs 107 and 123 (2x inlet and 2x outlet) Total = 104 samples. • Temperature every 30 minutes. • Bedload samples (x2) every 2 hours from the end trough. (HY 100-124 = 14 samples). • Velocity floats at varying discharges. • Video footage (x3 cameras). • Topographic laser profiles every 4 hours at 0.1 m section intervals over a 2.5 m x 2 m grid (26 sections).
Run 5 (Series F)	Sediment feed rate was proportional to discharge. Final hydrograph for 1 hour.	Constant discharge (0.313, 1.765, 3.217 l s^{-1})	0.008 kg s^{-1}	1 mm hr^{-1}	Fine	• Video footage (x3 cameras). • Water surface laser profiles at 0.5 m intervals over a 2.5 m x 2 m grid (6 sections) during the run. After draining dry surface profiles were taken at the same interval. • Velocity floats at the three discharges. • Final bed profile of the entire flume at 0.5 m intervals downstream.

*= Water was changed in the main reservoir tank at the end of the run

a

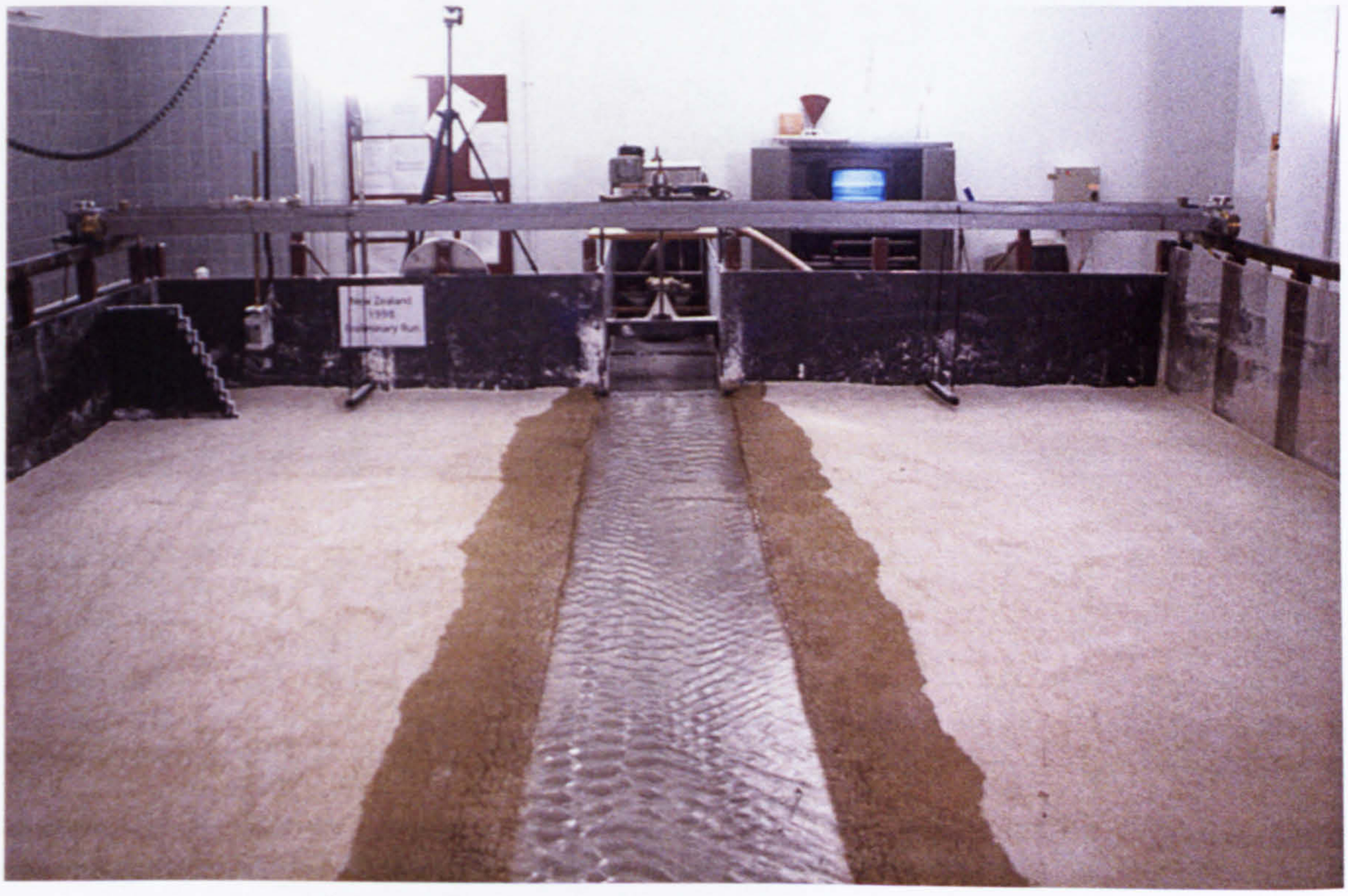

b

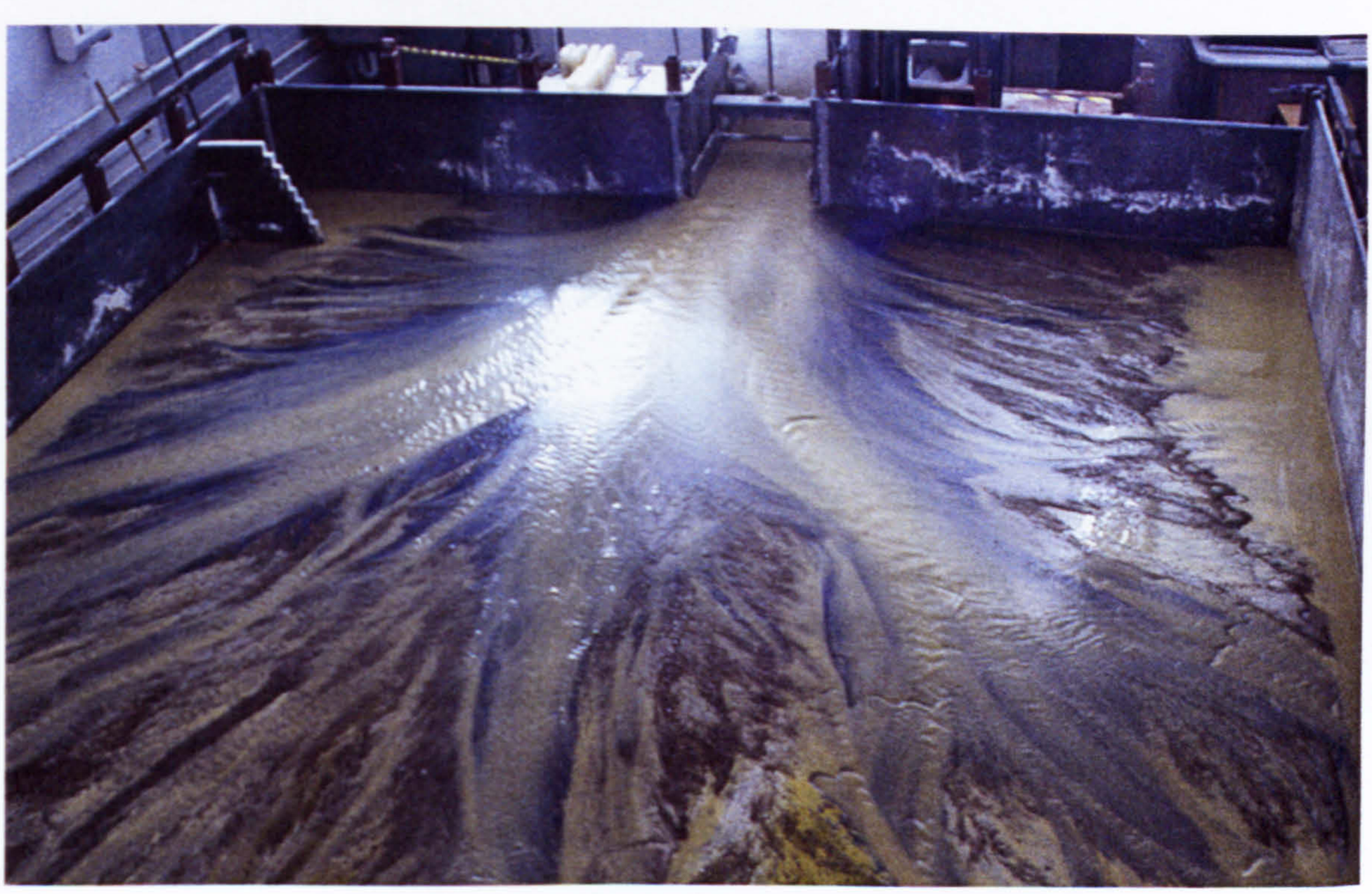

Figure 5.15. Oblique view of the Leeds flume facility (a) after initial water was turned on and (b) during experiment C. Flow enters the basin from the central feeder channel at the top and drains at the bottom of the image.

5.10 Measurements taken during the experimental runs

During the experiments a series of measurements were taken to quantify surface flow velocity, surface braidplain topography, suspended sediment/bedload concentrations and grain size, in order to characterise and validate the physical modelling (Table 5.4).

5.10.1 Video imaging

Four 1000 Watt halogen lamps were situated around the flume facility and were reflected off the white ceiling to provide a uniform lighting intensity over the stream table for videoing purposes. Three varying format video cameras were used in the observation of the developing fluvial system (Figure 5.10).

1. A Panasonic WV-CD130 colour Camera with a Molynx 4.8mm 1:1.8 wide-angle lens mounted directly above the centre of the flume provides images of a central area of approximately 3.8 m downstream x 2.5 m cross-stream. Signals from the video camera were fed into a S-VHS AG6720 time-lapse video recorder set on 48 hour mode to record a frame every 0.32 seconds. This camera was used to capture flow paths of plastic floats added in the feeder channel to allow the surface velocity to be measured.
2. A Sony DCR-VX1000E digital video camera with a Vivanco VC95 W 0.5 x 52 mm wide-angle lens was mounted alongside the Panasonic camera above the flume. One second of time-lapse footage was taken every 30 second time intervals. The 2 m x 2.5 m image covered the central portion of the flume basin.
3. A JVC GR-SX1 S-VHS-C video camera was mounted obliquely above the main feeder channel supported on a Perspex frame attached to the side of the feeder channel walls. One second of time-lapse footage was captured every 30 seconds.

Video images were captured using VidCap 4.1.2.3 with a compression rate of 1:15 and imported into Adobe Premiere 5.1, where they were spliced together allowing continuous overhead video footage to be observed and related to subsurface deposits. The video file was exported at 5000 % speed and at 768 x 576 pixels at 10 frames per

second (see accompanying CD). Individual frames were converted to .gif files for individual analysis.

5.10.2 Surface velocity floats

Average surface velocities were calculated from videos by measuring the distance travelled between frames of velocity floats and converted to mean flow velocity for both experiments. Surface velocity floats were added at different stages of the hydrograph to obtain an average velocity for calculation of flow and grain Reynolds numbers and Froude numbers. Mean velocities were calculated by multiplying the surface velocity by 0.8 from the formula of Prony (Graf, 1998, p12).

5.10.3 Sediment surface measurements

An infra-red Selcom SL5070 Class 3b laser (Figure 5.16) was used to measure the topography within a grid of dimensions 2.5 m downstream x 2 m cross-stream. A series of 26 predetermined cross-sectional profiles (Figure 5.17) were measured at 100 mm intervals downstream and at a coverage of 2267 points at 0.87 mm intervals (total 2 m) across-stream. The laser has an accuracy of ± 0.2 % of the vertical measurement range, which is equivalent to 0.14 mm.

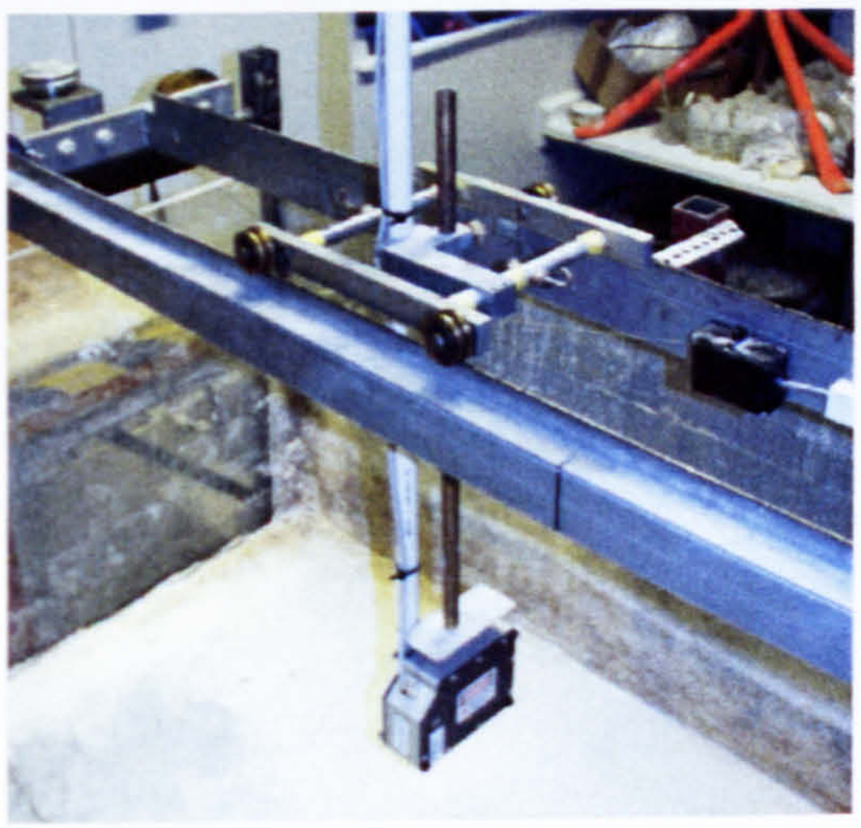

Figure 5.16. Photograph of the Selcom SL5070 laser unit mounted on an aluminium bridge and used for the measurement of surface braidplain topography.

From the starting position the laser-bed profiler, which is mounted on a trolley, travels in a cross-flume direction, driven by a stepper motor at a constant speed and controlled by the LabView software. Once moving, the trolley breaks an optical switch mounted on the supporting bridge and activates the data capture stream. The data stream from the laser is downloaded directly into a text file. Measurements at a frequency of 25 Hz are gathered over the measurement area and stopped when the trolley breaks the optical switch at the opposite end of the bridge, causing a time-out switch to be activated. The motor is then stopped by a timeout control in the LabView programme. To allow the measurement range of the laser (70 mm) to be adjusted to the elevation of the sediment surface as the system aggrades the laser unit was raised by 5 mm intervals after each survey.

Topographic profiles were taken of the entire basin area before the experiments commenced and then following every fourth hydrograph when the basin had been drained. A final profile was taken once all the experiments had been completed to determine the overall shape of the braidplain, and establish the volume of aggraded sediment and therefore, the mean capture ratio over the flume basin.

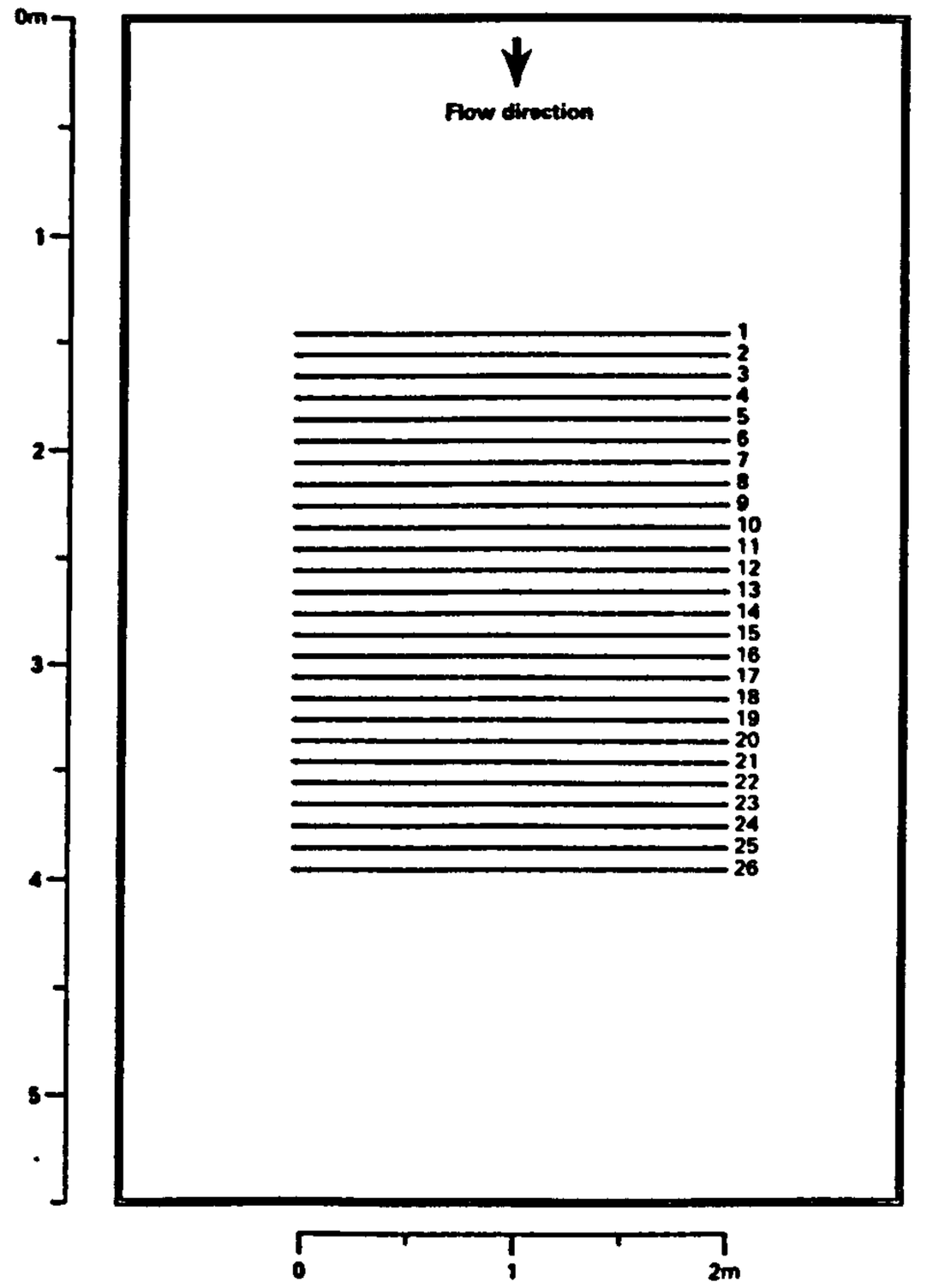

Figure 5.17. Diagram to show the plan view of the Leeds flume basin and the location of laser profiles and cut-section lines 1-26.

5.10.4 Suspended sediment and bedload

During the experiments, suspended sediment and bedload samples were collected at two hour intervals from the downstream end outlet mesh. Samples were always collected at a discharge of 0.31 l s^{-1}. Samples were taken at the end of each set of four hour hydrographs and at the beginning of the subsequent set of four hydrographs to capture any settling effects of suspended sediment during periods when the discharge was turned off. Water was changed in the reservoir tank after 40 hydrographs to avoid any mixing of the suspended sediment between series C and F grain size distributions. Suspended sediment concentrations were calculated by percentage weight and grain size distributions were measured for each sample on the Beckman-Coulter L5230.

5.11 Sectioning of the preserved sediment sequence for quantifying alluvial architecture

After completion of the experimental runs, the preserved sediment was left to air dry for five weeks. An initial vertical sediment surface was excavated using a 1 m wide steel guillotine mounted on the platform bridge and pushed vertically into the aggraded sediment. The surface was then cleaned with a trowel and sprayed with water to pick out the sedimentary architecture (Figure 5.18). Twenty-six faces were successively cut back perpendicular to the imposed palaeoflow direction (feeder channel) at intervals of 100 mm, which correlated to laser profiles taken during the experimental runs (Figure 5.17). Two spotlights were set up 3 m apart to illuminate the section and provide an even light intensity for photographing the section. A Nikon FS camera with a 50 mm lens, set at F11 and 1/15 speed, using Fuji 100 ASA film, mounted on a wooden board (placed vertically in the middle of the section face to minimise distortion) was used to take five successive across-section photographs with 10 % overlap. Photographs were assembled into photomontages for each cut section to allow identification and measurement of alluvial architecture. Acetate paper was placed over the photomontage and interpreted architecture drawn on and measured. Cut-sections were started 1.5 m downstream of the upstream basin wall to avoid the influence of the inlet channel.

a

b

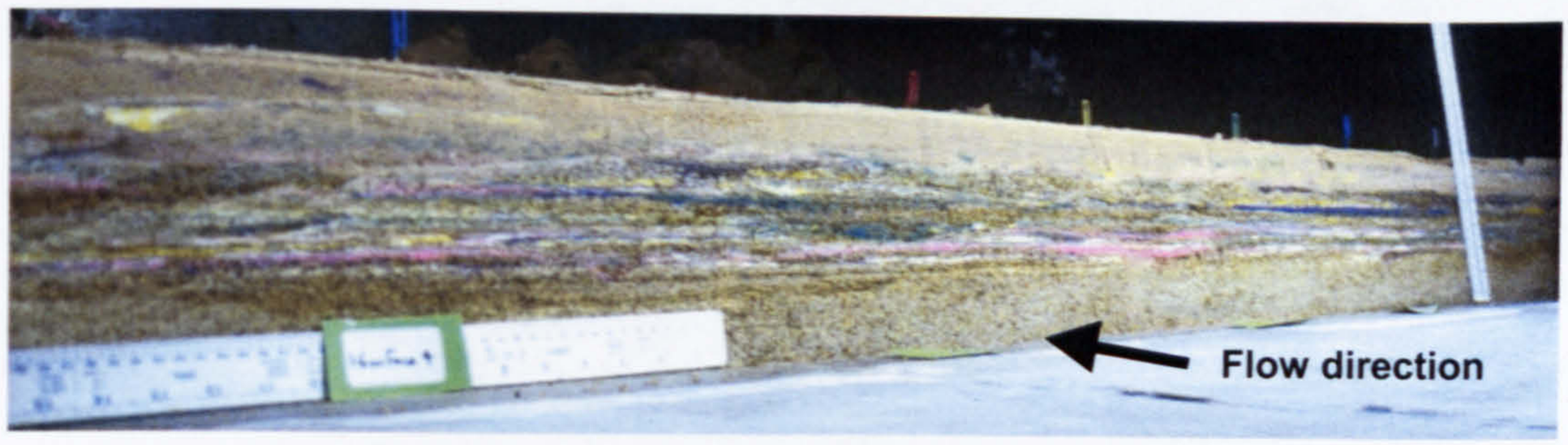

Figure 5.18. Sectioning procedure for the FSM sediment sequence (a) showing the section face being photographed following cutting of the aggraded sediments and (b) an example of the 2 m wide section exposure of alluvial architecture cut perpendicular to flow.

5.12 Implications of physical modelling for future alluvial architecture studies

Results from the physical modelling will have wider implications for the understanding of alluvial architecture, including: (1) investigating the differences between gravel-bed fluvial systems with varying grain size distributions; (2) allowing down-basin facies models to be constructed; and (3) providing the limits of grain size for physical modelling. These issues are addressed in Chapter 6.

5.13 Summary

The main conclusions from this chapter are:

1. Theoretical calculation of hydraulic flow parameters for FSM of the fine-grained Lower Ketch Member (Chapter 3) indicates that, Re* numbers are below the critical threshold for flow to be hydraulically rough and viscous forces to be minimised. Consequently, the use of coarse-grained prototypes such as the Canterbury Plains is recommended for FSM.
2. Three experiments were conducted to quantify the impact of grain size on braided channel morphology and alluvial architecture using boundary conditions derived from the Canterbury Plains, New Zealand. The Canterbury Plains provide suitable prototype data from both the modern Ashburton River and the Quaternary Canterbury braided river gravels for input to the FSM.
3. The Ashburton River displays a downstream fining of the grain size distribution over a 67 km distance from the current coastline. The exponential downstream fining curve fitted to D_{50} values taken from sites on the Ashburton River provides a diminution coefficient of 0.0322 ψ km^{-1}, which lies within the broad range documented for braided rivers.
4. While the magnitude of the grain size distribution diminishes downstream, the surface gravels in the Ashburton River show a conservation of the grain size distribution shape over a 44 km distance immediately preceding the Ashburton River Mouth.
5. Bulk grain size samples from the Quaternary Canterbury gravels exhibit a bimodal grain size distribution comprising ~20 % sand and ~80 % gravel. The shape of the grain size distribution for the gravel fraction of the Quaternary braided river deposits show a good match to the modern Ashburton River surface deposits.
6. Channel slopes from the modern Ashburton River reduce from ~0.009 to ~0.0046 between 44 km and 18 km upstream of the river mouth. FSM imposed a bed slope of 0.01 (above the upper limit of measured prototype slopes) to assist in the maintenance of hydraulically rough flow conditions.

Chapter 6. The influence of sediment supply grain size on alluvial architecture

6.1 Synopsis

This chapter quantifies the control of grain size on the surface channel morphology and subsurface alluvial architecture of a gravel-bed braided river using an aggrading generic-Froude scaled model of the Ashburton River (prototype), New Zealand. Results are presented from three physical modelling experiments, series C, M and F, which represent a fourfold change of the grain size distribution exhibited at the present day Canterbury Gravels coastal outcrop. A six-fold architectural element classification scheme is presented comprising of three coarse-grained architectural elements (primary channel fills, secondary channel fills, splays) and three fine-grained architectural elements (abandoned channel fills, erosional remnants, overbank fines), which are discussed in relation to formative surface morphology. Surface and subsurface verification between the model and prototype is offered and variations in size and frequency of occurrence of each architectural element quantified. The application of modelling data for interpretation of fluvial sequences exhibiting local and down-basin changes in channel-belt grain size are examined in relation to predicted alluvial architectural trends. A procedure for up-scaling is presented and the physical limits for modelling fine grain size distributions are reviewed.

6.2 Introduction and background to the braided river experiments

Field data were collected from the modern Ashburton River and late Quaternary Gravels of the Canterbury Plains, New Zealand (Chapter 5), in order to provide prototype information for conducting three 1:50 generic-Froude scaled modelling experiments. The main aims of the physical modelling were to:

1. Isolate the influence of grain size distribution on the surface channel morphology.
2. Quantify the impact of grain size distribution on the within channel-belt depositional geometries.

The principal findings from the field study (Chapter 5) established that: (1) the subsurface grain size distribution is strongly bimodal, and (2) the modern Ashburton River exhibits a downstream fining rate of 0.0223 mm km^{-1} while retaining the overall grain size distribution shape downstream. These characteristics of the Ashburton River were used to construct a methodology for the physical modelling (Chapter 5).

Three experiments, series C, M and F (Table 6.1) represented a fourfold change in grain size and were run using a scaled flood hydrograph (Chapter 5, Figure 5.14). Sediment was added synchronously with discharge and provided a total imposed aggradation rate of 1 mm hr^{-1}, where the capture ratio was equal to 1. The initial experimental surface was flat with a downstream gradient of 0.01, comparable to the upper reaches of the Ashburton River (Chapter 5, Section 5.6.6). Differences in feed rate between the three experiments arise from variations in bulk density between the each of the grain size distributions in order to maintain a capture ratio in the three experiments of 1.

Table 6.1. Summary of imposed conditions for the three FSM experiments used to compare the impact of sediment supply grain size on channel morphology and alluvial architecture.

Experiment series	Scaled D_{50} (mm)	Total run time (hr)	Mean sediment feed rate (kgs^{-1})	Imposed aggradation rate ($mm\ hr^{-1}$)	Actual aggradation rate ($mm\ hr^{-1}$)
F	0.19	45	8.0	1	0.82
M	0.39	28	7.9	1	0.72
C	0.78	88	9.7	1	0.82

Superposition of the three experimental grain size distributions (D_{50}) on to the present day downstream fining profile of the Ashburton River (Figure 6.1), shows series C is located in a position ~32 km upstream from the current coastline, series M at the Ashburton River Mouth, and series F, a position ~32 km downstream from the present coastline (i.e. offshore).

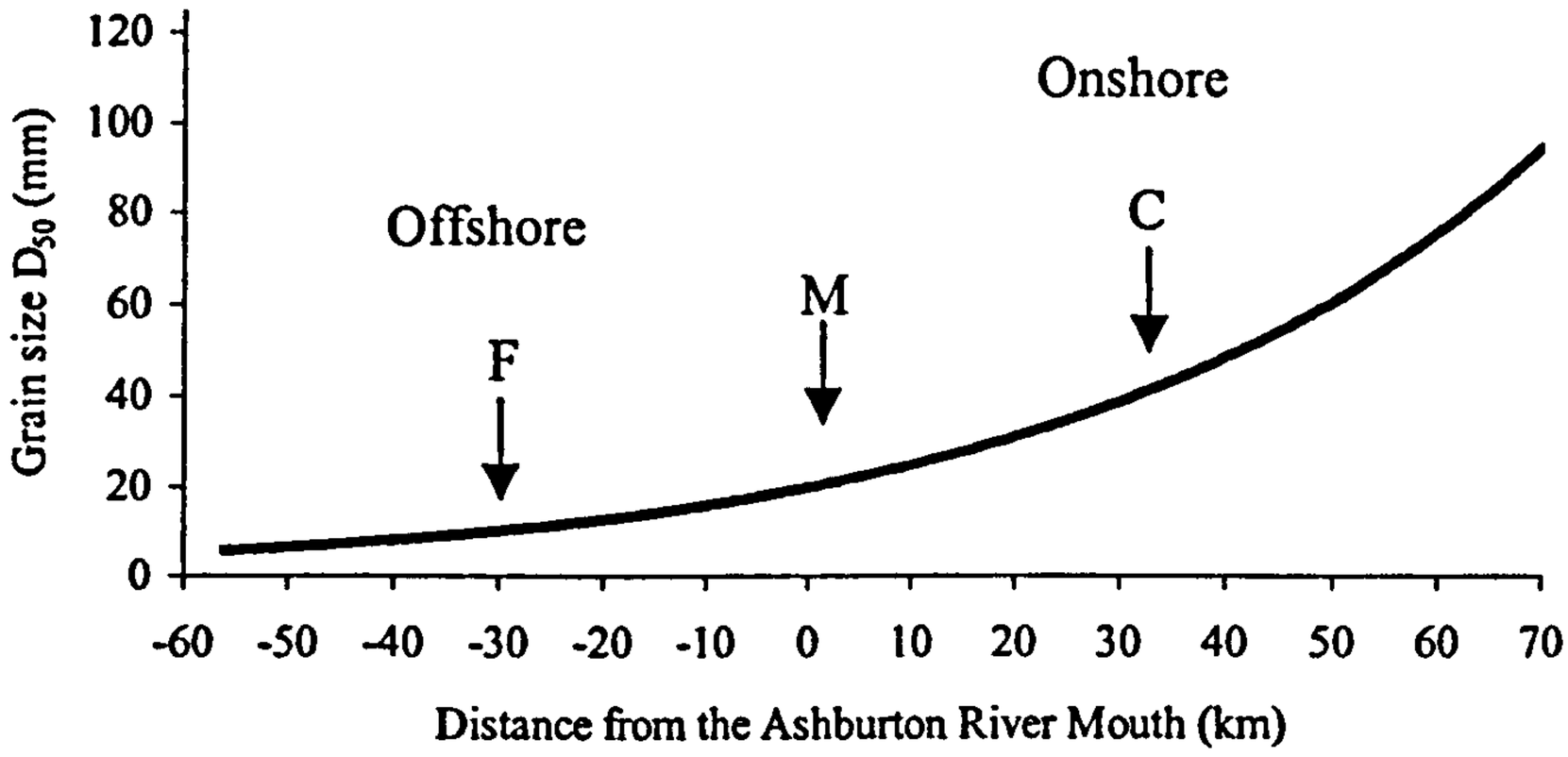

Figure 6.1. Exponential downstream fining curve based on D_{50} values for the modern Ashburton River with the superposition of the D_{50} values of the three scaled grain size distributions from series C, M and F.

6.3 Data analysis: field and flume

Data were also gathered from the modern Ashburton River and 50 km of exposed Quaternary Gravels between the Rakaia and Rangitata Rivers (Chapter 5, Figure 5.3a) in order to permit comparisons between the model and prototype. In order that FSM procedures are verified between the model and prototype, hydraulic flow parameters must show dynamic similarity. Warburton and Davies (1998) suggest that in satisfying dynamic similarity, kinetic and geometric similarity are also assumed.

Analysis of the channel morphology of the Ashburton River and the alluvial architecture of the Canterbury Gravels allows direct comparison of geometrical similarity between model channel morphology and cut-sections from the preserved model sedimentary architecture respectively. Alluvial architecture from both prototype and analogue were examined in an orientation perpendicular to the mean palaeoflow direction.

Analysis of the alluvial architecture was restricted to the current coastal outcrop because vegetation prevents observation of much of the alluvial architecture inland from the coastline.

6.4 Comparison of hydraulic flow parameters: field and flume

Mean flow conditions (Table 6.2) show broad agreement with those documented in braided rivers (e.g. Young and Davies, 1990) and for previous modelling experiments (e.g. Ashmore, 1991a; Hoey and Sutherland, 1991; Ashworth *et al.*, 1994; Warburton and Davies, 1994a, 1998). Mean Froude numbers in the model are below one, indicating subcritical flow conditions; although the observation of standing wave trains on the water surface indicate intermittent supercritical flow conditions. Flow Reynolds numbers are greater than 1000 and represent transitional to fully turbulent flow conditions. Mean grain Reynolds numbers for the three experimental grain size distributions fall below the critical value of 70 proposed by Yalin (1971) based on a version of the Shields diagram where the Shields curve becomes horizontal (Chapter 5, Figure 5.1). However, all three experiments produce Re* above the critical values recommended by other authors (Parker, 1979; Jaeggi, 1986; Ashworth *et al.*, 1994). During the experiments the presence of bedforms in the channels of series F and M was noted, which are discussed in Section 6.9.1. Hydraulic flow conditions for all three experiments show dynamic similarity with the prototype.

Table 6.2. A summary of mean key flow parameters calculated for the Ashburton River field study and physical modelling experiments series C, M and F.

Flow parameters	**Prototype**	**Model series**		
	Ashburton River	C	M	F
Grain D_{90} (m)	0.02	0.00179	0.00096	0.00050
Slope	0.007	0.013	0.014	0.015
Width (m)	9.97	0.18	0.28	0.31
Depth (m)	0.48	0.007	0.009	0.010
Mean velocity, U (ms^{-1})	1.74	0.24	0.26	0.28
Froude number, Fr	0.80	0.97	0.93	0.92
Flow Reynolds number, Re	501844	1495	2160	2627
Grain Reynolds number, Re*	2249	50	32	19

Note the flow parameters have been calculated assuming a rectangular cross-section and water temperature of 5°C in the prototype and 20°C in the model. Mean velocities for the physical model have been calculated from surface velocities multiplied by 0.8 (formula of Prony, in Graf, 1998). Values of Re* were calculated based on the D_{90} grain size.

An aggradation rate of 1 mm hr^{-1} was used in all three experiments. Using the time scale for the model (λ_t) to equal to $(\lambda_L)^{0.5}$, the aggradation rate is calculated at 0.14 mm hr^{-1} in the prototype. This aggradation rate is several orders of magnitude greater than

many long-term aggradation rates documented for fluvial systems (e.g. Sadler, 1981; Bentham *et al.*, 1993, Leeder *et al.*, 1996; Kraus, 1997), but sits within the documented range in the literature (10^{6}-10^{-3} m/1000years, Sadler, 1981).

6.5 Surface form and channel morphology: field and flume

Analysis of the series C, M and F focused on the characterisation and quantification of channel geometry, channel occupancy, duration of channel occupancy and braidplain slope. To establish the impact of changing grain size on surface form and channel morphology, analysis of the modern Ashburton River was undertaken to compare geometric similarity between model and prototype. In order to compare the distributions of geometric information (namely: width, depth and width/depth ratio) and verify the geometric similarity at the 95 % significance level the Kruskal-Wallis test for non-parametric data was employed (Appendix B).

6.5.1 Ashburton River channel geometries

Surveys were performed to quantify the distribution of channel geometries (bankfull width and depth) on four sites (A, represents two sites at equal distances upstream, B and C) down the course of the modern Ashburton River (Table 6.3). Data from the north Ashburton and south Ashburton River sites (A) have been amalgamated because both represent an equal distance from the Ashburton River Mouth (Chapter 5, Figure 5.3b).

Table 6.3. Comparison of channel geometries measured at four sites along the course of the modern Ashburton River.

Site		Depth (m)					Width (m)					
	Distance from river mouth (km)	n	mean	median	Standard deviation	max	min	mean	median	Standard deviation	max	min	W/D ratio
North Ashburton, A	43	7	0.29	0.31	0.07	0.39	0.17	9.41	8.64	2.33	13.17	6.79	32.5
South Ashburton, A	43	8	0.32	0.32	0.10	0.50	0.17	10.82	10.97	3.87	16.66	5.87	36.4
Ashburton Town, B	18	8	0.26	0.19	0.16	0.49	0.10	10.71	10.48	5.98	15.07	2.92	47.3
Ashburton mouth, C	0.5	8	0.26	0.26	0.12	0.50	0.11	8.87	7.68	3.43	13.94	4.49	37.8

Analysis of depth, width and width/depth ratio for the channels measured at four sites down the course of the Ashburton River reveal no significant change at the 95% confidence interval. These results (Table 6.3, Figure 6.2) suggest that the downstream

diminution of grain size have no significant effect on the channel geometry (either magnitude or shape) over a 43 km distance. An alternative interpretation may be that any impact that the grain size may have on the channel geometry is subordinate to other controls acting upon the Ashburton River such as discharge. The development of a wider channel-belt containing more active channels in the Ashburton River may be accommodating any increase in discharge that occurs downstream. A similar trend has been documented in the study of the braided Ashley River, New Zealand, by Warburton *et al.* (1993) who deduced that the number of channels in a transect across a river reach will increase rather than enlarge the existing channel geometries.

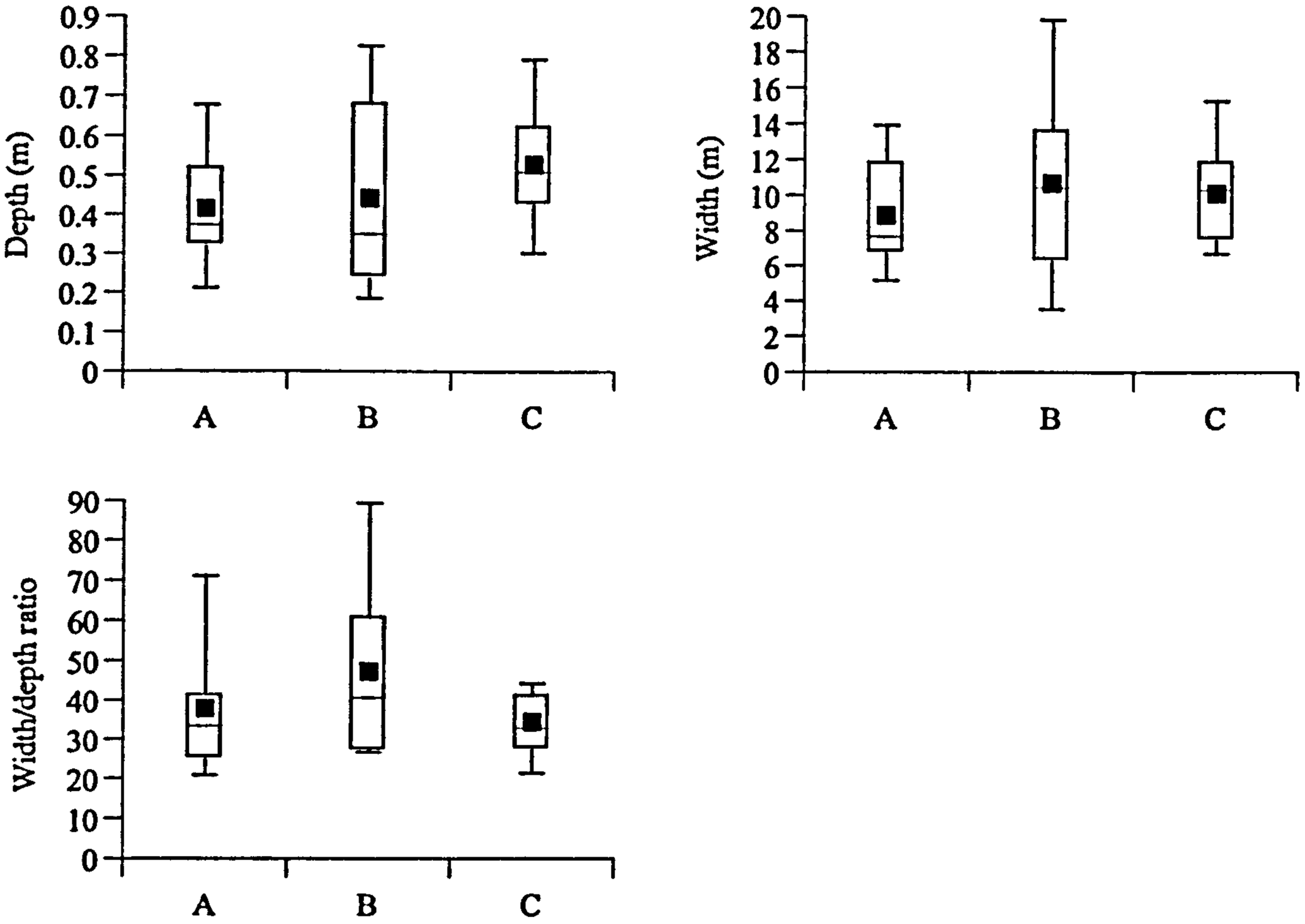

Figure 6.2. Box and whisker plots for the depth, width and width/depth ratios for three sites along the course of the Ashburton River, representing position (A) at 0 km (the Ashburton mouth), (B) 18 km (Ashburton Town) and (C) 43 km (Thompsons Track, North and South Branches) upstream from the present coastline.

However, a study on the Ohau River, New Zealand (Mosley, 1982) showed that as discharge increases existing channels become shallower and wider and merge, in addition to the generation of smaller channels with the same characteristics as those at lower discharges. Surveying of channel geometries in the Ashburton River took place during low summer discharges levels. Therefore, channel geometry measurements do not account for seasonal changes in discharge and any corresponding changes in

channel geometry, which highlight the drawback of field studies. The measurement of field channel geometries at high discharges is not often permissible due to the practical aspect of carrying out these studies (e.g. Warburton and Davies, 1998). Therefore, at the time of any particular field study, channel geometries will ultimately be a result of the magnitude and frequency of discharge effects occurring prior to that study. Physical modelling allows consistent discharge and frequency effects to be imposed on a scaled river, reducing the uncertainties described above. Therefore, to determine the relative effect of grain size on channel geometry, grain size must be first investigated in isolation from all other controls, a process that can be undertaken in FSM.

6.5.2 The geometry of the Ashburton model channels

To allow surface morphology to be characterised and compared between the three experiments channel geometries were measured. Bankfull width and depth measurements (Williams, 1978a) were gathered from laser profile information recorded at the end of every fourth hydrograph while the flume facility was left drained. Channel definition was assisted by the analysis of overhead video footage to corroborate the bankfull width. Figure 6.3a-c shows probability density functions of channel width in series C, M and F compared to the Ashburton River (Series 6.3d). Series C and M show similar PDF's to the Ashburton River, while series F exhibits a broader range of widths. Channel geometry results from series C, M and F are shown in Figures 6.4. In the three experiments, mean width/depth ratios (C=30, M=37, F=32) and 80 % of all the measured width/depth ratios sit within the range of the width/depth ratios measured from the Ashburton River (11-46) and agree with width/depth ratios documented in the literature (e.g. Parker, 1976, 1979; Ashworth *et al.*, 1994). A significant increase in the depth was noted between series C and M, and in width between series M and F. Furthermore, there was no significant difference in width/depth ratios of channels between the three experiments. These results suggest the relationship between grain size and channel geometry is ambiguous. Further discussion of these trends in channel geometry is found in Section 6.19.

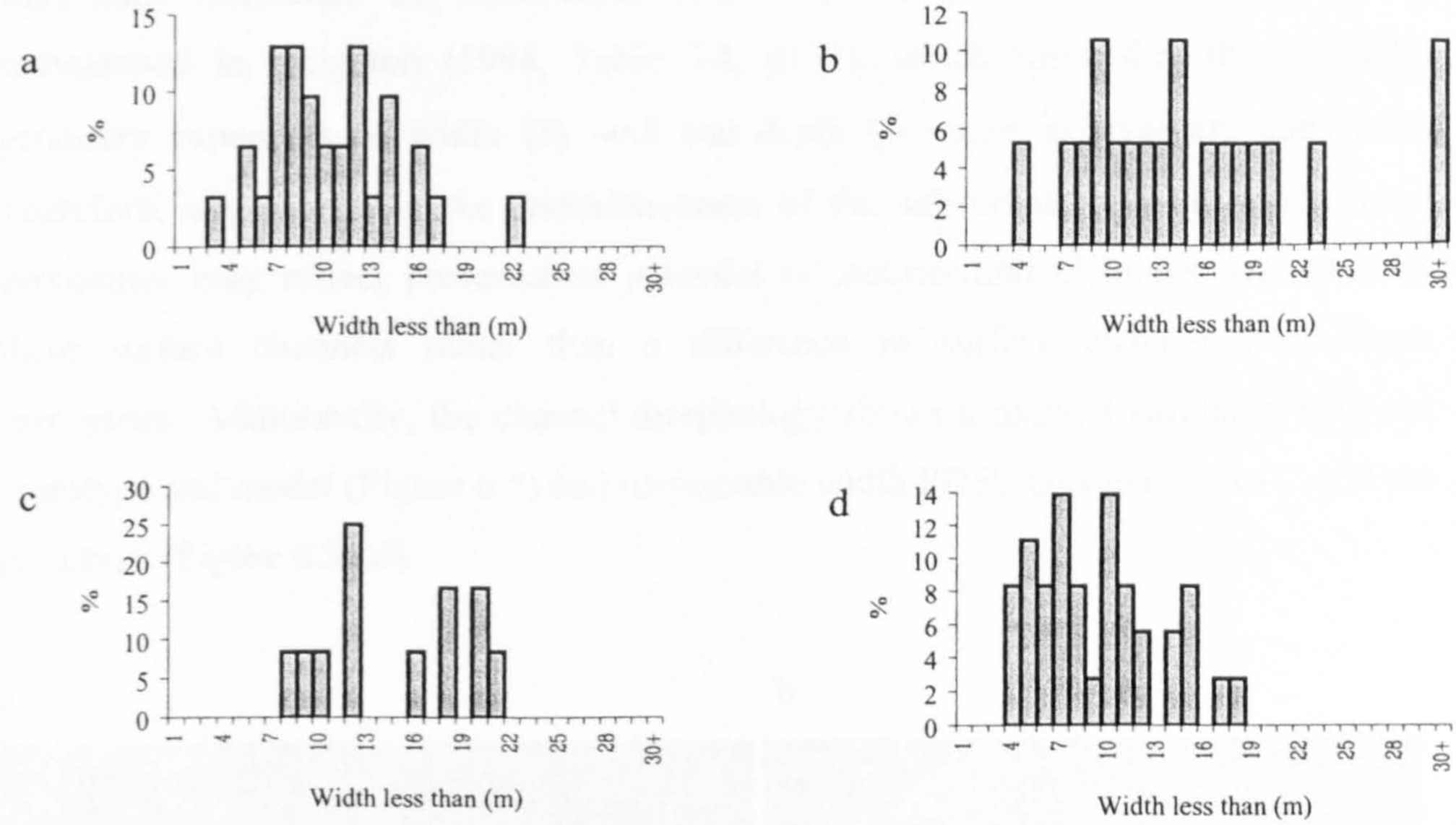

Figure 6.3. Probability density functions of channel widths for (a) the modern Ashburton River and physical modelling series (b) F, (c) M, and (d) C. Note: widths have been scaled up from the flume.

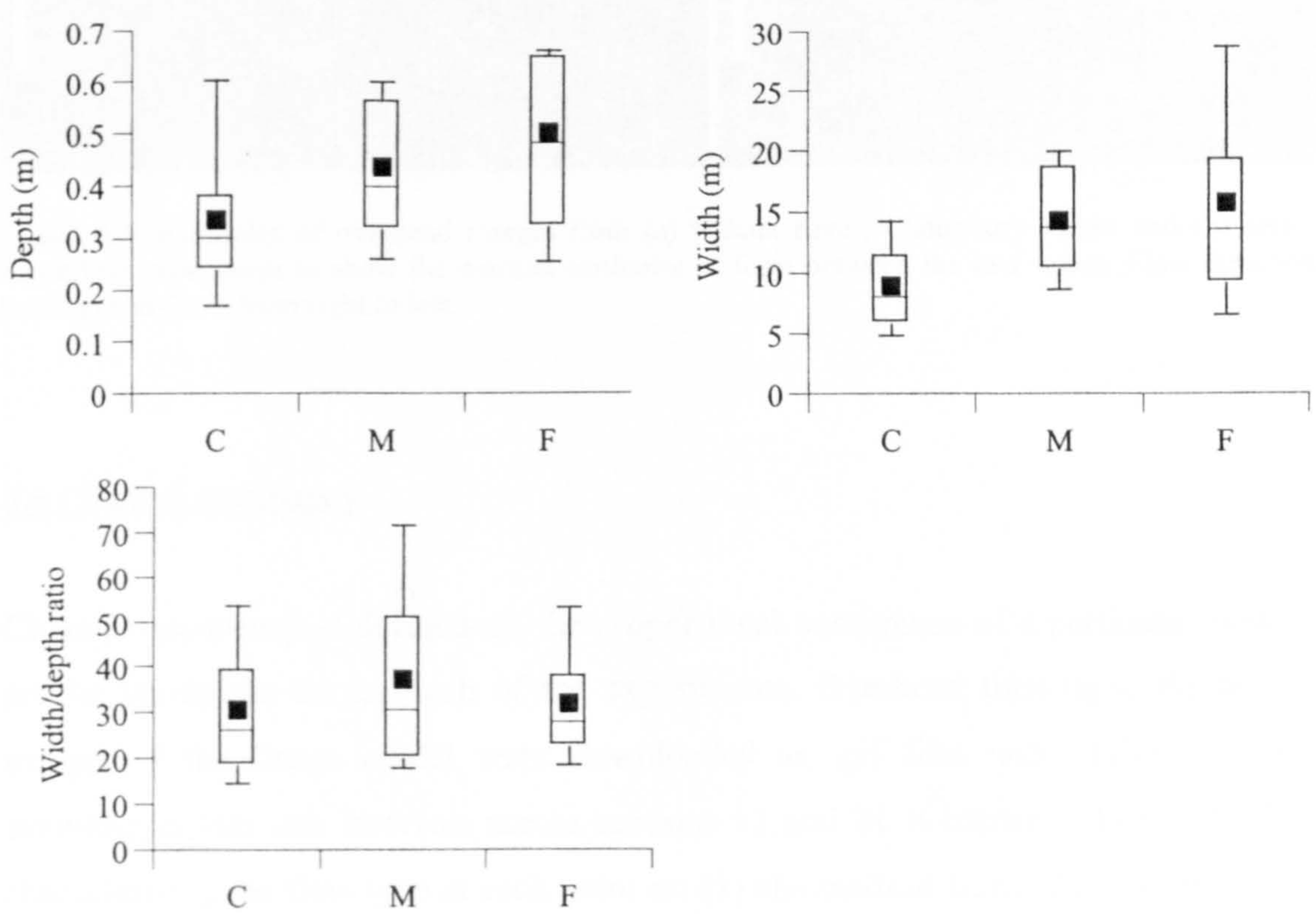

Figure 6.4. Box and whisker plots for depth, width and width/depth ratio distribution data from series C, M and F. Note the increase in width and depth between series C and F, but without a change in width/depth ratios. Note: widths have been scaled up from the flume.

Channel geometries within the Ashburton River and the physical model show no significant difference in width/depth ratio and are consistent with the studies summarised in Knighton (1998, Table 5.4, p173), which show that the hydraulic geometry exponents of width (*b*) ~0.5 and depth (*f*) ~0.36 in river are consistent. Therefore, any change in the width/thickness of the subsurface alluvial architectural geometries may reflect preservation potential of architectural elements deposited by these surface channels rather than a difference in surface channel width/depth geometries. Additionally, the channel morphology shows a marked similarity between prototype and model (Figure 6.5) and comparable width PDF's between series C and the prototype (Figure 6.3a,d).

a

b

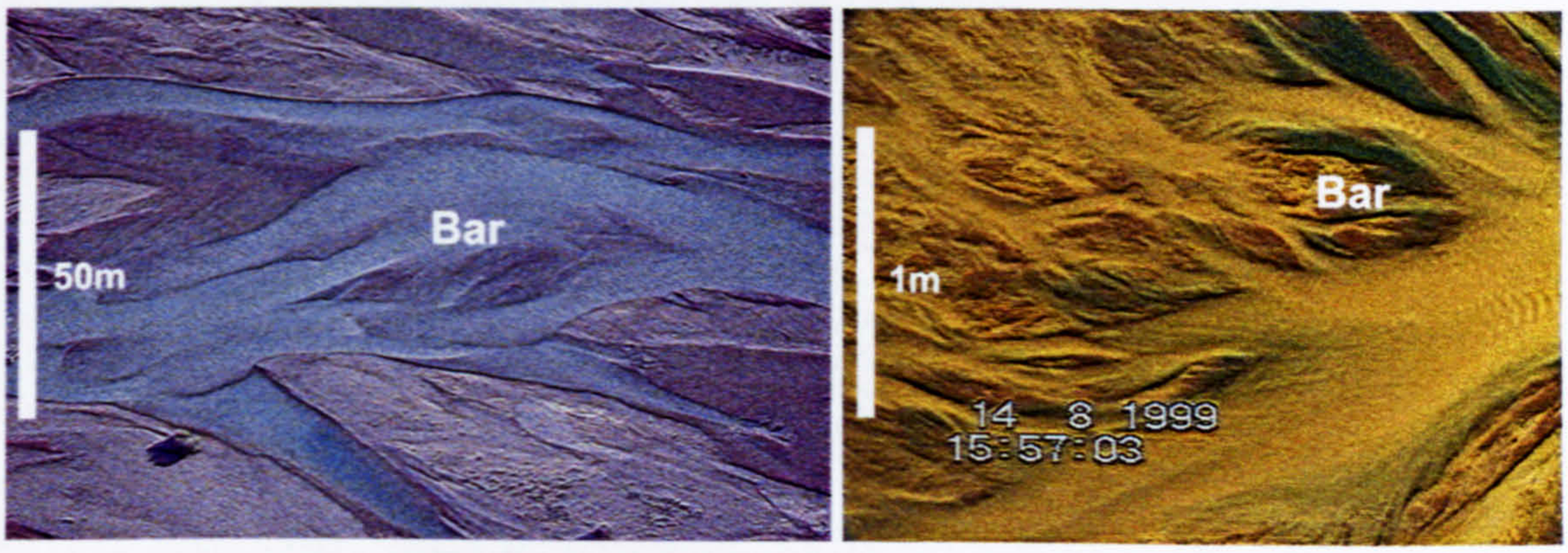

Figure 6.5. Examples of overhead images from (a) Rakaia River, Canterbury Plains and (b) series C modelling experiment to show the marked similarity of form between the two scales. Flow direction in both (a) and (b) is from right to left.

6.6 Channel occupancy

Channel occupancy is defined as: the proportional occurrence of a particular flow type on the braidplain during each of the experiments. Overhead time-lapse digital video images of the flume model were downloaded as .gif files and analysed by point sampling at 100 mm intervals across sections 11 and 21 (Chapter 5, Figure 5.17) and characterising the flow type at each point as: (1) channelised flow, (2) sheet flow, or (3) no flow/ponded water (Table 6.4). Images were collected at a frequency of one hour, at a discharge of 1.67 l s^{-1} following the peak of the hydrograph in all three experiments.

Table 6.4. Description of flow types observed within each of the three braided experimental runs.

Flow type	Description
Channelised flow	Channelised flow is confined flow, defined where the margins of the flow can be clearly observed. Channelised flow has mean width/depth ratios of 32, 37 and 30 in series C, M and F, respectively. When discharges are raised, channel banks are overtopped and the margins of the channel can become diffuse with the overbank flow. Channelised flow can diverge and converge as anabranch channels around a mid-channel bar or form chute channels that terminate in a chute lobe (cf. Southard *et al.*, 1984).
Sheet flow	Sheet flow is characterised by very diffuse margins between the channelised and the overbank deposits. Shallow flows that expand across the floodplain as flow overtops the channel margins as discharge rises.
No flow or ponded water	Areas of the basin that have become abandoned and may have ponded water or very shallow, slow-moving water allowing deposition of suspended sediment.

Results are displayed as stacked bar graphs (Figure 6.6) showing the proportion of time that the floodplain was occupied by channelised flow, sheet flow, or no flow. Comparison between the channel occupancy of series C, M and F shows a rise in the proportion of sheet flow occupying the floodplain from 8 % to 15 % to 25 % respectively. This change relates to a 213 % increase in the proportional occurrence of sheet flow between series C and F. However, this increase in sheet flow does not correspond to a decrease in the channelised flow. These flow categories are discussed in relation to surface form and resultant depositional architecture in Sections 6.9 and 6.10.1 respectively.

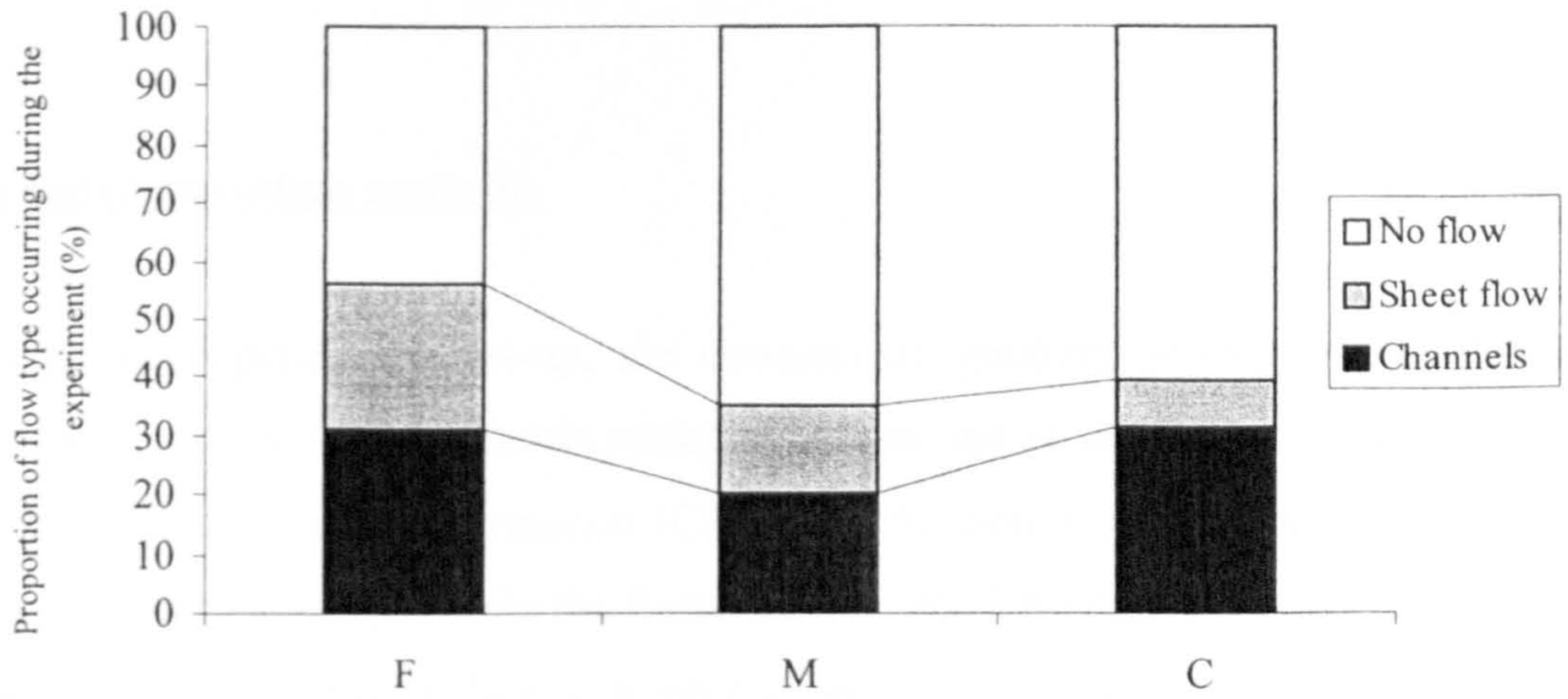

Figure 6.6. Comparisons of channel occupancy between the three experiments taken at a discharge of 1.67 l s^{-1}. An increasing proportion of the floodplain is occupied by sheet flow between series C and F.

6.7 Duration of channel occupancy

The duration of channel occupancy is defined as the period of time for which a channel occupies a point position on the braidplain before avulsing or migrating away from that point. The duration of channel occupancy was measured at four equally-spaced point locations across section lines 11 and 21 (Chapter 5, Figure 5.17) using the same sampling frequency as used for defining flow type (Section 6.6). The duration of channel occupancy is displayed as box and whisker plots in Figure 6.7. Although, series F appears to have a lower range of duration of channel occupancy, a Kruskal-Wallis non-parametric analysis of variance (Appendix B) between the three experiments shows no significant difference at a 95 % confidence limit.

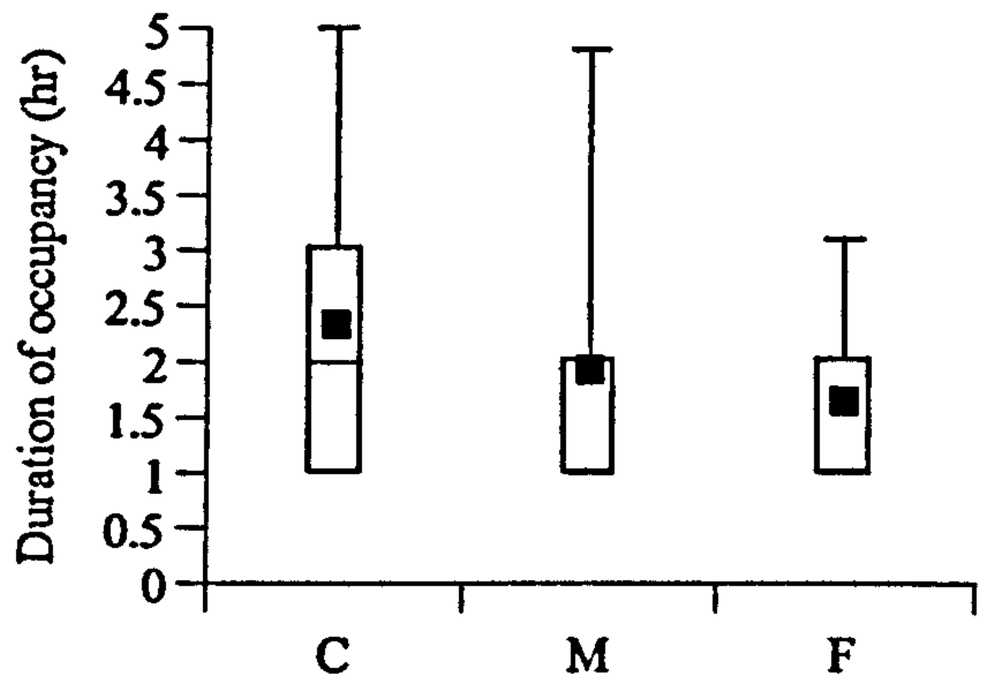

Figure 6.7. Duration of channel occupancy (see text for description) for series C, M and F, showing no significant difference between the three experiments. Note: the frequency of sampling was 1 hour, therefore any channel shifts below 1 hour will not be identified.

6.8 Sediment surface gradients

During the experimental set-up, the downstream gradient of the base of the flume facility was set at 0.01 to match prototype slopes and to increase Re* values (refer to Chapter 5). Laser data information (Chapter 5, Section 5.10.3) recorded at the end of every fourth hydrograph while the flume facility was left drained were used to calculate downstream sediment surface gradients (Figure 6.8). Results (Figure 6.9) show no significant difference in sediment surface gradients between C (0.0072-0.0165) and M (0.0119-0.0161) while significant differences exist in sediment surface gradients between series M and F (0.0144-0.0165). Nonetheless, all three series have similar maximum slope values (~0.0165, Figure 6.9).

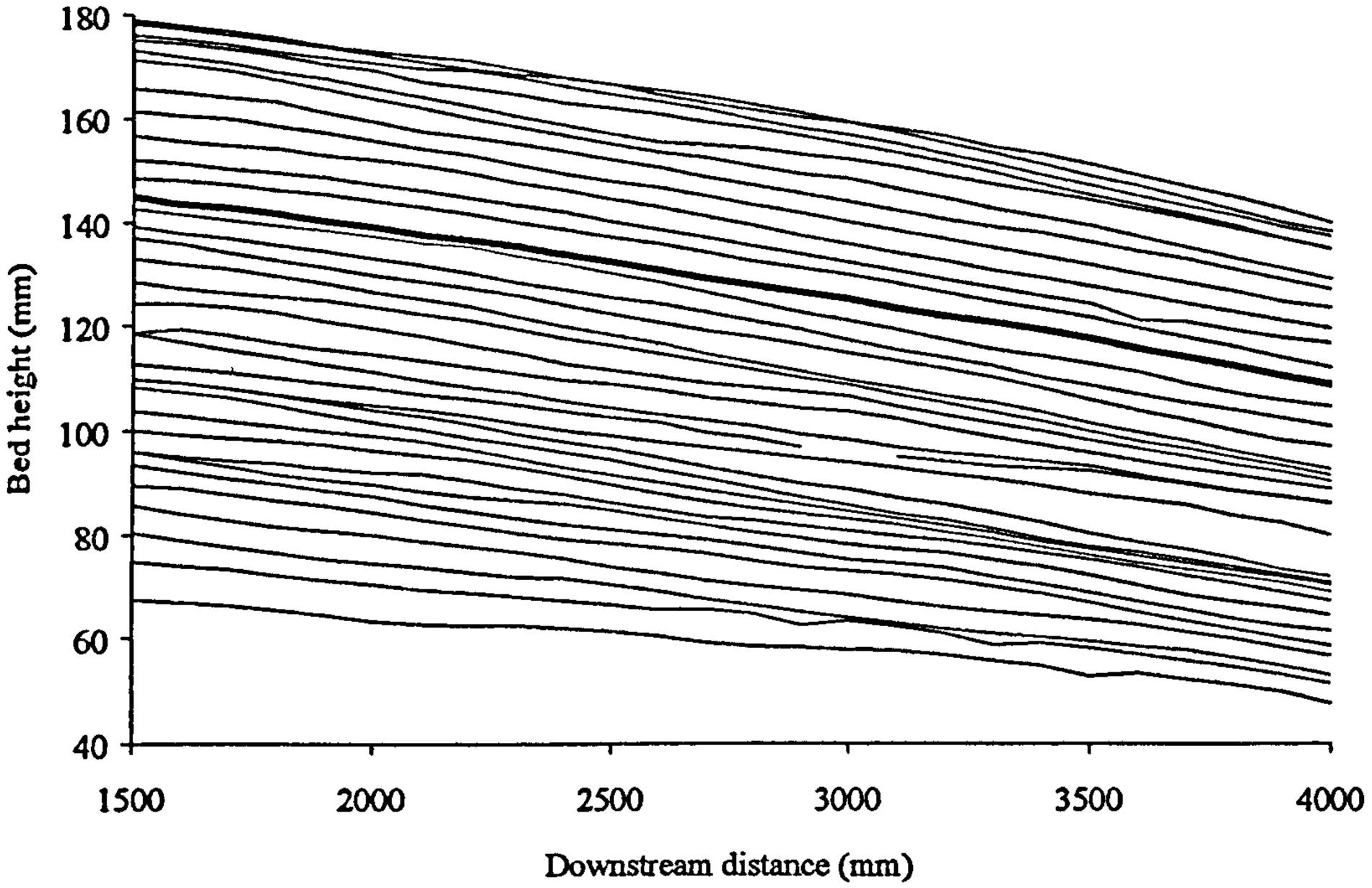

Figure 6.8. The development of downstream sediment surface gradients during the 125 hour experiment. The area between the lines represents sediment accumulation during four hour intervals. The bold line indicates where the grain size distribution was quartered. The gap in the line represents a section where no data were collected

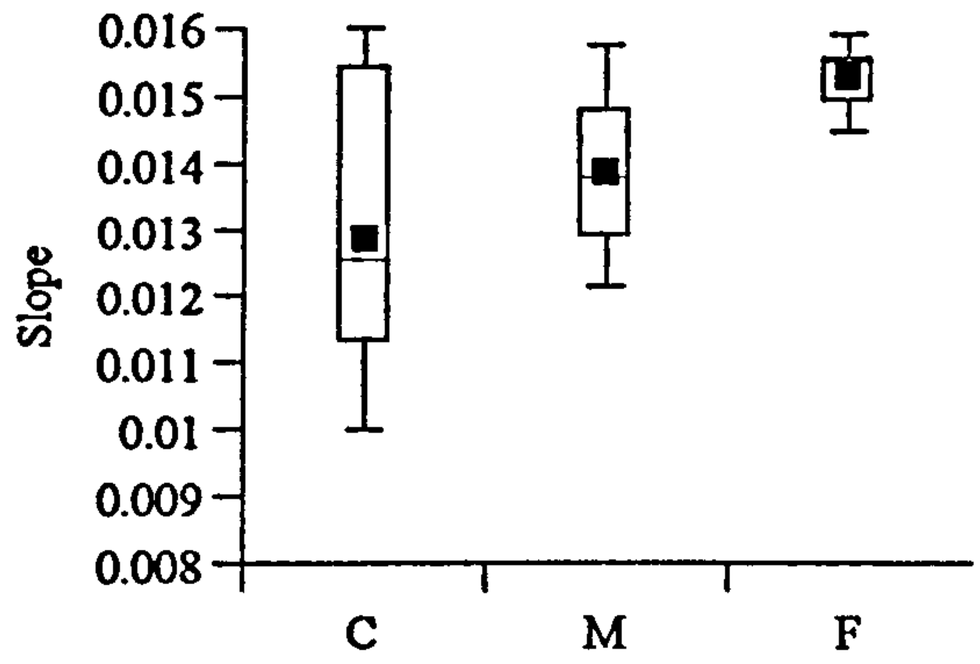

Figure 6.9. Box and whisker plots showing the range, upper and lower quartiles, mean and median values for downstream sediment surface gradients measured in series C, F and M.

In the three experiments downstream sediment surface gradients increased from an initial basin slope of 0.01 in combination with a reduction in the aggradation rate distally from the exit point of the feeder channel, to produce a low-angle alluvial braidplain surface. This low-angle braidplain development is most pronounced in the

series F and mean downstream sediment surface gradients increase sequentially in series C (0.013), M (0.014) and F (0.015) respectively. Downstream sediment surface gradient values are generally higher than those of the modern Ashburton River channels (Chapter 5, Section 5.6.5). Higher slope values in the model produce higher grain Reynolds numbers, which is beneficial for satisfying scaling laws (see Ashworth *et al.*, 1994).

Sediment aggrades immediately downstream of the feeder channel exit and aggradation rate decreases downstream (Figure 6.8). The smaller range of sediment surface gradients in series F may be the result of the differences in rate of sediment wave propagation downstream between the three experiments. Although no direct evidence was noted, the propagation of a sediment wave may be responsible for the differences in sediment gradient changes. The propagation of sediment waves has been noted in several previous braided river experiments (Ashmore, 1988; Hoey and Sunderland, 1991; Hoey, 1994; Warburton and Davies, 1994). Propagation of a sediment wave downstream results in a progressive reduction in sediment surface gradient over time. On reaching the downstream exit mesh the sediment wave increases the bedload transport rate. The increase in bedload transport rate is particularly pronounced at high discharges (cf. Peakall, 1995) when transport rate exceeds the capacity of the downstream mesh trapping sediment upstream of the mesh. This trapping of sediment increases the local aggradation rate immediately upstream of the mesh, which propagates upstream, progressively reducing downstream sediment surface gradient over time. The retention of the sediment is less pronounced in series F resulting in a more consistent downstream aggradation rate. Additionally, the range of sediment surface gradients is smaller in series F compared to series C and M, due to the capacity of the discharge to transport the sediment load more evenly across the developing braidplain. Simons and Simons (1987) noted in comparisons between gravel and sand bed rivers that sand bed rivers respond more rapidly to changes in discharge than gravel bed rivers. Although, the flume experiments described here are designed to scale a gravel-bed river, the relative response time for morphological change between the three experiments may be different, with series F responding more rapidly to discharge resulting in a narrower range of sediment surface gradients. In order that this response time can be investigated, the frequency of topographic bed surveys needs to be increased in future FSM to investigate the censoring effect of sampling frequency.

6.9 Surface morphological forms

Analysis of the overhead video footage allowed examination of the evolution of the sediment surface, which resulted in the classification of several geomorphological features described in Table 6.5 and shown in Figure 6.10.

Table 6.5. Summary of surface depositional forms from the three experiments, series F, M and C described from analysis of overhead video footage.

Surface form	Description and interpretation
Primary channels	Primary channels are broad with defined margins and commonly form anabranches around a mid-channel bar. During peak flows sediment is transported down the channels as migrating sediment lobes. The stalling of a sediment lobe within the channel often resulted in a narrowing of the channel to form a smaller secondary channel. Small, low relief-ridges and rhomboidal bedforms form on the head and sides of the sediment lobe indicating transitional flow Reynolds numbers and supercritical flow (Peakall *et al.*, 1996). Channels were observed to avulse by the mechanisms documented in Leddy *et al.* (1993). Channel filling and abandonment occurred by sediment lobe migration and blockage, often followed by passive filling (cf. Dreyer, 1990) and lateral accretion as the channel migrated across the braidplain. At low discharges in series F the formation of lunate bedforms within the channel was pronounced.
Secondary channels	Secondary channels are narrower than the primary channels and may form as a result of constriction or avulsion of a primary channel by sediment lobe migration (Leddy *et al.*, 1993). Secondary channels are often passively filled following abandonment or rapidly filled as a sediment lobe migrating down the main channel stalls at the confluence of the channel, resulting in fine- and coarse-grained channel fill deposits respectively. Secondary channels are also filled as splay deposition from the primary channels overtop the margins of the secondary channels and avalanches into the channels forming what may appear to be lateral accretion deposits in the subsurface. If complete abandonment from the primary channel occurs, water can pond within the channel enabling suspended sediment to be deposited as a fine-grained channel plug.
Chute crevasse channels and lobes	Chute crevasse channels form as the margins of primary channels are breached often by the avulsion mechanisms described in Leddy *et al.* (1993) initially forming a smaller channel that scours through the margins of the primary channel. Flow expands radially over the floodplain to deposit a lobe of sediment (cf. Southard *et al.*, 1984; Field, 2000) where flow becomes sheet-like. At lower discharges these sheet flows are concentrated into channels and dissect the sediment lobe. The subsurface expression of these chute channel and lobe would be similar to the secondary channels and splay deposits respectively, and are therefore, not differentiated in subsurface analysis.
Splays	Splays occur at high discharges when the channel margins are overtopped and sheet flow is initiated on the floodplain. This sheet flow deposits sediment onto the floodplain as a wedge shape, which tapers, away from the channel margin. Grain size can be observed to fine away from the channel (cf. Guccione, 1993).
Abandoned floodplain	Abandoned floodplain was defined as areas on the sediment surface where very shallow flows or no flow was occurring. Sedimentation in these in these areas occurs as suspension fallout, although no major morphological change occurs.

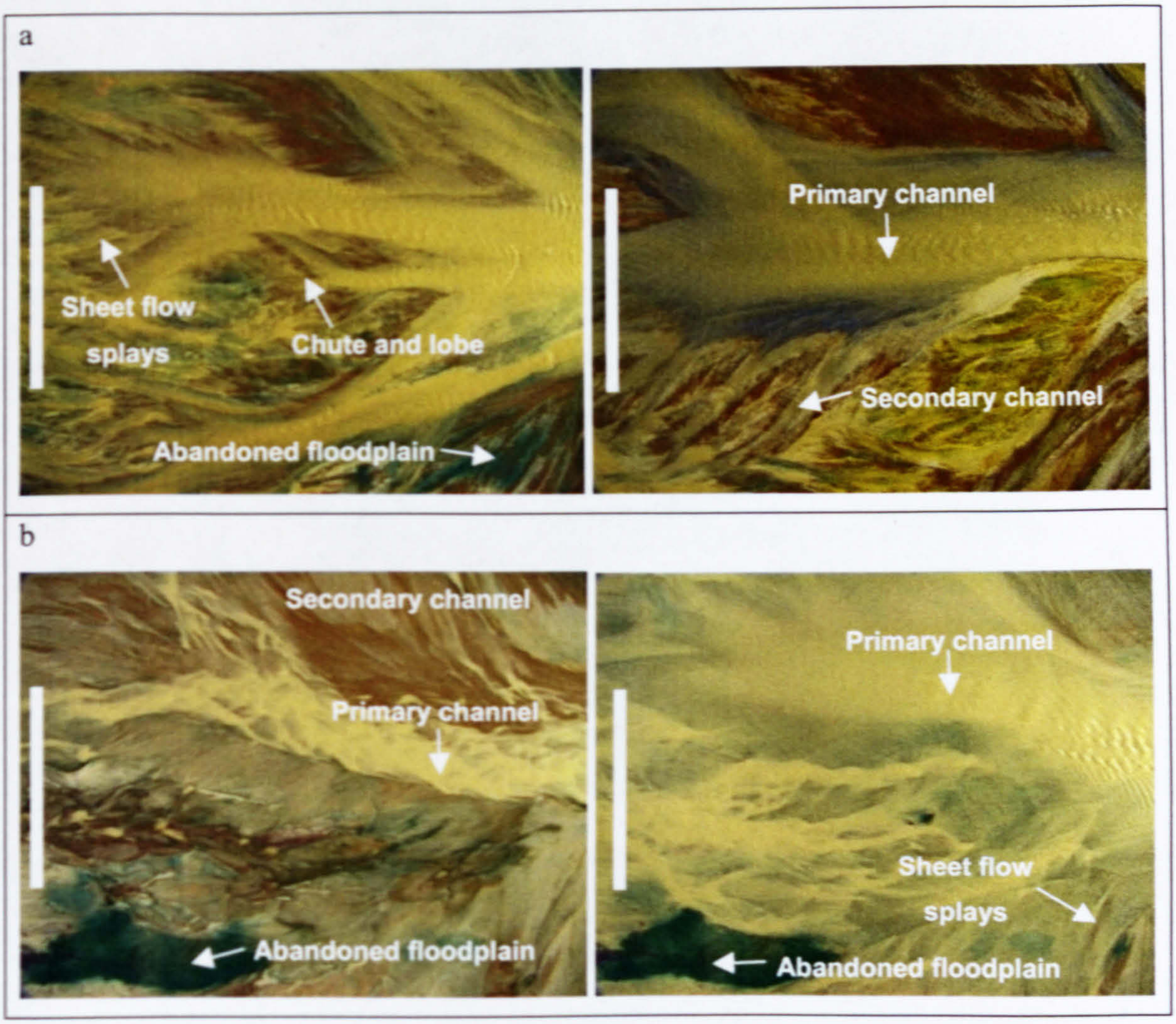

Figure 6.10. Examples of overhead video images showing the surface depositional forms described in Table 6.5, (a) from series C and (b) series F. Scale bar = 1 m. Flow direction is from right to left. Each image represents an area 2.5 m x 2 m.

6.9.1. Bedform generation

In series F and M, bedforms (Figure 6.11) were periodically observed to form in the primary channels during low discharge stages. The presence of ripple bedforms in physical models has been noted by Jaeggi (1986) to occur when grain Reynolds numbers drop below 5. Additionally, ripple formation has been noted to be particularly pronounced in medium or fine sands (Warburton and Davies, 1998). In order to establish if these bedforms were unscaled current ripples or scaled antidunes hydraulic flow parameters were analysed (Section 6.4).

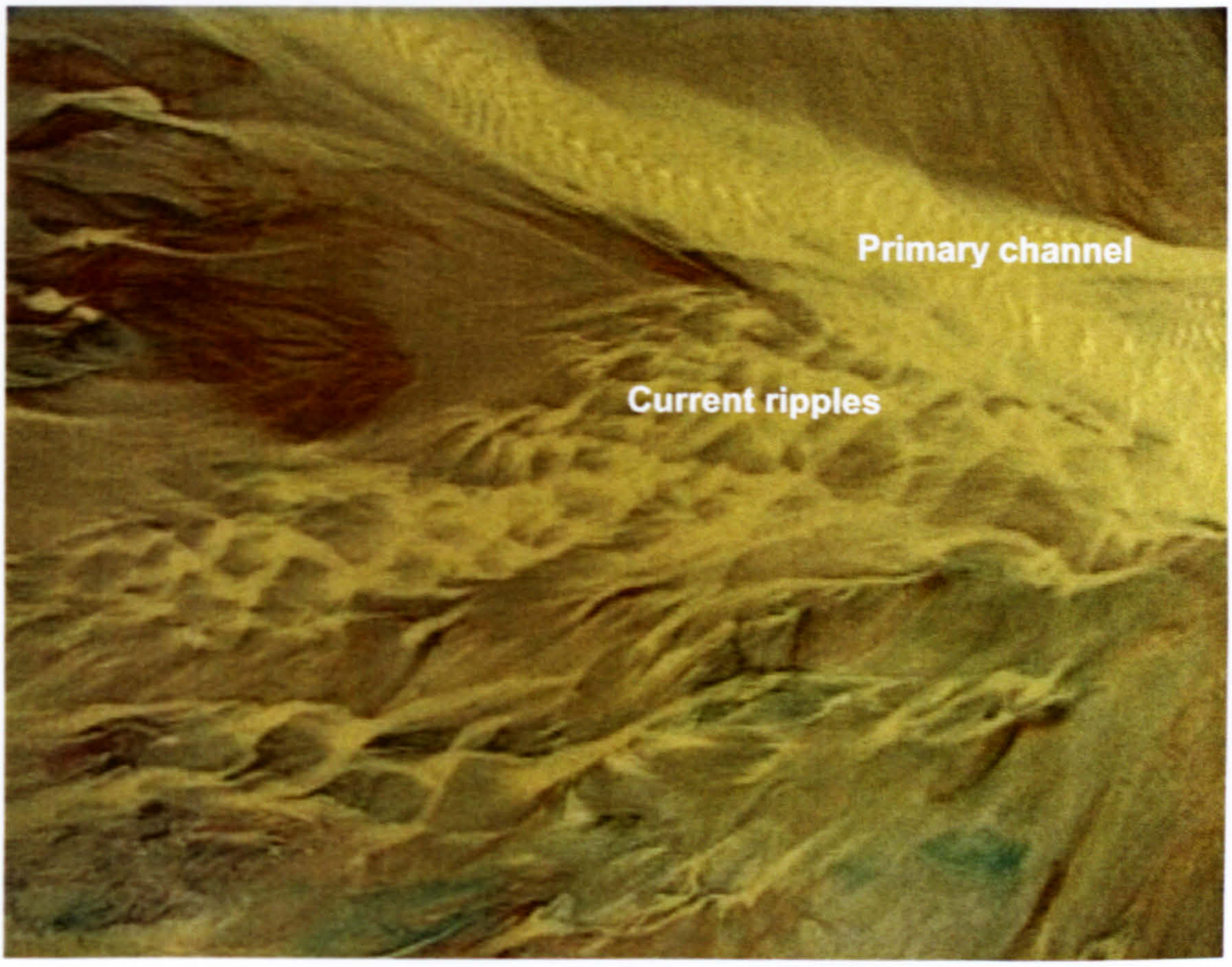

Figure 6.11. Overhead image of the braidplain showing the bedforms that form at low flow stage in series F and M (example from series F). Flow direction is from right to left and the images represents an area of braidplain of 2.5 m x 2 m.

Mean calculated Re* for series F and M are greater than the minimum Re* values required for modelling (Parker, 1979; Jaeggi, 1986; Ashworth *et al.*, 1994). However, locally the Re* may drop below the critical Re* required for hydraulically rough flow. D_{50} and D_{90} values were plotted against dimensionless boundary shear stress (Chapter 5, Equation 5.4) on the bedform phase diagram (Figure 6.12) of Allen (1983a). D_{50} values

for series F and M plot on the boundary of the ripple phase while D_{90} for series F and M plot within the dune phase and therefore are not forming at high enough shear stresses to be antidunes. Depending on local sediment sorting, finer-grained areas of the braidplain surface may intermittently develop ripples at the shear stresses plotted for series F and M in Figure 6.12. The D_{50} and D_{90} values of series C plot within the ranges of the dune and lower stage plane bed phases and are therefore, not subject to ripple propagation.

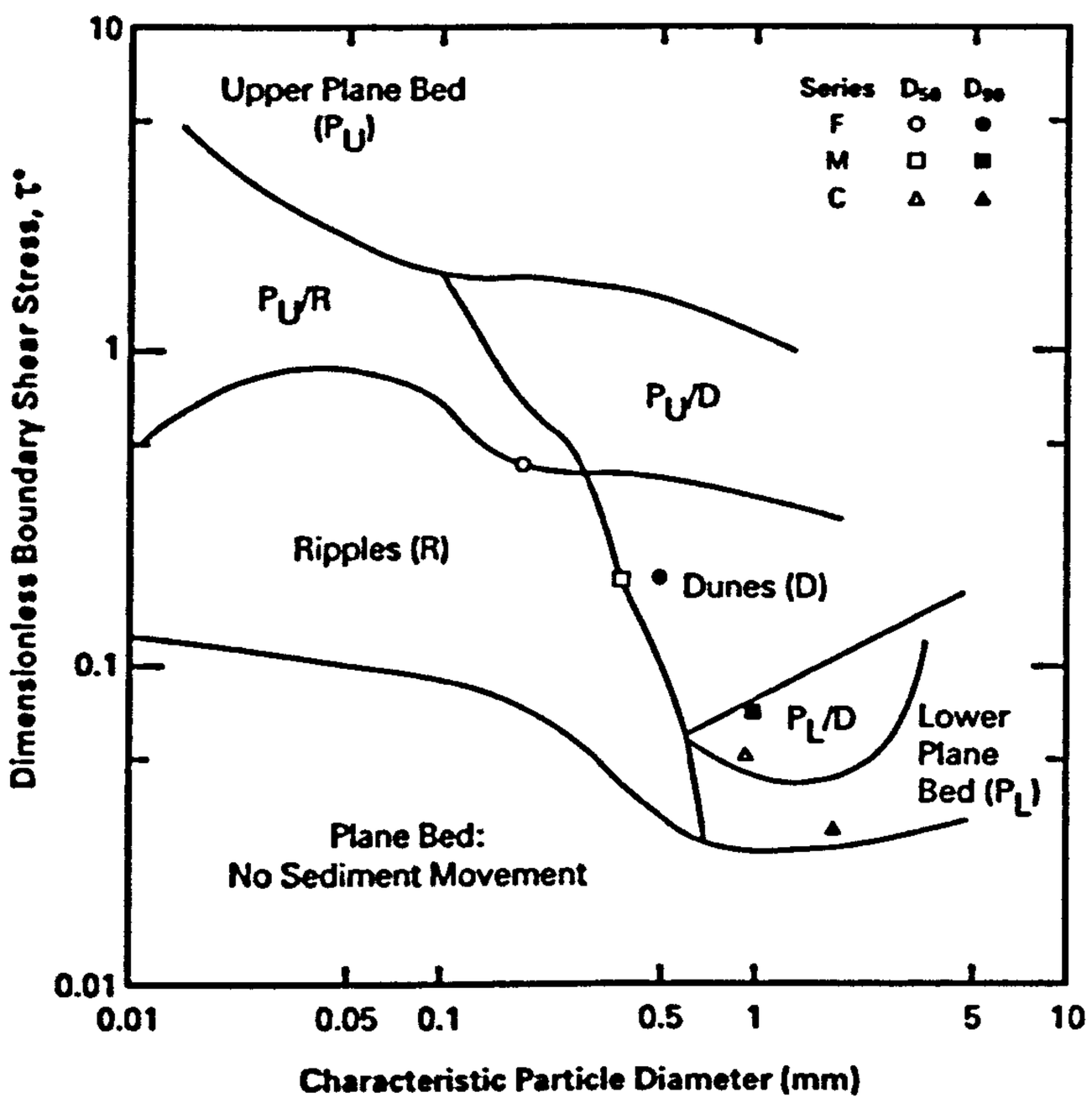

Figure 6.12. Phase diagram from Allen (1983a) showing the calculated dimensionless boundary shear stress for D_{50} and D_{90} values from experiment series F, M and C.

Local Froude numbers were calculated for two individual channels containing bedform development in series F and yielded values of 0.82 and 0.92, which are in the transitional range for the formation of antidunes (Leeder, 1982).

Further evidence that the bedforms (Figure 6.13) are not antidunes is observed when during falling hydrograph flow stages bedforms start to form while at high stages bedforms are sheared out. During experiment F the discharge was instantaneously halted at a discharge of 1.67 l s^{-1} and at a peak discharge of 3.21 l s^{-1} and the flume was allowed to rapidly drain. Analysis of the surface channel topography at peak discharge showed no evidence of bedform formation (Figure 6.13).

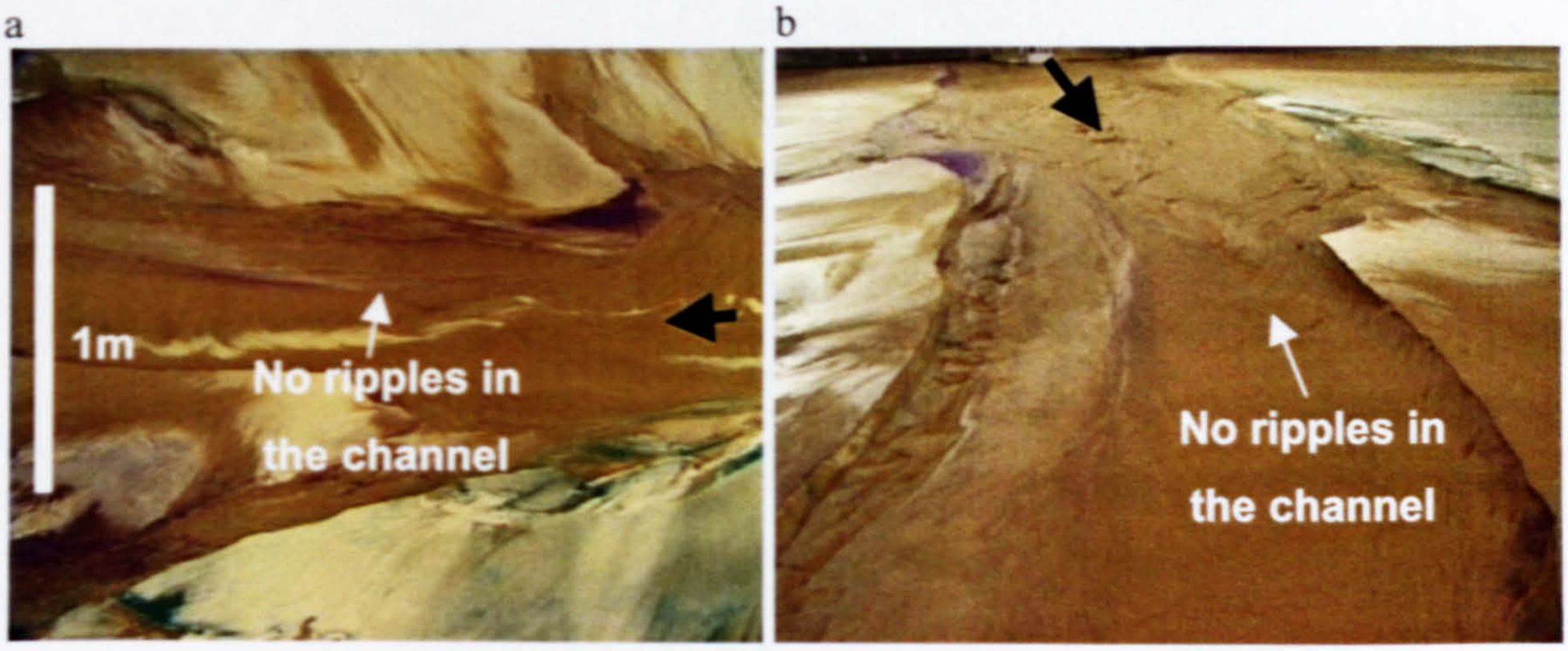

Figure 6.13. Overhead images of (a) a plan view and (b) an oblique view looking upstream following instantaneous drainage of the flume facility at 1.67 L s^{-1}, confirming that bedforms that disappear at higher shear stresses are ripples (see Figure 6.12). Black arrows indicate the flow direction.

Qualitative observations of the surface morphology of these evolving ripples show similar surface morphologies to the dune formation in the Platte River, Nebraska, USA, (cf. Blodgett and Stanley, 1980) and shows some scale distortion from the Ashburton River.

Evidence presented within this section suggests the bedforms observed in series F and M at lower discharge levels are ripples, which may not scale with the field prototype bedforms. These results provide physical modellers with important constraints on the magnitude of grain size scaled in the physical models. To avoid the formation of these bedforms, the use of series C grain size is recommended for future modelling. The scaling of finer-grained systems may be attempted by using a lower scaling ratio (e.g. 1:20, Ashworth *et al.*, 1994) or reducing the viscosity of the fluid, by heating the water.

6.10 Analysis of cut-faces

Sections were cut and photographed in panels perpendicular to flow, with a 10 % overlap for each of the three experiments. Six cut-faces (11, 13, 15, 17, 19, 21, Chapter 5, Figure 5.17) representing 0.2 m intervals in a downstream direction were analysed for classification and quantification of alluvial architecture for each experiment. Acetate overlays were used to trace and interpret the alluvial architecture. Architectural elements were defined and correlated to their formative surface processes via analysis of overhead video footage. The maximum width and thickness of all architectural elements were measured (Section 6.12) in addition to the construction of horizontal proportion curves (Section 6.11) in order to compare experimental datasets.

6.10.1 Classification of architectural elements

Initial classification of depositional architecture was based on comparisons with overhead video footage to provide surface-to-subsurface relationships. This methodology greatly benefits the understanding of depositional architecture and goes beyond the level of outcrop studies of alluvial architecture. A six-fold architectural element classification scheme (Table 6.6, Figure 6.14) was adopted. This scheme bears some resemblance to the architectural element scheme of Miall (1985), which has been criticised by Bridge (1993) because similar preserved structures may be formed by very different surface processes. For example, channel splays and crevasse lobes may exhibit similar parallel-bedded, two-dimensional depositional features in vertical section, but their planform geometries may differ. The sediment sequence of series F presented more difficulty in the interpretation of the cut-sections due to the homogeneity of sediment colour between element types. Coloured sediment added to define time horizons was often reworked by migrating bedforms and not commonly preserved in discrete horizons. Although architectural elements for all three experimental sequences appear common (Table 6.6), the internal fill of primary channel fills (architectural element A) in series F is dominated by trough structures as a result of ripple bedforms.

Table 6.6. Architectural elements observed within the flume sections and Quaternary Gravels of the Canterbury Plains. Elements A-C may include openwork deposits in field examples. Geometries for each of the architectural elements are presented for individual experiments in Tables 6.7 and 6.8.

Code	Architectural element	Sedimentary structure/ Texture	Depositional processes/ Interpretation surface morphology	Architectural element associations	Two-dimensional shape (perpendicular to palaeoflow) and mean W/T ratios	Comparison with architectural elements of Miall (1985)
A	Coarse-grained broad channel fills. Trough structures are observed in the internal channel fills of series F	Broad erosive bases with internally massive to weakly defined high angle cross-bedded. Broad tabular primary channel deposits. Coarse-grained trough structures filling broad erosive channel bases.	Results from major channel lobe or bar migration migration. Medium to coarse broad channel In series F trough structures results from bedform propagating and migrating down channels at low discharge stages.	C	Tabular	Gravel bars and bedforms, GB and lateral accretion, LA. Troughs show similarities to Sandy bedforms, SB
B	Coarse-grained channel fills	Arcuate convex lower surface filled with a massive or high angle cross-bedded fill. These may have a very coarse basal lag deposit. Ribbon-shaped secondary channel deposits	Results from the infilling of minor channels. Often as sheet splays flow into the channels from the adjacent major channels. Also plugging can occur as lobes stall in the channels or nodes of flow concentration. Convex-up ribbon form channel fill deposits of coarse grade sand with limited matrix. May be massive to steeply filled lateral accretion deposits	C	Arcuate	Channels, CH or scour hollows, HO
C	Medium-grained overbank splay deposits	Coarse overbank splay deposits. Low angle or horizontal parallel bedded elements. Often show small stacked fining-up sequences	Result from overbank splays from the channel margin or chute lobes can form on bar margins. Medium-grained, thin, laterally extensive splays often stacked to form a tabular unit.	A, F	Tabular-rhomboidal 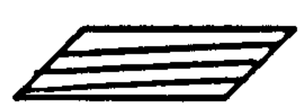	Laminated sands, LS and Parallel bedded gravels of GB

Table 6.6 continued.

Code	Architectural element	Sedimentary structure/ Texture	Depositional processes/ Interpretation surface morphology	Architectural element associations	Two-dimensional shape (perpendicular to palaeoflow)	Comparison with architectural elements of Miall (1985)
D	Fine-grained channel fills and nodes of flow concentration	Arcuate channel form. In the field, channel fills contain horizontal or cross-bedded laminations and pebbles maybe aligned along bedding planes.	Formed in slack water environments as minor channels are plugged at the upstream end and suspension fallout passively infills the channel form. Also form by nodes of flow concentration producing a deep scour hole during falling flow stages off a chute lobe. Often they only form the initial stages of abandonment.	D channel fills may form the base of type B channel fills.	Arcuate	Channels, CH
E	Erosional remnants	Irregular shaped fine-grained deposits. Field deposits are horizontally-laminated or cross-bedded.	Resulting from the subsequent erosion of fine-grained elements from their original form of drapes, bar-top fines and channel fills.		Random -irregular	
F	Fine-grained suspended sediment fallout deposits.	Fine-grained laminated deposits	The result of suspension fall-out of fines in the overbank environment. Coloured horizons denote substantial periods of floodplain abandonment over 8-12 hydrographs.	C	Tabular	Laminated sand sheet, LS or overbank fines, FF

a

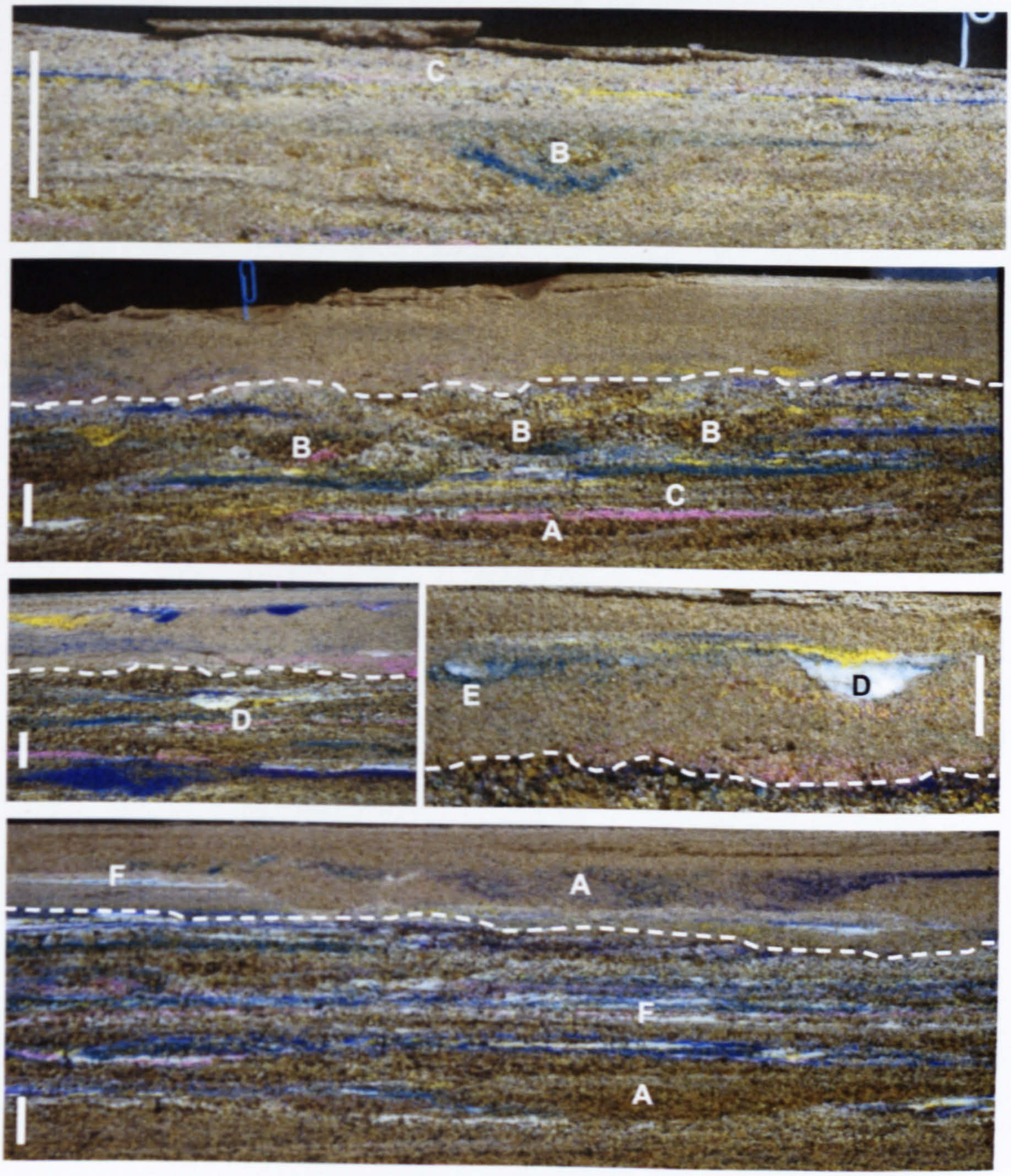

Figure 6.14 (a) Examples of architectural elements types A-F taken from the sections cut perpendicular to palaeoflow in the series C and F, where flow direction is into the page. Where A = primary channel fills, B = secondary channel fills, C = splay, D = fine-grained channel fills, E = erosional remnants, and F = overbank fines. Refer to Table 6.6 for sedimentary descriptions. The dashed line represents the boundary between series C at the base and series F at the top and the scale bar in each case is 20 mm.

b

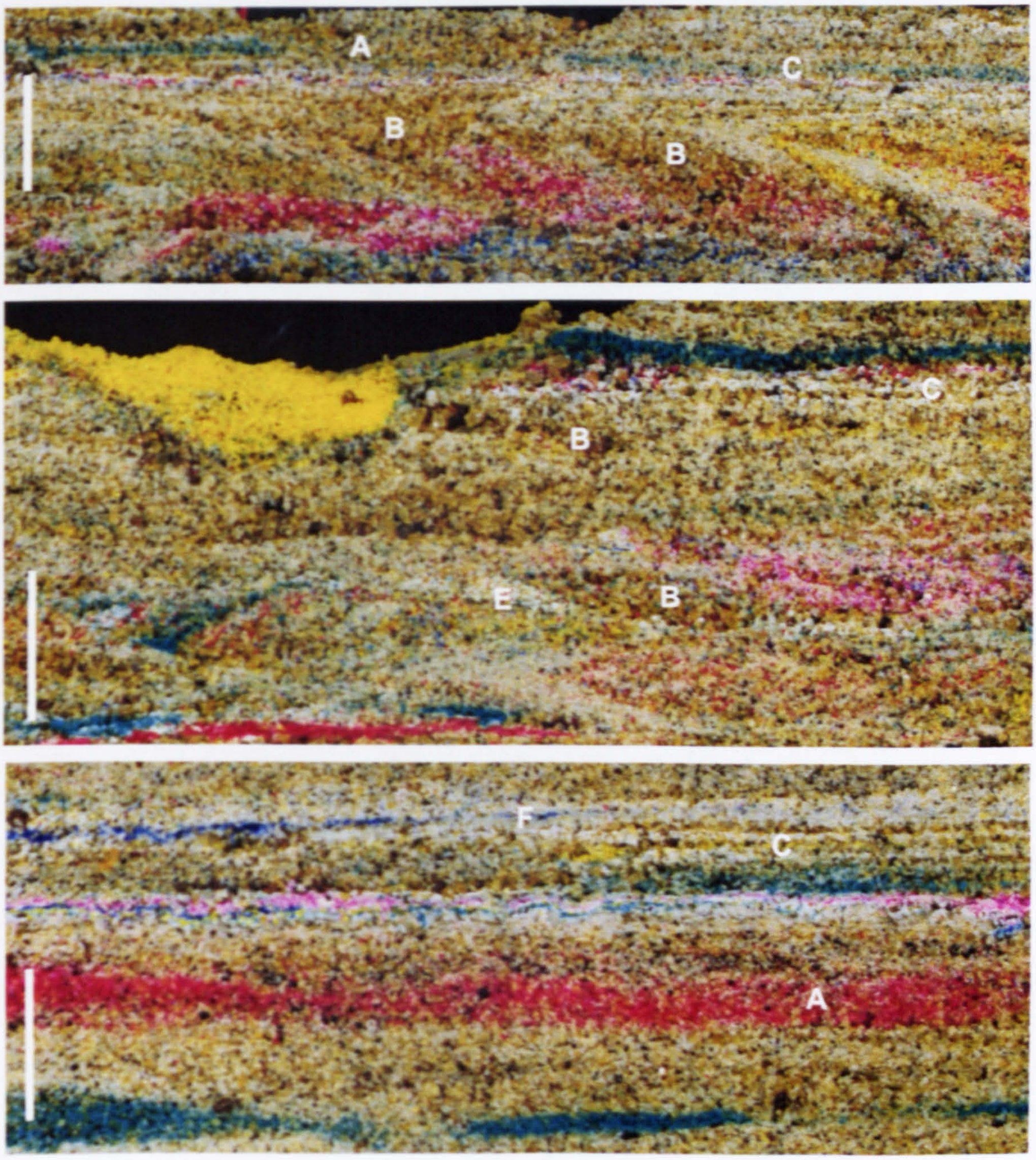

Figure 6.14 (b). Examples of architectural elements types A-F taken from the sections cut perpendicular to palaeoflow in series M. Where A = primary channel fills, B = secondary channel fills, C = splay, D = fine-grained channel fills, E = erosional remnants, and F = overbank fines. Refer to Table 6.6 for sedimentary descriptions. The scale bar in each case is 20 mm.

6.11 Frequency of occurrence of architectural elements

Horizontal proportion curves were constructed to characterise the relative proportion of architectural elements preserved in sequences from series F, M and C, using six cut-faces (11, 13, 15, 17, 19, 21, Chapter 5, Figure 5.17). These sections represented cross-sections at 0.2 m intervals in a downstream direction and were sampled at a 0.1 m horizontal spacing and a 0.005 m vertical spacing for the construction of horizontal proportion curves. Horizontal proportion curves were used to complement the data gathered on architecture element geometries (Section 6.10) by using the same sections. The use of horizontal proportion curves to depict spatially complex datasets provides a way of classifying cross-sections rapidly and reduces the uncertainties and subjectivity in the identification of all the boundaries of a particular architectural element. For example, where difficulties in exist in the identification of width because architectural elements may grade subtly into one another, the horizontal proportion curve method overcomes this problem by only characterising architectural element type using vertical profile sampling. Furthermore, previous studies have documented relative proportions of each architectural element as a percentage occurrence of the element type (Ashworth *et al.*, 1999), which again will bias the results towards the elements that are most easily identifiable. However, one disadvantage of horizontal proportion curves may be that they are influenced by the vertical and horizontal sampling frequency, which is explored further in Chapter 7, Section 7.8.1.

The percentage frequency of occurrence for each architectural element was calculated by summing the architectural element at each grid point for the sedimentary sequences from series C, M and F and results are shown in Figure 6.15. The additional assignment of a reference horizon, in this case the base of the flume facility allows the construction of vertical proportion curves (Figure 6.16).

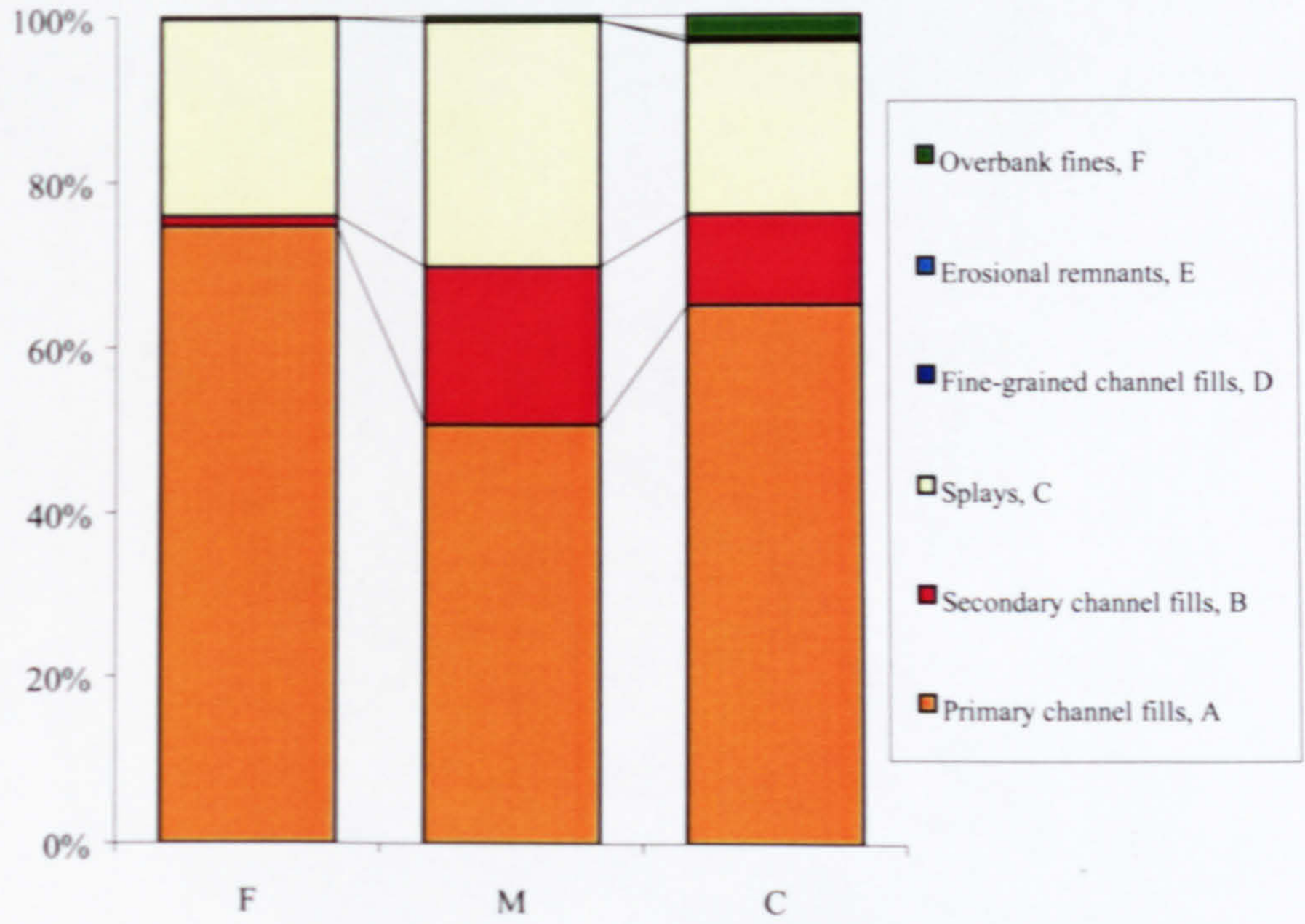

Figure 6.15. Frequency of occurrence for architectural elements observed in cut-sections from series F, M, and C.

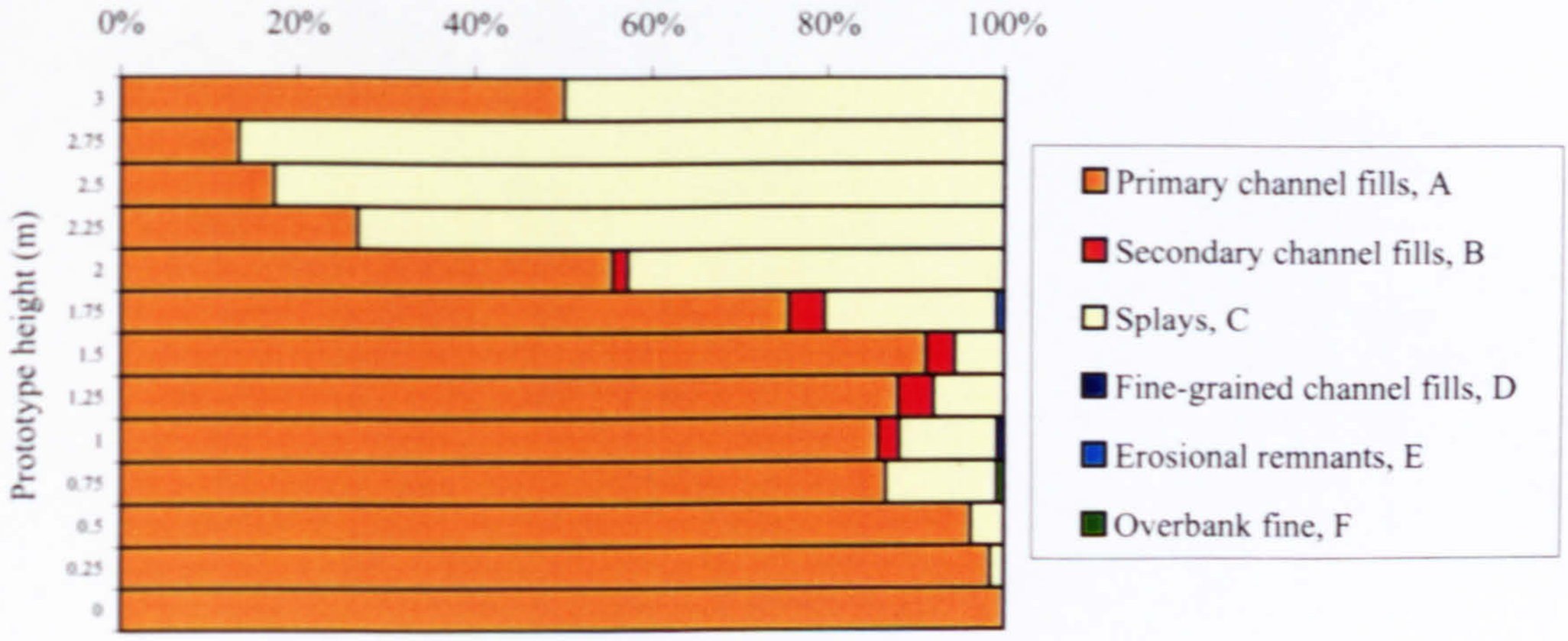

Figure 6.16. Vertical proportion curves for series F experiments, indicating an increase in the proportion of splay deposits towards the top of the sequences where the deposits became abandoned.

Analysis of the three experiments shows the preserved alluvial architecture is dominated by coarse-grained primary channel fill architectural elements (A), representing between ~70-80 % of the architectural element proportion with subordinate amounts of architectural element B (secondary channel fills deposits). Much of the internal fill of the channel deposits in series F is dominated by the reworking of sediment by ripples at low discharges. Analysis of the preserved splay deposits (C) shows there is a small increase in the proportion of this architectural element between series C and M, and a

decrease between M and F. The increase in occurrence of splay deposits between series C and M may be attributed to the increase in overbank sheet flow on the sediment surface between series C and M (Figure 6.6).

The proportion of fine-grained architectural elements (fine-grained channel fills, erosional remnants and overbank floodplain deposits) increases from 0.2 % - 0.6 % - 3.3 % in series F, M and C respectively. This increase in fine-grained deposits tentatively implies that more proximal coarse-grained deposits (gravel) may contain a higher proportion of fine-grained architectural elements (sand). However, these results need verifying with field analogues. Furthermore, the issue of whether the lower proportion of fine-grained architectural element observed between series C and F is a result of the progressive reduction in deposition of the fine particles between series C and F, or that the fine particles are deposited as interstitial fines within the coarse fabric rather than as discrete elements, is unclear. To resolve this issue in the future, grain size samples should be taken from all architectural elements to determine the proportion of interstitial fine-grained material preserved within the coarse-grained architectural elements. Possible reasons for the increase proportion of in fine-grained material preserved in discrete architectural element are explored in Section 6.11.1.

The top of the series F sequence displayed an increase in the preservation of splay architectural elements (Figure 6.16) that reflects the relationship between the time taken to rework the deposits and the length of time available before complete abandonment of the channel-belt occurs. Consequently, the sequence in series F may represent two forms of preserved deposits: (1) primary deposits and (2) reworked deposits. Therefore, the final preserved thickness of series F may only represent a completely reworked sequence when the deposits have exceeded approximately two formative channel depths of ~1 m when scaled up (cf. Figure 6.4 and Figure 6.16). The differences observed in the proportions of architectural elements between series C-M and C-F may be a result of series C deposits being fully reworked by subsequent experiments, whilst in the cases of series M and F, these top experimental sequences were relatively untouched. The implication from the FSM results suggest that when examining modern surface sediments some consideration is required for how representative the proportion of architectural elements in the immediate subsurface are to the proportions of architectural elements at depths below the level of several channel depths where increased reworking has occurred.

6.12 Two-dimensional architectural element geometry

Maximum widths and thickness were measured for 1063 coarse-grained and 663 fine-grained architectural elements in the three experiments. Architectural element geometries were compared between preserved experimental sequences. Table 6.7 shows summary statistics for the coarse-grained architectural elements and Table 6.8 for the fine-grained architectural elements (refer to Table 6.6 for element descriptions). Dimensions were measured on the photographs to an accuracy of ±0.5 mm (section data from series C and F had a 1:1 scaling of photograph to actual size, while series M involved an up-scaling by 1.31). A correction factor was applied to the photograph scale and scaled up by 1:50 for comparison with the prototype and the literature. For comparison box and whisker plots are presented (Figures 6.17-19) along with PDF's that have been plotted for the widths of all architectural elements (Figures 6.20-21) and for width/thickness ratios for the coarse-grained elements only (Figure 6.22).

Table 6.7. Geometrical dimensions for the coarse-grained architectural elements observed in the sections of the three experiments of series C (standard text), M (italics) and F (bold) grain size distributions

	Width (m)						Thickness (m)					
	n	Mean	Median	Standard deviation	Min	Max	Mean	Median	Standard deviation	Min	Max	W/T
A	215	7.52	6.85	3.57	1.75	19.20	0.42	0.40	0.16	0.15	1.13	19.24
	118	*6.74*	*6.72*	*2.60*	*1.11*	*15.13*	*0.41*	*0.42*	*0.19*	*0.08*	*0.95*	*19.85*
	97	**11.52**	**9.60**	**7.73**	**1.60**	**46.35**	**0.72**	**0.65**	**0.30**	**0.15**	**1.55**	**16.20**
B	106	3.31	3.01	1.44	1.10	7.20	0.49	0.46	0.17	0.18	0.98	7.09
	126	*2.19*	*2.06*	*0.73*	*0.65*	*3.97*	*0.39*	*0.36*	*0.14*	*0.10*	*0.86*	*6.00*
	29	**2.26**	**1.95**	**1.07**	**0.75**	**5.05**	**0.38**	**0.30**	**0.14**	**0.15**	**0.75**	**6.01**
C	218	6.17	5.50	3.10	0.65	16.55	0.21	0.20	0.10	0.08	0.58	33.75
	105	*7.71*	*6.87*	*4.13*	*1.34*	*21.60*	*0.19*	*0.17*	*0.09*	*0.06*	*0.46*	*46.92*
	49	**13.44**	**10.90**	**8.90**	**0.70**	**37.60**	**0.34**	**0.33**	**0.15**	**0.15**	**0.88**	**41.97**

Table 6.8. Geometrical dimensions for the fine-grained architectural elements observed in the sections of the three experiments of series C (standard text), M (italics) and F (bold) grain size distributions.

	Width (m)						Thickness (m)					
	n	Mean	Median	Standard deviation	Min	Max	Mean	Median	Standard deviation	Min	Max	W/T
D	9	1.30	1.50	0.42	0.60	1.85	0.14	0.13	0.04	0.10	0.20	9.94
	2	*0.19*	*0.19*	*0.11*	*0.11*	*0.27*	*0.03*	*0.03*	*0.01*	*0.02*	*0.04*	*8.50*
	7	**1.38**	**1.15**	**0.73**	**0.60**	**2.30**	**0.24**	**0.25**	**0.10**	**0.13**	**0.08**	**5.70**
E	206	0.67	0.49	0.51	0.08	2.45	0.07	0.05	0.05	0.03	0.35	11.46
	56	*0.47*	*0.38*	*0.31*	*0.10*	*1.56*	*0.04*	*0.04*	*0.02*	*0.02*	*0.13*	*14.00*
	25	**0.43**	**0.40**	**0.27**	**0.05**	**1.15**	**0.08**	**0.08**	**0.07**	**0.03**	**0.35**	**6.57**
F	218	1.65	1.25	1.35	0.15	8.85	0.08	0.05	0.06	0.03	0.35	24.76
	118	*0.59*	*0.44*	*0.62*	*0.08*	*4.85*	*0.05*	*0.04*	*0.04*	*0.02*	*0.19*	*17.11*
	22	**0.85**	**0.56**	**0.74**	**0.20**	**3.05**	**0.04**	**0.03**	**0.03**	**0.03**	**0.10**	**23.01**

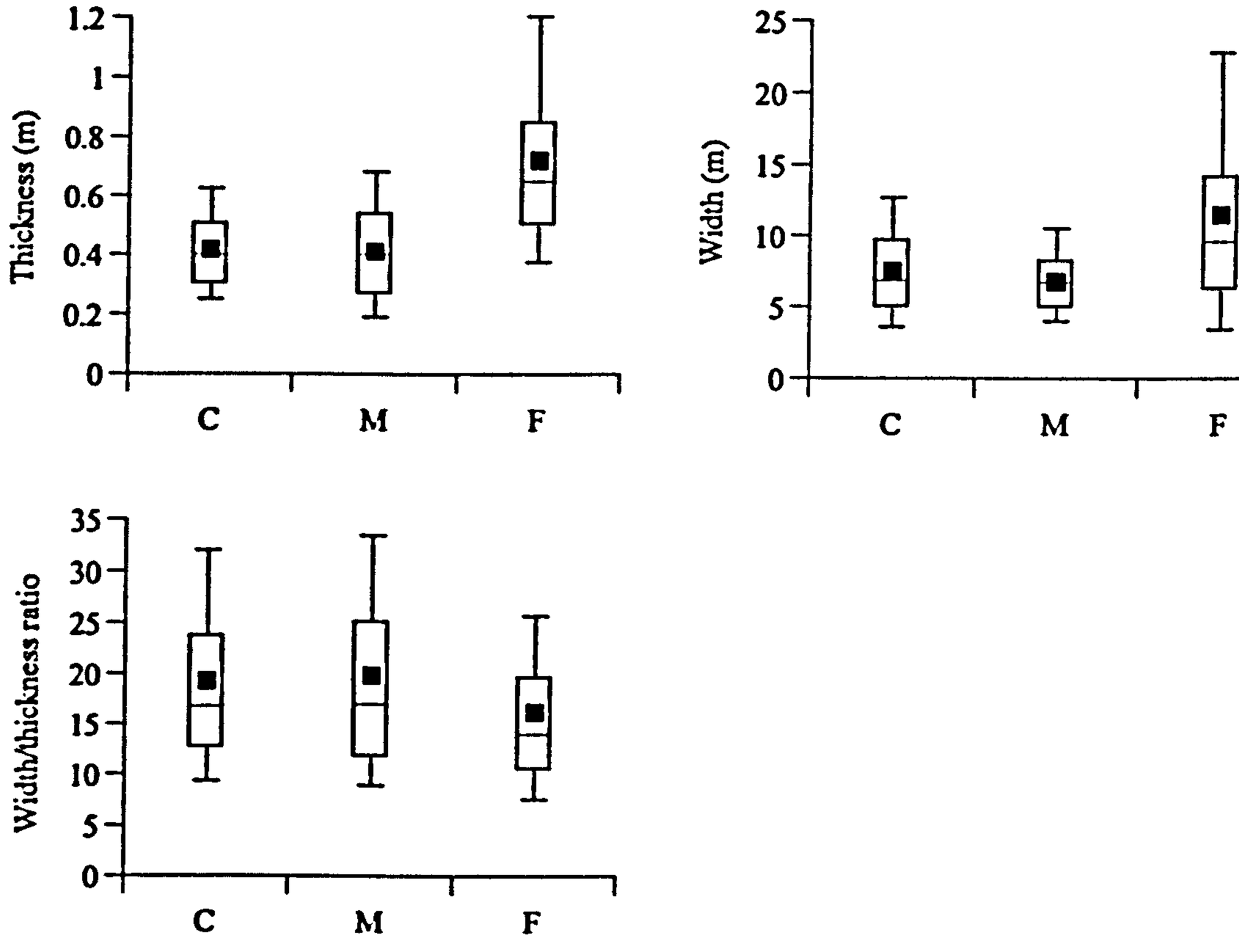

Figure 6.17. Geometrical information for architectural element A, primary channel fills.

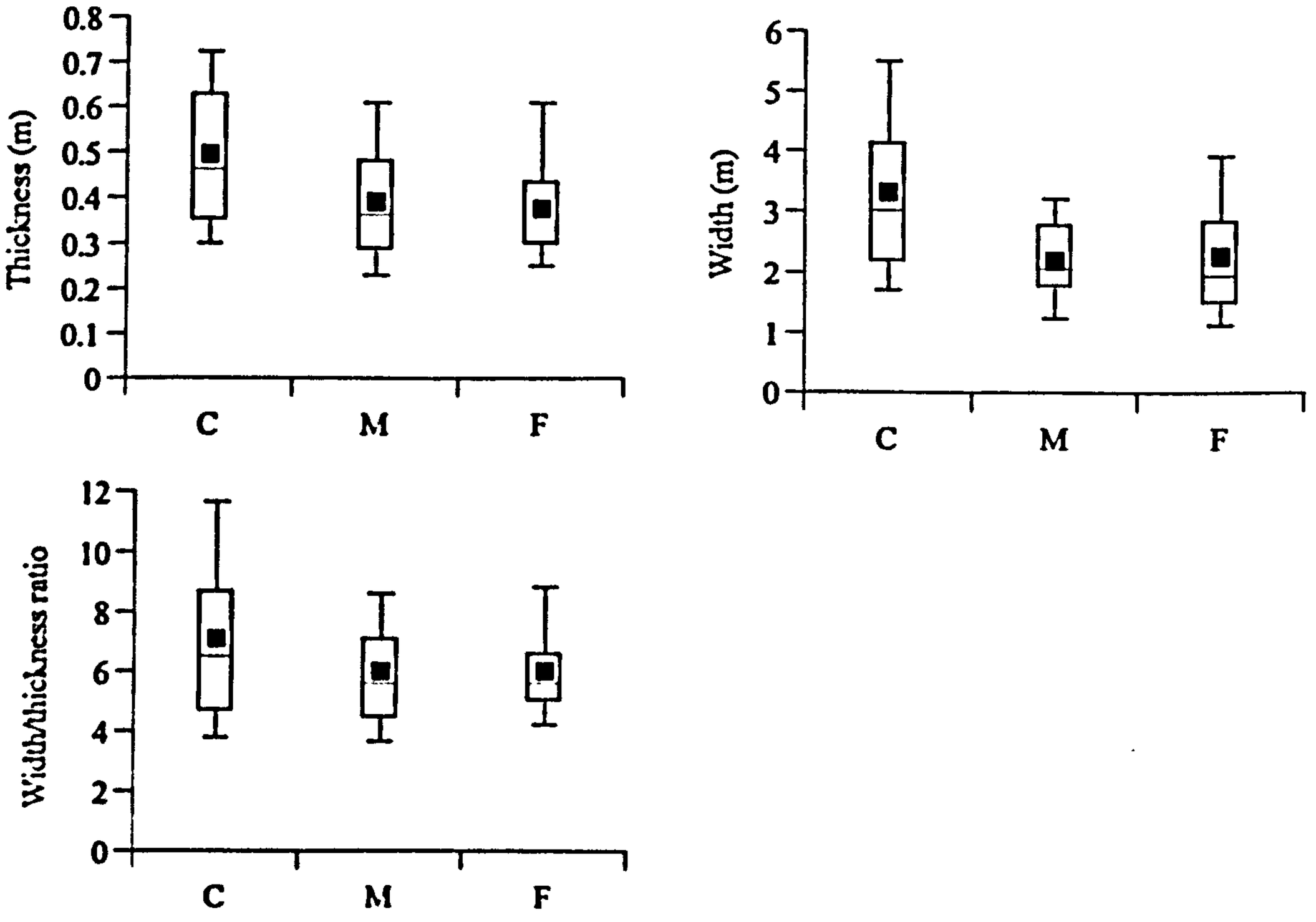

Figure 6.18. Geometrical information for architectural element B, secondary channel fills.

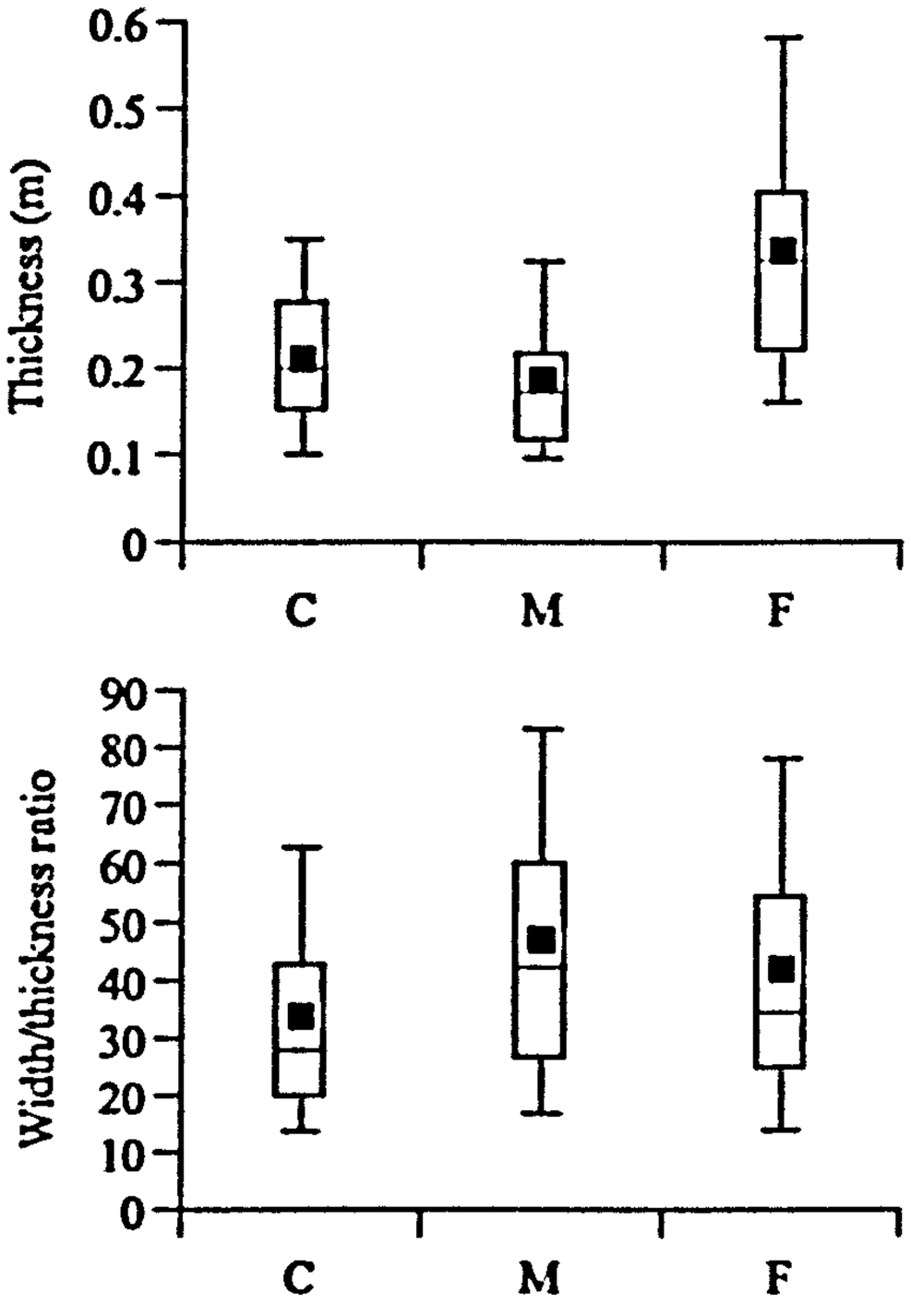

Figure 6.19. Geometrical information for architectural element C, splays.

The preservation potential of individual architectural elements is a function of initial depositional geometry and subsequent reworking within the aggrading channel-belt. No statistical significant difference in the geometry of primary channel fill deposits was recorded between series C and M, while a significant increase in the primary channel fill width and thickness was observed between series M and F, probably in relation to the larger formative channel depths in series F (Figure 6.4). Splay widths show a significant increase between C-M and then M-F, which may be related to the progressive increased proportion of sheet flow on the sediment surface between series C to F (Figure 6.6). No corresponding increase is observed with splay thickness and width/thickness ratios show a significant increase between series C and M, and no significant change between series M and F. These results are also reflected in the PDF's for architectural elements shown in Figures 6.20-22.

a

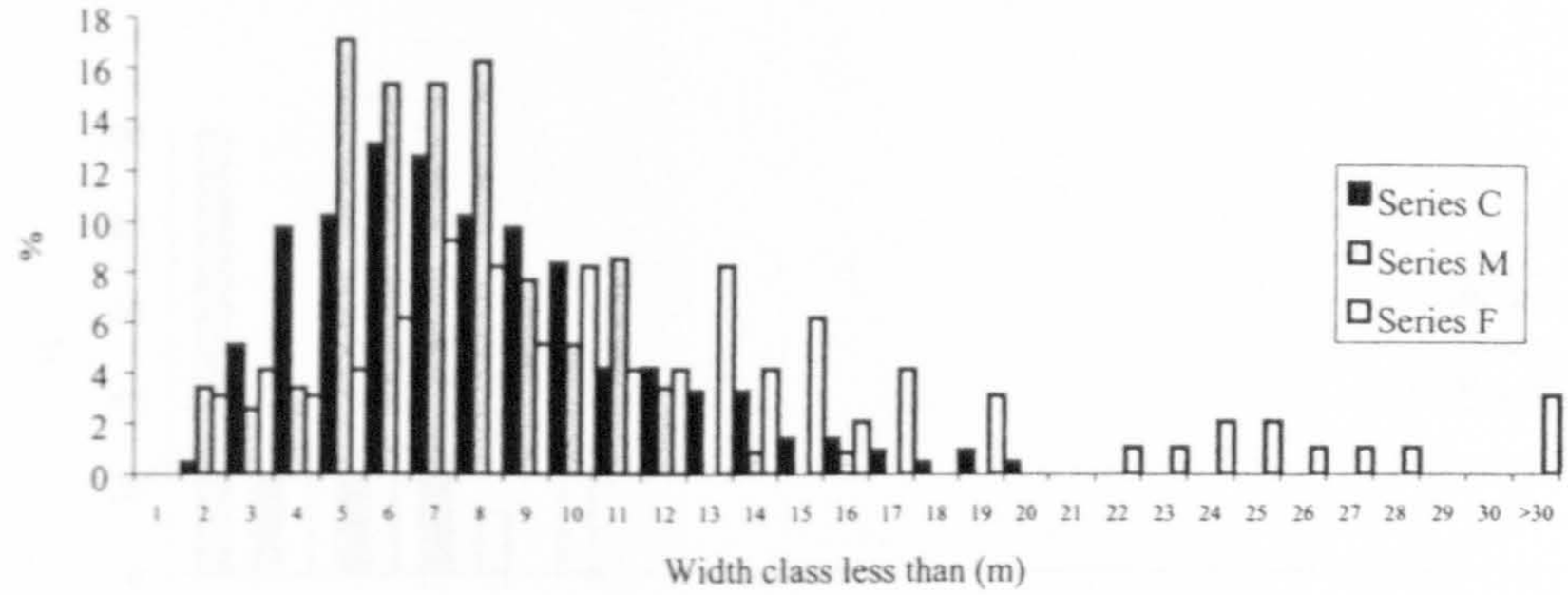

b

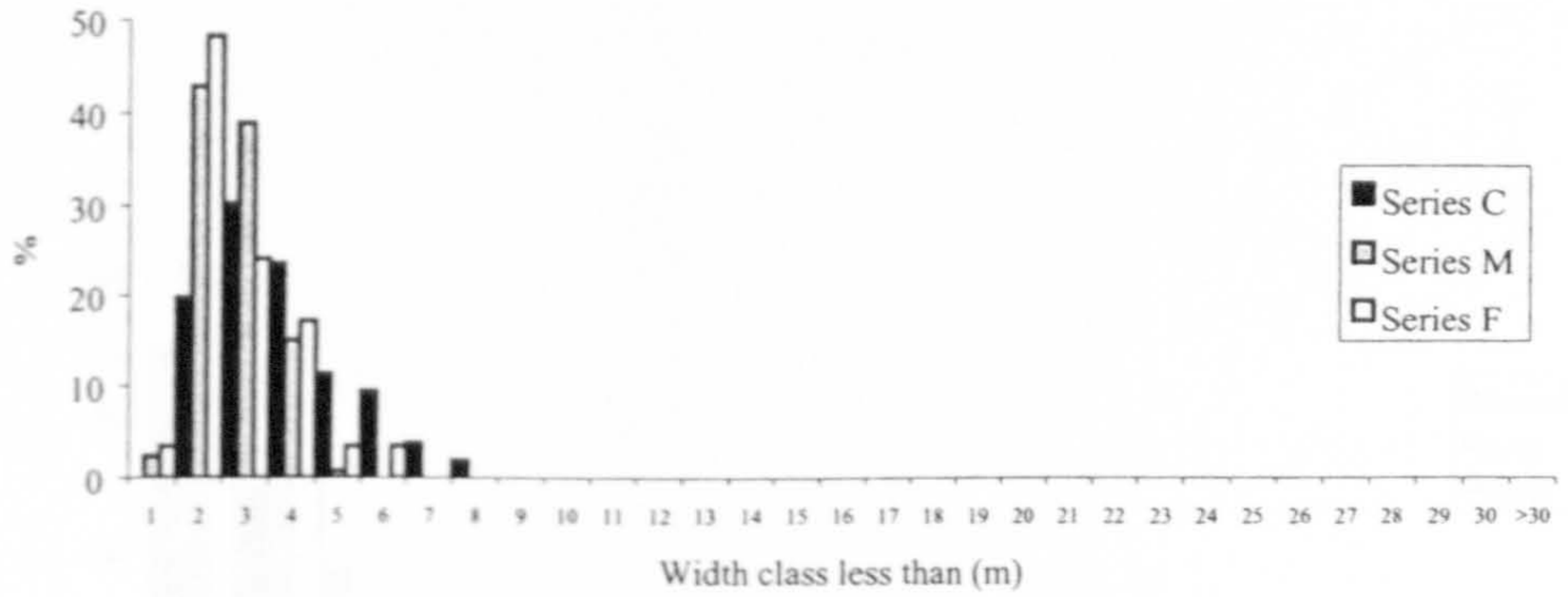

c

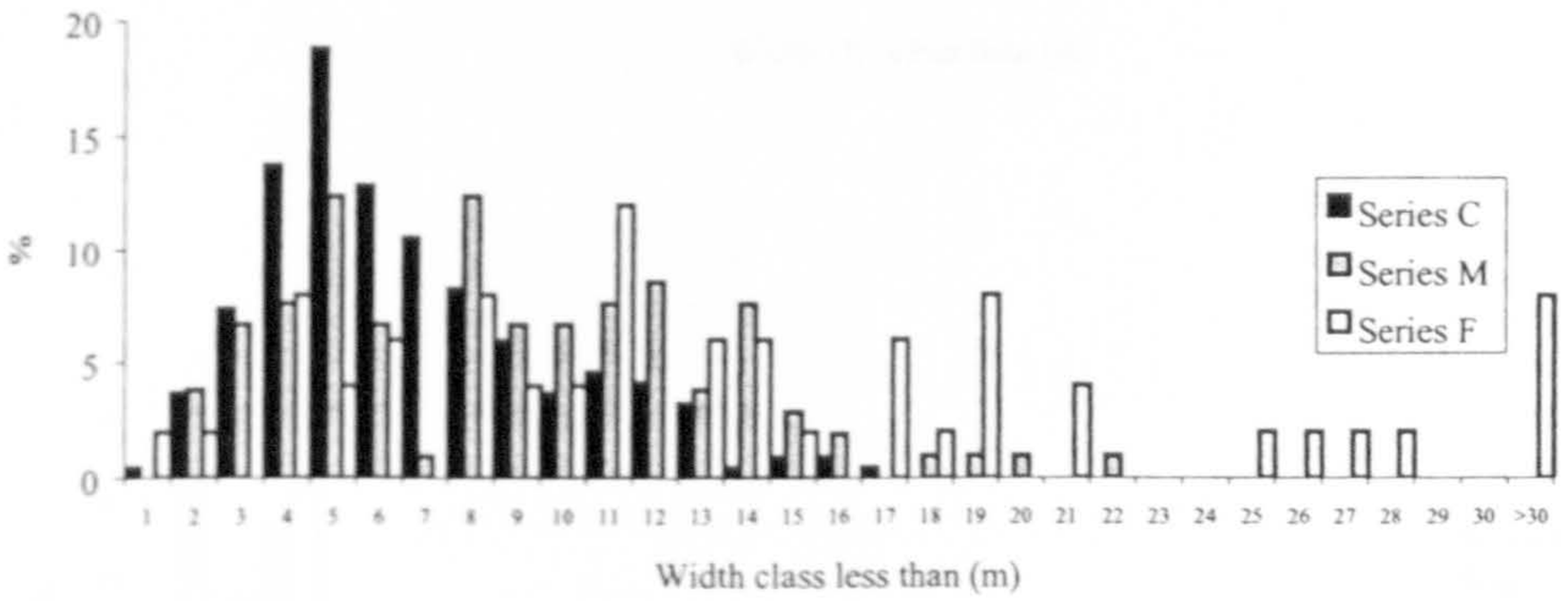

Figure 6.20. Probability density functions for width distributions of coarse-grained architectural elements (a) primary channel fills, (b) secondary channel fills, and (c) splays observed within the three experiments. Note the similarity of series C and M, but an extended width distribution of series F in (a) and (c).

a

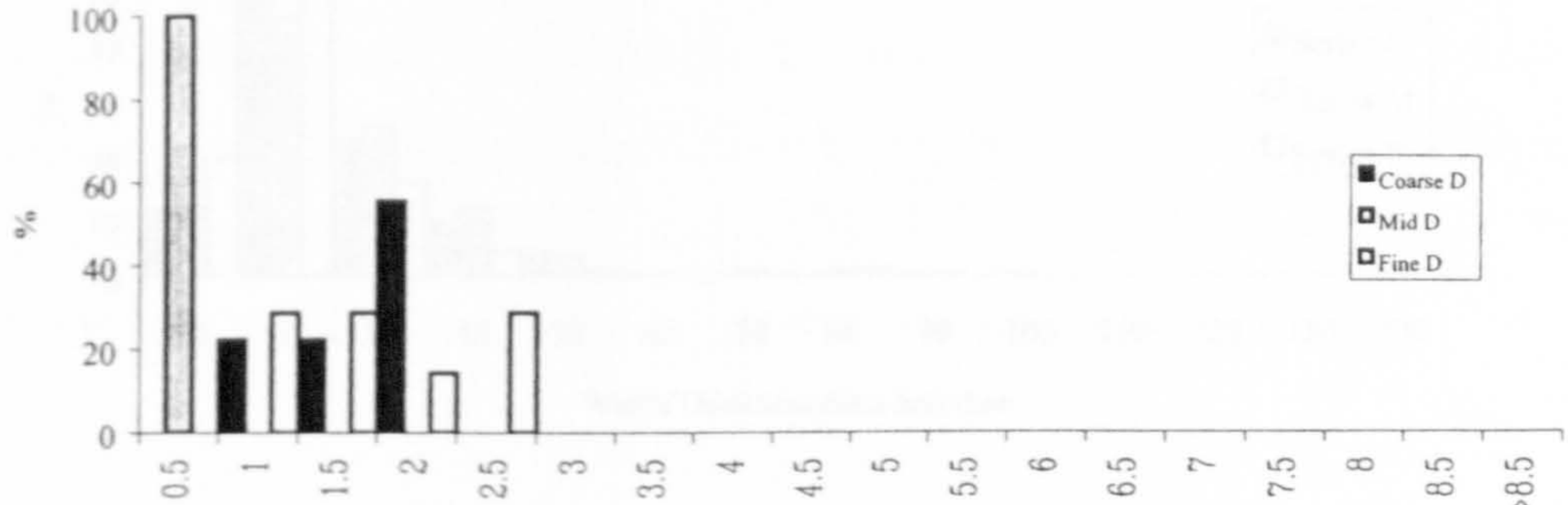

b

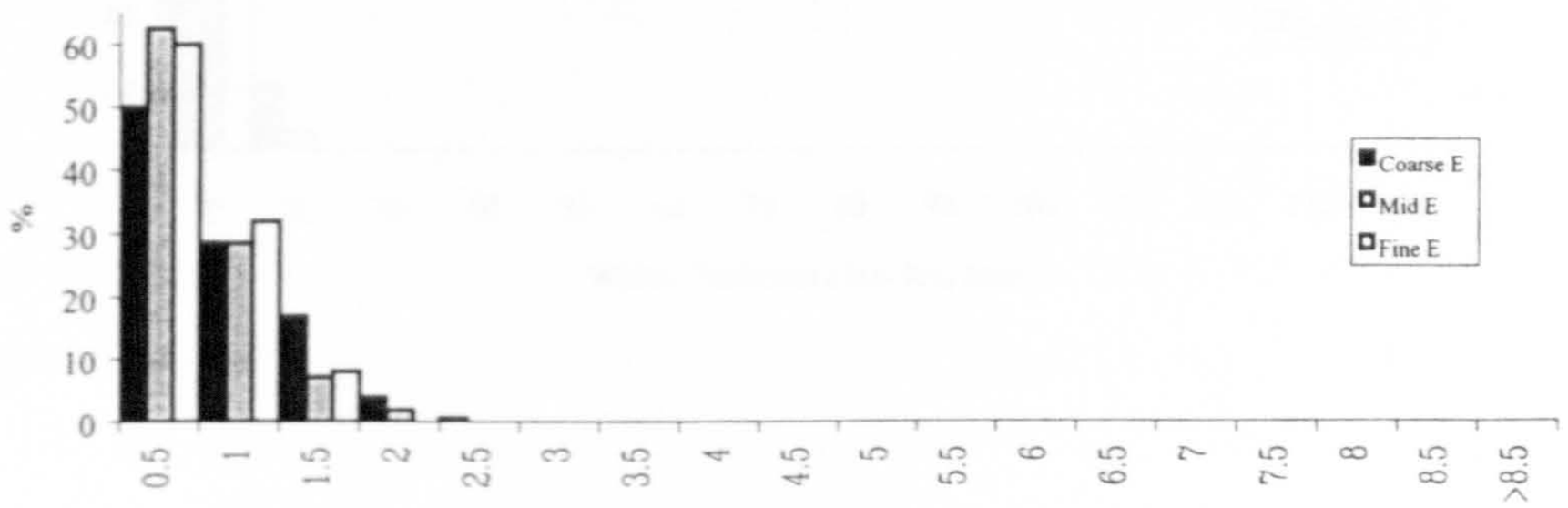

c

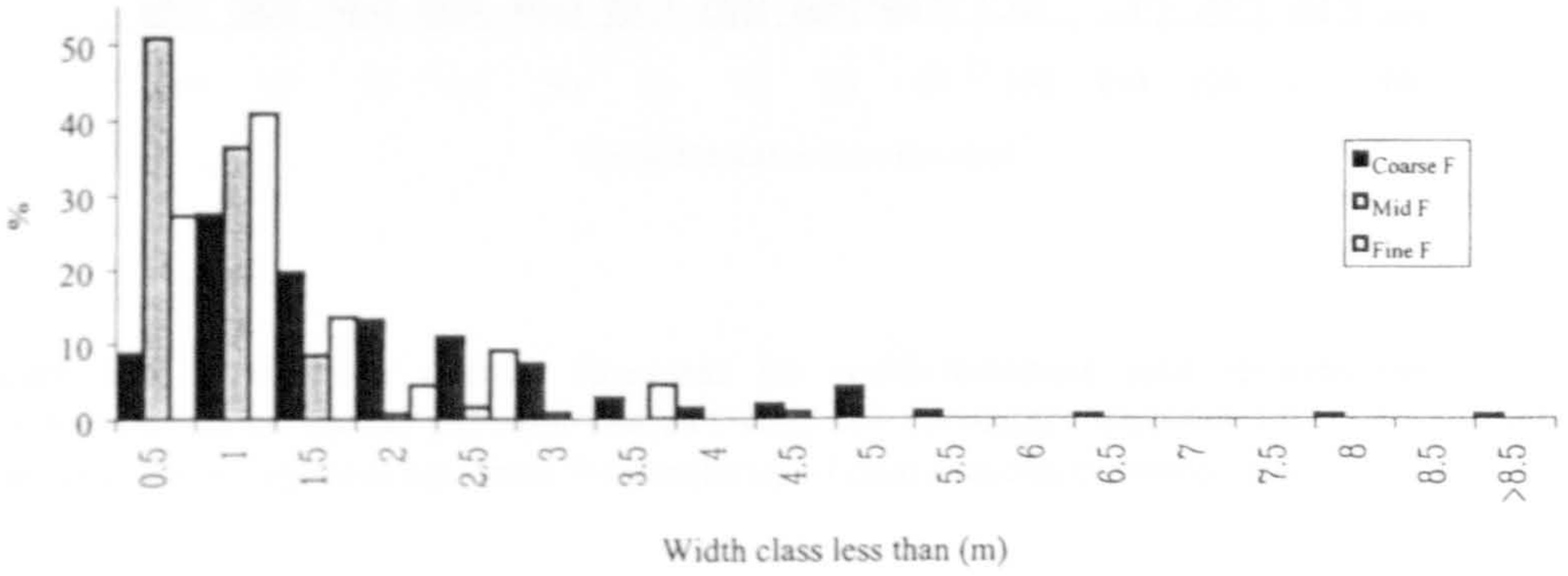

Figure 6.21. Probability density functions for the width distributions of fine-grained architectural elements (a) channel fills, (b) erosional remnants, and (c) overbank fines observed within series C, M and F.

a

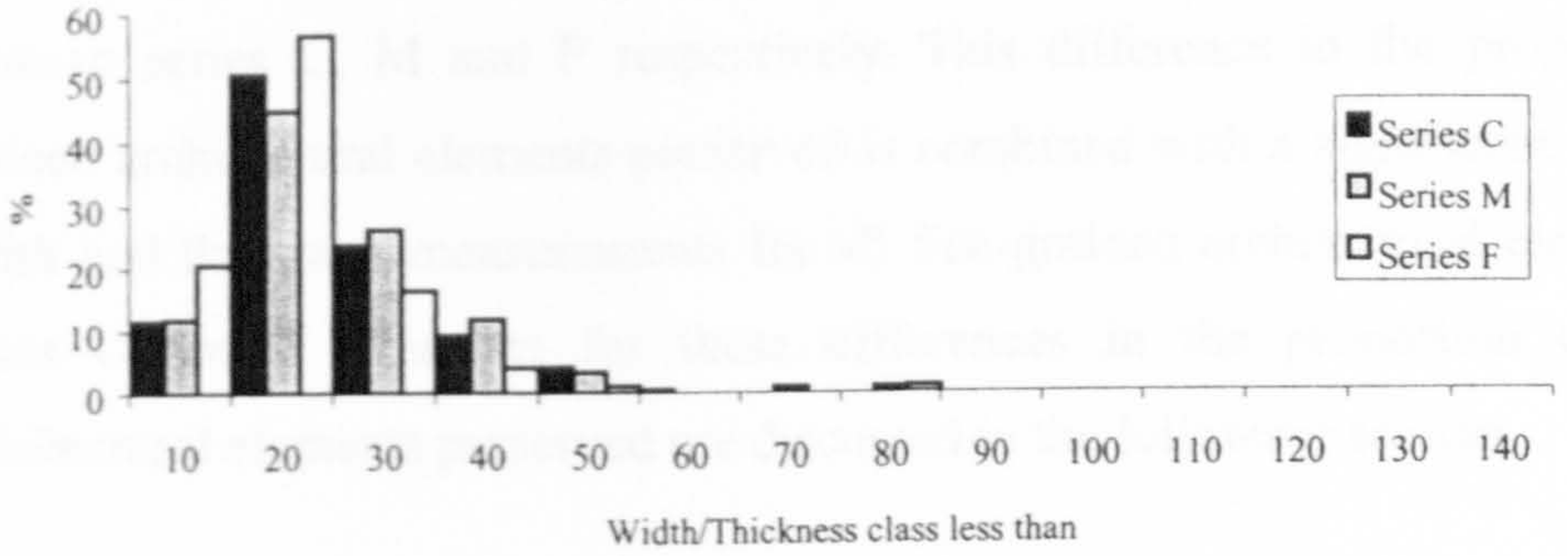

b

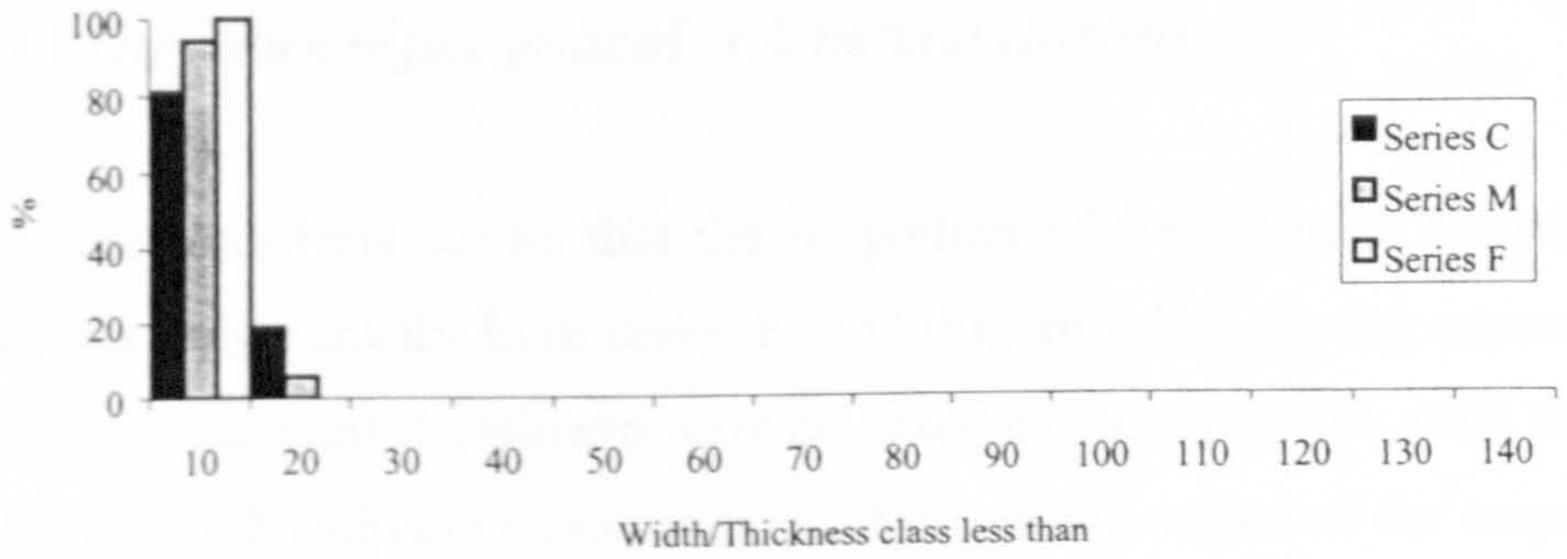

c

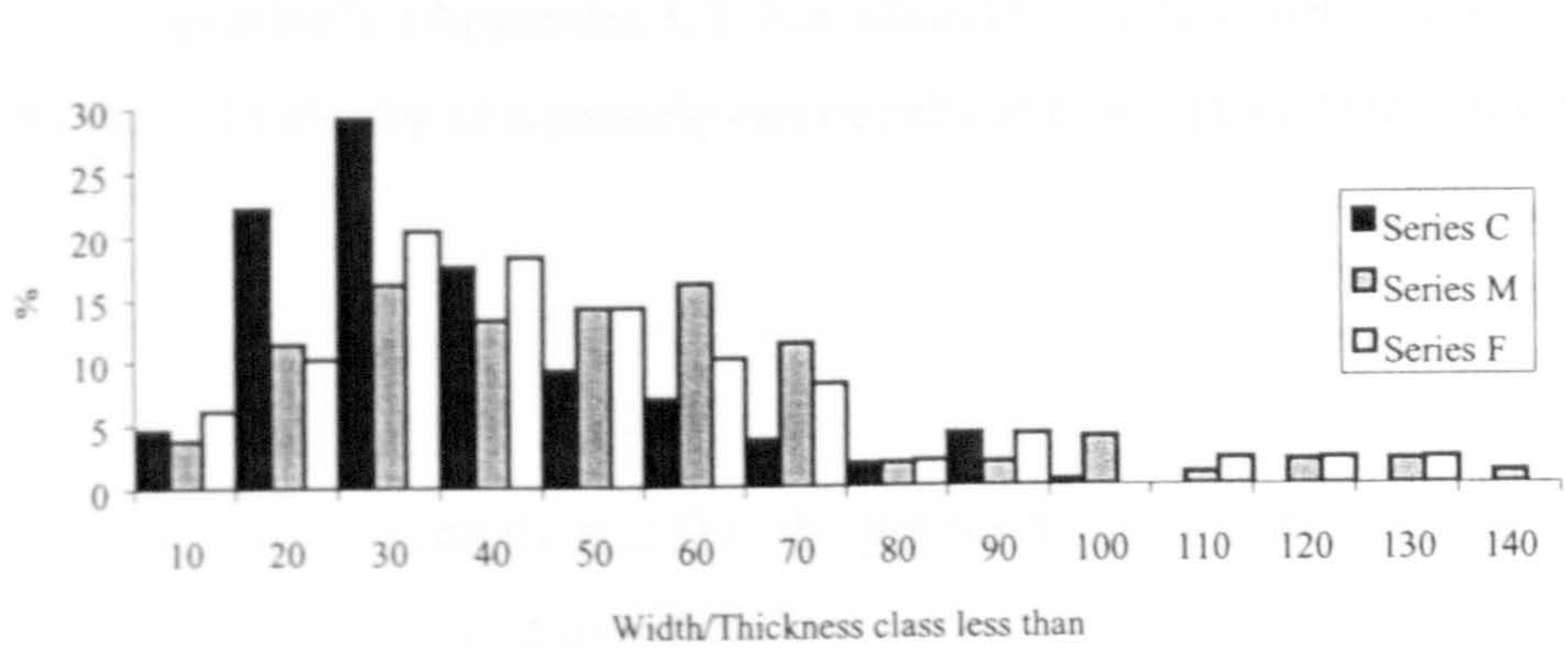

Figure 6.22. Probability density functions for width/thickness ratio distributions of coarse-grained architectural elements (a) primary channel fills, (b) secondary channel fills, and (c) splays observed within the three experiments. Note the similarity of distributions between series C, M and F.

Analysis of the stacked bar graphs for all three experiments (Figure 6.15) shows a decrease in the proportion of fine-grained elements (D-F) from 3.3 % to 0.6 % to 0.2 % between series C, M and F respectively. This difference in the proportion of fine-grained architectural elements preserved is combined with a significant decrease in the width and thickness measurements for all fine-grained architectural elements between series C and F. Reasons for these differences in the proportion of fine-grained architectural elements preserved are discussed in the following section.

6.12.1 Deposition of fine-grained architectural elements

Cut-section analysis shows that the proportion of fine-grained deposits (silica flour) increases progressively from series F to C (Figure 6.15). During experiments C and F samples of suspended sediment were collected and analysed for grain size distributions and suspended sediment concentrations. Average D_{50} values of the suspended sediment concentrations sampled for series F and C are 0.0011 mm (n=28) and 0.0015 mm (n=29) respectively (Appendix C). For particles smaller than 0.1 mm (Peakall *et al.*, 1996) the fall velocity of a particle can be related to the grain size using Equation 6.1:

$$U_f \propto D^2 \qquad \text{Equation 6.1}$$

where U_f is the fall velocity and D is the grain size. Therefore, settling velocities will be lower in series F compared to series C.

The differences in concentration of suspended sediment between series C and F can also be related to fall velocity using Equation 6.2 from Richardson and Zaki (1958). Figure 6.23 shows the results of suspended sediment concentrations measured during series F and C. Using suspended sediment concentrations from series C and F, the fall velocity of a spherical particle v_s', in a dispersion of other falling grains was calculated using Equation 6.2.

$$v_s' = v_s (1-C)^n \qquad \text{Equation 6.2}$$

where v_g is the fall velocity of a single grain (D_{50}) in an otherwise grainless fluid, C is the volume concentration of grains in the falling dispersion, and n is an exponent varying between 2.32 and 4.65. The calculation in the experimental runs has to be first converted to a volume percentage from a weight percentage by using densities of 1000 kg m^{-3} for water and 2650 kg m^{-3} for silica flour and sand. Figure 6.23 shows the suspended sediment concentrations increase at a greater rate in series F compared to series C.

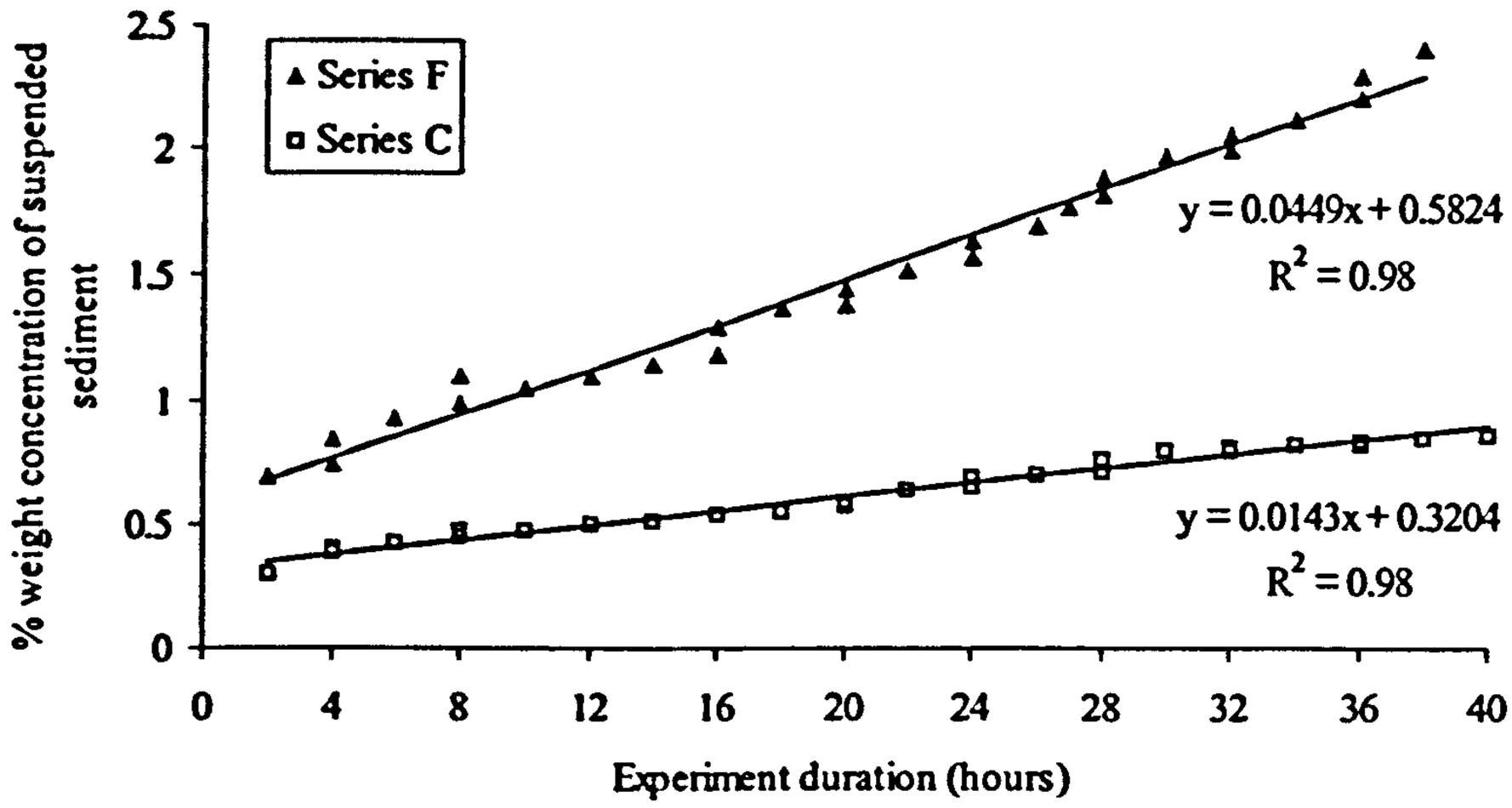

Figure 6.23. Running mean of suspended sediment concentrations by weight for series C and F, measured during at minimum discharge (0.31 l s^{-1}). Note the higher rates for series F compared to C.

Figure 6.23 shows that the higher concentration of suspended sediment in series F may cause lower fall velocities than in series C. Calculated settling velocities resulting from series C and F show the greater suspended sediment concentrations observed in series F (Figure 6.24) would result in lower fall velocities and consequently, fine suspended sediment would be inhibited from settling in series F. Moreover, lower fall velocities will keep the fine-grained material in suspension and prohibit fines being deposited and subsequently being preserved as fine-grained architectural elements.

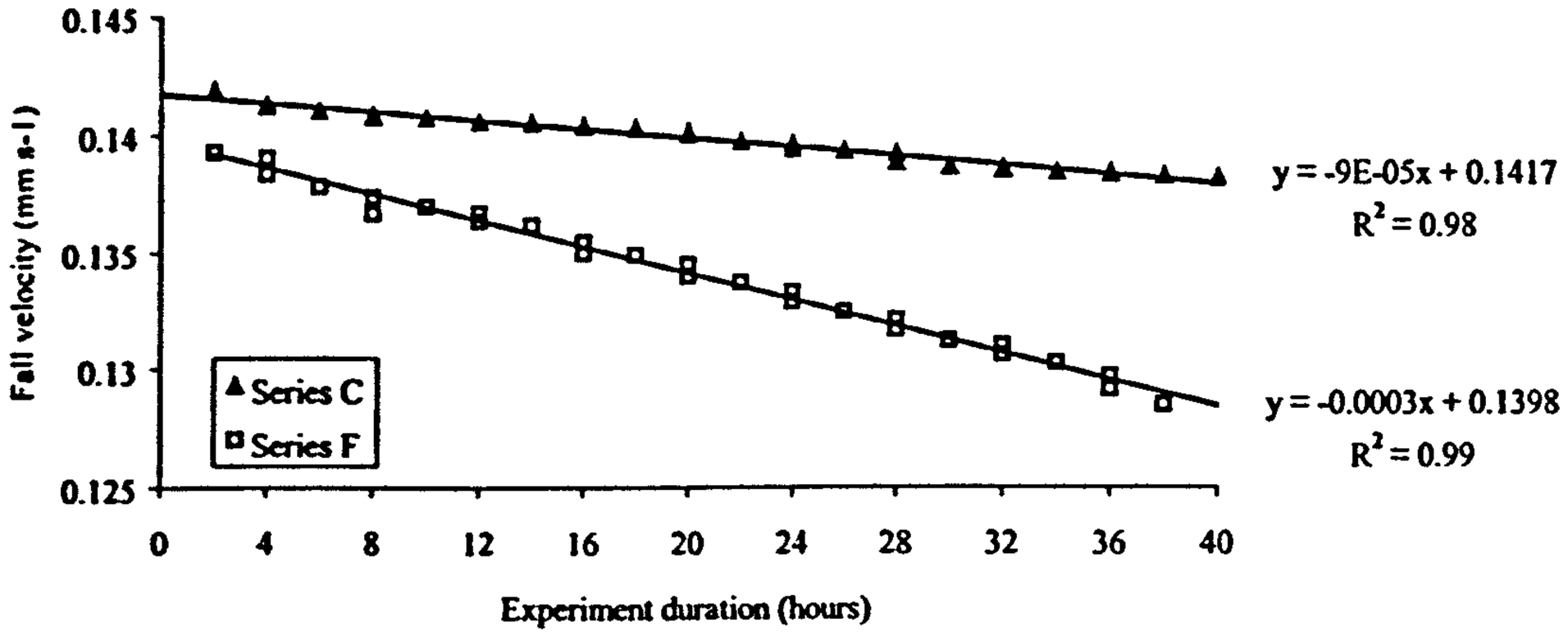

Figure 6.24. Calculated fall velocities for particles in suspension in series C and F based on sediment concentration presented in Figure 6.23. Note: the vertical exaggeration.

Possible reasons for the increase in the proportion of fine-grained architectural elements with an increasing grain size can be summarised by: (1) smaller D_{50} values of suspended sediment in series F causing a lower fall velocity of a particles in series F compared to series C, which inhibits the settling out of suspended sediment; (2) the higher suspended sediment concentrations in series F causing a reduced settling of fine-grained deposits, creating less opportunity for preservation of these fines; and (3) the higher aerial proportion of sheet flow and wider channels present on the sediment surface in series F may prohibit settling of fine-grained silica flour, by inhibiting the ponding of water.

If natural systems follow the same general trends, sand deposited in discrete architectural elements may have a higher frequency of occurrence in coarser-grained gravels (i.e. more proximal positions on the long profile). These results need further field study validation to assist in interpreting the occurrence and preservation potential of fine-grained deposits in fluvial sequences.

6.13 Preservation potential

Comparisons have been made between the mean values of surface channel geometries (width and depth) measured in Section 6.12 and the mean values of the preserved channel fill geometries (width and thickness) for all primary and secondary channel fill deposits (architectural elements A and B). The results displayed in Table 6.9 shows the mean values for preserved thickness in series C and F are greater than the means of the formative channel depths, while series M shows a lower preservation potential. All values lie above the range of 40-75 % for preserved channel fill thickness defined by Paola and Borgman (1991) who assume no deposition occurs. Therefore, as the physical model is an aggrading braided river system, the results may reflect the process of vertical aggradation and/or scour of the individual channels (described in Salter, 1993) to produce higher preserved thicknesses than those of Paola and Borgman (1991). Furthermore, this vertical thickening may be occurring in preference to lateral migration.

Mean values of preserved channel fill widths in all experiments are between 32-69 % of their original formative channel widths. Comparison of preserved geometries to formative width and depth, indicate width/thickness ratios of preserved channel fill geometries that are between 34-53 % of their original values. Therefore, channel fills are narrower than the formative channel widths suggesting that processes such as avulsion are occurring, which dissect the original channel fill deposits before aggradation allows the original channel geometry to be preserved. These results may suggest that avulsion is a more important process than lateral migration in creating the final preserved architectural form. These issues are addressed further in the discussion.

Table 6.9. Comparisons of formative channel width and depth data with preserved channel fill width and thickness data from the Ashburton model. The mean values of maximum channel depth were used.

Series	Surface channel geometries			Preserved channel fills			Surface/subsurface ratio		
Mean	Depth (m)	Width (m)	W/D	Thickness (m)	Width (m)	W/T	Thickness	Width	W/T
C	0.3	8.9	30.4	0.4	6.1	16.0	1.32	0.68	0.53
M	0.4	14.2	37.0	0.4	4.4	12.7	0.92	0.31	0.34
F	0.5	15.7	31.6	0.6	9.4	13.9	1.28	0.60	0.44
Maximum									
C	0.8	17.8	72	1.1	19.2	52.7	1.39	1.08	0.73
M	0.6	20.2	74	1.0	15.1	72.8	1.53	0.75	0.98
F	1.1	42.8	77	1.6	46.4	75.5	1.41	1.08	0.98
Minimum									
C	0.1	3.3	9.1	0.2	1.1	2.0	1.14	0.33	0.22
M	0.3	7.8	17	0.1	2.0	2.5	0.30	0.25	0.15
F	0.2	3.0	11	0.2	0.8	2.6	0.61	0.25	0.23

6.14 A summary of the impact of grain size on within channel-belt channel morphology and alluvial architecture

A summary of the statistical differences at the 95 % significance level between series C, F and M are displayed in Table 6.10. These results can be applied in two ways to alluvial architecture models: (1) as a comparison between different sediment sourced river systems or, (2) a comparison between reaches on the same river long profile exhibiting a downstream fining trend with no overall change in sorting.

Table 6.10. Summary information on the statistical differences using the Kruskal-Wallis test between series C - M - F, showing at the 95 % confidence limit the + represents a significant increase and – a significant decrease in the variables. Where no symbol is present, no significant differences between the series was found.

	Series	C⇒M	M⇒F
Surface channel morphology			
	Channel width	+	
	Channel depth		+
	Channel w/d ratio		
	Braidplain slope		+
	Duration of channel occupancy		
Architectural elements			
A (Primary channel fills)	Width		+
	Thickness		+
	W/T ratio		–
B (Secondary Channel fills)	Width	–	
	Thickness		–
	W/T ratio	–	
C (Splays)	Width	+	+
	Thickness	–	+
	W/T ratio	+	
D (Fine-grained channel fills)	Width*	–	+
	Thickness*	–	+
	W/T ratio*		
E (Erosional remnants)	Width	–	
	Thickness	–	
	W/T ratio	+	–
F (Overbank fines)	Width	–	
	Thickness	–	–
	W/T ratio		–

* Comparisons were conducted with a small sample number.

6.15 Three-dimensional element architecture

Previous physical modelling work by Ashworth and Best (1994) has showed that the shape of PDF's for shale lengths in both the downstream and cross-stream orientations were similar and therefore, architectural element dimensions may be considered isotropic. Wadman *et al.* (1979) and Haldorsen *et al.* (1987) assumed an aspect ratio, defined by width/length for shales of 0.33 for the Prudhoe Bay Field and used the same value to calculate shale volumes. Ashworth *et al.* (1994) measured aspect ratios for different sedimentary surface deposits in a scaled braided model, and found a mean of 0.47 and varied according to depositional element type. However, work by Ashworth and Best (1994) indicates that the surface aspect ratio of shales is subsequently modified as channels bifurcate at high angles to the mean flow direction causing a shift towards a more equant preserved depositional geometry. Although, the analysis of the surface channel morphology and alluvial architecture is confined to two-dimensional analysis in this thesis, future physical modelling may quantify the three-dimensional geometries of the architectural elements.

6.16. Comparison of prototype and model alluvial architectural

Qualitative analysis of alluvial architecture exposed in the Canterbury Plains cliff section at the present day coastline reveals similarities to the depositional architecture displayed in the FSM. Examples of architectural elements from the Canterbury Gravels are shown in Figure 6.25. In light of the results described in Section 6.12.1 highlighting the differences in the proportion and size of the fine-grained architectural elements (D-F) measured in the model, and the difficulties in identification of coarse-grained architectural elements (A and C) in the field as a result of weathering causing difficulties to distinguish lateral boundaries, quantitative comparison between prototype and model architecture has been confined to coarse-grained secondary channel fill deposits (architectural element B). Architectural element B is analogous to the coarse-grained channel fill depositional niche described in Ashworth *et al.* (1999).

Figure 6.25. Examples of architectural elements observed within the Canterbury Gravels, New Zealand. Where A = primary channel fills, B = secondary channel fills, C = splay, D = fine-grained channel fills, E = erosional remnants, and F = overbank fines. White scale bars represent 0.5 m.

Comparisons (Table 6.11) suggest prototype coarse-grained channel fills exhibit width and thickness magnitudes greater than double the magnitude of the mean width and thickness measurement in the model. Nevertheless, similar width/thickness ratios suggest a scaling factor may be applied to up-scale the model architectural datasets. Application of scaling factors requires further investigation.

Table 6.11. Two-dimensional geometries of coarse-grained channel fill architectural elements B measured from the Ashburton model and the Canterbury Gravels as documented in Ashworth *et al.* (1999).

	Canterbury Gravels coarse-grained channel fills		Ashburton model architectural element B	
	Width (m)	Thickness (m)	Width (m)	Thickness (m)
N	24	24	126	126
Mean (m)	6.79	1.25	2.19	0.39
Minimum (m)	3.52	0.65	0.65	0.10
Maximum (m)	15.8	2.26	3.97	0.86
Width/thickness ratio	5.45		6.00	

The difference in coarse-grained channel fill geometries may be a result of some of the underlying assumptions in the FSM. Firstly, the model only represents, at the reach scale, part of a single channel-belt system, therefore processes such as avulsion and migration may be limited, and secondly the model is a generic model of the Ashburton River and therefore not mimicking a specific reach. Consequently, while the surface channel geometries between prototype and model may scale on a ~1:1 basis (Section 6.5), the model is not capturing the natural depositional complexity imposed on the system by the interaction of multiple channel-belts of different sizes. From observation of the modern day Canterbury rivers, the Ashburton River is smaller than the Rakaia and Rangitata Rivers, and it is therefore not unreasonable to suggest that during the construction of the Canterbury Gravels a range of larger, differently sourced rivers than the current Ashburton River were also present. Consequently, while the surface channel geometries measured in Ashburton model may scale well between the Ashburton River channels the channel fill deposits do not account for the complete range of channel hierarchies. A comparison with the larger Rakaia and Rangitata Rivers to up-scaled model channels, shows that model channels may only be scaling second order channels. The issue of whether FSM can be directly up-scaled using a linear scaling needs consideration in future studies and the issue of up-scaling is explored further in the following section.

6.17 Scaling within physical modelling and application to analogue/reservoir studies

The issue of scaling is clearly central in the application of any one dataset to a different analogue, whether these data are derived or collected from modern or ancient sedimentary environments or physical models. Transferral and application of datasets derived from any one of these sources into reservoir models requires both appreciation of the scaling assumptions and a testing of the output. Clearly, an essential aspect of this

issue is the correct estimation and scaling of channel depth and testing of possible scale invariance of alluvial architecture across several orders of magnitude in physical scale. Sapozhnikov and Foufoula-Georgiou (1996, 1997) and Foufoula-Georgiou and Sapozhnikov working on fractal scaling suggested that braided rivers displayed similar anisotropic scaling (self-affinity), despite the three rivers in their study displaying marked differences in scale (0.5-15 km in braidplain width), slopes (0.007 - 0.00008), and types of bed material (gravel to sand). Sapozhnikov and Foufoula-Georgiou (1996, 1997) results are important guides for up-scaling physical modelling data to a range of fluvial outcrop and subsurface sequences.

When up-scaling FMS datasets, two scaling factors must be considered. Firstly, the length scale of the model, in this case 1:50, and secondly, a further scaling factor may be required to account for the larger first order channels that may not be represented in the model as discussed in Section 6.16.

In its simplest form, the relationship between physical modelling data and field data would require a linear scaling. The relative up-scaling between model and prototype may be based on a linear scaling ratio of maximum channel depth. For example, the Ashburton physical model experiments were undertaken at a scale ratio of 1:50 based on a prototype of the Ashburton River. Comparison between maximum channel depth in the model series C (0. 81 m, up-scaled) and maximum channel depth obtained from the modern Ashburton River (0.83 m) suggest that relationships follow a ~1:1 scaling based on the maximum channel depths. However, when the coarse-grained channel fill architectural elements B are compared between prototype and model (Section 6.12) this 1:1 ratio does not appear to account for the total amount of up-scaling required. Channel fill deposits from the Canterbury Gravels have a maximum thickness of 2.26 m, whereas the channel fill architectural elements (B) from the model have a maximum thickness of 0.86 m when up-scaled. This difference in maximum channel fill thickness implies a scaling factor of ~2.6 is required to up-scale the data from the model to the prototype.

The results suggest that whilst the FSM of the Ashburton River may be scaling well with the prototype Ashburton River over the entire hierarchy of channel geometries; the alluvial architecture from the FSM may be only scaling smaller channel orders.

Therefore, may not accounting for the different scales of channel-belts that may have contributed to the deposition of the Canterbury Gravels.

Additionally, comparisons of alluvial architecture between FSM and prototype are complicated by the interaction of formative channel size, aggradation and preservation rate and processes of avulsion and migration of channels, resulting in the erosion and dissection of alluvial deposits (discussed in Section 6.19). These relationships are difficult to quantify in field studies due to river size, limited time constraints and episodic changes in channel form (Warburton and Davies, 1998). Nevertheless, these links warrant further investigation in future studies. Peakall *et al.* (1996) also documented that vertical erosion and deposition operates on a much faster time frame than horizontal accretion in FSM (Warburton and Davies, 1998). This difference in deposition of horizontal and vertical accretion rates may result in a distortion in the size of scours and overbank splays preserved in aggrading river models and cause inconsistencies when comparisons are made between model and prototype.

6.18 Comparisons between geostatistics from physical modelling and documented outcrop studies

Whilst comparison of channel fill deposits between physical model and the prototype Canterbury Gravels has been undertaken in Section 6.16, comparison to literature studies is more problematic, again because the scale considered in the physical model is often different than that identified in the literature (channel scale versus channel belt scale). The majority of studies reported in the literature are concerned with channel sandbodies and in most cases refer to a range of sandbodies, many of which have been formed by deposition from: (1) the amalgamation of a series of channels or, (2) a single channel avulsing or migrating across an alluvial plain and constructing a series of stacked multilateral and multi-storey sandbodies. Analysis of the literature reveals a paucity of quantitative, within channel-belt alluvial architecture (Chapter 2, Table 2.3). Therefore, it is inappropriate to compare physical modelling datasets with many of these documented studies of channel-belt architecture because the physical model results present a level of resolution that is different to many outcrop analogue studies. Additionally, the large scatter of datapoints highlights the need to be highly critical in applying modern and ancient analogues and defining the parameters for modelling. Use

of general trend lines to compare the scaled datasets to previous literature studies should not be adopted without knowledge of the level of significance, errors and composition of the database.

The three physical modelling experiments were run under precisely known, repeatable conditions, while field datasets are the result of a combination of temporally variable controlling parameters. FSM must be scaled using the correct analogue. Therefore, the deposits described for the Lower Ketch Member (Chapters 3) and the Escanilla Formation (Chapters 4), which are not generic examples of a proglacial gravel-braided fluvial depositional environment, require further quantification of the scaling relationships between different fluvial systems before data can be applied from the Ashburton FSM. There is a need for further studies to be undertaken on a range of depositional settlings before the modelling dataset can be applied to all depositional environments. Where these experiments have compared the geometry of surface channels (Section 6.16) and architectural elements (Section 6.12) with specific outcrops from which prototype data were obtained, good agreement between physical model results and the field has been achieved.

6.19 Discussion

While some studies have included some river bed grain size parameter into channel pattern classification schemes (e.g. Leopold and Wolman, 1957; Schumm, 1960; Schumm, 1977), no fully quantitative models currently exist that compare the response of within channel-belt braided channel morphology and alluvial architecture to an imposed change in sediment supply grain size. The use of FSM has allowed the isolation and quantification of channel morphology and alluvial architecture in response to a change in sediment grain size. A bimodal grain size distribution was used to impose a fourfold change in grain size in a FSM while maintaining the overall grain size sorting to represent a reduction in grain size that takes place over a distance of ~64 km down the modern Ashburton River.

The results from series C, M and F suggest there are differences between the three experiments. This section identifies these differences and discusses their significance for improved understanding of braided alluvial architecture.

6.19.1 Channel geometry

Analysis of bankfull channel geometries from the Ashburton River reveals no significant change in the width, depth and width/depth ratios over a 43 km distance downstream. Results are consistent with the conservation of width and depth exponents in a range of fluvial systems (see Knighton, 1998, Table 5.4, p 172) and strengthen the suggestions of Bridge (1985, 1995) that grain size of sediment load may not have a major control on channel pattern. Alternatively, any changes in gradient or discharge that occur down the rivers course may counteract any morphological changes that occur as a result of in downstream grain size diminution (cf. Chew and Ashmore, 2001). FSM can isolate these effects by keeping all boundary effects constant with the exception of grain size.

The results from series C, M and F showed that the magnitude of the depths increased significantly from series C to M and widths increased significantly from M to F. This trend suggests that channels tend to increase firstly in depth and then width between series C and F. In spite of this, no significant change in the width/depth ratio is observed between the three experiments. The bimodality of the Canterbury Gravels grain size distribution used in the FSM mean the distributions only experiences a ~3 % shift in the proportion of coarse (gravel) to fine (sand) modes following a fourfold reduction in grain size (Chapter 5, Figure 5.6.4). Knighton (1998) reports that coarser bed load is often associated with wider, shallower channels and Parker (1979) predicted that for a given discharge, a 30 % increase in gravel load leads to a 40 % increase in width and a 25 % reduction in centre depth, ultimately increasing the width/depth ratio. Sambrook Smith (1996) suggested from analysis of Iseya and Ikeda's (1987) work that when surface sand content exceeds 30 % the bed changes from behaving as a gravel bed to behaving as a sand bed. These studies suggest that the relative proportions of the coarse (gravel) and fine (sand) modes of the grain size distribution may be more influential in determining individual width/depth ratios within in bimodal grain size supplied river rather than the absolute magnitude of change. Moreover, with the sand mode of the

Canterbury Gravel only representing between ~19 to ~22 % of the total distribution, levels may be below the critical threshold of sand proportion where the channels alter their geometry. Future modelling could focus on the impact on channel morphology and resultant alluvial architecture when a change in the relative proportions of sand to gravel modes is imposed on the fluvial system.

Results from series C, M and F show a general increase in channel widths and depths and an increase in sheet flow in the finer grain size distributions. Studies by Whipple *et al.* (1998) on experimental fan development show the opposite effect, with enhanced flow channelisation in sediment distributions with a D_{50} finer than 0.16 mm, due to the onset of significant suspended sediment transport and effect of cohesion of the fine-grained channel banks. The D_{50} grain size for series C, M and F was above 0.12 mm and therefore above the threshold grain size for channelisation documented in Whipple *et al.* (1998). Additionally, the use of non-cohesive silica flour in the Ashburton Model allows the channels to migrate and erode laterally.

While no significant change in the width/depth ratios of the channels was observed between series C and F there was an increase in the proportion of sheetflow on the braidplain. The increase in sheet flow between successively finer grain size distributions may correspond with the general increase in magnitude of bankfull channel geometries in the finer distributions representing a different scaling of the overall system.

6.19.2 Bedform generation

The development of bedforms within the channels of series M and F show a similar planform surface morphology to dunes migrating in the Platte River, Nebraska (Blodgett and Stanley, 1980). However, the low dimensionless shear stresses, locally low grain Reynolds numbers, subcritical flow conditions, and disappearance of bedforms at high discharges indicate these bedforms may be current ripples. Therefore, while the channel geometries may scale with the field prototype, the ripples may not be scaling with the prototype. The resultant impact on the alluvial architecture is that the internal fill of the primary channels (architectural element A) in series F may be dominated by the deposits of these migrating ripples. It is therefore recommended that future physical modelling be undertaken using a grain size distribution with a D_{50}

equivalent to series C to avoid the formation of unscaled bedforms and a scale distortion from prototype to model. In addition to this, calculations of flow parameters for scaled models of low net-to-gross fluvial sequences documented in Chapters 3 (Lower Ketch Member) and 4 (Escanilla Formation) at a 1:50 scaling would produce grain size distribution with D_{50} values of ~ 0.0015 mm (Chapter 5) and therefore may be influenced by scaling effects documented in Whipple *et al.* (1998). The problems of FSM of fine-grained fluvial systems could be addressed in the future by: (1) decreasing the scale ratio the prototype to model (e.g. 1:20; 1:10) while using a larger flume facility, and (2) relaxing the scaling of grain size and using a grain size distribution that is above the magnitude where non-scaled bedforms occur. The physical modelling described in this chapter has helped define the lower limit for FSM a 1:50 scaled grain size distributions of the Ashburton River.

6.19.3 Alluvial architecture and preservation potential

A six-fold architectural element scheme comprising of coarse-grained (primary channel fills, secondary channel fills, splays) and fine-grained (channel fills, erosional remnants, floodplain fines) element for the Ashburton model shows similarities with the Canterbury Gravels, New Zealand.

The preservation potential of individual architectural elements is a function of initial depositional geometry and subsequent reworking within the aggrading channel-belt. Therefore, based on the results that show the duration of channel occupancy in the three experiments showed no significant difference. Assuming that the duration of channel occupancy gives some indication of the stability of the channels, it may be proposed that architectural element geometries are principally dependant on the formative channel morphology and reworking. Results show that no significant difference in the geometry of primary channel fill architectural elements was recorded between series C and M, while a significant increase in the primary channel fill width and thickness was observed between series M and F. The significant increase in primary channel fill thickness between series M and F, are consistent with the increase in formative channel depth between series M and F. Splay architectural elements (C) show a significant increase in width between series C-M and M-F. Since sheet flows are responsible for the deposition of the splays, the increase in splay deposit widths can be, related to the

increased proportion of sheet flows occupying the sediment surface in progressively finer grain size distributions. Horizontal proportion curves reveal the proportion of splay deposits between series C and M also increases, providing further evidence that splay deposition is related to the proportion of sheet flow over the sediment surface. However, while there is a significant increase in the width and thickness of the splay deposits between series M and F, there is no corresponding increase in the proportion of splay deposits in relation to the channel deposits between these two experiments. Therefore, the depositional architecture appears to be the result of more complex relationships between processes, which are still not fully understood.

Further comparisons of the mean, minimum and maximum preservation potential percentages (e.g. bankfull channel depth/preserved channel fill thickness) of the coarse-grained channel-fill architectural elements in the three experiments show a decrease in the preserved width/thickness ratios in comparison to the formative channel width/depth ratios. The lower preserved thicknesses of channel-fill architectural elements within series M compared to series C and M may relate to the lower feed rates and subsequent, lower actual aggradation rates recorded in series M (Table 6.1). Analysis of the three experiments reveals that mean architectural element widths are smaller than, or approximately equal to formative channel widths. The mean thickness of the channel fill deposits generally responds to a lesser extent than the width in all three series and both series C and F are greater than their formative channel depth (cf. Salter, 1993). A reduction in width and channel fill thickening reduces the width/depth ratio. This reduction in width/thickness ratio of channel fill deposits from formative channel geometry may result from a process of vertical aggradation or scour (e.g. Salter, 1993), limited lateral migration and scour and dissection of underlying channel fill deposits. Peakall *et al.* (1996) suggests that since vertical erosion and deposition are much faster than horizontal accretion, there may be a distortion in the size of scours and overbank splays preserved in aggrading river models. However, identification of any major differences in preservation potential between the three experiments and the underlying processes that control these relationships are ambiguous.

6.19.4 Alluvial architecture models

Recent alluvial architecture models (e.g. Leeder *et al.*, 1993; Peakall *et al.*, 2000) suggest channel-belt avulsion results in sandbodies with ribbon geometries, while gradual channel-belt migration produces wider sheet-like sandbodies. If these models of alluvial architecture also apply to the within channel-belt scale architecture, the general reduction in channel fill widths in comparison to formative channel width implies that channel avulsion is the dominant mechanism controlling the within channel-belt architecture in the model. Future FSM work is required to quantify the relative importance of avulsion versus lateral migration of individual channels.

Series C, M and F were imposed with an equal aggradation rate (Table 6.1). Under conditions of similar aggradation rates, models of Bridge and Leeder (1979), Bryant *et al.* (1995) and Heller and Paola (1996) may predict a similar alluvial architecture for all three experiments. However, the proportion of channel fill to overbank deposits in the three experiments differed. While alluvial architecture models such as Bridge and Leeder (1979), Bryant *et al.* (1995), Mackey and Bridge (1995) and Heller and Paola (1996) provide theoretical scenarios for architectural stacking patterns between channel-belt sandbodies and floodplain deposits, they require testing before they can be scaled down to interpret the within channel-belt architecture. Consequently, the relationship of formative channel size and the proportion of overbank sheet flow versus channelised flow must play an important role in determining the proportion of channel to overbank deposition and thus stacking patterns. The results from this physical modelling must now be incorporated into some of the existing theoretical and computational models of alluvial architecture both at the channel-belt (e.g. Mackey and Bridge, 1995; Heller and Paola, 1996) and within channel-belt scale (e.g. Peakall, 1995; Ashworth *et al.*, 1999).

6.19.5 Preservation of fine-grained deposits

The proportion of fine-grained (sand) architectural elements fine-grained channel fills, erosional remnants and overbank floodplain deposits) increased from 0.2 % - 0.6 % - 3.3 % in series F, M and C respectively. The increase in fine-grained architectural elements in series C may result from: the lower suspended sediment concentrations and higher median grain size values for suspended sediment in series C creating higher

settling velocities. Additionally, the larger channel geometries in the series F suggest that a lower proportion of the braidplain is available for water to pond and allow fines to settle out in order to deposit fine-grained architectural elements. These findings are important for the construction of fluvial heterogeneity models where differences in permeability exist between the sand and gravel fractions. However, field studies are needed to identify the differences in the proportion of fine-grained material in outcrops with different grain size distributions.

6.19.6 Up-scaling of physical model datasets

The preserved alluvial architecture in FSM shows similar architectural elements to the Canterbury Gravels field prototype. While width/thickness ratios of secondary channel fill deposits (B) are comparable between field and model, the magnitude of the secondary channel fill deposits (B) geometries in the model are smaller than those measured in the outcrop. This difference in magnitude between prototype and model may be a result of the combination of different scale rivers coalescing to deposit the Canterbury Gravels and the assumptions of generic scaling principles. While physical modelling can provide valuable insight into understanding of controls on the rivers and their deposits, scaled models must be tested with a field analogue and cannot be applied to fluvial sequences without full appraisal of all the criteria listed in Chapter 4 for reservoir-analogue comparisons.

6.20 Limitations and potential benefits of future physical modelling

Physical modelling permits capture of some of the complexity of real systems, however a number of limitations can be identified. The limitations and results from the physical modelling have suggested that several factors be considered in future studies, including:

- Architectural element data obtained from series F, M and C are provided as two-dimensional measurements and use maximum width and thickness perpendicular to the mean palaeoflow direction to characterise shape. Quantification of the three-dimensional shape and spatial distribution of architectural elements from physical modelling is required in future modelling.

- The physical model only incorporates the use of one input source channel. Comparison with the field prototype suggests the Canterbury Gravels deposits were constructed from several braided rivers. Future FSM may assess the impact of several input channels with varying discharge on the alluvial architecture.
- The impact of changing the relative proportion of sand to gravel modes in a bimodal sediment distribution, changing discharge and sediment supply rate on channel braided rivers and alluvial architecture may be investigated.
- Field studies are required to investigate the proportion of fine-grained architectural elements deposited in relation to sediment supply grain size.
- Quantification of the rates and frequency of channel avulsion and migration is needed in order to test alluvial architecture models (e.g. Mackey and Bridge, 1995; Heller and Paola, 1996).
- The investigation of scaling relationships between different braided river systems. In future studies quantification of these scaling relationships is paramount for the application of FSM datasets to reservoir characterisation.

6.21 Summary

Seven conclusions can be summarised from the field and FSM of the Ashburton River:

1. Channel geometries (width, depth and width/depth ratio) from the modern Ashburton River study show no significant difference over a 43 km distance downstream in a river experiencing a downstream fining rate of 0.0322 ψ km^{-1}.
2. Three experimental runs, series C, M and F representing a quartering of the scaled Ashburton River grain size distribution show no significant difference in the channel width/depth ratios. However, a significant increase in channel depth was present between series C and M and an increase in width between series M and F, suggesting that channel geometries first deepen then widen as grain size is reduced.
3. A six-fold architectural element scheme comprising of coarse-grained (primary channel fills, secondary channel fills, splays) and fine-grained (channel fills, erosional remnants, floodplain fines) architectural element for the Ashburton model is presented, which are comparable to the alluvial architecture of the Canterbury Gravels, New Zealand.

4. Preservation potential of individual channel fill architectural elements (A and B) is a function of initial depositional geometry and subsequent reworking within the aggrading channel-belt. Results suggest that the process of local vertical channel aggradation or scour and avulsion may control the final channel geometry in preference to channel migration.
5. Splay architectural elements show a significant increase in width between C-M and M-F, which corresponds to the increased proportion of overbank sheet flow splay deposition between series C and F. The proportion of splay deposits between series C and M increases in combination with an increase in the proportion of overbank sheet flows and resultant increase in depositional width.
6. The proportion and size of fine-grained architectural elements increased between series F and C as a result of: lower suspended sediment concentrations, a larger suspended sediment median grain size creating higher settling velocities, smaller channels, and a lower proportion of sheet flow providing larger areas of abandoned floodplain for water to pond and allow fines to settle out.
7. In series M and F pronounced bedform formation occurred in the channels at low flow stages, which are current ripples. The presence of ripples and the calculation of low Re* numbers for fine-grained FSM provides lower grain size limits for future FSM.

Chapter 7. Application of combined core-physical modelling-outcrop approach to reservoir simulations: future potential

7.1 Synopsis

This chapter illustrates the potential of using an integrated approach to reservoir characterisation and provides details on how different scales of alluvial heterogeneity might benefit from the use of techniques discussed in Chapters 3-6. An exploration of the use of the outputs from physical modelling for fluvial reservoir characterisation is presented. A methodology is introduced for gaining the necessary inputs for specific pixel- and object-based reservoir simulations, which is founded on the assumption that architectural elements have a direct relationship to petrophysical attributes. The use of physical models to test the sensitivity of geostatistical techniques is also demonstrated. Recommendations for further work in the use of physical modelling datasets for reservoir characterisation are presented.

7.2 Introduction

Chapters 3 and 4 demonstrated the use of an outcrop analogue dataset to provide information on the inter-well scale alluvial architecture (<0.5 km) for a subsurface reservoir, using examples from the Carboniferous Southern North Sea and the Eocene Escanilla Formation, Spain. Chapters 3 and 4 highlighted the difficulty in obtaining the geometries of architectural elements at the within channel-belt scale. Chapter 6 described results from three physical modelling experiments that used different grain sizes distributions in order to quantify the impact of grain size on alluvial architecture. While physical models provide the ability to control the depositional system and isolate the main variable influencing the system, in order to make progress with their use in the hydrocarbon industry, the results have to be addressed in a manner in which to supply data to both the geological modeller and petroleum engineers. This involves combining the more traditional approaches of fluvial sedimentology and facies modelling with a more quantitative approach that incorporates the flow properties of individual facies. Existing reservoir simulation software requires the collection of geologic data for inputs and validation of the model outputs. With this in mind, data from outcrop and physical

models must be collected and related to petrophysical properties in order to run full flow simulations in a dynamic model. Therefore, this chapter has four main aims:

1. To highlight the scale of heterogeneities addressed by each of the core, outcrop and physical modelling statistics and emphasise the importance of an integrated approach.
2. To establish the link between architectural elements in the preserved stratigraphy of physical models and petrophysical properties for specific case studies.
3. To provide a methodology for the use of physical modelling datasets in reservoir characterisation, and show the potential use of these data for object-based modelling.
4. To present recommendations for future research.

7.3 Scales of heterogeneity

Cross (1991) highlights the need to treat and analyse each scale of heterogeneity within a reservoir in a manner that ensures they all complement each other (Table 7.1). The information from the physical model presented in Chapter 6 may fill the data gap between: (1) the channel-belt scale alluvial architecture, for example, sandbodies in Bridge and Leeder (1979), Mackey and Bridge (1995), Dreyer *et al.* (1993), Fielding and Crane (1987), and (2) the grain and bedform scale data that provides petrophysical information. Physical modelling can provide details on the smaller-scale, within channel-belt scale to nest within simulation models.

The need to predict performance from individual sandstone packages is clearly vital for exploitation strategies of a reservoir (Van der Graaff and Ealey, 1989) and physical modelling can quantify heterogeneity of the genetic sandbody and architectural element scale reservoir heterogeneities (>0.001 to 0.5 km). As the incorporation of increasingly smaller scales in simulation models is now becoming possible, the heterogeneities become more complex and the required inputs to these models are lacking.

Table 7.1. Scales of heterogeneity for consideration of fluvial reservoir performance, showing how different techniques provide data at different scales that complement each other as various aspects of the reservoir model are constructed.

Scale		Example	Most appropriate data source
Field scale	1 - 10 km	Formation scale	Seismic resolution
Reservoir scale	0.1 - 1 km	Channel-belt complexes	Outcrop analogue
Genetic sandbody scale	0.01 - 0.5 km	Architectural elements	Physical modelling experiments and field analogue application/verification
Small scale	0.01 - 1 m	Petrophysical properties/sedimentary structures	Physical modelling experiments down to the metre scale, field analogue and well data

7.4 Quantitative data needs for petroleum engineering

While in the past, many models for the interpretation of alluvial architecture and vertical facies types (e.g. Miall, 1977; Collinson, 1978) have been qualitative, there has been a lack of quantitative information gathered. Qualitative data allow conceptual models of inter-well reservoir heterogeneity to be constructed and may guide geologists in decision making. With the advancement of technology, a host of simulators are available to provide three-dimensional models of geological structure and flow path simulations. Reservoir modellers and petroleum engineers require quantitative datasets to run these simulation models. The key to providing data for the petroleum and hydrogeology industry is twofold: (1) to collate a database on the quantitative statistics for a range of depositional systems and scales, and (2) to quantitatively link facies/architectural elements to petrophysical attributes for the construction of flow cells. Only then can such data serve both as input data to reservoir models and test the output.

7.5 Advantages of using physical models over conventional methodologies

Physical modelling can investigate parameters that cannot be obtained fully from conventional outcrop studies that are inhibited by limited exposure, assignment of depositional model, and lack of three-dimensional definition of architecture. In outcrop studies, failure to classify all the architectural elements in any sequence introduces gaps in the data and a bias to those most easily identified deposits, such as channel fills. Therefore, physical modelling has a number of advantages over conventional outcrop analogue description because it can provide:

- an order of magnitude more datapoints than existing outcrop datasets that are often limited to two-dimensional exposure,
- information on the scales of heterogeneity that are currently poorly understood in three-dimensions within the channel-belt environment,
- X, Y, Z location data to permit down and cross-channel correlations,
- observation of the evolution of the depositional system via the use of a variety of overhead and oblique digital video cameras,
- an identification of 'true' palaeoflow direction and hence correction of depositional geometries,
- a sedimentary basin infilled under controlled conditions where the sediment source and depositional environment are known,
- several parameters that help constrain current reservoir models (e.g. geometrical characteristics) and test the sensitivity of the analysis technique to quantify the alluvial architecture,
- data that can test the output from both pixel- and object-based reservoir models,
- data that needs no correction for outcrop orientation, topographic distortion, or partial and complete lengths,
- data where lateral and vertical variations can be examined at the same resolution, which improves understanding of subsurface reservoir data, which typically, have a greater resolution in the vertical (e.g. cores) than in the horizontal.

7.6 Application of physical modelling to the characterisation of alluvial reservoirs

Permeability data is often up-scaled in current reservoir flow simulation models to the scale of the channel-belt sandbody as a result of the scarcity of geometrical data at the within channel-belt scale. Current models have been based on modern channel or channel-belt parameters, and applied to subsurface objects, such as channel-belt width, thickness and sinuosity. As the power of workstations increases a finer detail of alluvial architecture can be introduced. In order to apply physical model datasets to any particular subsurface study an appreciation of the depositional model for the reservoir is first required. Subsequently, the application of any physical modelling dataset needs to be correlated to flow cells and this requires an evaluation of the relationship between facies type and petrophysics, which is discussed in the proceeding section.

7.6.1 Relationships between petrophysical properties and lithofacies

Permeability is the most important quantifiable control in reservoir fluid flow simulations and a number of studies assume that permeability distribution pattern is a function of sedimentary facies and depositional process (Alexander, 1993). Petrophysical parameters are primarily controlled by grain size and sorting (Freeze and Cherry, 1979; Domenico and Schwartz, 1990, Brayshaw *et al.*, 1996; Robinson and Friedman, 2001) and secondly, by diagenesis (Hornung and Aigner, 1999). In Chapter 3 the link between lithofacies type in the Lower Ketch Member and permeability was made, and this is complementary to many studies of fluvial deposit in the literature that have also made the link in both reservoir wells (Begg *et al.*, 1989; Atkinson *et al.*, 1990; Lui *et al.*, 1996; Eschard *et al.*, 1998; Tye *et al.*, 1999; Vaughan *et al.*, 1999) and onshore outcrop (Ravenne *et al.*, 1988: Dreyer *et al.*, 1990; Miller *et al.*, 1990; Jacobsen and Rendall, 1991).

Lithofacies units with similar hydrogeological properties must be identified (Koltermann and Gorelick, 1996; Webb and Davis, 1999). This has been attempted by applying Miall's (1985a) concept of architectural element analysis to outcrop studies (Anderson, 1989; Phillips *et al.*, 1989). Hazen's equation (1893) has been applied by Anderson *et al.* (1999) to calculate hydraulic conductivity for several hydrofacies units

and uses the relationship of hydraulic conductivity to the square of the D_{10} grain size. This method is based on the assumption that the D_{10} is the effective diameter that controls hydraulic conductivity. Klingbeil *et al.* (1999) showed a reduction of 23 lithofacies types into 5 hydrofacies types for the fluvial gravels. This simplification to five fundamental hydrofacies suggests that several simple building blocks can be used in models with relative permeabilities. Permeability classes have been allocated to each of the resultant architectural elements to produce a relative scale of permeability as absolute values of hydraulic conductivity may be affected by scaling laws (Bradbury and Muldoon, 1990; Anderson *et al.*, 1999).

The Ivishak Formation, Prudhoe Bay (Tye *et al.*, 1999) was used in Ashworth *et al.* (2000) to provide permeability values via core comparison and calibration to the scaled braided river deposits of the Ivishak physical model of Ashworth *et al.* (1994). However, data from the Ivishak Formation is not an appropriate match for the entire architectural element scheme defined in the Ashbuton model (Chapter 6, Table 6.6). Therefore, two more appropriate examples to calibrate the Ashburton River model may be the deposits of Quaternary Stoughton Gravels, Winconsin (Anderson *et al.*, 1999, Figure 7.1) and the Quaternary Gravel deposits of the Singen Basin (Klingbeil *et al.*, 1999). Braided river deposits described in Quaternary Stoughton Gravels (Anderson *et al.*, 1999, Table 2) have been used to assign permeability values to architectural elements of the Ashburton model (Chapter 6) based on the similarity of grain size and sedimentary structure characteristics, which can be used to indicate facies type (Table 7.2). When coupled with the geometrical information from the Ashburton model section data, architectural elements can be assigned dimensional data in addition to flow properties, and distributed according to vertical proportion curves (Section 7.7.1) in any particular reservoir interval.

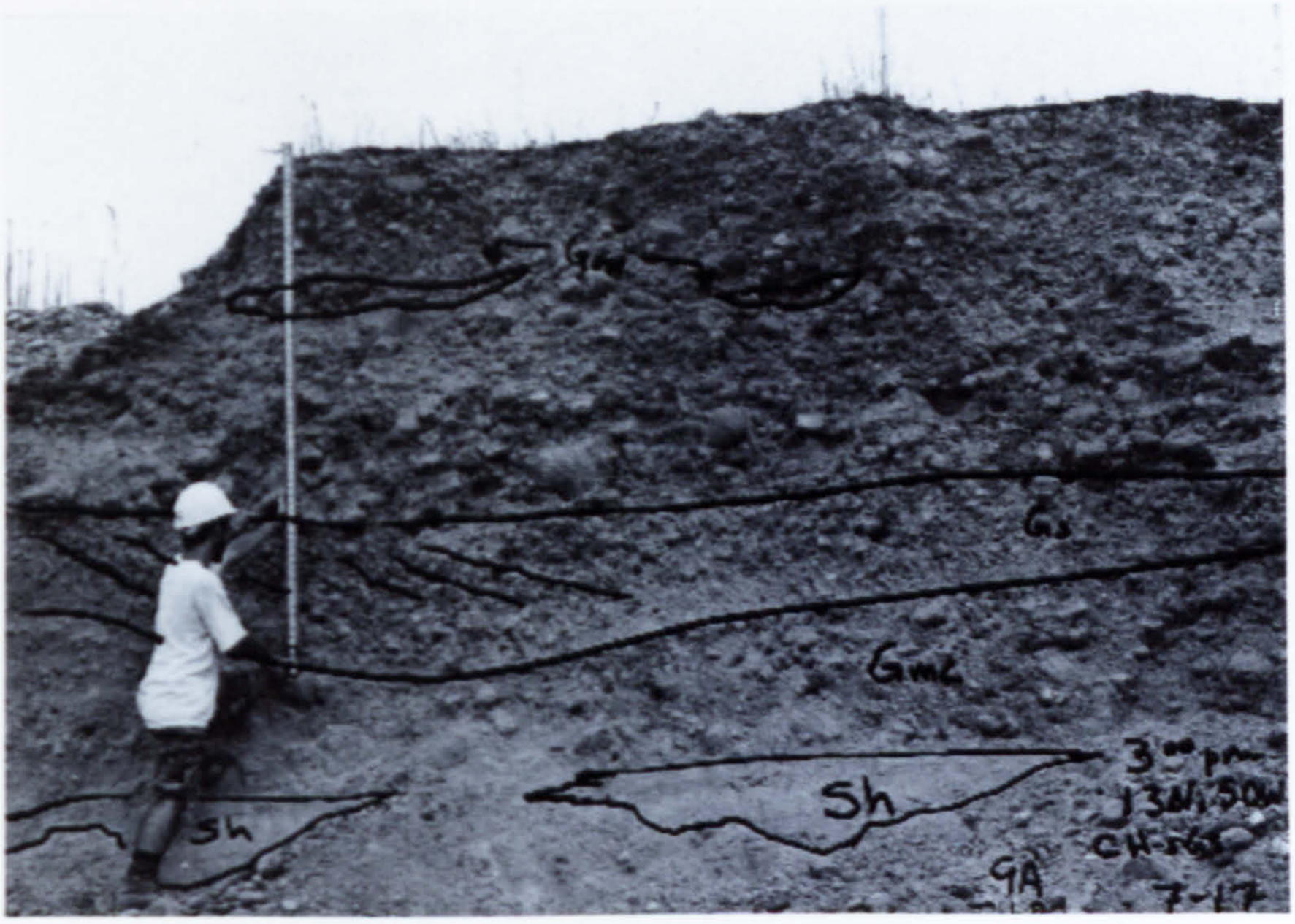

Figure 7.1. Photograph from Anderson *et al.* (1999) showing lithofacies Gs, Gm, and Sh within the Stoughton Gravel deposits used to apply permeability information to architectural elements from the Ashburton model.

Table 7.2. Assignment of permeability classes based on calibration of Soughton Outwash Gravels (from Anderson *et al.*, 1999) to architectural elements described in Chapter 6, Table 6.6.

Element code	Architectural elements description from the Ashburton model	Lithofacies similarities from the Stoughton site	Mean hydraulic conductivity (cm/s)	Permeability class
A	Primary channel fills	Gm/Gs	0.088-0.090	2
B	Secondary channel fills	Gmc	0.17	1
C	Splays	Gp	0.090	3
D	Fine channel fills	St/Sh	0.030	4
E	Erosional remnants	St/Sh	0.030	4
F	Overbank fines	St/Sh	0.030	4

The fine-grained architectural elements in the model (Table 7.2) have each been assigned an equal permeability class, because the internal structures are too fine to identify in the model, but the study of the fine-grained lithofacies in Anderson *et al.* (1999) shows both Sr and Sh lithofacies exhibit the same permeability. With field validation, differences in permeability between fine-grained architectural elements may be established and relative permeabilities adjusted accordingly. The application of this methodology is based on the assumptions that: (1) the architectural elements in field studies can be identified in the model and were deposited under a similar depositional environment, (2) there is a direct link between facies and petrophysics, and (3) the model has a linear scaling to the field prototype.

If each of these assumptions can be made, the model can be used to establish trends within the sequence. Care must also be taken when applying these models universally to fluvial deposits without full consideration and assessment of the controls acting upon the system at the time of deposition (Chapter 2, Table 2.1).

Vaughan *et al.* (1999) show how there may be a large range of porosity-permeability values in one facies type across any specific reservoir interval. It may therefore be appropriate to run a series of reservoir simulations using different petrophysical values found in specific areas of the field (i.e. proximal to distal trends). Hornung and Aigner (1999) documented that the highest porosities occur in proximal palaeogeographic positions on the alluvial plain and stratigraphically in the middle parts of macrocycles. Bal (1996) noted the presence of distinct large scale permeability trends within the Canterbury Gravels represented incised valley fills ~ 5-10 km wide that must be incorporated in geological models at the channel-belt scale.

7.7 A methodology for collecting data from physical modelling experiments for reservoir evaluation

Combined grain size and sedimentological analysis including sedimentary structures, grain size and grain size variation observed in each element type can give an indication of petrophysical attributes for each element. Petrophysical attributes can then be assigned to the various facies types or architectural elements observed in the physical model as described in Section 7.6.1. This section will highlight the potential of detailed sedimentological study of cut sections taken from the physical model to allow improved reservoir simulations to be undertaken at the within channel-belt scale of heterogeneity (i.e. 0.1-500 m). Several key steps are required in this process:

1. Identification of architectural elements observed in the cut sections (Chapter 6, Table 6.6). The shapes and geometry of the various architectural elements also need to be categorised at this stage.

2. Assignment of reference horizons. In this example from the Ashburton physical modelling experiment, the base of the flume basin was taken as the reference horizon and 60 vertical sequence logs were taken through the series C. Vertical proportion curves (Section 7.7.1) can be been calculated on the thickness of

sediments at each logged interval. This will subsequently allow model data to be used to populate the reservoir block by providing an estimate of the percentage of various facies at a specific reservoir interval. Physical modelling also allows a better temporal constraint than outcrop through the use of coloured sediment to act as time horizons across the sedimentary package.

3. Classification of lithofacies. Sequences through preserved sections of the Ashburton model were logged. Lithology was classified into three broad grain size categories: (1) silica flour, representing fine-grained sediment in the field (sands in the Ashburton prototype); (2) fine to medium sand; and (3) coarse sand (the later two categories representing gravel grade sediment in the field equivalent). Lithofacies units were also coded in terms of their architectural element type. Future modelling should more accurately constrain the grain size ranges and sorting for specific architectural element. The grain size of each type of architectural element should be sampled within the cut sections during the sectioning phase of the experiment, and be guided by previous classification of element categories (Chapter 6, Table 6.6). Each of the facies types or architectural elements can then be calibrated against specific reservoir facies and a hierarchy of heterogeneity within the reservoir assigned to the physical model architectural elements.

4. Assignment of petrophysical properties to the lithofacies observed in the physical model. Application of this methodology to the physical model cut sections allows a comprehensive hierarchy of flow units to be constructed for within channel-belt architectural elements. Petrophysical data from the Stoughton Gravels (Table 7.2) were assigned to the architectural elements described in Chapter 6, Table 6.6. The Stoughton Gravels are not an ideal match and refinement is possible by the use of grain size sampling of architectural elements from the model stratigraphy and the subsequent assignment of permeability based on grain size. These quantitative grain size data from the model architectural elements were not available in this study. However, this section illustrates how the method can be applied to a specific reservoir interval. For any specific modelling, calibration of specific petrophysical properties to lithofacies would be required for a reservoir model to be constructed (e.g. lithofacies from the Lower Ketch Member, Chapter 3). No distinction in the present example has been made between horizontal (K_h) and vertical permeability (K_v), although this may again be incorporated into future modelling.

5. Quantification of the scaling factor required to scale the physical model alluvial architecture up to the prototype scale (refer to Chapter 6, Section 6.17).

6. At the reservoir simulation stage, petrophysical data (core) are combined with physical model data including stop data (from vertical proportion curves, Section 7.7.2), geometries, shape, spatial distribution and sinuosity at the within-channel belt scale. The input from channel-belt and field scale datasets such as outcrop and seismic data can complete the hierarchy of scales needed for full flow simulation models. These steps are summarised in Table 7.3.

Table 7.3. A step-by-step methodology required to collect data from stratigraphic physical models to serve as inputs to object-based geological simulations.

Step	Procedure
	Data collection from the model
1	Identification of architectural elements in the cut sections and classification of shapes and geometries of architectural elements.
2	Assignment of a reference horizon and production of vertical proportion curves.
3	Quantification of grain size distribution for each of the architectural elements using sampling of grain size or a broad qualitative scheme. Comparison of vertical and lateral facies trends with the specific reservoir interval to calibrate the architectural elements.
	Calibration with the field studies
4	Assignment of petrophysical properties from the field prototype.
5	Quantification of channel geometries from the prototype and calculation of scaling factors needed to apply model datasets to the prototype.
6	Integration of the channel-belt and field scale datasets such as outcrop and seismic data.

Primary depositional petrophysical properties need to be isolated from diagenetic alteration, because diagenetic alteration may impact differently on the petrophysical properties of each facies type. Although this approach does not take into account any burial compaction or diagenetic effects that have altered the primary porosity and permeability trends, analysis of core would allow calibration of the model for field-specific applications.

7.7.1 Vertical proportion curves

Commonly, reservoir simulation models use input data from vertical proportion curves as stop data for models (Escard *et al.*, 1998). Vertical proportion curves provide data on a particular vertical sedimentary sequence parallel to a given reference horizon,

allowing rapid visualisation of the vertical organisation of lithofacies. These data allow reservoir simulators to distribute a lithofacies type in a particular horizon, defined by the cell size, according to the proportion of that facies type in any specific sequence. In core the proportions of any particular facies are based on the vertical thickness and involve using a reference horizon. These proportions may be ambiguous if a well-defined reference horizon is lacking.

Two vertical proportion curves are presented using data gathered from 60 vertical profiles from series C (Figure 7.2) and series F (Figure 7.3) in the Ashburton model. The base of the flume basin was used as the reference horizon and profiles have been up-scaled by the length scale of 50.

Figure 7.2 indicates two peaks in the channel fill proportions (elements A and B) above and below a peak in the overbank splays (element C) at 2.25 m. These types of data are important for showing the internal cyclicity associated with intrinsic variability of the fluvial system. The second example (Figure 7.3) shows the vertical proportion curve for series F, exhibiting a dominance of primary channel fill deposits, architectural element A (Chapter 6). Visual analysis of series F sequence exhibits a considerable increase in the proportion of splay deposits (element C) at the top of the sequence. This change from channel fill deposits to a more horizontal laminated unit at the top of sandbodies has been noted in deposits such as the Escanilla Formation (Chapter 4). Increased splay preservation towards the top of the sequences is also important for calculation of gross vertical permeability trends especially if channel-belts are stacked. An increase in splay deposits will affect the gross calculation of permeability across a specific sandbody. Changes in vertical sandbody permeability trends have been noted in braided (Richardson *et al.*, 1987a), meandering (Richardson *et al.*, 1987b) and ephemeral stream (North and Taylor, 1996) deposit sequences. Vertical proportion curves described in this section have highlighted the potential of physical models to constrain facies trends at the within channel-belt scale.

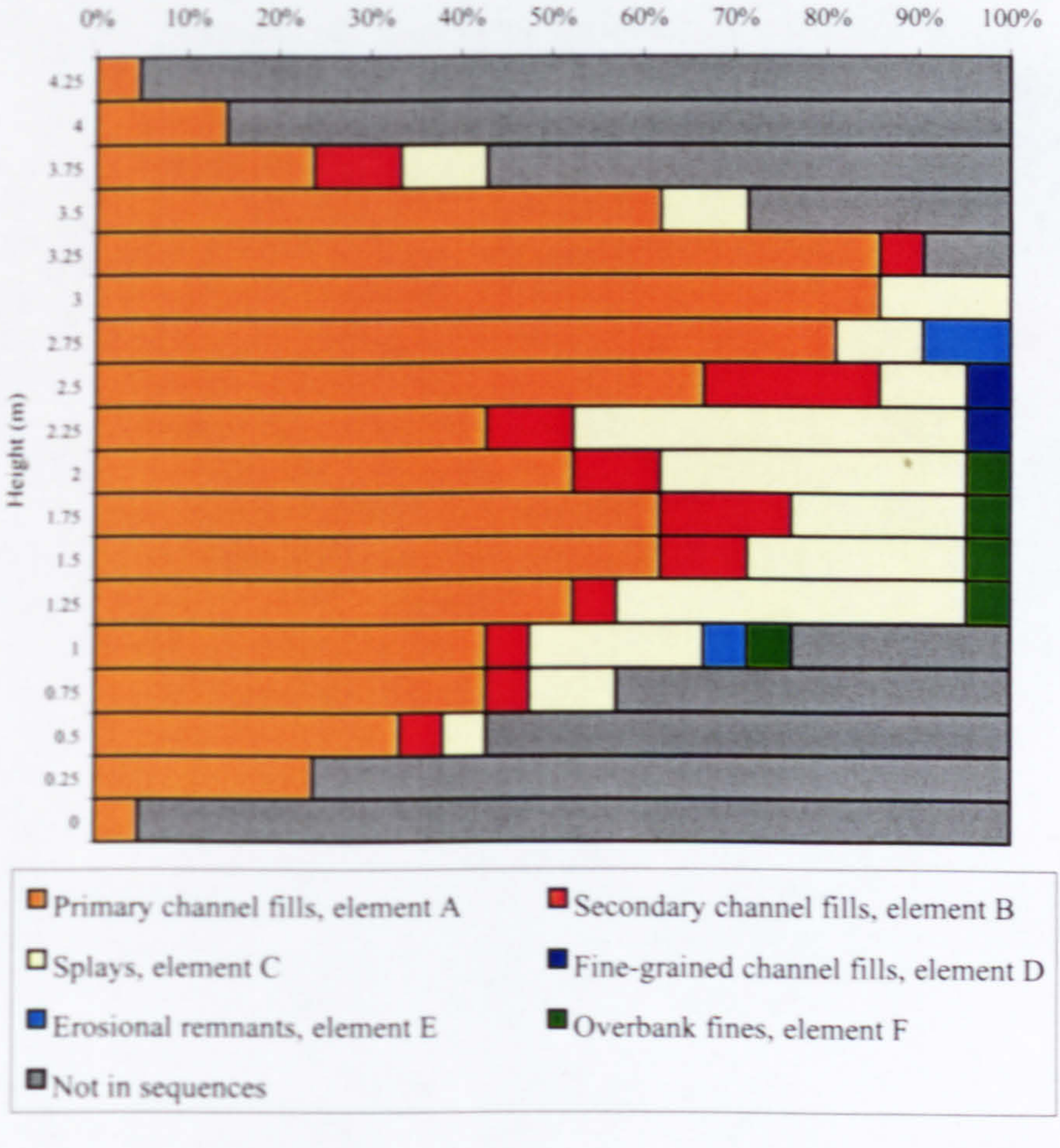

Figure 7.2. Vertical proportion curves for series C, showing a possible cyclicity with an increasing percentage of splay deposits (architectural element C) around the 2.25 m level, with two peaks either side of increased primary channel deposits (A). Note the sequence has been up-scaled by 1:50 (n =60).

Classification of vertical permeability profiles can be carried out on cut-sections from the physical model. By linking a series of these permeability profiles it is possible to pick out permeability trends within the physical model sections in cross-stream and downstream orientations.

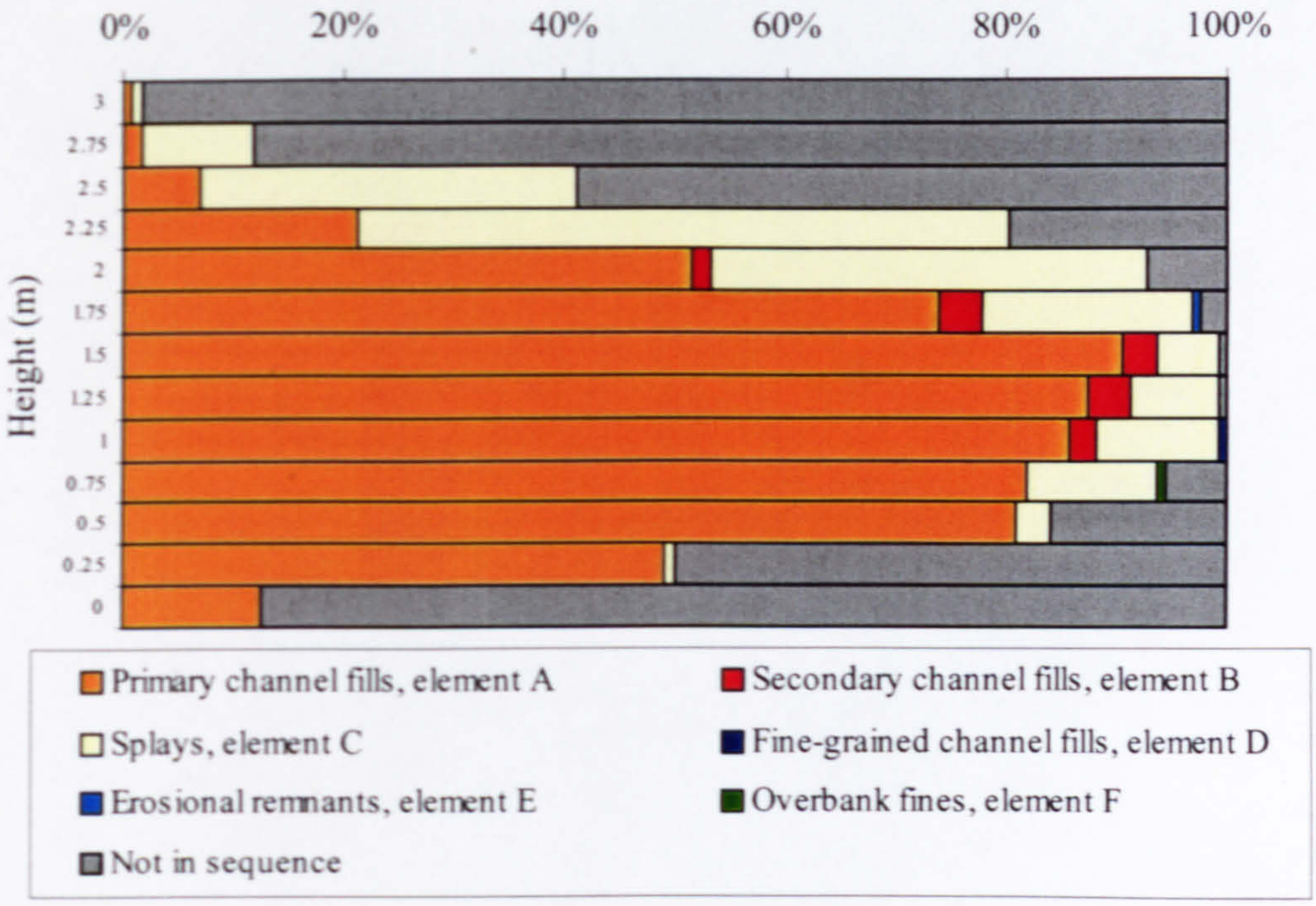

Figure 7.3. Vertical proportion curve for series F showing the dominance of channel fill deposition and an increase in the proportion of splay deposits towards the top of the sequences, reflecting the reworking towards the top of the sequence. Note the sequence has been upscaled by 1:50.

7.8 Data from physical models as input to object- and pixel- based reservoir simulation models

Table 7.4 summarises the inputs needed for object-based modelling (e.g. RMS software) and provides examples of how physical model datasets combined with conventional techniques can provide data for this type of simulation. Log data can provide vertical proportions curves that supply stop criteria for various architectural elements in the physical modelling. Using the methodology detailed in Section 7.7 and integrated field and physical model data, the parameters for a variety of reservoir simulation packages can be provided. Hirst *et al.* (1993) shows similar input parameters for reservoir simulation software to those illustrated in Table 7.4, which are currently being used in the hydrocarbon industry.

Table 7.4. Typical input parameters for a current fluvial reservoir modelling software simulators, ROXAR - RMS/STORM. The versatility of the physical modelling dataset allows provision of all parameters to cover a spectrum of methods for reservoir evaluation.

Modelling Criteria	Example from the physical model
Facies type	Fluvial
Body type	Coarse- and fine-grained architectural elements (Chapter 6).
Body shape	e.g. half cylinder, could be constrained more accurately if needed.
Thickness	Preserved thickness (e.g. probability distribution function, Chapter 6) modern and preserved available.
Width	Preserved width (e.g. probability distribution function, Chapter 6) modern and preserved available.
Orientation	Orientations of architectural element gathered from overhead video footage as a probability distribution function.
Amplitude	Overhead video footage of the developing model.
Wavelength	Overhead video footage of the developing model.
X-position	Reference horizon in the physical model.
Y-position	From a vertical reference position in the physical model
Z-position	Distance down-stream (section number)
Relative Z-position	Position in the physical model
Stop criterion	Percentage of each architectural element in a particular interval (e.g. vertical proportion curves)
Branch points	Overhead video footage of the developing model.
Branch locations	Overhead video footage of the developing model.
Erode/replace if	Estimates on preservation potential from superimposing topographic profiles onto cut sections in the physical model.

Physical modelling can provide a level of detail that is not commonly addressed in current reservoir simulation models. Within channel-belt alluvial architecture may be needed for future modelling exercises during secondary reservoir evaluation stages. Physical models also provide the potential to evaluate averaging and sampling frequency procedures, which are often used in up-scaling reservoir data. The following sections deal with averaging and sampling issues.

7.8.1 Altering grid size and sample averaging

Section 7.5 illustrated some of the advantages of using physical modelling for within channel-belt reservoir characterisation. In order to collect this data for input to reservoir simulators, issues of sampling frequency and averaging data must be addressed. In cored reservoir intervals, sampling is often much more detailed in the vertical than the horizontal orientation. Typically, in subsurface datasets <1 % of the volume of the reservoir is considered in order to classify the geological properties. Outcrop datasets suffer similar problems and commonly an exposed outcrop cannot be fully classified due to weathering, vegetation, and the ability of the geologist to define the margins of each architectural element. For example, Anderson *et al.* (1999) estimate that only 40 % of the outcrop volume using mapping and ground penetrating radar was used to classify the geological description of the site.

The section below explores the potential benefits of using physical modelling to test the sensitivity of the sampling frequency and averaging effects. The two examples shown below illustrate the effect of: (1) averaging the vertical data over the Ashburton model sequence (series C) from 60 vertical profiles (Figure 7.4), and (2) changing the vertical sampling frequency (Figure 7.5) for 60 vertical profiles through the model sequence (series C). Visual comparison of the two techniques suggests that the changing the sampling frequency will have different effects from averaging the data. In the example shown in Figure 7.4, averaging the data retains all the architectural element categories, while losing the vertical stacking patterns of elements by distributring elements equally within each of the horizons. Alternatively, reducing the sampling frequency (Figure 7.5) results in a progressive reduction in the number of architectural element categories represented in the sequence, starting with the most volumetrically insignificant (i.e. fine-grained architectural elements D-F). The differences in permeability between the fine- and coarse-grained architectural elements may be significant (Table 7.2) and the loss in fine-grained architectural elements will alter the total permeability balance of the sequence. This type of sampling and averaging information may have important ramifications for prediction of reservoir performance, especially in determining how well data in a single borehole represents the entire reservoir interval. This information will allow decisions on cell size for the reservoir simulation models to be made to capture the level of heterogeneity needed for realistic flow simulations. In order to

determine how the geostatistics of a particular reservoir sequence alter as a result of sampling and averaging procedures, future studies should quantify:

1. The sensitivity of altering sampling frequency on the proportion of architectural elements in vertical and horizontal proportion curves. Analysis of Figure 7.5 suggests that with decreasing sampling frequency there is a progressive reduction in the incorporation of fine-grained architectural elements.
2. The effects of up-scaling alluvial architecture by averaging the values with a constant sampling frequency over progressively larger reservoir volumes (cell sizes), which may affect the proportion and stacking of architectural elements within the sequence. This analysis may be carried out using a similar method to that described in Section 7.7. The problems of up-scaling data from the metre scale to a scale of tens to hundreds of metres suitable for modelling have been addressed by Mansoori (1994), Desbarats and Bachu (1994), Ewing (1997) and Kitandis (1997).
3. The impact of grid size and averaging effects on the vertical (K_v) and horizontal (K_h) permeability data, in order to determine whether the effects are isotropic. Analysis of geometrical data of architectural elements in the physical model (Chapter 6) shows all of the architectural elements have greater widths than thicknesses. This geometrical anisotropy may be reflected in any up-scaling and choice of grid spacing for flow cells in existing reservoir simulation models.

Incorporating petrophysical properties into this type of analysis allows the incorporation of variograms in future research. The variogram is a geostatistical tool that relates geological variability to physical distance in a reservoir (Kupferberger and Deutsch, 1999). Variograms need quantitative datasets in order to plot the distributions and therefore, in many cases the petrophysical properties are used to assess the attributes using a variogram. The use of geostatistics and variograms is becoming increasingly common to evaluate the spatial variation in any particular reservoir unit (Davis *et al.* 1992, 1993; Dominic *et al.*, 1998; Sahin *et al.*, 1998; Kupferberger and Deutsch, 1999). Often these techniques use datasets of the order of well spacing on the scale (0.5 km). Physical models from aggrading basins allow the variograms or proportion curves to be constructed at a much higher resolution than well data permits and consequently, the effect of changing sampling distance on the geostatistical reproducibility can be quantified.

a

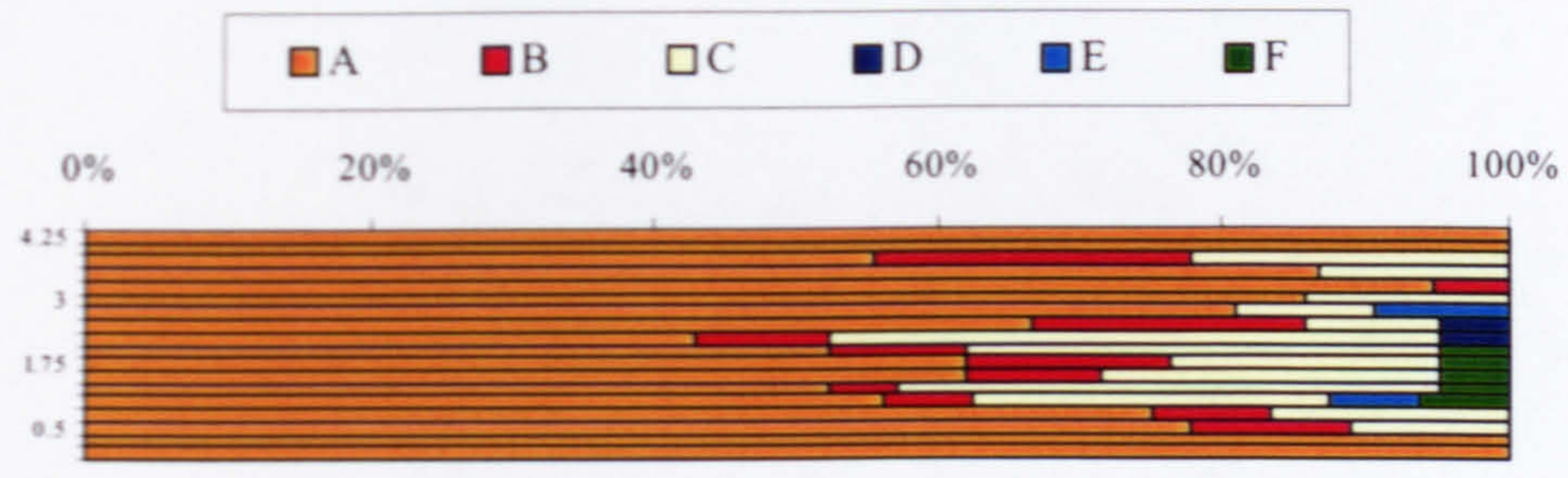

b

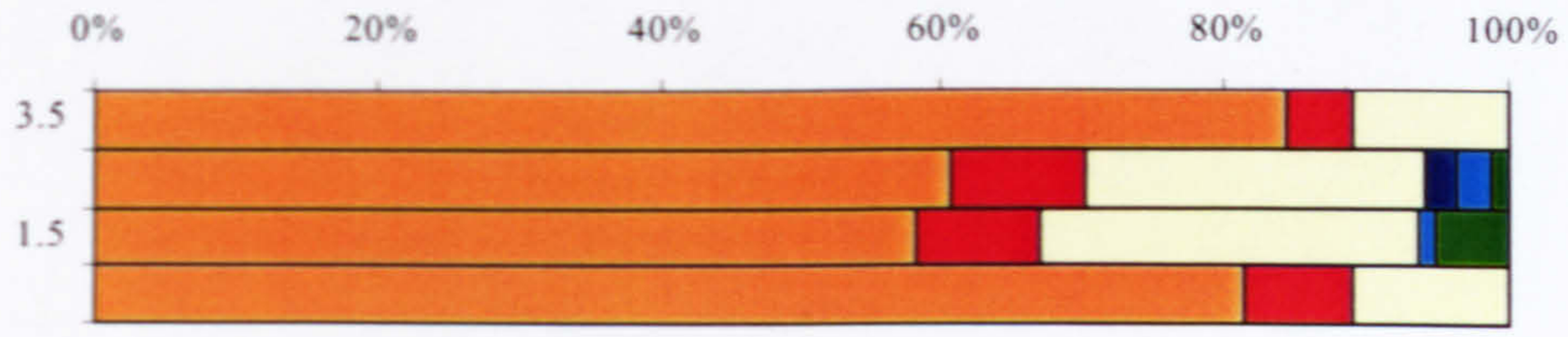

c

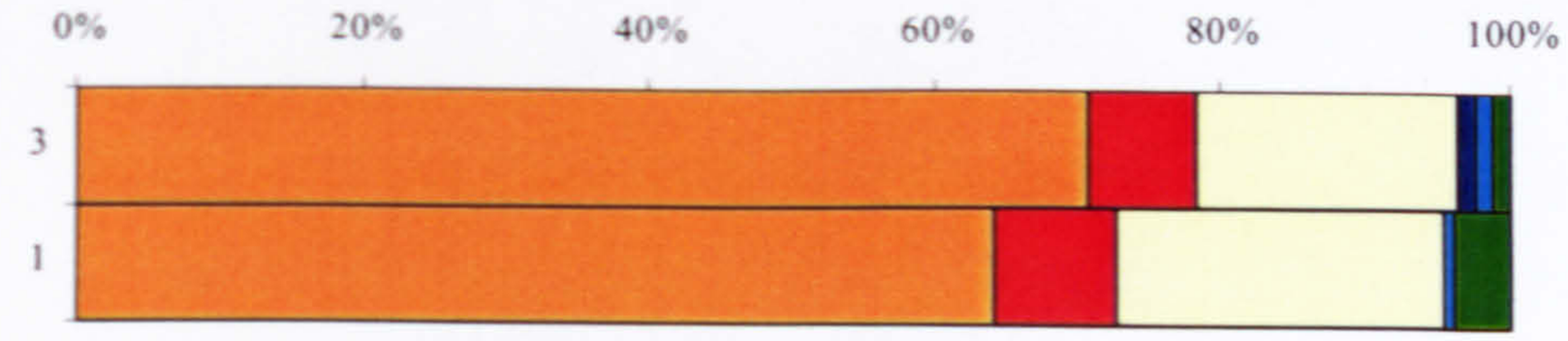

d

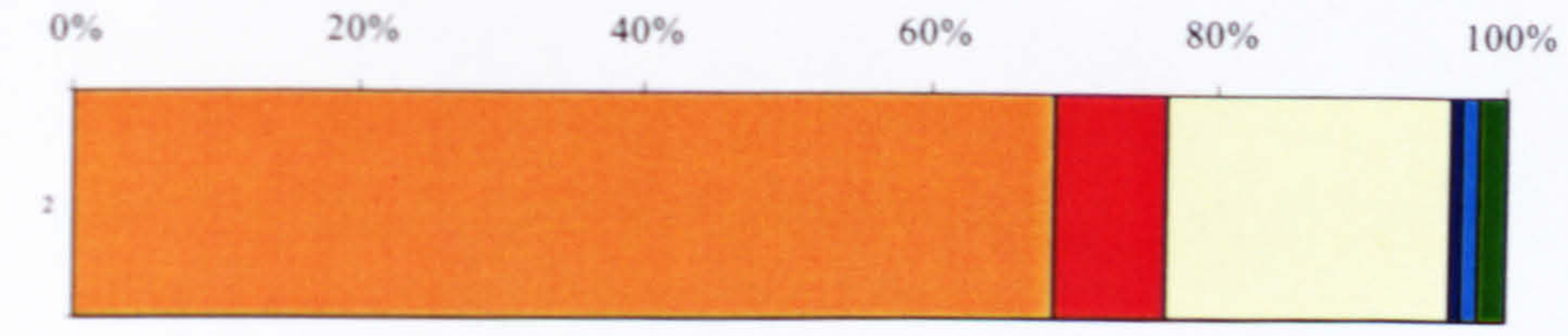

Figure 7.4. The effects of averaging the vertical facies data, whilst keeping the sampling frequency constant. Where A = Primary channel fills, B = Secondary channel fills, C = Splays, D = fine-grained channel fills, E = erosional remnants, and F = overbank fines. The small scale cyclicity that may be encountered in the (a) and (b) is lost when and averaged over greater vertical thicknesses (c and d). Also, because the data are averaged, the finer-grained architectural elements are distributed through the entire sequences (c and d) and not just concentrated in the centre of the sequences as shown in (a) and (b).

a

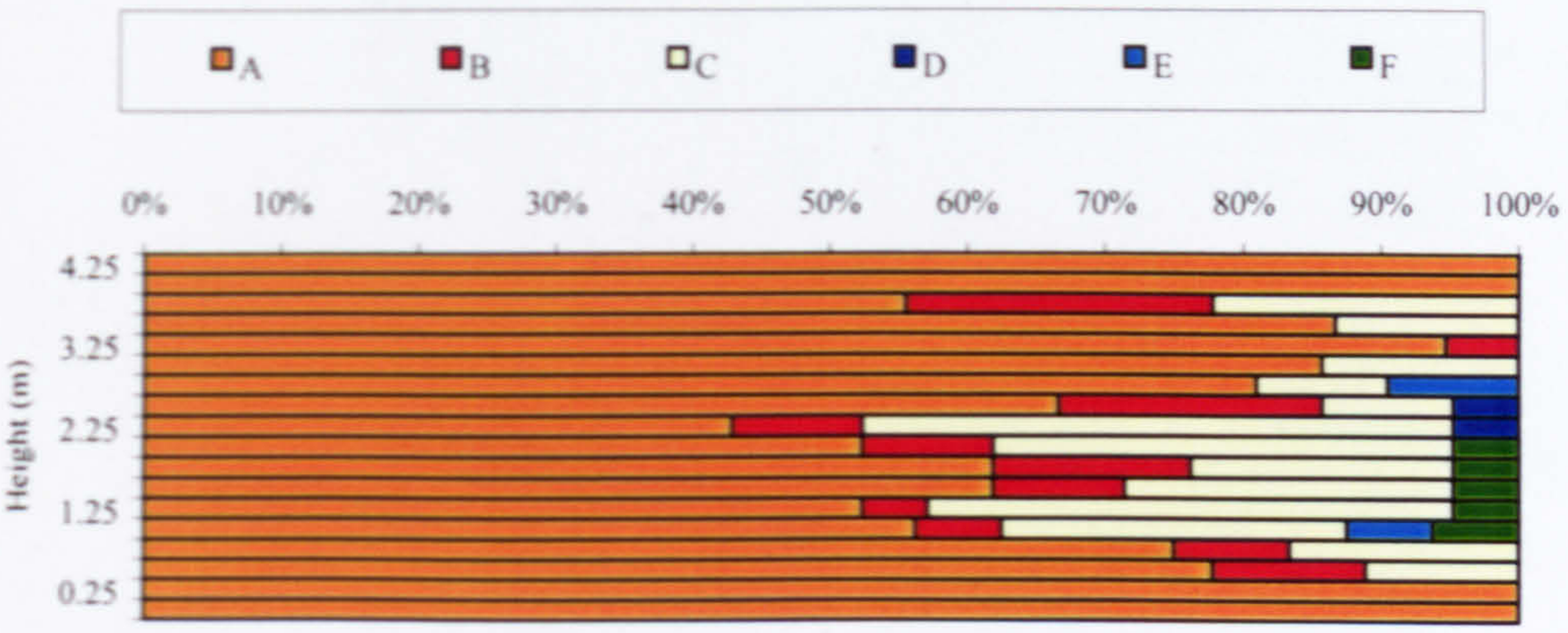

b

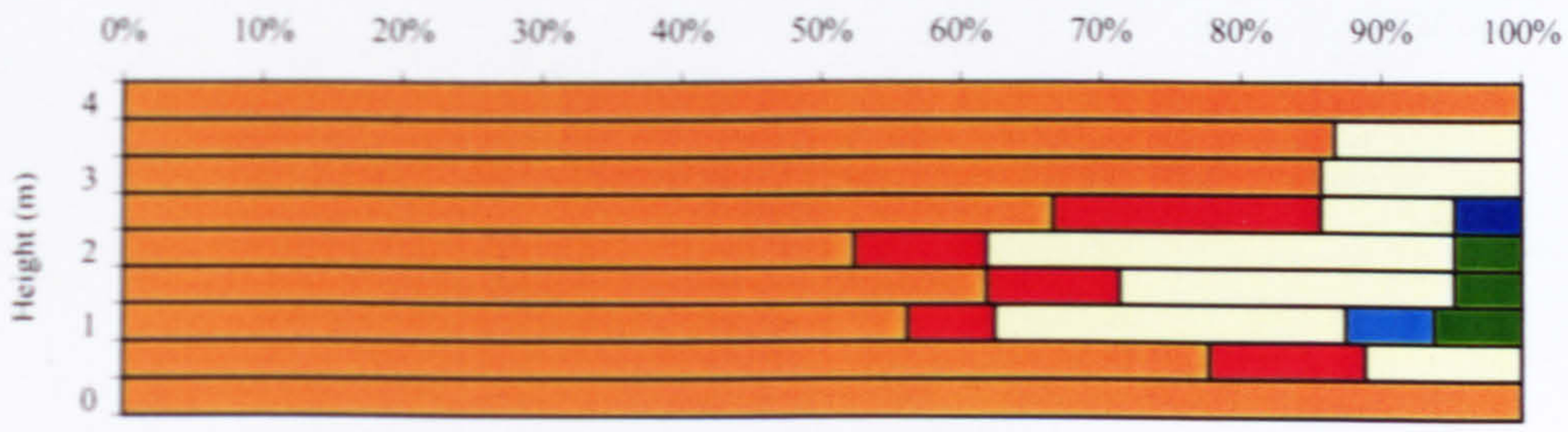

c

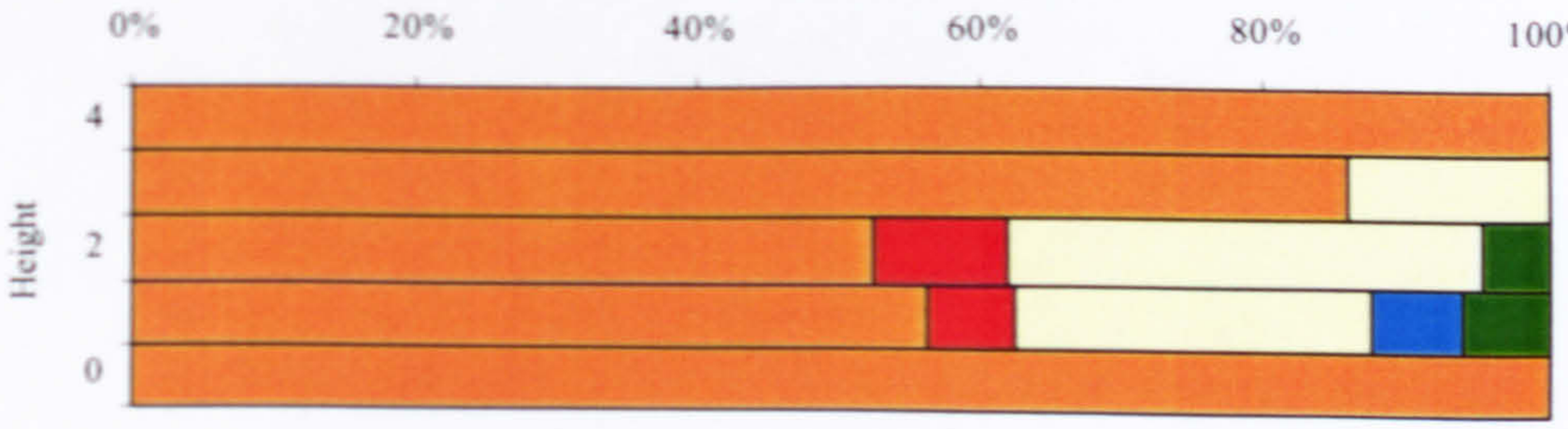

d

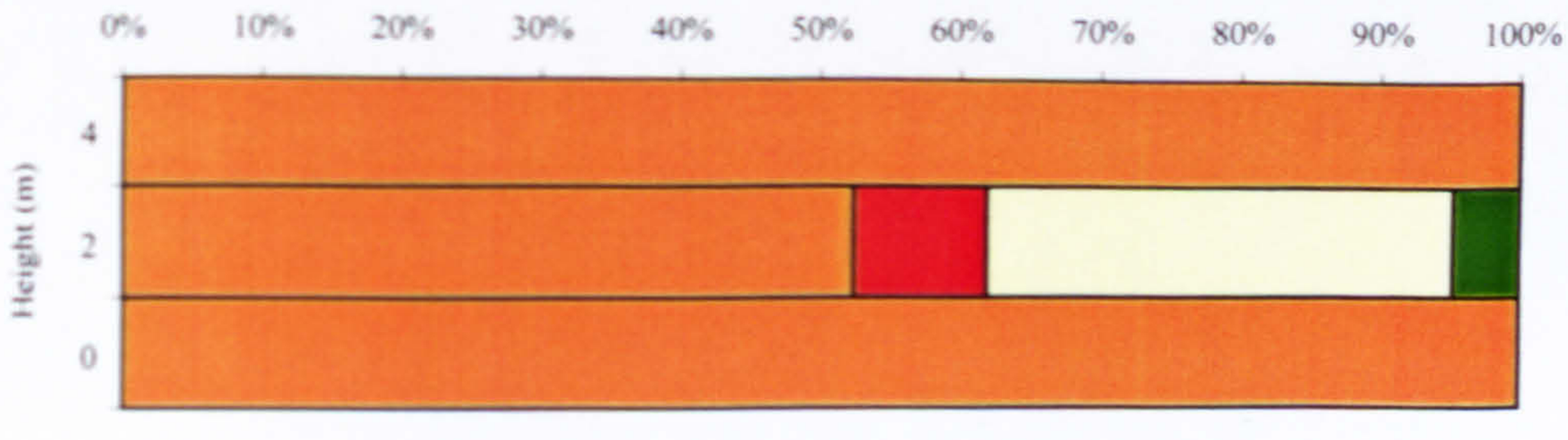

Figure 7.5. A diagram to illustrate the impact of the progressive doubling the vertical grid spacing (reducing the sampling frequency) using the model section data (a-d). Where A = Primary channel fills, B = Secondary channel fills, C = Splays, D = fine-grained channel fills, E = erosional remnants, and F = overbank fines. The most apparent differences are that as sampling frequency is reduced, primary channel fill deposits become over represented and a loss of some of the fine-grained elements (D and E) occurs.

7.9 Alternative analysis techniques

This chapter has detailed the future potential of how data from physical models can not only yield information on the controls of alluvial architecture but also provides a host of quantitative information to apply in hydrocarbon and aquifer geological studies. While Section 7.6 describes a methodology of assigning permeability to architectural elements based on comparisons of grain size and internal sedimentary structures, other approaches to this type of analysis may be used.

Work being carried out by Davis *et al.* (2000) on the sedimentary deposits from the experimental facility (Jurassic Tank) at St. Anthony Falls, University of Minnesota (refer to Paola, 2000; Stokstad, 2000) is focussing on the difference in facies permeability at a range of scales. The experimental facility is fed with a mixture of pale off-white sand and black coal grains to represent coarse- and fine-grained clastics respectively. The resultant depositional architecture comprises a mixture of the two materials (Figure 7.6). The composition of pale off-white sand and black coal grains within the sequence determines the greyness of each pixel covering the cut-section. Permeabilities are assigned to pixels based on this grey scale using the geometric mean of the two end members. Pixel size can be altered and the greyness becomes an average of the larger pixel size. This method can be used to address up-scaling effects and initial results showed effective permeability balance was not maintained as pixel size was increased (Davis *et al.* 2000).

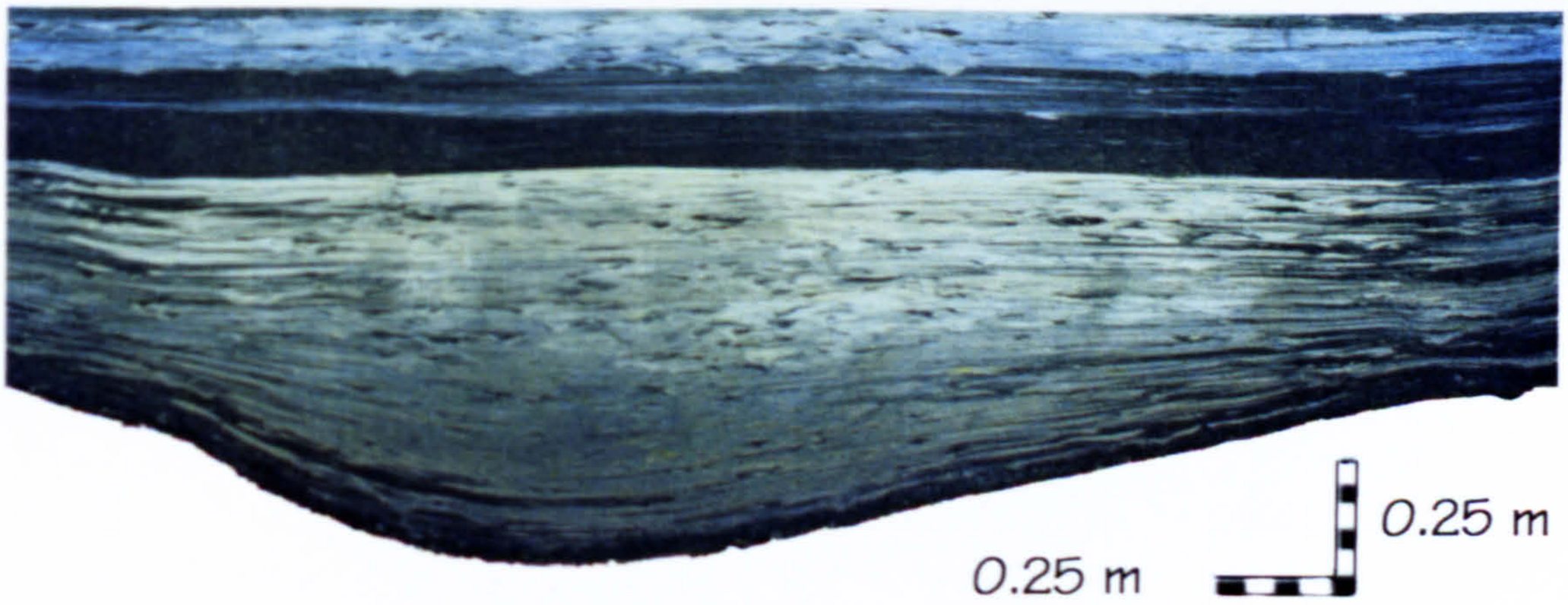

Figure 7.6. An example of the sectioned alluvial architecture from unscaled models from the experimental facility at St. Anthony Falls, University of Minnesota. Note palaeoflow direction was out of the page (Courtesy of Ben Sheets, University of Minnesota).

This methodology shows potential for use on a section from the Ashburton model, to allow rapid quantification of the flow through these coarse-grained architectural elements. An example of a cut section photograph from the Ashburton model is presented following conversion to a greyscale in Adobe Photoshop 5.0 (Figure 7.7a,b). This may yield important information on the permeability balance from these coarse-gravel braided river deposits and can be tested against the more time consuming methods of assigning specific permeability values of architectural elements described in Section 7.6. This type of analysis may also be used to test the effect of up-scaling the architecture, by using different pixel sizes to characterise the sequence. This technique may be more problematic when applied to the Ashburton model deposits as the range of grain sizes and colour are more varied than those used in the St. Anthony Falls Laboratory facility. General trends within the deposits show darker colours are associated with coarser grain sizes and therefore relative trends may be established. Conversion to a black and white scale (Figure 7.7c) highlights the coarse-grained channel fill deposits (elements A and B). This pixel-based analysis technique does not rely on the geologist to identify the alluvial architecture and relies of the assumption that greyness is linked to permeability and in turn facies type.

Alternative techniques to test conductivity may include mini-permeameter apparatus (e.g. Dreyer *et al.*, 1990) that may need to be adapted for use in small-scale physical models. To gain bulk conductivity, tracer or pump tests could be employed in future modelling experiments before the sequence is sectioned.

a

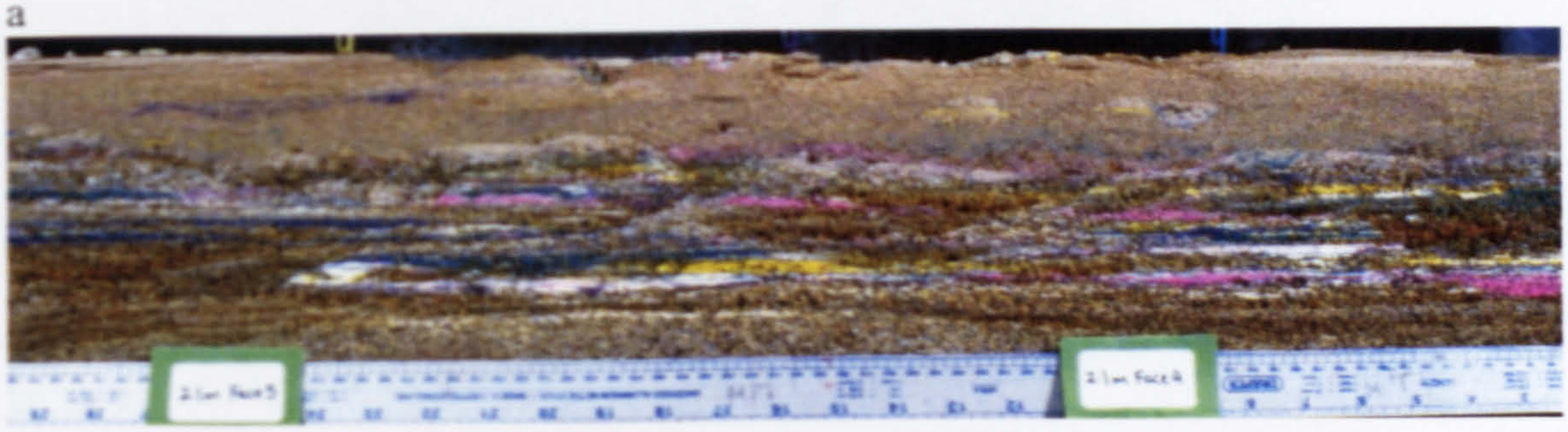

b

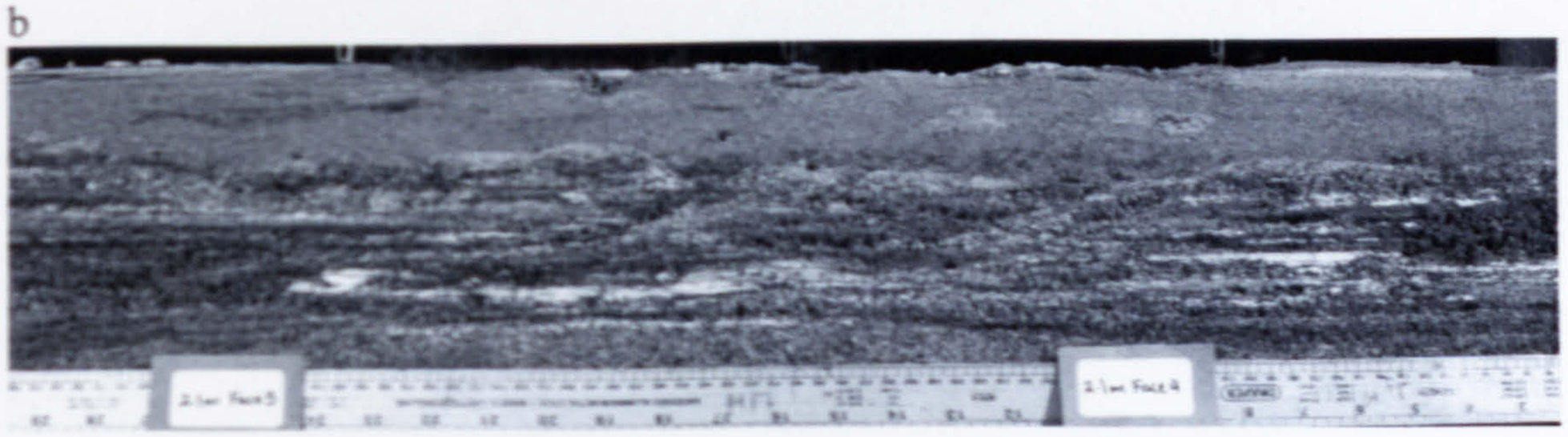

c

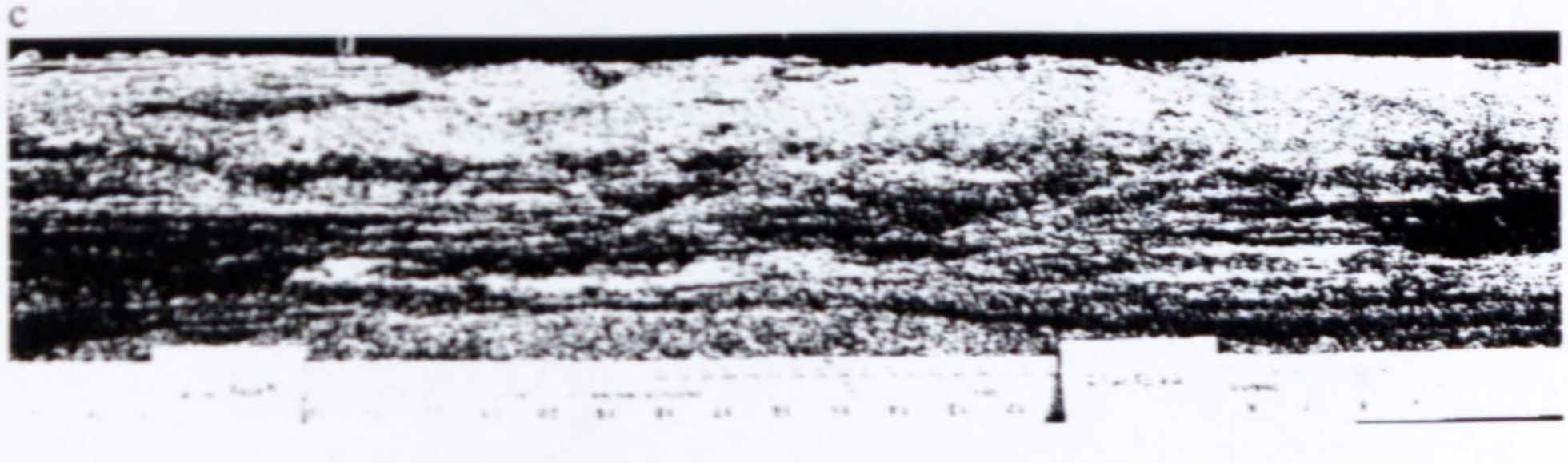

Figure 7.7. Examples of how the techniques using greyscale pixel analysis of Davis *et al*. (2000) to assign permeabilities could be employed on sections from the scaled Ashburton physical model (Chapter 6). Sections are cut perpendicular to the palaeoflow direction. (a), (b), and (c).

7.10 Recommendations

This chapter has explored the potential of physical modelling to provide information at the within channel-belt architecture scale to serve as direct input to current reservoir simulation software. A series of recommendations are made to continue this research theme.

- Future work on the physical model datasets needs to constrain more accurately the influence of changing the sampling grid and averaging the data when up-scaling at the within channel-belt scale.
- Alluvial architectural elements and channel-belt sandbodies are often considered as rectangular block in quantitative models (e.g. Bridge and Leeder, 1979; Mackey and Bridge, 1995) based on a maximum width and thickness measurements. Quantification of the three-dimensional shape of architectural elements in the physical model needs to be undertaken in order that future models are not reliant on this rectangular form.
- Incorporation of the within channel-belt architectural element heterogeneities into reservoir simulation models is required to validate the model outputs and test their impact on flow simulation models.
- Testing of the methods of conditioning outcrop width distributions (Visser and Chessa, 2000a,b) employed in Chapter 3, is required, using complete and partial sections of the alluvial architecture displayed in the physical model cut-section sequences.
- Permeability studies using a portable air permeameter to allow in situ measurements of unconsolidated sediments in physical models. Tracer tests and pump tests may also be used for bulk hydraulic conductivities.
- Analysis of scale invariance in fluvial systems is needed, coupled with an appreciation of the depositional model to enable application of physical modelling datasets to outcrop and subsurface studies to be carried out.
- Input the data into current reservoir simulation software such as IRAPS RMS or GeoQuest and test model sensitivity.

7.11 Summary

The main conclusions to the chapter are outlined below:

1. The potential of using a combined approach to fluvial reservoir evaluation is highlighted using both more traditional techniques of core and outcrop analogues studies together with aggrading basin physical models to address *all* scales of heterogeneity required for fluvial reservoir evaluation.
2. With direct correlations between within channel-belt architectural element/facies type and petrophysical properties, a methodology for collection of data from preserved stratigraphy of physical modelling is presented with the aims of: (i) providing vertical proportion curves to exhibit vertical facies trends within the model sequences; (ii) provide quantitative data to serve as inputs to object-based reservoir simulation models; and (iii) to assess the sensitivity of sampling grid size and sampling averaging in up-scaling of geological datasets.
3. The future potential benefits of using physical modelling are explored and several recommendations for future work are expressed. These are: (i) improved quantitative datasets for hydrogeological simulations; (ii) quantification of three-dimensional architectural element shape; (iii) sensitivity testing of geostatistical techniques; (iv) permeability studies; (v) application of physical models to different fluvial depositional environments and different scales of fluvial systems; and (vi) use of alternative pixel-based and permeability analysis techniques.

Chapter 8: Conclusions and recommendations for further work

8.1 Conclusions

This thesis has presented an integrated subsurface, physical modelling and field analogue approach to the investigation of allocyclic and autocyclic controls on river morphology and the prediction of alluvial architecture at both the channel-belt and within channel-belt scales. This chapter summarises the main conclusions of the thesis and presents ideas for further work.

8.1.1 Carboniferous of the UK Southern North Sea

1. Subsurface prediction of inter-well alluvial architecture and connectivity of the continental Barren Red Beds of the Upper Carboniferous, Lower Ketch Member, Tyne Field, UK SNS, is problematic, because of the lack of correlative marker horizons and low seismic resolution. The Lower Ketch Member exhibits a variety of discrete sandbodies nested within heavily oxidized fine-grained silts and a net-to-gross of 0.6. A new model for the depositional environment of the Lower Ketch Member is presented that proposes an alluvial plain developed that was traversed by a series of coarse-grained sandy, braided channel-belts in co-existence with extensive floodplains, which were subject to crevasse splay events. Palaeochannel depths were estimated as between 1.5 and 3.5 m and occurred within sandy, braided channel-belts with widths ranging between 100 to1100 m. The depositional model for the Tyne Field is consistent with the depositional model from the Ketch and Schooner Fields (Stone and Moscariello, 1999) and can be consolidated to produce a regional depositional model with the following characteristics: (i) predominant sediment supply was from the north, and (ii) proximal to distal trends exhibit a grain size diminution, lowering of net-to-gross and connectivity, and increase in pedogenesis to the south. Differentiating between the control of climate, base-level, sediment supply and tectonics as the main controlling mechanisms for the Lower Ketch Member alluvial architecture is ambiguous.

8.1.2 Onshore analogues for the UK Southern North Sea

1. Lithofacies characteristics and the proposed depositional model for the Tyne Field are dissimilar to UK stratigraphic outcrop analogues and onshore UK exposure is often limited to distances below typical well spacing (~0.5 km). Therefore, the application of onshore UK stratigraphic analogues for reservoir evaluation of the Lower Ketch Member is rejected.
2. The Eocene Escanilla Formation, Southern Pyrenees, Spain, is proposed as a suitable analogue for the Lower Ketch Member, Tyne Field, SNS. The depositional model proposed by Bentham *et al.* (1992, 1993) has been expanded in this thesis and new information regarding the occurrence of limestones containing freshwater biota and presence of oncoids suggest shallow lakes were pervasive on the floodplain. The increase in the proportion of sandbodies at the top of the Lower Escanilla Formation was consistent with the overall shallowing upward sequence exhibited within the Ainsa Basin. This thesis provides the first complete comparative study between the Tyne Field and an onshore analogue. Marked qualitative and quantitative similarities between the two sedimentary sequences give confidence in the analogue and permit the use of sandbody datasets that include information on width/thickness ratios, probability density functions, and channel-belt orientation for use in populating stochastic reservoir models. This thesis presents a case to show that while many modern fluvial systems exhibit extensive floodplains, grain size is the critical control on the preservation of floodplain deposits within the subsurface of the Escanilla Formation and the Lower Ketch Member.

8.1.3 Quantitative prediction of alluvial architecture

1. A review of the literature reveals several key considerations regarding the application of alluvial architecture datasets to the prediction of subsurface datasets, including: (i) the use of vertical facies profiles may be ambiguous in determining channel pattern; (ii) several channel patterns may have been responsible for the deposition of a particular sequence; (iii) a single channel pattern type may show a wide range in sandbody widths and thicknesses, and (iv) allocyclic and autocyclic controls also determine sandbody geometry. Consequently, the use of general trend

lines to predict sandbody geometry is not recommended. Instead, a match of all geological characteristics and the subsequent use of frequency distribution of sandbodies geometries may be more reliable. Quantitative datasets for reservoir-analogue studies are often too poorly-constrained to be applied reliably without a visit to the analogue outcrop. This study highlights the need to critically appraise reservoir and analogue studies by comparing: depositional environment, climate, grain size, lithofacies associations, formative channel depth, channel-belt widths, palaeoflow direction, orientation, sandbody and overbank geometries, basin setting, burial depth and compaction. A list of minimum requirements for a procedure for sandbody classification for full reservoir and analogue comparisons is presented to facilitate communication between geologists and the application of geometrical datasets between sedimentary sequences, without the necessity to visit the field.

2. This study shows that the use of single sandbody measurements for the comparison of reservoir-analogue sequences must account for compaction. A rationale is presented, which has ascertained that the sedimentary sequences from both the Lower Ketch Member and the Escanilla Formation have undergone minimal facies-dependent differential compaction and that much of the dewatering associated with standard shale burial compaction curves occurs during the formation of well-drained palaeosols.
3. The conditioning methods of Visser and Chessa (2000a,b) have been successfully used to adjust the partially exposed Escanilla sandbody distributions to provide an order of magnitude more data points than when only the completely exposed sandbodies are measured. The conditioning method also adds considerable information on the larger width distributions and failure to account for sandbody exposure results in an underestimation of sandbody widths. Empirical calculations of channel-belt width from cross-set data overestimated ~75 % of the measured channel-belt sandbody widths taken in the Escanilla field study. Empirical calculations of channel-belt width fail to capture the intrinsic variability of sandbody geometry.

8.1.4 Physical modelling of fine-grained systems

1. The direct 1:50 generic Froude-scaling of rivers supplied with fine-grain size distributions, such as the rivers responsible for the deposition of the Lower Ketch Member, is not possible without introducing significant distortion to the model. Theoretical calculations of scaled hydraulic flow parameters for the Lower Ketch Member produce grain Reynolds numbers below the critical level for flows to be hydraulically rough. The physical limits of grain size distributions needed for successful Froude-scaling modelling are explored in three braided (series C = coarse, M = medium, F = fine) river experiments. The presence of pronounced bedform development was noted within the channels of series F and M experiments. Phase diagram plots of D_{50} and D_{90} values fall within the dune/ripple/lower-stage plane bed field, and the disappearance of bedforms at higher flow stages suggest the bedforms represent current ripples. These current ripples do not scale with field prototype bedforms; and therefore this study may provide minimum grain size distribution limits to guide future physical scale modelling.

8.1.5 The impact of grain size on alluvial architecture

1. The Ashburton River displays a diminution coefficient of 0.0322 ψ km^{-1} and retains the grain size distribution shape along the length of river. Channels exhibit no significant change in geometry along the length of the Ashburton River, because either: (i) grain size has no significant impact on channel geometry compared to other controls, or (ii) downstream changes such as increasing discharge and reduction of downstream channel gradient counteract the impact of downstream grain size diminution on channel geometry. Physical modelling suggests other controls such as field discharge or sediment load may be more important controls on determining channel geometry.
2. This thesis is the first study that quantifies the influence of grain size on within channel-belt surface morphology and depositional architecture, using a unique 1:50 scaled model of the modern Ashburton River prototype. Three reach-scale, generic Froude-scaled modelling experiments, incorporating a fourfold change in grain size were conducted in a flume facility that permits aggradation. Changes in braided

channel morphology show that as grain size distribution is decreased by 50 % and 75 %: (i) channel geometries first deepen then widen, (ii) the proportion of overbank sheet flow increases, (iii) the duration of channel occupancy remains constant, and (iv) sediment surface gradients are significantly higher in series F. The surface morphology shows a marked similarity between the field prototype and model.

3. The two-dimensional geometry and frequency of occurrence of alluvial architectural elements are controlled by grain size. Architectural elements from FSM of the Ashburton River show that alluvial architecture is dominated by primary channel fill deposits and a fourfold change in the grain size distribution resulted in: (i) an increase in primary channel fill width and thickness between series M and F; (ii) an increase in splay width between series C and F; (iii) a higher proportion of preserved splay deposits between series C and M; and (iv) a decrease in the size and proportion of fine-grained architectural elements between series C and F. The reduction in preservation of fine-grained architectural elements between series C and F may be attributed to: (i) the smaller median grain size and lower fall velocity of particles in series F compared to series C, which inhibits the settling of suspended sediment; (ii) the higher suspended sediment concentrations in series F causing a reduced settling of fine-grained deposits, creating less opportunity for preservation of these fines; and (iii) the higher aerial proportion of sheet flow and wider channels present on the sediment surface in series F may prohibit settling of fine-grained silica flour.
4. Channel-belt architectural models such Bridge and Leeder (1979) and Heller and Paola (1996) cannot be scaled down to the channel scale without the incorporation of grain size controls. Preservation of channel fill geometry is determined by vertical channel aggradation, bed scour and deposit dissection by channel avulsion. These processes result in a reduction in the width/thickness ratio of channel fill deposits from their formative channel geometry.
5. Despite the presence of large amounts of fine-grained material in the Lower Ketch Member and the Escanilla Formation that is usually attributed to high aggradation or subsidence rates, it is difficult to unambiguously isolate aggradation as the mechanism controlling alluvial architecture. Existing alluvial architecture models (e.g. Bridge and Leeder, 1979; Bryant *et al.*, 1995; Mackey and Bridge, 1995; Heller and Paola, 1996) fail to incorporate downstream grain size changes.
6. Grain size distribution is critical to the interpretation of alluvial sequences. Sedimentary fluvial deposits displaying an increasing sandbody proportion relative

to overbank deposits up-sequence do not necessarily represent a change in aggradation rate or sediment supply rate. Alternatively, these sequences could result from a basinward facies shift associated with a modification of downstream fining trend or a progradation of the alluvial plain. Both a modification of the downstream fining trend and a basinward facies shift would alter the relative proportions of coarse- and fine-grained material being supplied to a particular location in the basin.

8.1.6 Integrated approaches to fluvial reservoir evaluation

1. Quantitative geometrical datasets for alluvial architecture within the published literature are biased towards the channel-belt scale architecture and there is a data gap concerning the within channel-belt alluvial architecture. This is the first study to explore the potential benefits of using preserved stratigraphy from physical models for the construction of both static and dynamic reservoir models at the within channel-belt scale. These physical modelling datasets complement analogue and subsurface datasets to address all the scales of heterogeneity required in full reservoir appraisal.
2. Alluvial architecture data from the physical model requires up-scaling to a prototype and then extrapolation to analogue deposits. This thesis shows that physical models scale well with maximum depth to the modern prototype, but require a further scaling factor to account for the full hierarchy of channel scales that may have been responsible for the deposition of the ancient prototype.
3. The Lower Ketch Member and literature studies show a direct relationship between architectural element/facies type and permeability, indicating that reservoir quality improves with increasing particle grain size and sorting. This direct correlation between within channel-belt architectural element/facies type and petrophysical properties allows a methodology for collection of data from preserved stratigraphy of physical modelling to be presented to: (i) provide vertical proportion curves to characterise vertical facies trends within the model sequences; (ii) provide quantitative data on the architectural element geometries to serve as inputs to object-based reservoir simulation models; and (iii) assess the sensitivity of sampling grid size and sampling averaging in up-scaling of geological datasets.

8.2 Recommendations for future work

This thesis provide significant advances in the understanding of fluvial reservoirs and lays the foundation for more detailed investigations. Fruitful avenues for future research could be:

1. Examination of core data from the Tyne Field now needs to be supplemented with investigation of wireline well data in order to investigate the alluvial architecture within the entire reservoir interval. In addition, an understanding of the Lower Ketch Member would be significantly enhanced by the incorporation of a wider study of the Southern North Sea Fields that have wells that penetrate the Carboniferous Barren Red Beds. A broader study would allow a more regional quantitative depositional model to be generated and assist in constraining downstream changes in channel-belt sandbody geometries. The development of a depositional model for the Lower Ketch Member and the Escanilla Formation should be complemented by the establishment of a modern day analogue (if it exists).
2. Future work should quantify the grain size distributions for individual facies types in both the Lower Ketch Member and the Escanilla Formation. Uncertainties associated with the contribution of illuvial material to the overbank deposits required quantifications through analysis of thin sections, in order to isolate the proportion of the grain size distribution supplied to the basin from fluvial processes.
3. Future work may focus on differentiating the palaeocurrent populations for individual channel sandstone body types. This may add particular value to the estimation of connectivity in the Lower Ketch Member, especially following the work of Mijnssen (1997) who identified sandbody orientation as the critical parameter affecting sandbody connectivity within the Schooner Formation, SNS. In addition, an assessment of cross-set thickness within individual sandbodies may assist the application of empirical relationships that predict channel-belt width (e.g. Bridge and Mackey, 1993) rather than taking a mean of all the set thicknesses measured in all the sandbodies.
4. Sandbody geometrical datasets from the Escanilla Formation do not provide information on the lateral and vertical basin wide stacking patterns. Bentham *et al.*, (1992) document a general increase in sandbody proportion up-section within the Escanilla Formation. The understanding of geometrical data from this thesis would be improved by the examination and quantification of stacking patterns, in addition

to the acquisition of more sandbody dimension data, to include shape, in different locations within the sequences to those used in this study. Oblique aerial photography of the main 20 km exposed ridge in the Ainsa Basin is recommended to quantify the basinwide alluvial architecture.

5. The conditioning method of Visser and Chessa (2000a,b) provides considerably more information on the longer width classes. Detailed stratigraphy from physical modelling sections provides well-constrained datasets that can be used to validate the conditioning method of Visser and Chessa (2000a,b). Preserved alluvial architecture from physical models provides only complete width or length distributions for which palaeocurrent direction is known. Preserved sections could be progressively obscured to simulate outcrop conditions and the sensitivity of the conditioning method to predict the width distributions may be tested against the completely exposed section.
6. Datasets gathered from both the Escanilla Formation and the preserved stratigraphy from the physical modelling provide the necessary geostatistics for stochastic reservoir simulation models at the channel-belt and within channel-belt scale architecture respectively. Opportunities exist to input these data into a geological modelling package such as ROXAR's RMS or Schlumberger's GeoQuest software packages in order to validate the outputs.
7. The physical model presented in this thesis is a simplification of the multiple controls that may act on or within one particular basin. The key now lies with the systematic isolation and incorporation of factors such as: (i) discharge magnitude and frequency, (ii) spatial and temporal variations in sediment supply rate, (iii) the density and sediment binding capacity of floodplain vegetation, and (iv) quantification of avulsion frequency and duration controls on stacking patterns.
8. A linear scaling was employed to up-scale physical modelling datasets of two-dimensional cross-sectional alluvial architecture. Sapozhnikov and Foufoula-Georgiou (1996, 1997) suggested that planform geometry of braided rivers exhibited an anisotropic scaling. Studies are required to both assess and validate the scaling relationships between reservoir-outcrop studies, model-outcrop studies and model-modern river studies in order that data may be up-scaled in an appropriate manner. Following the problems with the scaling of fine-grained systems in a physical model, a large study is needed of how subsurface geometries can be applied to fluvial systems at a range of scales. A study of the scale invarience of planform geometry between modern braided rivers is required. The failure to satisfy Froude-

scale model scaling laws for the fine grain size distributions such as observed in the Lower Ketch Member, make necessitate a study on the applicability of using coarse-gravel rivers to interpret sandy rivers by quantifying the scaling relationship between sand and gravel braided rivers.

9. Along a river course, grain size has been identified to alter in two ways: (i) by reducing the magnitude of particle sizes, and/or (ii) changing the overall sorting of the grain size distribution. This thesis investigated the first of these modifications. However, studies such as Parker (1979), Iseya and Ikeda (1987), Sambrook Smith (1996) and Knighton (1998) advocate that rivers supplied with a bimodal grain size distributions will undergo a change in river morphology (e.g. planform and cross-sectional geometry) when the relative proportion of gravel and sand modes alters beyond a critical threshold. A major opportunity exists to use physical modelling to isolate the impact of altering the modal proportion of a bimodal grain size distribution. Furthermore, the collection of grain size distribution data in modern rivers is often confined to the channel-belt. Grain size acquisition needs to be extended to include the floodplain to ascertain the extent to which changes in channel-belt sandbody proportions observed in the Escanilla Formation are the result of downstream fining trends or other controlling mechanisms (e.g. sedimentation rate and avulsion frequency).
10. Grain size has an impact on both the channel-belt and within channel-belt architecture. Consequently, the incorporation of grain size into alluvial architecture models (e.g. Bridge and Leeder, 1979; Mackey and Bridge, 1995; Heller and Paola, 1996) both at the channel-belt and within channel-belt scale is required. Incorporation of grain size would allow the construction of more comprehensive alluvial architecture models that could be tied back to the gross permeability structure.
11. This thesis has shown the direct link between facies/architectural element type and permeability. Sampling of grain size from architectural elements that have been defined in the physical model cut-sections is required, in order to quantify the qualitative link between architectural elements and permeability ascertained in Chapter 7. In addition, there is also need to investigate the permeability within individual architectural elements by calibrating with outcrop studies. Further opportunities exist to evaluate the effect of within channel-belt architecture on the permeability distribution of alluvial sequences, by: (i) performing airflow tests through the sequence to determine the connectivity of the sediment sequence in

three-dimensions, and (ii) the assignment of permeability to pixels based on the conversion of cut-section photographs to a greyscale and the assignment of a relative permeability on the grey intensity to act as a surrogate for facies type (e.g. Davis *et al.*, 2000). In addition, the effects of up-scaling and averaging of the alluvial architecture from the physical model sections warrants quantification to determine: (i) the importance of within channel-belt architecture on the permeability balance, and (ii) optimal flow cell size for simulation modelling.

References

ADAMS, J. 1980. Contemporary uplift and erosion of the Southern Alps, New Zealand. *Geological Society of America Bulletin*, 91, 1-114.

AHLBRANDT, T. S., ANDREWS, S. & GWYNNE, D. T. 1978. Bioturbation in eolian deposits. *Journal of Sedimentary Petrology*, 48, 839-848.

AIGNER, T., ASPRION, U., HORNUNG, J., JUNGHANS, W. & KOSTREWA. 1996. Integrated outcrop analogues studies for Triassic alluvial reservoirs: examples from southern Germany. *Journal of Petroleum Geology*. 19, 393-406.

AITKEN, J. F., QUIRK, D. G. & GUION, P. D. (1999) Regional correlation of Westphalian sandbodies onshore UK: implications for reservoirs in the Southern North Sea. *In*: FLEET, A. J. & BOLDY, S. A. R. (eds.) *Petroleum geology of Northwest Europe: proceedings of the 5th Conference*. Geological Society, London. 747-756.

ALEXANDER, J. 1993. A discussion on the use of analogues for reservoir geology. *In*: ASHTON, M. (ed.) *Advances in Reservoir Geology*. Geological Society Special Publication of London. 69, 175-194.

ALEXANDER, J., BRIDGE, J. S., CHEEL, R. J. & LECLAIR, S. F. 2001. Bedforms and associated sedimentary structures formed under super critical water flows over aggrading sand beds. *Sedimentology*, 48, 133-152.

ALEXANDER, J. & GAWTHORPE, R. L. 1993. The complex nature of a Jurassic multistorey, alluvial sandstone body, Whitby, North Yorkshire. *In*: NORTH, C. P. & PROSSER, D. J. (eds.) *Characterization of Fluvial and Aeolian Reservoirs*. Geological Society Special Publication. 73, 123-142.

ALEXANDER, J. & LEEDER, M. R. 1987. Active tectonic controls on alluvial architecture. *In*: EHTHRIDGE, F. D., FLORES, R. M. & HARVEY, M. D. (eds.) *Recent Developments in Fluvial Sedimentology*. The Society of Economic Paleontologists and Mineralologists, Special Publication, Tusla. 39, 243-252.

ALEXANDER, J. & LEEDER, M. R. 1990. Geomorphology and surface tilting in an active extensional basin, SW Montana, USA. *Journal of the Geological Society of America*, 147, 461-467.

ALLEN, J. R. L. 1970. *Physical Processes of Sedimentation*. London, Allen and Unwin, 248p.

ALLEN, J. R. L. 1978. Studies in fluviatile sedimentation: an exploratory quantitative model for the architecture of avulsion-controlled alluvial suites. *Sedimentary Geology*, 21, 129-147.

ALLEN, J. R. L. 1983a. Studies in Fluviatile Sedimentation: Bars, Bar-complexes and Sandstone Sheets (Low-Sinuosity Braided Streams) in the Brownstones (L. Devonian), Welsh Borders. *Sedimentary Geology*, 33, 237-293.

ALLEN, J. R. L. 1983b. River bedforms: progress and problems. *In*: COLLINSON, J. D. & LEWIN, J. (eds.) *Modern and Ancient Fluvial Systems*. Special Publication of the International Association of Sedimentologists, 6, 19-33.

ANDERSON, M. P. 1989. Hydrogeologic facies models to delineate lareg-scale spatial trends in glacial and glacio-fluvial sediments. *Geological Society of America Bulletin*, 101, 501-511.

ANDERSON, M. P., AIKEN, J.S., WEBB, E. K. & MICKELSON, D. M. 1999. Sedimentology and hydrogeology of two braided stream deposits. *Sedimentary Geology*, 129, 187-199.

ARCHARD, G., STAFFORD, J., BARDWELL, K. & BAGGE, M. 1998. A Review of techniques used to determine geological and thermal history in the Southern North Sea. *In*: DUPPENBECKER, S. J. & ILIFFE, J. E. (eds.) *Basin modelling; practice and progress*, Geological Society Special Publication, 141, 117-135.

ARCHIE, A. & LOPEZ-GOMEZ, J. 1999. Tectonic and geomorphic controls on the fluvial styles of the Eslida Formation, Middle Triassic, eastern Spain. *Tectonophysics*, 315, 187-207.

ARNOT, M. J., GOOD, T. R. & LEWIS, J. J. M. 1997. Photogeological and image-analysis techniques for collection of large-scale outcrop data. *Research Methods Papers, Journal of Sedimentary Research*, A67, 984-987.

ASHLEY, G.M. 1990. Classification of large-scale subaqueous bedforms: a new look at an old problem. *Journal of Sedimentary Petrology*, 60, 160-172.

ASHMORE, P.E. 1982. Laboratory modelling of gravel braided stream morphology. *Earth Surface Processes and Landforms*, 7, 201-225.

ASHMORE, P.E. 1988. Bed load transport in braided gravel-bed stream models. *Earth Surface Processes and Landforms*, 13, 677-695.

ASHMORE, P.E. 1991a. How do gravel-bed rivers braid? *Canadian Journal of Earth Sciences*, 28, 326-341.

ASHMORE, P.E. 1991b. Channel morphology and bed load pulses in braided, Gravel-bed streams. *Geografiska Annaler*, 73A, 37-52.

ASHWORTH, P. J. & BEST, J. L. 1994. The scaled modelling of braided rivers of the Ivishak Formation, Prudhoe Bay II: shale geometries and response to differential aggradation rates. Final BP project report, August 1994, 1-247.

ASHWORTH, P.J. & BEST, J.L. 1998. Discussion of: Use of hydraulic models in management of gravel-bed rivers (Warburton and Davies) *In*: Klingeman, P.C., Beschta, R.L., Komar, P.D. and Bradley, J.B. (eds.) *Gravel-bed Rivers in the Environment*, Water Resources Publications, Colorado, 539-540.

ASHWORTH, P. J., BEST, J. L., LEDDY. J. O. & GEEHAN, G. W. 1994. The physical modelling of braided rivers and deposition of fine-grained sediment. *In*: KIRKBY, M. J. (ed.) *Process Models and Theoretical Geomorphology*. John Wiley & Sons Ltd. 115-139.

ASHWORTH, P. J., BEST, J. L. & MORETON, D. J. 2000. Quantification of TAGI reservoir architecture and depositional geometries: Phase 1. Final Project Report for Anadarko Algeria Corporation, June 2000, 1-37.

ASHWORTH, P. J., BEST, J. L.& PEAKALL, J. 1997. Aggradation controls on the three dimensional architecture of braided alluvium: a combined field and flume modelling approach. NERC Grant GR9/01640, Final Report, 1-7.

ASHWORTH, P. J., BEST, J. L., PEAKALL, J. & LORSONG, J. A. 1999. The influence of aggradation rate on braided alluvial architecture: field study and physical scale modelling of the Ashburton River gravels, Canterbury Plains, New Zealand. *In*: SMITH, N.D. & ROGERS, J. (eds.) *Fluvial Sedimentology VI*, Special Publication of International Association of Sedimentologists, Blackwells, 28, 333-346.

ASPRION, U. & AIGNER, T. 1999. Towards realistic aquifer models: three-dimensional georadar surveys of Quaternary gravel deltas (Singen Basin, SW Germany). *Sedimentary Geology*, 129, 281-297.

ATHY, L. F. 1930. Density, porosity, and compaction of sedimentary rocks. *Bulletin of the American Association of Petroleum Geologists*, 14, 1-24.

ATKINS, R. A. E. & HICKS, S. R. 1979. Geophysical models along Ashburton River, Canterbury, New Zealand. *New Zealand Journal of Geology and Geophysics*, 22, 673-677.

ATKINSON, C. D. 1983. *Comparative sequences of ancient fluviatile deposits in the Tertiary South Pyrenean Basin, Northern Spain.* Unpubished PhD thesis, University of Wales. 350 pp.

ATKINSON, C. D. 1986. Tectonic control on alluvial sedimentation as revealed by an ancient catena in the Capella Formation (Eocene) of Northern Spain. *In*: WRIGHT, V. P. (ed.) *Paleosols - their Description and Interpretation.* Blackwell Scientific Publications, Oxford, 139-179.

ATKINSON, C. D., McGOWEN, J. H., BLOCH, S., LUNDELL, L. L. & TRUMBLY, P. N. 1990. Braidplain and Deltaic Reservoir, Prudhoe Bay Field, Alaska. *In*: BARWIS, McPHERSON & STUDLICK (eds.) *Sandstone Petroleum Reservoirs*. 7-29.

BAILEY, J. B., ARBIN, P., DAFFINOTI, O., GIBSON, P. & RITCHIE, J. S. 1993. Permo-Carboniferous plays of the Silver Pit Basin. *In*: PARKER, J. R. (ed.) *Petroleum Geology of Northwest Europe: Proceedings of the 4th Conference*, The Geological Society, London, 707-715.

BAL, A. A. 1996. Valley fills and coastal cliffs buried beneath an alluvial plain: evidence from variation of permeabilities in gravel aquifers, Canterbury Plains, New Zealand. *Journal of Hydrology (NZ)*, 35, 1-27.

BALDWIN, B. 1971. Ways of deciphering compacted sediments. *Journal of Sedimentary Research*, 41, 293-301.

BALDWIN, B. & BUTLER, C.O. 1985. Compaction curves. *Bulletin of the American Association of Petroleum Geologists*, 69, 622-626.

BASHER, L.R., TONKIN, P. J. & McSAVENEY, M. J. 1988. Geomorphic history of a rapidly uplifting area on a compressional plate boundary; Cropp River, New Zealand. *Zeitschrift fuer Geomorphologie. Supplementband*, 69, 117-131.

BEARD, D.C. & WEYL, P.K. 1973. Influence of texture on porosity and permeability of unconsolidated sand. *Bulletin of the American Association of Petroleum Geologists*, 57, 349-369.

BEER, J. A. & JORDEN, T. E. 1989. The effects of Neogene thrusting on deposition in the Bermejo Basin, Argentina. *Journal of Sedimentary Petrology*, 59, 330-345.

BEGG, S. H., CARTER, R. R. & DRANFIELD, P. 1989. Assigning effective values to simulator gridblock parameters for heterogeneous reservoirs. *Society of Petroleum Engineers*, November, 455-463.

BEHL, R. J. & KENNETT, J. P. 1996. Brief interstadial events in the Santa Barbara basin, NE Pacific, during the past 60 kyr. *Nature*, 379, 243-246.

BENTHAM, P. A. 1992. *The tectonostratigraphic development of the western oblique ramp of the South-Central Pyrenean thrust system, Northern Spain*. PhD Dissertation, University of Southern California, Los Angeles, USA. pp. 109-200.

BENTHAM, P. A., BURBANK, D. W., PUIGDEFABREGAS, C. 1992. Temporal and spatial controls on the alluvial architecture of an axial drainage system: Eocene Escanilla Formation, southern Pyrenean foreland basin, Spain. *Basin Research*, 4, 335-352.

BENTHAM, P. A., TALLING, P. J. BURBANK, D. W. 1993. Braided stream and flood-plain deposition in a rapidly aggradation basin: the Escanilla formation, Spainish Pyrenees. *In*: BEST, J. L. & BRISTOW, C. S. (eds.) *Braided Rivers*, Geological Society Special Publication. 75, 177-194.

BERGER, G. W. 1988. Dating Quaternary events by luminesence. *Geological Society of America, Special Paper*, 227, 13-49.

BESLY, B. M. 1987. Sedimentological evidence for Carboniferous and Early Permian paleoclimates of Europe. *Extrait Des Annales De La Societe Geologique Du Nord*, CVI, 131-143.

BESLY, B. M. 1988. Palaeogeographic implications of late Westphalian to early Permian red-beds, Central England. *In*: BESLY, B. M. & KELLING, G. (eds.) *Sedimentation in a Synorogenic Basin complex: The Upper Carboniferous of Northwest Europe*. Blackie, Champman and Hall, 200-221.

BESLY, B. M. 1990. Carboniferous. *In*: GLENNIE, K. W. (ed.) *Introduction to Petroleum Geology of the North Sea*, Blackwell Scientific Publications, Oxford, 90-119.

BESLY, B. M., BURLEY, S. D. & TURNER, P. 1993. The late Carboniferous "Barren Red Bed" play of the Silver Pit area, Southern North Sea. *In*: PARKER, J. R. (ed.)

Petroleum Geology of Northwest Europe: Proceedings of the 4th Conference. The Geological Society, London, 727-740.

BESLY, B. M. & CLEAL, C. J. 1997. Upper Carboniferous stratigraphy of the West Midlands (UK) revised in the light of borehole geophysical logs and detritial compositional suites. 1997. *Geological Journal.* 32, 85-118.

BESLY, B. M. & FIELDING, C. R. 1988. Palaeosols in Westphalian coal-bearing and red-bed sequences, central and northern England. *Palaeogeography, Palaeoclimatology, Palaeoecology*, 70, 303-330.

BESLY, B. M. & TURNER, P. 1983. Origin of red-beds in a moist tropical climate (Etruria Formation, Upper Carboniferous, UK). *In*: WILSON, R. C. L. (ed.) *Residual Deposits: surface related weathering processes and materials.* Geological Society Special Publication, 11, 131-147.

BEST, J. L. & ASHWORTH, P. J. 1997. Scour in large braided rivers and the recognition of sequences boundaries. *Nature*, 387, 275-277.

BIERMAN, P. R. 1994. Using in situ produced cosmogenic isotopes to estimate rates of landscape evolution; a review from the geomorphic perspective. *Journal of Geophysical Research, B, Solid Earth and Planets*, 99, 13, 885-13,896.

BLODGETT, R.H. 1985. Paleovertisols as indicators of climate. *Bulletin of the American Association of Petroleum Geologists*, abstract, 69, 239.

BLODGETT, R. H. & STANLEY, K. O. 1980. Stratification, bedforms, and discharge relations of the Platte braided river system, Nebraska. *Journal of Sedimentary Petrology*, 50, 139-148.

BLUCK, B. J.,1987. Texture of gravel bars in braided streams. *In*: Richards, K.S. (ed.) River Channels: environment and process. *Institute of British Geographers Special Publication*, 17, 159-178.

BLUM, M. D. & VALASTRO, S. 1994. Late Quaternary sedimentation, Lower Colorado River, Gulf Coastal Plain of Texas. *Geological Society of America Bulletin*, 106, 1002-1016.

BLUM, M. D. & TORNQVIST, T. E. 2000. Fluvial responses to climate and sea-level change: a review and look forward. *Sedimentology*, 47, Supplement 1, 2-48.

BOWN, T. M. 1982. Ichnofossils and rhizoliths of the nearshore fluvial Jebel Qatrani Formation (Oligocene), Fayum Province, Eygpt. *Palaeogeography, Palaeoclimatology, Paleoecology*, 40, 255-309.

BOWN, T. M. & KRAUS, M. J. 1987. Integration of channel and floodplain suites, 1. Developmental sequence and lateral relations of alluvial paleosols. *Journal of Sedimentary Petrology*, 57, 587-601.

BRADBURY, K. R. & MULDOON, M. R. 1990. Hydraulic conductivity determinations in unlithified glacial and fluvial materials. *ASTM Special Technical Publication = American Society for Testing and Materials Special Technical Publication*, 138-151.

BRAYSHAW, A.C., DAVIES, G. W. & CORBETT, P. W. M. 1996. Depositional controls on primary permeability and porosity at the bedform scale in fluvial reservoir sandstones. *In*: CARLING, P. A. & DAWSON, M. R. (eds.) *Advances in Fluvial Dynamics and Stratigraphy*, 373-394.

BRIDGE, J. S. 1985. Palaeochannel patterns inferred from alluvial deposits: A critical evaluation. *Journal of Sedimentary Petrology*, 55, 579-589.

BRIDGE, J. 1993a. Description and interpretation of fluvial deposits: a critical perspective. *Sedimentology*, 40, 801-810.

BRIDGE, J. S. 1997. Thickness of sets of cross strata and planar strata as a function of formative bed-wave geometry and migration, and aggradation rate. *Geology*, 25, 917-974.

BRIDGE, J. S., ALEXANDER, J., COLLIER, R. E. LL., GAWTHORPE, R. L. & JARVIS, J. 1995. Ground-penetrating radar and coring used to study the large-scale structure of point-bar deposits in three dimensions. *Sedimentology*, 42, 839-852.

BRIDGE, J. S., COLLIER, R. E. LL. & ALEXANDER, J. 1998. Large scale structure of the Calamus River deposits (Nebraska, U.S.A.) revealed using ground-penetrating radar. *Sedimentology*, 45, 977-986.

BRIDGE, J. & DIEMER, J. 1983. Quantitative interpretation of an evolving ancient river system. *Sedimentology*, 30, 599-623.

BRIDGE, J. S. & GABEL, S. L. 1992. Flow and sediment dynamics in a low sinuosity, braided river: Calamus River, Nebraska Sand Hills. *Sedimentology*, 39, 125-142.

BRIDGE, J. S., JALFIN, G. A. & GEORGIEFF, S. M. 2000. Geometry, lithofacies, and spatial distribution of Cretaceous fluvial sandstone bodies, San Jorge Basin, Argentina: outcrop analogue for the hydrocarbon-bearing Chubut Group. *Journal of Sedimentary Research*, 70, 341-359.

BRIDGE, J. S. & LEEDER, M. R. 1979. A simulation model of alluvial stratigraphy. *Sedimentology*, 26, 617-644.

BRIDGE, J. S. & MACKEY, S. D. 1993a. A theoretical study of fluvial sandstone body dimensions. *In*: FLINT, S. S. & BRYANT, I. D. (eds.) *The Geological Modelling of Hydrocarbon Reservoirs and Outcrop Analogues*, International Association of Sedimentologists, Special Publication, 15, 213-236.

BRIDGE, J. S. & MACKEY, S. D. 1993b. A revised alluvial stratigraphy model. *In*: MARZO, M. & PUIGDEFABREGAS, C. (eds.) *Alluvial Sedimentation*. Special Publication of the International Association of Sedimentologists, 17, 319-336.

BRIDGE, J. S. & MACKEY, S. D. 1995. Three-dimensional model of alluvial stratigraphy: theory and application. *Journal of Sedimentary Research*, B65, 7-31.

BRIDGE, J. S. & TYE, R. S. 2000. Interpreting the dimensions of ancient fluvial channel bars, channels, and channel belts from wireline-logs and core. *Bulletin of the American Association of Petroleum Geologists*, 84, 1205-1228.

BRIERLEY, G. J. 1996. Channel morphology and element assemblages: a constructivist approach to facies modelling. *In*: CARLING, P. A. & DAWSON, M. R. (eds.) *Advances in Fluvial Dynamics and Stratigraphy*, 263-298.

BRIERLEY, G. J. & HICKIN, E. J. 1985. The downstream gradation of particle sizes in the Squamish River, British Columbia. *Earth Surface Processes and Landforms*. 10, 597-606.

BRIERLEY, G. J. & HICKIN, E. J. 1991. Channel planform as a non-controlling factor in fluvial sedimentology: the case of the Squamish River floodplain, British Columbia. *Sedimentary Geology*, 75, 67-83.

BRISTOW, C.S. 1987. Brahmaputra river: channel migration and deposition. *In*: ETHERIDGE, F. G., FLORES, R. M. & HARVEY, M. D. (eds.) *Recent Developments in Fluvial Sedimentology*, Society of Economic Paleontologists and Minerologists Special Publications, 39, 63-74.

BRISTOW, C. S. 1993. Sedimentary structures exposed in bar tops in the Brahmaputra River, Bangladesh. *In*: BEST, J.L & BRISTOW, C.S. (eds.) *Braided Rivers*, Geological Society of London Special Publication, 75, 277-289.

BRISTOW, C. 1996. Reconstructing fluvial channel morphology from sedimentary sequences. *In*: CARLING, P. A. & DAWSON, M. R. (eds.) *Advances in Fluvial Dynamics and Stratigraphy*. 351-370.

BRISTOW, C.S. and BEST, J.L., 1993. Braided rivers: perspectives and problems. *In*: Best, J.L. and Bristow, C.S. (eds.) *Braided Rivers*, Geological Society of London Special Publication, 75, 1-11.

BROWN, A. R. 1986. Interpretation of three-dimensional seismic data. *American Association of Petroleum Geologists Memoir*, 42, 194.

BROWN, L. J., WILSON, D. D., MOAR, N. T. & MILDENHALL, D. C. 1988. Stratigraphy of the late Quaternary Plains, New Zealand. *New Zealand Journal of Geology and Geophysics*, **31**, 305-330.

BRYANT, I. D. & FLINT, S. S. 1993. *The Geological Modelling of Hydrocarbon Reservoirs and Outcrop Analogues*. Special Publication of International Association of Sedimentologists, **15**, Blackwells, London.

BRYANT, M., FALK, P. & PAOLA, C. 1995. Experimental study of avulsion frequency and rate of deposition. *Geology*, **23**, 365-368.

BURBANK, D. W., VERGES, J., MUNOZ, J. A. & BENTHAM, P. 1992. Coeval hindward- and foreward-imbricating thrusting in the south-central Pyrenees, Spain: Timing and rates of shortening and deposition. *Geological Society of America Bulletin*, **104**, 3-17.

BURNETT, A. W. & SCHUMM, S. A. 1983. Active tectonics and river response in Louisiana and Mississippi. *Science*, **222**, 49-50.

BURNETT, M. 1996. 3-D seismic expression of a shallow fluvial system in west central Texas. *Bulletin of the American Association of Petroleum Geologists*, **42**, 45-55.

CADLE, A. B. & CAIRNCROSS, B. 1993. A sandy bed-load dominated fluvial system deposited by lateral-accretion: Permian Karoo Sequence, South Africa. *Sedimentary Geology*, **85**, 435-455.

CAMERON, T. D. J. 1993. 5. Carboniferous and Devonian of the Southern North Sea. *In*: KNOX, R. W. O'B & CORDEY, W. G. (eds.) *Lithostratigraphic nomenclature of the UK North Sea*, 1-90.

CANT, D. J. & WALKER, R. G. 1978. Fluvial processes and facies sequences in the sandy braided South Saskatchewan River, Canada. *Sedimentology*, **25**, 625-648.

CARACUEL, J. E., CARDENAL, J., DELGADO-GARCIA, J. & GARCIA-LOPEZ, S. 2000. A simple photogrammetric method to improve quantitative image analysis in geoscience research. *Journal of Sedimentary Research*, 70, 1337-1340.

CARLSON, C. W. 1965. The relationship of free meander geometry to stream discharge and its geomorphic implications. *American Journal of Science*, 263, 864-885.

CARSON, M.A., 1984a. Observations on the meandering-braided river transition, the Cantebury Plains, New Zealand: Part One. *New Zealand Geographer*, 40, 12-17.

CARSON, M.A., 1984b. The meandering-braided river threshold: a reappraisal. *Journal of Hydrology*, 73, 315-334.

CARTER, L. & HERZER, R. H. 1979. The hydraulic regime and its potential to transport sediment on the Canterbury continental shelf. *New Zealand Oceanographic Institute Memoir*, 83.

CAUDILL, M. R., DRIESE, S. G. & MORA, C. I. 1997. Physical compaction of vertic palaeosols: implications for burial diagenesis and palaeo-precipitation estimates. *Sedimentology*, 44, 673-685.

CHANDLER, M. A., KOCUREK, G., GOGGIN, D. J. & LAKE, L. W. 1989. Effects of stratigraphic heterogeneity on permeability eolian sandstone sequence, Page Sandstone, Northern Arizona. *Bulletin of the American Association of Petroleum Geologists*, 73. 658-668.

CHAPPELL, J. 1983. A revised sea-level record for the last 300000 years from Papua, New Guinea. *Search*, 14, 99-101.

Chemostratigraphy of the Westphalian C/D sequences from wells 44/14-2, 44/18-1, 44/18-2Z and 44/18-4A. 1995, Chemostrat Consultants, 1-80.

CHEW, L. C. & ASHMORE, P. E. 2001. Channel adjustment and a test of rational regime theory in a proglacial braided stream. *Geomorphology*, 37, 43-63.

CHITALE, S. V. 1970. River channel patterns. *Journal of the Hydraulic Division*, 96, 201-221.

CHORLEY, R. J. 1967. Models in geomorphology. *In*: CHORLEY, R. J. & HAGGETT (eds.) *Models in Geography*, London, 56-96.

CHURCH, M. & KELLERHALS, R. 1978. On the statistics of grain size variation along a gravel river. *Canadian Journal of Science*, 15, 1151-1160.

CLARKE, M. L. & RENDELL, H. N. 2000. The development of a methodology for luminescence dating of Holocene sediments at the land-ocean interface. *In*: SHENNAN, I. & ANDREWS, J. E. (eds.) *Holocene land-ocean interaction and environmental change around the North Sea*, Geological Society Special Publications, 166, 69-86.

COJAN, I. 1993. Alternating fluvial and lacustrine sedimentation; tectonic and climatic controls (Provence Basin, S. France, Upper Cretaceous /Palaeocene). *In*: MARZO, M; PUIGDEFABREGAS, C (eds.) *Alluvial Sedimentation*, Special Publication of the International Association of Sedimentologists, 17, 425-438.

COLLIER, R. E. L. 1989. Modelling the role of differential compaction and tectonics upon Westphalian facies architecture in the Northumberland Basin. *In*: GUTTERIDGE, R. S & NOLAN, P. (eds.) *The role of tectonics in Devonian and Carboniferous sedimentation in the British Isles*, Occasional Publication Yorkshire Geological Society, 6, 189-199.

COLLINSON, J. D. 1978. Vertical sequence and sand body shape in alluvial sequences. *In*: MIALL, A. D. (ed.) *Fluvial Sedimentology*, Canadian Society of Petroleum Geologists, Memoir 5. 577-586.

COLLINSON, J. D. & JONES C. M. 1997. Stratigraphy and sedimentology of the Westphalian C/D Barren Red Beds in Quadrants 44 and 49, Southern North Sea. Collinson Jones Consulting Ltd., Volume 1 & 2.

COLLINSON, J. D., JONES, C. M., BLACKBOURN, G. A., BESLY, B. M., ARCHARD, G. M. & McMAHON, A. H. 1993. Carboniferous depositional systems of

the Southern North Sea. *In*: PARKER, J. R. (ed.) *Petroleum Geology of Northwest Europe: Proceedings of the 4th Conference*, The Geological Society, London, 677-687.

COOPER, D. 1995. Tyne development programme - version 2. ARCO Internal report. Confidential.

COOPER, D. & MERRYWEATHER, M. 1994. Tyne geological and Geophysical submission. 1, ARCO Internal Report. Confidential.

COWEN, G. 1989. Diagenesis of Upper Carboniferous sandstones: southern North Sea Basin. *In*: WHATELEY, M. K. G. & PICKERING, K. T. (eds.) *Deltas: Sites and Traps for Fossil Fuels*, The Geological Society Special Publication, 41, 57-73.

CROSS, T. A. 1991. Field-scale reservoir characterization. *In*: LAKE, L. W., CARROLL, H. B. & WESSON, T. C. (eds.) *Reservoir Characterization 2*, Academic Press, London, 493-496.

CROUZEL, F. & MEYER, R. 1977. Les calcaires lacustres du Miocene Aquitain-Participation des lacs a l'edification d'un ensemble molassique continental. *Sci Terre*, XXI, 237-250.

CUEVAS GOZOLA, M. C. & MARTINIUS, A. W. 1993. Outcrop data-base for the geological characterisation of fluvial reservoirs: an example from distal fluvial fan deposits in the Loranca Basin, Spain. *In*: NORTH, C. P. & PROSSER, D. J. (eds.) *Characterization of Fluvial and Aeolian Reservoirs*, Geological Society of London Special Publication, 73, 79-94.

DAVIES, D. K., WILLIAMS, B. P. J. & VESSELL, R. K. 1992. Models for meandering and braided fluvial reservoirs with examples from the Travis Peak Formation, East Texas. *Society of Petroleum Engineers*, Paper 24692, 321-329.

DAVIES, D. K., WILLIAMS, B. P. J. & VESSELL, R. K. 1993. Dimensions and quality of reservoirs originating in low and high sinuosity channel systems, Lower Cretaceous Travis Peak Formation, east texas, USA. *In*: NORTH, C. P. & PROSSER,

D. J. (eds.) *Characterization of Fluvial and Aeolian Reservoirs*, Geological Society Special Publication, 73, 95-121.

DAVIS, J.M., LOHMANN, R.C., PHILLIPS, F.M., WILSON, J. L. & LOVE, D.W. 1993. Architecture of the Sierra Ladrones Formation, central New Mexico:Depositional correlation structure. *Geology Society of America Bulletin*, 105, 998-1007.

DAVIS, M. J., HICKSON, T. A., HARRIS, D., PAOLA, C. PERSON, M. 2000. Characterisation of heterogenity and scaling behaviour in three-dimensional laboratory-derived sedimentary deposit. *Geological Society of America*, Abstracts. P144.

DAWSON, M. 1988. Sediment size variation in a braided reach of the Sunwapta River, Alberta, Canada. *Earth Surface Processes and Landforms*, 13, 599-618.

DEODHAR, L. A. & KALE, V. S. 1999. Downstream adjustments in allochthonous rivers: Western Deccan trap upland region, India. *In*: MILLER, A. J. & GUPTA, A. (eds.) *Varieties of fluvial form*, Wiley & Sons Ltd. 295-315.

DERAMOND, J., GRAHAM, R. H., HOSSACK, J. R., BABY, P. & CROUZET, G. 1985. Nouveau modele de la chaine des Pyrenees. *C.R. Ac. Sc. Paris*, 301, 1213-1216.

DESBARATS, A. J. & BACHU, S. 1994. Geostatistical analysis of aquifer heterogeneity from core scale to basin scale: a case study. *Water Resources Research*, 30, 673-684.

DEUTSCH, C. V. & WANG, L. 1996. Hierarchical object-based stochastic modelling of fluvial reservoirs. *Mathematical Geology*, 28, 857-880.

DIETRICH, W. E., KIRCHNER, J. W., IKEDA, H. & ISEYA, F. 1989. Sediment supply and the development of the coarse surface layer in gravel-bedded rivers. *Nature*, 340, 215-217.

DINGMAN, S. L. 1984. *Fluvial Hydrology*. W. H. Freeman, New York, p85.

DOMENICO, P. A. & SCHWATZ, F. W. 1990. *Physical and Chemical Hydrology.* New York, Jon Wiley & Sons, 824p.

DOMINIC, D. F., RITZI, R. W., REBOULET, E. C. & ZIMMER, A. C. 1998. Geostatistical analysis of facies distributions: elements of a quantitative facies model. *In*: FRASER, G. S. P., DAVIS, M. J. (eds.) *Hydrogeologic Models of Sedimentary Aquifers*, 137-146.

DOTT, R. H. & BOURGEOIS, J. 1983. Hummocky stratification; significance of its variable bedding sequences. *Geological Society of America Bulletin*, 93, 663-680.

DREYER, T. 1990. Sand body dimensions and infill sequences of stable, humid-climate delta plain channels. *In*: BULLER, T., BERG, E., HJELMELAND, O., KLEPPE, J. TORSAETER, O. & AASEN, J. O. (Eds.). *North Sea Oil and Gas Reservoirs 2*, Graham and Trotman, London. 337-351.

DREYER, T. 1993. Quantified fluvial architecture in ephemeral stream deposits of the Esplugafreda Formation (Palaeocene), Tremp-Graus Basin, northern Spain. *In*: MARZO, M. & PUIGDEFABREGAS, C. (eds). *Alluvial Sedimentation*, Special Publication of the International Association of Sedimentologists, 17, 337-362.

DREYER, T., CORREGIDOR, J., ARBUES, P. & PUIGDEFABREGAS, C. 1999. Architecture of the tectonically influenced Sobrarbe deltaic complex in the Ainsa Basin, northern Spain. *Sedimentary Geology*, 127, 127-169.

DREYER, T., FALT, L. M., HOY, T., KNARUD, R., STEEL, R. & CUEVAS, L. J. 1993. Sedimentary architecture of field analogues for reservoir information (SAFARI): a case study of the fluvial Escanilla Formation, Spanish Pyrenees. *In*: FLINT, S. S. & BRYANT, I. D. (eds.) *The Geological Modelling of Hydrocarbon Reservoirs and Outcrop Analogues*, Special Publication of the International Association of Sedimentologists, 15, 57-80.

DREYER, T., SCHEIE, A. & WALDERHAUG, O. 1990. Minipermeameter-based study of permeability trends in channel sand bodies. *Bulletin of the American Association of Petroleum Geologists*, 74, 359-374.

DRIESE, S. G. & MORA, C. I. 1993. Physico-chemical environment of pedogenic carbonate formation in Devonian vertic palaeosols, central Appalachians, USA. *Sedimentology*, 40, 199-216.

DRIESE, S. G., SIMPSON, E. L. & ERIKSSON, K. A. 1995. Redoximorphic paleosols in alluvial sequences and lacustrine deposits, 1.8 GA Lochness Formation, Mount Isa, Australia: Pedogenic processes and implications for paleoclimate. *Journal of Sedimenatry Research*, A65, 675-689.

DUBIEL, R. F. & SMOOT, J. P. 1994. Criteria for interpreting palaeoclimate from red beds - a tool for pangean reconstruction. Pangea: Global Environment and Resources, *Canadian Society of Petroleum Geologists*, Memoir 17, 295-310.

DULLER, G. A. T. 1996. Recent developments in luminescence dating of Quaternary sediments. *Progress in Physical Geography*, 20, 127-145.

EBERTH, D. A. & MIALL, A. D. 1991. Stratigraphy, sedimentology and evolution of a vertebrate-bearing, braided to anastomosing fluvial system, Culter Formation (Permian-Pennsylvanian), north-central New Mexico. *Sedimentary Geology*, 72, 225-252.

EMERY, D. & MYERS, K. 1996. *Sequence Stratigraphy*, Oxford : Blackwell Science.

ESCHARD, R., LEMOUZY, P., BACCHIANA, C., DESAUBLIAUX, J., PARPANT, J. & SMART, B. 1998. Combining sequence stratigraphy, geostatistical simulations, and production data for modelling a fluvial reservoir in the Chaunoy Field (Triassic, France). *Bulletin of the American Association of Petroleum Geologists*, 82, 545-568.

EVANS, D. J., MENEILLY, A. & BROWN, G. 1992. Seismic facies analysis of Westphalian sequences of the southern North Sea. *Marine and Petroleum Geology*, 9, 578-589.

EWING, R. E. 1997. Aspects of numerical methods in multiphase flows. *In*: DAGAN, G., NEUMAN, S. P. (eds.) *Subsurface Flow and Transport: A Stochastic Approach*, Cambridge University Press, 92-100.

FERGUSON, R. I. & ASHWORTH, P. J. 1991. Slope-induced changes in channel character along a gravel-bed river: The Allt Dubhaig, Scotland. *Earth Surface Processes and Landforms*, 16, 65-82.

FERGUSON, R. J. & BRIERLEY, G. J. 1999. Levee morphology and sedimentology along the lower Tuross River, south-eastern Australia. *Sedimentology*, 46, 627-648.

FERGUSON, R. I., HOEY, T., WATHEN, S. & WERRITY, A. 1996. Field evidence for rapid downstream fining of river gravels through selective transport. *Geology*, 24, 179-182.

FIELD, J. 2001. Channel avulsion on alluvial fans in southern Arizona. *Geomorphology*, 37, 93-104.

FIELDING, C. R. 1984. Upper delta plain lacustrine and fluviocustrina facies from the Westphilian of the Durham coalfield, NE England. *Sedimentology*, 31, 547-567.

FIELDING, C. R. 1986. Fluvial channel and overbankdeposits from the Westphalian of the Durham Coalfield, NE England. *Sedimentology*, 23, 119-140.

FIELDING, C. R. 1993. A review of recent research in fluvial sedimentology. *Sedimentary Geology*, 85, 3-14.

FIELDING, C. R. & CRANE, R. C. 1987. An application of statistical modelling to the prediction of hydrocarbon recovery factors in fluvial reservoir sequences. *In*: ETHERIDGE, F. G., FLORES, R. M. & HARVEY, M. D. (eds.) *Recent Developments in Fluvial Sedimentology*, Society of Economic Paleontologists and Minerologists, Special Publication, 39, 321-327.

FLUGEL, E. 1978. *Mikrofacielle Untersuchungsmethoden von Kalken*. Springer, Berlin Heidelberg, New York, 454pp.

FOGG, G. E. 1986. Stochastic analysis of aquifer interconnectedness with a test case in the Wilcox Group, East Texas. *Eos, Transactions, American Geophysical Union*, 67, pp.942.

FOGG, G. E. 1990. Architecture and interconnectedness of geologic media; role of the low-permeability facies in flow and transport. *Hydrogeology*, Selected Papers, 2, 19-40.

FOUFOULA-GEORGIOU, E. & SAPOZHNIKOV, V. B. 1998. Anisotropic scaling in braided rivers: An integrated theoretical framework and results from application to an experimental river. *Water Resources Research*, 34, 863-867.

FRANCIS, J. E. 1994. Palaeoclimates of Pangea - geological evidence. Pangea: Global Environment and Resources. *Canadian Society of Petroleum Geologists*, Memoir 17, 265-273.

FRASER, G. S. P., DAVIS, M. J. 1998. *Hydrogeologic Models of Sedimentary Aquifers.*

FREEZE, R. A. & CHERRY, J. A. 1979. *Groundwater: Englewood Cliffs*, N. J. Prentice-Hall, 604p.

FRENCH, R.H. 1985. *Open-channel Hydraulics*, McGraw-Hill, New York, 739 pp.

FRIEND, P. F. & SINHA, R. 1993. Braiding and meandering parameters. *In*: BEST, J.L & BRISTOW, C.S. (eds.) *Braided Rivers*, Geological Society of London Special Publication, 75, 105-111.

FRIEND, P. F. 1978. Distinctive features of some ancient river systems. *In*: MIALL, A. D. (ed.) *Fluvial Sedimentology*, Canadian Society of Petroleum Geologists, Memoir 5. 531-542.

FRIEND, P. F. 1993. Control of river morphology by grain-size of sediment supplied. *Sedimentary Geology*, 85, 171-177.

FRIEND, P. F., MAHMOOD, R. S., GEEHAN, G. & SHEIKH, K. A. 2001. Intermediate-scale architectural features of the fluvial Chinji Formation (Miocene), Siwalik Group, northern Pakistan. *Journal of the Geological Society of London*, 158, 163-177.

FRIEND, P. F., SLATER, M. J. & WILLIAMS, R. C. 1979. Vertical and lateral building of river sandstone bodies, Ebro Basin, Spain. *Journal of the Geological Society of London*, 136, 39-46.

FRITSCH, F. E. 1959. *The structure and Reproduction of Algae. 2*, Cambridge University Press, 939pp.

FROSTICK, L. E., REID, I. & LAYMAN, J. T. 1983. Changing size distribution of suspended sediment in arid-zone flash floods. *In*: COLLINSON, J. D. & LEWIN, J. (eds.) *Modern and Ancient Fluvial Systems,* Special Publication of the International Association of Sedimentologists, 6, 97-106.

GALLOWAY, W. E. & SHARP JR., J. M. 1998. Hydrogeology and characterization of fluvial aquifer systems. *In*: FRASER, G. S. P., DAVIS, M. J. (eds.) *Hydrogeologic Models of Sedimentary Aquifers*. 91-106.

GARRIDO-MEJIAS, A. 1968. Sobre la estratigraphia de los conglomerates Campanue (Santa Liestra) y formaciones superiores del Eocene (extremo occidental de la cuenca de Tremp-graus) Pirinco Central, Provincia de Huesca. *Acta Geologica Hispanica*. 3, 359-374.

GARRIDO-MEJIAS, A. 1973. *Estudio geologico y relacion entre tectonica y sedimntacion del Secundario y Terciario de la vertiene meridional pirenaica en su zona central (prov. Huesca y Lerida)*. Unpublished Doctoral Dissitation, Faculty of Science, Granada.

GAWTHORPE, R. L., COLLIER, R. E. LL., ALEXANDER, J., BRIDGE, J. S., & LEEDER, M. R. 1993. Ground penetrating radar: application to sandbody geometry and heterogeneity studies. *In*: NORTH, C. P. & PROSSER, D. J. (eds.) *Characterization of Fluvial and Aeolian Reservoirs*, Geological Society Special Publication, 73, 421-432.

GEEHAN, G. 1993. The use of outcrop data and heterogeneity modelling in development planning. *In*: ESCHARD, R. DOLIGEZ, B. (eds.) *Subsurface reservoir characterization from outcrop observations*, 53-64.

GEEHAN, G. & UNDERWOOD, J. 1993. The use of length distributions in geological modelling. *In*: FLINT, S. S. & BRYANT, I. D. (eds.) *The Geological Modelling of Hydrocarbon Reservoirs and Outcrop Analogues*, International Association of Sedimentologists, Special Publication, 15, 205-212.

GERMANOSKI, D. & SCHUMM, S.A. 1993. Changes in Braided river morphology resulting from aggradation and degradation. *The Journal of Geology*, 101, 451-466.

GIBB, J. G. 1978. Rates of coastal erosion and accretion in New Zealand. *New Zealand Journal of Marine and Freshwater Research*, 12, 429-456.

GIBB, J. G. 1986. A New Zealand regional holocene eustatic sea-level curve and its application to determination of vertical tectonic movements. *Royal Society of New Zealand Bulletin*, 24, 377-395.

GIBB, J. G. & ADAMS, J. 1982. A sediment budget for the east coast between Oamaru and Banks Peninsula, South Island, New Zealand. *New Zealand Journal of Geology and Geophysics*, 25, 335-352.

GIBLING, M. R. & RUST, B. R. 1990. Ribbon sandstones in the Pennsylvanian Waddens Cove Formation, Sydney Basin, Atlantic Canada: the influence of siliceous duricrusts on channel-body geometry. *Sedimentology*, 37, 45-65.

GILES, M.R., INDRELID, S.L. & JAMES, D.M.D. 1998. Compaction - the great unknown in basin modelling. *In*: DUPPENBECKER, S.J. & ILIFFE, J.E. (eds.) *Basin Modelling: Practice and Progress*, Geological Society, London, Special Publications, 141, 15-43.

GLENNIE, K. W. 1983. Lower Permian Rotliegend desert sedimentation in the North Sea area. *In*: BROOKFIELD, M. E. & AHLBRANDT, T. S. (eds.) *Eolian sediments and processes*, 11th international Association of Sedimentologists congress, Hamilton, ON, Canada.38, 521-541.

GLENNIE, K. W. & BOEGNER, P. L. E. 1981. Sole Pit Inversion Tectonics. *In*: ILLING, L. V. & HOBSON, G. D. (eds.) *Petroleum Geology of the Continental Shelf of*

North-West Europe, Proceedings of the second conference, Institute of Petroleum, London. 110-120.

GLOVER, B. W., POWELL, J. H. & WATERS, C N. 1993. Etruria Formation (Westphalian C) palaeoenvironments and volcanicity on the southern margins of the Pennine Basin, South Staffordshire, England. *Journal of the Geological Society of London*, 150, 737-750.

GOFF, J. R. & ASHMORE, P. 1994. Gravel transport and morphological change in braided Sunwapta River, Alberta, Canada. *Earth Surface Processes and Landforms*, 19, 195-212.

GORDON, I. & HELLER, P. L. 1993. Evaluating major controls on basinal stratigraphy, Pine Valley, Nevarda: Implications for syntectonic deposition. *Geological Society of America Bulletin*, 105, 47-55.

GOUDIE, A. 1973. The geomorphic and resource significance of calcrete. *Progress in Geography*, 5, 77-118.

GOUDIE, A. 1983. Calcrete. *In*: GOUDIE, A. S & PYE, K. (eds.) *Chemical sediments and geomorphology: precipitates and residua in the near-surface environment.* Academic Press, London, 93-131.

GRAF, W. H. 1998. *Fluvial Hydraulics: Flow and Transport Processes in Channels of Simple Geometry*. John Wiley & Sons, p12.

GRISSINGER, E. H. & MURPHEY, J. B. 1983. Present channel stability and late Quaternary valley deposits in northern Mississippi. *In*: COLLINSON, J. D. & LEWIN, J. (eds.) *Modern and Ancient Fluvial Systems*, Special Publication of the International Association of Sedimentologists, 6, 241-250.

GROLL, P. E. & STEIDTMANN, J. R. 1987. Fluvial response to Eocene tectonism, the Bridger Formation, Southern Wind River Range, Wyoming. *In*: ETHERIDGE, F. G., FLORES, R. M. & HARVEY, M. D. (eds.) *Recent Developments in Fluvial*

Sedimentology, Society of Economic Paleontologists and Minerologists Special Publications, 39, 263-268.

GUCCIONE, M. J. 1993. Grain-size distribution of overbank sediment and its use to locate channel position. *In*: MARZO, M. & PUIGDEFABREGAS, C. (eds.) *Alluvial Sedimentation*, Special Publication of the International Association of Sedimentologists, 17, 185-194.

GUPTA, A. 1983. High-magnitude floods and stream channel response. *In*: COLLINSON, J. D. & LEWIN, J. (eds.) *Modern and Ancient Fluvial Systems*, Special Publication of the International Association of Sedimentologists, 6, 219-227.

GUPTA, A. & FOX, H. 1974. Effects of High-Magnitude Floods on Channel Form; A Case Study in Maryland Piedmont. *Water Resources Research*, 10, 499-509.

GUSTAVSON, T. C., HOVORKA, S. D. & DUTTON, A. D. 1994. Origins of satin spar veins in evaporite basins. *Journal of Sedimentary Research*, A64, 88-94.

HALDORSEN, H. H. & CHANG, D. M. 1986. Notes on Stochastic shales, from outcrop to simulation Model. *In*: LAKE, L. W. & CARROLL, H. B. (eds.) *Reservoir Characterization I*, Academic Press, London, 445-485.

HALDORSEN, H. H., CHANG, D. M. & BEGG, S. H. 1987. Discontinuous vertical permeability barriers: a challenge to engineers and geologists. *In*: KLEPPE, J., BERG, E. W., BULLER, A. T., HJELMELAND, O. & TORSAETER, O. (eds.) *North Sea Oil and Gas Reservoirs I*, Graham and Trotman, London, 127-151.

HALDORSEN, H. H. & DAMSLETH, E. 1990. Stochastic modelling. *Journal of Petroleum Technology*, 404-412.

HAMLIN, R. H. B., WOODWARD, J. C., BLACK, S. & MACKLIN, M. G. 2000. Sedimentology fingerprinting as a tool for interpreting long-term river activity: the Voidomatis Basin, NW Greece. *In*: FOSTER, I. D. L. (ed.) *Tracers in Geomorphology*, Chichester : John Wiley, 473-501.

HANCOCK, G. S., ANDERSON, R. S., CHADWICK, O. A. & FICKEL, R. C. 1999. Dating fluvial terraces with (super 10) Be and (super 26) Al profiles; application to the Wind River, Wyoming. *Geomorphology*, 27, 41-60.

HARDEN, J. W. 1982. A quantitative index of soil development from field descriptions; examples from a chronosequence in central California. *Geoderma*, 28, 1-28.

HARTLAND, W. B., ARMSTRONG, R. L., COX, A. V., CRAIG, L. E., SMITH, A. G. & SMITH, D. G. 1990. *A geologic time-scale 1989*. Cambridge University Press, Cambridge, 263pp.

HARTLEY, A. J. 1993. Sedimentology response of an alluvial system to source area tectonism: the Seilao Member of the Late Cretaceous to Eocene Purilactis Formation. *In*: MARZO, M. & PUIGDEFABREGAS, C. (eds). *Alluvial Sedimentation*, Special Publication of the International Association of Sedimentologists, 17, 489-500.

HARVEY, A. M. 1969. Channel capacity and adjustment of streams to hydraulic regime. *Journal of Hydrology*, 8, 82-98.

HAYS, J. D., IMBRIE, J. & SHACKLETON, N. J. 1976. Variations in the Earth's orbit: pacemaker of the Ice Ages. *Science*, 194, 1121-1132.

HAZEN, A. 1892. *Some physical properties of sands and gravels with special reference to their filtration*. Lawrence, Mass., 24th Annual Report of the State Board of heath of Massachusetts for 1892, 24p.

HEDEMANN, H. A. & TEICHMULLER, R. 1971. III. Oberkarbon (Silesium); A, Der paralische Raum; 6, Die palaeogeographische Entwicklung des Oberkarbons. 3. Upper Carboniferous (Silesian); A, The paralic region; 6, The paleogeographical development of the upper Carboniferous. *Fortschritte in der Geologie von Rheinland und Westfalen*, 19, 129-141.

HELLER, P. L. & PAOLA, C. 1992. The large-scale dynamics of grain-size variation in alluvial basins, 2: Application to syntectonic conglomerate. *Basin Research*, 4, 91-102.

HELLER, P. L. & PAOLA, C. 1996. Downstream changes in alluvial architecture: An exploration of controls on channel-stacking patterns. *Journal of Sedimentary Research*, 66, 297-306.

HENDERSON, F.M. 1966. *Open Channel Flow*. Macmillan, New York, 463-484 pp.

HIRST, J. P. P. 1991. Variations in alluvial architecture across the Oligo-Miocene Huesca fluvial system, Ebro basin, Spain. *In*: MIALL, A. D. & TYLER, N. (eds.) *The three-dimensional facies architecture of terrigenous clastic sediments and its implication for hydrocarbon discovery and recovery*, Concepts in Sedimentology and Paleontology, 3, 111-121.

HIRST, J. P. P., BLACKSTOCK, C. R. & TYSON, S. 1993. Stochastic modelling of fluvial sandstone bodies. *In*: FLINT, S. S. & BRYANT, I. D. (eds.) *The Geological Modelling of Hydrocarbon Reservoirs and Outcrop Analogues*, International Association of Sedimentologists, Special Publication, 15, 237-252.

HOEY, T. B. 1994. Patterns of sediment storage in the Kowai River, Torlesse Range, New Zealand. *Journal of Hydrology (NZ)*, 32, 1-15.

HOEY, T. B. & BLUCK, B. J. 1999. Identifying the controls over downstream fining of river gravels. *Journal of Sedimentary Research*, 69, 40-50.

HOEY, T. B. & FERGUSON, R. I. 1994. Numerical simulation of downstream fining by selective transport in gravel bed rivers: Model development and illustration. *Water Resource Research*, 30, 2251-2260.

HOEY, T. B. & FERGUSON, R. I. 1997. Controls on the strength and rate of downstream fining above a river base level. *Water Resource Research*, 33, 2601-2608.

HOEY, T. B. & SUTHERLAND, A. J. 1991. Channel morphology and bedload pulses in braided rivers: a laboratory study. *Earth Surface Processes and Landforms*, 16, 447-462.

HOLLYWOOD, J. M., & WHORLOW, C. V. 1993. Structural development and hydrocarbon occurrence of the carboniferous in the UK Southern North Sea Basin. *In*:

PARKER, J. R. (ed.) *Petroleum Geology of Northwest Europe: Proceedings of the 4th Conference*, The Geological Society of London, 689-696.

HORNUNG, J. & AIGNER, T. 1999. Reservoir and aquifer characterisation of fluvial architectural elements: Stubensandstein, Upper Triassic, southwest Germany. *Sedimentary Geology*, 129, 215-280.

HUANG, H. Q. & NANSON, G. C. 1998. The influence of bank strength on channel geometry: An integrated analysis of some observations. *Earth Surface Processes and Landforms*, 23, 865-876.

HUGGENBERGER, P. 1993. Radar facies: recognition of facies patterns and heterogeneity estimation (Pleistocene Rhine gravel, N. E. Switzerland) *In*: BEST, J. L. & BRISTOW, C. S. (eds.) *Braided Rivers*, Geological Society Special Publication, 75, 163-176.

IMBRIE, J., HAYS, J. D., MARTINSON, D. G., McINTYRE, A., MIX, A. C., MORELY, J. J., PISIAS, N. G., PRELL, W. L. & SHACKLETON, N. J. 1984. The orbital theory of Pleistocene climate: support from a revised chronology of the marine δ18O record. *In*: BERGER, A. L., IMBRIE, J. HAYS, J., KUKLA, G. & SALTZMAN, B. (eds.) *Milankovitch and Climate, Part 1*, Dordrecht: D. Reidel, 269-305.

ISEYA, S. & IKEDA, H. 1987. Pulsations in bedload transport rates induced by a longitudinal sediment sorting: a flume study of sand and gravel mixtures. *Geografiska Annaler*, 69A, 15-27.

JACOBSEN, T. & RENDALL, H. 1991. Permeability patterns in some fluvial sandstones. An outcrop study from Yorkshire, North-east England. *In*: LAKE, L. W., CARROLL, H. B. & WESSON, T. C. (eds.) *Reservoir Characterization 2*, Academic Press, London. 315-338.

JAEGGI, M. N. R. 1986. Non distorted models for research on river morphology. Proceedings of the Synopsis on Scale Effects in Modelling Sediment Transport Phenomena, August 1986. *International Association of Hydrological Science*, 70-84.

JOHNSON, S. A., GLOVER, B. W. & TURNER, P. 1997. Multiphase reddening and weathering events in the Upper Carboniferous red beds from the English West Midlands. *Journal of the Geological Society of London*, 154, 735-745.

JONES, L. S. & HARPER, J. T. 1998. Channel avulsion and related processes, and large-scale sedimentation patterns since 1875, Rio Grande, San Luis Valley, Colorado. *Geological Society of America Bulletin*, 110, 411-421.

JONES, M., ASHWORTH, P. & BEST, J. 1999. From surface to subsurface: quantifying the preservation potential of braided alluvial architecture. Abstract, *British Sedimentological Research Group*, Annual Meeting, Edinburgh.

JONES, S. J., FROSTICK, L. E. & ASTIN, T. R. 1999. Climatic and tectonic controls on fluvial incision and aggradation in the Spanish Pyrenees. *Journal of the Geological Society of London*, 156, 761-769.

KELLY, S. B. & OLSEN, H. 1993. Terminal fans - a review with reference to Devonian examples. *Sedimentary Geology*, 85, 339-374.

KITANDIS, P. K. 1997. Groundwater flow in heterogeneous formations. *In*: DAGAN, G., NEUMAN, S. P. (eds.) *Subsurface Flow and Transport: A Stochastic Approach*, Cambridge University Press, 83-91.

KLINGBEIL, R., KLEINEIDAM, S., ASPRION, U., AIGNER, T. & TEUTSCH, G. 1999. Relating lithofacies to hydrofacies:outcrop-based hydrogeological characterisation of Quaternary gravel deposits. *Sedimentary Geology*, 129, 299-310.

KNIGHTON, A. D. 1987b. River channel adjustment - the downstream dimension. *In*: RICHARDS, K. (ed.) *River channels: environment and process*. Oxford, Blackwell, 95-128.

KNIGHTON, A. D. 1998. *Fluvial Forms and Processes*. Arnold, London.

KODAMA, Y. 1994a. Downstream changes in lithology and grain size of fluvial gravels, the Watarase River, Japan: Evidence of the role of abrasion in downstream fining. *Journal of Sedimentary Research*, A64, 68-75.

KODAMA, Y. 1994b. Experimental study of abrasion and its role in producing downstream fining in gravel-bed rivers. *Journal of Sedimentary Research*, A64, 76-85.

KOLTERMANN, C. E. & GORELICK, S. M. 1996. Heterogeneity in sedimentary deposits: A review of structure- imitating, process-imitating, and descriptive approaches. *Water Resources Research*, 32, 2617-2658.

KOSS, J. E., ETHRIDGE, F. G. & SCHUMM, S. A. 1994. An experimental study of the effects of base-level change on fluvial, coastal and shelf systems. *Journal of Sedimentary Research*, B64, 90-98.

KRAUS, M. J. 1987. Integration of channel and floodplain suites, 2. Vertical relations of alluvial paleosols. *Journal of Sedimentary Petrology*, 57, 601-612.

KRAUS, M. J. 1997. Lower Eocene alluvial paleosols: Pedogenic development, stratigraphic relationships, and paleosol/landscape associations. *Palaeogeography, Palaeoclimatology, Palaeoecology*, 129, 387-406.

KRAUS, M. J. & BOWN, T. M. 1993. Palaeosols and sandbody prediction in alluvial sequences. *In*: NORTH, C. P. & PROSSER, D. J. (eds.) *Characterisation of Fluvial and Aeolian Reservoirs*, Geological Society Special Publication, 73, 23-31.

KRAUS, M. J. & MIDDLETON, L. T. 1987. Contrasting architecture of two alluvial suites in different structural settings. *In*: ETHERIDGE, F. G., FLORES, R. M. & HARVEY, M. D. (eds.) *Recent Developments in Fluvial Sedimentology*, Society of Economic Paleontologists and Mineralogists Special Publications, 39, 253-262.

KRAUS, M. J. & WELLS, T. M. 1999. Recognizing avulsion deposits in the ancient stratigraphical record. *In*: SMITH, N.D. & ROGERS, J. (eds.) *Fluvial Sedimentology VI*, Special Publication of International Association of Sedimentologists, Blackwells, 28, 251-267.

KUPFERSBERGER, H. & DEUTSCH, C. V. 1999. Methodology for intergrating analog geologic data in 3-D variogram modelling. *Bulletin of the American Association of Petroleum Geologists*, 83. 1262-1278.

KVALE, E. P. & VONDRA, C. F. 1993. Effects of relative sea-level changes and local tectonics on a Lower Cretaceous fluvial to transitional marine sequence, Bighorn Basin, Wyoming, USA. *In*: MARZO, M. & PUIGDEFABREGAS, C. (eds.) *Alluvial Sedimentation*. Special Publication of the International Association of Sedimentologists, 17, 383-399.

LAKE, P. A. 1992 The biostratigraphy and palaeoenvironmental analysis of the Late Carboniferous section of the ARCO well 44/18-1.1-35.

LANGHAAR, H.L. 1980. *Dimensional Analysis and Theory of Hydraulic models*, Robert E. Krieger, Florida, 178 pp.

LASSETER, T. J. 1986. Reservoir heterogeneities and their influence on ultimate recovery. *In*: LAKE, L. W. & CARROLL, H. B. (eds.) *Reservoir Characterization 1*, Academic Press, London. 545-559.

LAWRENCE, D. T., DOYLE, M. & AIGNER, T. 1990. Stratigraphic Simulation of Sedimentary Basins: Concepts and Calibrations. *Bulletin of the American Association of Petroleum Geologists*, 74, 273-295.

LEATHERMAN, S. P., ZHANG, K. & DOUGLAS, B. C. 2000. Sea level rise shown to drive coastal erosion. *EOS Transactions*, 81, 55-58.

LECKIE, D. A. 1994. Canterbury Plains, New Zealand - implications for sequence stratigraphic models. *Bulletin of the American Association of Petroleum Geologists*, 78, 1240-1256.

LECLAIR, S. F., BRIDGE, J. S. & WANG, F. 1997. Preservation of cross-strata due to migration of subaqueous dunes over aggradaing and non-aggrading beds: comparison of experimental data with theory. *Geoscience Canada*, 24, 55-65.

LEDDY, J.O., ASHWORTH, P.J., and BEST, J.L. 1993. Mechanisms of anabranch avulsion within gravel-bed braided rivers: observations from a scaled physical model, *In*: BEST, J. L & BRISTOW, C. S. (eds.) *Braided Rivers*, Geological Society of London Special Publication, 75, 119-127.

LEEDER, M. R. 1973. Fluviatile fining –upwards cycles and the magnitude of palaeochannels. *Geological Magazine*, 110, 265-276.

LEEDER, M. R. 1975. Pedogenic carbonates and flood sediment accretion rates: a quantitative model for alluvial arid-zone lithofacies. *Geological Magazine*, 112, 257-270.

LEEDER, M.R. 1978. A Quantitative stratigraphic Model for Alluvium with special references to channel deposit density and interconnectedness. *In*: MIALL, A.D. (ed.) *Fluvial Sedimentology*, Canadian Society of Petroleum Geologists, Memoir 5, 587-596.

LEEDER, M.R. 1987. Tectonic and palaeogeographic models for Lower Carboniferous Europe. *In*: MILLER, J. M., ADAMS, A. E. & WRIGHT, P. V. (eds.) *European Dinantian Environments*. John Wiley, Chichester. pp 1-20.

LEEDER, M.R. 1980. *Sedimentology: Process and Product*. Allen & Unwin Inc. 344pp.

LEEDER, M. 1988. Devono-Carboniferous river systems and sediment dispersal from the orogenic belts and cratons of NW Europe. *In*: HARRIS, A. L. & FETTES, D. J. (eds.) *The Caledonian-Appalachian Orogen*, Geological Society Special Publication. 38, 549-558.

LEEDER, M. 1988a. Recent developments in Carboniferous geology: a critical review with implications for the British Isles and N.W. Europe. *Proceedings of the Geologists Association*. 99, 73-100.

LEEDER, M. R. 1993. Tectonic controls upon drainage basin development, river channel migration and alluvial architecture implications for hydrocarbon reservoir development and characterisation. *In*: NORTH, C. P. & PROSSER, D. J. (eds.)

Characterisation of Fluvial and Aeolian Reservoirs, Geological Society of London Special Publication, 73, 7-22.

LEEDER, M., BOLDY, S. R., RAISWELL, R. & CAMERON, R. 1990. The Carboniferous of the Outer Moray Firth Basin, quadrants 14 and 15, Central North Sea. *Marine and Petroleum Geology*, 7, 29-37.

LEEDER, M. R. & GAWTHORPE, R. L. 1987. Sedimentary model for extensional tilt block / half-graben basins. *In*: COWARD, M. P., DEWERY, J. F.& HANCOCK, P. L. (eds.) *Continental Extensional Tectonic*, Geological Society of London Special Publication, 28, 139-152.

LEEDER, M. & HARDMAN, M. 1990. Carboniferous geology of the Southern North Sea Basin and Controls on hydrocarbon prospectivity. *In*: HARDMAN, R. F. P. & BROOKS, J. (eds.) *Tectonic events Responsible for Britain's Oil and Gas Reserves*, Geological Society Special Publication, 55, 87-105.

LEEDER, M., MACK, G.H., PEAKALL, J. & SALYARDS, S. L. 1996. First quantitative test of alluvial stratigraphic models: Southern Rio Grande rift, New Mexico. *Geology*, 24, 87-90.

LEEDER, M. & STEWART, M. D. 1996. Fluvial incision and sequence stratigraphy: alluvial responses to relative sea level fall and their detection in the geological record. *In*: HESSELBO, S. P. & PARKINSON, D. N. (eds.) *Sequence Stratigraphy in British Geology*, Geological Society Special Publication, 103, 25-39.

LEEDER, M., RAISWELL, R., AL-BIATTY, H., McMAHON, A. & HARDMAN, M. 1990. Carboniferous stratigraphy, sedimentation and correlation of well 48/3-3 in the southern North Sea Basin: integrated use of palynology, natural/sonic logs and carbon/sulphur geochemistry. *Journal of the Geological Society of London*, 147, 287-300.

LENSEN, G. J. 1975. Earth-deformation studies in New Zealand. *Technophysics*, 29, 541-551.

LEOPOLD, L. B. 1992. Sediment size that determins channel morphology. *In*: BILLI, P., THORN, C. R. & TACCON, P. (eds.) *Dynamics of gravel-bed rivers*, Wiley & Sons Ltd. 297-311.

LEOPOLD, L. B. & MADDOCK, T. 1953. *The hydraulic geometry of stream channels and some physiographic implications*. United States Geological Survey Professional Paper 252.

LEOPOLD, L.B. & WOLMAN, M.G. 1957. *River channel patterns: braided, meandering, and straight*. Professional Paper 282-b, United States Geological Survey, 39-85.

LEOPOLD, L. B. & WOLMAN, G. M. 1960. River Meanders. *Geological Society of America Bulletin*, 71, 769-794.

LOPEZ-GAMUNDI, O. R., CESARI, S. N. & LIMARINO, C. O. 1993. Paleoclimatic significance and age constraints of the Carboniferous coals of Paganzo Basin, western Argentina. International Gondwana Symposium, 8, 291-298.

LORENZ, J. C., HEINZE, D. M., CLARK, J. A. & SEARLS, C. A. 1985. Determination of widths of meander-belt sandstone reservoirs from vertical downhole data, Mesaverde Group, Piceance Creek Basin, Colorado. *Bulletin of American Association of Petroleum Geologists*, 69, 710-721.

LOVELL, M. A., HARVEY, P. K., JACKSON, P. D., BREWER, T. S. WILLIAMSON, G. & WILLIAMS, C. G. 1998. Interpretation of core and log data-integration or calibration? *In*: HARVEY, P. K. & LOVELL, M. A. (eds.) *Core-Log Intergration*, Geological Society of London, Special Publication, 136, 39-51.

LUI, K., BOULT, P., PAINTER, S. & PATERSON, L. 1996. Outcrop analog for sandy braided stream reservoirs: permeability patterns in the Triassic Hawkesbury Sandstone, Sydney basin, Australia. *Bulletin of American Association of Petroleum Geologists*, 80, 1850-1866.

LUTHI, S. M. 1990. Sedimentary structures of clastic rocks identified from electrical borehole images. *In*: HURST, A., LOVELL, M. A. & MORTON, A. C. (eds.) *Geological Applications of Wireline Logs*, Geological Society of London, Special Publication, 48, 3-10.

MABIN, M. C. G. 1987. Early Aranuian sedimentation in the Rangitata Valley, mid Canterbury. *New Zealand Journal of Geology and Geophysics*, 30, 87-90.

MACDONALD, A. C. & HOLLAND, E. K. 1993. Sedimentology and shale modelling of a sandstone-rich fluvial reservoir: Upper Statfjord Formation, Statfjord Field, Northern North Sea. *Bulletin of American Association of Petroleum Geologists*, 82, 1156-1172.

MACKEY, S. D. & BRIDGE, J. S. 1995. Three-dimensional model of alluvial stratigraphy: theory and application. *Journal of Sedimentary Research*, B65, 7-31.

MACKIN, J. H. 1948. Concept of the graded river. *Bulletin of the Geological Society of American*, 59, 463-512.

MADER, D. 1985. Fluvial conglomerates in continental redbeds of the Buntsandstein (Lower triassic) in the Eifel (F.R.G.) and their palaeoenvironmental, palaeogeographical and palaeotectonic significance. *Sedimentary Geology*, 44, 1-64.

MANSOORI, J. 1994. A review of basic upscaling procedures; advantages and disadvantages. In: YARIS, J. M. & CHAMBERS, R. L. 1994. Stochastic modeling and geostatistics: principles, methods, and case studies, AAPG Computer Applications in Geology, 3. 65-74.

MARRIOTT, S. B. 1999. The use of models in the interpretation of the effects of base-level change on alluvial architecture. *In*: SMITH, N.D. & ROGERS, J. (eds.) *Fluvial Sedimentology VI*, Special Publication of the International Association of Sedimentologists, Blackwells, 28, 271-282.

MARSDEN, N. 1981. *Model simulation on the effect of vegetation on braided rivers.* Project Report, Department of Agricultural Engineering, Lincon College, Canterbury, New Zealand, 66 pp.

MARTIN, J. H. 1993. A review of braided fluvial hydrocarbon reservoirs: the petroleum engineer's perspective. *In*: BEST, J. L. & BRISTOW, C. S. (eds.) *Braided Rivers*, Geological Society Special Publication, 75, 333-367.

MARTINIUS, A. W. 2000. Labyrinthine facies architecture of the Tortola fluvial system and controls on deposition (late Oligocene-early Miocene, Loranca Basin, Spain). *Journal of Sedimentary Research*, 70, 850-867.

MATHEWS, W. H. 1967. A contribution to the geology of the Mount Tongarito massif, North Island, New Zealand. *New Zealand Journal of Geology and Geophysics*, 10, 1027-1039.

MATHIEU, Y., VERDIER, F., HOUEL, P. & FERNANDEZ, J. 1995. *Spain: Sandbody geometry and high sequence stratigraphy in fluvial deposits (Keuper Facies) of the Upper Triassic from outcrops and core-drill studies.* Field Trip Notes, AAPG International Conference, Nice, 35pp.

MAXWELL, J.C. 1964. Influence of depth, temperature, and geologic age on porosity of quartzose sandstone. *Bulletin of the American Association of Petroleum Geologists*, 48, 697-709.

MAYNARD, J. R., HOFMANN, W., DUNAY, R. E., BENTHAM, P. N., DEAN, K. P. WATSON, I. 1997. The Carboniferous of Western Europe: the development of a petroleum system. *Petroleum Geoscience*. 3, 97-115.

McLEAN, D. 1996. A report on the palynological analysis of the interval 14584.90' to 14705.80' in well 44/18-T1, ARCO British Ltd.1-11.

MERCADIER, C. G. L. & LIVERA, S. E. 1993. Applications of the formation micro-scanner to modelling of the Palaeozoic reservoirs in Oman. *In*: FLINT, S. S. & BRYANT, I. D. (eds.) *The Geological Modelling of Hydrocarbon Reservoirs and*

Outcrop Analogues. Special Publication of the International Association of Sedimentologists, 15, 125-142.

MERZ-PREIß, M. & RIDING, R. 1999. Cyanobacterial tufa calcification in two freshwater streams: ambient environment, chemical thresholds and biological processes. *Sedimentary Geology*, 126, 103-124.

MIALL, A. D. 1977. A review of the braided river depositional environment. *Earth Science Review*, 13, 1-62.

MIALL, A. D. 1978. Lithofacies types and vertical profile models in braided river deposits: A summary. *In*: MIALL, A. D. (ed.) *Fluvial Sedimentology*, Canadian Society of Petroleum Geologists, Memoir 5. 597-604.

MIALL, A. D. 1981. Alluvial Sedimentary Basins: Tectonic Setting and Sedimentary Architecture. *In*: MIALL, A. D. (ed.) *Sedimentation and Tectonics in Alluvial Basins*, Geological Association of Canada Special Paper, 23, 1-33.

MIALL, A. D. 1985. Architectural-element analysis; a new method of facies analysis applied to fluvial deposits. *Earth-Science Reviews*, 22, 261-308.

MIALL, A. D. 1988a. Architectural elements and bounding surfaces in fluvial deposits: Anatomy of the Kayenta Formation (Lower Jurassic), Southwest Colorado. *Sedimentary Geology*, 55, 233-262.

MIALL, A. D. 1988b. Reservoir Heterogeneities in Fluvial Sandstones: Lessons from Outcrop Studies. *Bulletin of the American Association of Petroleum Geologists*, 72, 682-697.

MIALL, A. D. 1996. *The geology of fluvial deposits : sedimentary facies, basin analysis, and petroleum geology*. Berlin London, Springer.

MUNSSEN, F. C. J. 1997. Modelling of sandbody connectivity in the Schooner Field. *In*: ZIEGLER, K., TURNER, P. & DAINES, S. R. (eds.) *Petroleum Geology of the*

Southern North Sea: Future and Potential, Geological Society Special Publication, **123**, 169-180.

MILLER, D. D., McPHERSON, J. G. & COVINGTON, T. E. 1990. Fluviodeltaic reservoir, South Belridge Field, San Joaguin Valley, California. *In*: BARWIS, McPHERSON & STUDLICK (eds.) *Sandstone Petroleum Reservoirs*, 109-130.

MJOS, R. & PRESTHOLM, E. 1993a. The geometry and organisation of fluviodeltaic channel sandstones in the Jurassic Saltwick formation, Yorkshire, England. *Sedimentology*, **40**, 919-935.

MJOS, R., WALDERHAUG, O. & PRESTHOLM, E. 1993b. Crevasse splay sandstone geometries in the Middle Jurassic Ravenscar Group of Yorkshire, UK. *In*: MARZO, M. & PUIGDEFABREGAS, C. (eds.) *Alluvial Sedimentation*, Special Publication of the International Association of Sedimentologists, **17**, 167-184.

MOHRIG, D., HELLER, P. L., PAOLA, C. & LYONS, W. 2000. Interpreting avulsion process from ancient alluvial sequences: Guadalope-Matarranya system (northern Spain) and Wasatch Formation (western Colorado). *Geological Society of America Bulletin*, **112**, 1787-1803.

MONTY, C. L. V. 1972. Recent algal stomatolitic deposits, Andros Island, Bahamas. Preliminary report. *Geol Rundschau*, **61**, 742-783.

MONTY, C. L. V. 1979. Scientific reports of the Belgian expedition on the Australian Great Barrier Reef, 1967. Sedimentology 2. Monospecific stromatolites from the Great Barrier Reef and their palaeontolgical significance. *Ann Soc Geol Belg*, **101**, 163-171.

MORRIS, P. H. & WILLIANS, D. J. 1999. Worldwide correlations for subaerial aqueous flows with exponential longitudial profiles. *Earth Surface Processes and Landforms*, **24**, 867-879.

MOSLEY, M. P. 1982. Analysis of the effect of changing discharge on channel morphology and instream uses in a braided river, Ohau River, New Zealand. *Water Resources Research*, **18**, 800-812.

MOSLEY, M. P. & ZIMPFER, G. L. 1978. Hardware models in geomorphology. *Progress in Physical Geography*, **2**, 438-461.

MOULINE, M. P. 1977. La place des formations stromatolitiques et oncolitiques dans l'analyse sequentielle des sediments fluviolacustres tertiaires du Castrais et de l'Albigeois. The position of stromatolitic and oncolitic formations in the sequential analysis of Tertiary fluvial lacustrine sediments of Castres and Albi. *Bulletin de la Societe d'Histoire Naturelle de Toulouse*, **113**, 132-146.

MUNZO, J. A., CASAS, J. M., MARTINEZ, A. & VERGES, J. 1988. *An introduction to the structure of the Southeastern Pyrenees, the Ter-freser cross-section.* Symposium on the Geology of the Pyrenees and Betics (Barcelona), Excursion Guide, 86pp.

MUTTI, E., SEGURET, M. & SGAVETTI, M. 1988. *Sedimentation and deformation in the Tertiary sequences of the Southern Pryenees.* American Association of Petroleum Geologist, Mediterranean Basins Conference Field Trip 7, Excursion Guidebook, 1-126.

MYROW, P. M. 1990. A new graph for understanding colors of mudrocks and shales. Journal of Geological Education, **38**, 16-20.

NAMI, M. & LEEDER, M. R. 1978 Changing channel morphology and magnitude in the Scalby Formation (M. Jurassic) of Yorkshire, England. *In*: MIALL, A. D. (ed.) *Fluvial Sedimentology*, Canadian Society of Petroleum Geologists, *Memoir 5*. 431-440.

NEWELL, A. J., TVERDOKHLEBOV, V. P. & BENTON, M. J. 1999. Interplay of tectonics and climate on a transverse fluvial system, Upper Permian, Southern Uralian Foreland Basin, Russia. *Sedimentary Geology*, **127**, 11-29.

NICKEL, E. 1982. Alluvial-fan-carbonate facies with evaporites, Eocene Guarga formation, southern Pyrenees, Spain. *Sedimentology*, **29**, 761-796.

NICKEL, E. 1983. Environmental significance of freshwater oncoids, Eocene Guarga formation, southern Pyrenees, Spain. *In*: PERYT, T. M (ed.) *Coated grains*, Springer 308-329.

NORTH, C. P. 1996. The prediction and modelling of subsurface fluvial stratigraphy. In: CARLING, P. A. & DAWSON, M. R. (eds.) *Advances in Fluvial Dynamics and Stratigraphy*, 395-508.

NORTH, C. P. & TAYLOR, K. S. 1996. Ephemeral-fluvial deposits: Integrated outcrop and simulation studies reveal complexity. *Bulletin of the American Association of Petroleum Geologists*, **80**, 811-830.

O'BRIEN, P.E. & WELLS, A.T. 1986. A small alluvial crevasse splay. *Journal of Sedimentary Petrology*, **56**, 876-879.

OBORN, L. E. & SUGGATE, R. P. 1959. *Sheet 21-Christchurch (1st ed.) Geological map of New Zealand, 1:250000.* Department of Science and Industrial Research, Wellington.

OLSEN, H. 1987. Ancient ephemeral stream deposits: a local terminal fan model from the Bunter Sandstone Formation (L. Triassic) in the Tonder-3, -4 and -5 wells, Denmark. *In*: FROSTICK, L. & REID, I. (eds.) *Desert Sediments: Ancient and Modern*, Geological Society Special Publication, **35**, 69-86.

OLSEN, H. 1990. Astronomical forcing of meandering river behaviour: Milankovitch cycles in Devonian of East Greenland. *Palaeography, Palaeoclimatology, Palaeoecology*, **79**, 99-115.

OLSEN, H. & LARSON, P. H. 1993. Structural and climatic controls on fluvial depositional systems; Devonian, North-East Greenland. In: *In*: MARZO, M. & PUIGDEFABREGAS, C. (eds.) *Alluvial Sedimentation*, Special Publication of the International Association of Sedimentologists, **17**, 401-423.

ORTON, G. J. & READING, H. G. 1993. Variability of deltaic processes in terms of sediment supply, with particular emphasis on grain size. *Sedimentology*, **40**, 475-512.

OSTERKAMP, W. R. 1980. Sediment-morphology relations of alluvial channels. *Proceedings of the Symposium on Watershed Management, American Society of Civil Engineers*, Boise, 188-199.

OUCHI, S. 1985. Response of alluvial rivers to slow active tectonic movement. *Geological Society of America Bulletin*, **96**, 504-515.

PAOLA, C. 1988. Subsidence and gravel transport in alluvial basins. *In*: KLEINSPEHN, K. L. & PAOLA, C. (eds.) *New Perspectives in basin analysis*, Springer-Verlag, New York. 231-243.

PAOLA, C. 2000. Quantitative models of sedimentary basin filling. *Sedimentology*, **47**, Supplement 1, 121-178.

PAOLA, C. & BORGMAN, L. 1991. Reconstructing random topography from preserved stratification. *Sedimentology*, **38**, 553-565.

PAOLA, C., HELLER, P. L., ANGEVINE, C. L. 1992. The large-scale dynamics of grain-size variation in alluvial basins, 1: Theory. *Basin Research*, **4**, 73-90.

PAOLA, C., PARKER, G., SEAL, R., SINHA, S. K., SOUTHARD, J. B. & WILCOCK, P. R. 1992. Downstream fining by selective deposition in a laboratory flume. *Science*, **258**, 1757-1760.

PARKER, G. 1976. On the cause and characteristics scales of meandering and braiding in rivers. *Journal of Fluid Mechanics*, **76**, 457-480.

PARKER, G. 1979. Hydraulic geometry of active gravel rivers. *Journal of the Hydraulics Division, American Society of Civil Engineers*, **105**, HY9, 1185-1201.

PARKER, G. 1991. Selective sorting and abrasion of river gravel, 1: Theory. *Journal of Hydraulic Engineering*, **17**, 131-149.

PARKER, G. 1991. Selective sorting and abrasion of river gravel, 2: Applications. *Journal of Hydraulic Engineering*, **17**, 150-171.

PEAKALL, J. 1995. *The influence of lateral ground-tilting on channel morphology and alluvial architecture.* Department of Earth Science, University of Leeds, Unpublished Ph.D. thesis.

PEAKALL, J. 1998. Axial river evolution in response to half-graben faulting: Carson River, Nevada, U.S.A. *Journal of Sedimentary Research*, **68**, 788-799.

PEAKALL, J., ASHWORTH, P.J. & BEST, J.L. 1996. Physical modelling in fluvial geomorphology: principles, applications and unresolved issues, *In*: RHOADS, B.L. & THORN, C.E.(eds.) *The Scientific Nature of Geomorphology*. Wiley and Sons, 221-253.

PEAKALL, J., ASHWORTH, P. J. & BEST, J. L. In review. Physical scale modelling of meander bend evolution and depositional architecture. *Journal of Sedimentary Research.*

PEAKALL, J., LEEDER, M., BEST, J. & ASHWORTH, P. 2000. River response to lateral ground tilting: a synthesis and some implications for the modelling of alluvial architecture in extentional basins. *Basin Research*, **12**, 413-424.

PEAKALL, J. & WARBURTON, J. 1996. Surface tension in small hydraulic river models – the significance of Weber number. *Journal of hydrology (NZ)*, **35**, 199-212.

PEARCE, T.J. 1995. *Chemostratigraphy of Westphalian C/D sequences from wells 44/14-2, 44/18-1, 44/18-2Z and 44/18-4A*. Chemostrat. Consultants, 80pp.

PEARCE, T.J., BESLY, B. M., WRAY, D.S. & WRIGHT, D.K. 1999. Chemostratigraphy: a method to improve interwell correlation in barren sequences - a case study using onshore Duchmantian/Stephanian sequences (West Midlands, U.K.). *Sedimentary Geology*, **124**, 197-220.

PERRIER, R. & QUIBLIER, J. 1974. Thickness changes in sedimentary layers during compaction history; methods for quantitative evaluation. *Bulletin of the American Association of Petroleum Geologists*, **48**, 507-520.

PERYT, T. M. 1981. *Phanerozoic oncoids - an overview*. Facies 4, 197-214.

PHILLIPS, F. M., WILSON, J. L. & DAVIS, J. M. 1989. Statistical analysis of hydraulic conductivity distributions: a quantitative geological approach. *Proceedings of*

New Field Techniques for Quantifying the Physical and Chemical Properties of Heterogeneous Aquifers. National Ground Water Association, Columbus, Ohio.

PUIGDEFABREGAS, C., MUNOZ, J. A. & MARZO, M. 1986. Thrust belt development in the eastern Pyrenees and related depositional sequences in the southern foreland basin. *In*: ALLEN, P. A. & HOMEWOOD, P. (eds.) *Foreland Basins*, Special Publication of the International Association of Sedimentologists, **8**, 229-246.

PUTNAM, P. E. 1983. Fluvial deposits and hydrocarbon accumulations: examples from the Lloydminster area, Canada. *In*: COLLINSON, J. D. & LEWIN, J. (eds.) *Modern and Ancient Fluvial Systems*, Special Publication of the International Association of Sedimentologists, **6**, 517-532.

PYE, K. 1983. Red beds. *In*: GOUCIE, A. S. & PYE, K. (eds.) *Chemical sediments and geomorphology; precipitates and residua in the near-surface environment*, Academic Press, London, 227-263

QUIRK, D. G. 1993. Interpreting the Upper Carboniferous of the Dutch Cleaver Bank High. *In*: PARKER, J. R. (ed.) *Petroleum Geology of Northwest Europe: Proceedings of the 4th Conference.* The Geological Society of London, 697-706.

QUIRK, D. G. 1997. Sequence stratigraphy of the Westphalian in the northern part of the Southern North Sea. *In*: ZIEGLER, K., TURNER, P. & DAINES, S. R. (eds.) *Petroleum Geology of the Southern North Sea: Future and Potential*, Geological Society Special Publication, **123**, 153-168.

QUIRK, D. G. & AITKEN, J. F. 1997. The structure of the Westphalian in the northern part of the southern North Sea. *In*: ZIEGLER, K., TURNER, P. & DAINES, S. R. (eds.) *Petroleum Geology of the Southern North Sea: Future and Potential.* Geological Society Special Publication, **123**, 143-152.

RAMOS, A. & SOPENA, A. 1983. Gravel bars in low-sinuosity streams (Permian and Triassic, central Spain) *In*: COLLINSON, J. D. & LEWIN, J. (eds.) *Modern and Ancient Fluvial Systems*, Special Publication of the International Association of Sedimentologists, **6**, 301-313.

RAMOS, A., SOPENA, A. & PEREZ-ARLUCEA, M. 1986. Evolution of Bunsandstein fluvial sedimentation in the northwest Iberian Ranges (Central Spain). *Journal of Sedimentary Petrology*, **56**, 862-875.

RATCLIFFE, B. C. & FAGERSTROM, J. A. 1980. Invertebrate Lebensspuren of Holocene floodplains: their morphology, origin and paleoecological significance. *Journal of Paleontology*, **54**, 614-630.

RAVENNE, C. & BEUCHER, H. 1988. Recent development in description of sedimentary bodies in a fluvio deltaic reservoir and their 3D conditional simulations. *Society of Petroleum Engineers*, **Paper 18310**. 463-475.

RAVENNE, C., ESCHARD, R., GALLL. A., MATHIEU, L., MONTADERT, L. & RUDKIEWICZ, J. L. 1987. Heterogeneities and Geometry of Sedimentary Bodies in a Fluvio-Deltaic Reservoir. *Society of Petroleum Engineers,* **Paper 16752**, 115-122.

READ, W. A. & DEAN, M. 1982. Quantitative relationships between numbers of fluvial cycles, bulk lithological composition and net subsidence in a Scottish Namurian basin. *Sedimentology*, **29**, 181-200.

READING, H.G., 1986. *Sedimentary Environments and Facies*, (2nd ed.), Blackwell.

REINFIELDS, I. & NANSON, G. 1993. Formation of braided river floodplains, Waimakariri river, New Zealand. *Sedimentology*, **40**, 1113-1127.

REPKA, J. L., ANDERSON, R. S. & FINKEL, R. C. 1997. Cosmogenic dating of fluvial terraces, Fremont River, Utah. *Earth and Planetary Science Letters*, **152**, 59-73.

RETALLACK, G. J. 1984. Completeness of the rock and fossil record: some estimates using fossil soils. *Paleobiology*, **10**, 59-78.

RETALLACK, G. J. 1986. Fossil soils as grounds for interpreting long-term controls on ancient rivers. *Journal of Sedimentary Petrology*, **56**, 1-18.

RETALLACK, G.J. 1993. Late Ordovician paleosols of the Juniata Formation near Potters Mills, Pennsylvania. *In*: DRIESE, S.G. (ed.) *Paleosols, Paleoweathering and Paleoatmospheric CO2; Paleozoic Paleosols of Central Pennsylvania*, University of Tennessee, Department of Geological Sciences, Studies in Geology, **22**, 33-50.

REYNOLDS, A. D. 1999. Dimensions of Paralic sandstone bodies. *Bulletin of the American Association of Petroleum Geologists*, **83**, 211-229.

REYNOLDS, D. J., STECKLER, M. S. & COAKLEY, B. J. 1991. The role of the sediment load in sequence stratigraphy; the influence of flexural isostasy and compaction. *Journal of Geophysical Research, B, Solid Earth and Planets*, **96**, 6931-6949.

RHY, G. H. 1974. *A proposed standard lithostratigraphic nomenclature for the Southern North Sea and an outline structural nomenclature for the whole of the (UK) North Sea.* Institude of Geological Science Report 74/8.

RICE, S. 1999. The nature and controls on downstream fining within sedimentary links. *Journal of Sedimentary Research*, **69**, 32-39.

RICE, S. & CHURCH, M. 1998. Grain size along two gravel-bed rivers: statistical variation, spatial pattern and sedimentary links. *Earth Surface Processes and Landforms*, **23**, 345-363.

RICHARDS, K. 1982. *Rivers : form and process in alluvial channels.* London : Methuen, pp358.

RICHARDSON, J. F. & ZAKI, W. N. 1958. Sedimentation and fluidisation, *Trans. Insititue of Chemical Engineers*, **32**, 35-53.

RIDER, M.H. 1990. Gamma-ray log shape used as a facies indicator: critical analysis of an oversimplified methodology. *In*: HURST, A., LOVELL, M.A. & MORTON, A.C. (eds.) *Geological Applications of Wireline Logs*. Geological Society Special Publication, **48**, 27-37.

RIDING, R. 1983. Cyanoliths (Cyanoids):oncoids formed by calcified Cyanophytes. *In*: PERYT, T. M (ed.) *Coated grains*, Springer. 276-282.

RIDING, R. & VORONOVA, L. 1983. Recent freshwater oscillatoriacean analogue of the Lower palaeozoic calcareous alga Augulocellularia. *Lethaia*, **15**, 105-114.

RITCHARDSON, J. G., SANGREE, J. B. & SNEIDER, R.M. 1987a. Braided stream reservoirs. *Journal of Petroleum Technology*, December 1987, 1499-1500.

RITCHARDSON, J. G., SANGREE, J. B. & SNEIDER, R.M. 1987b. Meandering stream reservoirs. *Journal of Petroleum Technology*, December 1987, 1501-1502.

ROBINSON, J. W. & McCABE, P. J. 1997. Sandstone-body and shale-body dimensions in a braided fluvial system: Salt Wash Sandstone Member (Morrison Formation), Garfield County, Utah. *Bulletin of the American Association of Petroleum Geologists*, **81**, 1267-1291.

ROBINSON, D. A. & FRIEDMAN, S. P. 2001. Effect of particle size distribution on effective dielectric permittivity of saturated granular media. *Water Resources Research*, **37**, 33-40.

ROBINSON, R. A. J. & SLINGERLAND, R. L. 1998. Origin of fluvial grain-size trends in a foreland basin: the Pocono Formation on the Central Appalachian Basin. *Journal of Sedimentary Research*, **68**, 473-486.

ROURE, F., CHOUKROUNE, P., BERASTEGUI, X., MUNOZ, J. A., VILLIEN, A., MATHERON, P., BAYRET, M., SEGURET, M., CAMARA, P. & DERAMOND, J. 1989. ECORS deep seismic data and balanced cross-sections:geometric constraints to trace the evolution of the Pyrenees. *Tectonics*, **8**, 41-50.

ROWLEY, D. B., RAYMOND, A., TOTMAN PARRISH, J., LOTTES, A. L., SCOTESE, C. R. & ZIEGLER, A. M. 1985. Carboniferous paleogeography, phytogeography, and paleoclimatic reconstructions. *International Journal of Coal Geology*, **5**, 7-42.

RUDKIEWICZ, J. L., SUERILLOT, D., GALLI, A. & GROUP HERESI. 1990. An integrated software for stochastic modelling of reservoir lithology and property with an example from the Yorkshire Middle Jurassic. *In*: BULLER, A. T., BERG, E., HJELMELAND, O., KLEPPE, J., TORSAETER, O. & AASEN, J.O (eds.) *North Sea Oil & Gas Reservoirs II,* Graham & Trotman. 399-406.

RUHE, R. V. 1965. *Quaternary paleopedology.* The Quaternary of the United States. 755-764.

RYDER, R. T., FOUCH, T. D. & ELISON, J. H. 1976. Early Tertiary sedimentation in the western Uinta Basin, Utah. *Geological Society of America Bulletin*, **87**, 496-512.

SADLER, P. M. 1981. Sediment accumulation rates and the completeness of stratigraphic sections. *Journal of Geology*, **89**, 569-584.

SAHIN, A., GHORI, S. G., ALI, A. Z., EL-SAHN, H. F., HASSAN H. M. & AL-SANOUNAH, A. 1998. Geological controls of variograms in a complex carbonate reservoir, Eastern Province, Saudi Arabia. *Mathematical Geology*, **30**, 309-322.

SALTER, T. 1993. Fluvial scour and incision: models for their influence on the development of realistic reservoir geometries. *In*: NORTH, C. P. & PROSSER, D. J. (eds.) *Characterization of Fluvial and Aeolian Reservoirs*, Geological Society Special Publication, **73**, 33-51.

SAMBROOK SMITH, G. 1996. Bimodal fluvial bed sediments:origin, spatial extent and processes. *Progress in Physical Geography*, **20**, 402-417.

SAMBROOK SMITH, G. H. & FERGUSON, R. I. 1995. The gravel-sand transition along river channels. *Journal of Sedimentary Research*, **A65**, 423-430.

SAMBROOK SMITH, G. H. & FERGUSON, R. I. 1996. The gravel-sand transition: flume study of channel response to reduce slope. *Geomorphology*, **16**, 147-159.

SAPOZHNIKOV, V. & FOUFOULA-GEORGIOU, E. 1996. Self-affinity in braided rivers. *Water Resources Research*, **32**, 1429-1439.

SAPOZHNIKOV, V. & FOUFOULA-GEORGIOU, E. 1997. Experimental evidence of dynamic scaling and indications of self-organised criticality in braided rivers. *Water Resources Research*, **33**, 1983-1991.

SCHNEIDER, J., SCHRODER, H. G. & LE CAMPION-ALSUMARD, T. 1983. Algal micro-reefs-coated grains from freshwater environments. *In*: PERYT, T. M. (ed.) *Coated Grains*, Springer, Berlin, 284-298.

SCHREIBER, B. C. 1980. Evaporites. *In*: HOBSON, G. D. (ed.) *Developments in Petroleum Geology*, 87-138.

SCHUMM, S.A. 1960. *The shape of alluvial channels in relation to sediment type*. U. S. Geological Survey Professional Paper, Report: **P 0352-B**, 17-30.

SCHUMM, S. A. 1977. *The fluvial system*. John Wiley and sons.

SCHUMM, S. A. 1981. Evolution and response of the fluvial system, sedimentologic implications. *In*: ETHRIDGE, F.G. & FLORES, R.M. (eds.) *Recent and ancient non-marine depositional environments: models for exploration*, SEPM Special Publication, **31**, 19-29.

SCHUMM, S. A. 1993. River response to baselevel change: implications for sequence stratigraphy. *Journal of Geology*, **101**, 279-294.

SCHUMM, S. A. & BRAKENRIDGE, G. R. 1987. River responses. *In*: RUDDIMAN, W. F. & WRIGHT, H. E. (eds.) *North America and adjacent oceans during the last deglaciation*, Geological Society of America, 221-240.

SCHUMM, S. A. & LICHTY, R. W. 1963. *Channel widening and flood-plain construction along Cimarron River in southwestern Kansas*, U. S. Geological Survey Professional Paper, Report: **P 352-D**, 71-88.

SCHUMM, S.A. & KHAN, H.R. 1972. Experimental Study of Channel patterns. *Geological Society of America Bulletin*, **83**, 1755-1770.

SCHUMM, S.A., MOSLEY, M. P. & WEAVER, W. E. 1987. *Experimental Fluvial Geomorphology*, Wiley, New York.

SCHUSTER, M. W. & STEIDMANN, J. R. 1987. Fluvial sandstone architecture and thrust induced subsidence, North Green River Basin, Wyoming. *In*: ETHERIDGE, F. G., FLORES, R. M. & HARVEY, M. D. (eds.) *Recent Developments in Fluvial Sedimentology*, Society of Economic Paleontologists and Minerologists Special Publications, **39**, 279-286.

SCLATER, J.G. & CHRISTIE, P.A.F. 1980. Continental stretching: an explanation of the post-mid-Cretaceous subsidence of the central North Sea Basin. *Journal of Geophysical Research*, **85**, 3711-3739.

SEAL, R., TORO-ESCOBAR, C., CUI, Y., PAOLA, C., PARKER, G., SOUTHARD, J. B. & WILCOCK, P. R. 1998. Downstream fining by selective deposition; theory, laboratory, and field observations. *In*: KILINGEMAN, P. C., BESCHTA, R. L, KOMAR, P. D. & BRADLEY, J. B. (eds.) *Gravel-bed Rivers in the Environment*, International Gravel-Bed Rivers Workshop, 61-84.

SEIFERT, D. & JENSEN, J. L. 2000. Object and pixel based reservoir modelling of a braided fluvial reservoir. *Mathematical geology*, **32**, 581-603.

SERRA, O. 1987. Sedimentological applications of wireline logs to reservoir studies. *In*: KLEPPE, J., BERG, E. W., BULLER, A. T., HJELMELAND, O. & TORSAETER, O (eds.) *North Sea Oil and Gas Reservoirs*, Graham and Trotman. 277-299.

SHACKLETON, N. J. & OPDYKE, N. D. 1973. Oxygen isotope and palaeomagnetic stratigraphy of equitorial Pacific core V28-238: oxygen isotope temperatures and ice volumes on a 105-106 year scale. *Quaternary Research*, **3**, 39-55.

SHANLEY, K. W. & McCABE, P. J. 1993. Perspectives on the sequence stratigraphy of continental strata. *Bulletin of the American Association of Petroleum Geologists*, **78**, 544-568.

SHAW, J. & KELLERHALS, R. 1982. The composition of recent alluvial gravels in Alberta river beds, *Alberta Research Council, Bulletin*, **41**, 151.

SHIELDS, A. 1936. Anwendung der Aehnlichkeitsmechanik und der turbulenzforschung auf die geschiebebewegung (The application of dimensionless analysis and the investigation of turbulence and bedload movement). *Mitteilung der Preussischen versuchsanstalt fuer Wasserbau und Schiffbau*, Heft 26, Berlin.

SHINN, E.A. & ROBBIN, D.M. 1983. Mechanical and chemical compaction in fine-grained shallow-water limestones. *Journal of Sedimentary Petrology*. **53**, 595-618.

SHUSTER, M. W. & STEIDTMANN, J. R. 1987. Fluvial-sandstone architecture and thrust-induced subsidence, northern Green River basin, Wyoming. *In:* ETHERIDGE, F. G., FLORES, R. M. & HARVEY, M. D. (eds.) *Recent Developments in Fluvial Sedimentology*, Society of Economic Paleontologists and Minerologists Special Publications, **39**, 279-285.

SIEGENTHALER, C. & HUGGENBERGER, P. 1993. Pleistocene Rhine gravel:deposits of a braided river system with dominant pool preservation. *In*: BEST, J.L. & BRISTOW, C.S. (eds.) *Braided Rivers*, Geological Society Special Publication, **75**, 147-162.

SIMONS, D. B. & SIMONS, R. K. 1987. Differences between gravel-and sand-bed rivers. *In*: THORNE, C. R., BATHURST, J. C. & HEY, R. D. (eds.) *Sediment transport in gravel bed rivers*. John Wiley & Sons Ltd. 3-15.

SINGH, H., PARKASH, B. & GOHAIN, K. 1993. Facies analysis of the Kosi megafan deposits. *Sedimentary Geology*, **85**, 87-113.

SKORSTAD, A., HAUGE, R. & HOLDEN, L. 1999. Well conditioning in a fluvial reservoir model. *Mathematical Geology*, **31**, 857-872.

SMITH, A. G. 1994. Climatic influences on continental deposition during late stage filling of an extensional basin, south-eastern Arizona. *Geological Society of America Bulletin*, **106**, 1212-1228.

SMITH, A. G. 1996. Tertiary stages and ages, and some distinctive stratigraphic approaches. *In*: FRIEND, P. & DABBRIO, C. J. (eds.) *Tertiary basins of Spain: the stratigraphic record of crustal kinematics*. Cambridge Univ. Press, New York, 3-5.

SMITH, D. 1976. Effect of vegetation on lateral migration of anastomosed channels of glacier meltwater river. *Geological Society of America Bulletin*, **87**, 857-860.

SMITH, N.D. & PEREZ-ARLUCEA, M. 1994. Fine-grained splay deposition in the avulsion belt of the lower Saskatchewan river, Canada. *Journal of Sedimentary Research*, **B64**, 159-168.

SMITH, N.D., CROSS, T.A., DUFFICY, J.P. & CLOUGH, S.R. 1989. Anatomy of an avulsion. *Sedimentology*, **36**, 1-23.

SMITH, R. J., THRASHER, G. P. & BEGGS, J. M. 1994. *Quaternary sedimentation in the Canterbury Region, eustatic influences on braidplain development.* Unpublished Confidential Client Report 513916:10. Institute of Geological and Nuclear Science Ltd. 84p.

SMITH, R. M. H. 1990. Alluvial paleosols and pedofacies sequences in the Permian Lower Beaufort of the Southwestern Karoo Basin, South Africa. *Journal of Sedimenatry Petrology*, **60**, 258-276.

SMITH, S. A. 1990. The sedimentology and accretionary styles of an ancient gravel-bed stream: the Budleigh Salterton Pebble Beds (Lower Triassic), southwest England. *Sedimentary Geology*, **67**, 199-219.

SOONS, J. M. 1963. The glacial sequence in part of the Rakaia valley, Canterbury, New Zealand. *New Zealand Journal of Geology and Geophysics*, **6**, 735-756.

SOONS, J. M. & GULLENTOP, F. W. 1973. Glacial advance in the Rakaia Valley, New Zealand. *New Zealand Journal of Geology and Geophysics*, **16**, 425-438.

SOUTHARD, J.B., SMITH, N.D. & KUHNLE, R.A. 1984. Chutes and Lobes: Newly Identified elements of braiding in shallow gravelly streams. *In*: KOSTER, E.H. &

STEEL, R.J. (eds.) *Sedimentology of Gravels and Conglomerates*, Canadian Society of Petroleum Geologists, **Memoir 10**, 51-59.

STANLEY, K. O. & FAGERSTROM, J. A. 1974. Miocene invertebrate trace fossils from a braided river environment, Western Nebraska, U.S.A. *Palaeogeography, Palaeoclimatology, Paleoecology*, **15**, 63-82.

STANLEY, K. O., JORDE, K., RAESTAD, N. & STOCKBRIDGE, C. P. 1990. Stochastic modelling of reservoir sand bodies for input to reservoir simulation, Snorre Field, northern North Sea, Norway. *In*: BULLER, A. T., BERG, E., HJELMELAND, O., KLEPPE, J., TORSAETER, O. & AASEN, J.O (eds.) *North Sea Oil & Gas Reservoirs II*, Graham & Trotman. 91-101.

STEAR, W. M. 1983. Morphological characteristics of ephemeral stream channel and overbank splay sandstone bodies in the Permian Lower Beaufort Group, Karoo Basin, South Africa. *In*: COLLINSON, J. D. & LEWIN, J. (eds.) *Modern and Ancient Fluvial Systems*, Special Publication of the International Association of Sedimentologists, **6**, 405-420.

STEEL, R. J. & THOMPSON, D. B. 1983. Structures and textures in Triassic braided stream conglomerates ("Bunter" Pebble Beds) in the Sherwood Sandstone Group, North Staffordshire, England. *Sedimentology*, **30**, 341-367.

STERNBERG, H. 1875. *Untersuchungen uber Langen-und Querprofil geschiebefuhrender Flusse: Zeitschrift fur Bauwesen*. **25**, 483-506.

STEVENS, M. A., SIMONS, D. B. & RICHARDSON, E. V. 1975. Non-equilibrium river form. *Journal of the Hydraulics Division, American Society of Civil Engineers*, **101**, HY5, 557-566.

STOKSTAD, E. 2000. Seeing a world in grains of sand. *Science*, **287**, 1912-1915.

STOLUM, H. 1991. Fractal heterogeneity of clastic reservoirs. *In*: LAKE, L. W., CARROLL, H. B. & WESSON, T. C. (eds.) *Reservoir Characterization 2*, Academic Press, London, 579-605.

STONE, G. & MOSCARIELLO, A. 1999. Integrated modelling of the Southern North Sea Carboniferous Barren Red Measuresusing production data, geochemistry, and pedofacies cyclicity. *Society of Petroleum Engineers,* **Paper 56898.**

SUGGATE, R. P. 1963. The fan surfaces of the central Canterbury Plain. *New Zealand Journal of Geology and Geophysics*, **6**, 281-287.

SUGGATE, R. P. 1965. Late Pleistocene geology of the northern part of the South Island, New Zealand. *New Zealand Geological Survey Bulletin*, 77.

SURINACH, E., MARTHELOT, J., GALLART, J., DIAGNIERES, M. & HIRN, A. 1993. Seismic images and evolution of the Iberian crust in the Pyrenees. *Tectonophysics*, **221**, 67-80.

SYMONDS, R. A. & VAN DIJK, C. P. J. 1995. *Sedimentology, Petrography and Reservoir Properties of core 1-4, Well 44/18-4A*, Final Report, 1-30.

TIPPETT, M. J. & KAMP, P. J. 1995. Geomorphic evolution of the Southern Alps, New Zealand. *Earth Surface Processes and Landforms*, **20**, 177-192.

TODD, S. P. 1996. Process deduction from fluvial sedimentary structure. *In*: CARLING, P. A. & DAWSON, M. R. (eds.) *Advances in Fluvial Dynamics and Stratigraphy*. 299-350.

TODD, S. P. & WENT, D. J. 1991. Lateral migration of sand-bed rivers; examples from the Devonian Glashabeg Formation, SW Ireland and the Cambrian Alderney Sandstone Formation, Channel Islands. *Sedimentology*, **38**, 997-1020.

TORNQVIST, T. E. 1994. Middle and late Holocene avulsion history of the River Rhine (Rhine-Meuse delta, Netherlands). *Geology*, **22**, 711-714.

TROTTER, F. M. 1953. Reddened beds of Carboniferous age in north-west England and their origin. *Proceedings of the Yorkshire Geological Society*, **29**, 1-19.

TROTTER, F. M. 1954. Reddened beds in the Coal Measures of south Lancashire. *Bulletin of the Geological Survey of Great Britain*, **5**, 61-80.

TUCKER, M. E. 1978. Triassic lacustrine sediments from South Wales: Shore zone clastics, evaporites and carbonates. *In*: MATTER, A. & TUCKER, M. E. (eds.) *Modern and Ancient Lake Sediments*, Special Publication of the International Association of Sedimentologists, **2**, 205-224.

TUNBRIDGE, I. P. 1981. Sandy high-energy flood sedimentation - some criteria for recognition, with an example from the Devonian of S.W. England. *Sedimentary Geology*, **28**, 79-95.

TURNER, P. 1980. *Continental red beds*. Developments in sedimentology, Elsevier Sci. Publ. Co., Amsterdam, Netherlands, **29**, 536 pp.

TURNER, P., HIRST, J. P. P., & FRIEND, P. F. 1984. A palaeomagnetic analysis of Miocene sediments at Pertusa, near Huesca, Ebro Basin, Spain. *Geological Magazine*, **121**, 279-290.

TYE, R. S. 1991. Fluvial-sandstone reservoirs of the Travis Peak Formation, East texas basin. *In*: MIALL, A. D. & TYLER, N. (eds.) *The three-dimentional facies architecture of terrigenous clastic sediments and its implications for hydrocarbon discovery and recovery*. SEPM. Concepts in Sedimentology and Paleontology, **3**, 172-188.

TYE, R. S., BHATTACHARYA, J. P., LORSONG, J. A., SINDELAR, S. T., KNOCK, G. D., PULS, D. D. & LEVINSON, R. A. 1999. Geology and stratigraphy of fluvio-deltaic deposits in the Ivishak Formation: Applications for development of Prudhoe Bay Field, Alaska. *Bulletin of the American Association of Petroleum Geologists*, **83**, 1588-1623.

VAIL, P. R., MITCHUM, R. M. & THOMPSON III, S. 1977. Seismic stratigraphy and global changes of sea level; Part 4, Global cycles of relative changes of sea level. *Memoir - American Association of Petroleum Geologists*, **26**, 83-97.

VAN DE GRAAF, W. J. E. & EALEY, P. J. 1989. Geological modelling for simulation studies. *Bulletin of the American Association of Petroleum Geologists*, **73**, 1436-1444.

VAN DER NEUT, M. & ERIKSSON, P. G. 1999. Palaeohydrological parameters of a Proterzoic braided fluvial system (Wilgerivier Formation, Waterberg Group, South Africa) compared with a Phanerozoic example. *In*: SMITH, N.D. & ROGERS, J. (eds.) *Fluvial Sedimentology VI*, Special Publication of International Association of Sedimentologists, Blackwells, **28**, 381-392.

VAUGHAN, A., HANSEN, T., CARDON, H. & RADCLIFFE, N. 1999. Litho-flow facies prediction in alluvial fan/fluvial system, Central North Sea. *Petroleum Geoscience*, **5**, 409-419.

VISSER, C. A. & CHESSA, A. G. 2000a. A new method for estimating lengths for partially exposed features. *Mathematical Geology*, **32**, 109-126.

VISSER, C. A. & CHESSA, A. G. 2000b. Estimation of length distributions from outcrop datasets - application to the Upper Permian Cutler formation, Utah. *Petroleum Geoscience*, **6**, 29-36.

WADMAN, D. H., LAMPRECHT, D. E. & MROSOVSKY, I. 1979. Joint geologic/engineering analysis of he Sadlerochit reservoir, Prudhoe Bay field. *Journal of Petroleum Geology*, **31**, 933-940.

WALDERHAUG, O. & MJOS, R. 1991. Sandbody geometry in fluvial systems - an example from the Jurassic of Yorkshire, England. *In*: LAKE, L. W., CARROLL, H. B. & WESSON, T. C. (eds.) *Reservoir Characterization 2*, Academic Press, London, 701-703.

WALKER, T. R. 1967. Formation of red beds in modern and ancient deserts. *Geological Society of America Bulletin*, **78**, 353-368.

WARBURTON, J. & DAVIES, T. 1994a. Variability of bedload transport and channel morphology in a braided river hydraulic model. *Earth Surface Processes and Landforms*, **19**, 403-421.

WARBURTON, J. & DAVIES, T. R. H. 1998. Use of hydraulic models in management of braided gravel-bed rivers. *In*: KILINGEMAN, P. C., BESCHTA, R. L, KOMAR, P. D. & BRADLEY, J. B. (eds.) *Gravel-bed Rivers in the Environment*, International Gravel-Bed Rivers Workshop, 513-542.

WARBURTON, J., DAVIES, T. R. H. & MANDL, M. G. 1993. A meso-scale field investigation of channel change and floodplain characteristics in an upland braided gravel-bed river, New Zealand. *In*: BEST, J.L & BRISTOW, C.S. (eds.) *Braided Rivers*, Geological Society of London Special Publication, **75**, 241-255.

WEBB, E. K. & ANDERSON, M. P. 1996. Simulation of preferential flow in three-dimensional, heterogeneous conductivity fields with realistic internal architecture. *Water Resources Research*, **32**, 533-545.

WEBB, E. K. & DAVIS, J.M. 1998. Simulation of the spatial heterogeneity of geologic properties: an overview. *In*: FRASER, G. S. P. & DAVIS, M. J. (eds.) *Hydrogeologic Models of Sedimentary Aquifers*, 1-13.

WEBB, E. K. 1994. Simulating the Three-Dimensional Distribution of Sedimentary Units in Braided-Stream Deposits. *Journal of Sedimentary Research*, **B64**, 219-231.

WEBER, K. J. 1980. How Heterogeneity affects oil recovery. *In*: LAKE, L. W. & CARROLL, H. B. (eds.) *Reservoir Characterization 1*, Academic Press, London, 487-544.

WEBER, K. J. 1986. Influence on fluid flow of common sedimentary structures in sandbodies. *Society for Petroleum Engineers*, **Paper 9247**. 1-7.

WEBER, K. J. 1993. The use of 3-D seismic in reservoir geological modelling. *In*: FLINT, S. S. & BRYANT, I. D. (eds.) *The Geological Modelling of Hydrocarbon Reservoirs and Outcrop Analogues*, Special Publication of the International Association of Sedimentologists, **15**, 181-188.

WELLMAN, H. W. 1979. An uplift map for the South Island of New Zealand, and a model for uplift of the Southern Alps. The origin of the Southern Alps. *Royal Society of New Zealand Bulletin*, **18**, 13-20.

WELLS, N. A. 1983. Transient streams in sand-poor redbeds: early-Middle Eocene Kuldna Formation of northern Pakistan. *In*: COLLINSON, J. D. & LEWIN, J. (eds.) *Modern and Ancient Fluvial Systems*, Special Publication of the International Association of Sedimentologists, **6**, 393-403.

WELLS, N. A. & DORR, J. A. 1987. A reconnaissance of sedimentation on the Kosi alluvial fan of India. *In*: ETHRIDGE, F. G., FLORES, R. M. & HARVEY, M. D. (eds.) *Recent developments in Fluvial Sedimentology*, The Society of Economic Paleontologists and Mineralogists, **39**, 51-61.

WERRITTY, A. 1992. Downstream fining in a gravel-bed river in Southern Poland: Lithological controls and the role of abrasion. *In*: BILLI, P., HEY, R. D., THORNE, C. R. & TACCONI, P. (eds.) *Dynamics of Gravel-bed Rivers*, John Wiley & Sons Ltd. 333-346.

WHIPPLE, K. X., PARKER, G., PAOLA, C. & MOHRIG, D. 1998. Channel dynamics, sediment transport, and the slope of alluvial fans: Experimental study. *Journal of Geology*, **106**, 677-693.

WHITE, C. D. & WILLIS, B.J. 1999. A method to estimate length distributions from outcrop data. *Mathematical Geology*, **32**, 389-419.

WHITE, C. D. & WILLIS, B.J. 2000. Quantitative outcrop data for flow simulation. *Journal of Sedimentary Research*, **4**, 788-802.

WILLIAMS, G. P. 1978a. Bankfull discharge of rivers. *Water Resources Research*, **14**, 1141-1158.

WILLIAMS, H. & SOEK, H. F. 1993. Predicting reservoir sandbody orientations from dipmeter data: the use of sedimentary dip profiles from outcrop studies. *In*: FLINT, S. S. & BRYANT, I. D. (eds.) *The Geological Modelling of Hydrocarbon Reservoirs and*

Outcrop Analogues, Special Publication of the International Association of Sedimentologists. **15**, 57-80.

WILLIAMS, P. F. & RUST, B. R. 1969. The sedimentology of a braided river. *Journal of Sedimentary Petrology*, **39**, 649-679.

WILLIS, B. J. & BEHRENSMEYER, A. K. 1994. Architecture of Miocene Overbank Deposits in Northern Pakistan. *Journal of Sedimentary Research*, **B64**, 60-67.

WILLIS, B. J. 1993a. Ancient river systems in the Himalayan foredeep, Chinji Village area, northern Pakistan. *Sedimentary Geology*, **88**, 1-76.

WILLIS, B. J. 1993b. Evolution of Miocene fluvial systems in the Himalayan foredeep through a two kilometre-thick succession in northern Pakistan. *Sedimentary Geology*, **88**, 77-121.

WILSON, D. D. 1976. Hydrogeology of Metropolitan Christchurch. *Journal of Hydrology (NZ)*, **15**, 101-120.

WILSON, D. D. 1985. Erosional and depositional trends in rivers of the Canterbury plains, New Zealand. *Journal of Hydrology (NZ)*, **24**, 32-48.

WIZEVICH, M. C. 1991. Photomosaics of outcrops: useful photographic techniques. *In*: MIALL, A. D. & TYLER, N. (Eds.) *The Three-dimensional Facies Architecture of Terrigeneous Clastic Sediments and its implications for hydrocarbon discovery and recovery*, Concepts in Sedimentology and Paleontology **3**, SEPM, 21-24.

WIZEVICH, M. C. 1993. Depositional controls in a bedload-dominated fluvial system: internal architecture of the Lee Formation, Kentucky. *Sedimentary Geology*, **85**, 537-556.

WOLCOTT, J. 1988. Nonfluvial control of bimodal grain size distributions in river-bed gravels. *Journal of Sedimentary Petrology*, **58**, 979-984.

WOLMAM, G.M. & MILLER, J.P. 1960. Magnitude and frequency of forces in geomorphic processes. *Journal of Geology*. **68**, 54-74.

WOOD, L. J., ETHRIDGE, F. G. & SCHUMM, S. A. 1993. The effects of rate of base-level fluctuation on coastal-plain, shelf and slope depositional systems: an experimental approach. *In*: POSAMENTIER, H. W., SUMMERHAYES, C. P., BILAL, U. & ALLEN, G. P. (eds.) *Sequence Stratigraphy and Facies Associations*. Special Publication of the International Association of Sedimentologists. **18**, 43-53.

WORTHINGTON, P. F. 1990. Sediment cyclicity from well logs. *In*: HURST, A., LOVELL, M. A. & MORTON, A. C. (eds.) *Geological Applications of Wireline Logs*, Geological Society Special Publication, **48**, 123-132.

WRIGHT, V. P. 1990. Estimating rates of calcrete formation and sediment accretion rates in ancient alluvial deposits. *Geological Magazine*, **127**, 273-276.

WRIGHT, V. P. 1992. Paleopedology: stratigraphic relationships and empirical models. *In*: MARTINI, I. P. & CHESWORTH, W. (eds.) *Weathering, soils and Paleosols: Developments in Earth Surface Processes 2*, Ch.18, 475-497.

YALIN, M.S. 1964. Geometrical properties of sand waves. *Journal of the Hydraulics Division, American Society of Civil Engineers*, **90**, 105-119.

YALIN, M.S. 1971. *Theory of Hydraulic Models*, Macmillan, London, 266 pp.

YARIS, J. M. & CHAMBERS, R. L. 1994. *Stochastic modeling and geostatistics: principles, methods, and case studies*. AAPG Computer Applications in Geology, **3**.

YOUNG, W. J. & DAVIES, T. R. H. 1990. Prediction of bedload transport rates in braided rivers: a hydraulic model study. *Journal of Hydrology (NZ)*, **29**, 75-92.

YU, B. & WOLMAN, M. G. 1987. Some dynamic aspects of river geometry. *Water Resources Research*, **23**, 501-509.

ZIEGLER, P. A. 1990. Collision related intra-plate compression deformations in western and central-Europe. *Journal of Geodynamics*, **11**, 357-388.

Appendix A: Tyne Field sedimentary core logs

The following pages display sedimentary core logs taken from eight well (Figures A1-A8) from the Ketch Member of the Tyne Field reservoir, Southern North Sea, UK. Well locations are shown in Chapter 3, Figure 3.1.

Well Number: *44/18–1* Core Numbers: *1,2,3* Drillers Depth: *12,393.00' – 12,429.20'* Well Deviation: *4°*

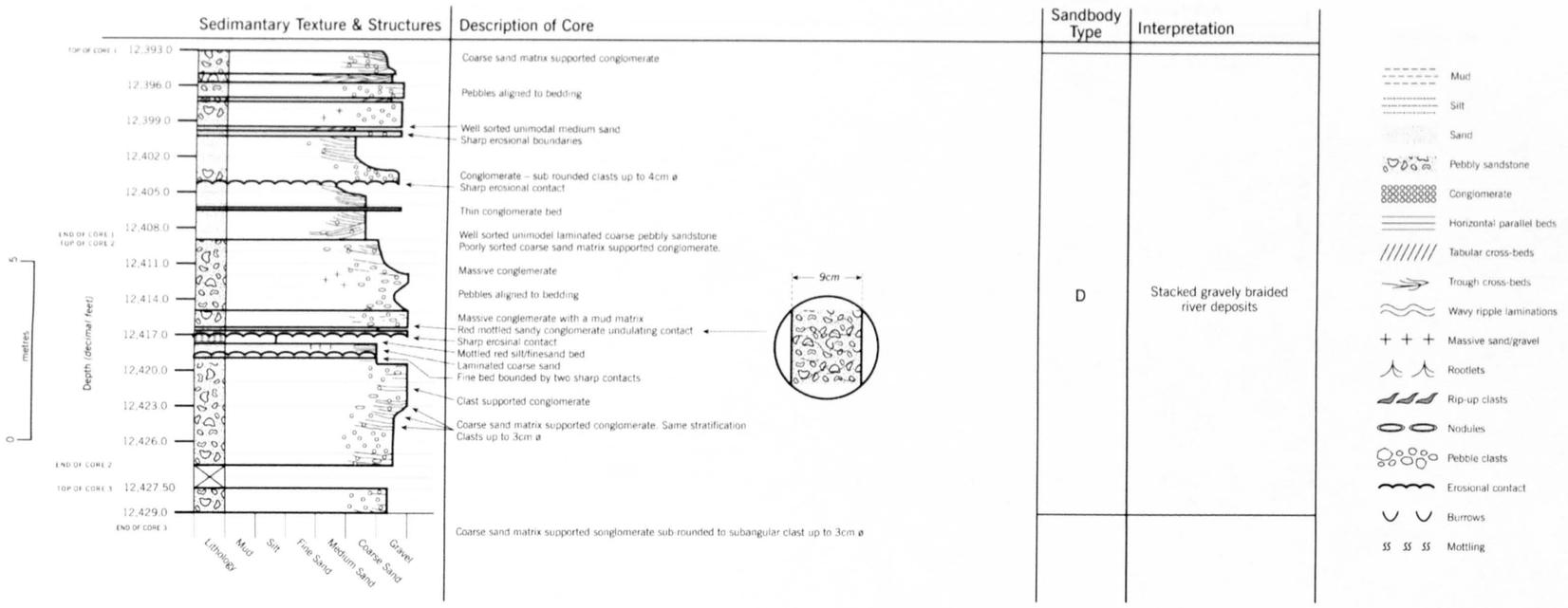

Date Logged: *10/2/98* Tyne Field Logs David Moreton

Well Number: *44/18–T1* Core Number: *2* Drillers Depth: *14,582.00' – 14,706.90'* Well Deviation: *28°*

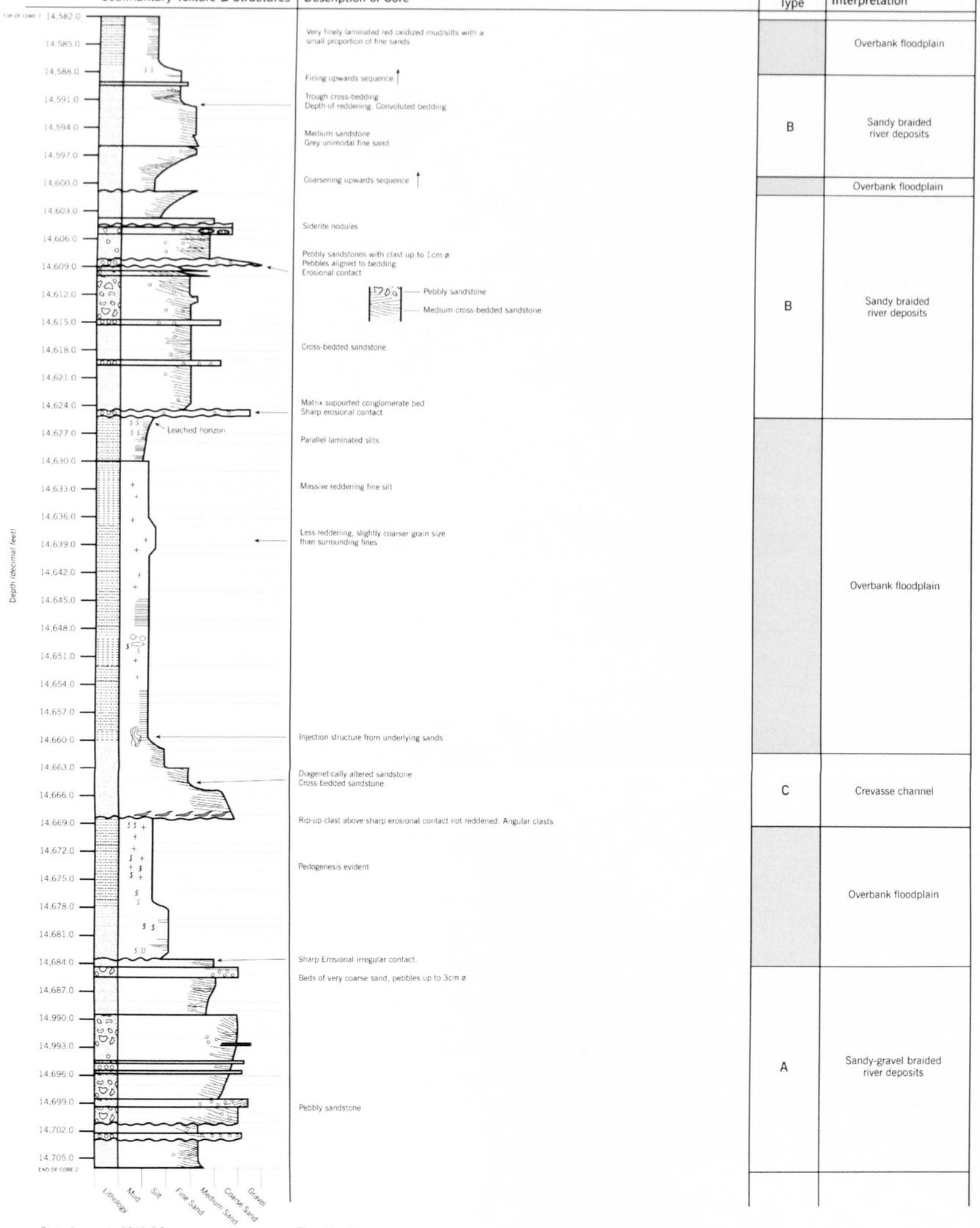

Date Logged: *12/1/98*

Tyne Field Logs

David Moreton

Well Number: *44/18–T2* Core Numbers: *1,2,3* Drillers Depth: *13,236.00' – 13,397.20'* Well Deviation: 24°

Depth (decimal feet)	Sedimantary Texture & Structures	Description of Core	Sandbody Type	Interpretation
TOP OF CORE 1 13,236.0		Unimodel, well sorted trough cross-bedded medium sand		
13,239.0		Very few pebble clasts. <1%	A	Sandy braided river deposits
13,242.0		Fining upwards sequence. A few quartz clasts rip-up clasts of mudstone at base		
13,245.0		Clast supported conglomerate, rounded – subrounded. Clasts up to 2cm ø ina a coarse sand matrix Sandstone lenses with cross-bedding Sharp erosinal incision boundary		
13,248.0		Red overbank laminated mud-siltstone (oxidized)		
13,251.0		Mottled silts		Overbank floodplain
13,254.0				
13,257.0		Planar laminated sands Fining upwards sequence from pebbly sands to floodplain mud/silts Grey unimodel well sorted sand. Some laminations		
13,260.0		Medium grained, homogeneous well sorted sand.		
13,263.0		Trough cross-bedded sandstones		
13,266.0		A few pebbles <1%		
13,269.0		Grey coarse sand laminated with pebble quartz clasts up to 3cm ø. The sand unit is interbedded with conglomerates bed of rounded – subrounded clasts.		
13,272.0		Cross bedded coarse pebbly sandstone		
13,275.0				
13,278.0		Large quartz clast 8cm ø		
13,281.0		Brown matrix supported laminated coarse sand, pebble clasts upto 10% of unit	A	Gravel-pebbly sand braided river deposits
13,284.0				
13,287.0		Very angular clasts up to 2cm ø in clast supported conglomerate bed		
13,290.0				
13,293.0				
13,296.0				
END OF CORE 1 TOP OF CORE 2 13,297.0		Coarse sand conglomerate, subangular clasts upto 3cm ø		
13,300.0		Smaller angular clasts up to 1cm ø, poorly sorted pebbly sandstone. Grading present Cross bedded pebbly sandstone		
13,303.0		Sub-rounded to subangular clasts. Poorly sorted clasts aligned to bedding 5-10% clasts Poorly sorted, clast supported conglomerate bed – rounded clasts upto 3cm ø with coarse sand matrix		
END OF CORE 2 TOP OF CORE 3 13,306.50		Laminated sandstone at the base of unit.		
13,309.50		Thick red oxidized floodplain mud/siltstones some mottling		
13,312.50		Finely laminated horizons		
13,315.50		Pedogenesis evident		Overbank floodplain
13,318.50		Small pyrite nodules with leached halo Massive, well sorted, unimodal sandstone Some laminations		
13,321.50		Unit of coarse pebbly sand with subrounded clasts upto 2cm ø ranging from <1% clasts to 20%		
13,324.50		Stratified pebbly sandstone		
13,327.50		Graded bedding		
13,330.50		Series of small fining upwards sequences with conglomeratic layer at base (sometimes clast supported) to a fairly clean unimodal well sorted sand at top.		
13,333.50				
13,336.50				
13,339.50		Angular clasts up to 2cm ø		
13,342.50		Sharp boundary with clay rip up clasts at base		
13,345.50		Fine mud fill (grey)		
13,348.50		Homogeneous unimodal well sorted laminated medium sandstone.		
13,351.50				
13,354.50		Gradational boundary Clast upto 1cm ø		
13,357.50		Coarse pebbly sandstone with clasts up to 1cm ø and 2% of total unit		
13,360.50		Coarse homogeneous, unimodal well sorted sandstone		
13,363.50				
13,366.50		Angular clast supported conglomerate. Clast up to 1.5cm ø		
13,369.50		Coarse quartz pebble sandstone		
13,372.50		Sharp erosional contact cutting down into floodplain muds/siltstones.		
13,375.50		Sharp contact with underlying sands		
13,378.50		Unimodal well sorted sand Irregular boundary between conglomerate and sandstone Conglomerate		
13,381.50		Clast supported conglomerate, with matrix coarse sand Mudstone bed, 3cm thick Unimodel well sorted laminated medium sand		
13,384.50		erosional boundary laminated grey mudstone conglomerate		
13,387.50		Matrix supported coarse sand conglomerate unit Laminated pebbles aligned to bedding Clasts up to 2cm ø mainly quartz Clasts range from 1% to 80% (clast supported) of the unit		
13,390.50				
13,393.50			D	Vertically stacked gravel braided river deposits
13,396.50 END OF CORE 3				

Lithology: Mud, Silt, Fine Sand, Medium Sand, Coarse Sand, Gravel

Mud
Silt
Sand
Pebbly sandstone
Conglomerate
Horizontal parallel beds
Tabular cross-beds
Trough cross-beds
Wavy ripple laminations
Massive sand/gravel
Rootlets
Rip-up clasts
Nodules
Pebble clasts
Erosional contact
Burrows
Mottling

0 metres 5

Date Logged: *10/2/98*

Tyne Field Logs

David Moreton

Well Number: *44/18–2Z* Core Numbers: *1,2,3* Drillers Depth: *12,892.00' – 13,265.00'* Well deviation: *45°*

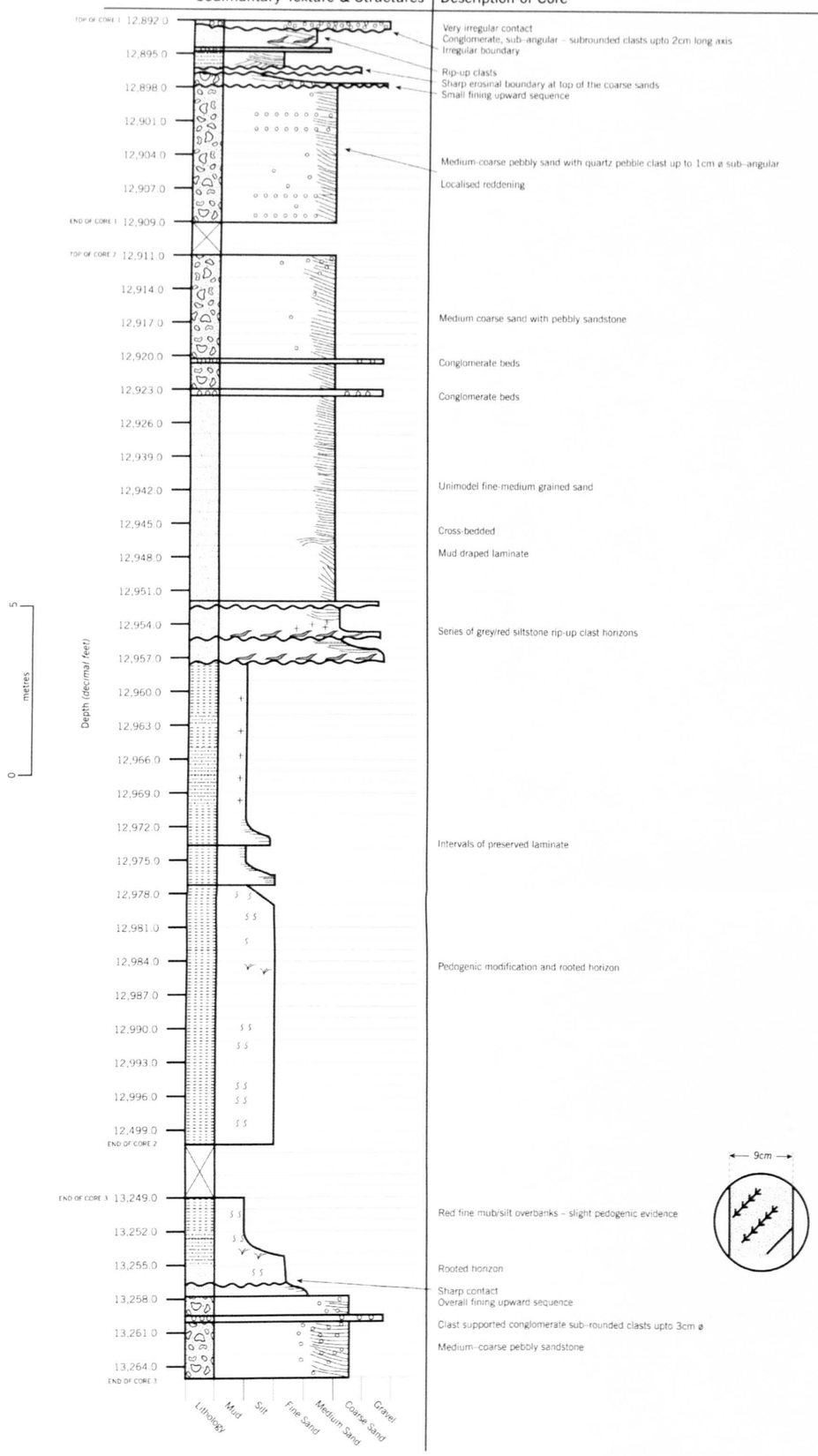

Date Logged: *10/2/98*

Tyne Field Logs

David Moreton

Well Number: *44/18–T3a* Core Numbers: *1 & 2* Drillers Depth: *21,154.00' – 21,256.00'* Well Deviation: 64°

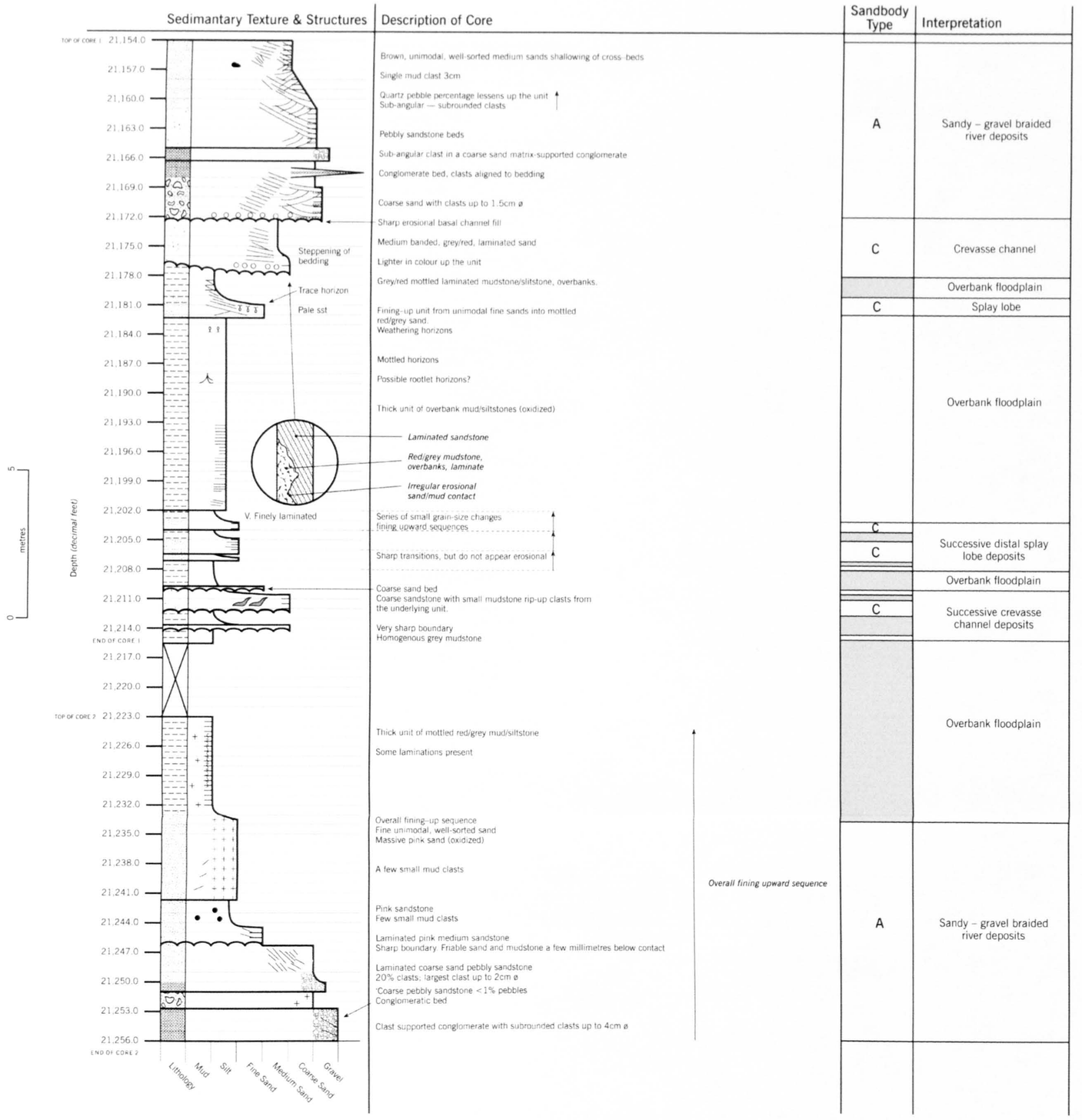

Date Logged: *11/2/98* Tyne Field Logs David Moreton

Well Number: *44/18–4A* Core Numbers: *1 & 2* Drillers Depth: *12,208.00' – 12,374.20'* Well deviation: *4°*

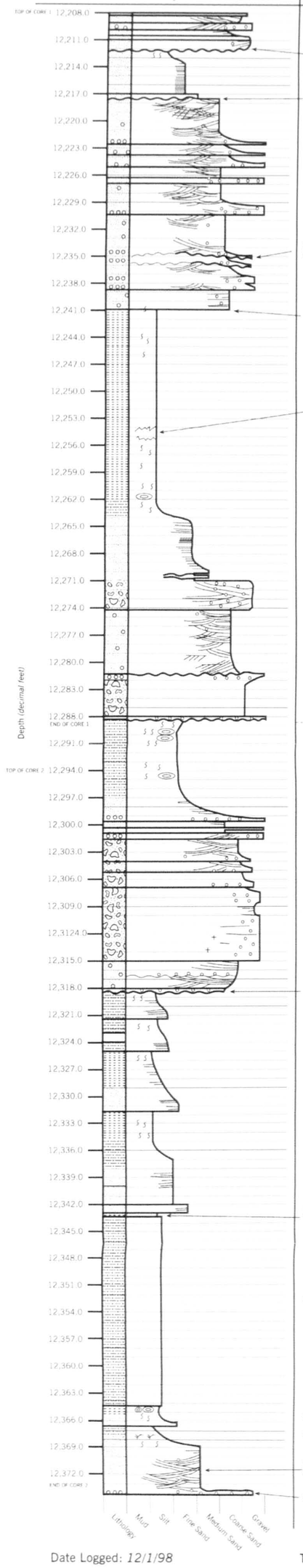

Date Logged: *12/1/98* Tyne Field Logs David Moreton

Well Number: *44/18a–T5* Core Numbers: *2 & 3* Drillers Depth: *18,058.00' – 18,173.50'* Well Deviation: 54°

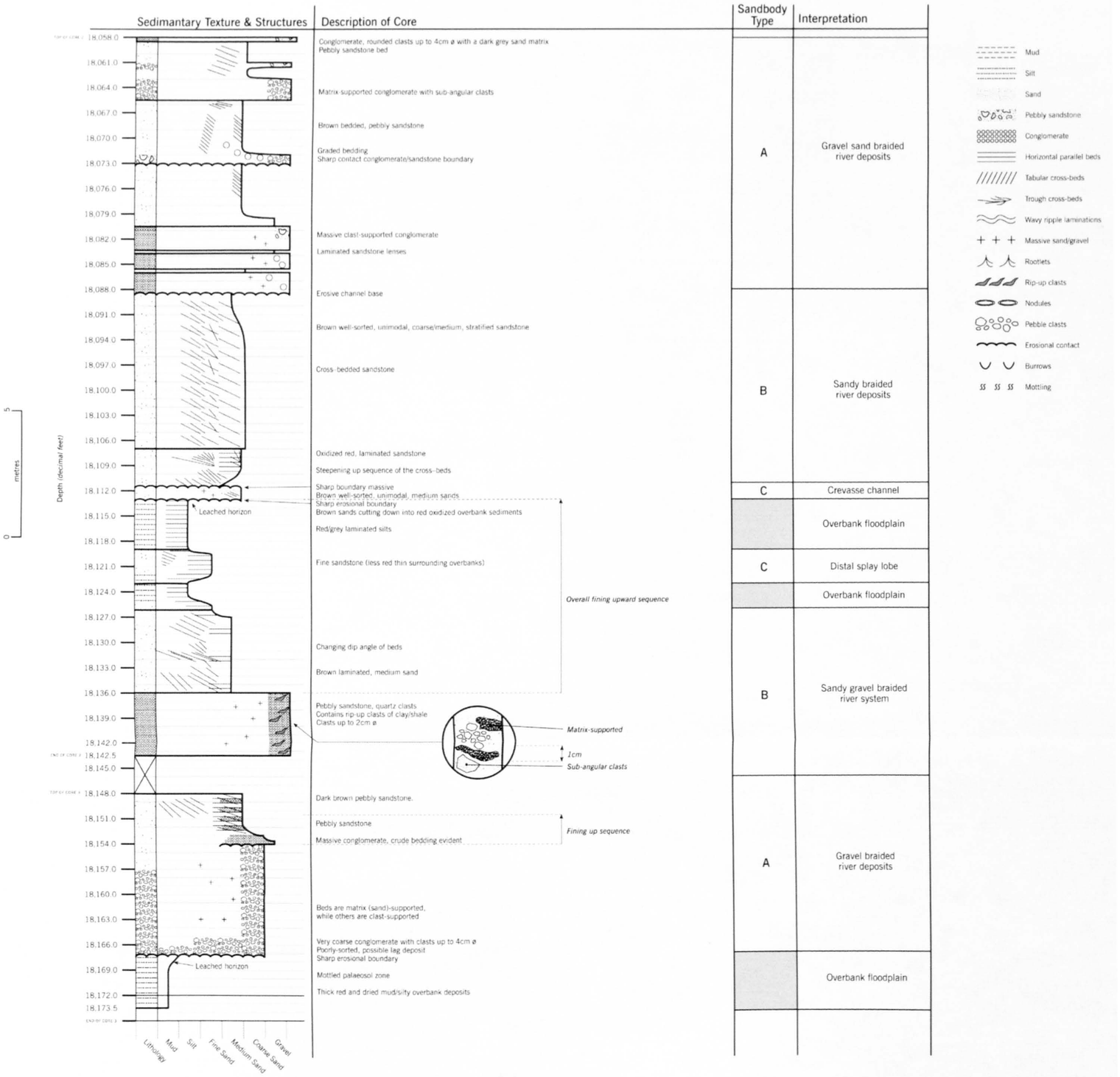

Date Logged: *12/1/98* Tyne Field Logs David Moreton

Well Number: *44/18a–5* Core Number: *2* Drillers Depth: *12,455.00' – 12,566.00'* Well Deviation: *0°*

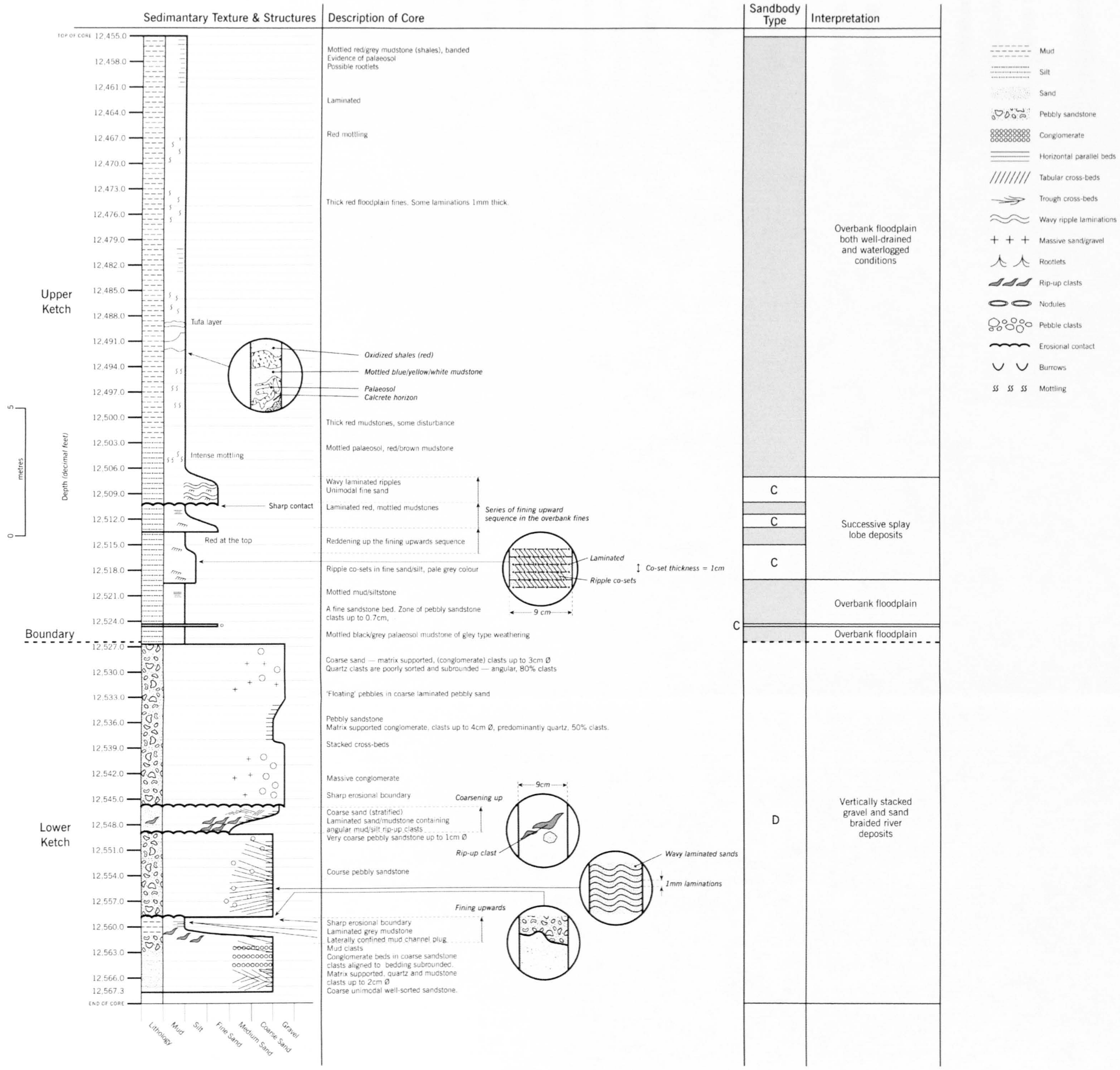

Date Logged: *10/2/98*

Tyne Field Logs

David Moreton

Appendix B: Kruskal-Wallis Test: Analysis of variance by ranks

The nonparametric Kruskal-Wallis one-way analysis of variance, is a test of the equality of medians for two or more populations. Nonparametric implies that there is no assumption of a specific distribution for the population. The Kruskal-Wallis hypotheses are:

H_0: the population medians are all equal versus,

H_1: the population medians are not all equal.

An assumption for this test is that the samples from the different populations are independent random samples from continuous distributions, with the distributions having the same shape.

The Kruskal-Wallis test uses the ranks of the data rather than their raw values. The values are first ranked from low to high, disregarding which group each value belongs. If two values are the same, then they both get the average of the two ranks for which they tie. The smallest number gets a rank of 1. The largest number gets a rank of *N*, where *N* is the total number of values in all the groups. The ranks are then summed in each group. If the sums of the ranks are very different, the P value will be small. If the P value is greater than 0.05 (95 % significance level) then there is no difference between the population medians.

The Kruskal-Wallis test was performed using MiniTab 12.2 for comparison of channel geometry and architectural element distributions in Chapter 6.

Appendix C: Grain size for suspended sediment samples

D_{50} values for samples of suspended sediment taken during series C and F are presented in Table C1 and were used to establish relative fall velocities for each experiment (Chapter 6, Section 6.12.1).

Table C1. D_{50} values for samples of suspended sediment taken from series C and F.

D_{50} (microns)	
Series C	Series F
4.837	2.11
3.529	1.467
1.95	0.895
2.325	1.174
2.061	1.016
1.153	1.072
1.663	1.169
1.715	0.568
1.524	1.254
1.563	1.129
0.969	1.046
1.226	1.407
1.366	1.165
1.521	0.749
1.269	1.003
1.269	1.027
1.134	0.932
1.09	1.071
1.074	0.992
0.763	1.044
1.042	1.014
0.947	1.04
0.955	1.08
1.22	0.79
0.787	1.057
0.929	0.965
0.805	2.308
0.794	1.688
	0.866
Mean	Mean
1.481	1.141

Appendix D: Supplementary CD

A supplementary CD is provided in a web-browsable format to provide additional information to support this thesis, which includes:

1. Lithofacies for the Lower Ketch Member, Tyne Field, Southern North Sea.

2. Extra images of sandbody types from the Escanilla Formation.

3. Overhead video footage from generic-Froude-scaled modelling of the Ashburton River from the series C and F.

In order to access the CD, double click on the 'Thesis CD May 2001' folder and then the 'index.htm' file. The index page will open in either Internet Explorer or Netscape. Click on the above contents to access the information. Video files will open in the Netscape window or in Windows Media Player within Internet Explorer.